

**National Academy of Sciences of Ukraine (NASU)
Frantsevich Institute for Problems of Materials Science of NASU
Ukrainian Materials Science Association "Composites"
INTEM LTD (Ukraine)**

Under auspices of



INTERNATIONAL CONFERENCE

**"Science for Materials in the Frontier
of Centuries:
Advantages and Challenges"**



20030110 024

PROCEEDINGS OF CONFERENCE

Editor: Academician, Professor Valery V. Skorokhod

**4-8 November 2002
Kyiv, Ukraine**

REPORT DOCUMENTATION PAGE

Form Approved OMB No. 0704-0188

Public reporting burden for this collection of information is estimated to average 1 hour per response, including the time for reviewing instructions, searching existing data sources, gathering and maintaining the data needed, and completing and reviewing the collection of information. Send comments regarding this burden estimate or any other aspect of this collection of information, including suggestions for reducing the burden, to Department of Defense, Washington Headquarters Services, Directorate for Information Operations and Reports (0704-0188), 1215 Jefferson Davis Highway, Suite 1204, Arlington, VA 22202-4302. Respondents should be aware that notwithstanding any other provision of law, no person shall be subject to any penalty for failing to comply with a collection of information if it does not display a currently valid OMB control number.

PLEASE DO NOT RETURN YOUR FORM TO THE ABOVE ADDRESS.

1. REPORT DATE (DD-MM-YYYY)
19-11-2002

2. REPORT TYPE
Conference Proceedings

3. DATES COVERED (From - To)
4 November 2002 - 8 November 2002

4. TITLE AND SUBTITLE

Science for Materials in the Frontier of Centuries: Advantages and Challenges
Vol. 2

5a. CONTRACT NUMBER
F61775-02-WF042

5b. GRANT NUMBER

5c. PROGRAM ELEMENT NUMBER

5d. PROJECT NUMBER

5d. TASK NUMBER

5e. WORK UNIT NUMBER

6. AUTHOR(S)

Conference Committee

7. PERFORMING ORGANIZATION NAME(S) AND ADDRESS(ES)

Institute for Problems of Materials Science
3 Krzhyzhanovsky Str.
Kyiv 03142
Ukraine

8. PERFORMING ORGANIZATION
REPORT NUMBER

N/A

9. SPONSORING/MONITORING AGENCY NAME(S) AND ADDRESS(ES)

EOARD
PSC 802 BOX 14
FPO 09499-0014

10. SPONSOR/MONITOR'S ACRONYM(S)

11. SPONSOR/MONITOR'S REPORT NUMBER(S)
CSP 02-5042

12. DISTRIBUTION/AVAILABILITY STATEMENT

Approved for public release; distribution is unlimited.

13. SUPPLEMENTARY NOTES

14. ABSTRACT

The Final Proceedings for Science for Materials in the Frontier of Centuries: Advantages and Challenges,
4 Nov 02 - 8 Nov 02

- I. Fundamental problems of materials science including phase transformations, reaction kinetics, deformation of materials, materials modeling, and surface phenomena.
- II. Prospective materials for functional and structural purposes as composites, ceramics, amorphous and nano-crystalline materials, quasi-crystals, fullerenes, nano-tubes, intermetallics, eutectic materials, hard alloys and cermets.
- III. Materials processing routes including materials synthesis in the bulk and dispersed states, self-propagating high-temperature synthesis, powder formation, sintering, joining, and coating.
- IV. Characterization of materials properties using non-destructive methods, microscopy, spectroscopy, acoustics, and X-ray

15. SUBJECT TERMS

EOARD, Materials, Metals & alloys, Polymers, Ceramics

16. SECURITY CLASSIFICATION OF:

a. REPORT
UNCLAS

b. ABSTRACT
UNCLAS

c. THIS PAGE
UNCLAS

17. LIMITATION OF
ABSTRACT
UL

18. NUMBER
OF PAGES

793

19a. NAME OF RESPONSIBLE PERSON
Charles H. Ward, Lt Col, USAF

19b. TELEPHONE NUMBER (Include area code)
+44 (0)20 7514 3154

Standard Form 298 (Rev. 8/98)
Prescribed by ANSI Std. Z39-18

AQ F03-03-0435

**This conference is dated
to 50th Anniversary of Frantsevich
Institute for Problems of Materials
Science of National Academy of Sciences
of Ukraine**



DISTRIBUTION STATEMENT A
Approved for Public Release
Distribution Unlimited

VOLUME II

AQ F03-03-0435

LIST OF ABBREVIATIONS

NASU	– National Academy of Sciences of Ukraine
RAS	– Russian Academy of Sciences
NASB	– National Academy of Sciences of Belarus
NSAU	– National Space Agency of Ukraine
PAS	– Polish Academy of Sciences
BAS	– Bulgarian Academy of Sciences
SB	– Siberian Branch of RAS
KSC FEB	– Khabarovsk Science Center of Far East Branch
NTUU “Kiev Polytechnical Institute”	– National Technical “University of Ukraine “Kiev Polytechnical Institute”

**EXTENDED ABSTRACTS ARE PUBLISHED IN ORIGINAL
PRESENTED BY THEIR AUTHORS**

**ORGANIZING COMMITTEE DOES NOT RESPONSIBLE FOR
QUALITY AND CONTENT OF THESE MATERIALS**

***Scientific Secretary of Conference
L. CHERNYSHEV***

***SECTION II. PERSPECTIVE
MATERIALS
OF FUNCTIONAL
AND STRUCTURAL
PURPOSES: POSSIBILITIES
OF OBTAINING NEW LEVEL
OF PROPERTIES***

UNMIXED SYSTEMS AS THE NEW CLASS OF PERSPECTIVE MATERIALS FOR MODERN TECHNIQUE

Bashev V.F., Dotsenko F.F., Ryabtsev S.I., Beletskaya O.E., Kutseva N.A., Balyuk Z.V.
Dniepropetrovsk National University, Dniepropetrovsk, Ukraine

The formation of metastable (including solid amorphous) states in immiscible (unmixed) systems is of great fundamental and practical interest as it can open a new class of perspective materials specifically for microelectronics, radio building and TV. Among such alloys are the systems W-Ba, Ni-Ba, C-Cu, Fe(Ni, Co)-Ag with both components having the bcc or the fcc lattice. These systems are characterized by anomalously high positive values of heat of formation. Calculated within the modernized semi-empirical Miedema model these are 170 kJ/mol (W-Ba system), 105 kJ/mol (Fe-Ag system), 59 kJ/mol (Ni-Ag system). Calculations of the energetic effects of mixing in this model are based on the contact interactions at the boundary which separates heterogeneous metals taking account also of atomic size differences. The Miedema model excluding atomic size effects gives good results for the heats of dissolutions of liquid metals. Therefore it was of interest to establish the correlation between the structure and properties of sputtered alloys. In order to obtain the above alloys over the whole range of concentrations an improved method of ion-plasma sputtering in a vacuum is used. An additional acceleration of Ar ions impinging on the target, and hence an great increase in the kinetic energy of sputtered atoms depositing on to the ceramic glass substrates, was achieved by using a specially designed device in the sputtering apparatus. This produced a considerable additional acceleration of the bombarding ions in the final part of their trajectories just before striking the target surface. As a result there is a stream of sputtered atoms with large dispersion in energy and in direction. Due to sufficient mixing in the vapour favorable conditions are realized for the formation of highly non-equilibrium phases on substrates.

In conditions of modern 3-electrod ion-plasma sputtering (IPS) was investigated film non-equilibrium system "carbon-copper". It was established that during the same technological conditions carbon is fixed in amorphous and alloys C-Cu and copper - in crystalline state. Thus in film C - 12at. %Cu alloys besides crystalline compounds: copper ($a=0,3628$ nm), new

metastable diamond-like phase ($a=0,4476$ nm) and hexagonal graphite ($a=0,2428$ nm, $c=0,6556$ nm) is founded and an amorphous carbon. The energy of connection between carbon atoms more than in two times bigger energy connection in graphite. According to transmission electron data in C-Cu alloys with $c<59,5\%$ (at.) it is observed formation of "really copper" of areas among which the diamond-like structure is situated. The C - 22.6% Cu alloy has the higher electrical resistance among all receiving alloys. Here the highest intensity of diamond-like peaks is observed. During the treatment coalescence of pseudocrystals of Cu passes with decreasing of square of contact with carbon composite. This leads to change in carbon structure: passage from diamond-like structure to carbon structure with significant (~in 100 times) decreasing of electrical resistance. Changing of resistance is connected with decomposition of amorphous composite also. But decomposition of diamond-like phase influences more significant on electrical resistance of films, than decomposition of amorphous phase. Maybe received in hard conditions of modern IPS high resistance diamond-like is strong semiconductor.

The structure of Fe - (22,6.48,6) at.% Ag film alloys in as-sputtered state represents the mixture of supersaturated solid ($a=0,4084$ nm) solution on Fe-base and microcrystalline Fe. The structure of Ni - (27.42) at.% Ag films alloys represents of amorphous structure with precise value of TCR $\sim 2 \cdot 10^{-6} \text{ K}^{-1}$.

Magnetic properties these films have been measured by vibrating sample magnetometer. The coersivity of Fe - 22,6 at.% Ag films after treatment is about 2 kOe when the H is athwart to sheet of films. In the case the H is parallel to sheet of films coersivity was 140 Oe. The value of coersivity in Fe-Ag films can be likened to a H_c of hardmagnetic films Fe-Nd-B system. It should be recorded that there is the thickness of Fe-Ag film in 10^3 times was smaller than thickness of Fe-Nd-B films.

The next perspective unmixed systems are W-Ba and Ni-Ba film alloys. A limitation of traditional method of receiving of emissive cathodic knots is that it does not possibility to obtain homogeneous emissive alloys from unmixed components, high adhesion metals (Ba, Sr, Ca) on W-substrate to reach miniature geometrical forms of cathodic knots.

By using the modernized 3-electrod method of ion-plasma sputtering the amorphous phase in W(Ni) – Ba film alloys was received in wide concentration intervals. After this treatment (900 – 1000 K) mosaic system of alternating microareas W, Ni or Ba) with different electron density and work of exit have been formed. Received areas (W, Ni) with high density of emissive current of electrons and high work of exit become the effective electron donors, which are joining to microareas (Ba, Sr, Ca) with low work of exit (1,4 eV). Thus this method makes possible electrons from areas with high electron density and high values of work of exit to leave this surfaces by the way of similar "tunneling". These electrons have considerably lesser energy as compared with traditional conditions. It guarantees total high electron emissive density of miniature film emissive cathodic knots at relatively low temperatures of

emissive surfaces. Marking in one cycle by thermal way on the final stage of ion-plasma sputtering of mosaic targets the protective layer of Mg on the emissive surface cathodic knots makes possible of long preservation these knots in atmosphere conditions. Deliverance of surface of cathodic film knots from Mg – layer passes automatically at heating and preparation cathodic knot to work's state.

This method secures the following advantages: 1) the possibility of receiving emissive film unmixed alloys in wide concentration intervals; 2) improving and restoring emissive characteristics of film alloy by the way of cycle treatment; 3) the possibility of application of straight warming up emissive surface by electric current; 4) accommodating with high density of miniature cathodic point knots on the area for new improved colour TV-kinescopes.

Thus the proposed method of 3-electrod ion-plasma sputtering opens the new class of film alloys with improved physical properties.

ELECTRON BEAM WELDING OF γ -TITANIUM ALUMINIDE

Zamkov V.N., Sabokar V.K., Vrzhyzhevsky E.L.

E.O.Paton Electric Welding Institute of the NAS of Ukraine, Kyiv, Ukraine

Interest in γ -TiAl based alloys is dictated by their unique properties. They possess high heat resistance and thermal stability and, at the same time, relatively low density ($3.8-3.9 \text{ g/cm}^3$) [1]. However, at normal temperatures these alloys have low ductility, which makes their treatment much more difficult and hampers their commercial application. Therefore, utilization of γ -TiAl in different-application structures will be determined to a high degree by development of efficient processes for their treatment, including welding.

Because of low ductility (up to a temperature of 700°C), γ -TiAl alloys are very sensitive to stresses formed under conditions of non-uniform heating during welding, and their welded joints are susceptible to transverse cold cracking. It is suggested in [2, 3] that preheating of weld edges should be used to prevent formation of the above cracks, as this method leads to a decrease in the rate of growth of temporary stresses during welding and lowers the level of residual welding stresses. However, the above studies contain no unambiguous recommendations for a preheating temperature at which the crack-free welded joints could be guaranteed.

Investigations were conducted on samples of γ -alloy Ti-48Al-2Nb-2Mn, 4-17 mm thick, cut from an ingot and subjected to isostatic treatment at a temperature of 1260°C and pressure of 171 MPa for 4 hours, and to subsequent stabilizing annealing at 1015°C for 50 hours.

As shown by calculation methods, the larger the thickness of a metal welded, the higher the rigidity of a plate and the higher the preheating temperatures. In this case the level of stresses formed in welding under the effect of the welding cycle temperature gradient will not exceed tensile strength of the metal, and no cracks will be formed in a welded joint.

The samples were welded using the UL-144 machine equipped with the ELA 60/60 power unit. Preheating was performed in a welding chamber by scanning a low-power electron beam over the surface of a workpiece. The preheating temperatures were 400 , 500 and 600°C . Welding with full penetration of edges was performed in a single pass using no filler metal.

The character of variations in temperature along the weld axis and peculiarities of formation of longitudinal temporary and residual stresses were established by calculating temperature fields in EBW, allowing for preheating. Relatively low thermal conductivity of the alloy favours that temperature field in a plate retains its non-uniformity for a long time after completion of welding. Therefore, temporary stresses in the weld metal increase with cooling of a sample down to the initial welding temperature. It was shown that the level of residual tensile stresses along the weld at a preheating temperature of 400°C was not in excess of tensile strength of the alloy at a normal temperature, which accounted for the absence of cracks in the plates welded using preheating to 400°C .

Mechanical tests of welded joints showed that metal in the as-welded condition had σ_t equal to $332.8-353.6 \text{ MPa}$.

Annealing after welding at temperatures of $800-900^\circ\text{C}$ for 10-15 min leads to a fundamental decrease in the probability of formation of transverse cold cracks, owing to a decrease of almost 2 times in residual welding stresses in the plates. This heating was performed immediately after the end of welding using the same procedure as that employed for preheating.

Mechanical tests showed dependence of σ_t upon postweld annealing. Thus, in the as-welded condition + annealing σ_t is equal to $459.0-522.0 \text{ MPa}$. A substantial difference in the values of σ_t of welded samples without annealing and after annealing can be explained only by the presence of residual welding stresses in a welded plate, which are decreased as a result of annealing.

It has been established that annealing at 800°C for 10 min immediately after welding favours development of lamellar structure in all regions of a welded joint. However, the observed microstructural transformations can hardly cause an increase in strength of the welded joint. It can be concluded that the main cause of this phenomenon does lie in a decrease in residual stresses.

Heat treatments were conducted in a vacuum furnace for 5-25 hours in the $(\alpha+\beta)$ region of the

alloy to form the most favourable structure in terms of mechanical properties of welded joints.

The main structural characteristic of a heat-treated welded joint is formation of a Widmanstatten structure in all its regions.

The best mechanical properties of γ -titanium aluminide Ti-48Al-2Nb-2Mn ($\sigma_t = 513-528$ MPa, $\sigma_{0.2} = 480.8-499.0$ MPa) and the optimal structure ensuring such properties were achieved after annealing at 1260 °C for 25 hours. The presence of the Widmanstatten structure, which is formed as a result of the $\gamma \rightarrow \alpha$ transformation, has a favourable effect on ductile properties of the alloy.

Conclusions

1. To prevent formation of transverse cracks in EB welded joints of alloy Ti-48Al-2Nb-2Mn, 4-17 mm thick, it is recommended to subject workpieces to a temperature of 400-500 °C.
2. To decrease the level of residual stresses, it is necessary to subject welded joints immediately after welding to annealing within a temperature range of 800-900 °C.

3. To provide the optimal structure and mechanical properties of welded joints in γ -titanium aluminide, it is necessary to conduct annealing at 1260 °C for 25 hours.

References

1. Ivanov V.I., Yasinsky K.K. Efficiency of application of heat-resistant alloys based on intermetallics Ti_3Al and $TiAl$ for operation at temperatures of 600-800 °C in aircraft engineering. – 1996. – No. 3. – P. 7-12, 93.
2. Titanium aluminide: electron beam weldability / R.A.Patterson, P.L.Martin, V.K.Damkroger, L.Christodoulou // Welding J. – 1990. – 69, No. 1. – P. 39-44.
3. The effect of postweld heat treatment on the structure and properties of electron beam welded Ti-48Al-2Cr-2Nb / C.M.Jensen, H.Zhang, W.A.Baerslack, T.J.Kelly // Abs. of Papers Presented at 79th AWS Annual Meeting. – Miami: AWS, 1998. – P. 179-180.

ADVANCED LIGHT ALLOYS METALLIC SYSTEMS FOR THE FUTURE: PROGRESS IN HIGH - CURRENT ELECTRONICS AND DYNAMIC (STRUCTURAL) APPLICATIONS

Tkachenko V.G.

Frantsevich Institute for Problems of Materials Science, National Academy Science of Ukraine,
Kiev Ukraine

This report use aims to exchange and disseminate basic ideas in the field of designing advanced metallic alloy systems between research scientists and engineers throughout the world. The emphasis is placed on the original research, both analytical and experimental, in various aspects of the approach when outstanding new advances are made in existing areas of physics of metals and electronic materials science and new areas have been developed to definite stage.

I. Stimulated Diffusion in Excess Vacancy Supersaturated Solid Solutions with Cluster - Forming Structure.

The effect of inducing the excess (non - intrinsic, structural) vacancies with mobile interstitials (hydrogen atoms and the like) as well as of forming the diffusive mobile clusters of "excess vacancy - solute" are predicated theoretically and then supported in a series of experiments. In search of the generalized approach, the results obtained are analyzed and summarized in terms of solute - stimulated diffusion concept and of a structure - clustering model with the estimates of the rate of relaxation and the activation parameters of diffusion at the temperature range of 77 - 1000K by means of structure - sensitive methods of measurements (discrete Q^{-1} temperature spectra, mechanical hysteresis loops, electron - positron annihilation on vacancies, electroresistivity, etc.). The excess vacancy concentration is found to exceed the values of thermally equilibrium vacancies in pure metals by two - three orders. As a consequence, it changes the classical vacancy - type mechanism of diffusion in the substitutional subsystem (HCP Mg-Ba) facilitating the formation of diffusive nanoclusters with different bonding energies. Then accelerated short - range diffusion in solid solutions is developed by the mixed (partly - through excess vacancy sites, partly - through interstices) cluster diffusion mechanism typical for above solid solutions and responsible for thermally activated deviation of solute diffusivity from classical (Arrhenius) behavior at low temperatures as well as for the appearance of high - temperature anomalies in electrical resistance (FCC Al-Li), change the interstitial - to -substitutional - type

mechanism of diffusion with increasing temperature (HCP Be-C), and deviation from Vegard's law predicting a linear dependence of atomic volume as function of solute concentration.

II. Crystals Systems with Advanced Quantum Yield of Photoemission.

Development of the high - current UHF electronics stimulated exploring the photoemissive materials with enhanced quantum yield (Y , 10^{-3} - 10^{-2} electron/photon) in the ultraviolet spectral range, which have to maintain their properties at the technical vacuum conditions (10^{-5} - 10^{-6} Torr) under the influence of the intensive laser irradiation (10^6 - 10^7 Wt/sm²), strong (100MV/m scale) accelerating electric fields. It is known that conventional semiconductors being technological basis of the modern solid state physics prove to be synthesized in situ become unstable even in ultra high vacuum especially under the influence of intensive laser irradiation. Pure metals also could hardly be used there because of low Y - value in this spectral range. Advanced metallic alloy systems appear to be a suitable tool to increase photoemissivity of the some perspective metals of IIA and IIIB subgroups of Periodic Table (particularly, magnesium and aluminium) for producing extremely bright, high repetition rate devices.

Generalized results are presented which concern with perspective aluminium and magnesium alloys possessing new combination of bulk (structural) and surface (emissive) properties. The linear dependence of quantum yield on a photon energy in the $Y^{1/2}$ - $h\nu$ theoretical coordinates is in agreement with Fowler's law for near - free - electron model. Under the available and classified data of paramagnetic susceptibility, Auger - electron, X - ray and - UV - photoelectron spectroscopy for decaying solid solutions (FCC Al-Li) possessing true (lattice) solubility as well as eutectic alloys (HCP Mg-Ba) with nanophase structure differing effective solubility only on the structural defects the reliable correlation between improved quantum yield of photoemission and increased local density of occupied states of valence electrons near the Fermi surface is for the first time established which is determined by a volume portion of a crystalline

structure of their solid solutions if the energy of a quantum exceeds photoelectric work function.

On this basis the concepts of segregated solid solutions and diffusion clustering a structure are developed, and nanocluster segregation model for nanophase materials is suggested which relates electron structure and optic properties with their solute composition closed to corresponding chemical compounds and describes rapid decomposition with formation of hydride - like segregation and/or prephase (GP - zone) "precipitates". The new regularities allow to formulate physical principles of doping the light metals IIA and IIIB subgroups of Periodic Table necessary for creation of perspective photoemissive materials with increased quantum efficiency, which can be used for replacement of semiconducting photoemitters, ineffective in strong electric fields and technical vacuum. They are based on recognizing of the decisive contribution of chemical binding state change for solid solutions or its hybridization in nanocluster as emission - active centers providing stable quantum yield, in particular, on the nature of hybridization of Ba - and Mg atomic orbits (s,p,- d - electron configurations) for eutectic alloys with cluster - forming structure.

Using preliminary activation of sample surface by a pulsed excimer XeCl laser irradiation and studying the observed photoelectron energy - distribution data as well as the quantum yield's spectral characteristics within the photon energy range up to 11 eV one can demonstrate a two - three order - magnitude improvement in the quantum efficiency of the metallic alloy (massive) photocathodes compared to corresponding pure metals (aluminum and magnesium). On this basis are evidenced a possibility of principle and advantages for producing (branching) the monoenergetic electron beams in a nanosecond range using Mg-Ba,X and Al-Li,X alloy systems to facilitate the solution of one of the key problem of the accelerative technique requiring creation of laser - controlled photoelectron gun with shot (nanosecond) current pulses.

Maximum quantum yield of these advanced binary and ternary alloy systems is characterized by an optimum combination of volume - controlled properties ensuring the most effective redistribution of partial DOS near the Fermi level, and surface localization of a dipole moment (double electrical layer consisting from volume - diffusible and polarized atoms of alloying elements) with a minimum of photoelectric work function for excited valance electrons.

The existence of universal relationship between the fundamental macro -, micro, - and submicro (electron) levels is outlined for the investigated metallic alloy systems. For example, Li as alloying element increases macroscopic elastic modulus, grain boundary contribution into strengthening/softening effects and quantum yield photoemission. The level of their photoemissive properties is attributed by nature of chemical bonding to be formed as well as relative electronegateness (ionization energy) which increases within third period (Na, Mg, Al) and reduces in subgroup (IIA - Be, Mg,Ca,...Ba) with increasing atomic number of elements.

III. Steady Progress of Structural Light Alloys.

Two group of structural magnesium alloys are being developed in industrial use to meet requirements for further developments of technical progress: (i) high creep - resistant, light and more cheaper magnesium alloys for automobile, radio engineering and other dynamic applications; (ii) .high temperature - strength magnesium based alloys containing Y, Sc, Th RE as alloying elements for high - loaded details applications in industrial use (aircrafts, helicopters, automobile engines). Taking into consideration seller's price of the RE which restrict their adoption in a mass production, aerospace,- acoustician,- and car designers are interested in development of lower cost, high creep - resistant and light structural materials not containing the RE is possible in order to use them in dynamic applications in which a low moment of inertia, good static stiffness and high resistance to deformation at evaluated temperatures are essential. In the present research the main attention is given to magnesium alloys of Mg - Al,Ca,Ba,X system of eutectic origin as well as discontinuous SiC (Al_2O_3) particle - reinforced magnesium matrix composites to be produced different routs of advanced processing. The evaluated temperature creep and unit strength properties appear to be significantly better (at the creep limit of 65 MPa and 160 °C) than that of the commercially available MgAZ91D alloy with divorced eutectics (Dow Chemical Corp., USA).

New generation superlight alloys of HCP Be-Al,Mg,Si system can be successfully utilized in precision aerospace navigational instrumentation such as gyroscope components requiring materials with high microyield strength and good dimensional stability as well as precision optical components for high quality metal optic mirrors with an extremely high stiffness - to weight ratio and an excellent thermal conductivity.

POWDER TITANIUM INTERMETALLIDES

I.I.Ivanova, A.N.Demidik

Institute for Problems of Materials Science NASU, Kiev, Ukraine

Within the last decade high-temperature strength and heat resistance lightweight alloys attract a great attention. Such alloys are of great interest for aircraft, space and transport industry. The most promising materials of this class are titanium based alloys. In addition to traditional materials of Ti-V, Ti-V-Nb, Ti-Zr-Nb types, new materials based on intermetallide compounds, especially titanium aluminides, are intensively developed [1,2]. Such compounds are distinguished by high-temperature strength but they show low plasticity at room temperature. Their production by smelting is rather complicated and the most of developments are dedicated to the production of intermetallides based materials by powder metallurgy methods. Processes of intermetallides preparation in Ti-Ni, Ti-Al, Ti-Si systems have been studied in this work. The intermetallides have been prepared by high-energy milling of powders followed by sintering. Titanium has been used both as electrolytic powder and as titanium hydride powder. Powders milling and mixing have been carried out in the vibration mill at a 1:10 ratio of blend and balls. Specific surface of powders and degree of lattice distortion have been determined after milling.

Investigation of powders milled has shown that considerable dispersion is achieved only for silicon and titanium hydride powders that have size of particles less than 1 μm . Titanium, nickel and aluminium powders milling has not resulted in substantial changes of dispersity. However, the shape of particles changes rather considerably.

Measurement of specific surface and lattice distortion has shown that optimum milling time is 3-5 h what has been taken for the subsequent preparation of Ti-Al, Ti-Ni, Ti-Si mixtures using titanium or titanium hydride powders.

Microstructural study of particles in powder mixtures has shown the following. In Ti-Al mixtures the titanium flat particles that have size about 50 μm are partially covered with an aluminium layer preventing further disintegration of titanium. The same situation is observed in Ti-Ni mixtures but in this case titanium particles are covered with a thinner nickel layer (1-2 μm) and less uniformly.

In the Ti-Si system, at first, active silicon dispersion occurs during joint milling. Then silicon particles are forced into the flat titanium plates. Processes of the alloy formation that follows the mechanical alloying pattern are absent in all systems.

Synthesis of Ti_3Al , TiNi , Ti_5Si_3 intermetallides has been studied under different conditions for sintering in vacuum. The specimens with a density of 75-80% have been compacted from the blend prepared. The specimens compacted correspond to the compositions of above intermetallides. Results of X-ray diffraction analysis are given in Table 1. Phases are shown in order of the decrease in intensity. In all the systems the formation of intermetallides results in only the intense exothermic reaction.

In this case fusion or growth and destruction of specimens are observed.

Table 1. Phase composition of specimens from titanium based mixtures

System	Sintering temperature, $^{\circ}\text{C}$	Sintering time, h	Phase composition	Note
Ti-Ni	770	1	$\gamma_{\text{sol}}\text{Ni}+\text{Ti}+\text{Ti}_2\text{Ni}+\text{Ni}_3\text{Ti}$	Ni ₃ Ti traces Exothermic reaction. Specimens are fused
	770	3	$\text{Ti}_2\text{Ni}+\text{Ni}_3\text{Ti}+\text{Ti}$	
	900	2	$\text{Ti}+\gamma_{\text{sol}}\text{Ni}+\text{Ti}_2\text{Ni}$	
	1000	2	TiNi	
Ti-Al	475	24	$\text{Ti}+\text{Al}+\text{Al}_3\text{Ti}$	Exothermic reaction. Growth and deformation of specimens
	620	5	The same	
	900	6	Solid sol. $\text{Ti}+\text{Al}_3\text{Ti}+\text{Ti}_3\text{Al}+\text{TiAl}+\text{Al}$	
	1080	4	The same	
Ti-Si	700	2	Ti+Si	Ti ₅ Si ₃ traces
	800	2	Ti ₅ Si ₃	Exothermic reaction.
	900	2	Ti ₅ Si ₃	Destruction of specimens

At lower sintering temperatures for the systems studied interaction between components does not practically occur or the multiphase material forms. The material contains a number of solid solutions and compounds. When sintering time is increased, subsequent homogenization proceeds rather slowly. Thus, experiments conducted have not allowed the preparation of intermetallides that would have the

given compositions. Experiments have not allowed the preservation of specimens shape and size.

At the next stage synthesis of compounds with titanium introduced as hydride has been studied. Results of X-ray diffraction analysis are given in Table 2. As follows from the data obtained, titanium hydride sharply intensifies synthesis for

Table 2. Phase composition of specimens from TiH₂ based mixtures

System	Sintering temperature, °C	Sintering time, h	Phase composition	Note
TiH ₂ -Ni	600	3	Ti+Ni+NiTi+Ni ₃ Ti	Ni ₂ Ti traces
	770	3	Ti ₂ Ni+Ni ₃ Ti	
	900	3	TiNi	
TiH ₂ -Al	475	24	Ti+TiAl ₃ +Ti ₃ Al	Ti traces
	620	5	Ti+Ti ₃ Al+TiAl	
	900	6	Ti ₃ Al+Ti	
	1080	4	Ti ₃ Al	
TiH ₂ -Si	900	2	Ti ₅ Si ₃	
	1100	2	Ti ₅ Si ₃	

all the considered systems. In this case fusion and destruction of specimens are not observed. Sintered Ti₃Al and TiNi intermetallides have a density more than 90% of theoretical one and strength on a level with analogous materials produced by smelting.

During sintering Ti₅Si₃ specimens change their size very little but they show low strength. Ti₅Si₃ particles formed are weakly connected between each other. This is likely due to the presence of covalent bonds in the TiSi system.

Thus, introduction of titanium hydride has resulted in substantial activation of synthesis. Possible causes of this effect have been considered.

Structures of mixtures with titanium and its hydride proved to be quite different. In the first case the mixture represents rather large titanium particles covered with aluminium or nickel layer. In the second case diffusion paths are by 1-2 order of magnitude less than those in the mixtures with pure titanium.

It should be noted that titanium hydride decomposition that begins at 300-400 °C results in formation of atomic hydrogen. Reduction of residual oxide films present on aluminium and silica particles is possible thermodynamically in the atomic hydrogen medium.

High intensity of interaction in the mixtures with titanium hydride has been verified by differential thermal analysis (DTA) of Ti-Al, TiH₂-Al mixtures heating [3]. In heating Ti-Al specimens the noticeable exothermic effects are not observed up to a temperature of melting aluminium. The intensive reaction begins in going over the melting point.

The reaction results in formation of a number of compounds. DTA of heating the specimens with titanium hydride has shown that synthesis shifts to the temperature range lower than the point of melting aluminium. In this case the solid-phase reaction proceeds so intensively that above 600-620 °C pure aluminium is no longer in specimens (Table 2). Absence of liquid phase has provided the formation of the material having high density (94-95% of theoretical one).

Thus, the use of titanium hydride gives significant advantages in production of titanium intermetallides. Substantial intensification of diffusion processes occurs due to the optimum component distribution within the blend and reduction of surface oxide films. Therefore, synthesis begins at considerably lower temperatures than in the case of pure titanium what allows us to avoid an intense reaction with high exothermic effect. This circumstance allows the production of the material having high density and the preservation of the product shape after synthesis. This is a significant advantage of the technology as low plasticity of intermetallides makes the process of the following compaction rather complicated.

1. Bania P.G. An advanced alloy for elevated temperatures//JOM, 1988.-40(3)-P.20-22.
2. Kim Y.W., Dimiduk D.M. Progress in the understanding of gamma titanium aluminides//Ibid.-1991.-43(8)-P.40-47.
3. Ивасишин О.М., Демидук А.Н., Саввакин Д.Г. Использование гидроксида титана для синтеза алюминидов титана из порошковых материалов//Порошковая металлургия.-1999.-N9-10.-С.63.

AN INFLUENCE OF COOLING RATE ON A STRUCTURE AND MECHANICAL BEHAVIOR OF TI-SI CAST ALLOYS

Mazur V., Kapustnikova S., Shportko A., Podrezov Yu.⁽¹⁾, Bega N.⁽¹⁾

National Metallurgical Academy of Ukraine, 4 Gagarin Ave., 49635, Dnipropetrovsk, Ukraine

⁽¹⁾Institute for Problems of Materials Science, National Academy of Science of Ukraine,
3 Krzhizhanovski Str., 252180, Kyiv, Ukraine

The composites Ti-Si are intended for production of small details of engines and compressors, such as wheel rotors both stators of turbochargers and compressors, bodies of pre-chambers of diesel engines, heat-shield attrition-resistant inserts in the piston of forced diesel. These details are distinguished by major difference of cross-sections. Hence their solidification happens in a broad band of cooling rates. Thus the study of effect of a cooling rate at solidification of alloy on parameters of its structure and its properties is actual.

Materials and technique of researches

Iodide titanium and zirconium, silicon and aluminum of high cleanliness have been applied as raw materials. Smelting of alloys has been carried out in the plasma-arc furnace with skull tilted crucible, plasma formation gas helium has been used. After smelting of an alloy, overheating up to given temperature and certain endurance at this temperature the melt has been poured out in copper wedge – shaped mould.

The local cooling rate has been determined by means of the Institute of Light Alloys resumptive diagram using a dependence of a dendrite structure parameter of primary β - dendrites of cooling rate.

Light microscope JENAPHOT 2000, X-ray diffractometer DRON 2,0, EDAX was used for study microstructure and phase composition of experimental alloys. The volumetric share of structural constituents was determined by means quantitative processing of the images with the help of software Image Expert. A hardness of the samples was determined with help Rockwell press. A micro-hardness was tested with the PMT-3 tester. The basic mechanical characteristics of a material (Young's modulus, bending strength, relative elongation) was determined by four-dot bend with help test machine CERAMTEST with computer registration of experimental data.

Results of experiment and discussion

The diagram of change of local cooling rate depending on distance from an edge of a wedge looks like falling down exponent.

The maximal cooling rate ($3 \cdot 10^3$ K/s) is fixed in near-surface layers of wedge-shaped ingot. Characteristic microstructure corresponds to it: light primary dendrites of formed β - solid solution with mutual - orthogonal branches and dark etched eutectic constituent. With removal from a surface cooling parameter of dendrite structure is in steps increased. The morphology of transformed β -dendrites is changes also: the not numerous short dendrite branches lose mutual ortogonality and dendrites accept wrong rounded form. It is necessary to note, that zones with both structural types of dendrites simultaneously quite often are observed.

With removal from an edge of a wedge the share of the β -dendrites of the second type grows. The branching of the β -dendrites decreases, their branches are made thicker. The external contour of β -dendrite becomes more and more rounded. The precipitations of dot crystals apparently of secondary titanium silicides are observed at the cross-sections of rounded transformed β -dendrites. The liquation contours well appreciable on sections of orthogonal β -dendrites have disappeared completely. In the parcels solidified with the minimal speed of cooling the rounded crystals of the transformed β -phase are lost with attributes of dendritic structure and turn in rounded grains with irregular rounded interface with interdendritic eutectic.

The volumetric share of transformed β -dendrites depends on local rate of cooling of alloy. The minimal share of β -dendrites is located near an edge of a wedge. With distance from an edge it rises, asymptotically coming nearer to 75 %. The equilibrium value of a volumetric share of β -dendrites for an alloy of the given concentration is 76 %.

The measurement of micro-hardness of transformed β -dendrite has fixed its maximal value near an edge of a wedge. With removal from an edge the micro-hardness of β -dendrite asymptotically comes nearer to value $H_{\mu} = 1850$ MPa.

In micro-zone of an ingot, where light microscopy effectively permits microstructure of eutectic, eutectic colonies of complex micro-morphology are fixed. The central part of colonies is formed by silicide rods. They form close packed package framed by lamellar environment. The metal matrix here forms a basis of eutectic. It is known, that eutectics with a continuous matrix and ramified tillers of reinforcing (here - silicide) hases is referred as skeletal eutectics (Fig.1).



Fig.1. Skeletal eutectic ($\beta + \text{Ti}_5\text{Si}_3$), 200^x

A matrix of the eutectic of other type is formed by a non-metal phase while branched phase is represented by metallic solid solution. The eutectics of such type are named ledeburite-like under the name of eutectic of white cast iron which has the same type of micro-structure. Phase composition of cast is presented with equilibrium α , Ti_5Si_3 and metastable β and TiSi phases. An occurrence of silicide TiSi in a researched alloy represents the great interest because this silicide enters into a subsystem $\text{Ti}_5\text{Si}_3 - \text{Si}$ and is absent in alloys of a subsystem $\text{Ti} - \text{Ti}_5\text{Si}_3$ in equilibrium conditions. For finding - out of the factors stimulating formation of silicide TiSi in wedge-shaped casts the following experiments have been carried out.

1. Two wedge-shaped ingots Ti- 2.9Al- 4.1Si- 4.7 Zr have been filled in mould after overheating of the melt 1650°C and 1800°C.
 2. Wedge-shaped ingots of an alloy Ti- 3Al- 6Si- 5Zr have been made after overheating 1800°C.
- From obtained data it follows that the intensity of (210) interference from a TiSi lattice raises with

increase of concentration of silicon and temperature of overheating of the melt. After annealing at 650°C during 1 hour interferences of TiSi disappeared.

The given data allow to assume, that structure of initial melt plays the main role in formation of metastable silicide TiSi. Apparently with increase of concentration of silicon and temperature of overheating the probability of formation of cluster with TiSi stehiometry increases. Probably the crystals TiSi is nucleated on the basis of them and then grow.

The dependence of hardness of an alloy with cooling rate is investigated. It is shown that the maximal hardness corresponds to zones of the cast which are formed at the maximal cooling rate ($3 \cdot 10^3 \text{K/s}$). With reduction of cooling rate the hardness is decreased. It can be explained by influence of two factors: - with reduction of cooling rate a supersaturation of β -dendrites by silicon and others alloying elements is decreased; - with reduction of cooling rate of an alloy the volumetric share of transformed β -dendrites having plasticity large than eutectic constituent is increased. The tests of samples for a four-dot bend are carried out at room temperature. The micro-deformations curve are constructed with the help of the computer program. The basic mechanical characteristics: the modulus of elasticity E, bending strength σ , deformation ϵ at the moment of destruction are given in the Table.

Cooling rate	The mechanical characteristics		
	E, GPa	σ , MPa	ϵ , %
10^0	129	1337	0,063
10^1	129	625	0
10^2	131,5	1582	0,2

The analysis of the data shows, that the highest mechanical characteristics corresponds to high cooling rate which provides with formation of rather uniform structure of greater volumetric share of orthogonal β -dendrites and skeletal eutectic.

Conclusion

1. A cooling rate has effective influence on both the microstructure and mechanical behavior of Ti-Si based alloys.
2. A solidification under high cooling rates results in highest mechanical characteristics of alloys. It can be explained by formation of favorable microstructure: fine-branched β -dendrites and skeletal eutectic with metallic matrix and branched silicide phase.

AN INFLUENCE OF OVERHEATING OF A MELT ON A STRUCTURE AND MECHANICAL BEHAVIOR OF TI-SI CAST ALLOYS

Mazur V., Kapustnikova S., Shportko A., Levitsky M.⁽¹⁾, Miroshnichenko V.⁽¹⁾

National Metallurgical Academy of Ukraine, 4 Gagarin Ave., 49635, Dnipropetrovsk, Ukraine

⁽¹⁾Physical and Technological Institute of Metals and Alloys, National Academy of Science of
Ukraine, 34/1 Vernadsky ave., 03680, Kyiv, Ukraine

Introduction

At research of some physical properties of the melts in temperature interval three interesting features a polyterm of these properties are established.

1. Sometimes anomalies or even jumps are observed on polyterms of viscosity, density, luminosity at the certain temperatures.

2. At heating higher than the certain temperature and cooling of liquid alloys the hysteresis of the properties polyterms is observed. Hence the high-temperature structural state of a melt is capable to be kept long time.

3. At measurement of viscosity of the melt during isothermal endurances oscillatory character of change of this property is observed. Time of a relaxation of viscosity values is changed from several minutes till several hours. Special experiences have shown, that one of reason of the instability can be processes of slow reorganization of structure of liquid alloys.

This information is rather important for a choice of a temperature mode of a fusion of multi-component alloys to provide a maximum level of strength, plasticity and other service properties. Optimization of a temperature mode of a melt enables to save power resources.

An absence of the data on temperature dependences of physical properties of titanium alloys can be explained by their high reactionary ability.

Therefore a study of influence of overheating temperature of a melt on structure and a level of properties of the solidified ingot is actual task.

Materials and technique of researches

In-situ titanium base composite Ti-3Al-4Si-5Zr is used as material of researches.

An electric plasma-arc furnace is used. The melting was carried out in copper cold wall crucible. Temperature of a melt is supervised with the help the W-Re thermocouple. The melt is poured out in graphite cylindrical mould after

heating to the given temperature and endurance at this temperature within 10 minutes. In total 9 ingots of diameter of 60 mm in height of 120 mm was melted from overheating temperatures in range 1510 – 2000 °C. A chemical composition of ingots is defined by spectral analysis.

Microstructural researches are carried out on microscope JENAPHOT - 2000, X-ray examinations are executed with help diffractometer DRON-2,0 in Cu K α -radiation. Distribution of alloying elements in different phases is studied on X-ray microanalyzer MS-46 CAMECA by methods of scanning in the area and on a line and at quantitative definition by dot method. Volume fractions of structural components are defined on microphotos with quantitative processing of images with the help of computer software Image Expert.

Measurements of hardness of alloys is carried out on Rockwell device.

Short-term and long hot hardness are defined in interval of temperatures 25 – 900 °C.

The most important mechanical characteristics (σ , E, ϵ) were determined by tests for four-dot bend.

Results of experiment and their discussion

Two structural constituents are fixed: transformed primary β -dendrites and inter-dendritic eutectic, including titanium silicides and transformed β -Ti solid solution.

Primary β -dendrites have different morphology in dependence of their localization and overheating temperatures. In a superficial layer of all ingots β -dendrites have well expressed mutual - perpendicular branches. These dendrites form a columnar zone of ingots. They are nucleated on a surface of a crucible and grew in a radial direction to the center of an ingot. The second type of β -dendrites are lost with attributes of dendritic structure and turn in rounded grains. They are localized in central part of ingots. It is necessary to note that zones with both structural types of dendrites simultaneously are observed quite often.

II. PERSPECTIVE MATERIALS OF FUNCTIONAL AND STRUCTURAL PURPOSES: POSSIBILITIES OF OBTAINING NEW LEVEL OF PROPERTIES

The eutectic constituent includes three structural types of eutectic: quasicutectic i.e. eutectic with superfine differentiation of eutectic phases and the common chemical composition which is distinguished from concentration of an equilibrium eutectic point; eutectic with silicide matrix and the branched β -phase which usually is referred as ledeburite-like; eutectic with metallic (β -Ti) matrix and silicide branched phase submitted by dendritic branches as cores or plates. It is skeletal type eutectic.

The probability of formation of each types of primary β -dendrites and eutectic depends on distance of the given micro-site from a surface of an ingot and overheating temperature of a melt. With approach to a surface of an ingot the volume fraction of β -dendrites is decreased. The maximal volume fraction of β -dendrites is observed in an ingot, solidified after overheating up to 2000 °C, and the minimal one after overheating up to 1600 °C. Orthogonal dendrites have eutectic layer between branches of approximately identical thickness while in sites with rounded dendrites the eutectic is distributed more non-uniformly.

The results of study of localization of structural constituents show that more favorable distribution takes place in ingots solidified after overheating 1600-1900 °C.

Phase composition of all ingots presented by the next phases: α -Ti, β -Ti, Ti_5Si_3 and metastable Ti-Si silicide. The probability of formation of TiSi is increased with raising of overheating temperature. The given data allow to assume, that structure of initial melt play the main role in formation of metastable TiSi silicide. Apparently with increase of temperature of a melt a probability of formation of cluster with TiSi stoichiometry is increased. The TiSi crystals are nucleated on the basis of them and then grow.

Hardness HRC grows when overheating temperature is increased. The influence of melt overheating temperature on the strength and elastic characteristics is given in Table 1.

The analysis of the obtained results shows, that the maximal values of durability are received after overheating temperatures 1740, 1750 and 1900°C. Nonlinear dependence of structural characteristics and properties of ingots on melt overheating temperature does not allow to explain their change

only by influence of heat reserved by liquid metal, superheated up to various temperatures. More suitable the following hypothesis is represented. We assume, that in an interval of temperatures of overheating of the melt between 1510 and 1560 °C and also 1940 and 2000 °C there are the structural reorganizations of a liquid phase connected with change of parameters of the short-range order (coordination numbers and radius of coordination spheres) and also stoichiometry of various clusters. According to modern representations it will result in distinction of microscopic kinetics of nucleation and growth of phase constituents.

Table 1.

Temperature of melt, °C	Mechanical characteristics		
	E, GPa	σ , MPa	ϵ , %
1560	136,9	1235	< 0,1
1600	142,0	1346	0,10
1740	129,7	1381	0,20
1750	129,3	1358	0,12
1900	143,3	1357	0,10
1940	138,0	1126	0
2000	123,0	1077	0,01

Conclusion

It is found that maximal level of strength is provided with choice of overheating temperature of a melt in the range 1600-1900 °C. It can be explained by formation of the best structural characteristics of an alloy: fine-branched orthogonal dendrites of β -Ti solid solution and skeletal eutectic (β + Ti_5Si_3).

Two critical overheating temperature intervals 1510-1560 and 1940-2000 °C are found. The ingots which are solidified after this overheats are characterized by extensive zones of coarse and very coarse β -dendrites and quasi-eutectics. These structural characteristics drop out of a general structural line, which characterizes change structural constituents with temperature of overheating. The assumption of influence of structural reorganizations in a liquid alloy at these temperatures on kinetics of crystallization is expressed.

HIGH-STRENGTH ALUMINUM-BASED ALLOYS HARDENED BY QUASICRYSTALLINE NANOPARTICLES

**Lotsko D.V., Milman Yu.V., Miracle D.B.⁽¹⁾, Sirko O.I., Yefimov M.O., Bilous A.M.,
Danylenko M.I., Neikov O.D., Voropayev V.S.**

I.M.Frantsevych Institute for Problems of Material Science of NAS of Ukraine, Kyiv, Ukraine

⁽¹⁾Air Force Research Laboratory, Materials and Manufacturing Directorate, Wright-Patterson, USA

Traditional strengthening mechanisms for Al alloys developed for last eight decades [1] permitted to obtain the upper limit of tensile strength σ_f to 660 MPa in sheets [2]. In our investigations this level was increased to 800 MPa in rods due to alloying with Sc. Last decade by a group of Japanese scientists headed by Prof. A.Inoue there were proposed new high-strength Al-based alloys with σ_f to about 1500 MPa that are described in reviews [1, 3]. For hardening these alloys the nonequilibrium phase effects (the creation of nonperiodic structures in particular) were used. The latter included amorphous and quasicrystalline icosahedral phases (I-phases). Maximum σ_f was obtained in melt-spun ribbons. In bulk materials with I-phase produced from argon-atomized powders σ_f was to 850 MPa in combination with the elongation $\delta \approx 10\%$. Last two years some works of German [4] and Romanian [5] scientists in this subject were published.

High strength and good ductility in Al alloys with I-phase are expected, when the I-phase is in the state of uniformly distributed nanosize particles of spherical morphology. It is caused by a special deformation mechanism of the I-phase [3]: a room temperature deformation is connected with the formation of approximant crystalline phases on a subnanoscale that takes place in phason defects. The formation of these phases is as a rule accompanied by changing the chemical composition provided by diffusion from α -Al matrix. The refinement of I-phase particles to nanoscale size in Al-rich alloys introduces a high density of phason defects to the I-phase and facilitates alloy ductility.

High-strength Al+I alloys were produced on the base of the systems Al-R-EM and Al-R-LM, where R = rare-earth metals, EM = Ti, Zr, Hf, Nb, Ta, Cr, Mo, W, and LM = Mn, Fe, Co, Ni, Cu, in Al-rich composition range above 92 at. % Al. Elevated temperature alloys were developed on the base of Al-Fe-Ti-M systems with M = Cr, V, Mn [1, 3, 6]. An alloy $\text{Al}_{93}\text{Fe}_3\text{Cr}_2\text{Ti}_2$ appeared the best. Its σ_f at 300 °C was 350 MPa, which exceeds the air-force goal level and did not change after annealing the sample at 300 °C for 1000 h [1].

Hardening by I-phase nanoparticles was found also in maraging steels [7].

We studied structure and mechanical properties of rapidly quenched alloys of Al-Fe-Cr-Ti system with additional alloying with Zr and Sc. The investigation was carried out with melt-spun ribbons and powder alloys. Powders were produced by an original water-atomization technique developed in the IPMS. In ribbons $\text{Al}_{93}\text{Fe}_3\text{Cr}_2\text{Ti}_2$ of 25 μm in thickness and $\text{Al}_{92.8}\text{Fe}_3\text{Cr}_2\text{Ti}_2\text{Sc}_{0.2}$ of 45 μm in thickness we obtained I-phase particles of 15-50 nm in size (Fig. 1).

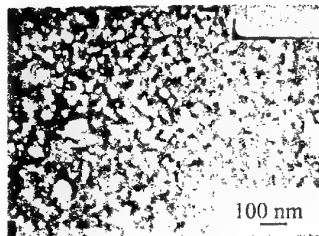


Figure 1. Quasicrystalline particles in $\text{Al}_{93}\text{Fe}_3\text{Cr}_2\text{Ti}_2$ melt-spun ribbon, dark field image

In addition we manufactured the ribbon $\text{Al}_{84.2}\text{Fe}_7\text{Cr}_{6.3}\text{Ti}_{2.5}$ that according to [6] shall be almost completely quasicrystalline (Fig. 2).

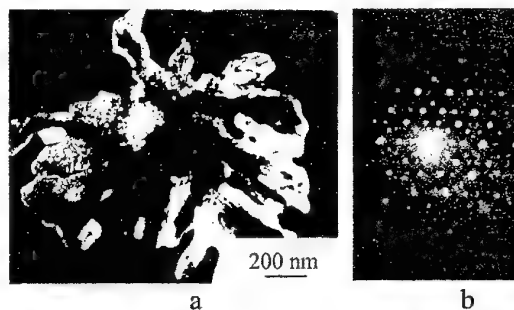


Figure 2. Structure, dark field image (a) and electron diffraction pattern of 5-fold symmetry (b) of a particle in $\text{Al}_{84.2}\text{Fe}_7\text{Cr}_{6.3}\text{Ti}_{2.5}$ ribbon

Experiments with ribbon annealing have shown (Fig. 3) that ribbon hardness remains

practically unchanged after annealing at 400 °C. A drop of hardness after annealing at higher temperatures is caused by vanishing the I-phase and appearing crystalline intermetallics ($\text{Al}_{23}\text{Ti}_9$ and $\text{Al}_{13}(\text{Cr,Fe})_2$) accompanied by their coagulation.

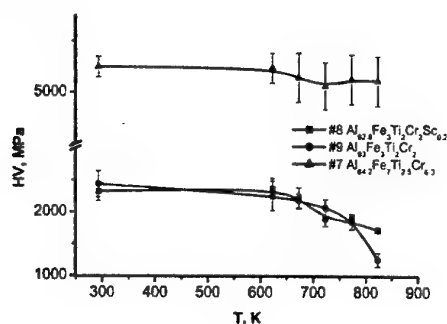


Figure 3. Change of hardness of AlFeCrTi(Sc) ribbons after annealing for 1 h

X-ray investigation confirmed a high level of phonon and phason distortions in small I-phase particles that were higher than in purely quasicrystalline ribbon 5 and 2 times respectively. It provided about 1 % of plastic strain while ribbon bending. In the ribbon $\text{Al}_{93}\text{Fe}_{0.7}\text{Cr}_{4.3}$ (ribbon 4) I-phase particles were of 100-700 nm in size, and its hardness was as low as 1200 MPa.

For producing powder alloys we used powder fractions 1: (~ 63) μm and 2: (63-100) μm . For powders of $\text{Al}_{93}\text{Fe}_3\text{Cr}_2\text{Ti}_2$ and $\text{Al}_{92.8}\text{Fe}_3\text{Cr}_2\text{Ti}_2\text{Sc}_{0.2}$ alloys in both of them together with I-phase a large amount of $\text{Al}_{23}\text{Ti}_9$ intermetallic was revealed, a small changing of composition permitted to obtain powders with only icosahedral second phase (alloys #3-8 in Table). To preserve I-phase it was necessary to carry out powder consolidation at temperatures not exceeding 400 °C (see Fig. 3). In alloys except 6 powder billets were degassed and vacuum forged at 400 °C, but their extrusion to rods of 9 mm in diameter (extrusion ratio 7.7) was possible only after heating the die to 500 °C and the billet to 400 °C. Alloy 6 was extruded in an evacuated aluminum capsule without forging with heating to 420 °C both die and billet. The rod 9 was produced by consolidation of crushed ribbon. Samples from rods with gauge diameter of 3 mm were tested in an Instron-type machine at a strain rate of 10^{-3} s^{-1} .

I-phase was preserved only in the rod 6 (of 70-200 nm in size). In other rods including rod 9 crystalline intermetallics were formed to 400 nm in size. Rods were also distinguished by very small grain size of α -Al matrix – less than 1 μm .

Evidently, the existence of small I-phase particles in powders facilitated the formation of small uniformly distributed intermetallic particles while thermomechanical treatment at temperatures exceeding the temperature of quasicrystal stability.

Thus, Al alloys from water-atomized powders hardened by fine quasicrystalline particles or intermetallic particles formed on their base can have strength higher than 300 MPa at 300 °C. Note that Sc and Zr increased the elevated temperature strength of powder alloys.

Table. Composition and tensile mechanical properties of rods from powder alloys

#	Composition	T, °C	$\sigma_{0.2}$, MPa	σ_U , MPa	δ , %
1	$\text{Al}_{93}\text{Fe}_3\text{Cr}_2\text{Ti}_2$	20	538	574	1.0
2	$\text{Al}_{92.8}\text{Fe}_3\text{Cr}_2\text{Ti}_2\text{Sc}_{0.2}$		520	567	0.7
3	$\text{Al}_{93.4}\text{Fe}_{2.6}\text{Cr}_{2.8}\text{Ti}_{1.2}$		469	561	5.1
4	$\text{Al}_{93.7}\text{Fe}_{2.6}\text{Cr}_{2.8}\text{Ti}_{0.6}\text{Zr}_{0.3}$		-	536	0.1
5	- " - fraction 2		-	539	0.2
6	- " - fraction 2, extrusion in capsule		618	649	0.6
7	$\text{Al}_{93}\text{Fe}_{2.6}\text{Cr}_{2.8}\text{Ti}_{1.2}\text{Zr}_{0.4}$		-	627	0.1
8	$\text{Al}_{94.7}\text{Fe}_{2.6}\text{Cr}_{2.7}$		398	459	11
9	$\text{Al}_{93}\text{Fe}_3\text{Cr}_2\text{Ti}_2$, extruded ribbon		-	449	0
1	$\text{Al}_{93}\text{Fe}_3\text{Cr}_2\text{Ti}_2$	300	255	294	2.5
2	$\text{Al}_{92.8}\text{Fe}_3\text{Cr}_2\text{Ti}_2\text{Sc}_{0.2}$		271	315	2.9
3	$\text{Al}_{93.4}\text{Fe}_{2.6}\text{Cr}_{2.8}\text{Ti}_{1.2}$		269	313	2.7
4	$\text{Al}_{93.7}\text{Fe}_{2.6}\text{Cr}_{2.8}\text{Ti}_{0.6}\text{Zr}_{0.3}$		313	343	1.5
5	- " - fraction 2		297	328	1.5
6	- " - fraction 2, extrusion in capsule		274	303	1.9
8	$\text{Al}_{94.7}\text{Fe}_{2.6}\text{Cr}_{2.7}$		221	247	3.1
9	$\text{Al}_{93}\text{Fe}_3\text{Cr}_2\text{Ti}_2$, extruded ribbon		321	360	1.7

1. Inoue A., Kimura H.M. // Proc. Mater. Res. Soc. Symp., Warrendale, PA, 1999. - 553. - P. 495.
2. Fridlyander I.N. // Mater. Sci. Forum. - 2000. - 331-337. - P. 921.
3. Inoue A. // Progr. Mater. Sci. - 1998. - 43. - P. 365.
4. Manaila R., Popescu R., Jianu A. et al. // J. Mater. Res. - 2000. - 15, No. 1. - P. 56.
5. Schurack F., Eckert J., Schultz L. // Acta mater. - 2001. - 49. - P. 1351.
6. Kimura H.M., Sasamori K., Inoue A. // J. Mater. Res. - 2000. - 15, No. 12. - P. 2737.
7. Nilsson J.-O., Liu P., Dzugutov M. // Proc. Mater. Res. Soc. Symp., Warrendale, PA, 1999. - 553. - P. 513.

LOW TEMPERATURE MECHANICAL PROPERTIES OF BULK NANOSTRUCTURED TITANIUM PROCESSED BY SEVERE PLASTIC DEFORMATION

Bengus V.Z., Tabachnikova E.D., Natsik V.D.

B. Verkin Institute for Low Temperature Physics & Engineering of National Academy of Sciences
of Ukraine, Kharkov, Ukraine

Successful technical applications of titanium and its alloys as structural materials became possible due to their high specific strength and high plasticity, which are not decreasing at cryogenic temperatures owing to propitious peculiarities of plastic deformation mechanisms of titanium. Using of severe plastic deformation through Equal Channel Angular Pressing (ECAP) and the additional thermo-mechanical treatment made possible to obtain in the Institute of Physics of Advanced Materials (Ufa, Russia) nano-structured (NS) states (with the 100 nm average grain size) of bulk commercially pure Ti VT-1-0 [1]. So small grain dimension allowed hoping for essential increasing of mechanical characteristics in comparison with a usual polycrystalline state of Ti.

This short report presents experimental data evidencing a high strength state of the bulk NS VT-1-0 Ti at the ambient and cryogenic temperatures and its sufficient plasticity resource.

Deformation and failure of titanium have been studied in three structural states: State 1 – the average grain size is 15 μ m – the initial state. State 2 – the average grain size is 0.3 μ m – processed by intensive plastic deformation through 8 runs of ECAP. State 3 – the average grain size is 0.1 μ m – processed by 8 runs of ECAP followed by 75 % strain cold rolling and subsequent annealing at 300 C during 1 hour.

Mechanical characteristics were studied under a uniaxial compression with the $\sim 4 \cdot 10^{-4} \text{ s}^{-1}$ strain - rate with a 10 kN/mm stiffness testing machine at temperatures 300, 77 (in liquid nitrogen) and 4,2 K (in the liquid helium 4). Samples for compression were rectangular prisms 2x2x7 mm cut by electro-erosion. An accuracy of the stress measurements was ± 3 MPa and that of the strain measurements was ± 1 %.

Measurements were carried out for specimens cut along (\parallel) and across (\perp) the ECAP axis. Measured mechanical characteristics: a "stress-strain" curve " σ - ϵ ", the conventional yield stress σ_y (determined by the method of intersection of tangents to the deformation curve at its initial part), the ultimate plastic strain ϵ_{ul} before failure and a failure mode –

found by data averaging for 3-5 tested specimens of each kind. Morphology of the failure surfaces was usually studied by the TESLA BS-300 scanning electron microscope.

Deformation curves " σ - ϵ ", of the bulk NS-Ti are of a staged character, as distinct from a "parabolic" one, which is typical of ordinary polycrystals. This may be a consequence of a discrete mode of plastic deformation, typical of NS-state [2], which is caused by difficulty of cross-slip (due to the small grain dimension or due to a grain-boundary type of mobile dislocations).

Conventional yield stresses σ_y of bulk Ti at 300, 77, 4,2 K for the three available structural states (with the different average grain size d) under the compression parallel (\parallel) or perpendicular (\perp) to the specimens axis for initial and NS-Ti are given in the Table 1 (it is worth noting that σ_y of initial Ti are in good accordance with literature data [3]).

Table 1. Conventional yield stresses σ_y of bulk Ti at 300, 77, 4,2 K for the three available structural states (with the different average grain size d) under the compression parallel (\parallel) or perpendicular (\perp) to the specimens axis for studied titanium.

State	Axis orientati- on	σ_y , GPa		
		300 K	77 K	4.2 K
1, $d=15\mu$	\parallel	0.44	0.78	0.97
	\perp	0.50	0.90	1.03
2 $d=0.3\mu$	\parallel	0.65	0.87	1.24
	\perp	0.87	1.33	1.47
3 $d=0.1\mu$	\parallel	1.00	1.32	1.67
	\perp	1.14	1.55	1.79

It is seen that σ_y values of bulk NS-Ti are substantially higher than for initial state 1. At 300 K (even under straining parallel to the ECAP axis) the σ_y value in the state 3 (~ 1 , 1 GPa) is more than twice exceeds σ_y of initial titanium. At 77 K ($\sigma_y \approx 1,3$ GPa) and at 4,2 K ($\sigma_y \approx 1,7$ GPa) it is almost 1,7 times larger. These values achieve σ_y of the VT-6 alloy (~ 0.9 GPa at 300 K, 1.4 GPa at 77K, 1.6 GPa at 4.2 K [3]).

Ultimate plasticity σ_{ul} before failure in bulk NS-Ti is rather high and comparable with that of the coarse-grained rod-like Ti at a uniaxial tension (18-20% at the state of supply [4]). Even in the least ductile state 3, at 4.2 K it is equal to 12% for (\parallel) and 4.3% for the (\perp) orientations. This evidences that cold brittleness is absent in the bulk NS-Ti obtained through ECAP. It can be considered as a potential structural material with a high specific strength, for engineering applications at cryogenic temperatures.

Explanation of unusual mechanical behavior of nanostructured titanium at low temperatures, and possibility of prognosis of its mechanical properties demand knowledge of microscopic mechanisms of its low temperature deformation.

It is known that low temperature deformation in polycrystalline titanium realizes by intra-granular slip and twinning [4]. In nanostructured Ti twinning in grains is suppressed because grains dimensions are smaller than dimensions of the critical nuclei of twins. Therefore only intragranular slip is possible in nanostructured titanium. Besides, a possibility of intergranular slip (grain-boundary sliding) supposed possible in nanostructured titanium.

Direct experimental observations of grain boundary sliding in nanostructured Ti at low temperatures are not yet available. But some indirect indications exist about such possibility.

Discovering of the ductile shear failure mode (catastrophic slipping-off of one part of a specimen relative to another) [5] under the low temperatures compression (with the $4 \cdot 10^{-4} \text{ s}^{-1}$ strain-rate) of the nanostructured Ti can be considered as the most important indirect indication.

Similarly to bulk metallic glasses [6] such slipping-off is accompanied by extreme local adiabatic heating along the failure surface up to more than 882 C that is evidenced by the "vein" pattern [5]. It is caused by the high failure stress, near sound velocity of plastic shear, the small thermal conductivity of titanium. Preliminary qualitative theoretical consideration of the process allows concluding [5] that at large plastic deformations of nanostructured titanium unstable localized grain boundary sliding must extend macroscopically by the high-speed motion of grain boundary dislocations.

Another indirect indication of grain boundary sliding can be a small value of the SD-effect that may be explained by small Burgers vectors of grain boundary dislocations [7].

In explanations of low temperature anomalies of the NS-Ti also an internally stressed state of nanostructured titanium processed by ECAP must be taken into consideration as well as its modification by the thermal anisotropy internal microstresses (spreading through each grain). These latter ones arise under cooling of titanium in nanocrystalline as well as in polycrystalline state owing to the anisotropy of the thermal expansion coefficient of titanium grains, which belongs to the hexagonal symmetry group.

These factors allow explaining of anomalies of the Hall-Petch relations in the nanostructured titanium and large anisotropy of the yield stress of its rods at 77 K (see Table 1).

Further thermal activation analysis of low temperature plastic deformation of the nanostructured titanium and SEM and TEM electron microscopy observations will give more possibilities for understanding microscopic mechanisms of low temperature deformation of nanostructured titanium.

The authors would like to thank R. Z. Valiev and V. V. Stolyarov for supplying the specimens of Ti for this study and for very fruitful discussions of the results.

This work has been carried out with a partial support of the INTAS-99-01741 and INTAS-2001nano-320 Projects.

References

1. R.Z.Valiev, R. K., Islamgaliev, I.V. Alexandrov, Bulk nanostructured materials from severe plastic deformation. Progress in Materials Science vol. 45, (2000) pp. 103 – 189.
2. A. Vinogradov, Scripta Materialia, vol. 39 (1998), p.p. 797-805.
3. V.N.Kovaleva, V.A.Moskalenko, Cryogenics, vol. 29 (1989) p.p. 1002-1005.
4. R. A. Ul'yanov, V. A. Moskalenko, Metallography & Thermal Treatment of Metals, № 10, October (1966) p. p. 48-51 (in Russian).
5. V.Z. Bengus, E.D. Tabachnikova, K. Csach, J. Miškuf, V.V. Stolyarov, R.Z. Valiev, V. Ocelik, J.Th.M. De Hosson, in: Science of Metastable and Nano-crystalline Alloys. Structure, Properties and Modelling, Eds. A.R.Dinesen, M.Eldrup et al., Riso National Laboratory, Roskilde, Denmark (2001) pp. 217-222.
6. V. Z. Bengus, E. D. Tabachnikova, J. Miskuf, K. Csach, V. Ocelik, W. L. Johnson, V. V. Molokanov, Journal of Mater. Science, v.35 №17, (September 2000) pp. 4449-4457.
7. E. D. Tabachnikova, V. Z. Bengus, V.V. Stolyarov, G. I. Raab, R.Z. Valiev, J. Miskuf, K. Csach, Mater. Sci. Eng. A, v. 309-310 (2001) pp. 524-527.

HIGHLY EFFECTIVE DISPERSION STRENGTHENED MATERIAL BASED ON COPPER POWDER OF DISCOM[®] TRADE MARK FOR CURRENT REMOVING INSERTS OF PANTOGRAPHS OF HIGH SPEED ELECTRIC TRAIN

Shalunov E.P., Lipatov Ya. M., Wendland St.⁽¹⁾, Shalunova N.B.

Scientific and Technological Company TECHMA Ltd, Cheboksary, Russia

⁽¹⁾RÖTECH G.m.b.H., Mühlheim-an-der-Ruhr, Germany

The most important element of the pantograph current-collecting device of electric trains is a current-removing insert directly contacting a contact wire of the railway electric net. This insert is supposed to remove current from the contact wire and direct it to the electric drive of the train. The more effective the current-removing insert fulfils its functions, the more efficiently electric net energy is used by the electric train. But the operating efficiency of the current-removing insert itself can be evaluated, first and foremost, according to the energy loss amount at it.

It is evident, that the higher electrical conductivity of the insert material, the less the loss of power being emitted as heat is. Since power may be partially lost directly in the contact between the contact wire and the current-removing insert, then transition resistance of this contact R_K should be as low as possible.

From the experimental formula [1]

$$R_K = 100\% \frac{\rho_0}{2} \left(\frac{1}{\varepsilon_w} + \frac{1}{\varepsilon_s} \right) \sqrt{\frac{H_s}{P}},$$

where ε_w and ε_s - electrical conductivity in % from electrical conductivity of copper (IACS) related to materials of the contact wire of the mains and current-removing insert;

ρ_0 - specific electrical resistance of copper, $\times 10^{-6}$ $\Omega \cdot \text{sm}$;

H_s - contact hardness of a softer material of the contact pair, $\times 10^6$ g / sm^2 ;

P - the contact effort, g

it follows, that to reduce R_K it is necessary that the material of both the contact wire and the current-removing insert should be of the highest electrical conductivity and the contact hardness H_s of the softest material of the contact pair at the same contact effort P should be the highest.

To achieve the lowest power loss in the railway electric net contact wires are produced conventionally from copper alloying it with small additions of silver, tin and other elements. Material hardness of such wires makes up 80...120 HB.

As regards minimization of power loss as heat, copper also could be the best material for current removing inserts. But inserts run under the condition of high voltage (from 1500 up to 25000 V) and strong current (from 700 up to 2800 A) electric contact, sliding at that, which is accompanied by the processes of sparking and arcing aggravating due to rain, snow and ice on the contact wires.

The warming caused by arc and friction in the contact pair is added to self-warming of the current-removing inserts due to the current loss in them and in the place of their touching with contact wires. The temperature on current removing inserts at electric train moving at the speed of up to 120 km/h can reach 200...300°C, that is higher than copper recrystallization temperature. That is why instead of pure copper there have been used its alloys containing alloying elements such as Ni, Fe, Cr, Zr and others. For instance, current removing inserts made of bronze CuCrZr are applied by railways of Spain, Italy and other states.

To cut down the wear of contact wires there was added from 2 up to 20% of graphite to copper alloys produced by means of powder metallurgy resulting in considerable reduction of hardness and electrical conductivity of the insert material and increasing power losses in it, and it also caused the increase of wear of the inserts themselves.

As the speed of electric train movement increases up to 160...250 km/h the temperature of current removing inserts exceeds the recrystallization temperature of the best heat resistant bronze, and the bronze became unacceptable for application in the current removing inserts of high speed electric trains. Sintered materials based on iron saturated with

lead and tin alloy and even materials based on carbon became substitutes for bronze. The former contains lead harmful for health, and the latter possesses electric conductivity 0,04...0,06% IACS that presupposes power consumption increase from electric net by 5...10% as compared with copper inserts [2]. Besides, carbon base inserts are quickly worn out and require frequent substitutes.

Scientific & Technological Company TECHMA Ltd. has developed a new highly effective Oxide and Carbon Dispersion Strengthened material (OCDS-Copper) C 0/97 on copper powder base of Cu-Al-C-O system of DISCOM® Trade Mark [3].

The basic physical and mechanical characteristics of this material are as follows:

Electrical conductivity, % IACS.....	88...92
Hardness	70...74HRB
Ultimate tensile strength, N/mm ²	410...460
Conditional tensile yield limit, N/mm ²	350...390
Relative elongation, %.....	20...23
Recrystallization temperature, °C.....	over 800
Compression ultimate strength, N/mm ²	1800...2000
Relative compression settling, %	63...67

After having been heated at 800°C within 1 hour the solidity characteristics of the material become lower not more than by 10...15 %.

Thanks to its high heat resistance and electrical conductivity the material developed can be applied not only as current removing inserts of high speed electric trains (over 160 km/h), but also it can be considered as a wear resistant material for contact wires of the electric net of railways, and it can also be applied for collector stripes and current supplying rings of tractive electric engines of powerful electric locomotives.

Current removing inserts of various sizes are manufactured from OCDS-Copper C 0/97 of DISCOM® Trade Mark by means of technology of mechanical and chemical activation of the initial powder substance in attritors and hot extrusion of the granulate obtained into stripes; such inserts are delivered for high speed electric trains (over 160 km/h) to the Italian Railway via the German firm RÖTECH G.m.b.H.

When installing into a pantograph current-collecting device, a graphite insert preventing the contact wire from wearing is fixed between the above inserts. In case when the collecting device design doesn't provide for an additional graphite insert, a current removing insert itself can be made as "a comb", the space between the cogs of the

comb being filled with graphite. The insert can be also made as a package of alternating stripes produced from OCDS-Copper DISCOM® C 0/97 and graphite.

The introduction of the new design of current collection device runners to the Russian electric trains according to the patent of PhD V.Berent [4] stipulating the application of a spring-loaded carbon insert between current removing inserts, and design application of the current removing inserts made of the material C 0/97 DISCOM® combined will make it possible to get an ideal design of the electric high speed train current collecting device to ensure the minimal wear not only of the current removing inserts, but also of the contact wire and to cut down power consumption in the railways electric net by 5...10 % as compared with the application of carbon-graphite and graphite current removing inserts.

Highly effective Oxide and Carbon Dispersion Strengthened composite material based on copper powder (OCDS-Copper) of DISCOM® Trade Mark C 0/97 is produced in accordance with Technical Requirements of the Italian Railway FS 305977 and Technical Requirements TU 1479-002-13092819-2001 registered by State Standard of Russia No. 002575.

Sources of Information:

1. R.Holm. Electric Contacts. Berlin: Springer - Verlag, 1958, 464p.
2. E.P. Shalunov, A.L. Matrosov, S. Wendland. Railway Transport Energy Saving Due to the Application of Dispersion Strengthened Composite Material of DISCOM® Trade Mark in its Current - Collecting Device. - In: Effective Energy Systems and New Technologies. Proc. 1-th Int. Conf. Kazan. December 4-6, 2001, pp. 23-24.
3. E.P. Shalunov, V.A. Dovydenkov, V.S. Simonov. Anwendung der hocheffizienten dispersionsgehärteten Werkstoffe auf Pulverkupferbasis in den Teilen von Motoren und Kraftanlagen der Transportmittel. - In: Powder Metallurgical High Performance Materials. Proc. 15-th Int. Plansee Seminar. Reutte/Tyrol, Austria. May 28 - June 1, 2001, vol. 4, pp.126-149.
4. V. Ya. Berent, Russia, Patent of Russia No. 2112668, MKI 6B 60L 5/08. A runner of the locomotive current-collecting device. Published in IB 10.06.98.

HIGH-STRENGTH RAPIDLY SOLIDIFIED P/M ALUMINUM ALLOYS

**Neikov O.D., Milman Yu.V., Sirko A.I., Lotsko D.V., Zakharova N.P., Danylenko M.I.,
Laptev A.V., Patsyna R.V., Tokhtuev V.G., Voropaev V.S., Samelyuk A.V.**

I.M.Frantzevych Institute for Problems of Materials Science, 3 Krzhizhanovsky Str., 03142 Kyiv,
Ukraine

The strongest wrought aluminum alloys developed on the base of Al-Zn-Mg-Cu system have found a wide application in various fields of engineering [1-3]. The present paper focuses on the effect of Sc, Zr and other TM (transition metal) alloying additions on the structure and mechanical properties of Al-Zn-Mg-Cu alloys manufactured by P/M technology. Rapidly solidified powders produced by the WA-N process of high-pressure water atomization of the melt [4] were used. Powder size fractions of (0-63) μm and (63-100) μm were separated. Powder compacts, cold pressed to about 30 % porosity, were subjected to hot vacuum dehydration. On completing the degassing, the briquettes were consolidated by vacuum pulse pressing under at a pressure of 1.0 GPa without cooling vacuum. The prepared preforms were extruded at a temperature of 400 $^{\circ}\text{C}$ to produce rods of 6 mm in diameter (extrusion ratio $\lambda = 17$). Rods were subjected to T6 heat treatment (aging at 120 $^{\circ}\text{C}$ for 24 h after quenching from 465 $^{\circ}\text{C}$).

The structure of powders and compacts was studied by optical metallography (OM), scanning and transmission electron microscopy (SEM and TEM), and X-ray diffraction (XRD). The powder surface and microchemistry were examined by (OM) and (SEM). The cooling rate while crystallization v was estimated from the dendritic parameter d according to the empirical formula $d = Av^{-n}$, where $A = 100$ and $n = 0.41$ [5]. Tensile strength and ductility of rods were determined for samples with gauge diameter of 3 mm tested at a deformation rate of 10^{-3} s^{-1} . The ultimate tensile (UTS) and yield (YS) strengths were determined, along with the tensile elongation (EL). High-alloyed alloys of 3 compositions were compared (Table 1).

Table 1. Chemical composition of alloys

Alloy #	Content of elements, wt. %	
	Zn + Mg + Cu	Zr + Sc + Mn
1P	14.0	-
2P	13.7	1.5
3P	16.2	1.5

A characteristic dendritic structure, with well developed branches, was observed in powder particles of alloy 1P (Fig. 1), and its scale became finer with the decrease of grain size, evidently, due to the difference in cooling rates while particle formation. In alloys with (Sc + Zr) additions such structure was preserved in particles smaller than about 40-50 μm . In coarser particles subdendritic grains were observed (Fig. 2a) with crystallization centers containing Sc and Zr (Fig. 2b). Small grains of about 4 μm in size were formed in this case. This structure corresponded to the estimated cooling rate of about $4 \cdot 10^3 \text{ s}^{-1}$, and this rate seems to be limiting for the precipitation of primary particles while melt cooling. For particles with dendrite structure the estimated cooling rates were in the interval of $10^3 - 10^5 \text{ s}^{-1}$.

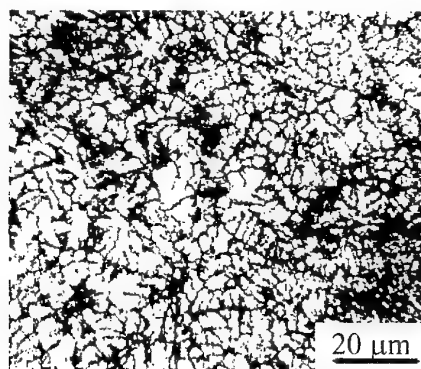


Fig. 1 Structure of a 200 μm powder particle of the alloy 1P, OM image

In dendrite and subdendrite boundaries inside of powder particles X-ray spectral microanalysis revealed a net of layers with an increased concentration of the main alloying elements Zn, Mg and Cu (Fig.2b). Evidently, the are eutectic layers [2], and our experiment shows that their formation cannot be retarded by cooling rates on the level of 10^5 s^{-1} .

In extruded rods in T6 condition these layers transformed to particles of 0.4-1.5 μm in size that were distributed rather uniformly. XRD investigation of these rods reveals the availability of MgZn_2 and T-phases [2] that practically vanished after prolonged annealing (to 99 h) at

120 °C. These particles shall give a very small contribution to alloy hardening.

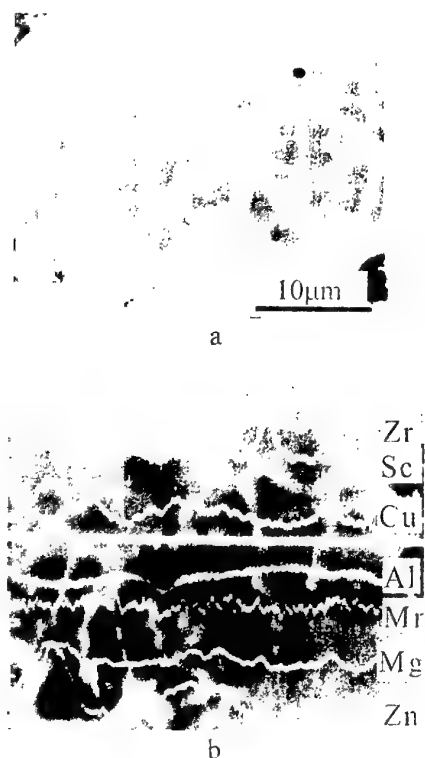


Figure 2. Microstructure and composition of a particle of 100 μm in size in 2P alloy powder: a – SEM photo in COMPO condition; b – changing the intensity of element spectral lines along the secant

The room-temperature mechanical properties for P/M rods of alloys under investigation are summarized in Table 1.

Table 2. Mechanical properties of P/M rods
Ø6 mm in T6 condition

Alloy #	Powder fraction, μm	HV, MPa	YS, MPa	UTS, MPa	El, %
1P	63-100		742	763	3.7
2P	63-100	2325	717	779	3.2
3P	0-63	2350	774	816	3.4

The main hardening agent in alloys based on Al-Zn-Mg and Al-Zn-Mg-Cu systems in T6 condition is the metastable η' -phase that precipitates during aging in the form of very small (to 10 nm in size) secondary dispersoids, coherently bound with the matrix [2, 6]. Such particles in our case are shown in Fig. 3a. The second hardening agent is a polygonal cellular

structure with cell size less than 1 μm that was observed by TEM in all P/M alloys. Evidently, recrystallization in P/M alloys is retarded by oxide films from particle boundaries. Both of these factors form hardening in the rod 1P. As seen from Table 2, alloying with Sc and Zr changed the mechanical properties insignificantly, in spite of the presence of Mn that shall give a solid solution hardening [2]. Coherent $\text{Al}_3(\text{Sc}_{1-x}\text{Zr}_x)$ intermetallics (Fig. 3b) evidently make a contribution to rod strength, but Sc somewhat increases particle size of the η' -phase [6], and the results may compensate each other. In this case Sc additions are useful to improve some other properties, e.g. corrosion resistance. Strength characteristics of the rod 3P are increased (Table 2) mainly by the increased amount of the η' -phase due to a higher content of Zn. Note that using the smallest powder fraction permitted to obtain in this P/M rod the plasticity higher than 3 %.

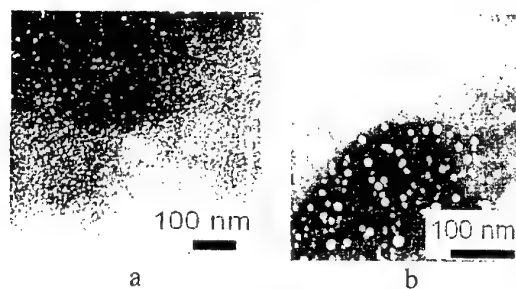


Figure 3. Secondary dispersoids in the P/M rod of 2P alloy in T6 condition, TEM, dark field image formed by particle reflections: η' -particles (a) and $\text{Al}_3(\text{Sc}_{1-x}\text{Zr}_x)$ particles (b)

The work was partially financed by STCU (project P061).

Reference

1. Zolotarevsky Yu. // Mater. Sci. Forum. -- 1997. -- 242. - P.181.
2. Aluminum and Aluminum Alloys, ASM Speciality Handbook, 1993.
3. Fridlyander I.N. Wrought Aluminum Industrial Alloys. -- Moscow: Metallurgia, 1979. -- 209 p.
4. Neikov O.D., Krajnikov A.V. // Mater. Sci. Forum. --1996. -- 217-222. -- P. 1649.
5. Eskin G.I. // Tekhnologia Legkikh Splavov. -- 2000. - No. 2. -- P. 17.
6. Senatorova O.G., Uksusnikov A.N., Legoshina S.F. et al. // Mater. Sci. Forum. -- 2000. -- 331-337. -- P. 1249.

COMPACTING DYNAMICS OF THE WC-Co CEMENTED CARBIDES DURING HOT IMPULSE PRESSING IN VACUUM

Kovalchenko M.S., Laptev A.V.

I.N. Frantsevich Institute for Problems of Materials Science, the Ukraine NAS, Kyiv, Ukraine

The experience of powder metallurgy development in recent decades points out the forcing tend to use of external actions for the formation of structure and properties of sintered materials. Thermal-mechanical actions are related to such ones that enable to produce an effect on materials by the way of variation of such factors as temperature, rate, character, and type of mechanical loading. The use of the materials thermal-mechanical processing enables to diminish the problems connected with features of mesostructure imperfections in porous media being caused by random particles packing on initial stages of powder technology [1, 2]. In this context a hot impulse pressing has to be considered as one of effective methods for thermal-mechanical treatment of porous materials, and it creates the favorable prerequisites for its use in cemented carbides processing. The results of theoretical and experimental study of hot impulse pressing in vacuum of the WC-Co cemented carbides are cited in the present paper.

The hot impulse pressing occurs during an impact of a mass M with initial velocity v_0 on deformable body under its elastic limit is described by a dynamic second order differential equation

$$\ddot{x} + (r/M)\dot{x} + (c/M)x = 0, \quad (1)$$

and beyond the elastic limit of the body—by a third order equation as follows

$$\ddot{x} + \alpha_3\dot{x} + \alpha_2\ddot{x} + \alpha_1 = 0. \quad (2)$$

Here $\alpha_1 = \frac{cg}{Mb}$, $\alpha_2 = \frac{c}{M} \left(1 + \frac{r}{b} \left(1 + \frac{g}{c} \right) \right)$,

$$\alpha_3 = \frac{c+g}{b} + \frac{r}{M}; \quad \frac{1}{c} = \frac{1}{c_m} + \frac{1}{c_s}; \quad c_s = \frac{\tilde{K}S}{l_s};$$

$$b = \frac{ZS}{l_s}; \quad g = \left(\frac{\partial P}{\partial e} \right) \frac{S}{l_s}; \quad c_m = \text{elastic rigidity of the}$$

impact machine; c_s = the same of deformable body; \tilde{K} = effective bulk elastic modulus, Z = volumetric viscosity, $\partial P/\partial e$ = bulk modulus of strain hardening, S = cross-section area, and l_s = deformable body length; r = effective viscous

resistance of surrounding medium [3]. The points over the variables indicate differentiation in respect to time. The equation (1) corresponds with an autonomous second order dynamic system, and equation (2) with an autonomous third order dynamic system. The solution of the second order system is a periodic one when $c/M > r^2/(4M^2)$. As to the third order dynamic system, its periodic solution corresponds with small and large the control parameter α_3 , and in the intermediate case the solution is nonoscillating.

The experimental study of hot impulse pressing is carried out in a laboratory vacuum impact machine, had specially designed and made for this purpose. The maximum impact energy can be reached 10 kJ, collision velocity over 12 m/sec, and temperature up to 1700 °C. The machine has the elastic rigidity of 347 MN/m, and the reduced mass of 105.5 kg during impact. It enables to treat preforms, which have a diameter up to 50 mm and a height up to 30 mm. The machine has a strain-gauge assembly unit for oscillogram recording as well as frequency module for registration of the initial impact velocity. The oscillogram data processing is carried out in a computer with the programs written in FORTRAN programming language. Integration of digitized data array gives the velocity data for each point of the oscillogram, and following integration of the array obtained enables to compute the change in total height of the mechanical system, height of its elastic elements as well as height of deformable body vs. time. Further differentiation of the table data of the deformable body height gives the values of viscous flow rate, being needed for determination of viscous resistance of the body during hot impulse pressing. The letter is determined as a ratio of force (from the oscillogram) to the viscous flow rate above.

As an example, the Fig. 1 depicts the experimental oscillogram that represents the inertial force, arising as a result of dynamic impact action on the heated preform of cemented carbide, vs. time. The time dependence of change in the total height of the mechanical system (machine), the height of elastic elements of the machine and

deformable body (the preforms of cemented carbide) as well as the deformable body height is shown in Fig. 2. It is seen that the change in the height of porous deformable body gives the main contribution into the total elongation of the mechanical system.

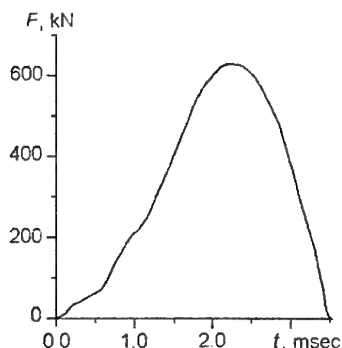


Figure 1. The force F vs. time t during impulse hot pressing of the WC+15 mass % Co cemented carbide at the temperature of 1050 °C with the initial impact velocity of 9.35 m/sec.

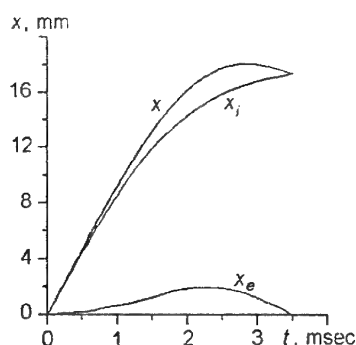


Figure 2. The change in the total height x of the system, height of its elastic elements x_e , and height of deformable body x_i vs. time t during hot impulse pressing of the WC+15 mass % Co cemented carbide body at the temperature of 1050°C with the initial impact velocity of 9.35 m/sec.

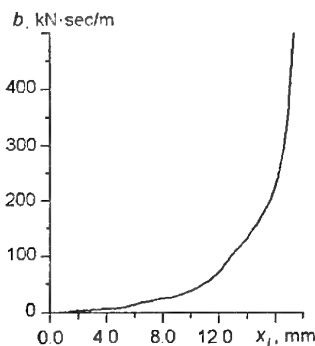


Figure 3. The viscous resistance b of the WC+15 mass % Co cemented carbide body at the

temperature of 1050 °C vs. time t during hot impulse pressing.

The viscous resistance of preform is progressively increased as its height is decreased that corresponds with a general dependence of porous body bulk viscosity upon its relative density. It is found down that an estimated shear viscosity of the matrix, forming porous body, is decreased in the course of densification. It may be caused by a mechanic-thermal effect due to energy dissipation in deformable body as well as the change of deformation mechanism. As it follows from the analysis carried out, the behavior of the cemented carbide preform during hot impulse pressing is in agreement with the dynamics of the process.

Comparison of the data for mechanical properties of the WC+20 mass % Co hot-impulse-pressed as well sintered (in vacuum) specimens (Fig. 4) shows that the process in study besides total the elevation of strength enables to rise a Weibull's modulus of the cemented carbides that essentially improves their operating reliability.

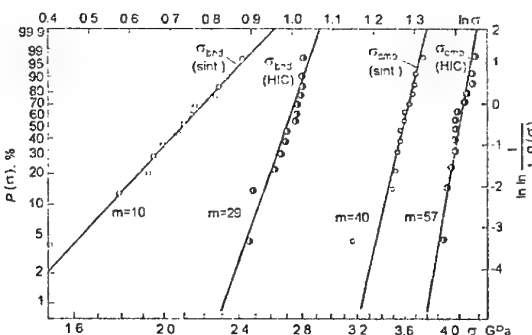


Figure 4. The Weibull statistic distribution of transverse rupture strength σ_{bnd} as well as compression strength σ_{cmp} for sintered (sint.) and hot impulse compacted (HIC) WC+20 mass % Co cemented carbide; m is a Weibull's modulus.

References

- [1] R. German: Particles packing characteristics, MPIF, Princeton, 1989.
- [2] A.N. Nikolenko, M.S. Kovalchenko: A hierarchic structure, levels of description, models classification and the analysis of powder metallurgy materials compacting, *Poroshkovaya Metallurgiya* (1989) No 6, 29-33.
- [3] M.S. Kovalchenko: The dynamics of mechanical actions on materials. Periodic and aperiodic movements of the autonomous dynamic system, *ibid.* (1997) Nos 3/4, 113-122.

GLASS-COMPOSITE ABRASIVE-CONTAINING MATERIALS OF TOOL ASSIGNMENT

Shilo A., Bondarev E., Kukharevko S.

V.N.Bakul Institute for Superhard Materials of the National Academy of Sciences of
Ukraine, Kiev, Ukraine

The need of an industry of the developed countries in abrasive tools from superhard materials (SHM) continuously increases. For last 10-20 years manufacture of abrasive SHM tools on ceramic bonds, for example, in the countries of Europe, has increased in 3-5 times. A defined complex of properties approached to demanded, can have the composite materials on glass bond.

The properties of glass materials on basis of two systems are investigated: sodium-boron-silicate and lead-zinc-borate, which can be a basis of abrasive tools on ceramic bonds. The complex of properties describing glass as binding for SHM is investigated. It includes temperature of sintering and flowing, chemical activity, wear resistance, wetting ability and adhesion of a melt of a glass in relation to SHM and fillers, durability of deduction of SHM in glass matrix, crystallizing ability, kinetics of sintering of glass powders and composites, thermal conduction, mechanical and other properties.

To provide for a demanded level of interaction of components of composites and their high aggregate stability in heterogeneous melts of systems "glass - filler" the physico-chemical and technological aspects of interphase adhesion appearances were investigated.

The regulation of properties of CBN- and diamond-containing composites by means of a modification of structure of glass bonds is realized at the expense of use of glasses of various chemical structure or modifying them by oxides, use of fillers of various functional assigning, and also application of different modes of manufacture of composites.

In systems "glass - SHM - filler" the materials possessing new properties at the expense of use of adhesion-active to SHM and fillers of glasses, described by the increased ability to moisten and to keep grains of SHM, and also distinguished from known by high wear resistance and antifrictional properties are obtained.

For reaching the given properties of glass-composite binding materials a traditional process of sintering in a free condition, high-speed low-temperature process of thermoplastic pressing and "solution" technology are used.

The diamond tool on ceramic bonds has found a use on finishing operations of machining of steel products and nonmetal materials, and tool from CBN - at grinding and honing of hardened steel.

Ceramic bonds are applied to manufacture of the following types of the diamond tool:

- The grinding instrument for sharpening the cutting instrument from hard-facing alloys together with a steel;
- Short-grained bars for finishing dimensional treatment of bearing rollers from hardened steels;
- Blocks - bars for a finish machining of steel nicks of gear-wheels of hydraulic pumps both bent shafts of tractor and automobile drives;
- Elastic wheels for draft and fair grinding of non-metallic materials (glass, ceramics, self-colour stones).

The instrument from CBN has recommended itself on operations of draft and fair sharpening, and also operational development with refrigeration and without it of hardened intractable steels. Such instrument effectively works at outside and interior grinding, and also honing of quenched steel articles(workpieces). The instrument ensures grinding steels with productivity 600 mm³/minute and more.

The serviceability of the instrument from CBN on ceramic bonds is tested at treatment of cutting tools from steels P6M5, P9K5, P9M4K8, P12Φ3K10M3 and others at the machine-building plants of Ukraine and other countries of CIS, and also Poland, Bulgaria and China.

SUPERHARD CARBON FILMS WITH PREDOMINANTLY sp^2 BONDS

Kulikovskiy V., Bohac P.⁽¹⁾, Kurdyumov A., Jastrabik L.⁽¹⁾

Frantsevich Institute for Problems of Materials Science, Ukraine National Academy of Sciences,
Kiev, Ukraine

⁽¹⁾Institute of Physics, Academy of Sciences of the Czech Republic, Prague

The high hardness of amorphous carbon films (a-C) is usually linked to the presence of a high percentage of sp^3 bonds. Such films are called diamond-like carbon (DLC). The higher the sp^3/sp^2 ratio, the harder film. Recently, it was shown that some hard films contain a high number of sp^2 bonds [1]. The structural origin of the very high hardness of such films is still a subject of discussion and investigation.

In this paper we attempt to find the connection between the hardness, intrinsic stress, and structure of a-C films obtained by magnetron sputtering of carbon by varying the Ar pressure, the substrate bias and gas mixtures of Ar + CH₄ or Ar + O₂.

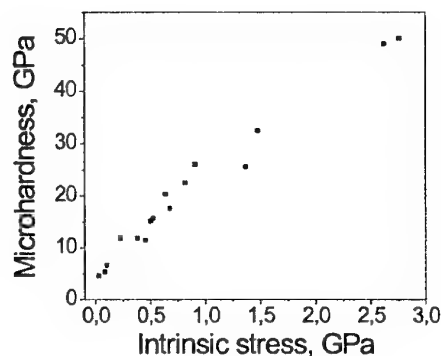
The substrate-target distance was 50 mm. The total working gas pressure was approximately 0.17-2.8 Pa for a-C and 0.17-0.5 Pa for a-C:H and a-C:O deposition. The discharge power was varied from 300 to 960 W, but was mainly at 960 W. Bias up to -150 V was induced due to 13.56 MHz power source applied to the substrate carrier. Substrates were not specially heated.

The film thickness was approximately 1.5 μ m for the majority of films. The film structure was investigated by Raman spectroscopy, and also by transmission electron diffraction (TED) using a filter of an elastically scattered electrons. Electrical resistivity of the films was determined using standard four-point probe measurements. The microhardness measurements were carried out on a Fisherscope H100 apparatus at a growing load of up to 10 mN. The intrinsic stresses were calculated using Stoney's classical equation. Thick films on Si(111) substrates (size 20×8×0.5 mm) were used for measurement of the microhardness and determination of the intrinsic stress. Thin films (30-60 nm) were prepared on KCl substrates for the investigation by TED.

Fig. shows a strong dependency of the microhardness on intrinsic stress for all the thick (approx. 1.5 μ m) a-C and a-C:H films obtained at different values of discharge power (300-900 W), Ar or Ar+CH₄ pressure (0.17-3.3 Pa) and negative substrate bias (from 0 up to -100 V). The higher intrinsic stress, the harder film. The decrease in Ar

pressure from 2.8 to 0.17 Pa leads to an increase in the microhardness and intrinsic stress and an decrease in electrical resistivity.

Such behavior of the film properties could be explained by an decreasing amount of absorbed gas on the boundaries of clusters that improves their interconnection. Note that at low Ar pressure, when the mean free path λ of sputtered C atoms is equal or larger than the cathode-substrate distance L , the energy not only of the Ar ions, but of every



carbon atom arriving at the substrate, is of several eV. This is already sufficient to remove (re-sputter) the gas impurities weakly bound to the growing film. In such a case, the value of the microhardness can be approximately 25 GPa without any ion bombardment. A decrease in λ/L leads to a reduction in the average energy of condensing C atoms and as a result to a decrease in bonds between adjacent clusters.

Similar, but more pronounced changes in microhardness, intrinsic stress and resistivity are observed when even a small amount of oxygen or methane is added to the argon. It has been shown on our 1.5 μ m thick carbon films (a-C, a-C:O and a-C:H) that with increasing of negative substrate bias and/or decreasing of O₂ or CH₄ pressure, the resistivity decreases with simultaneous increase in the microhardness and compressive stress. The a-C films condensed under ion bombardment at the discharge power of 960 W and substrate bias of -100 V showed the highest microhardness of 50

GPa and the lowest resistivity (0.01 - 0.05 Ω cm). The same result was achieved by decreasing these values to 300 W and -60 V respectively. This increase in microhardness and intrinsic stress and simultaneous decrease in resistivity to very low value against previous cases can mainly be explained by the re-sputtering of weakly bound gas impurities on the boundaries of clusters. This leads to enhancement of the contacts between adjacent clusters and a decrease in the electron scattering on numerous cluster boundaries. In addition, it leads to an increase in the intrinsic stress due to formation of the dense, incoherent boundaries of clusters. An increase in the film hardness can be caused by this growth process and also by a displacement of C atoms by Ar ions into subsurface positions.

Thermal annealing of the hard films took place in vacuum at the temperatures: 300, 500, 700 and 820 °C during 1 h at every temperature. After measuring, the same set of samples was used again for the next annealing cycle.

After annealing in vacuum at different temperatures was found that the microhardness and intrinsic stress of the hardest a-C film do not correlate each other. The annealing up to 500 °C leads to increasing microhardness (up to 65 GPa) at simultaneous decreasing intrinsic stress (from 4.2 to 2.3 GPa). It means the high microhardness of the deposited film is defined not only by the intrinsic stress, but the film microstructure. High level of the intrinsic stress induced by ion subimplantation during film growth is needed mainly for the formation of the dense nanostructure with strong interaction between atoms at the grain boundaries, even if they occupy incoherent positions. The possible sliding along prime planes within clusters is difficult, due to the high disordering within clusters and high compressive stress, which, in turn, can bind these planes. In any way, if such sliding is possible, it is realized partially during film growth under compressive stress. That is why these films demonstrate not only the high hardness, but high elasticity (80-90 %). Further annealing of the hardest film at 700 and 820 °C leads to some decrease in the microhardness, however, its value remains enough high ($H \sim 40$ GPa). The intrinsic stress of thick a-C film does not relax completely

at annealing up to 820 °C as it was observed for ta-C thin ones. It indicates strongly compressed film nanostructure which is stable up to temperature of recrystallization (≥ 900 °C).

Microhardness and intrinsic stress are closely related to the film structure. The density of the hardest films is equal to $2.2 \div 2.4$ g/cm³ and close to that for graphite (2.26 g/cm³). Raman spectra from these films show asymmetrical band near 1550 cm⁻¹ that indicates the presence of considerable number of sp² bonds. The electron diffraction patterns from thin carbon films, prepared at the same conditions as thick hard ones, contain three strong visible haloes. The first, small angle halo appears only if the film contains fragments of graphite-like structure and corresponds to the diffraction from (002) graphite planes. It was shown for the first time that the interplane distance d_{002} could be shortened down to approximately 0.300 nm in the hard graphite-like carbon films obtained with ion bombardment. The considerable decrease of d_{002} can be explained by the highly stressed sp² structure of our films. Such a structure was observed for bulk graphite under high pressure (see e.g. [2]). Also, we have developed and substantiated a simple procedure using the transmission electron diffraction data to determine whether the amorphous carbon film is graphite- or diamond-like [3]. This procedure is based on the comparison of calculated and real position of the maximum of the third halo. For our films this procedure gave the same first coordination sphere radius as for graphite independently of whether the film is under stress or not.

Thus, all the data indicate an sp² bonding configuration of the hard carbon films deposited.

The sp² hard carbon films presumably consist of cross-linked randomly oriented dense clusters, bonded to each other through incoherent boundaries on which high stresses are accumulated. The fewer the gas impurities on these boundaries are, the stronger is the bonding between the clusters. In this way a continuous rigid network is formed. The high compressive stress can result in the strong bonding between the cluster boundaries, on which a small concentration of sp³ sites may be occurring.

[1]. I. Alexandrou, H.-J. Scheibe, C.J. Kiely, et al., Phys. Rev. B, 60 (1999) 10903.

[2]. R.W. Lynch, H.G. Drickamer, J.Chem.Phys. 44 (1966) 181.

[3]. V. Kulikovskiy, K. Metlov, A. Kurdyumov, P. Bohac and L. Jastrabac, Diamond Relat. Mater. (2002), to be published.

PERSPECTIVES OF NANOSTRUCTURE MATERIALS APPLICATION FOR CUTTING AND PRODUCTION OF A WIRE

Panov V.S., Malochkin O.V.

Moscow State Steel and Alloys Institute (Technological University), Moscow, Russia

The perspectives of development of various branches of modern mechanical engineering depend on a level of development and introduction of new ceramic constructional materials with special properties, which could provide necessary operational reliability of details of designs and be characterized by a complex of the given properties at high temperatures 1000-1500°C and above, including high sizes of hardness and wear resistance, durability and stability to oxidation.

The problem of mechanical properties is one of key in a general problem of technical ceramics, as the common fault - their fragility in a wide range of temperatures is inherent in refractory not metal connections. The efforts of the researchers basically are directed on overcoming of this lack, by means of development of principles of structural designing for increase of resistance to fragile destruction. Thus the researchers proceed from representations about indissolubility of interrelation of all elements of a sequence: technology - structure - mechanical properties - operational characteristics.

In this connection last years the increased interest of the researchers to study nanosized powders is observed on the zirconia basis. It is caused, as by necessity of expansion of existing representations about a structure and properties of the given materials, and perspective of their use for the qualitatively new appendices in various industries. It is necessary to note, that, despite of intensive study, structure and nanosized powders phase structure especially received is strong nonequilibrium conditions, are investigated insufficiently. As modeling system $ZrO_2-Yb_2O_3$ was chosen.

In work the representations about kinetic of zirconium allocation from a solution are advanced at sol-gel synthesis and the mathematical model of the given process allowing to assume law crystallization of stabilized zirconia powders particles (the centers, stabilized, of particles of a zirconia powder is offered are formed in one stage and have two directions of effective growth). Kinetic of phase formation is investigated in a course of sol-gel synthesis of zirconia

particles with the various contents of ytterbia and the effect of gelation time on the average size of particles is established.

The mathematical model allowing to expect density of materials from with various duration, stabilized is created achievable at any given pressure in an interval 0 - 2,5 t/sm² and to optimize parameters of processes of pressing and sintering. The complex researches of physical and mechanical properties of a composite material on a zirconia nanosized powders basis are executed. The given researches have allowed to determine the optimum contents of the stabilizing additive ytterbia), which there were equal 2% appropriate to the maximal importance of durability (923 MPa), K_{IC} (13,3 MPa×m^{1/2}) and hardness (16,7 GPa).

The unknown laws of phase formation in process of sol-gel synthesis and subsequent heat treatment in system $ZrO_2-Yb_2O_3$ in process of crystallization are established earlier. The temperature dependence of durability and K_{IC} of a composite material of optimum structure is investigated: the monotonous decrease of durability and K_{IC} with increase of temperature is established.

The scientific results of work have allowed developing technology of reception of a composite material and coatings on a zirconia nanosized powders basis with high physical-mechanical properties.

STRUCTURAL ENGINEERING OF NANOCRYSTALLINE MATERIALS FOR CONSTRUCTION APPLICATION

Podrezov Yu.N.

Frantsevich Institute for Problems of Material Science NAS of Ukraine, Kiev, Ukraine
podrezov@materials.kiev.ua

The last decade has seen an important development that drastically changed the status of nanostructural materials as a branch of material science. Instead of being exotic and purely descriptive object they are increasingly resorting to very useful and carefully investigated type of structure. This achievement owns much to introduction of nanostructural materials as the main elements in super-tiny electronic plates. Undoubtedly, so-call functional materials and its unique electromagnetic properties have priority in such investigation. The wave of publication about mechanical behavior for this class of materials immediately followed, too.

Severe plastic deformation is more preferable method, which gives the possibility to create nanocrystalline structure in a macroscopic volume. Traditional deformation methods (elongation, compression, ruling, draft and so on) give such possibility on a very thin samples (thin foil or thin wire). In the last case the comparison of the mechanical properties of the materials with a different deformation degree is hindered by scale effect. The creation of new high deformation methods offers ample scope both for strain hardening theory and for deformed materials structure engineering. Equal canal angel pressyre (ECA) method was created by Segal et al. Simple shift uniform deformation of high intensity can be achieved on a macro sample 15x15x150 mm without exchanging of its sizes. Other method based on the deformation by twist extrusion (TE). scheme was proposed by Beygelsimer et. al. The creation of shift uniform deformation without sizes exchanging allows to carry out repeated deformed treatment in the different (or the same) direction of deformation and as the result to control structure formation process under high deformation degrees.

AL-Mg-Sc alloys deformed by ECA - pressure method demonstrate the record value of superplastic deformation 2400% when speed of deformation 10^{-3}sec^{-1} is usual for superplasticity, and moreover keep the superplastic ability up to high speed deformation $10^{-1}-1\text{sec}^{-1}$. After ECA - pressure deformation titanium has maximum strengthening (yield point is 800-900 MPa) that improves its application in medical branch. Extremely high fracture toughness in high deformed Fe-Armco after (ECA) pressure was obtained in our previous works.

These results and some other experimental data demonstrate high ability and good perspective of severe plastic deformation methods. But achievement of high strength in deformed materials with nanostructure is essentially more complicate task then it follows from microscopic theory of strength. According to the models of this theory strength of materials is connected with structural size dimension by Hall - Petch equation $\sigma_T = \sigma_0 + \kappa_y d^{-1/2}$ or its Holt variation for cells materials $\sigma_T = \sigma_0 + \kappa_y d^{-1}$. The extrapolation to nano scale of grain or cell size dimension theoretically predicts a very high strength of nanocrystalline materials. But experimetal results demonstrate essentially worse situation. A. W. Tompson reviewed experimental data from variety of investigation obtained on high deformed Fe - Armco wires. In this graph we add our data obtained on Fe - Armco deformed by (ECA) pressure.

Some important conclusion about interconnection between structural evolution and strengthening of high deformed materials is followed from these results. Firstly, it is the change of strengthening mechanism from grain size sensitivity (Hall - Petch equation) to cell size sensitivity (Holt equation) at critical

grain size $d < 0,4 \mu\text{m}$. Secondly, it is the theoretical possibility to obtain super high strengthening in nanocrystalline Fe- Armco. It follows from experimental data (see dashed line) that extrapolation of experimental data to nanostructure sizes (10 nm) gives the value of yield point for such material approximately 6000 MPa. But the thread conclusion restricts such possibility. Difficulty is amplified due to the fact that cells or subgrain size in armco-Fe obtained by different methods of severe plastic deformation (ruling, draft, EC-pressure), can not be less than 100 nm. As the result, the yield point for such material is only 1000 MPa.

MULTISTAGE HIGH STRAIN RATE SUPERPLASTICITY OF MICROCRYSTALLINE ALLOYS

Kamalov M.M., Myshlyaeva M.M., Medvedev A.S., Myshlyaev M.M.⁽¹⁾

Institute of Solid State Physics RAS, Chernogolovka, Russia

⁽¹⁾Baikov Institute of Metallurgy and Material Science RAS, Moscow, Russia

INTRODUCTION: Scientists and technologists have been displaying recently an active interest in aluminium-lithium alloys due to unique combination of their properties, namely, an increased elastic modulus, sufficiently high strength and low density. Nowadays much work is in progress aimed at improvement of properties of these alloys, also by forming in them nano- and microcrystalline structure via intensive plastic deformation. It is generally acknowledged herewith that equal-channel angular pressing (ECA-pressing) is one of the most promising methods to achieve the goal. In this work precisely this method was employed for the formation of a microcrystalline structure. The object to study was the prospective lightest (density $2.47 \text{ g}\cdot\text{cm}^{-3}$) corrosion resistant weldable alloy 1420 (Al-5.5%Mg-2.2%Li-0.12%Zr). It is superplastic and is widely used to fabricate workpieces of a complicated profile. Typical characteristics of its superplasticity (SP) are as follows: strain to failure is 350% and the coefficient of strain rate sensitivity of stress is 0.45 at a strain rate of $5 \times 10^{-3} \text{ s}^{-1}$ at $T=480^\circ\text{C}$ [1].

PROCEDURES, RESULTS AND DISCUSSION: The rods (20 mm in dia, 70 mm in length) were produced by sequentially ECA-pressing the material for 10 passes at 370°C . Structure and phase state were studied by an electron microscopy (JEM-100CX). Three sample sections, i.e. normal to the rod axis and two mutually perpendicular and parallel to the rod axis were examined. Flat samples (0.85 mm in thick, 5 mm in gauge length) to be tested under tension in Instron machine were prepared.

The investigations showed. Rods demonstrated grained structure. About 50% of grains measured from 0.5 to $3 \mu\text{m}$, grains measuring from 3 to $5 \mu\text{m}$ made up 30-40%, from 5 to $8 \mu\text{m}$ – 10-20%. Normally, the grains exhibited subgrains containing both individual dislocations and dislocation cells and tangles. The subgrain misorientations were $2-8^\circ$. The subgrain boundaries consisted of dislocations. Often they were quite regular dislocation networks and single-row walls. They

measured from 0.3 to $2 \mu\text{m}$, depending on the grain size. Fractured and broken subgrain boundaries were frequent. Dislocation motion and migration of subgrain boundaries were observable when examining the structure. In individual cases bent extinction contours were observed that is suggestive of the occurrence of internal stresses. The rods demonstrated numerous particles of the Al_2LiMg phase of various sizes and configurations and small particles of the δ' (Al_3Li) phase. The formers were found in the grain and subgrain interiors and at their boundaries as well as on dislocations. In the latter case particles were small.

The diagrams describing the connection of true stress σ with true strain e were experimentally obtained. They showed three stages of plastic deformation. The first one was rather continuous stage of deformation hardening. The second stage was characterized by constancy σ . The third one was a stage of monotonous fall of σ with increase in e value. This stage was the most continuous in true strain and, consequently, in elongation. To determine the true strain rates in these stages we obtained a dependence of \dot{e} on e using the same testing conditions. This dependence showed that strain rates 10^{-2} s^{-1} and 10^{-3} s^{-1} corresponded to the first and the third stages, correspondingly. The former indicated strain rate is characteristic for SP deformation (SPD) at the expense of sliding inside grains [2]. The last indicated strain rate is typical for SPD of fine-grained materials, when SP is conditioned by grain boundary sliding [3,4].

Studies of the dependence of deformation up to failure on the initial strain rate and testing temperature (T) showed that the range of $365-400^\circ\text{C}$ and $\dot{e}_{in}=1.7 \times 10^{-2} \text{ s}^{-1}$ were the most optimum to attain the largest strain. The greatest value of the attained elongation was 1878%. Note (see Introduction) that this alloy, not subjected to ECA-pressing, exhibited the SP elongation (350%) and its SP manifested itself at a much higher temperature (480°C) and a noticeably smaller strain rate ($5 \times 10^{-3} \text{ s}^{-1}$).

The analysis of the collected experimental data with take into account the ones presented in literature showed that the connection among $\dot{\epsilon}$, σ and T can be well described by the known relationship:

$$\dot{\epsilon} = \dot{\epsilon}_0 \times \exp(-U/kT) = A \sigma^n T^{-1} \times \exp(-U/kT), \quad (1)$$

where $n = 2$, and U – activation energy of SPD, k – Boltzmann constant, A – constant. Estimation of value n and U were evaluated using standard techniques. According to our experiments $n = 2.235$ and $U = 1.4$ eV in the first stage and $n = 2.3$ and $U = 0.98$ eV in the third stage. The experimental values n coincide with rather a high accuracy in the value $n = 2$ in Eqn. (1). Using these values of n and U values of parameters $\dot{\epsilon}_0 = 5 \times 10^{10} \text{ s}^{-1}$ and $A = 1.6 \times 10^6 \text{ K} \cdot \text{mm}^2 \cdot \text{MPa}^{-1} \cdot \text{s}^{-1}$ were calculated. The aforementioned of SPD activation energy value of $U = 1.4$ eV corresponds to self-diffusion energy (1.4 – 1.5 eV) inside of grain [5]. The value of $U = 0.98$ eV corresponds to grain boundary self-diffusion energy $Q_{sp} = W + R_{gb} = 0.99$ eV, where $W = 0.8$ eV [5] – vacancy formation energy and $R_{gb} = 0.19$ eV [6] – vacancy migration energy along grain boundaries or dislocations (pipe diffusion). The obtained different values of activation energy which correspond to the first and third stages point to the presence of plastic deformation under different mechanisms during these stages. Thus, the second stage is a transitory one and transforms from one mechanism to another.

TEM studies were carried out to investigate structure of the samples subjected to tensile straining. The first stage shows overall continuous rearrangement of structure with domination of hardening processes over dynamic recovery ones, and active sliding inside grains. As a result, the grains became elongated in the strain direction. Elongation of grains decreased during the deformation in the third stage. As a result, the grains became elongated in the strain direction. Elongation of grains decreased during the deformation in the third stage. By the end of the stage grains became nearly equiaxed. Important

circumstances attract attention in the whole stage: Absence of dislocations in many grains and the presence of fine Al_2LiMg particles in them and in grain boundaries. The important fact is also that Al_2LiMg particles make chains in grains and situated as grain boundary profiles. All these points to continuous and overall dynamic recrystallization with grain boundary sliding and migration. One should note that the described herewith in agreement with aforesaid activation energies.

CONCLUSION: The structure and mechanical behaviour of the ECA pressed 1420 alloy have been studied in SP conditions. Three stages of SPD have been shown. The data showing intra-grain sliding during the hardening stage and dynamic recrystallization with participation of grain boundary sliding and migration during the stage of the decrease of true stress have been obtained. It has been shown the elongation up to 1878% corresponds to alloy, and $n \approx 2$ and $m \approx 0.45$ for both stages.

ACKNOWLEDGEMENT: The support from the Russian Foundation for Basic Research (Projects 02-02-81021 and 02-02-96413) is greatly appreciated.

REFERENCES:

1. Novikov I.Y., Portnoi V.K., Konstantinov I.L., Kolobnev N.I. Physical metallurgy of aluminium alloys, Nauka, Moscow, 1985.
2. Likhachev V.A., Myshlyaev M.M., Sen'kov O.N. Laws of the Superplastic Behavior of Aluminum in Torsion, Lawrence Livermore National Laboratory, Livermore, 1987.
3. Grabskii M.V. Structural superplasticity of metals, Metallurgia, Moscow, 1975.
4. Kaibyshev O.A. Plasticity and superplasticity of metals, Metallurgia, Moscow, 1975.
5. Friedel J. Dislocations, Pergamon press, Oxford, 1964.
6. Stark J.P. Diffusion in solids, Energiya, Moscow, 1980.

DEVELOPMENT OF HIGH-HARDNESS WEAR RESISTANT BORON-CONTAINING COMPOSITE MATERIALS

Makarenko G.N., Timofeeva I.I., Bykov A.I., Gridneva I.V., Fedorus V.B., Buzhenets E.I.,
and L.P. Isaeva

Institute for Problems of Materials Science, National Academy of Sciences of Ukraine, Kiev,
Ukraine

A great number of composite materials on the base of boron carbide and its compounds for different applications have been known. Among these are the B_4C - MeB_2 composites possessing high hardness, wear resistance, strength, and chemical inertness.

A study of the hard phase indicates that the formation of the boride proceeds through the stage of formation of the corresponding carbide. In this case, its further interaction with boron carbide proceeds practically under the conditions of a solid-state reaction. This fact was used in development of a new method of preparing dense specimens from the B_4C - MeB_2 composition in a wide concentration range. It provides reaction sintering, activates the interaction of mixture particles, and not only facilitates the conditions of preparing high-density products, but also makes it possible to form a highly disperse structure in them.

In the present work, the mechanism of interaction of boron carbide with carbides of transition metals was investigated, the regularities of formation of the boride phase were elucidated, and optimum conditions of formation of the fine crystalline structure of the materials during reaction sintering under conditions of high pressures were established.

Hot pressing was carried out in graphite dies on a laboratory lever press, in which pressure was maintained constant automatically. The mass of powder samples was fixed and was controlled after hot pressing. Temperature was recorded with a self-recording optical temperature sensor (with an accuracy of $\pm 20^\circ C$). An external pressure was applied after heating up to a set temperature. Investigations were performed in the temperature range 1700-2000 $^\circ C$ under pressures from 5 to 15 MPa with an exposure for 1-5 min at a set temperature. High pressure sintering was carried out in a lens-type pressure chamber with a diameter of the working channel of 6 mm. Heating was performed by passing current through a graphite heater.

During the formation of boron carbide by the reaction $B_4C + MeB_2 = 2MeB_2 + 3C$, free carbon precipitates, which decreases significantly the quality of the composite material. In order to bind free carbon, boron and boron silicide were added to the mixtures.

According to X-ray phase analysis, under the conditions of hot pressing and high-pressure sintering, the interaction in the B_4C - MeB_2 system proceeds through the stages of formation of lower borides. As the sintering temperature and the exposure time are increased under constant pressure, the reaction proceeds more completely. However, the end phase MeB_2 forms at a temperature above 1800 $^\circ C$. As the temperature of high-pressure sintering is raised, the diboride content increases. According to our data, the reaction proceeds completely at a temperature of 2000 $^\circ C$ and under a pressure of 3 GPa.

An increase in the boron content of the mixture favors the formation of the boride phase. Boron silicides affect most essentially. This is likely to be connected with their decomposition at temperatures above 1420 $^\circ C$ and the appearance of reactive boron and silicon atoms. After treatment of the mixtures with the participation of B_4Si under analogous thermobaric conditions, besides boron carbide, in the end product, diboride of the corresponding metal and silicon carbide were detected.

According to metallographic analysis data, in all alloys, boron carbide grains, small diboride grains, located along B_4C grain boundaries, and very small silicon carbide grains, partially dispersed in boron carbide grains, are present.

It has been known that intracrystalline nanoinclusions increase greatly the mechanical properties of the materials. The microhardness (measured with a load on the indicator 2 H) of the B_4C - MeB_2 materials prepared under conditions close to optimum ones appeared to be higher than that of pure B_4C , namely, 42-45 GPa against 28 GPa.

Thus, the process of pressure reaction sintering of the powder mixtures of boron carbide with titanium, zirconium, and vanadium carbide results in the formation of a heterophase material of set composition through the stages of formation of lower borides.

In conditions of hot pressing under high pressure, boron and boron silicide additives favor the reaction to proceed completely. The promising compositions of the initial mixtures in terms and directions of optimization of thermobaric sintering conditions were determined.

Wear Resistant Composite Materials and parts, Manufactured by Hot Pressure Treatment

Serdyuk G.G., Sakhnenko A.V., Pavligo T.M.,
Svistun L.I. ⁽¹⁾, Plomodyalo R.L. ⁽¹⁾, Plomodyalo L.G. ⁽²⁾

I.N.Frantsevich Institute for Problems of Materials Science of NAS of Ukraine

⁽¹⁾ Kuban State Technological University, Krasnodar, Russia

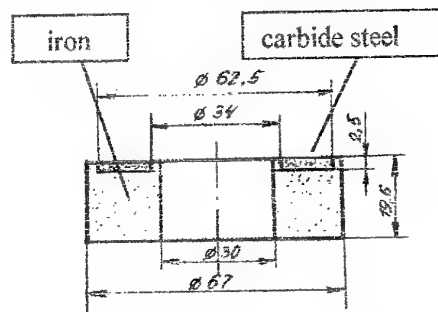
⁽²⁾ Technological Enterprise "Tool", Krasnodar, Russia

Wear resistant composite structural materials are intended to supply reliable and durable work of friction units of modern machines, mechanisms, devices in conditions of significant loadings and speeds, at high and low temperatures, at limited greasing or in general at its absence, in vacuum, aggressive gas and liquid environments. The basic principle of maintenance of high wear resistance of a material is creation of its heterogeneous structure. The artificial introduction of hard (firm) inclusions into strong elastic-plastic matrix from a metal powder is one of the methods of the creation of such structure. Classical example is material ПС5 with hard glass particles which are inserted into the ferrous matrix by mixing of iron, graphite (2,5 %) and glass (5...10 %). After heat treatment of the material the glass particles have hardness 8...12,0 GPa and sizes 20...60 microns with hardness 5...6 GPa of metallic matrix. The mechanical properties of dense metal-glass materials are determined by durability of a matrix (at the smaller glass contents the strength is higher), and tribotechnical characteristics (wear intensity, friction coefficient) have the optimum values if the volume contents of a glass is 12...25 % [1].

The crushing of structure promotes reduction of distance between dislocation barriers and consequently increase exploitation characteristics of materials. So, for a metal-glass material on a basis of carbonil iron increase of wear resistance and essential increase of the durability and plasticity characteristics (strength on break on ~30 %, on a bend - on ~70 %, shock viscosity - in 2,5 ... 4 times) is observed simultaneously.

Metal-glass materials are used for manufacturing of the loaded parts of friction units (gear wheels, cams, condense rings, details of weaver's machines, agricultural machine-building products). The material ПС5, was obtained by hot pressing in shells used for manufacturing of gears of "lunohod" running sites. Hot forging condense rings was produced for basic rollers of caterpillar tractors.

At development of new wear resistance material technologies and products the idea greatest possible (from the technological and economic points of view) crushing of initial



powders is realized. Carbide steels of the marks KCT-1 (P6M5K5-KT20), KCT-2 (6X6B3MΦC-KT20), KCT-3 (P6M5K6-KHT20), KCT-4 (6X6B3MΦC-KHT20) are produced by hot isostatic pressing and subsequent deformation processing (rolling, forging). Tool steel is served as matrix of wear resistance material, and the role of hard inclusions allocated in regular intervals is carried out by TiC or TiNC particles (30 % on volume). Initial size of particles of used powders is no more then 20 microns. After heat treatment materials have hardness HRA85...89 and are used for cutting and deforming tool, for stamp and another wear resistant tool or parts of friction units [2].

At enterprise Inter-Kontakt-Prior Ltd the hot forging technology is developed for a bmetal product serving as a support of the chisel tool (fig.).

The working part of a product is made of carbide steel KCT-1, case is executed from an iron powder (with 1%C). Mixture P6M5K5+20%TiC is ground in an attritor up to average particle size of 1...1,2 microns. contains A thin layer of a nice powder 1 is there between layers of iron and carbide steel. It's necessary for reliable merging of layers at termomechanical tratement. The detail is forged from temperature 1200 °C up to a dense status. After heat treatment the carbide steel layer gets hardness HRC 60...62. At operating conditions wear resistance of the

working carbide steel layer is not below wear resistance of tungsten which was used for working layer earlier.

Literature

1. Порошковая металлургия. Материалы, технология, свойства, области применения: Справочник / Отв. ред. И.М.Федорченко-Киев: Наук. Думка, 1985. – 624 с.

2. Карбидосталь «Д» - деформированный композиционный материал для режущего и износостойкого инструмента / Ю.Ф.Бокий, В.Т.Зубкова, А.Ф.Прохоров и др. // Запорожье: РИО «Издатель», 1991. – 3 с.

NONCARBON NANOTUBES AND THEIR 2D CRYSTALS. REVIEW

Pokropivny V. V.

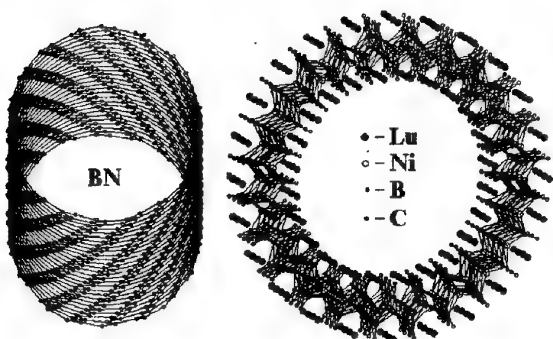
Institute for Problems of Materials Science of NAS of Ukraine, Kiev, Ukraine

Recent progress is shortly reviewed in the research of noncarbon (inorganic) nanotubes (N-NTs) on base of the boron carbonitride $B_xC_yN_z$, boron nitride BN, and sulphides WS_2 , MoS_2 , selenides $NbSe_2$, khalogenides $NiCl_2$, oxides SiO_2 , TiO_2 , V_2O_5 of transition metal, et al., synthesized by arc discharge, laser ablation, chemical reactions, electron irradiation, incapsulation, and membrane-templating methods. Their atomic and electronic structure, the thermodynamic, elastic, vibrative, optic properties are considered shortly in couple with numerous promising applications [1].

Any layered compounds with weak interlayer interaction are possible to be rolled up into nanotubes [1,2]. This given an impetus in a prediction, synthesis and study of large class of noncarbon NTs, such as: 1) mixed NTs, such as $C_xB_yN_z$, C_2BN , C_3B , C_3N_4 ; 2) carbon NTs, intercalated by metals, carbides B_4C , chlorides $FeCl_3$, and other compounds; NTs on base of: 3) boron nitride (BN-NTs) [2]; 4) dichalcogenides of transition metals MeX_2 , where $Me=Mo$, W , Nb ; $X= S$, Se , Te ; 5) khal-cogenides, for example $GaSe$; 6) oxides MoO_3 , SiO_2 , Al_2O_3 , V_2O_5 , TiO_2 ; 7) khalogenides $NiCl_2$; Layers of BC_2N , BN , MoS_2 , $NbSe_2$, $PbSe$, C_3N_4 , $GaSe$, MoO_3 , LaB_2C_2 , etc., offer as building units of N-NTs.

Nanotubes, fullerenes and onions one can consider as new kinds of layered ultrafine particles, which attached much attention of material scientists long time ago. Decrease of dimensionality under wrapping of two-dimensional (2D) layers into 1D nanotubes offers the other reason (ex-cept dimension) of structural phase transition $2D \rightarrow 1D$ and their exeptional properties too.

Atomic structure of chiral BN-NT and $LuNiBC$ -NT is shown for example in figure.



Noncarbon NTs as well as C-NTs are unique quantum objects, the solenoids and quantum nanocoils of which can be used as inductors, magnetic storage, etc.

BN-NTs are semiconductors with a constant band gap. In contrast to C-NTs the gap and electron structure of BN-NTs are governed by a chemistry, rather then its diameter and chirality. Conductive band resemble a band of near free electrons, resulting an electron conducting gas to be confined inside walls of NTs.

High stiffness and axial strength of BN-NTs in couple with sharpness of tip closed by cup, give a base to use this NTs as probe in atomic force and other probe microscopy.

Nanotubes of dichalcogenide $2H-WS_2$ type are shown to be as effective nanolubricants, because they rotate rather then slide during friction, acting as nanobearings, that make them indispensable in the units of forthcoming microelectromechanical systems (MEMS) and nanodevices.

Boron nitride NTs were suggested to serve in kinds of piezoelectric transducers and hypersound generators. Also 2D supercrystals of vibrating NTs were predicted to be used as gain media for phonons generation.

For development of unique nanomaterials and nanodevices the 2D nano-crystals of N-NTs rather then single NT are required. Therefore, a frontier of fullerene science is moved now in the research of quasi 1D arrays, ropes, bundles, and 2D crystals of NTs.

Materials science aspects for synthesis of 2D nanocomposites, photonic crystals and nanomembranes, built from the nanotubes was reviewed in couple with their physical properties and promising applications [3].

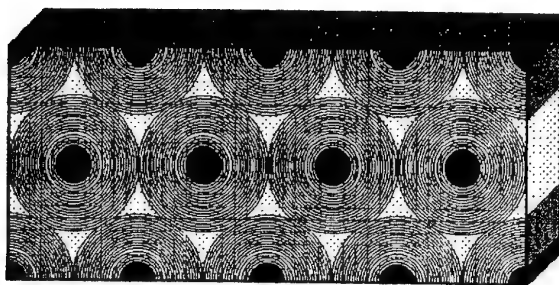
Electrochemical template synthesis is widely used for preparation of highly-ordered 2D crystals of parallel-NTs on base of metal and semiconductor compounds by CVD or PVD technique within both the inner walls of membrane nanochannels or outer walls of brush-like arrays of nanorods. This technique is compatible with standard lithographic processes and thus enables future integration of such nanotube 2D arrays with silicon ultra low scale integrated circuits (ULSI)..

II. PERSPECTIVE MATERIALS OF FUNCTIONAL AND STRUCTURAL PURPOSES: POSSIBILITIES OF OBTAINING NEW LEVEL OF PROPERTIES

expected to reveal exclusive optical properties that opens ways for novel promising applications as waveguides, birefringent lenses and prisms, switches, gain media for micro-lasers, superconductors and other devices from microwave to ultraviolet range. Small size of N-NTs makes possible to extend abilities of photonic crystals in lasing, operating and guiding of electro-magnetic waves.

Luminescence properties, small radius of tip, high melt temperature and alignment level of 2D lattices built from N-NTs make them attractive in kinds of emitters for extremely high resolution displays.

2D nanocomposite of superconducting NTs (MgB_2 , NbSe_2 -NTs, etc.) was predicted to be a record room T_c superconductor [4].



Capacity for a storage of hydrogen and other gases in N-NTs is expected to have advantage over the C-NTs. For example, formation of boranes B_nH_n inside and outside the BN-NTs, or TiH_2 inside Ti-encapsulated BN-NTs is helpful for using them as membrane materials for batteries and fuel cells, capacitors and chemical filters.

Noncarbon NTs are anticipated to have great potential as chemical reagents and catalysts. For example, the TiO_2 NTs are expected to be used in the preparation of catalysts, adsorbents, and deodorants with high activities, because their specific area is greatly increased.

Coaxial complex $\text{SiC-SiO}_2\text{-BN-C}$ nanocables promises great potential as a semiconductor - insulator - semiconductor/ metal heterojunction.

Many other layered compounds are forecasted to be wrapped in nanotubes, namely: 1) Layered compounds, built from 4-, 6-, 8-, 10-, 12- rings, such as (4,8) BN-rings and hole C_3N_4 rings. 2) Intercalated chalcogenides like a $\text{MeX}_2\text{-(pyridine)}_{1/2}$, PbSe/ NbS_2 , forming multilayered coaxial heterostructures. 3) Rare-earth and actinide borocarbides such as YB_2C_2 , LuNiBC , ThB_2C . 4) Pirovskites - oxides, chalcogenides, sulphides of $\text{A}^m\text{B}^n\text{X}_p$ ($m+n=-3p$) general formula, where A and B are the metal

atoms, $\text{X} = \text{F}, \text{Cl}, \text{Br}, \text{O}^{2-}, \text{S}^{2-}$. 5) Minerals such as khrisotile and galuassite, formed natural microtubes. 6) Two-dimensional Zr and Ti phosphates of $\text{Zr}(\text{HPO}_4)_2\text{H}_2\text{O}$ type, uranyl-phosphates of $\text{Me}(\text{UO}_2\text{PO}_4)_n\text{H}_2\text{O}$ type, vanadyl-phosphate $\alpha\text{-VOPO}_4$, and their intercalators. 7) Noncarbon compounds with tetrahedral anions of glazerite $\text{K}_3\text{R}(\text{EO}_4)_2$ type, where R is rare-earth element, $\text{E} = \text{As}, \text{V}, \text{P}$ and of palmerite type (arsenates, vanadates, phosphates of $\text{Me}_3(\text{EO}_4)_2$ general formula, where $\text{Me} = \text{Sr}, \text{Ba}$, molybdates $\text{Me}_3\text{R}(\text{MoO}_4)_4$, where $\text{Me} = \text{Rb}, \text{K}$, and many others. Here one can relate thin polymeric covers on channels of mesoporous materials and nanotubular ropes. Hence theoretically the variety of N-NTs is very vast.

In contrast to C-NTs, the non-carbon layers may be wrapped not only in nanotubes, but in another spiral forms, for example, MoS_2 microribbons, SiO_2 helicoids, Cr_2GaN whiskers, and other kinds until unknown.

One can conclude that investigation of noncarbon NTs lies in a starting point, because a majority of theoretically possible N-NTs was not synthesized yet. In the course of time the C-NTs would be considered as model objects, because the properties of complex N-NTs are more multifarious. Another ones, such as piezoelectric properties are absent for C-NTs in general. Many of nanodevices, developed on base of C-NTs, such as field transistors, emitters, nanomanipulators, nanogears, etc., appear to be realized more successful on base of N-NTs, rather than C-NTs.

Synthesis, investigation and application of novel noncarbon nanotubes and their 2D materials appear to be the main direction in development of materials science and nanotechnology of near future.

1. Pokropivny VV. Noncarbon nanotubes. Review. // Powder Metallurgy.-I. Synthesis methods. N9/10 (2001); II. Kinds and structure. N11/12 (2001); III. Properties and applications N3/4 (2002).
2. Pokropivny VV, Skorokhod VV, Kurdyumov AV, Olcinik GS, Bartnitskaya TS, et al. Boron nitride analogues of fullerenes (fulborenes), nanotubes, and fullerites (fulborenites). J.Solid State Chemistry. 154; 214-222 (2000);
3. Pokropivny VV. Two-dimensional nanocomposites. Review. // Powder Metallurgy.-I. Structure and synthesis. N5/6 (2002); II. Properties and applications N7/8 (2002).
4. Pokropivny V.V. Composite on base of 2D nanotubular lattice as ideal high- T_c superconductor// Physica C.-351, N4.-P.71-77 (2001).

FERRITIC STEEL INTERCONNECT FOR REDUCED TEMPERATURE SOFC

Shemet V., Pirón Abellán J., Singheiser L., Quadakkers W.J.

Institute for Materials and Processes in Energy Systems, Forschungszentrum Jülich, D-52425
Germany

Metallic materials for be used as interconnects in SOFCs should fulfil a number of specific requirements. Crucial properties of the materials are high oxidation resistance in both air and anode environment, low electrical resistance of the oxide scales formed on the alloy surface as well as good compatibility with the contact materials. Additionally, the value of the coefficient of thermal expansion (CTE) should match with those of the other cell components. These requirements can potentially be achieved with high chromium ferritic steels, however, previous studies have shown that none of the commercially available ferritic steels seems to possess the suitable combination of properties required for long term reliable cell performance.

One of the most important problems found during stack operation using metallic interconnect materials is the formation of volatile chromium oxides and/or oxy-hydroxides at the cathode side of the cell leading to serious deterioration of the cell performance. Several authors proposed various protective coating types to prevent the deleterious effect of volatile Cr-species.

Recently, a new class of FeCrMn(Ti/La) ferritic steels, see Table 1, has been developed to be used as construction materials for SOFC interconnects. In the present study, the long term oxidation resistance of some of these FeCrMn(Ti/La) steels in both air and simulated anode gas has been studied and compared with the behaviour of a number of commercially available ferritic steels. Main emphasis was put on the growth and adherence of the oxide scales formed during exposure, their contact resistance at service temperature as well as their interaction with various perovskite type contact materials.

Table 1. Studied model and semi-commercial FeCrMn(Ti/La) alloys

Steels design	Major features
JS-1	high Mn, Ti, La
JS-2	high Mn, low Ti, La
JS-3	low Mn, Ti, La

The model ferritic Cr steels with variation in Mn, Ti and La content were manufactured by Krupp/Thyssen NIROSTA (KTN). The main features of the various studied alloy types are given in Table 1.

Fig. 1 shows the oxidation behaviour under cyclic oxidation conditions for several FeCrMn model alloys with and without Ti and La additions compared with the behaviour of some of the most promising commercial ferritic steels. The JS-1 alloy and the commercial alloy ZGM232 show the highest weight changes mainly due to the extensive internal oxides formed beneath the scale. The other studied alloys show similar oxide scale growth rates because either no internal oxides are present at all or they appear in form of very fine internal precipitates. Both commercial alloys 1.4509 and 446, exhibit substantial scale spallation during the oxidation test but the chromium concentration is still sufficiently high to re-form the chromia based scale.

Fig. 2 shows the oxidation behaviour of JS-1 and JS-3 alloys oxidized in both air and simulated anode gas. A general tendency is that the oxide scales formed in anode gas are slightly thinner than those formed on air. As has previously been reported for Cr-based alloys, for all studied alloys the scales formed in the anode gas generally possess better adherence than those formed in air or oxygen.

Fig. 3 shows the instantaneous K_p -values at 50h determined during isothermal oxidation in air for a number of FeCrMn alloys with and without Ti and La additions and compared with a number of other SOFC relevant alloys as function of the reciprocal temperature. The addition of Ti to the FeCrY alloy leads to a substantial increase in the oxidation rate. The enhancement increases with increasing Ti content, in agreement with previous findings related to the behaviour of NiCr-based alloys in steam reforming gas. Comparing the alloys FeCrMn and JS-1 it is clear that in the entire range of temperatures studied, only minor changes in the Mn, La and Ti contents can

substantially affect the oxidation rate. Based on these findings, suitable oxidation resistance of the ferritic steels requires adequate addition and careful control of these elements in the alloy. By optimum additions of the oxygen active elements, oxidation rates can be achieved which are similar to those of the chromium based ODS alloy $\text{Cr5Fe1Y}_2\text{O}_3$, which has frequently been proposed as interconnect material for high temperature SOFC's.

The electrical resistances of the oxides scales formed on different FeCrMn(Ti/La) alloys during 500h exposure at 800°C are shown in Figure 4. The results are compared with data obtained for a number of commercial alloys, i.e., 1.4742 (X10CrAl 18), 1.4509 (X2CrTiNb 18), alloy 446 and alloy ZGM232. The values obtained for alloys 1.4509, 446 and ZGM232 show a very wide scatter range, although on all three materials, the oxide formed mainly consists of a duplex $\text{MnCr}_2\text{O}_4/\text{Cr}_2\text{O}_3$ scale. The highest values of approximately $20 \Omega\text{cm}^2$ were obtained for the commercial alloy 1.4742 which has in some cases been considered as a potential candidate to be used as interconnect in intermediate temperature SOFCs. These high values can be explained by the fact that this alloy, depending on the exact alloy composition and surface treatment, in some cases tends to form a very protective alumina scale, which, however, possesses a very poor electrical conductivity. In contrast, the new JS-3 alloys show very low contact resistance values of approximately $10 \text{ m}\Omega\text{cm}^2$, i.e., values which are two to three orders of magnitude smaller than that of the commercial alloy 1.4742.

Conclusions

Commercial high Cr ferritic steels as interconnect material have large drawbacks because the materials tend to exhibit scale spallation during long term oxidation, especially under cyclic oxidation conditions. Besides, the formed oxide scales frequently exhibit high electrical resistances. These effects are mainly related to a poor control of the oxygen active minor alloy constituents. For these reasons, new alloys of type FeCrMn(Ti/La) were developed to be used as interconnect materials for SOFCs. These alloys form oxide layers with low growth rates being constituted by a duplex $\text{MnCr}_2\text{O}_4/\text{Cr}_2\text{O}_3$ scale. The formation of the external spinel layer considerably reduces the chromium evaporation. Also, it has been demonstrated that this type of scale has a

low contact resistance, i.e., almost three orders of magnitude lower than that of alumina-rich scales frequently formed on commercial ferritic steels.

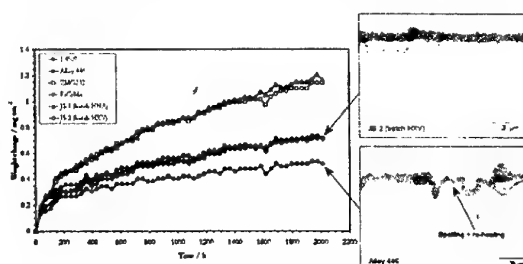


Fig. 1. Oxidation behaviour of commercial and model ferritic steels at 800°C in air.

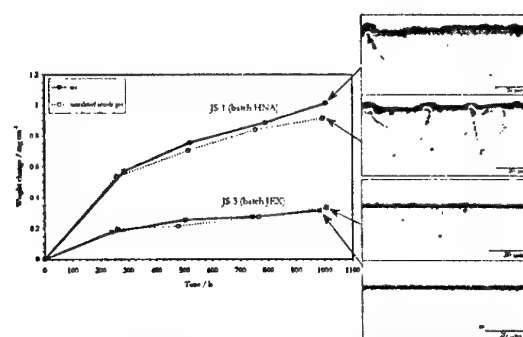


Fig. 2. Oxidation behaviour of selected model ferritic steels at 800°C in $\text{Ar}/4\%\text{H}_2\text{-}2\%\text{H}_2\text{O}$

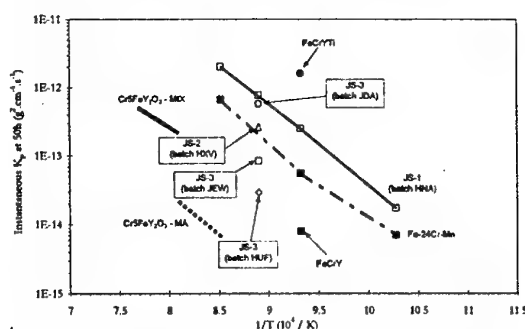


Fig. 3. Instantaneous K_p values as function of temperature during isothermal oxidation in air

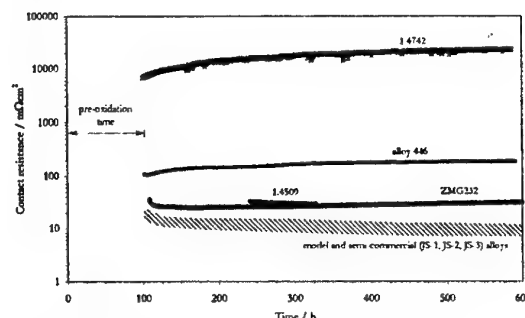


Fig. 4. Contact resistance of commercial ferritic steels and model alloys at 800°C in air.

ANALYSIS STRESS-STRAIN STATE OF DIAMOND-SiC COMPOSITE MATERIAL

Grygoryev O. M., Stepanenko A. V., Bega M. D.

Frantsevich Institute for Problems of Materials Science, NAS of Ukraine, Kyiv

Operation and strength properties of the diamond based composites on to a great extend are determined by their stress-strain state.

The present research is devoted to the analysis of the internal stress in composites diamond-Silicon carbide which arises due to differences in thermoelastic properties of components.

Samples of composite were produced by infiltration of liquid silicon into diamond powders compacts at high pressure and temperature. The grain size of powders was varied from 80/63 to 10/7 μm

Theoretical analysis of residual stresses was carried out by using the statistical theory [1]. The experimental investigation was fulfilled by XRD-methods. Shifts and broadening of diffraction curves of diamond and SiC were measured as respects of corresponding lines of the Si-powder etalon. Stressed state of composite was studied by the shifts and widths of the diffraction curves in accordance with article [2].

Volume concentration SiC was defined by means of determination intensity of lines phases in the specimens with using factor reference intensity ratio (RIR), which were found by theoretical calculation for equivolumetrical composition mixture.

As the thickness of reflecting layer is much more of the size grains any of the phases (0.5 μm in SiC and 60 μm in diamond) than the volumetric stress state was researched. The components of principal stresses versus composite composition are determined. For measurements were used line (331) in diamond and (333)-(511) in SiC.

Calculation of microstresses in composite was performed by the approximation method using approach of Reuss. Satisfactory fit of calculation and experimental values of residual stresses into phases was found

As a result of theoretical and experimental investigation was established:

1) Mismatch of elastic and thermal characteristics of investigated phases results in inverse of sign of internal stresses when the pressure of sintering is increased ($P_s^{\text{inv}} \sim 2 \text{ GPa}$) – Figure 1;

2) For specimens were obtained at the real conditions of production the level of the residual stresses is high (Figure 2) and tensile stresses in diamond and compressive stresses in SiC reach 0.5 GPa and 2.3 GPa respectively if $C_{\text{SiC}}=15 \text{ vol. \%}$.

3) The increase of grain size of diamond powder from 10/7 to 80/63 μm and an additional use of small fractions has resulted in reduction of contents of SiC in composite from 20 vol. % to 11 vol. %; reduction of tensile stresses in diamond from 0.7 GPa to 0.35 GPa and increase compressive stresses into SiC from 2.5 GPa to 2.8 GPa.

Changing of microstresses in diamond is proportionally to changing of pseudomacro stresses, that is microstresses in diamond we may interpret as dispersion of pseudomacro stresses.

But, the structure of SiC is characterized some significant distinction. The lattice period of created β -SiC ($a=0.4356 \text{ nm}$) is less than period of standard β -SiC (Figure 3). Microstresses into SiC is much larger in comparison with diamond and don't depend on pseudomacro stress level and substantially were defined his faulty conditions.

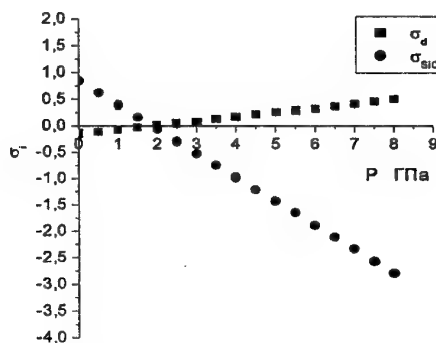


Figure 1. Residual stresses in phase of composite as function of the sintering pressure.

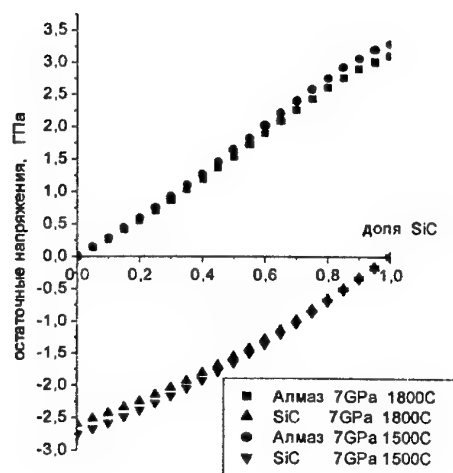


Figure 2. Residual stresses in phase of composite as function of content of SiC.

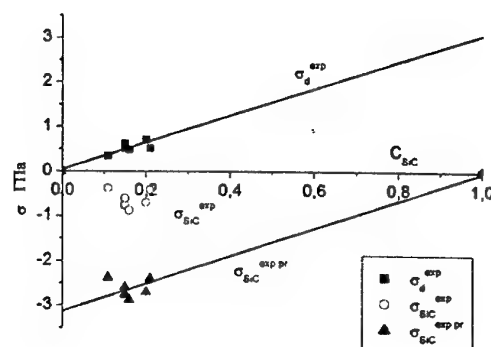


Figure 3. Pseudomacro stresses in composite as function of content of SiC.

1. Григорьев О. Н., Трефилов В. И., Хорошун Л. П. Остаточные напряжения в двухфазных керамических материалах // Материалы III Всесоюзного симпозиума "Технологические остаточные напряжения". - Москва: Из-во АН СССР. -1988. - С. 129-133.

2. Григорьев О. Н., Кривошей Г. С., Перепелица Н. И., Хорошун Л. П. Внутренние напряжения в квазибинарных композитах на основе Si_3N_4 // Заводская лаборатория. - 1992. - № 10. - С. 37-39.

HIGHLY TEXTURED POLYCRYSTALS OF DIAMOND-LIKE PHASES OF BN

Britun V.F., Kurdyumov A.V., Petrusha I.A.⁽¹⁾

Frantsevich Institute for Problems of Materials Science, National Ukrainian Academy of Sciences,
Kiev, Ukraine

⁽¹⁾ Bacul Institute of Superhard Materials, National Ukrainian Academy of Sciences, Kiev, Ukraine

Highly textured polycrystals of diamond-like (HTP-DL) boron nitride phases (wurtzitic - wBN and cubic - cBN) are of interest as the basis for new superhard materials engineering. Such interest is caused by HTP-DL properties some of which are close to those of cBN monocrystals and some - may exceed of monocrystal properties (for example hardness, toughness, resistance to wear). The advantage of HTP-DL is determined also by the fact that they could be more easily obtained as compared to cBN monocrystals. In this connection we must also note that the growing of wBN monocrystals is impossible in principle because wBN is a metastable phase and transforms into cBN under heating. At the same time the method of HTP-DL samples making with sizes of the order of 1 cm has been already developed. This method is based on the crystal-oriented transformations of graphite-like phases into diamond-like ones in highly textured CVD materials [1].

In the present work we discuss the features of HTP-DL obtaining and its texture characteristics. Two types of HTP-DL are compared: one based on rhombohedral and another on hexagonal graphite-like BN modifications. The highly textured plates of rBN were used as starting samples. The texture investigations were performed by means of x-ray diffractometry and x-ray transmission texture photography method described in [2]. The unlimited axial texture with the [001] axis is characteristic to starting CVD-BN (the (001) basal planes of graphite-like BN were oriented mainly parallel to the surface of CVD plates). The texture scattering angle ($\Delta\rho/2$) was near $\pm 3^\circ$. The rBN phase was used both for realization of series of crystal-oriented transformations rBN-wBN-cBN, and hBN modification obtaining. The rBN - hBN transformation was carried out in high pressure apparatus at $p=3\text{ GPa}$ (to prevent BN decomposition) and $T > 2500\text{ K}$. The data of x-ray diffraction show that thermal treatment of rBN leads to its full transformation to hBN. The hBN inherited rBN texture and grain sizes. This phenomenon may be explained by crystal-oriented transformation that developed as diffusion

rearrangement of (001) layers without nucleation and growth of new grains. But such mechanism of transformation causes the polytype stacking faults formation. At the same time the concentration of turbostratic stacking faults in hBN was very low, and this was an important condition for coherent diffusionless transition of hBN into dense phases.

The HTP-DL samples were obtained by hBN or rBN compression in toroid-type apparatus at $p=7,7\text{ GPa}$. The HTP-DL texture evolution was investigated in temperature range from 300 up to 2800 K.

Phase transformation of rBN into dense phases is developed by buckling mechanism and leads to wBN formation if $T < 1500\text{ K}$. The following orientation relationships $(001)w//[101]r$ and $[210]w//[212]r$ are formed. These relationships are confirmed not only by transmission electron microscopy but also by x-ray texture photography. The HTP-DLs based on cBN are formed at $T > 2000\text{ K}$ by coherent wBN - cBN transition, and this leads to the orientation relationships between dense phases : $(111)s//[001]w$ and $[112]s//[210]w$. The x-ray texture photographs of HTP-DL samples obtained from rBN are shown in Fig.1.

The local recrystallization of cBN and destruction of texture was fixed in some samples at $T > 2300\text{ K}$. However detailed study of these HTPs showed that grain growth is connected with impurity diffusion to the BN specimen from the walls of high pressure apparatus. If the special shield is used the recrystallization does not begin up to 2800 K.

The main peculiarities of rBN-based HTP-DL structure is the triple texture formation in every monocrystal grain. Such texture begins to form as a result of rBN twinning before transformation occurs. Formation of substructure with high density of twins is accompanied by (101) planes rotation to the position normal to CVD plate surface. During the development of phase transformations rBN - wBN - cBN, the rBN planes transform into (001) wBN and {111} cBN planes so these planes of dense phases are oriented normally to the surface of HTP-DL plates. The grain structure of dense phases

is characterized by submicron sizes resulted from diffusionless character of phase transformations.

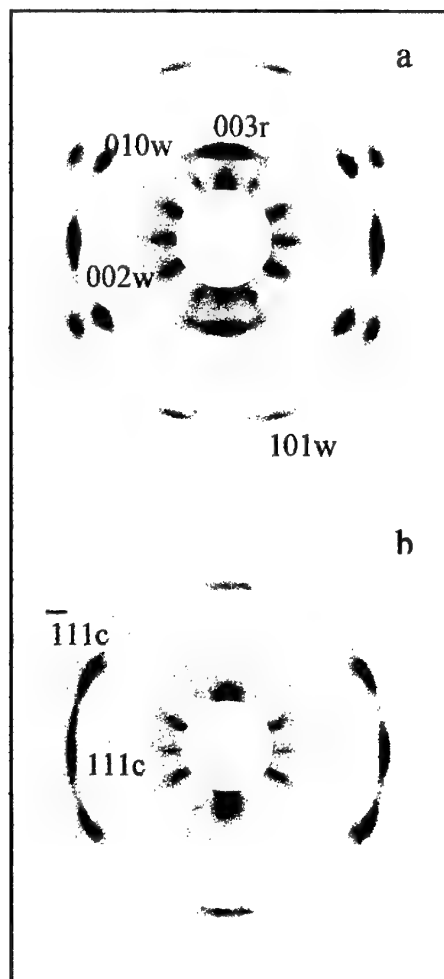


Fig.1 The x-ray texture photographs of HTP-DL obtained from rBN: wBN (a) and cBN (b).

In the case of hBN used as initial modification, the transformation mechanism is puckering. At the first stage the hBN transforms into wBN with orientation relationships $(001)w // (001)h$ and $[210]w // [210]h$. The main structure feature of wBN formed from CVD hBN was the high concentration of intrinsic type stacking faults. Such faults are inherited from hBN structure and accelerate the wBN - cBN transformation. Therefore it is difficult to obtain HTP with pure wBN structure from hBN. In both mechanisms of transformations the stage wBN - cBN is realized at $T > 1500$ K with identical orientation relationships.

We must note also that transformations by buckling mechanism occur at lower temperatures than transformations by puckering mechanism. For example: rBN - wBN transformation at 1500 K leads to almost 100% amount of dense phase, whereas hBN - wBN transition at the same p,T conditions leads to amount of dense phases not more than 10%.

The triple texture does not form during hBN transition, so this scheme of HTP obtaining can lead to more perfect texture. But texture scattering angle of HTP dense phases strongly depends on the scattering of initial CVD BN texture. The texture photograph of cBN phases (in mixture with hBN) formed on puckering mechanism is shown in Fig. 2. The main feature of this type texture is the orientation of $(001)w$ and $(111)c$ planes parallel to surface of initial CVD BN plate. So, the orientations of $(001)w$ and $(111)c$ planes in HTP-DLs formed by different mechanisms differ in rotation by 90° . This difference must lead to difference in HTP-DL properties.

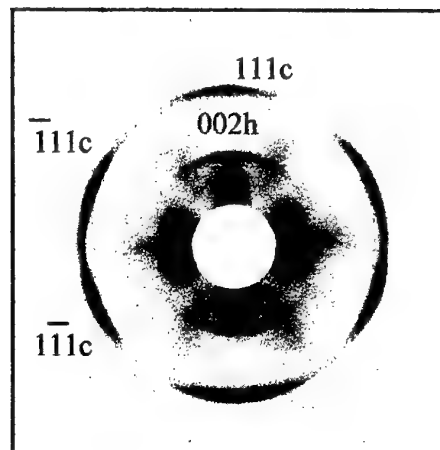


Fig.2 The x-ray texture photograph of HTP-DL obtained from hBN.

References

1. V.F.Britun, A.V.Kurdyumov, I.A.Petrusha. // Superhard materials, 2000, №2, p.3-7
2. V.F.Britun, A.V.Kurdyumov, V.B.Zelyavskii and I.A.Petrusha. // ibid. 2001, №4, p.7-14.

THE STRUCTURE AND PROPERTIES OF A HARD ALLOY COATING DEPOSITED BY HIGH-VELOCITY PULSED PLASMA JET ONTO A COPPER SUBSTRATE

Tyurin Yu.N., Pogrebnyak A.D.⁽¹⁾, Zadkevich M.L., Kolisnichenko O.V.

Paton Institute of Electric Welding, Kiev, Ukraine

⁽¹⁾Institute of Surface Modification, Sumy, Ukraine

Using a plasmatron operating in specially calculated regimes, tungsten carbide (WC) based coatings were deposited onto a copper crystallizer plate. It was found that a local hardness of the WC-Co coating may reach up to 1.3×10^4 N/mm² and the coating adhesion to substrate may be as high as 270 MPa. The elemental and phase compositions of coatings were studied by Rutherford backscattering spectroscopy, X-ray diffraction, and transmission electron microscopy with electron diffraction.

The surface morphology and depth-composition profiles of the coatings were studied by optical and scanning electron microscopy. The coating is composed of WC crystal grains with hexagonal close packed (hcp) lattice, α - and β -Co grains, and cubic WC grains. The average size of the hcp WC grains is 0.15 μ m and that of the cobalt particles is about 25 nm. In addition, the grain boundaries contain W₃Co₃C particles with an average size of 15 nm.

Pulsed beams of charged particles and plasmas have been extensively used for the surface modification of various materials since the beginning of 1980s [1-4]. The action of such concentrated energy fluxes upon a solid sample leads to a high-rate ($10^{-3} - 10^{-8}$ s) heating of the surface layer followed by its rapid quenching with a fast heat removal in depth of the processed target. As a result, the target material exhibits significant structural and phase transformations, including the formation of metastable phases, dispersed nanoinclusions, amorphous layers, and high densities of dislocations and nonequilibrium point defects frequently accompanied by the ion-beam-induced mixing [1,2]. Pulsed energy fluxes are also employed for depositing thin films, applying coatings, and obtaining dispersed nanoparticle powders [2]. In particular, by introducing a WC-Co powder (VK-12 grade) into a pulsed high-velocity plasma jet, one may obtain a coating of this composition with good adhesion to a copper crystallizer plate (solving this task is important for the molding technology).

The sample coatings were prepared using a pulsed plasmatron supplied with a VK-12 powder

with an average particle size of 35-56 μ m. Using preliminary mathematical modeling and variation of the plasmatron parameters, nozzle geometry, the distance from the nozzle to substrate surface, and the reaction chamber dimensions, we determined optimum values of the pulsed plasma jet velocity, plasma temperature, and optimum nozzle to substrate spacing.

These parameters were as follows: jet plasma temperature, 2.4×10^4 K; jet velocity, ~ 7 km/s; jet power density, up to 10^7 W/cm²; nozzle to substrate spacing, 30 mm. The gas mixture components and powdered material were supplied to the plasmatron in a continuous regime. The jet pulse duration was 0.3 ms.

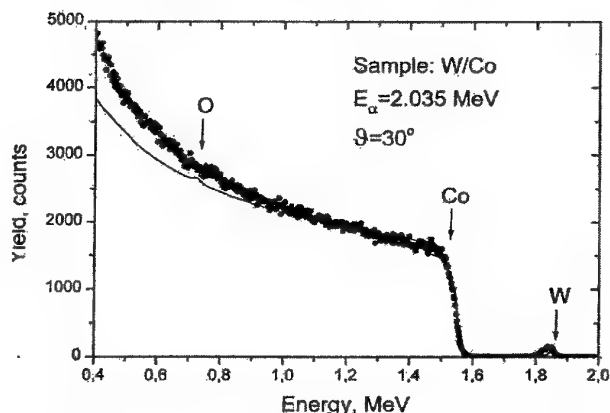


Fig. 1. RBS He⁴⁺ spectrum of a WC-Co coating on a copper crystallizer surface.

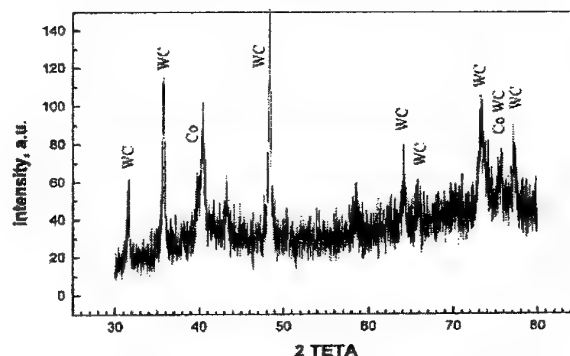


Fig. 2. X-ray diffractogram (CuK α radiation; Sunya, Japan) of a WC-Co coating deposited by a pulsed plasma jet onto a copper crystallizer surface.

Figure 1 shows the Rutherford backscattering (RBS) spectrum of He^+ ions for a tungsten carbide-cobalt coating. As is seen, the spectrum displays the peaks of tungsten and oxygen and a kinematic threshold of Co. The relative content of Co, W, C, and O in the surface layer with a thickness of 2.8 μm corresponded to the following composition: WC_{89} ; Co_8 ; C_2 ; O_2 .



Fig. 3. Micrograph of the transverse cross section of a WC-Co coating on a copper substrate with indenter pyramid marks: (1) in the middle of the coating; (2) near the film-substrate interface; (3) at the film-substrate interface.

Note that the concentration of tungsten on the film surface was very small (~ 1 at. %), while the carbon concentration reached 30 at. %. As is known [7,8], the tungsten carbide films deposited by the HVOE and HEP techniques are characterized by the tungsten content increased up to 84.38 and 87.98%, respectively. This may even be accompanied by the partial amorphization of complex phases at the carbide and cobalt grains [8]. The cobalt content also changed to reach 12.98% (HVOE) and 9.22% (HEP), while the carbon concentration decreased from 4.09% in the initial powder to 2.5% (HVOE) and 2.52% (HEP). In our case, the coating contained phases which were mostly present in the initial powder, although some other phases formed in the course of rapid quenching appeared as well.

The X-ray diffraction analysis performed on a DRON-3 diffractometer using K_α -Cu radiation showed that the main phase in the coating was WC with an hcp lattice. The presence of other phases was evidenced by reflections in the 37° - 47° angular interval (Fig. 2). Unfortunately, the diffraction peaks observed in this interval exhibited overlap, hindering the identification of phases. The interplanar spacings calculated for the reflections that could be resolved suggested the presence of the following phases: W_2C , Co_7W_6 , Co_3W , W, and Co. Complex phases occurring in the intergranular regions may be amorphous, in agreement with

[8,9]. This state is explained by a high-temperature cycle involved in the coating formation.

Additional analysis of the sample structure and phase composition was performed with the aid of the transmission electron microscopy with electron diffraction. According to these data, the coating has a poly-crystalline structure including grains of the hcp WC phase and the cubic α -Co, β -Co, and WC phases. The average size of the hcp WC grains is 0.15 μm and that of the cobalt particles is about 25 nm. In addition, the grain boundaries contain $\text{W}_3\text{Co}_3\text{C}$ particles with an average size of 15 nm. A dislocation substructure was observed inside the cubic WC grains.

Figure 3 shows a micrograph of the transverse cross section of a WC-Co coating with prints of a diamond indenter pyramid used for the microhardness measurements (scale: 1 cm \sim 200 μm). As is seen from this image, the coating contains local regions possessing significantly different microhardnesses (ranging from 8×10^3 to 1.3×10^4 N/mm 2). The adhesion of coating to substrate was determined for the films deposited onto M-00 grade copper plates. This characteristic, determined after about ten measurements of the groove made by a diamond pyramid scribing the sample surface, was calculated by the formula $H_u = 4P/b^2$ (here P is the load and b is the groove width). The results of these measurements showed that the adhesion is on the average 250 MPa (ranging from 210 to 280 N/mm 2).

REFERENCES

1. V. I. Boiko, A. N. Valyaev, and A. D. Pogrebnyak. *Usp. Fiz. Nauk* **169** (11), 1243 (1999).
2. A. N. Valyaev, Kishimoto Naoki, and A. D. Pogrebnyak. *Modification of Materials Properties and Synthesis of Thin Films under Irradiation by Intense Electron and Ion Beams* (Vostochno-Kazakhstanskii Tekhnicheskii Univ., Ust'-Kamenogorsk, 2000).
3. V. L. Yakushev, B. A. Kalin, and V. I. PoFskikh, *Metally*, No. 4, 74 (1994).
4. Yu. N. Tuyrin and A. D. Pogrebnyak. *Surf. Coat. Technol.* **III**, 269 (1999).
5. A. D. Pogrebnyak, Yu. N. Tyurin, Yu. F. Ivanov, et al., *Pis'ma Zh. Tekh. Fiz.* **26** (21), 53 (2000) [*Tech. Phys. Lett.* **26**, 960 (2000)].
6. *Surface Modification and Alloying by Laser, Ion and Electron Beams*, Ed. by J. M. Poate, G. Foti, and D. C. Jacobson (Plenum, New York, 1983; Mashinostroenie, Moscow, 1987).
7. J. Nerz, B. Kushner, and A. Rotolico, *J. Therm. Spray Technol.* **1** (2), 147 (1992).
8. C. J. Li, A. Ohmori, and J. Harada, *J. Therm. Spray Technol.* **5** (1), 69 (1996).
9. R. B. Bhagat, M. F. Amatean, A. Papyrin, et al., *ASM Thermal Spray Society*, 1997, pp. 361-376.

HYDROGEN-OXYGEN INTERPLAY IN HYDRIDES OF OXYGEN-STABILIZED Zr- AND Ti-BASED INTERMETALLIC COMPOUNDS

Zavaliy I.Yu.

Physico-Mechanical Institute, National Academy of Sciences of Ukraine,
5, Naukova Str., Lviv, 290601, Ukraine; zavaliy@ipm.lviv.ua

The presence of oxygen interstitial atoms even at low concentrations leads to the formation of new phases in *d*-metal systems. Such phases in Zr(Ti)-based systems of $A_3B_3O_x$ and $A_4B_2O_x$ stoichiometries with Ti_2Ni type of structure and A_3BO_x with Re_3B type demonstrated interesting peculiarities of hydrogen absorption/desorption properties on the dependence of oxygen content. A review of recent results on the hydrogenation properties and H-induced phase-structural transformations of these compounds will be presented in this report. The influence of hydrogen-oxygen interplay on gas and electrochemical hydrogen absorption-desorption properties will be discussed.

It has been shown, that the existence of oxygen-stabilized η -phase with Ti_2Ni type of structure in Zr-V alloys facilitates the activation process, accelerates the hydride formation and, in a number of cases, leads to higher hydrogenation capacity [1]. The formation of hydrides with the highest capacity can be reached by the decrease of oxygen content in the alloy down to $Zr_3V_3O_{0.6}$ composition. The single-phase η - $Zr_3V_3O_{0.6}D_{10.5}$ deuteride was synthesized and studied by X-ray and neutron diffraction [2]. The crystal structure of η -phase hydrides was analyzed to predict the hydrogenation capacity in dependence of oxygen content for a wide range of oxygen-containing compounds with Ti_2Ni structure type.

η - $Zr_4Fe_2O_{0.6}$ and η -(Zr,Hf) $_2$ Fe demonstrated the substantial difference between the hydrogenation capacity of oxygen-containing and oxygen-less compounds [3]. However, the increase of hydrogen storage capacity of η - $Zr_4Fe_2O_{0.25-0.6}$ was observed with the decrease in oxygen content, the maximum reached H/f.u.=9.8. Slight crystal structure transformation of η - $Zr_4Fe_2O_{0.25}$ saturated hydride in comparison with parent compound was identified [4]. The increase of metal matrix stability with the rise in O-content was observed in hydrogenation disproportionation route for $Zr_4Fe_2O_x$ alloys [5].

XRD studies of the annealed $(Zr,Ti)_4Ni_2O_{0.6}$ alloys demonstrated the presence of η -phase as a dominant in the whole range of substitution [6]. The presence of oxygen leads to the stabilization of η - $Zr_4Ni_2O_{0.6}$ compound instead of Zr_2Ni (CuAl $_2$ -type) as well as η - $ZrTiNiO_{0.3}$ instead of ZrTiNi C14 Laves phase. The hydrogen storage capacity was observed

to be 1.22-1.25 H/M for $(Zr_{1-x}Ti_x)_4Ni_2O_{0.3}$ alloys ($x=0.25-0.75$). Hydrogenation does not cause the crystal structure transformations of parent η -phase and the volume expansion ~15 % has been observed. Insertion of oxygen atoms in metal matrix of $(Ti_{1-x}Zr_x)_4Ni_2O_x$ results the increase of pressure on *p-c-T* plato. This accompanies by the decrease of hydrogen desorption temperatures and the increase of discharge capacity upon electrochemical cycling.

A_3B phases with Re_3B -type of structure in Zr-based systems can dissolve oxygen up to A_3BO stoichiometry (Zr_3Fe , Zr_3Co) or can be stabilized by oxygen, when the compound does not exist in the binary system (Zr_3NiO). The hydrogenation properties of oxygen-containing $Zr_3Fe(Co)O_x$ and oxygen-stabilized Zr_3NiO_x compounds were studied. In this report new results about the formation of Zr_3NiO_x hydrides ($x=0.4$; 0.6; 0.8; 1.0) will be analyzed. The insertion of oxygen atoms leads to the decrease of hydrogen storage capacity from $Zr_3NiO_{0.4}H_{6.5}$ up to $Zr_3NiOH_{5.3}$. On the contrary, the value of hydrogen induced lattice expansion increases with the increase of oxygen content from $\Delta V/at.H = 2.333 \text{ \AA}^3$ for $Zr_3NiO_{0.4}$ up to 3.047 \AA^3 for $Zr_3NiO_{1.0}$ [7]. For investigated compounds the influence of inserted oxygen on the hydrogen storage capacity is much lower in comparison with that for Ti_2Ni -type phases. Obtained crystallographic data demonstrated that the hydrogenation of both kinds of structures (Ti_2Ni - and Re_3B -type) is accompanied by redistribution of oxygen atoms. The features of hydrogen absorption-desorption properties of the studied compounds will be analyzed from their application point of view as hydrogen storage, getter or electrode materials for Ni-MH batteries.

- [1] I.Zavaliy. *J.Alloys and Comp.*, 291 (1999) 102-109.
- [2] I.Zavaliy, W.Yelon, P.Zavalij, *et al. J. Alloys and Comp.*, 209 (2000) 75-82.
- [3] I.Zavaliy, A.Riabov, V.Yartys, G.Wiesinger *et al. J. Alloys and Comp.*, 265 (1998) 6-14.
- [4] I.Zavaliy, V.Pecharsky, R.Cerny, G.Wiesinger *et al. J. Alloys and Comp.* Will be published.
- [5] I.Zavaliy, V.Yartys, O.Gutfleisch, I.R.Harris, Abstracts of ICHMS'2001, Crimea, Ukraine. P.334-337.
- [6] I.Zavaliy, G.Wojcik, G.Mlynarek *et al. J. Alloys and Comp.*, 314 (2001) 124-131.
- [7] I.Zavaliy, R.Cerny, I.Kova'chuk, I.V.Saldan. Abstracts of ICHMS'2001, Crimea, Ukraine. P64-67.

ADVANCE CERAMIC: SELF STRENGTHENING EUTECTIC REFRACTORY COMPOUND COMPOSITES, PRESENT AND FUTURE

Paderno Yu.B., Paderno V.N., Filippov V.B.

Frantsevich Institute for Problems of Material Sciences of NAS of Ukraine, Kiev, Ukraine

The nonoxigen metallike refractory compounds – borides, carbides, silicides etc are distinguished by very high melting temperatures (upto 4000°C), high hardness (upto 40-50 GPa), high strength, especially at high temperatures. But simultaneously they are very brittle. The main reason of such brittleness is their specific chemical nature – the big contribution of a rigid covalent bond [1].

These features from one side restrict the wide application of such kind of materials in constructions. From the other side they open the possibility to use them as reinforcement components different composite materials. Usually such materials consist from the relatively plastic matrix phase, in which there are distributed particles or in many cases, fibers of more strong refractory compounds [2, 3]. Such strengthening extends the temperature limits of using of related construction materials. Nevertheless, there are limited by relatively low melting matrix.

The high temperature conditions demand the construction of composite materials consisted only from refractory compounds.

In this case the component materials have to satisfy the main demand – the absence of interaction at high temperatures. In many cases this situation for nonoxigen refractory compounds is fulfilled, especially between boride and carbide or different boride phases.

In all cases the configuration of composite component phases is one of main parameters which determine the mechanical properties of the whole material. The configuration and the interaction in the phase's boundaries control the trans – or intercrystalline fracture character, its temperature dependence.

One of most effective method of strengthening is the creation of the composites in which the strengthening phase is represented by fibers or whiskers. In this case mostly there are achieved the mechanical characteristics which are much

more than they are proper for individual components.

There exist different technological methods to prepare composite materials having refractory compound strengthening phase. Some methods provide the precipitation of previously compacted powders or fibers of compound by liquid metals. The hard alloys are the example of recrystallization through liquid phase. The most common for refractory compounds are methods of powder metallurgy – sintering or hot pressing.

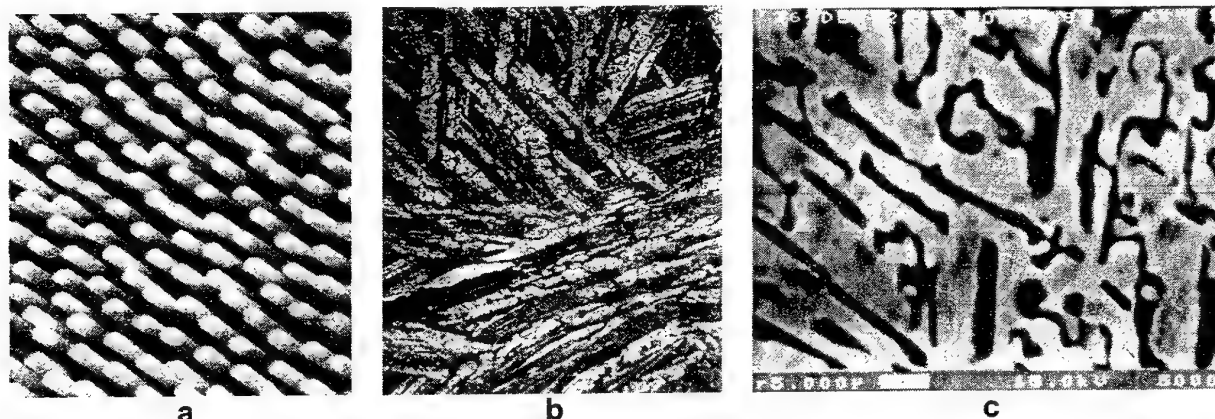
In recent years the big attention is paid to the directional crystallization process, which in the case of eutectic mixtures permits to obtain "in situ" composites. The structure of such composites is determined by such factors as the volume fraction of component phases, crystallochemistry correlation of the both phases structures, technological processes parameters etc [4-6].

It is known that the quasibinary constitutional diagrams of refractory compounds in many cases represent eutectic kind of diagram [7]. It permit to suppose that the directional crystallization process may be used for the creation of new kinds of based on these materials composite materials.

We studied the structure of directionally crystallized pseudobinary eutectic compositions in some $Me^I B_6 - Me^II B_2$ (Me^I : La, Sm, Eu, Gd, Ca; Me^II : Ti, Zr, Hf, V, Nb, Ta) systems, $MoSi_2 - MeB_2$ system, $B_4C - MeB_2$ (Me : Ti, Zr, Hf, Nb, Mo) systems.

It was shown that, according [5], the kind of obtained structure is determined in the greater extent by the volume fraction of component phases (Fig. 1,a,b). The big difference in the crystal structures and chemical bonds character results in more complicate structure (Fig. 1,c).

It is important to note, that in the most of these systems the mutual solid solubility of both phases is absent or negligible small, which determines their stability at high temperatures.



The typical structures of the directionally crystallized eutectic composites.
a) $\text{LaB}_6 - \text{ZrB}_2$ (needle - like structure, $V_1/V_2 = 83/17$)2565
b) $\text{CaB}_6 - \text{TiB}_2$ (lamellar structure, $V_1/V_2 = 97$)
c) $\text{B}_4\text{C} - \text{NbB}_2$ ("Chinese script" structure)3000

The perfection of obtained structures is influenced by technological parameters of processes – the crystallography direction of crystallization, temperature rate of crystallization etc.

By optimal parameters it is possible to obtain structures consisted from single crystal matrix of the main refractory phase, in which there are uniformly distributed needle-like single crystals of the second refractory phase [8].

It is worth to note that for instance, $\text{MeB}_6 - \text{MeB}_2$ composites may be considered as any model materials.

These both phases may be formed by different rare-earth and d-transition metals correspondingly with changing of such phases parameters as cell dimension, thermal expansion coefficient etc. Moreover, it is possible to use not only individual borides but their solid solutions, that permits to obtain the continuous changing of these parameters.

These peculiarities may be used, particularly, for investigation of fundamental rupture characteristics of fiber reinforced composites, as the function of interphases strains, of friction between fiber and matrix during its pulling etc.

By introducing of any third element, which has any solubility in both boride phases, also it is possible to change the character of interaction between components.

The realization of physical properties, proper to the main matrix phase with simultaneously reinforcement permit to use, for instance, LaB_6 based materials as effective and thermal shock resistant thermoemitters, EuB_6 based materials as strong neutron absorber materials etc.

References

1. V.Trefilov, Yu.Milman, O.Grigoriev, Prog. Cryst. Growth and Charact., **16**, 225, 1988.
2. Modern Composite Materials, ed.L.G.Broutman, R.H.Krock, Massachusetts, 1967.
3. Fiber based composite materials, ed.I.N.Francevich, D.M.Karpinos, Naukova Dumka, Kiev, 1970.
4. G.Chadwick, Progr. Mater. Sci.**12**, 971, 1963.
5. D.Cooksey, D.Munson, M.Wilkinson, H.Hellawell, Phil. Mag. **10**, 745, 1969.
6. Yu.Taran, V.Mazur, The structure of Eutectic Alloys, Ed. Metallurgia, M., 1978.
7. S.Ordanian, Ogneupory, №9-10, 11, 1992.
8. Yu.Paderno, in Advanced Multilayered and Fibre-Reinforced Composites, NATO ASY Ser., **3**, p.353, 1998.

HIGH-PRESSURE SYNTHESIZED MgB_2 WITH HIGH CRITICAL CURRENT DENSITY AND IRREVERSIBLE FIELD, POSITIVE INFLUENCE OF Ta ON SUPERCONDUCTIVE CHARACTERISTICS

Prikhna T.A.⁽¹⁾, Gawalek W.⁽²⁾, Savchuk Ya.M.⁽¹⁾, Sergienko N.V.⁽¹⁾, Moshchil V.E.⁽¹⁾,
Dub S.N.⁽¹⁾, Wendt M.⁽²⁾, Melnikov V.S.⁽³⁾, Surzhenko A.B.⁽²⁾, Litzkendorf D.⁽²⁾,
Nagorny P.A.⁽¹⁾, Schmidt Ch.⁽²⁾

⁽¹⁾Institute for Superhard Materials of the Nat'l Ac. Sci of Ukraine, Kiev, Ukraine

⁽²⁾Institut für Physikalische Hochtechnologie e.V., Jena, Germany

⁽³⁾Institute of Geochemistry, Mineralogy and Ore-Formation of the Nat'l Ac. Sci of Ukraine Kiev,
Ukraine

Magnesium diboride can be easily synthesized under ambient, elevated or high pressures. The characteristics that are important for practical applications of a material as a superconductor, such as critical current density (j_c), irreversible magnetic field (H_{ir}), etc. are very sensitive to the material density, impurity content and structural defects. High-pressure (HP) synthesis and sintering are promising methods for manufacturing of the bulk MgB_2 superconductive material and available high-pressure apparatuses with 100 cm³ working volume can allow us to use the bulk MgB_2 for practical application such as electromotors, flying wheels, bearings, etc.

We obtained a bulk materials with the following critical current densities j_c in 1 T field: 570 kA/cm² at 10 K, 350 kA/cm² at 20 K and 40 kA/cm² at 30 K. Besides, the materials demonstrated high mechanical characteristics (microhardness, fracture toughness, Young modulus).

We have found that the Ta presence during HP synthesis (especially) or sintering process (in the form of a foil that covered the sample and as an addition of Ta powder of about 2 -10 wt.% to the starting mixture of B and Mg or to MgB_2 powder) increases the (j_c) in the magnetic fields up to 10 T and the H_{ir} of MgB_2 -based bulk materials.

We succeeded in the HP synthesis of MgB_2 -based materials with j_c and H_{ir} higher than those reported by Kijoon H. P. Kim et al. [1] Fig.1, i.e. with the highest ones that ever have been reported for bulk MgB_2 .

High-pressure synthesized or sintered samples have a multiphase nanostructure. As SEM study shows the matrix phase of the samples consists mainly of Mg, B, O. The black grains or single

crystal inclusions (from the micron or even less to dozen microns in size) of Mg-B phase (MgB_2) are distributed in the matrix.

We observed the strong evidences that Ta absorbs gases during synthesis and sintering to form Ta_2H , TaH and $\text{TaN}_{0.1}$ and prevents from or reduces the formation of MgH_2 (both with orthorhombic and tetragonal structures) as well as essentially reduces the amount of impurity nitrogen and oxygen in black MgB_2 . No Ta-Mg, Ta-B or Ta-Mg-B compounds have been found.

The samples with higher j_c and H_{ir} have the higher density of Mg-B (MgB_2) inclusions in their matrix, i.e. the higher amount of black grains. Besides, in the samples with better superconductive properties, these black Mg-B inclusions contain a higher amount of boron than that in the samples with worse superconductive characteristics while the amount of magnesium is about the same. The samples with better superconductive properties also contained a higher amount of unreacted magnesium in the matrix phase.

Positive influences of Ta are much more pronounced in the synthesis process than in the sintering one. The presence of Ta extends the temperature region of synthesis of a material with high j_c and H_{ir} .

The results of investigations of mechanical properties are given in Table 1. The black inclusions (MgB_2 single crystals) have hardness higher than that of sapphire.

The attained level of superconductive and mechanical properties of the high-pressure synthesized MgB_2 and the possibility to produce

large bulk MgB_2 products make this material very promising for practical applications.

Choi, Min-Seok, Park & Sung-Ik Lee, "Origin of the high DC transport critical current density for the MgB_2 superconductor", *cond-mat/0103176*.

Reference

1. Kijoon H. P. Kim, W. N. Kang, Mun-Seog Kim, C.U. Jung, Hyeong-Jin Kim, Eun-Mi

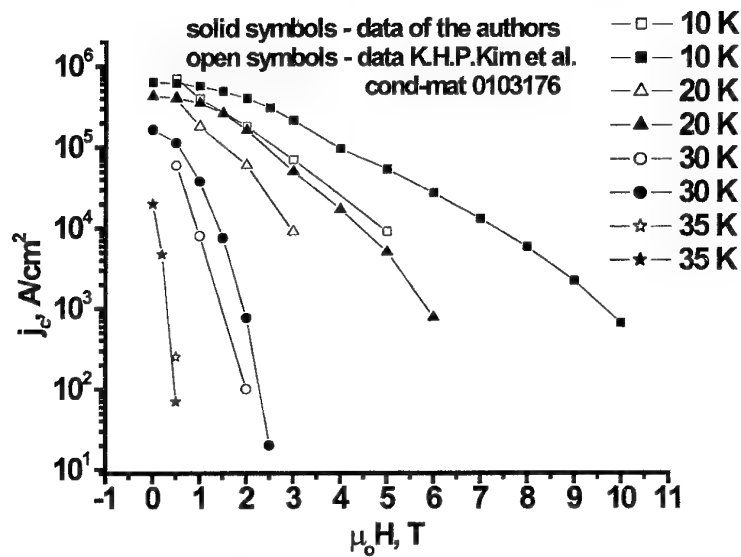


Fig.1. Data on critical current density j_c vs. magnetic field μH_0 for the bulk MgB_2 samples: solid symbols - high pressure synthesized at 2GPa, 800 – 900 °C, 1h from Mg and B by the authors; open symbols - high pressure sintered from MgB_2 powder at 3 GPa, 950°C by K.H.P. Kim et al. [1].

Table 1. Results of micro-(Vickers indent) and nanohardness (Berkovich indent) investigations of the sintered MgB_2 samples

Characteristics	Matrix phase of the samples	Single crystal MgB_2	Sapphire, Al_2O_3
60 - mN-load			
Nanohardnes, H_B , GPa	17.4 ± 1.1	35.6 ± 0.9	31.1 ± 2.0
Young modulus, E, GPa	213 ± 18	385 ± 14	416 ± 22
4.96 N-load			
Vickers microhardness, H_v , GPa	17.1 ± 1.11	-	-
147.2-N load			
Fracture toughness, K_{Ic} , $\text{MN/m}^{-3/2}$	7.6 ± 2.0	-	-
Vickers microhardness, H_v , GPa	10.12 ± 0.2	-	-

SILVER - CARBON COMPOSITE MATERIALS HIGH IN CARBON. STRUCTURE AND PROPERTIES

Minakova R.V., Zatovskiy V.G., Kryachko L.A., Lukovich V.V., Cartuzov V.V.,
Golovkova M.E., Yenevich V.G., Susidko V.L.⁽¹⁾

Frantsevich Institute for Problems of Materials Science NAS of Ukraine, Kiev, Ukraine

⁽¹⁾ Ukrzaliznytsia, Kiev, Ukraine

Ag-C composite materials (CM), with 3-60 % carbon (by weight) are traditionally used in switching devices as explosive and sliding contacts. The phenomenon of electrical erosion of explosive contacts from Ag-C CM with 3-5 % carbon (graphite) and a different dispersivity of its particles were investigated, for example, in [1,2]. The detected features of influence of the graphite particles sizes in CM on structural changes in a working layer have shown, that the nature of the physic-chemical phenomena under influence of arc discharge is not completely found out, and the opportunities of structure optimization are not reached one's limit. The information about behaviour of explosive contacts with heightened contents of graphite up to 60-wt % (up to 90 vol. %) the practically are unknown, though these materials are widely used in relay systems. In the given work of a research results explosive contacts material erosion (asymmetric pair) are submitted: stationary contact, containing 40 % Ag and 60 % carbon (graphite) of a type BAP112Д (Russia) and movable one from silver. The purpose of this research is the exploration of optimization opportunities of structure and properties of CM Ag-C with the heightened content carbon, for achievement of required functional properties of contacts and reliability of the relay equipped by them. The testing of contacts are carried out in the mix of the relay Ж3ТА (Ukraine) with an operating time $2 \cdot 10^6$ cycles. The switched current - direct ($U = 24$ B), load - inductive, varied from 0,40 up to 0,12 H by resistance from 1500 up to 214 Oh, that corresponds to a current from 18 up to 126 Ma. The shape, sizes of erosion traces and their structural features were investigated by the methods of optical structural analysis, scanning electronic microscopy etc.

The analysis of structural changes in a working layers of asymmetric pair contacts testifies to localization of discharge operation and heterogeneity of trace depth on the occupied area with increase of a switched current. A series of erosive trace representative features, which can be attributed to the following basic aspects of

electroerosive destruction were observed in a selected interval of loads. First of them - failure and ablation Ag-C material of a stationary contact, occurs in a solid phase with settling out of the fine flaky graphite particles and of the silver spherical particles on movable contact. The particles of graphite of CM are dividing, sublimating, acquiring of carbon black character; the particles of silver are burning-off, spheroidizing and fractionally evaporating. Apparently, the features of morphology of movable contact working layer are concerned with it, fig. 1. Other mode of failure of CM of the stationary contact working layer is concerned with removal of graphite in a gas phase, burn-off of silver particles, shaping in its crystallization of a porous skeleton. The character of secondary structure with increase of discharge current force testifies to a preferential role of carbon in forming arc discharge. Thus carriers of charges are the products of carbon (graphite) interaction with oxygen, their decomposition and ionization. With increase of commutation number the porous skeleton on the basis of silver is deformed. Under effect of a thermal stream of discharge burn-off of these skeleton sites occurs. The bad wetting of graphite by silver melt causes the consolidation of these sites in extended fields, and formation continuous grid or fragments of this grid in the cells of which grains of graphite and their conglomerates were founded, fig. 2. This fact and knobs toroidal shape on a surface of movable contacts testify to a saved role of graphite as generator of discharge carriers during an investigated amount of commutation cycles. To find an explanation of experimentally detected mode failure the simulation of discharge thermal stream influence on CM Ag-C with the different contents of graphite and size of elementary volume in a modeled composite was undertaken. Elementary volume of graphite in CM was chosen as cube, with sides covered by continuous silver layers. Simulation of chosen parameters influence on a temperature field in elementary volume and time of

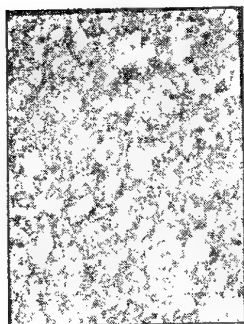


Fig. 1 - Working layer surface structure after test movable contact within the relays



Fig. 2 - Working layer secondary structure after test stationary contact within the relays

heating of graphite up to temperature sublimation were carried out with the help of the decision thermal conduction three-dimensional task [3]. The computer realization of mathematical model has allowed to establish regularity of the temperature distribution in elementary volumes at given their size (40, 80 and 100 microns), thermal stream (10^9 - 10^4 W) and of graphite and silver ratio (0,903-0,729). It is found, that the more elementary volume, the more variance between temperature at its center (T_1) and a rim, boundaries of graphite and silver coverage (T_2). This result confirms an opportunity of destruction of graphite in a gas phase in conditions, when the silver was not heated yet to temperature of boiling, fig. 3.

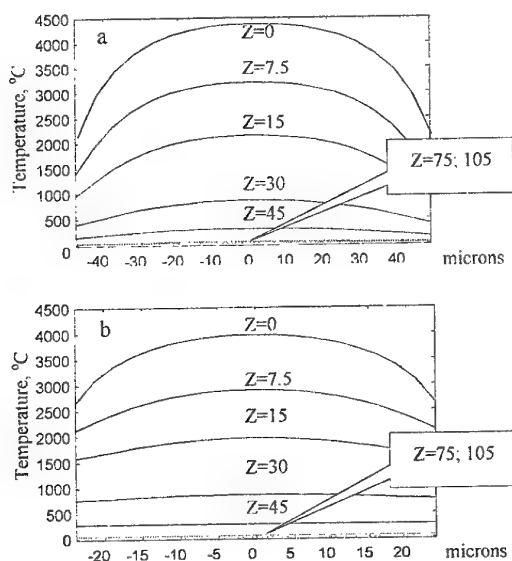


Fig. 3 - Model representations about heat distribution in composite elementary volume (their size: a - 80; b - 40 microns)

The dates of theoretical simulation confirm an opportunity of a skeleton formation on the basis of

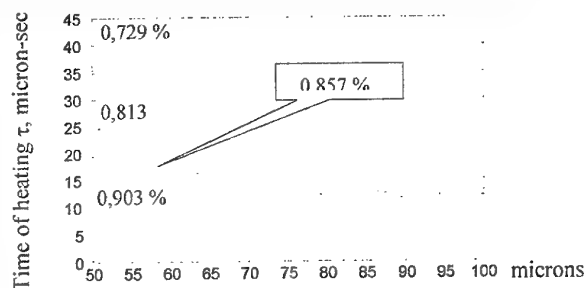


Fig. 4 - Influence of the basic components content ratio and elementary volume size on its heating time

silver. They testify also that a basic principle of formation of CM with the heightened contents of graphite should be creation of silver matrix structure in a composite. Its saving with increase of an amount of an operating age cycles will promote stability of transition resistance in these conditions. The chosen technological cycle gives such opportunity. Precision regulation granulometric composition of graphite and the distribution of silver in a technological cycle take into account necessity of saving at a required level of resistance welding. It is assumed that it is achieved as a result of an ejection role heightening of a structural component on the silver basis from a surface of a stationary contact. Besides is established, that the alignment of temperature in CM on depth occurs faster with lowering of the graphite elementary volumes size, and the working surface is heated faster at their integration, fig. 4. With increase of the graphite contents and of the elementary volume size the time of its heating up to temperature close to sublimation temperature is reduced. This fact and interaction in a system C-O, heightening of a role stripped influence on arc discharge of interaction products will favor of explosive contacts erosion lowering.

REFERENCES

1. Малышев В.М., Румянцев Д.В. Серебро. - М.: Металлургия, 1976. - С. 151-152.
2. Philip C. Wingert, Sam E Allen, Richard C. Resignation The Effect of Graphite Size and Processing on the Performance of Silver-Graphite Contacts - IEEE Transactions on Components, Hybrids and Manufacturing technology, Vol.15. - N 2. - April 1992. - P. 154-159.
3. Minakova R.V., Grekova M.L. Modeling of Composite Materials and Electrical Erosion During Electrical Discharge Machining //Proceedings of the International Symposium ISECTA'93. - Almaty, Kazakhstan, June 21-25. - 1993. - P. 231 - 236.

ORGANIC-INORGANIC NANOSTRUCTURAL COMPOSITE COATINGS PREPARED BY SOL-GEL PROCESSING

**Shilova O.A., Tarasyuk E.V., Shevchenko V.V.⁽¹⁾, Klimenko N.S.⁽¹⁾, Hashkovsky S.V.,
Shilov V.V.⁽¹⁾**

Institute of Silicate Chemistry of Russian Academy of Sciences, St. Petersburg, Russia

⁽¹⁾Institute of Macromolecular Chemistry, Ukraine National Academy of Sciences, Kyiv, Ukraine

Sol-gel technology has experienced an explosive growth in two past decades and research achievements in this field are very fruitful. [1,2]. Among sol-gel products are known different kinds of materials such as glass, ceramics, organic-inorganic hybrids composites as well as coatings, fibers, membranes. Here temperature-resistant glass-ceramic and organic-inorganic hybrids coatings prepared using sol-gel synthesis are considered with a point of view of their properties and application.

Temperature-resistant ceramic coatings formed by sol-gel method from sols containing fillers are extremely perspective for application as electric insulating and radiotolerant coatings for electrical engineering and power industry including nuclear power stations. The approach to prepare such coatings has been developed by A. Borisenko and co-workers [3,4]. Now these investigations are actively developed because the new requirements to such coatings are appeared. Except for electrical parameters, such properties as elasticity and flexibility are important operating ones. These parameters are especially critical for using in different miniature electric engineering devices. It is known organic or polymeric additives are involved in sols to increase elasticity of sol-derived hybrid organic-inorganic materials and coatings [1,5]. Different types of organic-inorganic hybrids: CERAMERS, ORMOCERS, ORMOSILs and ORMOLYTs as well as films, coatings and membranes based on such materials have been successfully synthesized.

The organic-inorganic hybrid materials are usually prepared by various routes or by means of introduction of inorganic particles into organic materials or by means of plasticization of inorganic materials by organic substances such as polymers [1,6,7]. The corresponding hybrid nanomaterials and coatings are now the following new generation of "designer materials". One of effective ways of preparing such materials is the sol-gel method.

Here we search for ways of improvement of ceramic coating flexibility keeping at the same time good electrical properties of theirs. The approach for improving bending strength of the corresponding temperature-resistant flexible ceramic electric insulating coatings is considered. The first investigations have carried out by us and published elsewhere [8-10]. Here we have extended a number of high-molecular additives used in the starting sols.

Starting suspensions, based on both tetraethoxysilane (TEOS)-derived modified sols and high disperse fillers such as Cr_2O_3 , are used to deposit the coatings on metals and alloys. The low and high molecular substances are tested as additives for improving flexibility of the ceramic coating. As organic low and high molecular weight components were taken hydroxyl containing substances with various amounts of OH groups such as glycerol (three OH groups), poly(ethylene glycol) (PEG) of molecular weight 300 (two OH end groups), branched polyurethaneurea (BPUM) of molecular weight 4200 (six OH end groups), as well as three-arm hyperbranched polymer (HPB) (twelve OH peripheral groups). The influence of organic components on both sol stability and suspension covering capacity was estimated visually as well as by means of both the viscosity and sol wetting ability measurements.

The results of research of both bending and electrical strength of the flexible hybrid organic-inorganic insulation formed on nichrome wire are discussed. The results of investigations of chemical and phase structure of the coatings obtained by heat treatment at temperature from 500 to 1100° C using DSC, thermal analysis and as well X-ray diffraction techniques are represented. Both the electron probe microanalysis and scanning electron microscopy studies was carried out using Camebax microanalyzer.

The parameters of the flexible electric insulation are high enough for extremely thin coatings (8-25 mkm). It was important that the additive influences positively on both bending strength and electric strength of the coatings. The value of breakdown voltage reaches 550 V for the line wire and 240 V for the wire of coil winding, in the case of a coil diameter 8mm. The additives used by us lead to increase the bending strength value by a factor of 1.5-4 in comparison with those of the pure ceramic coatings. It is worth to mention that a thickness of the coatings prepared by the one-step deposition process from the suspensions containing BPUM and HPB is far larger than the thickness of the coatings prepared using other additives or without ones.

The SEM-image of the glassceramic coating as well as the hybrid coating prepared using BPUM, as an additive, are shown in Figure.

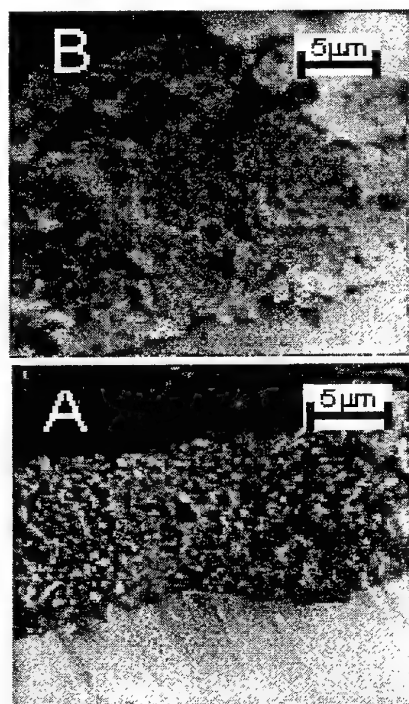


Fig. SEM-image of a cross section of the hybrid organic-inorganic coating formed using the suspension with BPUM (B) and the silicate glassceramic coating without BPUM (A).

The hybrid coating is thicker and of less dense structure than ceramic coating. The latter also exerts a salutary effect on winding of wires on coils due to reduction of cohesion forces and increase of adhesive forces of the coating to a substrate.

Thus, incorporation of the above-mentioned organic low and high molecular weight additives into the suspension of a type: TEOS-derived modified sol / Cr_2O_3 leads to increase of a flexibility of the ceramic coatings obtained. At that the electrical strength value is not worsened and at the expense of increasing thickness of coatings even is raised.

References

1. Brinker C.F., Scherer G.W. Sol-Gel Science: The Physics and Chemistry of Sol-Gel Processing. San Diego: Academic Press, Inc. 1990, P.908.
2. Mackenzie J. D., 11th International workshop on glasses, Ceramics, hybrids and nanocomposites from gels, September 16-21, Abano Terme, Italy. Abstracts. University of Padova, 2001, P.246.
3. Nikolaeva L.V. and Borisenko A.I., Thin Layer Glass Enamel and glass-ceramics coatings ("Nauka", Leningrad, 1980) P.88
4. Nikolaeva L.V. and Borisenko A.I., J. Non-Crystal. Solids, 1986, 82, P.343.
5. Matsuda A., Matsuno Y., Tatsumisago M. and Minami T., J. Am. Ceram. Soc., 1998, 81, 11, P.2849.
6. Schubert U., Proceeding of 11th International Workshop on Glasses, Ceramics, Hybrids and Nanocomposites from Gels», Italy. Padova. 16-21 September 2001. – J. Sol-Gel Sci. & Techn., 2002 (in press).
7. Pomogailo A.D., Uspekhi Chemistry (Russia), 2000, 69, 1, P.60-83.
8. Shilova O.A., Hashkovsky S.V., Shilov, V.V., Shevchenko V.V., Gomza Yu.P., Klimenko N.S., Tarasyuk E.V., Voprosy Chem. & Chem. Techn., 2001, 4, P.77.
9. Shilova O.A., Hashkovsky S.V., Kuznetsova L.A., Proceeding of 11th International Workshop on Glasses, Ceramics, Hybrids and Nanocomposites from Gels», Italy, Padova, 16-21 September 2001. – J. Sol-Gel Sci. & Techn., 2002 (in press).
10. Shilova O.A., Hashkovsky S.V., Tarasyuk E.V., Shilov V.V., Shevchenko V.V., Gomza Yu.P., Klimenko N.S., Proceeding of 11th International Workshop on Glasses, Ceramics, Hybrids and Nanocomposites from Gels, Italy, Padova, 16-21 September 2001. – J. Sol-Gel Sci. & Techn., 2002 (in press).

THE MODERN TENDENCIES OF R&D IN THE FIELD OF BIO CERAMICS BASED MATERIALS

V.A. Dubok, E.A. Shevchenko, A.V. Shinkaruk

Frantsevich Institute for Problems of Material Science of the National
Academy of Sciences of Ukraine, Kiev, Ukraine

The main driving force of R&D of bioceramics is its market price and humanitarian value of these developments. Restoration and maintenance of health and functions of a human organism quickly becomes the most essential priority during peaceful progress of high technology society. The example of USA is very indicative in this respect as far as before events of September 2001 expenditures on health in the USA have been almost equal to the total spending on army and state. Diseases of bone tissue confidently take the third place (after cordial - vascular and cancer diseases) among reasons of death and disablement of the population. By number of visits to clinics (taking into account dentistry problems) bone diseases took the first place long ago. The people having completely healthy bone tissue can be found extremely rarely.

During two last decades bioceramics proved high efficiency and reliability at different surgical operations of bone tissue restoration. Among all synthetic implanted materials the bioceramics causes the least disturbances in human organism, to the greatest degree harmonizes with natural processes of bone tissue restoration and promises the most rapid progress in further improvement. Besides the restoration of bone tissue the bioceramics have a lot of others medical application – can be used as drug delivery systems, sorbents, ion exchangers, food additives. Applying the modern principles of biomimetics permits to plan new more substantial usage of bioceramics based materials for restoration of human's health, designing of new pharmaceuticals, etc. The listed factors explain considerable attention researchers and

surgeons to investigation of the materials and improvement methods of their medical application.

In addition to applied usage in surgery, research and modification of fundamental properties of bioactive ceramics assigned for bone tissue restoration opens path to study and modeling the processes of functioning of the alive bone which is the most perfect of all known nanostructured materials (and generally - to study principles of designing of nanostructured materials). Even now, on the basis of inexact and imperfect knowledge it can be asserted that quantity and complexity of miscellaneous fundamental phenomena and processes, that are utilized by the Nature for construction and functioning of a bone, much more exceeds the complexity of processes, for example, in chips of big integrated circuits. The precision of assembling of bone elements exceeds on the orders of value the same parameters of integrated circuits.

Besides, the same path of research of fundamental properties of bioactive ceramics is indispensable for development of biosensors – materials and microdevices for control and monitoring of different systems of an organism, as well as sensors for technical systems. The selection of hydroxyapatite (HAP) as main basis for biosensors was made in fact by nature on its own, as the HAP is the only inorganic matter selected by the nature for functioning of the most perfect product of the nature - the human being. Just therefore some modifications of synthetic HAP guarantee full biocompatibility and equilibrium of the implanted material with human organism, and do not cause any disturbances or

violations of the bioenvironment. Therefore, taking into account the multiplicity and variability of HAP properties, only on its basis it is expedient to design microdevices for monitoring internal systems of living organism.

The ways to improve medical applications of bioceramics are based, first of all, on investigation of methods of modifications of those physical parameters of bioceramics, which determine functioning of inorganic components of a bone in an alive organism. The set of these properties appears rather miscellaneous. Being based just on simplest ideas about surface modification of HAP crystals of bone, absence of OH groups and presence of carbonate radicals and other elements in the bone HAP, electrostatic nature of interaction of butt-ends of bone HAP crystals with untwined and charged butt ends of collagen molecules, this set includes such phenomena as adsorption, formation of solid solutions with some elements and salts, formation and physics of local charged centers in HAP microcrystals, mechanoelectric effects etc. Taking into consideration role of bone mineral as the main reservoir of ions in the living body (for it contains about 99 % of the total body calcium, 85 % of body phosphorus, 90 % of body sodium and 50 % magnesium), it is very important to study transport of different ions and electrons in imperfect HAP crystals and all related phenomena. Interesting results on interaction of bone HAP crystals with organic molecules were received by EPR and DNMR methods.

The fundamental approach to study and control of properties of bioceramics as well as last data of detailed researches of bone mineral component has resulted in considerable modification of bioceramics. Except of usual division of these materials on bioinert, bioactive and resorbed ceramics the concept of

biofunctionalization of ceramics have appeared which includes imparting to surface layer or volume of ceramics the special properties boosting particular reaction of biochemical and cellular systems of an organism. In the best developments all these kinds of bioceramics (or some of them) are integrated in one implant executing a given functions. At the same time it is necessary to take into consideration the general principle of multilateral interaction of implanted material and organism - corrosion of bioceramics as result of complex interconsistent action of different systems of organism and complex changes in the organism due to action on the organism of the biomaterial and products of its corrosion. All this knowledge allows proceeding to bioimitation - restoration with the help of implants made on the basis of modified bioceramics of some particular physiological and functional properties of separate organs of the organism. The number of tasks which can be solved by such method is permanently growing at the expense of new knowledge and technological capabilities - for example, already now speech goes about formation with the help of bioceramics separate micro blood vessels and nerve fibers.

The outlined way of R&D of the newest generation of bioceramic implants based on biomimetic engineering requires to integrate the latest data in different branches of science and wide technological capabilities. It explains concentration of such developments in large multiple-discipline scientific institutes or rather large-scale firms with big scientific potential as well as existence of fair quantity of counterfeits and low-grade bioceramic implants.

Acknowledgement

The authors gratefully acknowledge the financial support of STCU Grant No.1641

LITHIUM-CONDUCTING SOLID ELECTROLYTES BASED ON SOLID SOLUTIONS $\text{La}_{2/3-x}\text{Li}_{3x/4/3-2x}\text{Me}_2\text{O}_6$ (Me=Nb; Ta)

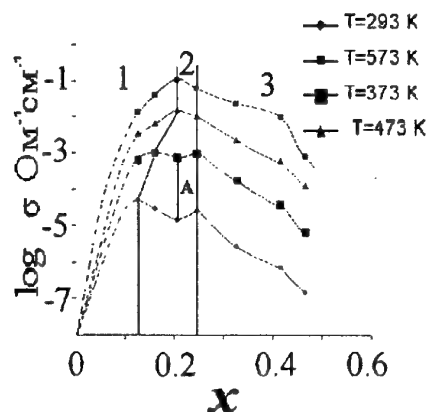
Gavrilenko O.N., Belous A.G., Pashkova Y.V.

V.I. Vernadskii Institute of General and Inorganic Chemistry of National Academy of Science of
Ukraine, Kyiv, Ukraine

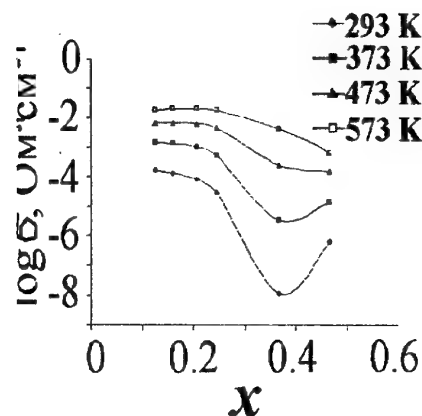
The problem of production of lithium solid-state power sources with high characteristics is intimately bound with a problem of synthesis of a solid electrolyte. The search for basic phases for new chemically and thermally resistant electrolytes is highly actual one. The complex oxides $\text{La}_{2/3-x}\text{Li}_{3x/4/3-2x}\text{Nb}_2\text{O}_6$, have been obtained by substitution of Li^+ for La^{3+} in lanthanum niobate with the structure of defect perovskite $\text{La}_{2/3}\text{Nb}_2\text{O}_6$ [1]. These phases can be promising ones because of the presence of rigid framework structure of crystalline lattice, migration channels and vacancies which provide free transport of charge carriers - the ions of lithium.

The purpose of this work was the investigation of synthesis conditions, phase transformations, crystal-chemical peculiarities, and electrophysical properties of the systems $\text{La}_{2/3-x}\text{Li}_{3x/4/3-2x}\text{Me}_2\text{O}_6$ (where Me = Nb; Ta).

The phase transformations accompanying synthesis of lithium-containing lanthanum niobates and tantalates with the structure of the defect perovskite have been investigated. It has been marked out the peculiarities of phase-formation in the system of lanthanum - lithium tantalates to consist in a higher order of structural transformations and the formation of lithium-containing tantalate based on non-lithium structure with the defect perovskite type. In the systems examined the optimum requirements to the processing of single-phase materials have been determined. The temperature and concentration ranges of single-phase materials as well as their homogeneity regions have been defined. The nature of solid solutions $\text{La}_{2/3-x}\text{Li}_{3x/4/3-2x}\text{Me}_2\text{O}_6$ (Me=Nb; Ta) was studied by means of analysis of concentration dependence of their crystallographic parameters. Both substitution and intercalation solid solutions have been determined to form within the homogeneity regions (Figure). Both concentration and temperature dependence of the conductivity of the materials synthesized have been examined.



a)



b)

Figure The isotherms of the ionic conductivity ($\log \sigma$) in the systems: a) $\text{La}_{2/3-x}\text{Li}_{3x/4/3-2x}\text{Nb}_2\text{O}_6$; b) $\text{La}_{2/3-x}\text{Li}_{3x/4/3-2x}\text{Ta}_2\text{O}_6$ (x - lithium concentration).

The lithium ions conductivity has been calculated taking into account the use of turn off electrodes according to Ref. [2]. Electron component of the conductivity was measured at DC (0.5 V). At 570 K this value did not exceed 0.05 %. The correlation between lattice parameters, chemical composition, and transport properties of $\text{La}_{2/3-x}\text{Li}_{3x/4/3-2x}\text{Me}_2\text{O}_6$ (Me=Nb; Ta) has been determined.

The results allow the assumption that there is an opportunity in enhancement of the conductivity by means of modifying structure towards an increase in the quantity of mobile lithium ions, vacancies and/or sizes of migration channels.

The influence of dispersion medium on the formation, microstructure and properties of lithium-containing lanthanum niobate has been also investigated. By means of XRD, electron spectroscopy, and electrophysical measurements the dispersion of the mixture of raw components in both aqueous and alcohol mediums, in comparison with that of acetone, has been shown to accelerate the formation of the perovskite phase and provide

the formation of the ceramics with higher both density and conductivity values.

Thus, lithium-containing lanthanum niobates and tantalates have been shown to be the promising basis for the production of solid state electrolytes with high lithium ion conductivity.

References

1. *E.I. Burmakin*. Solid state electrolytes with the cation conductivity of the alkali metals, in Russian, M: Nauka. 1992. 263 p.
2. Lines M.E. // *Phys. Rev. B*. 1979. V. 19. p.1189.

DIELECTRIC CERAMICS BASED ON COMPLEX NIOBATES

$\text{La}_{2/3-x}\text{Na}_{3x}\text{Nb}_2\text{O}_6$ AND $\text{Nd}_{2/3-x}\text{Na}_{3x}\text{Nb}_2\text{O}_6$

Ovchar O.V., Mischuk O.D.

V.I. Vernadskii institute of General and Inorganic Chemistry NAS of Ukraine, Kyiv, Ukraine

Introduction

When developing communication systems operating at UHF frequency range a need arises in the utilization of the materials with a high dielectric permittivity ($\epsilon > 100$). These materials are urgent for the producing resonant elements of filtering or oscillating devices (solid-state oscillators- DRO, UHF filters). The effective size of these elements decrease in the proportion to $\epsilon^{1/2}$ when increasing the permittivity of the materials utilized. Another important requirements to UHF dielectric materials are also both low dielectric loss in operating frequency region ($\text{tg}\delta$) to provide high Q-factor of a resonant element and high temperature stability of the permittivity determined by its temperature coefficient (τ_ϵ).

To date the materials based on barium lanthanides solid solutions $\text{Ba}_{6-x}\text{Ln}_{8+2x/3}\text{Ti}_{18}\text{O}_{54}$ are generally used as high-permittivity temperature stable UHF materials. However, the ϵ values of these materials do not mostly exceed 100, that does not allow the efficient solution of miniaturization problem. That is why the search and investigation into the new dielectric materials with the permittivity of above 100-200 still remain to be an essential scientific problem of UHF technique.

High- ϵ materials desired could be synthesized, in particular, when using solid solutions of ferro- and antiferroelectrics with the different temperature of the phase transitions as the basis for the further material development [1]. To this aim, amongst others the source materials based on the complex niobium oxides with the defect perovskite structure could be considered as the most promising candidates.

On the one hand sodium niobate (NaNbO_3), which has the perovskite structure, is known to be antiferroelectric one with the phase transition temperature of above 300°C [2] with the permittivity characterized by the positive temperature coefficient ($\tau_\epsilon > 0$) near the room temperature. On the other hand it is known that the niobates of rare-earth elements ($\text{Ln}_{2/3}\text{Nb}_2\text{O}_6$, where $\text{Ln} = \text{La} - \text{Nd}$), have the structure of the defect perovskite, in which 4/3 of crystallographic sites in the sublattice of rare-earth element are

vacant. However, there are only few data related to electrophysical properties of the niobates of rare-earth elements $\text{Ln}_{2/3}\text{Nb}_2\text{O}_6$. When examined electrophysical properties of the niobates $\text{La}_{2/3}\text{Nb}_2\text{O}_6$ and $\text{Nd}_{2/3}\text{Nb}_2\text{O}_6$ at low frequencies (10^3 - 10^4 Hz) the authors of [3,4] measured the high values of their permittivity ($\epsilon = 200$ и 50 respectively). However, it is difficult to make correct conclusions on the trends of high ϵ in the studied objects when basing only on low-frequency measurements because of the presence of low-frequency polarization mechanisms. Moreover, the analysis of the literature data [5] allows for the assumption that around the room temperature niobates of rare-earth elements $\text{Ln}_{2/3}\text{Nb}_2\text{O}_6$ (where $\text{Ln} = \text{La} - \text{Nd}$) could have the negative temperature coefficient of permittivity ($\tau_\epsilon < 0$).

Recently, it has been confirmed the formation of wide-range region of solid solutions in the systems $\text{Ln}_{2/3}\text{Nb}_2\text{O}_6 - \text{NaNbO}_3$ (where $\text{Ln} = \text{La}, \text{Nd}$) with the perovskite structure [6,7]. However, the data on their electrophysical properties are still not examined. Therefore, the target of the work presented was to investigate both the dielectric properties, and their temperature trends as well, of the materials in the following systems: $(1-3x/2)\text{La}_{2/3}\text{Nb}_2\text{O}_6 - 3x\text{NaNbO}_3$ and $(1-3x/2)\text{Nd}_{2/3}\text{Nb}_2\text{O}_6 - 3x\text{NaNbO}_3$ over the wide frequency and temperature ranges, and the possibility of producing temperature stable UHF dielectrics with high permittivity based on the systems examined.

Results and discussion

Ceramic materials in the system $\text{Na}_2\text{O} - \text{Ln}_2\text{O}_3 - \text{Nb}_2\text{O}_5$, where $\text{Ln} = \text{La}, \text{Nd}$, have been synthesized by solid phase reaction technique from extra pure raw reagents. Dielectric properties (ϵ and $\text{tg}\delta$) of sintered polycrystalline samples with the chemical compositions $\text{La}(\text{Nd})_{2/3-x}\text{Na}_{3x}\text{Nb}_2\text{O}_6$ within the x -range of $0 \leq x \leq 2/3$ have been examined within the frequency range of 10^4 - 10^{10} Hz.

When investigating niobates of rare-earth elements $\text{La}_{2/3}\text{Nb}_2\text{O}_6$ and $\text{Nd}_{2/3}\text{Nb}_2\text{O}_6$ the anomalies of unknown nature on the temperature dependencies of dielectric parameters ($\epsilon(T)$ and

$\text{tg } \delta(T)$ have been revealed in the MW range (10^9 - 10^{10} Hz), which are not related with the materials processing. When decreasing ionic radii of rare-earth element from that of lanthanum to that of neodymium the anomaly's temperature region shifts towards higher temperatures (Fig.1). When increasing the measurement frequency the temperature behavior of the permittivity of the niobates $\text{La}_{2/3}\text{Nb}_2\text{O}_6$ and $\text{Nd}_{2/3}\text{Nb}_2\text{O}_6$ changes its trend (τ_ϵ changes its sign in the vicinity of the room temperature). This behavior of the dielectric parameters in the materials with the composition $\text{Ln}_{2/3}\text{Nb}_2\text{O}_6$ could be related with the presence of high concentration of structural vacancies in the sublattice of rare-earth element.

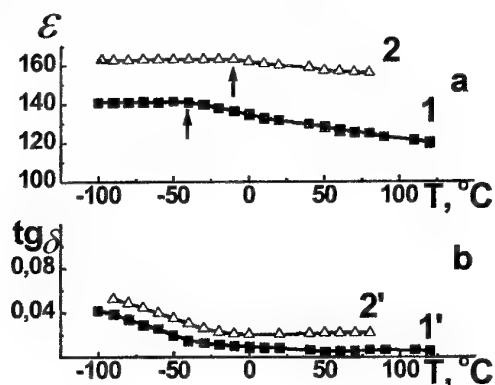


Fig.1. Temperature dependencies of the permittivity ϵ (a) and dielectric loss tangent $\text{tg } \delta$ (b) of the materials with the chemical composition $\text{La}_{2/3}\text{Nb}_2\text{O}_6$ (1,1'); $\text{Nd}_{2/3}\text{Nb}_2\text{O}_6$ (2,2') at the frequency 10^{10} Hz.

Within the range of the chemical compositions corresponding to $5/12 < x < 7/12$ - in the case of La containing materials- as well as in that range corresponding to $6/12 < x < 7/12$ - in the case of Nd containing compositions- spontaneously polarized state was observed in the materials $\text{Ln}_{2/3-x}\text{Na}_{3x}\text{Nb}_2\text{O}_6$ characterized by the maximum on the temperature dependence of the permittivity (Fig.2). Moreover, the noticeable hysteresis has been revealed on the dependence $\epsilon(T)$ for these materials without the changes subject to increasing measurement frequency from 10^6 to 10^9 . Observed behavior of the permittivity versus temperature and frequency denote the possible heterogeneity of the compositional ordering due to the presence of the ordered domains within the disordered matrix [8].

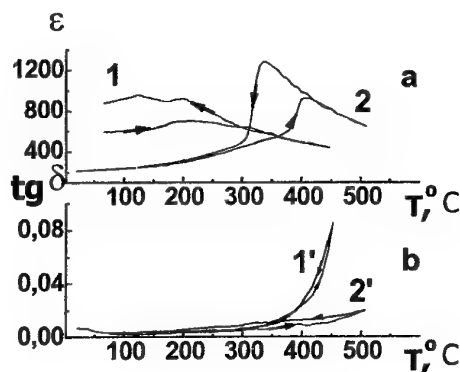


Fig.2. Temperature dependencies of the permittivity ϵ (a) and dielectric loss tangent $\text{tg } \delta$ (b) at 10^6 Hz: 1,1' - $\text{La}_{1/6}\text{Na}_{3/2}\text{Nb}_2\text{O}_6$; 2,2' - NaNbO_3 .

changes its sign in the vicinity of the room temperature) whereas the decrease in the concentration of structural vacancies accompanied this results in a decrease in the relaxation contribution to the value of the dielectric loss.

The results of the investigation of electrophysical properties in studied materials denote the potential possibility in producing dielectric materials with high and temperature stable permittivity subject to the chemical composition in the systems $(1-3x/2)\text{Ln}_{2/3}\text{Nb}_2\text{O}_6 - 3x\text{NaNbO}_3$. The materials synthesized have been used in the producing coaxial dielectric resonators (CDRs) for the frequency range of 200 to 300 MHz which have been tested and exhibit average values of unloaded Q-factor.

References

1. Venetsov Y.N., Politova E.D., Ivanov S.A. Ferro- and antiferromagnetics of barium titanate family (in Rus). - M: Chem, 1985.
2. Smolensky G.A., Bokov V.A., Isupov V.A., et al Ferroelectrics and antiferroelectrics (in Rus). - L: Science. 1971.
3. Sych A.M., et al // (in Rus) Inorg. Mat. - 1973. -IX, № 11. -p.1947-1950.
4. Sych A.M., Golub A.M. // (in Rus) Progress in chemistry. - 1977. -XLVI, iss.3. -p.414-444.
5. Masuno K. // J. Phys. Soc. Japan. - 1964. -19, № 3. - p.323-328.
6. Pivovarova A.P., Strahov V.I., Melnikova O.V. // (in Rus) Inorg. Mat. - 1999. -35, № 9. -p.1118-1119.
7. Fedorov N.F., Pivovarova A.P., Melnikova O.V., Morozova E.V. // (in Rus) J. Inorg. Chem. - 1979. - XXIV, iss. 12. -p.3350-3353.
8. Paltnikov M.N., Sidorov N.V., Sandler V.A., Stefanovich S.Y., Kalinnikov V.T. // (in Rus) Inorg. Mat. - 1997. -33, № 9. -p.1135-1142.

INVESTIGATION OF PROPERTIES OF CASTED METALLIC COMPOSITE MATERIALS

Kondratenko V., Kasakov S.⁽¹⁾, Knokhin V.⁽¹⁾, Vinoviy V.⁽²⁾

Iron and Steel Institute after Z. I. Nekrasov of NAS of Ukraine, Dnepropetrovsk, Ukraine

⁽¹⁾OJS "Dneprospeksstal" after A.N.Kuzmin", Zaporozhye, Ukraine

⁽²⁾"New Technologies & Materials Institute" Ltd, Dnepropetrovsk, Ukraine

During last years the original resource-saving technology of receiving of layered/sandwich steel composites with high level of properties was developed and mastered. Technology foresees the using of non-convenient high-efficient method of two-layer ingots manufacture - liquid-to-liquid casting. The method proposed does not require both the capital investments and sufficient reconstruction of steel making and teeming processes.

The proposed techniques was used for manufacture of different kind of metal products (periodic profile, sheet and section stock, calibrated rod for fixing bolts etc.) and from various type of steel combination ("low carbon-high carbon steels", "low carbon - low alloyed steels", "high alloyed- low alloyed steels") [1].

The developed layer/sandwich steels allow to save in surface layer the properties and compound of high- and mid-alloyed steels, which traditionally used in manufacturing metal structures of responsible applications (chemical industry, machinery, industrial and civil construction sector, etc.). Besides is reducing by up to 20% alloying elements/materials consumption and cutting the production cost of metal structures.

This paper presents some results of microstructure researches of cool-rolled sheets 1,2-2,0 mm from cast sandwich composite from chromium-containing high-alloyed steel (08Cr18Ti).

The macrostructure of metals of sheet's cross section consists of three layers.

The surface layers had the same thickness (up 100 μm to 300 μm) from both side of sheet and were made from steel containing 0,08 % C and 18,0 % Cr.

The inner layer was performed from steel with 0,08 ... 0,12 % C and 13,0 % Cr.

The "liquid sandwich" technique ensures an identical thickness of a surface layer through length and breadth of products.

The reduction of the chromium content, carbide quantity and the iron contents increase in an internal layer reduces the strength and raises plastic characteristics of multilayer sheets.

With increase of surface layer thickness, the plasticity parameter is reduced and some increase of strength property of multilayer sheets is observed.

The creation of ferrite martensite structure in an

internal layer of cold rolled multilayer sheets allows to raise strength and to reduce the plastic characteristics of products. The properties totality set of multilayer sheets will be determined by thickness of a superficial layer, of quantity and of products of ferrite and austenite decomposition ratio after cooling with various speeds.

High-chromium composite sheet metal with low carbon content in inner layer consists of chromium-containing ferrite with different quantity of carbides.

The increasing of carbon content in inner layer of sheet up to 0,12% led to appearance of austenite by temperatures 850-920° C.

The cooling of sheet metal from austenite state temperatures with different velocities allows to received the range of various structures in inner layer (fig.1).

Thus, by intensive cooling with cooling rate more than 9,4°C/s the inner layer consists of initial ferrite and martensite (originated from undercooled austenite).

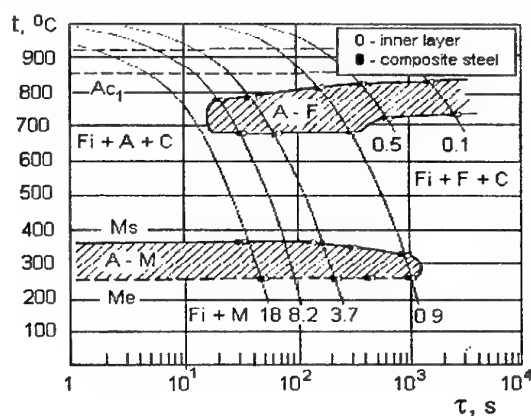


Figure 1. The thermokinetic diagram of phase transformations at heating and cooling of chromium alloyed multilayer steels.

In the cooling rate interval up 0,9°C/s to 9,4°C/s the undercooled austenite in inner layer's structure had been decomposed on ferrite and martensite. By lowering of cooling rates the share of the latter decreased from 100 to 3...5%.

The cooling of composite sheets with velocities

lower than 0,9^bC/s resulted to formation in the inner layer the range of structures: initial ferrite, ferrite originated from austenite and chromium carbides [2].

Microroentgenspectral analysis showed that in inner layer, iron content was greater and chromium and titanium contents were smaller then in surface layer (Table 1).

Table 1: Concentration of leading chemical elements in layers of sheet from sandwich composite

Layer	Chemical elements content, %		
	Fe	Cr	Ti
Surface	80,0-81,0	19,0-19,5	0,5-0,6
Inner	85,0-86,0	13,0-14,0	0,35-0,45

The grain size distinction in surface and inner layers of cold-rolled sheets had been stipulated, first of all, of different chemical compounds (quantity of crystallisation nucleus in first and second melts). In second turn, the grain size depends of ingots casting conditions and also, deformation and heat treatment parameters.

The transition boundaries from surface layers to inner are 5...15 microns width and are characterised by a smooth changing of the chemical elements content - iron, chromium, titanium, silicon.

The boundaries passing as between dendrite and secondary grains as through grain body because are formed in liquid condition. This and lack of spills are the main advantages of developed method of composite manufacture as compared other known techniques.

Investigation of fracture of composite sheet samples showed that surface layer is stronger and low plastic than inner and had inter-crystallite type of destruction. In cells of fracture was observed nitride non-metal inclusion. The character of destruction in transition zone had mixed type with majority of places of tough failure.

The fracture of inner layer's metal of sandwich composite is tough with bowl-shaped cells with middle and big sizes.

The majority of non-metal inclusions in sandwich composites represented of chromium carbides and titanium nitrides. Distribution of inclusions was uniform through sheet length and layer thickness.

The smaller concentration of chromium and it carbides and also lot of iron in inner layer resulted to increasing plastic properties of composite in whole. Tensile strength and yield point in

elongation of composite sheet were approximately on 20% low and relative elongation was in 1,15...1,2 once greater, than values inherent to surface layer steel (08Cr18Ti).

A layered structure and raised plasticity of sandwich composite ensure high values of ductility of hot rolled sheet at various temperatures $KCU_{+20} = 159 \text{ J/cm}^2$, $KCU_{-40} = 93 \text{ J/cm}^2$. With increasing of surface layer thickness, the relative elongation lowered and strength properties of sandwich sheets increased.

The sheet with such properties guarantees the large reliability of work of articles in aggressive mediums and at dynamic loads, for example of coaches for transportation of chemically active substances, in motor -vehicle construction industry etc., in that number for manufacture of articles by punching, including deep extrusion.

The corrosion and heat resistance of the composite sheet (estimated on a losing of a mass at temperature 815^oC) allows to recommend sandwich sheets for manufacture of knots of system of exhaust gas of motor and also in a food-processing industry.

The perfect mechanical and working properties of rolled steel products (high-strength, plasticity, wear- and corrosion resistance, etc.) achieve through the optimal composition and ratio of layers in composite steel products and also by means of fine steel microstructure which makes high-quality defect-free boundary between the layers formed in liquid state. The proposed technology has been tested and showed high-efficiency in production of various types of rolled steel products.

References

1. Casted metallic composite for mass application/V. Kondratenko, V.Leybenzon, Yu. Dmitriev, V.Polyakov, S.Kazakov, A.Stovpchenko // Proc.of the 10 Int. Metallurgy and materials congress (24-28 may 2000).-Istanbul (Turkey): ITF-CME,2000.-v.-p.1831-1838 (ISSN 1301-3637 (Volume set), ISBN 975-395-382-8.)
2. V. M. Kondratenko, M. F. Evsukov, S. S. Kasakov, V.G. Knohin., "Fundamental and applied problems of metallurgy ", Vol. 3, pp. 279-285, 1999 (in Russian).

NEW LEVEL OF MATERIAL PROPERTIES FOR AUTOMOBILE AND TRACTOR FRICTION ASSEMBLIES

Dmitrovich A.A.

Powder Metallurgy Institute of NAS of Belarus (Minsk, Belarus)

Development of automobiles, tractors and building machines has reached such a level when requirements for different units, assemblies and materials can be compared to those for specialized machines. Operational conditions of these assemblies differ in variety of operational parameters - sliding speed, specific loading and properties of environment - and are characterized by constant increase of their energy loading. Thus, maximal friction work in disc brakes of modern heavy «BELAZ» trucks is 9×10^3 J/cm² at sliding speed of 80 m/sec and pressure 5 MPa.

Having good heat-conductivity, high friction coefficient and wear-resistance, sintered friction materials can operate at high specific loading and sliding speed having high serviceability. Nowadays we observe tendency to substituting common polymer friction materials with sintered ones.

A number of research centers in Belarus and abroad are constantly carrying out intense works for creation new materials. According to the information provided by foreign scientists the total productional volume of friction materials based on iron will grow from 320.000 tons in 1998 to 428.700 tons in 2005, i.e. average annual growth - 6% [1]. Such tendency can be explained by increasing productional capacities of machine-building enterprises and bringing new production to a commercial level.

Modern sintered materials are characterized by the following values:

1. Friction materials working in oil:

Dynamic friction coefficient - 0.05-0.14;

Static friction coefficient - 0.09-0.18;

Maximal friction power - 2-4 W/mm².

2. Friction materials working in dry environment:

Dynamic friction coefficient - 0.25-0.50;

Static friction coefficient - 0.45-0.8;

Maximal friction power - 2-5 W/mm².

Friction copper-based materials are normally used in oil environment. Powder Metallurgy Research Institute have carried out works for substituting

expensive copper substrate of these materials to iron one.

One of such materials is «ШИАДЕФ» - a sintered friction material [2 - 3] - which is based on alloying steel powder produced from processed slurry of bearing production.

«ШИАДЕФ» has dynamic friction coefficient of 0.07-0.14; wearing rate of $2-5 \times 10^{-9}$. At the same time advantages of this materials are better seen in heavy-loaded friction assemblies (specific friction work up to 850 J/cm², initial sliding speed up to 70 m/sec). Friction coefficient of «ШИАДЕФ» material is 1.3-1.4 times higher and its wear-resistance is 1.5-2 times higher comparing the same of the MK-5 material. This was determined during comparative testing of friction discs produced from these materials in a T-150 tractor gearbox.

Complex testing carried out jointly with experts from Minsk Tractor Works have proved high characteristics of the developed material which enabled to establish batch production of these friction discs for friction assemblies of MTZ tractors. Nowadays, production of friction discs with «ШИАДЕФ» friction powder coating is 5.000-6.000 pcs/month. At the same time they are planning to increase productional capacities by starting production of new nomenclature for tractors of 150-250 hp.

«ШИАДЕФ-999/Л» sintered friction material is used in «dry» clutches of tractors (160-180 hp) and its bringing to a commercial level is currently coming to the end. The material has friction coefficient not less than 0.35 at speed approx. 30 m/sec and specific loading - up to 1.5 MPa, providing the necessary service life of 10000 hours.

A significant peculiarity of this material is aluminium nitride as a friction component. Having low thermal expansion coefficient ($4.8 \times 10^{-6} 1/^\circ\text{C}$), good heat-conductivity and heat-shock resistance AlN provides effective removing

of temperature from a friction zone and high wear-resistance of a friction pair [4-6].

«ШАДЕФ-999/Л» is characterized with high friction properties during operation with pig iron (СЧ18, СЧ20 and others) - friction coefficient 0.35-0.42, wearing rate up to 10 mkm/km, maximal possible specific friction power - 6-7 W/mm². Tests carried out at inert-brake stand C-140 (MTZ) have showed that a one-disc clutch with nominal force of pressing springs of 900 kg, equipped with 12 friction linings (6 linings - 45 cm² on each side of the driven disc) from «ШАДЕФ-999/Л» material has the following properties:

static break-away torque - 105-135 kgm on a heated clutch and 90-107 kgm on a non-heated one;

average wearing rate of the linings - 0.270-0.330 mkm/cycle.

Good results were achieved during testing a this new material in clutches of machine produced at Lipetsk Tractor Works.

«ШАДЕФ-2С» material was developed to operate in friction assemblies without lubrication with a steel counter-body. Full-scale testing of the «ШАДЕФ-2С» material were carried out in friction assemblies of crawlers produced at Volgograd Tractor Works. Works for introducing analog material based on iron into brake assemblies of crawlers (150 hp) produced at Altaysky Tractor Works are being carried out.

Together with «BELAZ» experts we are carrying out experiments for development and testing material for disc brakes of heavy pucker trucks with loading capacity of 130-200 tons. Preliminary testing of the developed material have showed its high tribotechnical characteristics - friction coefficient 0.50-0.55 at wearing rate not more than 20 mkm/km.

Together with Cheboksary Tractor Works we are carrying out works for exchange of copper-based МК-5 material used in friction assemblies now by

the other material having high stability in changing friction torque when braking.

Thus, Powder Metallurgy Research Institute have developed a number of friction materials for application in different operational conditions which are not worse than their foreign analogs according to their characteristics. It is first time when production of friction elements was established basing on powder produced from slurry of bearing industry (Fig.1).

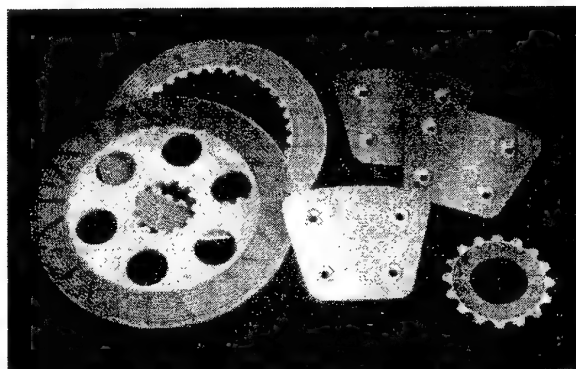


Figure1. Friction discs and linings.

References

1. Auto industry consumption to spur the P/m market// Metallurgia.- 1998.- 65, №9.-с.р/ms.
2. А.с. СССР №1039240
3. Генкин В., Дмитриевич А., Жарин А., Фишбейн Е. Новый фрикционный материал для работы в условиях смазки./Порошковая металлургия. Вып.2. СЭВ. Москва, 1985.
4. Mroz Thomas J. (Jr). Aluminium nitride // American Ceramic Society Bulletin.- 1992. Vol.71, №5.- P.782, 784.
5. Грабис Я.П., Хейдемакс Г.М., Рошманс Д.М., Миллер Т.Н. Синтез нитрида алюминия в высокотемпературном потоке азота/ В кн.: Высокотемпературный синтез и свойства тугоплавких соединений. Рига, 1979, С.42-50.
6. Заявка 63-100069 Япония, МКИ С04В 35/58 Форукава дэнки коге к.к.-№61 -243364.

MAGNETIC PROPERTIES OF CONDENSED MATTER

Lashkarev G.V.

Institute for Problems of Materials Science of NASU

Magnetic susceptibility (MS) of condensed matter which does not possess magnetic order in initial state is considered. MS is an universal thermodynamic characteristics containing vast information about chemical bond, electron spectrum, electronic structure of components and impurities with unfilled inner d- and f-shells, phase transitions, electronic state of charged defects of structure etc.

The components of MS in dielectrics, semiconductors and metals are analyzed. Information about solid state characteristics which is connected with each of these components are discussed.

Theoretical, experimental and empirical methods for separation of MS components are considered. The examples of such separation are presented. A connection of these components with spin paramagnetic resonance, nuclear magnetic resonance and magneto-optical Faraday rotation is shown.

Special interest is attracted to narrow-gap semiconductors. The results of MS researches of IV-VI single crystals pure and doped by noncentral and paramagnetic impurities, are considered. An information about band structure, electron spectra, structure phase transitions due to interband electron-phonon interaction and to noncentral ions obtained out of MS studies is presented. It was shown at the first time the effect of renormalization of electron spectra on MS of narrow-gap semiconductors. This influence was confirmed theoretically later and is due to the change of the narrow band gap in the vicinity of the phase transition temperature as well as to the fluctuations of order parameter.

Except semiconductors MS measurements are convenient for study of phase transitions of different solid states. MS behavior is connected with different parameters of investigated object such as following - electron density of states, band spectrum characteristics, crystal lattice distortion, appearance of temperature independent paramagnetism. Hydrogen intercalates of NbSe₂

represent structure phase transition accompanied with a change of electronic properties. This transformation had been thoroughly researched by method of MS.

Our investigations of MS of semiconductor Pb_{0,30}Sn_{0,60}Mn₁₀Te had led to discovery of ferromagnetic ordering in manganese doped semiconductors. It was firstly shown that indirect interaction between magnetic ions via holes at their high concentration (Ruderman-Kittel-Kasuya-Iosida mechanism) is responsible for ferromagnetic transition. This research gave an impulse for systematic investigations semiconductors doped by manganese, such as GaMnAs and ZnMnO. Magnetic researches had substantiated the appearance of new direction of modern electronics - spinelectronics, where electron spin is used in microelectronics instead of (or in addition to) electron change.

Investigation of MS allowed to discover new effects connected with dispersion of bulk materials or lowering their dimensionality. Porous silicon as against to bulk one displays ferromagnetic properties with Curie temperature ~ 500° K.

Magnetic properties of NbSe₂, MoSe₂ and WSe₂ undergo dramatic transformation at their dispersion to dimensions of nanosize particles. In the case of NbSe₂ (metallic type of conduction) a transition from the state of Pauli paramagnetics to diamagnetics occurs at lowering of particles sizes to 25-140nm. MoSe₂ and WSe₂ are diamagnetics in initial state. Due to dispersion up to particle sizes 15-95nm MS changes a sign and diselenides become Pauli paramagnetics. Observed effects are discussed.

A separation of MS components attracting related results of some other characteristics as ESR, NMR, optical Faraday effect, electrical properties etc. allows to obtain wide information about condensed matter.

NANOCRYSTALS OF SEMICONDUCTORS IN ORDERED ORGANIC MATRICES: GROWTH AND PROPERTIES

Savin Yu.N., Tolmachev A.V.

Institute for Single Crystals, NAS of Ukraine, Kharkov, Ukraine

One of the prospective direction in the development of nanotechnology is the working out of hybrid organic-nonorganic structures on the base of metal and semiconductor nanoparticles in the ordered metalloorganic matrices [1]. The efficiency of nucleation and growth processes of a nanostructures in such matrices is due to the possibility to make a large supersaturation (order 10^{14} metal ions can be introduced in the polar planes of Langmuir-Blodgett (LB) films), the small activation energy of the ion diffusion along the these planes and organic matrix-nonorganic particle interphase interaction. In addition the nucleation and growth processes depend on the composition of organic films and their structures and consequently are the matrix controlled [2].

In present work we discuss the peculiarities of the growing of semiconductor nanocrystals of the sulphides of lead, cadmium and zinc in the ordered metalloorganic matrices in the framework of the diffusion decomposition of solid solution.

The nanocrystal growing process in-situ passed by two stages. 1. The formation of the multilayer molecular films at the solid substrates by LB technology. 2. The carrying out of the solid phase synthesis of nonorganic phase in the volume of organic matrix consisting of $(C_{17}H_{35}COO)_2Me$ molecules, ($Me=Pb, Cd, Zn$) by ion-exchange reactions (the treatment of metalloorganic films in gas atmosphere or in the solution containing the cations-precursors S^{2-}). The authors assume that two stage process of the nanocrystal growth is the principle peculiarity of the phase formation in the ionomer matrices. The MeS seed nucleation is induced by the diffusion flow of negative ions S^{2-} from environment making to the supersaturation in the matrix solid solution. At next stage the MeS precursors (molecular clusters or MeS molecules) created by the ion-exchange reactions form the nonorganic phase seeds owing to their aggregation.

The experimental study of PbS, CdS and ZnS nanocrystal nucleation and growth kinetics shown (Fig. 1.) a number of essential differences of the phase transformation processes passed in multilayer LB

matrices respect to the classic Lifshitz-Slyozov-Wagner (LSW) theory [3,4]. In the first, the growth of the nanocrystal average size $\langle R \rangle$ depending on the duration treatment of LB films in sulphur environment (H_2S atmosphere or Na_2S water solution) at the beginning of treatment the size increasing is more slowly than it follows from LSW theory for "normal" growth stage, the value of exponent $n < 0.5$ in equation $\langle R \rangle \sim t^n$ (in LSW theory $n=0.5$, and $\langle R \rangle$ depends on the initial Me concentration and treatment temperature. At the prolonged exposition the decreasing of n is observed. This is likely due to the transition to the slow growth stage MeS nanoparticles.

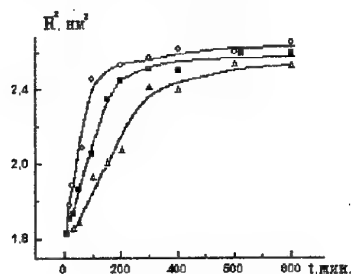


Fig.1 The square of average radius of PbS (○), CdS (△) and ZnS (□) nanocrystals vs time treatment of LB films in H_2S atmosphere.

Secondly, MeS precursor concentration in LB matrix is increased vs time as $X_{MeS} = X_0[1 - \exp(-dt/l^2)]$, where X_0 is the concentration of metal ions before treatment, D is diffusion constant for S^{2-} ions, l is the characteristic length. So the original stage of precursor formation and consequently the rise of supersaturation are in fairly good agreement with Fick classic diffusion law. The experimental data show the nucleation velocity of MeS precursors in the range of a large initial metal concentration in the matrix (corresponding to the stoichiometric composition of the lead stearate LB films) exceeds the velocity of MeS "absorption" by nanocrystals. Thirdly, if supersaturation is absent in the matrix (this takes place at the prolonged treatment in the sulfur media) The rise of the average size and concentrations of nanoparticles are ended. Fourthly, for all studied matrices, which are distinguished by the stoichiometric compositions the

increasing of the nanocrystal size as their concentration proceed at room temperature.

The phase decomposition model in the multilayer metalorganic matrices proposed by the author is based on the supposition that there are two diffusional flows in the metalorganic matrices along the polar planes - diffusion flow of the sulfur ions initiating the phase decomposition of metalorganic matrix after the ion-exchange reactions S^{2-} with the $-(COO)_2Me$ molecular matrix fragments, and the diffusion flow MeS molecular precursors. The diffusion constants of these processes are different and depend on the metal ion concentration in matrix. At the small Me concentration the velocity of the generation of MeS precursors is equal or less of the seed absorption one. Therefore the growth mechanism at the origin growth stage is near practically to the classic LSW mechanism accounting the size confinement of the diffusion processes in multilayer films. At large initial Me concentrations the velocity of the precursor generation can be more than the absorption velocity. Owing to the violation the stationary conditions in the matrix can arise the local saturations which result in the increasing of the velocity of a seed formation at the simultaneous growth of average seed size. It is essential to draw attention to the fact of appearance of a big seeds which are not typical for the initial stage of the phase decomposition in classic systems (for example, glass matrix). The seeds have a large surface energy and therefore are in the metastable state. The distance between them in matrix is order of one or some MeS lattice constants, consequently the seed aggregation to a large seeds is energetically favorable. The nanoparticle grows in the plane disc form and their axes azimuthal orientation is not correlated. Therefore the electron diffraction of the nanocrystals in matrix corresponds to the polycrystals (Fig 2).

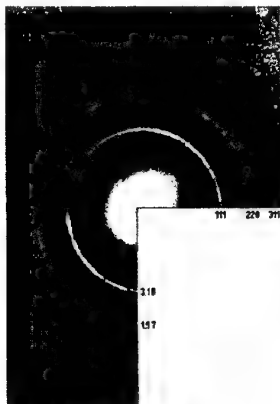


Fig.2. Electron diffraction of PbS nanocrystals grown in LB films.

It is found from the optical absorption spectra measurements that the MeS nanocrystals grown in LB matrices are in quantum confinement state [5]. (Fig3).

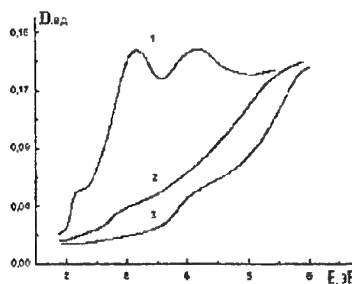


Fig.3. Optical absorbance of PbS(1), CdS(2) and ZnS (3) nanocrystals in LB films.

The most value of the size quantization energy of electro-hole pairs in PbS nanocrystals is ~ 1.5 eV. The influence of the matrix on the energetic structure of PbS nanocrystals is discussed on an example of the lead sulfide nanocrystals grown in the lead stearate LB films. The size quantization energy of the ground E_s and first E_p states of $e-h$ pairs are analyzed within effective mass approximation. The average radius of nanocrystals $r \approx 1.7$ nm and the potential barrier height at the contact between the semiconductor and matrix $V_e \approx 4.5$ eV are calculated. It is suggested that the finite barrier height is due to the action of electric fields of $\sim 10^7$ V/m in the contact regions with breaking the polar symmetry of dipole arrangement of matrix molecules with respect to the surfaces of growing planar nanocrystals.

References.

1. A.J. Bard. *Integrated Chemical Systems A Chemical Approach to Nanotechnology*, Wiley, New York, 1994.
2. A.G. Fedorov, Yu.N. Savin, I.A. Shneiderman, and A.V. Tolmachev, *Funct Matter*, **6**, 556 (1999).
3. I.M. Lifshitz and V.V. Slesov, *J. Phys. Chem. Solids* **19**, 35 (1961).
4. C. Wagner, *Z. Electrochem.* **65**, 581 (1961)
5. Yu.N. Savin, A.V. Tolmachev, *JETP Letters*, **75**, 135 (2002).

DEVELOPMENT OF MULTILAYERED Si_3N_4 -BASED CERAMIC COMPOSITES HAVING AN ABILITY TO ARREST CRACKS

Gogotsi A.G., Lugovy M.I.⁽¹⁾, Slyunyayev V.N., Orlovskaya N.A.⁽²⁾

Institute for Problems of Strength, Kiev, Ukraine

⁽¹⁾Frantsevich Institute for Problems of Materials Science, Kiev, Ukraine

⁽²⁾Drexel University, Philadelphia, USA

Elaboration of layered ceramic composites is widely considered now to be the most efficient way to enhance service performance and reliability of ceramic-based structural materials. The main requirement for the composites is their ability to make resistance to crack propagation in achieving a limit state. Besides, if their ability to bear mechanical (prolonged or cyclic) load is critical point, the inelasticity, being usually associated with damage accumulation, and sub-critical crack growth should be avoided. This means that constituent layers of the composite need to be elastic and strongly bounded each other. The necessity for the composites being used under intensive mechanical loads gives rise to demand of obtaining high strength of outer layers. Specifically, obtaining compressive stresses in outer layers is one of key elements of the strategy. Thereby, a marked increase of surface damage resistance and crack arresting can be achieved in such a way.

At the moment there is insufficient elaboration of modeling and simulation to understand the limits of stress and fracture toughness increasing of layered composites with respect to compact materials of pure components, possibilities to predict a response of such materials under loading. The lack of systematic study in this field creates some difficulties to develop the high reliable ceramic layered composites. Particularly, at present there have been only a few systematic studies to explore the ability of layered composites to arrest cracks.

The investigation of crack arresting of Si_3N_4 -based layered composites along with elaboration of possible ways of computational and practical optimization of their structure to increase this ability was made in this work.

Symmetrical layered composites $\text{Si}_3\text{N}_4/\text{Si}_3\text{N}_4\text{-xTiN}$ ($x=10, 20, 30, 50, 70$ and 100 wt. %) prepared similarly to [1] were studied. The addition of different amounts of TiN to Si_3N_4 in one of layers was used to ensure varying levels of internal stresses in both layers. Magnitudes of the residual compressive stresses (σ_c) in Si_3N_4 layers

and tension (σ_t) stresses in $\text{Si}_3\text{N}_4\text{-xTiN}$ layers were calculated by using of the following equations:

$$\sigma_c = \frac{E_c' E_t' f_t (\alpha_t - \alpha_c) \Delta T}{E_c' f_c + E_t' f_t},$$

$$\sigma_t = \frac{E_c' E_t' f_c (\alpha_c - \alpha_t) \Delta T}{E_c' f_c + E_t' f_t},$$

where ΔT is the difference in temperature between the actual temperature and the joining one,

$E_c' = E_c / (1 - \nu_c)$, $E_t' = E_t / (1 - \nu_t)$; α_j , E_j , f_j are the Poisson ratio, the coefficient of thermal expansion, the Young modulus and the volume fraction of the j -th component, respectively.

Calculations have shown that typical magnitudes of compressive and tensile residual stresses were in the ranges $100 \text{ MPa} - 1 \text{ GPa}$ and $100 - 500 \text{ MPa}$, respectively, increasing in the order corresponding to the titanium nitride contents.

The ability of the composites to arrest cracks was assessed preliminarily by computer simulation. It was supposed that total thickness of the composites along with residual stress magnitudes (compressive and tensile) is specified. The [2] procedure of calculating stress intensities using a weight function was adopted for the simulation. It was found that apparent fracture toughness of the composites depends substantially on sequence of layer thickness and not only on internal stress magnitude. It was shown also that the sequence can be adopted in such a way that crack shielding, i.e. increased fracture toughness of layered composite (compared with monolithic specimens) be produced not only in compressive layers but also in tensile ones. Now the work is in progress to determine conditions so as to provide enhancement of shielding in process of crack growth.

To examine composites as for their ability of cracks arresting, dozens of tests were conducted on compositions containing from 10 to 100% TiN in their tensile-stressed layers. The V-notches with tip radii of an order of 10-15 μm served as stress concentrators. The depth of the notches was 0.6-0.65 of the specimen height, being 4-5 mm (specimens of large height we ground down to such sizes). Characteristic load-deflection diagrams are shown in Fig. 1.

It is clear from Fig. 1 that the developed procedure provides the arrest of cracks, and the compositions under study, judging from these diagrams, fall into the order corresponding to their titanium nitride contents. An interesting feature of many of these diagrams is "hysteresis" loops recorded during specimen unloading and their further loading. It was connected probably with the amount of energy dissipated by wake effect during "artificial" unloading and loading of specimens. The mechanism determining such "hysteresis" (Fig. 1) is under study.

The mechanism of crack arresting is found to be the most effective in the compositions with the 70 % TiN containing layers. In 10 % TiN containing specimens a propagating crack did not arrest under our loading conditions, though their catastrophic failure typical of single - phase silicon nitride ceramics and particulate composites on their basis did not occur.

The microscopic analysis of fractured specimens demonstrated that tensile-stressed layers containing of 70 % and 100 % TiN display multiple channel cracks formed during specimen sintering that is probably determined by the insufficient strength of these layers. However, the propagating crack, fracturing the specimens, was not always coming through channel cracks in first case. In 50 % TiN specimens, channel cracks appeared not so often and propagating cracks deviated, coming through compressed layers, and crossed tensile-stressed layers in the loading plane. But it was not noticed that their paths included channel cracks. In 30 % TiN specimens the paths of the main cracks were less branched, and desired bifurcation on their way were not revealed. Note that lack of the bifurcation in the specimens was in accord with theoretical evaluation of this effect made in [3].

In the majority of cases, besides recording load-deflection diagrams and acoustic emission, the polished lateral surface was examined after each unloading of specimens by an optical microscope (x1000). It was established that in specimens with high TiN contents cracks did not

practically propagate in the direction of loading, and even they did not always start from the tip of a V-notch. They were branching, one crack could first appear; with further loading, another one could propagate, and so on. As a whole, the fracture pattern appeared to be very far from the models examined by linear fracture mechanics that is the basis for the modern methods of evaluation

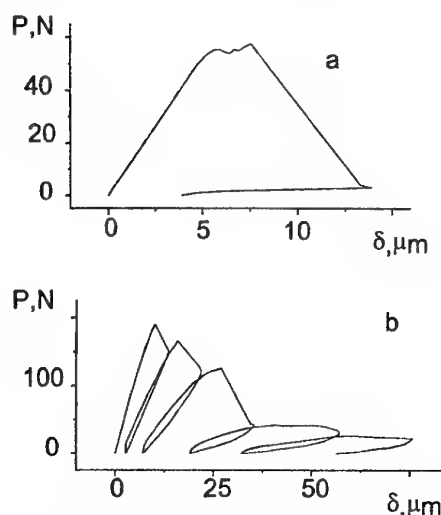


Figure 1. The load-deflection diagrams of layered composites: a) $\text{Si}_3\text{N}_4/\text{Si}_3\text{N}_4$ -10 wt.% TiN; b) $\text{Si}_3\text{N}_4/\text{Si}_3\text{N}_4$ -70 wt.% TiN.

of fracture toughness of ceramic materials. However, retarded fracture patterns of 30 % TiN specimens were closer to these models. Attempts to use critical stress intensity factors or to apply the compliance method rather popular in such investigations were of no success.

The work has supported by European Commission (Grant INCO-Copernicus ICA2-CT-2000-10020)

1. Yaroshenko V., Orlovskaya N., Einarsrud M.-A., Kovylayev V. Multilayered and Fibre-Reinforced Composites: Problems and Prospects. Ed. by Y.M.Haddad, Kluwer Academic Publishers, pp. 285-295, 1997
2. Blattner A.J., Lakshminarayanan R., Shetty D.K. Toughening of layered ceramic composites with residual surface compression: effects of layer thickness. Engineering Fracture Mechanics, 68 [1], pp. 1-7 (2001)
3. Lugovy M., Orlovskaya N., Slyunyayev V., Gogotsi G., Kubler J., Sanchez-Herencia A.J. Crack bifurcation features in laminar specimens with fixed total thickness. Composites Science and Technology, 62 [6], pp. 819-830 (2002)

CREATION OF HEAT-INSULATION OF INTERNAL SURFACES OF ELEMENTS OF INTERNAL-COMBUSTION ENGINES WASTEGATE LINE

Ved Valeriy

National Technical University "Kharkov Polytechnic Institute", Kharkov, Ukraine

Increase of the coefficient of efficiency of internal combustion engines and capacity of transport means are achieved mainly on the account of raising operating temperatures in engines. Advanced design solutions and development of new heat-resistant alloys ensure the tendency of 50-60 K growth per decade of such temperatures in the world propulsion engineering. However, cooling engines techniques are limited, and upper range of temperatures of using metal alloys is practically achieved. Qualitative shift in the development of propulsion engineering can be made only on the basis of application of ceramics with special properties. However, creation of an adiabatic ceramic internal combustion-engine with perfect operational parameters remains the perspective of the distant future.

In the nearest time essential increase of coefficient of efficiency of engines being designed, decrease of fuel consumption and toxicity of waste gases can be achieved with the usage of effective internal heat-insulation of the gas wastegate line - channels of cylinders heads, in which the heat loss makes up 85%, and manifolds.

Heat-insulation of engines gas channels redistributes heat flows with corresponding decrease of loss of power being taking away to the engine cooling system, enhances energy content of used gases with the following their wearing in the turbine, raises the effective efficiency with the simultaneous improvement of indicated efficiency on the account of heat loss decrease. High surface purity of gas channels being achieved by means of the erosion-resistant layer of heat-insulation can reduce aerodynamic resistance to a gas flow. Internal thermal protection must facilitate also the decreasing of the value of gas corrosion of elements of the wastegate line because of the realized possibility of their exploitation at lower temperatures. The rise in temperature of waste gases decreases their toxicity and gives a possibility to use alternative kinds of fuel in engines.

Famous propulsion engineering firms, for example Porsche, for increasing the degree of adiabaticity of augmented engines install test bed engines with ceramic insertions of the simplest forms into outlet channels of cylinders heads of

aluminum titanate. Information about creation in engines of lengthy heat-insulated outlet channels of complicated configurations is not found in literature.

A new class of ceramic materials characterized by visco-plastic statuses at high temperatures is created [1]. This peculiarity of the created ceramics allows to relax by the structure compliance the attached to it thermal and mechanical stresses that have predetermined its anomalous structure.

Materials of this class found their practical realization in the developed technology of forming heat-insulated erosion-resistant coatings of internal surfaces of components of complicated configurations and of unlimited length. A distinctive peculiarity of this technology is that the coating is being formed directly in the process of the casting of the metal on mold cores [2]. For this before the core will be filled with the molten metal the surface of the core is covered by the sequence of several different as to their functionality layers from the developed ceramic materials of inorganic nature which are transformed to a composition coating in the process of crystallization and subsequent cooling of the liquid metal (cast iron or alloys on the basis of aluminum).

In the developed heat-insulated ceramic coatings the layer, which is directly exposed to the gas flow, is produced to be very thick and firm for providing it with erosion resistance. In order to decrease aerodynamic resistance, the working surface of this layer should have a high degree of purity. This parameter is achieved by means of covering the mold core with a transient layer from materials, which soak into interstice of the mold core and give it a shining smooth surface. Further, while technological drying of the mold core having a multi-layer coating, the transient layer covered for the provision of channel purity is sublimated. Insignificant gap, which appears in connection with this between the core and the coating, serves as a compensator of extension while enhancing the volume of the core in the process of metal casting.

The coating layer facing the metal and carrying out directly heat-insulated functions is produced to be porous and optimally firm. The surface of this layer, which further will contact the

metal, is made to be maximally developed for increasing the mechanical constituent of coating adhesion to the metal and is saturated with chemical compounds facilitating the achievement of the small angle of edge wetting by the cast iron or aluminum depending on the type of metal being cast. The thickness of the heat-insulated layer determines the total thickness of the whole coating and can vary within the limits of 1 to 10 mm.

In order to make heat-insulated and especially erosion-resistant layers of coatings, materials have been developed on the basis of oxides and their compounds with maximum temperature coefficients of linear expansion equal to the cast iron [3].

The peculiarity of the new class of materials, on the basis of which the coatings have been created, is presence in their structure of an amorphous phase ensuring the visco-plasticity. Crystallization of this amorphous phase taking place in the materials of the coating at high temperatures and being a function of time is accompanied by the growth of their volume, which can reach 25% depending on the composition of amorphous phase. Such growth of volume considerably condenses the material of the coating increasing its erosion resistance and causing appearing of radical stresses reinforcing adhesion to metals.

For optimizing parameters defining the reception of a predetermined structure of the coating, the thermometry of the process of their forming while casting outlet elements of channels of cylinders heads of cast iron have been carried out [4]. On the basis of the analysis of continuing redistribution of temperatures in the heat system a possibility of receiving thermally unloaded ceramic heat-insulated coatings has been determined.

Investigations of materials properties of the developed coatings [5] showed that they are characterized by a small coefficient of heat conductivity - 0,1 W/m·K at temperatures higher than 800 K. It is one order lower than ceramics' one based on titanate aluminum.

In order to assess the working capacity limit of the developed coatings, they were put on trial in as internal heat insulation of elements of outlet channels of cylinders heads of internal combustion engines under conditions which several times exceed possible operational ones.

Thermocyclic tests of composition coatings have been conducted under considerable velocity of gas flows (325 ± 25 m/s) heating channels walls - the coating - till the temperature of 1100 K with the

subsequent cooling by the air (100 ± 20 m/s) in the regime: heating 30 s, cooling 60 s.

The coatings withstood without changes the test programme intended for conducting 51 heating changes. At the same time, the coating with the thickness of 2 mm created gradient of temperatures of 290 K at maximum temperatures on the coating. Calculations carried out on the basis of thermal characteristics of the coating defined that difference of temperatures, which can be created by the coating, must be higher in connection with the possibility of warmth redistribution to jointed metal walls of the elements of the engine wastegate line. This was confirmed by 100-hour experiments conducted with the engine wastegate line heat-insulated elements connected between each other by the end-walls through heat-insulation at temperatures of the wall of the outlet channel of cylinders heads of the engine of 1175 K and at gas flow velocity of 35 - 40 m/s. Under these conditions, the coating with the thickness of 2 mm creates on it the difference in temperatures of 520 K. At the same time, gradient of temperatures on the metallic part of the tested elements in the sections perpendicular to gas flows corresponded to 1,5 K/mm and was a constant magnitude along the length of the heat-insulated cylinders heads.

List of references: 1. Ведь В.Е. Технология нанесения теплозащитных покрытий внутренних поверхностей деталей газового тракта ДВС // Авиационно-космическая техника и технология: Сб. научн. тр. - Вып.5. - Харьков: ХАИ. - 1998. - С. 441 - 445. 2. Ведь В.Е., Лещенко В.А., Гусева Н.И., Верба А.Г. Энергоэффективные нагревательные устройства на основе термостойкой керамики // Интегровані технології та енергозбереження. - 2001. - №2. - С. 23 - 27. 3. Ведь В.Е., Завгородний Ю.Н. Гусева Н.И. Верба А.Г. Определение температурного коэффициента линейного расширения оксидов и их поликристаллических смесей // Вестник Национального технического университета "ХПИ": Сб. науч. тр. Тем. выпуск "Физико-химические проблемы керамического материаловедения" - Вып. 18-Харьков: НТУ "ХПИ". - 2001. - С.79 - 85. 4. Ведь В.Е. Термометрия процесса формирования теплозащитных покрытий каналов ДВС при отливке чугуна // Вестник Харьковского политехнического института: Сб. научн. тр. - Вып. 56.-Харьков: ХГПУ. - 1999. - С.57 - 60. 5. Ведь В.Е. Оценка эффективности тепловой изоляции головок цилиндров ДВС // Интегровані технології та енергозбереження. - 1999 - №2.- С.81 - 85.

SYNTHESIS AND INVESTIGATION OF COMPLEX REFRACTORY OXIDES WITH SPHENE AND PSEUDOBROOKITE STRUCTURE

Grigoryan R., Grigoryan L.⁽¹⁾

Institute of Structural Macrokinetics RAN, Chernogolovka, Russia

⁽¹⁾Institute of Chemical Physics Problems RAN, Chernogolovka, Russia

Compounds of sphene structure are inclined to form solid solutions with wide areas of homogeneity. These solid solutions are distinguished by unique electrophysical properties. Of the most interest is investigation of possible introduction of 3d and 4d element atoms into sphene lattice instead of calcium, titanium, tin, and silicon. Our work is dedicated to study of pseudobinary systems of CaTiSiO_5 - CaSnSiO_5 , CaTiSiO_5 - YFeTiO_5 and YFeTiO_5 - YFeSnO_5 . The samples were synthesized in low-temperature plasma of hydrogen-oxygen flame [1]. It differed from the conventional ceramic method by high speed and low power and labor consumption. X-ray analysis proved that the samples of the same composition synthesized by both methods were almost completely identical (before the investigation all the samples were subjected to roasting at 1173 K during 4 h with the following quenching by fast cooling).

CaTiSiO_5 - CaSnSiO_5 system is a continuous series of solid solutions with a general formula of $\text{CaTi}_{1-x}\text{Sn}_x\text{SiO}_5$. They are crystallized in a sphene structure. The introduced Sn^{4+} ions occupy distorted octahedron interstices previously occupied by Ti^{4+} ions in an oxygen pack. It results in an increase in the elementary cell parameters and the samples density.

The determined elementary cell parameters of CaTiSiO_5 [$a=(7.061\pm0.004)$ Å, $b=(8.710\pm0.005)$ Å, $c=(6.568\pm0.005)$ Å, $\beta=(113.86\pm0.04)^\circ$, $v=369.5$ Å³, $z=4$, sp.gr. $P2_1/a$, $d_{\text{X-ray}}=3.522$ g/cm³, $d_{\text{pycn}}=3.48$ g/cm³] and CaSnSiO_5 [$a=(7.07\pm0.01)$ Å, $b=(8.78\pm0.01)$ Å, $c=(6.57\pm0.01)$ Å, $\beta=(113.86\pm0.05)^\circ$, $v=373.0$ Å³, $z=4$, $d_{\text{X-ray}}=4.684$ g/cm³, $d_{\text{pycn}}=4.61$ g/cm³] are in agreement with the available literary data [2, 3]. It has been established [3] that at $T<(615\pm15)^\circ\text{C}$ in this system there is an area of nonmixing (dissolving maximum at $\text{Ti/Sn}=3/1$).

All the solid solutions are of semiconducting character. Fig. 1 represents a dependence of the sample electric conductivity on its composition.

Electric conductivity is strongly dependent on temperature (Fig. 2). For instance, the increase in temperature from 500 up to 625 K results in the increase of $\text{CaTi}_{0.2}\text{Sn}_{0.8}\text{SiO}_5$ specific electric conductivity by a factor of 10^2 .

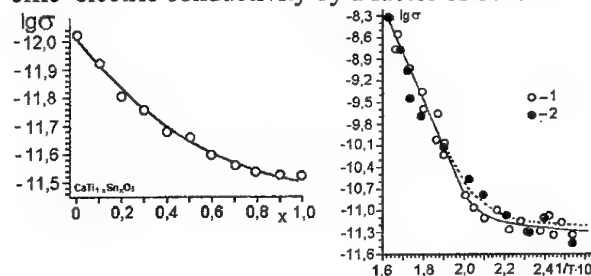


Fig. 1. $\text{CaTi}_{1-x}\text{Sn}_x\text{SiO}_5$ samples: specific electric conductivity as a function of composition.

Fig. 2. CaSnSiO_5 (1) and $\text{CaTi}_{0.2}\text{Sn}_{0.8}\text{SiO}_5$ (2) samples: electric conductivity as a function of temperature.

In the system of CaTiSiO_5 - YFeTiO_5 two phases of a variable composition are formed with a wide area of homogeneity. α -phase ($0\leq x\leq0.45$) is crystallized in sphene lattice. Substitution of up to 45 % Ca^{2+} and Si^{4+} does not result in a significant variation of the lattice. Fe^{3+} ions occupy oxygen surrounding voids which were previously filled by Si^{4+} ions, and Y^{3+} ions occupy polyhedral voids earlier filled by Ca^{2+} ions. Mössbauer spectra of α -phase have some lines corresponding to three states of iron. Introduction of less electropositive yttrium instead of calcium leads to an increase in the covalence share of M-O bond and the sample electric conductivity.

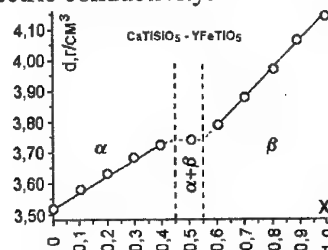


Fig. 3. $\text{Ca}_{1-x}\text{Y}_x\text{TiSi}_{1-x}\text{Fe}_x\text{O}_5$ samples: density as a function of composition

β -phase samples ($0.55\leq x\leq1.0$) are crystallized in rhombic syngony in pseudobrookite

structure (Table 1). Ti^{4+} ions occupy octahedral oxygen interstices. Substitution of Ca^{2+} for Y^{3+} results in the lattice ordering. Fe^{3+} ions have unusual coordination that can be described as distorted tetrahedron [4]. In the whole concentration interval introduction of Fe^{3+} ions leads to an increase in the sample density (Fig. 3).

Table 1.

Elementary cell parameters of β -phase samples of $\text{Ca}_{1-x}\text{Y}_x\text{TiSi}_{1-x}\text{Fe}_x\text{O}_5$ system

x	a, Å	b, Å	c, Å
0,6	9,61±0,05	8,31±0,05	3,81±0,05
0,8	9,95±0,05	9,12±0,05	3,86±0,05
1,0	10,746±0,002	9,922±0,002	3,849±0,002

Substitution of Ca^{2+} and Si^{4+} ions for Fe^{3+} and Y^{4+} ions results in an increase in electric conductivity and dielectric permeability and a decrease in the forbidden zone width of the samples of both phases. In the α -phase area the dielectric permeability stays practically invariable while the specific electric conductivity is increased by a factor of 10^2 . Such a considerable increase in electric conductivity indicates a decrease in current carriers concentration. It proves a decrease in the ionicity degree of the chemical bond of metal-oxygen in the crystal. In the β -phase area the specific electric conductivity grows insignificantly while the dielectric permeability increases more than twice.

YFeTiO₅-YFeSnO₅ system is single-phase. All the samples of $\text{YFeTi}_{1-x}\text{Sn}_x\text{O}_5$ are crystallized in pseudobrookite structure. Substitution of Ti^{4+} ions for Sn^{4+} ions does not lead to significant changes in the crystal lattice in the whole concentration interval (Fig. 4). Only a slight increase in the elementary cell volume is observed. It is explained by a difference in the effective ion radii of Ti^{4+} and Sn^{4+} . The parameters of the elementary cell are linearly dependent on the composition. However, the changes in the sample densities are more remarkable and linear (Fig. 4).

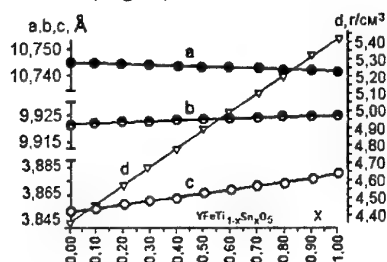


Fig. 4. Elementary cell parameters of

$\text{YFeTi}_{1-x}\text{Sn}_x\text{O}_5$ samples as a function of composition.

The elementary cell parameters of YFeSnO_5 [$a=(10.742\pm0.005)\text{Å}$, $b=(9.925\pm0.005)\text{Å}$, $c=(3.878\pm0.005)\text{Å}$, $z=4$, $v=413.450\text{ Å}^3$, $d_{\text{X-ray}}=5.516\text{ g/cm}^3$, $d_{\text{pycn}}=5.42\text{ g/cm}^3$] differ insignificantly from those of NdFeTiO_5 ($a'=10.599\text{ Å}$, $b=8.746\text{ Å}$, $c'=4.134\text{ Å}$) [5].

Comparison of Mössbauer spectra of Sn^{119} has indicated that isomeric shift of Sn^{4+} ions in SnO_2 is lower than that in YFeSnO_5 . It proves higher covalence degree of Sn-O bond in YFeSnO_5 than in SnO_2 . The same result was obtained for SnO_2 and Fe_2SnO_5 [5].

Substitution of Ti^{4+} ions for Sn^{4+} ions results in an increase in electric conductivity and dielectric permeability and a decrease in the sample forbidden zone width.

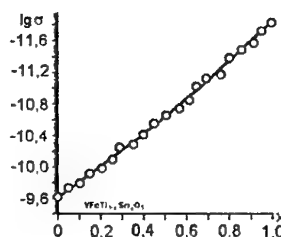


Fig. 5. Specific electric conductivity of $\text{YFeTi}_{1-x}\text{Sn}_x\text{O}_5$ samples as a function of composition.

References:

1. R.A. Grigoryan, G.G. Babayan, L.A. Grigoryan, Synthesis of compounds with sphene and pseudobrookite structure in low-temperature plasma. In "Khimiya i tekhnologiya redkikh i rasseyannykh elementov". Issue 2, Erevan: izd. EGU, 1981, p.269.
2. J.A. Speer, G.V. Gibbs, The crystal structure of synthetic titanite, CaTiOSiO_4 , and the domain texture of natural titanite. Am. Mineral, 1976, v. 61, p. 238 - 247.
3. C.L. Hollanbaugh, P.E. Rosenberg, Substitution of Ti for Si in titanite and new end-member cell dimension for Titanite. Am. Mineral, 1983, v. 68, No. 1-2, p.177 -180.
4. A.Wells, Structural inorganic chemistry. M: Mir, V. I, II, 1987, v. III, 1988.
5. D.A. Khramov, M.A. Glazkova, N.S. Ovanesyan and others, Cationic distribution and peculiarities of tin-containing pseudobrookite transition into the state of spin glass. Vestnik SPbGU, ser. 4, v. 3 (No. 18), p.118.

SOME ASPECTS OF THERMOEXFOLIATED GRAPHITE PRODUCTION AND ITS APPLICATION

**Kozhan O.P., Bondarenko B.I., Kurganskyi M.P., Sergienko O.A., Korsak Yu.V.,
Strativnov .V.**

The Gas Institute of National Academy of Sciences, Kyiv, Ukraine

Thermoexfoliated graphite (TEG) is a product of multistage thermal and chemical processing of natural graphite, capacity of which manufacturing in our country is the largest in Europe. The technology of TEG obtaining is investigated in detail [1,2].

The Graphite of the Zavallya Combine of type GAK-2 is oxidized by mixture of concentrated sulphuric acid and hydrogen superoxide. Then it is washed, vacuum-filtered and dried out. The technology of continuous drying of oxidized graphite is investigated in spouted bed device to decrease losses of sulphuric acid from bisulfate complex, and to avoid of a partial exfoliation of graphite. Air with temperature of 200°C serves as a drying agent. Drying machine provided with continuous drying of oxidized graphite from initial moisture of 40% to final one of 1-2%.

Exfoliation of oxidized graphite is realized in continuous gas furnace with temperature of working zone 900-1100 °C by original technology. The obtained material with bulk density of 3÷5 g/dm³ is forwarded to the bunker-store by pneumatic transport.

Thermoexfoliated graphite has ability to take some form without binding substances addition. The material can be transformed into sheets or volumetric products by rolling or pressing.

According to their chemical nature the graphite materials have chemical stability, high heat and electric conductivity, stability under radiation, low factor of friction, friendly to environment. Alongside with it, materials have elastic - plastic properties, which are important for sealing materials. Thus, products from TEG represent a new class of graphite materials with an unique set of useful properties, which make them rather perspective for the most various conditions of application, including extremal ones. A temperature range of their application without loss of properties is from cryogenic temperatures up to +2000°C (in vacuum and protective medium) and up to 600°C on air.

The most important technological operation in technology of a graphite sheet obtaining is rolling of a graphite powder. As a result of continuous rollings it is possible to obtain thin graphite foil (thickness 0,2÷1,0 mm), cardboard (thickness 1÷3 mm) and also a sheet reinforced with a wire-net or a metal foil. The graphite foil, besides its basic purpose, also serves as raw material for obtaining of more composite materials: sealing rings, waved graphite plaits, strings, etc.

Strength of articles depends on such properties as pressability of TEG source powders with different density, and from method of compaction. (Preliminary compaction TEG powder before pressing is compulsory operation, which is necessary to obtain the articles with the rather large size, in other case we need very big size pressform).

The diagram of pressing of noncompacted ($\rho = 5$ g/dm³) and compacted ($\rho = 100$ g/dm³) powder TEG is shown at fig.1. The Bending strength of pressed articles from same source powders is shown at fig.2.

The following conclusions can be done from above-mentioned data:

1. The preliminary compaction of a source powder decreases strength of pressed articles (twice up to $\rho = 1,8$ g/cm³).
2. Rings, which are pressed from preliminary winded graphite foil, are stronger than ones from non-winded powder.
3. The graphitic articles must be pressed up to 1,4-2,0 g/cm³ to have maximal strength (pressure - from a fig.1.)

Above-mentioned data are used for realisation of technology of graphite powder rolling, because the TEG rolling process can be considered as continuous pressing.

The rolling line for continuous graphite sheets producing of width 300 mm has been designed and erected.

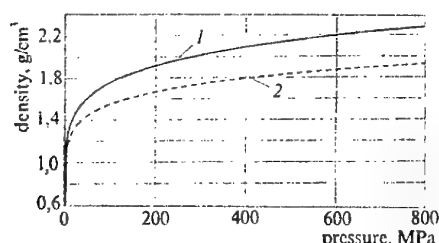


Fig.1. Pressing diagram for compacted and noncompact TEG powder:

- 1- noncompact powder (5 g/cm^3),
2- compacted powder (100 g/cm^3)

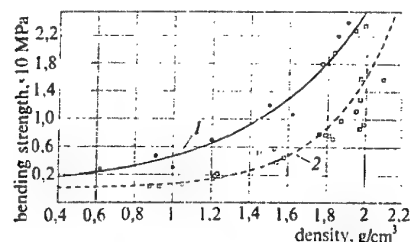


Fig.2. Bending strength of pressed articles with different density: 1- noncompact powder (5 g/cm^3), 2- compacted powder (100 g/cm^3)

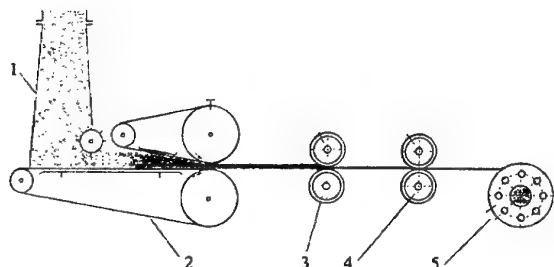


Fig.3. Scheme of graphite sheets production:
1 – loading hopper, 2- preliminary compacting rolling mill, 3 – first finish housing, 4- second finish housing, 5 – bobbin

The line consists of preliminary compaction mill and of two stands of rolls for finish rolling. The rough – rolling mill has two conveyors, which are located with angle $5 - 20^\circ$ to one another.

The noncompact TEG powder is dispensed to loading hopper by pneumatic transport, and then it is pressed between conveyors to $400-600 \text{ g/dm}^3$. Dependence of graphite sheets quality from rolling velocity, an angle between two conveyors, bulk density of TEG powder and other parameters have been investigated. It has been established that optimal rate of compacting on each stage of rolling takes place. If the rate of compacting is too much, the sheets have structure inhomogeneous like an ear swelling. This phenomenon has been also discovered in cases, when rolling velocity was too much. This is why the rolling velocity in

our experiments was not more than $0,5 \text{ m/min}$. Desired characteristics (thickness and density) of graphite sheet obtained after finish rolling. The rotating speed of all three pair of rolls has been coordinated in every cases of operation. Both conveyors have been provided with ribbons from stainless steel.

Under a rolling speed of $0,1 - 0,5 \text{ m/min}$ it was possible to obtain the elastic graphite sheets with a thickness from $0,2 \text{ mm}$ up to $2,0 \text{ mm}$ and density $800 - 1200 \text{ g/dm}^3$.

The tensile strength of a sheet is about $4 \div 6 \text{ MPa}$. It is found that the tensile strength of the sheets from compacted powder was much lower.

Described method gives possibility to obtain the gaskets and sealing articles. It is one of ways of the sealing materials deficit abatement.

Besides that we deal with TEG powder as very perspective sorbent for emergency spillage removal of different organic liquids from water surface and from the ground [3].

Literature

1. Махорин Е.Е., Кожан А.П., Веселов В.В. и др. Вспучивание графита в плотном и взвешенных слоях.// Химическая технология.- 1987.-№2.- с.43-49
2. Махорин Е.Е., Кожан А.П. и др. Способ получения терморасширенного графита и устройство для его осуществления. Авт. Свид. СССР № SU1664743 A1. Опубл. 23.07.91, бюл. № 27.
3. Бондаренко Б.І., Кожан О.П. Спосіб очищення ґрунту від нафтопродуктів графітовим сорбентом. Патент України UA41858A. 17.09.2001 р. Бюл. № 8.

ASSESSMENT OF THE STATE OF THE BINDER PHASE OF WC-Co CEMENTED CARBIDES BY THEIR FRACTURE TOUGHNESS

Loshak M.G., Alexandrova L.I.

Bakul Institute for Superhard Materials of the National Academy of Sciences of Ukraine, Kiev, Ukraine

For many years the performance of WC-Co-base composite materials was evaluated through the use of bending strength (R_{bm}) and impact strength which are an integral test result as the above characteristics essentially depend on specimen shape and size, porosity and crack-type defects, and surface layer state. The fracture toughness characteristics are free of this disadvantage.

Recently, a great number of papers were devoted to the fracture toughness tests to determine the strength and wear resistance of cemented carbides. Attempts have been made to correlate the fracture toughness of cemented carbides, on the one hand, and other mechanical characteristics, microstructure parameters and wear resistance, on the other hand. Analysis of theoretical and experimental studies on this problem and the authors' experimental results offers an idea of possible application of the fracture toughness to evaluate the quality of cemented carbide products.

To measure the fracture toughness of cemented carbides the values of critical stress intensity factor K_{IC} and of elastic energy release rate G_{IC} are used. In the present work the fracture toughness (K_{IC}) was measured in 3-point bending of a 5x5x35 mm beam specimen. Analysis of a variety of methods and results of K_{IC} tests of cemented carbides suggests that the specimen precracking procedure is one of the most important features of the K_{IC} measurement technique. Following methodical principles of the fracture mechanics, the test specimens should have initiated sharp cracks. In some cases tests specimens were precracked by electric-discharge-machining with the use of a tungsten wire or a copper foil. In doing so, from the notch tip, due to thermal action, fracture-initiating microcracks appear. The K_{IC} values for specimens containing an initial (fatigue) crack and for those containing an electric-discharge-machined crack are correlated. Therefore, the electric discharge precracking of a specimen, as a more simple procedure was used in the present work.

Two groups of WC-Co specimens of various Co content were tested. Cemented carbides of the first group were produced on the base of commercially

available tungsten carbide WC (tungsten reduction temperature = 1170K, carbide-formation temperature = 1720K); cemented carbides of the second group were produced on the base of high-temperature WC carbide (tungsten temperature reduction = 1470K, carbide-formation temperature = 2470K). Cemented carbides of the first group varied in Co-content but contained WC grains of the same mean size ($\bar{d}_{WC} = 2 \mu m$), whereas cemented carbides of the second group varied both in composition and in grain size.

Figure 1 shows the results of fracture toughness tests. It is seen that a batch of carbides containing WC grains of the same size shows a roughly linear increase in the K_{IC} value with Co content. The same is reported by other authors. An agreement between curve 1 and curve 2 (see Fig.1) suggests that the K_{IC} value does not depend on the carbide phase properties. With equal Co content, the grain size dependence of K_{IC} is either linear (curve 1, Fig. 2), or almost linear, but in all cases the K_{IC} value increases with \bar{d}_{WC} . Chermant and Osterstock [1] defined a linear relation between K_{IC} and both cobalt mean free path \bar{l}_{Co} with \bar{d}_{WC} being constant and square root of mean WC particle diameter with constant value of Co mean free path. Thus, the main parameters which control the K_{IC} value are the volume content of Co (V_{VCo}) and Co mean free path \bar{l}_{Co} which varies directly with \bar{d}_{WC} . The bending strength (R_{bm}) which is a standardized characteristic for the evaluation of cemented carbide quality, is also dependent of V_{VCo} and \bar{d}_{WC} values. But in case of V_{VCo} increase from 9 to 20% when $\bar{d}_{WC} = 1.4 \mu m$ R_{bm} increases by 13%, while K_{IC} increases by 30% [2]. On the other hand we have shown that R_{bm} essentially depends on the existence of pores which act as stress raisers, whereas the fracture toughness is unaffected by this factor.

Taking account of this evidence as well as the fact that R_{bm} essentially depends on the surface layer state, whereas K_{IC} does not, there is little sense in finding correlation between K_{IC} and R_{bm} .

It follows from the above statements that K_{IC} of cemented carbides is defined by a binding phase content and state. But the state of the binding phase which is a solid solution of tungsten and carbon in cobalt depends not only on its geometrical dimensions [$\bar{l}_{Co} = f(V_{VCo}, \bar{d}_{wc})$] but on its composition as well. An increase in the binding phase hardness due to the solution of an added amount of tungsten increases the K_{IC} value. The degree of tungsten and carbon solubility in cobalt essentially depends on the total carbon content in a cemented carbide and cooling conditions. Under otherwise identical conditions (V_{VCo} and \bar{d}_{wc}) variation of K_{IC} will show the binder phase state. The results of investigations into the optimization of conditions of strengthening cemented carbides by heat treatment and defining the mechanism of the process, may be taken as an example of the use of the fracture toughness criterion for the evaluation of the cemented carbide quality. It follows from the section through the Co-WC line in the ternary phase diagram of the W-Co-C system that by quenching sintered carbides one can control the degree of the solubility of tungsten and carbon in the binding cobalt phase. After quenching, the cemented carbide permeability decreases by 15-30% and the coercive force by 7-12% as compared with the initial state. These data and the results of X-ray analysis provide support for the increase of the tungsten content in the binder by 1-5% depending on the cemented carbide composition and heat treatment conditions. In turn, the change in the binder state correlates well with the value of the carbide fracture toughness. In some cases where other criteria remained unchanged before and after heat strengthening of cemented carbides, it was the degree of the K_{IC} value increase that

allowed the optimal quenching conditions to be determined. Specifically, this criterion enabled one to show the possibility and expediency of strengthening very fine-grained carbides by quenching.

Thus, K_{IC} which is specimen size independent represents a material property and allows comparison of fracture toughness of cemented carbides that are entirely different in composition and structure.

On the other hand, products of crack-containing cemented carbides of low plasticity are not intended for use under operating conditions. The K_{IC} parameter does not allow a unique determination of product performance. This follows from test results obtained on high-temperature WC-base cemented carbides: with equal V_{VCo} , \bar{d}_{wc} the K_{IC} values for alloys from conventional and high-temperature carbides are equal, whereas the durability of high-temperature WC-base cemented carbides is 3 to 5 times that of conventional cemented carbides.

At the same time when developing modern processes of cemented carbide production, which involve the use of new gaseous media when sintering, alloy additives, heat treatment, etc., the determination of the binder phase state from the K_{IC} parameter of the cemented carbide allows a controlled improvement of the process.

REFERENCES

1. J.L.Chermant, F. Osterstock Fracture toughness and fracture of WC-Co composites // Mat. Sci.-1976.- V.11.- P.1939-1951.
2. M.J. Murray, C.M. Perrott Fracture toughness of sintered carbide measured by the double torsion method // in Advances in Hard Material Tool Technology. Carnegie press. - 1976.- P.314-323.

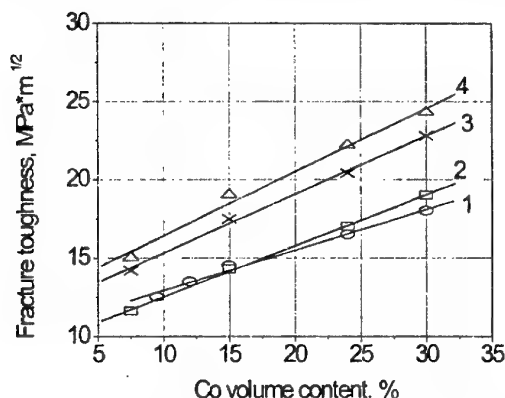


Fig. 1. Fracture toughness as a function of the Co volume content: 1 is the first group of cemented carbides, $\bar{d}_{wc} = 2 \mu m$; 2,3,4 are the second group of cemented carbides, $\bar{d}_{wc} = 2.5, 3.5, \text{ and } 9 \mu m$, respectively.

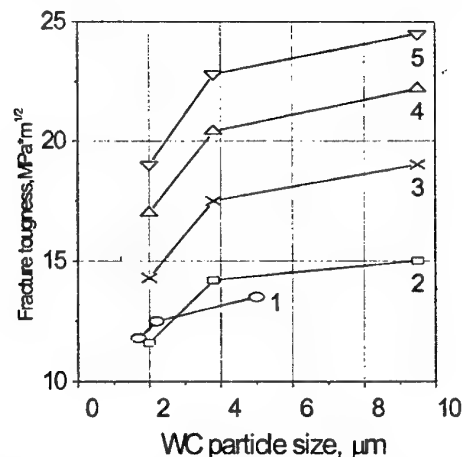


Fig. 2. Fracture toughness as a function of WC particle size: 1 is the first group of cemented carbides, $V_{VCo} = 10\%$; 2,3,4,5 are the second group of cemented carbides, $V_{VCo} = 8, 15, 24, \text{ and } 30\%$, respectively.

ECONOMICALLY REINFORCED CAST COMPOSITE MATERIAL (CCM) - SUCCESSFUL TECHNOLOGICAL DECISION FOR MASS MACHINE BUILDING

**Zatulovsky S.S., Kastornov A.G.⁽¹⁾, Zatulovsky A.S., Kosinskaia A.V., Kostenco A.D.⁽¹⁾,
Sharai E.V.**

Physico-Technological institute of metals and alloys of the NAN of Ukraine, Kiev, Ukraine

⁽¹⁾Frantsevich Institute for Problems of Materials science of the NAN of Ukraine, Kiev, Ukraine

Increase in longevity and reliability of car details and other machines in consequence of using of CM on the base of aluminium alloys is actual and important problem, all known giant automobile companies works in decision of which. The amounts of light metals using in autoindustry quickly increase. For instance, at present time a car of AUDI A8 mark consists at 34 % from aluminium details and only 40% of steel products. The alternatives of CM using for above mentioned purposes in practice does not exist. However expansion of CM using in autoindustry and other areas of mass machine-building be hold because of reinforcing elements high cost: SiC or Al₂O₃. In addition, fibrous crystals are scarce, expensive and give the disperse of characteristics.

The analysis of information from available literature has shown that oxides and row of compounds on their base have the high refractory, chemical stability in greater interval of the temperature and can be a perspective material for reinforcing of aluminium alloy. For study aluminosilicate be chosen, which have high temperature of melting (to 1900 °C), density (2200-2500 kg/m³) is not far to density of melted aluminium. The area of warm-up stability of aluminosilicate exceeds the aluminium alloys by 900 °C, which allows to forecast increasing of CM thermostability.

There are CM on the base of matrix alloy of mark AK12M2MrH, reinforced by particles from aluminosilicate (100-300 mcm) and silicon carbide (10-150 mcm). To define the perspective reinforcing systems, are organised comparative tribotechnical test of CM. For comparison, used samples which be sliced from piston body of "Икарыс" bus (the alloy type AK12M2MrH).

Tribotets carried by the friction machine MT68 at dry and fluid friction mode by conterbody from steel 65Г under normal loading P=6,3 kg/sm² and 12,7 kg/sm² and velocities of

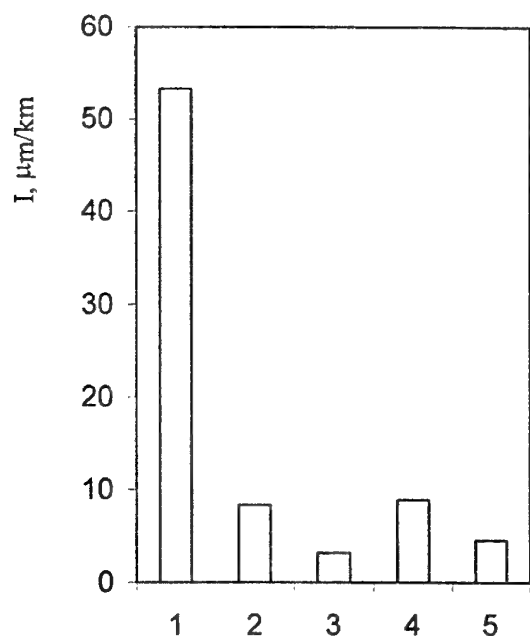
slide V=5, 10, 15 m/s. (Ill.1. P=6,3 kg/sm²; a) V=5 m/s; b) V=10 m/s).

Alloy	Contents of components, % of mass							Phase composition
	Si	Mg	Cu	Fe	Mn	Ti	Ni	
AK12M2MrH	11,2	0,58	2,08	1,01	0,33	0,078	0,95	α-solid solution; α(FeAlSi); CuAl ₂ needle-shaped and lamellar Crystals of primary Si
«Икарыс»	12,2	1,06	1,26	0,64	0,072	0,13	1,0	α-solid solution; CuAl ₂ Plates of primary Si

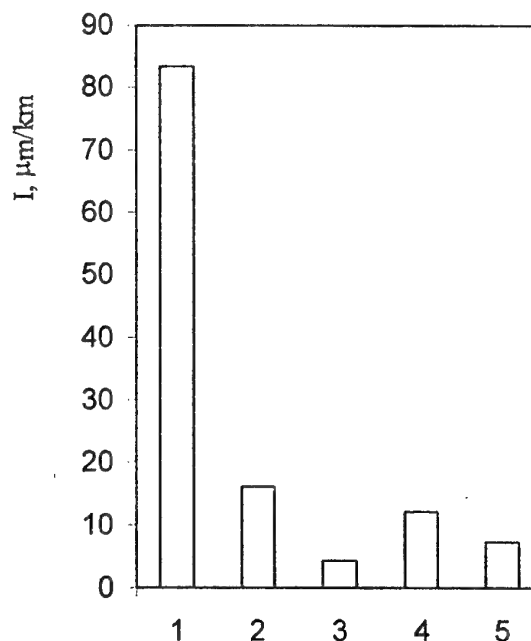
The results of the test have shown that reinforced CM with aluminosilicate particles and silicon carbide far less abrades, than piston from aluminium "Икарыс" alloy. From presented variants, the CM reinforced by aluminosilicate particles has preference in wear resistance. Herewith, the variant when content of reinforcing SiC phase is 5%, as well as at 3-4 % of aluminosilicate, both have closed value of wear-out. At increasing of amount of SiC in CM before 15%, then wearability reduction similar one then increase of aluminosilicate amount before 6-8%.

CM triboindex change with increasing of velocities of slide and loading (Ill.2): wear-out increase of the samples. At containing 6-8% of reinforcing phase, CM work more effectively. For event of contents 3-4% of aluminosilicate, with increasing of loading before 12,7 kg/sm² and velocities of slide over 10 m/s at conditions of dry friction, CM destruction are determined.

II. PERSPECTIVE MATERIALS OF FUNCTIONAL AND STRUCTURAL PURPOSES: POSSIBILITIES OF OBTAINING NEW LEVEL OF PROPERTIES



III. 1a.
P = 6,3 kg/sm²; V = 10 m/c.



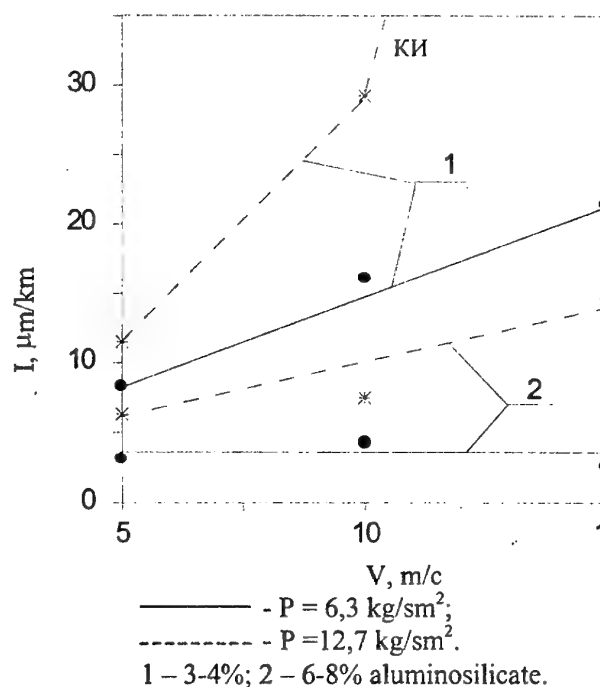
III. 1b.
P = 6,3 kg/sm²; V = 5 m/c.

1 – Poston alloy «Икарис»; 2 – 3-4% aluminosilicate; 3 – 6-8% aluminosilicate; 4 – 5% SiC; 5 – 15% SiC.

The identical results are got at tribotests of CM at friction with lubricant. The loss of mass and friction coefficient in these case decrease by 25-30%.

Intensive wetting of aluminosilicate grains by aluminium is determined by CM structure studies. The connecting zone formed as a result of partial interaction of phases. By means of X-ray spectral microanalysis of CM on interaction border of non-metallic component enrichment by copper is defined, but aluminium alloy – by silicon and calcium. Sometimes aluminosilicate grains impregnation by aluminium is discovered. Probably discovered phenomena's promote to increase of toughness of the reinforcing and matrix joining.

Data are indicating that economically reinforced materials at aluminium base are perspective for increasing of reliability and longevity of the piston-con-rod group of details of cars and tractors, others tribo-details in units of friction of mechanisms and agricultural machines, processing and others technology of mass machine building.



III.2

MECHANICAL PROPERTIES OF THE COMPOSITES IN-SITU BASED ON TITANIUM-BORIDE EUTECTIC

T.Ya. Velikanova⁽¹⁾, O.O. Bilous⁽¹⁾, A.A. Bondar⁽¹⁾,
L.V. Artyukh⁽¹⁾, S.O. Firstov⁽¹⁾, D. Miracle⁽²⁾

⁽¹⁾Frantsevich Institute for Problems of Materials Science of NAS of Ukraine, Kiev, Ukraine

⁽²⁾Air Force Wright Laboratory, Materials and Manufacturing Directorate, Wright-Patterson AFB, OH USA

The development of titanium-boride composites becomes noticed in last years and has been dominated by attempts to prepare materials by powder metallurgy techniques. Data on as-cast *in-situ* titanium composites containing borides is rather scarce. However, it is known that negligible porosity and high thermal stability of the eutectic structure can be great advantages of as-cast composites in comparison with powder-based approaches. For the binary Ti-B system, a uniform eutectic structure (Ti) + TiB is observed at the boron content of 7.5 at.%. The volume content of reinforcing phase in the binary alloy is ~10 %, and the hardness is found to be quite high at room temperature (1.5-2 GPa). The hardness decreases with increasing temperature to 0.25 GPa at 700°C.

It is known that the strength characteristics of alloys may be increased significantly by rational alloying. The influence of Al, Si, Ge, Sn, Zr, V, and Nb additions on the strength of as-cast eutectic (Ti) + (TiB) alloys was investigated in the present work.

The strength characteristics of the eutectic alloys under investigation have been estimated by hot hardness measurements in a vacuum in the temperature interval from RT to 800°C. Such an approach is shown to be a good express method of yield stress estimation. As it follows from our special experiment, the values of yield stress obtained by compression tests were in good correlation with the estimated yield stress as HV/3. The binary Ti_{92.5}B_{7.5} eutectic alloy was chosen for investigation as a basis. The alloying with Al (from 4.3 to 12.8 at.%) marked increase in hardness in the full temperature range under investigation. Thus, for the alloy containing 12.8 at.% Al, at RT the hardness is by two times higher and at 700°C it is four times higher than for the base binary eutectic alloy. The appearance of α_2 phase in the alloy at 30 at.% Al increases the hardness to 4.2 GPa at RT and to 2.8 GPa at 700°C. Taking into account that Al is a promising alloying addition, the eutectic alloy Ti₈₄Al_{8.5}B_{7.5} containing 10 at.%

Al in the matrix was chosen for investigation as a base ternary alloy.

The influence of two groups alloying additions (*d*- and *p*-elements) on mechanical properties of the binary Ti_{92.5}B_{7.5} and ternary Ti₈₄Al_{8.5}B_{7.5} eutectic alloys was investigated. Alloying of the binary (Ti) + (TiB) eutectic alloy (composition Ti_{92.5}B_{7.5}) by *d*-elements (such as V and Nb) increases the hardness at temperatures up to 500°C (to ~4 GPa for V and to ~3 GPa for Nb at RT), while additions of *p*-elements (such as Ge and Sn) to the binary eutectic alloy increased the hardness in the full temperature interval under investigation. Ge was found to be somewhat more effective in hardening than was Sn (e.g. 3.8 GPa at RT and 0.7 GPa at 700°C for the alloy Ti_{87.4}Ge_{5.1}B_{7.5}). The maximal values of hardness are obtained in alloys containing intermetallic phase together with boride.

The contribution of each alloying component under investigation to hot hardness was analyzed. The relative influence of fourth component additions on the hardness of the ternary eutectic alloy Ti₈₄Al_{8.5}B_{7.5} is almost the same as the influence of the third one on the hardness of the binary alloy Ti_{92.5}B_{7.5}. As a result of the joint influence of the fourth component and Al, the hardness of quaternary alloys reaches significantly higher values, e.g. 4.5 GPa at RT and 2.3 GPa at 700°C for the alloy Ti_{78.9}Al_{8.5}Ge_{5.1}B_{7.5}.

The metal matrix was shown to play a significant part in the high temperature strength properties of eutectic composites. The starting temperature of sharp softening for the eutectic alloy coincides with that of its matrix. Aluminium has the best influence on this temperature.

Acknowledgements. This research was supported by the Air Force Office of Scientific Research (USA) under the STCU Project P-060. The authors thank D.B. Borysov, M.P. Burka, P.S. Martsenyuk, T.O. Shapoval, T.I. Tsyganenko for technical assistance.

EFFECT OF OXYGEN MODIFICATION AND HDDR-PROCESS ON ELECTROCHEMICAL CHARACTERISTICS OF METAL HYDRIDE ELECTRODES BASED ON TITANIUM-NICKEL ALLOYS

Saldan I.V., Zavaliiy I.Yu.

Karpenko Physical-Mechanical Institute of the NAS of Ukraine,
5, Naukova Str., 79601 Lviv, Ukraine, e-mail: zavaliiy@ipm.lviv.ua

Alloys of the Ti-Ni system were the first materials studied as hydride electrodes in secondary chemical power sources [1]. Hydrogen absorption capacity of the Ti_2Ni intermetallics is about 2.9 at.H/f.u., which value corresponds to 498 mA×h/g discharge capacity when the electrochemical desorption of hydrogen completes. However, practically observed discharging capacity of electrodes on the basis of Ti_2Ni is much lower, 160–200 mA×h/g. Moreover, during 5–10 charge-discharge cycles the capacity substantially drops. So, this deviates the research interest from this class of compounds onto other systems. Nevertheless, low cost of the Ti-Ni alloys and the possibility of enhancement of their technical characteristics remain them in the list of prominent electrode materials for Ni-MH batteries. This work is further studies (see also [2]) of oxide modification influence on charging-discharging of metal hydride electrodes on the basis of Ti_2Ni compound. We applied also the preliminary treatment by the hydrogenation - disproportionation - desorption - recombination (HDDR) route for the study of its influence on electrode characteristics of alloys through increase of their homogeneity and microstructural uniformity. This technology is applied in preparation of permanent magnets on the basis of intermetallics of RE metals. The Ti_2Ni alloys easily disproportionate in hydrogen when heated above 200 °C, this allowed us to propose the HDDR technology for preliminary treatment of metal hydride electrode materials.

The synthesis of hydrides of $Ti_4Ni_2O_{0.3}$, $Ti_{3.8}Zr_{0.2}Ni_2$, $Ti_{3.8}Zr_{0.2}Ni_2O_{0.3}$ alloys and their electrochemical charge-discharge testing were conducted according to procedures described in [2]. The only phase constituent in $(Ti,Zr)_4Ni_2O_x$ alloys was found to be the η -phase with the structure of Ti_2Ni (η -Fe₃W₃C) type. Thanking to the insertion of oxygen atoms into crystal lattice and their influence on absorbed hydrogen, oxide-modified alloys are characterised by enhanced hydrogen desorption and increased pressure of the p-c-T plateau [3]. We suggested that oxide-stabilised IMC could have better electrochemical discharge characteristics as well.

The results of charge-discharge tests showed that capacity of the $Ti_{3.8}Zr_{0.2}Ni_2O_{0.3}$ -based metal hydride electrode is almost twice higher than that of oxygenless alloys. These results correlate with data for $Ti_4Ni_2O_x$ ($x=0; 0.3$) alloys and indicate that the rise in capacity under conditions of oxide modification is general for this type of alloys. Such modification is obviously prominent for other types of intermetallics used as metal hydride electrodes, which structures could accommodate atoms of oxygen or other non-metal elements.

The following regime of the HDDR process was applied for the $Ti_4Ni_2O_{0.3}$ compound: disproportionation in hydrogen – 700°C, 10 h; desorption-recombination in vacuum by heating up to 750 °C with 1 h dwelling. As shown by X-ray diffraction, the disproportionation did not result in complete degradation of the η -phase into TiH_x and $TiNiH_x$ (Ni). This confirms that oxide modification complicates the disproportionation process. After recombination we received a material, which X-ray diffraction pattern showed better homogeneity and microstructural uniformity of the sample. The discharge capacities of starting, disproportionated and recombined samples were studied during 10 cycles. A single phase $Ti_4Ni_2O_{0.3}$ alloy, obtained through the HDDR processing, during 10 cycles showed 20–40 % higher discharging capacity with much lower drop compared to the non-treated $Ti_4Ni_2O_{0.3}$ alloy (265–150 mA×h/g). This fact is an indication of the positive influence of the HDDR – process on electrode characteristics of the alloy through the refinement of its microstructure.

1. Buchner H.. *Energiespeicherung in Metallhydriden*, Springer, Vienna, 1982.
2. Zavaliiy I., Wojcik G., Mlynarek G., Saldan I., *et al.* Phase-structural characteristics of $(Ti,Zr)_4Ni_2O_{0.3}$ alloys and their hydrogen gas and electrochemical absorption-desorption properties // *J. Alloys and Comp.* 2001. Vol. 314. P. 124–131.
3. Takeshita H., Tanaka H., Kiyobayashi T., Takeichi N., Kuriyama N. Hydrogenation characteristics of Ti_2Ni and Ti_4Ni_2X ($X=O,N,C$) // *J. Alloys and Comp.* 2002. Vol. 330–332. P. 517–521.

WORK UP OF A NEW POWDERED MATERIAL FOR SUPPORTS OF SUBMERGED ELECTRIC MOTORS

Kurilov G.V.

The open joint-stock company Special Design-technology Office of Submerged Electric equipment
"Potential", Kharkov, Ukraine

The loss control on friction and deterioration of mobile articulations of machines and gears is one of most serious problems of modern engineering.

The in-service experience of the plant electro-rotary pumps (PERP) has shown, that the thrust bearings have poor reliability [1]. To ensure indispensable reliability of activity of parts and clusters in any conditions, it is important to pick up an optimum structure of an antifriction stuff.

Now clusters of friction are equipped by sliding bearings, which one can work both with lubrication, and without it. The bearing boxes working with lubrication, have some essential lacks (not a constructibility, sensitivity irregularities in lubrication etc.), they cannot be used for activity in extreme conditions. In such conditions specially relevant for modern engineering, can work self-lubricating bearing boxes received more often by powder metallurgical techniques.

The powder metallurgical techniques give large capabilities for creation high-performance composite self-lubricating stuffs. They allow is more differentiated to operate antifriction properties, integrating in one stuff of carrier the basis of indispensable strength and plasticities from a miscellaneous kind by dopes playing a role of firm lubrications, or dopes actuating processes of formation of indispensable frames of a stuff and secondary frames rubbing layers.

Traditionally basis metallic self-lubricating stuffs is cuprum, which one gives protecting films of oxides, has moderate predilection to grasping, provides fast run-in. For increase of efficiency of cuprum it dope by members, which one will derivate with cuprum solid solution (tin, nickel, iron, aluminium etc.) [2]. The greatest distribution was received stuffs which are generatrix as a result of doping of cuprum, on a steel substrate with sintered bronze layer, porous bronze, impregnated lubrication, and bronze-graphite stuffs.

The porous tinned bronze usually contains from 6 up to 12 % of tin. Bronze has optimum properties (keeping it within the limits of 9÷11%). At such structure the formation of frame of solid solution with high strength properties is provided. Bronze-graphite stuffs contain from 1 up to 25% of graphite depending on the working conditions of stuffs. Whereas the graphite does not interact neither with cuprum, nor with tin, it esteem as the component, executing role of firm lubrication. The film is permanently restored at mechanical damages to separate surface segments of friction.

The properties of bronze and bronze-graphite can be considerably improved by doping by such components as a titanium, nickel, lead, zinc etc., and also introducing of matters playing a role of firm lubrication [2].

The efficiency of operating of firm lubrication keeping in self-lubricating stuff is determined by capacity to derivate on a friction surface solid, permanently restored separating layer so-called secondary frames or film handicapping originating and development of grasping.

The introducing of firm lubrications in sintered antifriction stuffs began from application of graphite [2]. The graphite renders specific influencing on properties of a stuff: than lower is the contents of graphite, a stuff for activity especially is suitable at high loads, but than higher is the contents of graphite, the more perspectively stuff for activity at high speeds of friction with small loads.

The disulphide of molybdenum MoS_2 concerns to number of conventional most studied firm lubrications, the greasing operating which one is conditioned by features of a crystalline constitution (lamination) and series of other specific properties - high adhesion to metallic surfaces and small energy of a cleavage [3].

The desire to receive an antifriction powdered material serviceable at different modes of friction, results that in stuff enter some components improving the same properties. So, graphite enter together with a disulphide of molybdenum and boron nitride. Thus the mass lobe of graphite reaches 0,5÷5,0; disulphide of molybdenum - 0,5÷5,0; and boron nitride - 0,4÷2,0%.

The expediency of the simultaneous introducing of several firm lubrications is explained that they variously behave in the different operation conditions and by that supplement one another.

The poor reliability of bearing assemblies has resulted in necessity of mining of a new antifriction stuff from several variations of powdered materials on the basis of cuprum: БГр4 ТУ16-509.015, БрОГ10-1, МКБр2 and БрОГ10-2 ТУ16-538.393-83, and also БрОГ10-2 with the component 2% MoS₂ and 4% MoS₂, the characteristics which one met to values: a porosity - 7÷10%; density - (7,7÷7,8) · 10³ kgs / m³; hardness - 50÷80 % HB.

The set forth above stuffs were subjected to lab tests. The tests were conducted on supports of a new design at rotation rate $n=50 \text{ s}^{-1}$ (3000 promptness in minute) and load $P=1800\div2100 \text{ N}$, that has compounded unit load on a support 1,2÷1,5 MPa and corresponds to actual conditions of loading of a support.

Determining parameters were a friction coefficient (μ) and temperature apart 0,2÷0,5 mms from a zone of friction (t). The results of tests compared to serially used supports made by a method of a casting of bronze БрО4Ц4С17 with babbit cover by depth 1÷1,5 mms with a «playing leg» and without it.

The outcomes of the conducted lab tests of supports from powdered materials БГр4, МКБр2, БрОГ10-1 and БрОГ10-2 in matching with serially used have shown following:

- by the highest friction coefficient the stuff БГр4 ($\mu=0,04\div0,06$; $t=60\div80^\circ\text{C}$) differs;
- the intensity of wearing of a stuff БГр4 is much higher, than other investigated stuffs;
- with increase of load the friction coefficient for all studied stuffs decreases;
- for serially used supports a friction coefficient $\mu=0,01\div0,03$; and temperature in a zone of friction $t=30\div50^\circ\text{C}$.

The analysis of outcomes demonstrates, that by the best characteristics differ БрОГ10-2, and also МКБр2 and БрОГ10-1. However, having a good wear resistance as contrasted to babbit, these stuffs have a friction coefficient approximately in 2 times above, than serially used supports. As is established [2, 3] earlier, one of ways of a decrease of a friction coefficient is the introducing in a stuff of the components of a disulphide of molybdenum within the limits of 2÷4% with a different variation of the components of graphite.

One more series of lab tests was conducted, which one has shown, that the component has not given 1÷2% MoS₂ in БрОГ10-2 of an appreciable decrease of a friction coefficient, though its decreasing was watched.

Then by a trial and error method and variations of members, having taken for the basis the stuff chemistry Cu=82%, Sn=5%, Zn=5%, C=1%, MoS₂=2% was obtained a stuff having friction coefficient $\mu=0,01\div0,02$ (equal friction coefficient of a pair steel - babbit) following chemistry, in large-scale mining in %: tin - 1,5÷9,0; a boron - 0,05÷0,1; graphite - 1,0÷3,0; zinc - 1,0÷4,0; a disulphide of molybdenum - 1,0÷3,0; oxide of a boron - 0,7÷1,0. The stuff has received notation ДО4Ц4Гр2Мс3Б [4].

As the practice used in supports of thrust bearings a powdered material ДО4Ц4Гр2Мс3Б has shown differs by a high wear resistance, with a low friction coefficient (0,01÷0,03) and provides temperature in a zone of friction 40÷60°C. The decrease of a friction coefficient is conditioned by the introducing of firm lubrications - graphite and disulphide of molybdenum, and also application of a method of cladding of a disulphide of molybdenum at a sintering.

1. Исследование надежности упорных подшипников протекторов ПЭД. Отчет ХИМЭСХ, Харьков, с. 20.
2. Федорченко И.М., Пугина Л.И. Композиционные спеченные антифрикционные материалы. Киев, «Наукова думка», 1980, с. 400.
3. Исследование возможности применения в погружных электродвигателях деталей, полученных методом порошковой металлургии. Отчет СКТЕ ПЭ НОЗ.85041-373. Харьков, 1987, с. 101.
4. Гребень А.М., Курилов Г.В. и др. А. с. 1455743 (СССР) от 01.10.88. Спеченный материал на основе меди и способ его получения.

SOME PECULIARITIES OF TITANIUM ALUMINIDE PRODUCING BY THE METHOD OF ELECTROSLAG REMELTING

Ryabtsev A.D., Troyansky A.A., Pashynsky V.V., Mastepan V.Yu.

Donetsk National Technical University, Donetsk, Ukraine

One of most perspective directions in the field of development of titanium alloys, with high strength and simultaneously with high thermal stability widespread in the world in last years is the development of alloys on the base of intermetallides Ti_3Al and $TiAl$. They may be used in aircraft engines, explosion engines and as material for structural applications for static loading in high-temperature environment. Intermetallides of $TiAl$ system are more light than nickel and titanium superalloys, they don't demand the protection from high-temperature oxidation, more cheaper and have rather high strength (ultimate tensile strength at 1473 K is more than 100 N/mm²). They may be the competitors to nickel superalloys not only for aerospace applications, but in other branches of industry. Main disadvantages of titanium aluminides are the low plasticity, that is not correspond to necessary level of fracture toughness, and difficulties of processing of parts with complicated shape.

Wide application of alloys on $TiAl$ -base is restrained by the absence of effective and non-expensive technologies of their manufacturing. Producing of $TiAl$ -based alloys deals with difficulties, connected with differences in melting and evaporation temperatures and densities of components. Technologies of their manufacturing is very complicated and multi-stage. Methods of powder metallurgy in combination with mechanical alloying demands very prolonged grinding of components and prolonged treatment at high pressure and temperature.

In current time there are small quantity of publications about application of technologies of especial electrometallurgy, electroslag remelting in particular, to produce the alloys of $Ti-Al$ system. Development of rather simple and non-expensive methods of $Ti-Al$ system intermetallides is very actual, but not solved problem now.

Analysis of technological possibilities of ESR process permits to make an assumption concerning possibility of its application for $Ti-Al$ alloys manufacturing. In current work the results of using of chamber electroslag remelting process for this purpose are described.

Electroslag remelting was carried out in chamber ESR furnace A-550, in copper water-cooled crucible 115 mm in diameter and 450 mm in length. Water-cooled chamber was mounted directly on the top of the crucible. System was designed with corresponding sealing to provide vacuum or excessive pressure of gases in working space. Before melting the chamber was vacuumed, and after that filled by argon. During melting the excessive pressure of argon 15 kPa approximately was maintained to compensate the leakage through different seals.

To carry out the experiments, the combined titanium-aluminium consumable electrodes were used. In first series of meltings titanium part of electrode was made from pressed rectangle blocks 30x40x200 mm of titanium sponge (TG-120 grade). Average density of pressed material was 2810 kg/m³. Aluminium part of electrode was made from electrotechnical aluminium plates.

In second series of experiments titanium part of electrode was made from block of titanium rods 16 mm in diameter of VT1-0 grade. Aluminium part of electrode was made from electrotechnical aluminium rods with triangle cross-section. This rods were mounted uniformly around titanium part of electrode.

The powder of CaF_2 with high purity and cheap of metallic Ca were used as the base of flux. CaF_2 was annealed at temperature 973 K during 3 hours. Flux was melted directly in crucible with using of "solid" start. The calcium evaporates from the mixture $CaF_2 - Ca$ during its melting and vapours of calcium decrease the partial pressure of oxygen and nitrogen above the slag pool to the magnitude 10^{-13} kPa.

Manufactured ingots had smooth lateral surface and porosity in top part of ingot. Inner surface of pores is clear and has not the differences in color with another metal. Therefore there is not the oxidation inside the pores. Obviously porosity has shrinkage nature. Metallographic investigations show that metal of ingot is rather uniform. Inclusions of aluminium and titanium are absent. Traces of cutting tool on the surface of machined ingot show that metal has residual plasticity at room temperature, but chips, formed

during cutting have the appearance of uniform powder with bright faces. Phase composition of material was investigated by the method of X-ray structural analysis. Analysis of obtained result shows that main phase is the titanium aluminide $TiAl$. But some of reflections on diffractogram could not be identified as belonging to $TiAl$. Most probable second phase is $TiAl_3$. This conclusion is confirmed by the results of metallographic analysis that determines the presence in structure of alloy matrix the small volume (2-5% of sample section surface) of second phase precipitation. They are located on boundaries of dendrites of matrix phase. Measurement of density and resistance to high-temperature oxidation shows that obtained material has the magnitude of these characteristics, corresponding with published earlier for γ -titanium aluminide.

Obtained ingots were cut along the central longitudinal axis. One half of every ingot was used to determine chemical composition (see table), another – to study the macro- and microstructure in cast condition.

Table
Chemical composition of experimental ingots

Ingot	Location of testing at height of ingot	Al content, %	Ti content, %
Ingot #1	Top	51,9	45,5
	Middle	52,2	46,13
	Bottom	43,6	54,5
Ingot #2	Top	54,5	40,0
	Middle	46,8	47,9
	Bottom	37,6	59,75

Obtained ingots have high porosity and brittleness and they can not be used directly for producing of different parts. This material may be considered as semi-product. Therefore on next step of investigation the attempt to investigate the effect of treatment by high pressure at increased temperature on structure and properties of $TiAl$ was made. Peculiarities of behavior of materials of this type at temperature-deformation influence are investigated insufficiently now, but results of preliminary investigations give the evidence of possibility to increase the complex of mechanical properties in result of such treatment.

In order to do this, the material of ingots was subjected to grinding in ball mill to the powder with particle size 3-7 microns. Plates 3x10x40 mm in size were made from the powder by pressing. After that they were subjected to sintering at temperatures 1533 (regime 1) and 1693 K (regime 2) and at two-

step regime (2 subsequent treatment at 1533 and 1693 K with intermediate cooling) (regime 3). In all cases specimens were cooled after sintering with furnace (cooling rate 80-100 K/hour). Samples after sintering at 1693 K had the traces of partial melting, despite theoretical temperature of solidus line is equal to 1723 K. It may be explained by the influence of pressure (500 kgf/cm²), that may cause the decreasing of phase transformation temperature.

Specimens, sintered at different regimes were subjected to phase X-ray analysis, microhardness measurement and microstructure examination. All specimens have two-phase structure with residual porosity. They consist of mixture of γ and α_2 phases. The most coarse precipitation of α_2 -phase (30-35 microns) was formed in specimens, sintered in accordance with regime 1. It is 3 times higher then after regime 2 and 2 times higher then in specimens sintered at regime 3 (size of $TiAl_3$ precipitations 15-20 microns). These samples have large number of fine pores and microhardness of them is decreased. The minimal porosity was found in specimens after regime 2. They have most fine precipitations of second phase (5-10 microns). The refining of precipitations may be caused by process of phase transformation during the partial melting of material at high temperature, crystallisation of molten metal and decomposition of solid solution during cooling. These complex processes cause the changes in structure of sintered material.

To confirm the assumption concerning the phase composition of sintered specimens, the X-ray analysis was carried out. In sintered material after all regimes the considerable quantities of oxides and another impurities were not found. Only two main phases: $\gamma - TiAl$ and α_2 were determined.

CONCLUSION: Fulfilled work confirms the principal possibility of manufacturing of ingots of intermetallic compounds on $TiAl$ base by the method of electroslog remelting in chamber furnace under active flux. Obtained ingots have typical for cast material structure and increased porosity (up to 15%). Cast metal has high chemical and structure homogeneity. It is confirmed by the results of chemical, X-ray, metallographic analysis and microhardness test results.

The effectiveness of using of high-temperature sintering under external pressure for treatment of such materials as titanium aluminides with low plasticity was confirmed.

DEVELOPMENT OF ADVANCED TECHNOLOGIES FOR PRODUCTION OF HARD ALLOY ROLLS FOR MODERN ROLLING MILLS

Pashynsky V.V., Sydorenko D.G.⁽¹⁾, Kulik A.I.⁽¹⁾, Kashyryn V.P.⁽¹⁾

Donetsk National Technical University, Donetsk, Ukraine

⁽¹⁾Scientific Production Company "Donix", Donetsk, Ukraine

SPC "Donix" first in Ukraine begins the production of hard-alloy rolls of disc type up to 215 mm in diameter and 35 kg weight [1]. Technical-economical characteristics of rolls producing and their performance depends on technological scheme of their manufacturing. Traditional sintering (TS) is the most simple and non expensive method, but when large-size parts are produced, some technological problems appear. It is very difficult to obtain the low porosity and high precision of semiproduct size. Most effective technology from the point of view of maximal service properties is the hot isostatic pressuring (HIP). But its realization demands special complicated and expensive equipment. It increases the production cost. Therefore development of new technologies is problem of great practical interest. One of potentially effective technologies is the method of hot vacuum pressuring (HVP).

In this case the hydraulic press is used to produce the necessary loading and formation of semiproduct passes in mold with high precision. Besides lower cost of equipment this process is more flexible because complex regimes with programmed variations of temperature and pressure may be fulfilled.

Therefore two different ways of technology development were chosen by specialists of SPC "Donix" on pilot scale study of investigations:

1. Development of improved technology of sintering on the base of using of powder mixtures with controlled granulometric composition and chemical composition.
2. Development of new modifications of HVP process.

Used for traditional sintering new hard alloy materials with regulated granulometric composition and additions of small volumes of special carbides permit to produce rolls 170 mm in diameter with weight up to 15 kg with high mechanical properties and low porosity. Developed material "TC-15" on the base of tungsten carbide with cobalt-nickel binder content 15% permits to start the commercial manufacturing of disc rolls for finishing stands of modern rolling mills.

On the base of obtained experience the second stage of works was started. Main aim was the

development of new technology of HVP. To realize this process, the special unit for hot pressuring was designed and built. It has the following features:

- Process may be carried out in vacuum or protective atmosphere.
- Special design of resistive heater from electroconductive carbon composite material is used. Shape of heater provides the uniform temperature field in working space of unit.
- Press auxiliaries are made from high-strength carbon filament composite. It provides producing of the semi-product with minimal machining tolerance, long working life of auxiliaries and small specific contribution of their cost to overall productive cost.
- Control system permits to regulate with high precision the magnitude of pressure and velocity of its changing.

Technical equipment of the shop includes the section of powder hard alloy mixtures preparation. Producing of large size rolls 215 mm in diameter and 35 kg in weight demands the solving of series of difficult problem. Further improvement of developed materials for traditional sintering permits to overcome the many of shortcomings of this method and now rolls with diameter 215 mm and 85 mm in width are produced in commercial scale. But main problem of this technology is wide range of machining tolerances and increased part of semi-products with defects of macrostructure. Using of HVP permits to avoid these problems, but another problems may arise. In materials with high content of binder the non-uniform distribution of it may form during pressuring. This structure has decreased resistance to crack growth and fatigue life. To solve this problem, special investigation problem was fulfilled. It is established that to obtain the uniform structure, the velocities of temperature and pressure increasing must be strictly controlled in accordance with special program. New regimes were developed and this variant of HVP obtained own name "sintering, activated by external pressure" (PS). In result of implementation of new technology, manufacturing of large-size

parts with high quality by the PS method was started too.

Now there are two variants of technologies of large rolls production:

- Sintering of materials with regulated granulometric composition (TS-RG)
- Sintering, activated by external pressure (PS)

Therefore two types of rolls are now in commercial exploitation. Certain quantity of rolls before developing of PS-process was produced by ordinary HVP method. In order to analyze of advantages and shortcomings of both technologies, the laboratory investigations and monitoring of industrial experience of different rolls using was carried out. The criteria of roll durability, such as the volume of rolled metal per 1mm of diameter decreasing in result of roll grinding and overall volume of rolled metal for the period of working life of roll, are integral and demand very prolonged time to determine. To obtain the responsive information, the investigation of groove profile after every working cycle of roll was fulfilled. Preliminary analysis shows that there are most critical stands on every rolling mill with maximal wearing of rolls. Therefore rolls from this stands were used for monitoring of wearing. For example, most severe conditions for 170 mm rolls take place during rolling of wire rod 5,5 mm in diameter and maximal wearing is on finish stand (stand #28 for rolling mill PC-1 of Krivoy Rog integrated metallurgical plant). Investigations were fulfilled on rolls, produced by TS-RG, HVP and PS method. Results of exploitation of rolls of firm "SANDVIK" were used as comparative.

Initial measurement was fulfilled by photographing of groove profile with x10-20 magnification with using of digital camera EPSON-600 (resolution 860x1200). The error of linear dimension measurement was less than 0.01 mm. Visual evaluation of wear was fulfilled by the comparing of initial profile and profile after working cycle. To obtain quantitative information, the following characteristic were measured:

- Increasing of groove cross-section area after working cycle S (mm²)
- Maximal linear deviation of profile after working cycle from initial h (mm)

Measurement was fulfilled with using of special software package of image analysis "IMAGE TOOL 2.0". After the specific characteristics per 1000 ton of rolled metal were calculated.

The linear wearing of working surface is 10-15% higher than characteristics of best world products. But despite of difference, value of wearing

much lower than recommended magnitude of removed layer in result of rolls grinding.

Analysis of obtained results permits to conclude:

1. Material, obtained by TS-RG process has more equilibrium structure with high degree of carbide phase recrystallization and uniform distribution of binder. It provides the high resistance to thermal fatigue wearing and resistance to brittle fracture. But for this method the deviations of density and porosity are higher than for HVP and PS methods.
2. Material, obtained by HVP has high stability such parameters as density and hardness and very low porosity. But for increased content of binder, the non-uniform distribution of them may occur.
3. Implementation of PS-process permits to obtain the increased quality in comparison with HVP-process with very narrow tolerances for main parameters and uniform microstructure

Tolerances for PS process are shown in table

Table. Parameters of material TC-15 for rolls, processed by PS-method

Parameter	Nominal value	Tolerance
Bending strength, kgf/mm ²	285	+/-10
Hardness, HRA	87	+/-1
Density, g/cm ³	14,00	+/-0,05
Velocity of ultrasound waves m/s	6430	+/-15

Therefore, developed technological processes TS-RG and PS permits to produce the high-quality rolls up to 215 mm in diameter with productive cost lower than for HIP- process. In order to determine the advantages and shortcomings of new variants of processes, further collection of information about results of commercial working of items is necessary.

REFERENCES

1. A.G. Manshylyn, V.V. Nazarenko, S.V. Trukhanov and other. The certain aspects of organization of the hard alloy rolling mills producing by the method of the hot vacuum pressuring.- *Metal i litie Ukrainy*, 2000, #5-6 pp. 38-40.

INFLUENCE OF HIGH PRESSURE AND NITROGEN ON STRUCTURAL KINETIC MODIFICATIONS IN AUSTENITE OF Fe-Cr-Mn-Ni ALLOY

Bilousov M.M.

(Donetsk Phys.& Tech. Institute of the NAS of Ukraine, 72. R. Luxemburg St., Donetsk, 83114,
Ukraine. e-mail: bil.@hpress.dipt.donetsk.ua)

Abstract. A plastic strain at stage of fragmentation and phase ($\gamma \leftrightarrow \alpha$) transformation under high pressure is accompanied by structural - kinetic modifications in austenite of high-nitrogen steels, that promotes shaping of elements and complexes with nanocrystallstructure.

Initiation of phase transformation in metastable alloys by way of straining under high-pressure promotes shaping of materials with nanostructures [1,2]. The metastable state has been formed by a straining between diamond pyramids with superposition of a shift component [3,4]. The chamber (Bridgeman's method), was used enabling: a) to distort a material immediately in clusters of the testing machine; b) to conduct structural - kinetic researches immediately in the chamber of a microscope and of a diffractometer. The pressure was evaluated using loads on pyramids and was calibrated using displacement of R_1 and R_2 lines of luminescence of a ruby.

The results of experiment have shown, that: Dependence of force F on depth h of an indenter intrusion has stage character (fig.1): a) $P \leq 1 \text{ GPa}$ -stage of elastic behaviour; b) $P \leq 10 \text{ GPa}$ -stage of a plastic strain with fragmentation of elements of structure; c) $P > 10 \text{ GPa}$ -stage of structural - phase strengthening and secondary elastic behaviour.

After straining up to $P \leq 10 \text{ GPa}$ the alloy remained single-phase (γ -phase) in both ranges of pressure variation and density of nitrogen ($0.06 \div 0.57\% \text{ N}$). The α -phase was not registered by means of X-ray diffraction, however up to 10% of a magnetic phase (recalculated on $\alpha\text{-Fe}$) had been found.

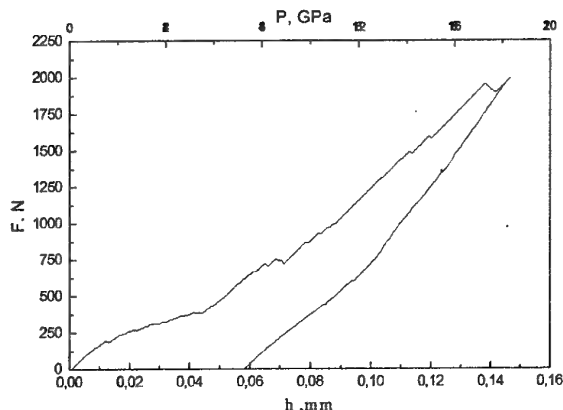


Fig.1 Dependence of force F on depth h of an indenter intrusion.

The lattice constant monotonically diminished with pressure for all range of density of nitrogen. The widening and intensity of lines (111) and (220) is nonmonotone varied, that correlated with beginning of fragmentation of elements of structure (fig.2).

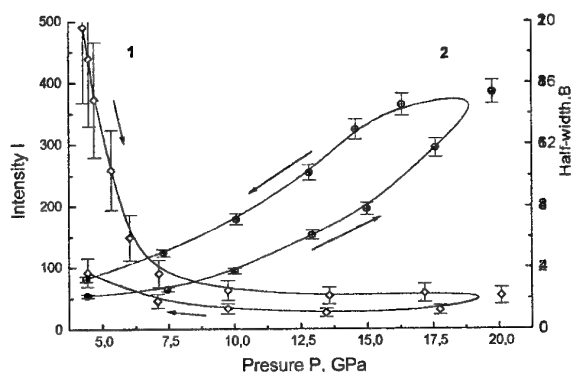


Fig.2 Baric dependence of the intensity I (curve1) and half-width B (curve2) of the X-ray line (220) of the γ -phase of HNS.

At pressure $P \geq 20$ GPa diffuse scattering has considerably increased. Near to a line (111) of the γ -phase new lines were detected, which were identified by a pair of $(110)_\alpha$ and $(110)_\beta$ lines of α -phase (fig.3).

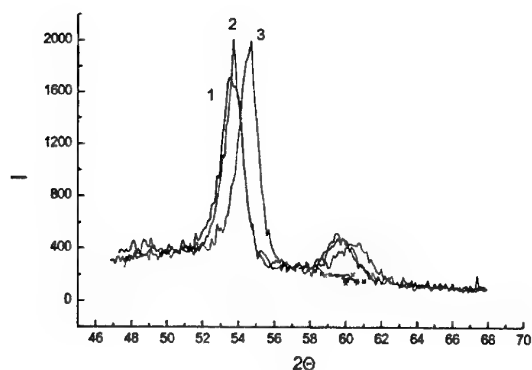


Fig.3 XRD investigation at pressure $P \geq 20$ GPa:

- 1) $C_n = 0.08\% \text{ N}$;
- 2) $C_n = 0.30\% \text{ N}$; 3) $C_n = 0.57\% \text{ N}$.

The quantitative treatment of diffractograms and electronograms has

shown presence of elements and complexes with nanocrystal structure.

Formation of α -phase and elements with nanostructure was facilitated at padding superposition of a shift component

Summary.

It is shown, that the course of a plastic strain at stage of fragmentation and phase ($\gamma \leftrightarrow \alpha$) transformation under high pressure is accompanied by structural - kinetic modifications. It promotes shaping of elements and complexes with nanocrystal structure in austenite of high-nitrogen steels.

References:

- [1]. K. Lu. Mater. Sci. Eng. Reports. Vol. R16. (1996). p. 161-221.
- [2]. R.Z. Valiev. Nanostruct. Mater. Vol. 6. (1995). p. 73-82.
- [3]. J. Dunstan. Rev. Sci. Instrum. Vol.60. (1989). p. 3789-3795.
- [4]. K. Takemura, O. Shimomura. Rev. Sci. Instrum. Vol. 60. (1989). p. 3783-3788.

UNIDIRECTIONAL SOLIDIFICATION AND COLD-ROLLING OF NON-STOICHIOMETRIC TWO PHASE NI-RICH SUPERALLOYS

Borodians'ka H. Yu., Kotko A.V., Hirano T.⁽¹⁾

Francevich Institute for Problem of Materials Science, Kiev, Ukraine

⁽¹⁾National Institute for Materials Science, Tsukuba, Japan

1. INTRODUCTION

Nickel-base superalloys are widely used in applications requiring strength at high temperature¹⁻¹². The main obstacle to nickel aluminides as potential materials for use at elevated temperatures is their low room temperature ductility in polycrystalline form. At high temperatures, the grain boundaries that are normal to the principal stress axis constitute sources of weakness and preferential nucleation sites for cracks, which may eventually lead to the failure. It was established that grain boundaries of Ni₃Al are intrinsically brittle^{5,6}. The brittleness of polycrystalline Ni₃Al is argued to be due to poor of grain boundary cohesion strength^{7,8} and the inadequate number of independent slip systems⁹.

This metallurgical problem was solved by Aoki *et al.*², Liu *et al.*⁵, who discovered that small microalloying additions of boron to Ni-rich compositions greatly improve the ductility and change the fracture mode from intergranular to transgranular.

Recent studies T. Hirano *et al.*, however, found that B-free Ni₃Al may be significant ductilized by the unidirectional solidification using a floating zone method (FZ-UDS) without any alloying elements^{10,11}. Stoichiometric Ni₃Al, in single crystal form, is quite ductile and can be strained to tensile test as high as 60% of elongation, even though they have polycrystalline form with columnar structure¹²⁻¹⁴. In addition, the directionally solidified materials have more ductility than that of the boron-doped alloy.

As is well known that impossible to fabricate Ni₃Al foil by cold rolling cast polycrystalline alloys due to severe intergranular brittleness³. However, ductility is not enough to cold roll to thickness below 800μm even this material has an addition of boron. Taking advantage of high ductility of unidirectional solidified materials one of the authors found that the fabrication of ductile thin foil of stoichiometric Ni₃Al by cold rolling without intermediate annealing would be possible. This technique successfully fabricated large-area foils and these cold-rolled foil, after heat treatment, showing 5% tensile elongation at room temperature¹⁵.

Using the same technique we investigated possibility of growing two phase (γ-γ') Ni-rich superalloy without additions with compositions of 22 - 16 at%Al by FZ-UDS. The first purpose of this study was to show the differences in solidification behavior of the non-stoichiometric Ni-rich composition in comparison with

stoichiometric Ni₃Al. The second purpose was to fabricate cold-rolled foils. In addition, we present here scanning electron microstructures of the samples before and after cold rolling. We expected that prepared thin foils could be promising materials for high-temperature aerospace and automobile applications as light-weight high-temperature structural materials, for example, honeycomb structure.

2. EXPERIMENTAL PROCEDURE

The raw materials of Ni-rich superalloy are prepared by the same way as in the previous report¹⁷. All rods Ni-rich crystals are produced by the floating zone technique (FZ-UDS). The Al-content of the as-grown crystal was determined by using wet chemical method in the central part of the crystal. The results agreed fairly well with nominal compositions within 0.4 at%, as listed in Table I.

The as-grown crystals were 9 - 13 mm in diameter and 120 mm in length. The resultant rods were cut along the growth direction and longitudinal sections were subjected to metallographic observations. X-ray Laue diffraction have been used to check the crystal structure and for controlling the growing orientation. Disk samples for the X-ray Laue diffraction were cut perpendicularly to the growth direction.

Cold rolling specimens (1.7 × 8-10 mm in cross section and 80-100 mm in length) were cut from the ingots with the longest dimension parallel to the growth direction by an electrical discharge machine. The cold rolling was carried out along the longest dimension at room temperature by using four-high mills with a back-up roll diameter of 360 mm and a working roll diameter of 120mm and the rolling speed of 3.5m/min. The amount of reduction in thickness per pass was about 0.1mm. The cold-rolling operations were performed without intermediate annealing.

The microstructure before and after the cold rolling were examined by optical and scanning electron microscopy. Since the differences in composition between the matrix and γ'-phase was relatively small, the contrast in absorbed or backscattered electron images was only slight, and it was often necessary to lightly etch specimens before examination. The surfaces of the specimens were mechanically polished with emery papers and finished with 0.05 μm alumina powder suspension, then etched in the Marble reagent (5g CuSO₄, 20 ml HCl and 20 ml H₂O).

3. RESULTS AND DISCUSSION

3.1 Growth and microstructure of as-grown crystals

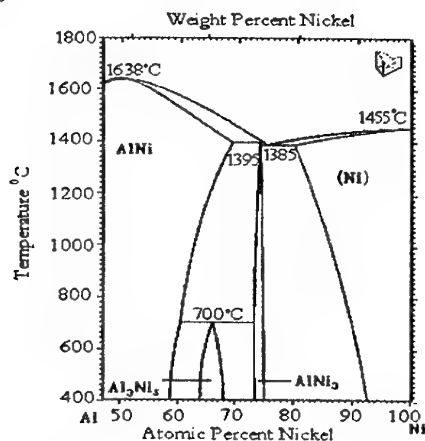
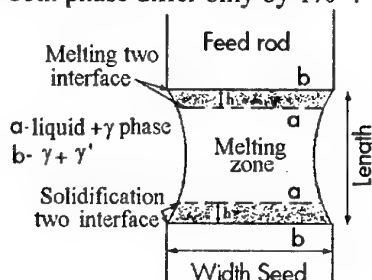


Fig. 1. The nickel-rich region of the Ni/Al system¹⁸

Nickel-rich region of the Ni/Al phase diagram (Fig. 1) shows that the γ -phase, Ni, exists over a wide range of composition, with a maximum melting point of 1455 °C. The γ' -phase, Ni_3Al , also exists over a range of composition less 24.4 at%Al is produced via a eutectic reaction at 1385 °C¹⁸.

In our case this leads to formation of two surfaces of melting and solidification interfaces (Fig. 2) during of crystal growth by FZ-UDS. The Al concentration influence on the distance (h) between surfaces, the spacing of which increases with the decreasing of Al content. It indicates that both the phases (γ and γ') grew non-simultaneously from the liquid. But the structure of stoichiometric Ni_3Al is formed at the planar solidification interface; both the phase (γ' and β) grew simultaneously from the liquid¹⁹. Such statement is in a good agreement with the Ni/Al phase diagram (Fig. 1), because when Ni-rich alloys are cooled from the melt, primary γ dendrites separate out (liquid \rightarrow liquid + γ). At the eutectic temperature, the remaining liquid freezes as a two-phase mixture of γ - γ' . Cooperative growth of these two phases is possible with the same crystallographic orientation because the edge length of the cubic unit of both phase differ only by 1%¹⁹.



2. Schematic of the molten zone

However, the little changes in the molten zone, the slight differences in the composition of raw materials or solidification conditions could modify

the nucleation process moved the system into a very unstable character of crystal's growth. This leads to difficulties of preparation the large single crystal, of two-phase Ni-rich composition from liquid. In previous study¹¹, it was found to be very difficult to grown stoichiometric Ni_3Al (γ') single crystals because of γ' -phase growing simultaneously from liquid with β -NiAl, but β -phase is not stable below the solidification temperature.

Instead, we successfully grew a single crystal 70mm length with high rest Ni-content the Ni-16Al alloy of [001] orientation and three big elongated grains of Ni-18Al composition, Table I. The same seed crystal was used for all alloys, but crystals happened to grow in different orientations. As stated above, it can be due to instability at the initial stage of the floating-zone process. In the case of Ni-20Al we grew only polycrystalline form. However, more grains of the above composition were elongated along the growth direction and the grain boundaries were found mainly low-angle (less than 12°) that allowed the future cold rolling. Only one composition Ni-22Al was formed at the uniform solidification interface nearly same as stoichiometric Ni_3Al ¹¹, because γ -phase concentration was lowest. The columnar-grained structure of two-phase alloy was formed along the growth direction.

Table I. Chemical composition and as-grown structure of FZ-UDS two-phase Ni-rich crystals.

Nominal composition	Al content, at %	As-grown structure
Ni-16Al	15.9	single crystal
Ni-18Al	18.1	large elongated grains
Ni-20Al	19.7	polycrystal with low-boundary grains
Ni-22Al	21.6	columnar structure

SEM microstructures of the as-grown crystals are shown in Fig.3.□The descriptive groupings, which are of course subjective, were round, moderately cuboidal, very cuboidal, irregular, and irregular faceted. The distribution of γ' is illustrated in Fig. 3(a) through (d). The γ' particles ranged from a cuboidal shape, as in Ni-16Al, to irregular faceted, as in Ni-22Al alloy. The Fig. 3(a, b) shows, that Ni-16Al and Ni-18Al are two-phase crystals, where discontinuous networks of γ -phase (gray) containing γ' -phase (black) are visible. The average particle size of γ' in Ni-16Al and Ni-18Al alloys were 150 nm and 300-500 nm, respectively.

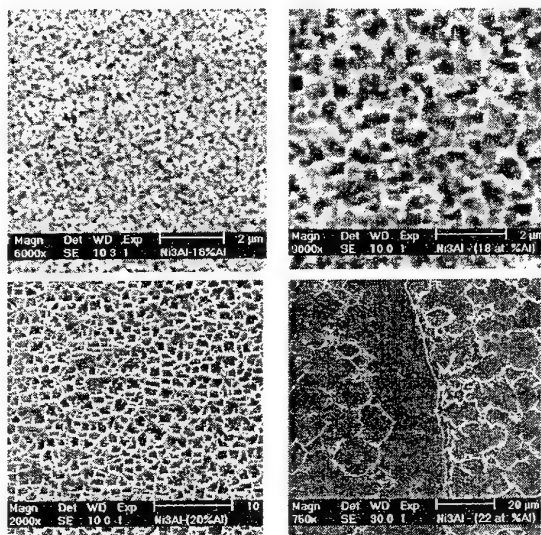


Fig. 3. SEM microstructures of as-grown crystals.

In the Ni-20Al and Ni-22Al the irregular precipitates were formed by the apparent coalescence of many smaller cuboidal precipitates (Fig. 3(c,d)); while the irregular faceted particles, which occurred in conjunction with a dispersion of small precipitates, formed during solidification and displayed a crystallographic faceting nature of the γ' interface. The cuboidal particles of γ' -phase (Fig. 3 (c)) were generally grouped and ordered in a square array.

The as-growth Ni-22Al microstructure consists of cored dendritic arms in the direction of crystal growth axis. The cores of the dendrites are composed of two-phase mixture of residual γ (nickel solid solution) in γ' (Ni₃Al). The average γ' irregular faceted size was found to be $\sim 25 \mu\text{m}$.

The processing conditions for all studied alloys, i.e. melting temperature, rate of growing, cooling regime were the same. However, γ' -particle size varied from alloy to alloy and became larger with increasing aluminum content. In addition, only slight variations in γ' precipitate size existed between the top and bottom of the bars.

3.2 Cold-rolling, texture and microstructure of as-rolled crystals

Here we present successful fabrication of thin foils of two-phase Ni-rich superalloys by cold rolling of directionally solidified ingots. Thin foil of 200 μm in thickness was successfully produced with 80% reduction in thickness at room temperature without intermediate annealing. Fig. 4 shows the appearance of the specimens after 80% reduction for all alloys. The Ni-16Al, Ni-18Al and Ni-20Al foils have a good surface quality. The surface is smooth, flat and crack free at the edge of the specimen. During cold-rolling one foil of Ni-16Al after 50% reduction was eventually bent double (Fig. 4(a)). However, no cracks appeared. Single cracks were observed only along the high-angle grain boundaries in polycrystalline part of alloys. It is well known that this type of

stoichiometric Ni₃Al grain boundaries has a typical brittleness and two-phase Ni-rich superalloys are not an exception (Fig. 4(c)), but the low-angle grain boundaries of the alloy prepared by FZ-UDS are crack-resistant (Fig. 4(b)).

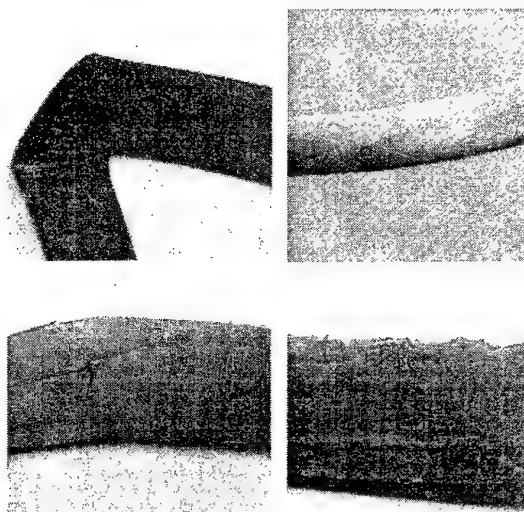


Fig. 4. General view of as-rolled foils.

Table II. Results of crystal growth and cold rolling: orientation, final cold rolling reduction, reduction when cracking starts, rolling texture.

Sample	Orientation	Final reduction %	Reduction where cracking start %	Rolling texture
Ni-16Al	$\langle 100.83.8 \rangle$	80	—	$\{110\}\langle 102 \rangle$ + $\{110\}\langle 121 \rangle$
Ni-18Al	$\langle 0.10.0.0.9 \rangle$	76	60	$\{110\}\langle 771 \rangle$
	$\langle 0.30.0.0.9 \rangle$	82		+ $\{110\}\langle 121 \rangle$
Ni-20Al	—	80	62	$\{110\}\langle 116 \rangle$
Ni-22Al	—	80	28	$\{110\}\langle 241 \rangle$ + $\{110\}\langle 121 \rangle$

The foils of Ni-18Al and Ni-20Al composition have the cracking initiation along high-angle grain boundaries after 60 % reduction (Table II). However, we successfully prepared large-area foils. The specimen of Ni-22Al did not break up to about 80% reduction but many cracks were observed at the edge of the specimen (Fig. 4(d)) after 28 % reduction. Such behavior during cold rolling can be related to the evolution of rolling texture. There are some differences among the samples, as shown in Table II. Sample Ni-20Al has only strong $\{110\}\langle 116 \rangle$ texture. Samples Ni-16Al, Ni-18Al and Ni-22Al have a general weak texture $\{110\}\langle 121 \rangle$, however, a strong $\{110\}$ texture has some scatters around rolling direction $\langle 102 \rangle$, $\langle 771 \rangle$ and $\langle 241 \rangle$, respectively. It can be dependent of the initial orientation of the sheet, but the details are not known. However, note that the rolling plane $\{110\}$ of two-phase Ni-rich superalloys are the same as the stoichiometric Ni₃Al¹⁵.

It should be noted that polycrystalline γ - γ' alloys could be cold-rolled without the addition of ductility enhancing elements.

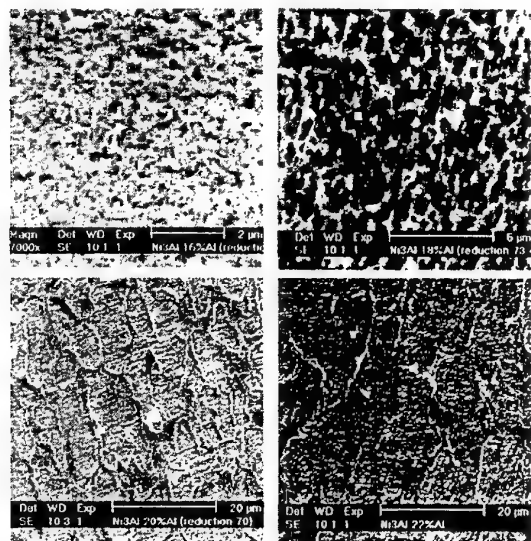


Fig. 5. SEM microstructures of as-rolled crystals

Fig. 5 shows the SEM micrographs of the polished and subsequently slightly etched specimens after cold rolling. The γ' precipitates are visible stretching along rolling direction and their form changes (comparison of Fig. 3 and Fig. 5): a) from cuboidal to rectangular (Fig. 3(b), Fig. 5(b)); b) irregular facets to elongated facets or rectangular (Fig. 3 (c, d) and Fig. 5 (c, d)). The grains were elongated uniformly toward the rolling direction and long slip traces are observed in the elongated grains. The slip traces run straight from one grain boundary to the other grain boundary, which indicates that substantial dislocations can transfer across even random grain boundary from one grain to the adjacent grain similar to the case in the directionally solidified columnar grains.

4. CONCLUSIONS

The influence of non-stoichiometry of Ni/Al alloys on the behavior of system during crystal growing had been studied. It was found that both the phases (γ and γ') grew non-simultaneously from the liquid, however, the structure of stoichiometric Ni_3Al is formed at the planar solidification interface; both the phase (γ' and β) grew simultaneously from the liquid. The crystals of two-phase Ni-rich superalloy with compositions of 16 - 22 at%Al were successfully prepared by FZ-UDS. The microstructure of those alloys in as-grown crystals consists of γ' precipitates in a γ -phase solid solution matrix.

It was found to be possible to prepare the large-area foils of the polycrystalline two-phase Ni-rich superalloys at room temperature by cold rolling. Total reduction of 80 % from the initial sheet was obtained. No heat treatment was performed on the sheet during the entire rolling process. It can be noted that such thin foils were produced from brittle intermetallic compound two-phase Ni-rich

superalloys without any alloying elements and without intermediate annealing treatment. The foils were so thin that it could be bent elastically.

REFERENCES

- [1] Aoki, K. and Izumi, O., *Trans. JIM*, **19**, 145 (1978).
- [2] Aoki, K. and Izumi, O., *Trans. JIM*, **19**, 203 (1978).
- [3] Pope, D. P. and Ezz, S.S., *Int. Mater. Rev.*, **29**, 136 (1984).
- [4] Stoloff, N. S., *Int. Mater. Rev.*, **34**, 153 (1989).
- [5] Lui, C. T., White C.L., and Horton J.A., *Acta metall.*, **33**, 213 (1985).
- [6] White, C.L. and Stein, D.F., *Metall. Trans.*, **A9**, 13 (1978).
- [7] Takasagi, T. and Izumi, O., *Acta metall.*, **33**, 1247 (1985).
- [8] Massner, R. P. and Briant, C. L., *Acta metall.*, **30**, 457 (1982).
- [9] Aball and Smallman, R.E., *Acta metall.*, **14**, 1517 (1966).
- [10] Hirano, T., *Scripta metall. mater.*, **25**, 1747(1991).
- [11] Hirano, T. and Mawari, T., *Mater. Res. Soc. Symp. Proc.*, **228**, 891 (1993).
- [12] Hirano, T. and Kainuma, T., *ISIJ International*, **31**, 1134 (1991).
- [13] Hirano, T. and Mawari, T., *Intermetallics*, **3**, 23 (1995).
- [14] Golberg, D., Demura, M., Hirano, T., *J. Crys. Growth*, **186**, 624 (1998).
- [15] Demura, M., Hirano, T. and Umezawa, O., unpublished
- [16] Hanada, S., Watanabe, S., and Izumi, O., *J. Mater. Sci.*, **21**, 203 (1986).
- [17] Hirano, T., *Acta metall. mater.*, **38**, 2667 (1990).
- [18] Massalski, T. B., "Binary Alloy Phase Diagrams" Am. Soc. Metals, Metals Park, Ohio. (1986) pp. 140-142
- [19] F.J. Bremer, M.Beyss, E. Karthaus, A.Hellwig, T. Schober, J.-M. Welter and H. Wenzl. *J. Crys. Growth* **87**, 185-192 (1988).
- [20] Madelcine Durand-Charre, "The Microstructure of Superalloys", Gardon and Breach Sci. Pub. (1997) pp.127.
- [21] E.F. Bradley (editor), *Superalloys*, Am.Soc. Metal, Metal Park, Ohio (1988) p. 31.

BIOMIMETIC RECEPTION OF HYDROXYAPATITE COATINGS

Kryshanovska A.S., Korovnikova N.I., Savin Yu.N., Tolmachev A.V.

Institute for Single Crystals of NAS of Ukraine, Kharkov, Ukraine

It is known, that calcium hydroxyapatite $\text{Ca}_{10}(\text{PO}_4)_6(\text{OH})_2$ (HAp) is a structural analogue and main composite of inorganic part of bone and tooth fabrics of organism. It is widely used as powders, as monocrystals in orthopaedics and stomatology due to its high biocompatibility. The special interest is represented by coats on a HAp basis, allowing to give made from bioinert materials implant proper HAp of property. There are various expedients of drawing of such coatings. The new opportunities for their reception are unclosed at use of properties of a structured organic matrix containing functional groups of an anionic type, to boost origin, to check and to guide growth of inorganic crystals (process biological mineralization or a biomimetic method). Last allows to shape inorganic coatings with given properties: in density, sizes of crystals, quantity and shape of pores etc.

In the given work the optimum requirements of reception of coats from HAp by a biomimetic method on surfaces, modified monomolecular film of stearic acid put expedient Langmuir-Blodgett are found. The nanocrystal coating of HAp were grown on modified quartz, silicon and sapphire substrates from water solutions $(\text{NH}_4)_2\text{HPO}_4$, CaCl_2 and NH_4OH (at a variation of concentrations of precursors, pH of medium) with the subsequent exsiccation and annealing. The received samples were explored by XPS, of the phase analyses, IR-spectroscopy, electronic microscopy and electronic microdiffraction.

The XPS data of the element analysis show stoichiometric a relation of calcium to phosphorus equal 1.67, relevant to a phase HAp.

The X-ray phase analysis testifies to presence of the phase of HAp (~90 %) and small quantity (~10 %) CaO in samples.

The basic reflections of the received coatings on the diffractogram are presented, which is reference for structure HAp.

There are strips of stretching vibrations of ions it ($\nu=3575 \text{ cm}^{-1}$), groups PO_4^{3-} ($\nu=1090, 1040, 963 \text{ cm}^{-1}$), reference for HAp IR-absorption spectra is model.

According with the experimental data received by an electronic microscopy (Fig) HAp films are polycrystalline (sizes of crystals is ~50-100 nm) and porous (sizes of pores - 100 nm). The grain edges are not sharp, confirming the amorphization of the nanocrystal surfaces. The possible reason is the presence of not completely reacted calcium at phase transformations.

In accordance with the experimental results of an electronic microdiffraction, nanocrystals have hexagonal structure with parameters of a lattice relating to a crystalline structure of HAp. They are oriented by a plane (011) respect to a normal of a surface.

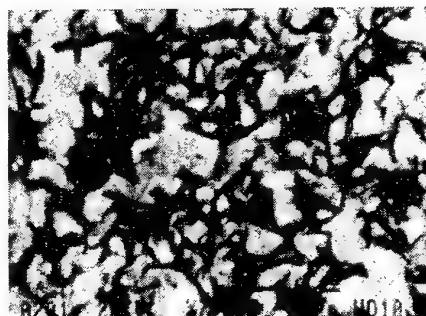


Fig. Electron microscopy image of hydroxyapatite coating on the quartz substrate.

NANOCRYSTALLINE DIAMOND-SiC CERAMICS

**Ekimov E.A., Palosz B.⁽¹⁾, Lojkowski W.⁽¹⁾, Gierlotka S.⁽¹⁾, Filonenko V.P., Antanovich A.A.,
Kuzin N.N., Slesarev V.N.**

Institute for High Pressure Physics, Russian Academy of Sciences, Troitsk, Moscow region, Russia

⁽¹⁾High Pressure Research Center, Polish Academy of Sciences, Warsaw, Poland

Dynamically synthesized nanodiamond is a promising material for obtaining superhard compacts. Abrasive properties of explosive diamond powders with the nanostructure of grains (shock-synthesized polycrystalline nanodiamond powder) are better than those of powders produced from natural and synthetic single crystal diamond [1]. We have previously shown that infiltrating polycrystalline nanodiamond powder by liquid Si under high pressure is an attractive approach to the synthesis of solid nanocrystalline diamond [2]. However, the question of infiltration mechanism and some structural peculiarities of the material with nanostructure were still unclear.

The starting nanodiamond, DALAN (Russia) was a 0.05 to 5 μm grain-graded powder. According to x-ray and TEM data, grains of the powder consisted of 3-10 nm crystallites. The polycrystalline nanodiamond powder contains a certain amount of gas impurities close to that in microcrystalline static-synthesized diamonds (Fig.1).

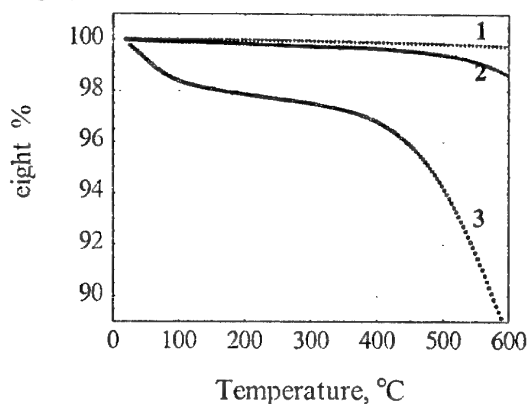


Fig. 1. Thermal gravimetric analysis (in helium) of the DALAN powder (2) in comparison with the behaviour of cluster diamond (3) and static-synthesized one (1).

The DALAN powder was subjected to heating in the 800-2200 $^{\circ}\text{C}$ temperature range at 7.7GPa to investigate the behavior of open pores, whose presence is important for the infiltration. Our

experiments showed that all compacts, except for samples obtained at 800 $^{\circ}\text{C}$, contain graphite. For the sintering temperature ranges 800 - 1400 and 1600 - 2000 $^{\circ}\text{C}$, the samples reach the Vickers hardness equal to 15GPa and 20 - 25GPa and the density equal to 90 - 95 and 80 - 85 % of the theoretical one, respectively (Fig. 2). Higher density values for the samples treated in the lower temperature range point out that these compacts contain pores permeable for He during density measurements (helium pycnometry). In addition, both a lower hardness and lower amount of the graphite phase are evidently connected with the presence of open pores in diamond compacts obtained in the lower temperature range.

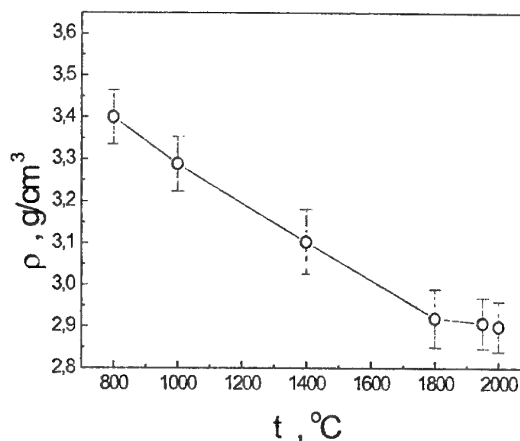


Fig.2. The dependence of sample density of the DALAN compact ($P=7.7\text{GPa}$, $\tau=6\text{min}$) on the sintering temperature.

In infiltration experiments under pressure (7.7GPa), molten Si penetrated into nanodiamond and filled pores between diamond grains. Subsequently Si reacted with carbon to form nanocrystalline SiC.

Hardness of infiltrated samples was measured by two methods. There are the microhardness and depth sensing indentation methods. Typically, the

Vickers microhardness measurements at the 9.8N indenter loading yielded the average hardness equal to 51 ± 3 GPa for composites. Being determined from the length of indentation-induced cracks, the fracture toughness coefficient was equal to 10 ± 3 MN/m^{3/2}. The depth and load sensing indentation technique was used to test the homogeneity of diamond-SiC composite in hardness and determine the Young's modulus as well. The average depth and area of indentation imprints of the Vickers pyramid were $0.82 \mu\text{m}$ and $8.1 \mu\text{m}^2$, respectively. From the area with sizes about $50 \times 50 \mu\text{m}$, taken in the middle of the diamond-SiC compact, the average both a hardness and the Young's modulus were found to be 60 ± 11 GPa and 550 ± 70 GPa, respectively. The standard deviation up to 20% for the hardness data and hardness data themselves are typical for polycrystalline diamond materials, whereas the Young's modulus of the nanocomposite is rather close to that of SiC. From our point of view, this circumstance clearly indicates a substantial role of the SiC binder in the mechanical behaviour of this nanocomposite. We did not detect any pores in the compacts of nanodiamond infiltrated with silicon (Fig.3).

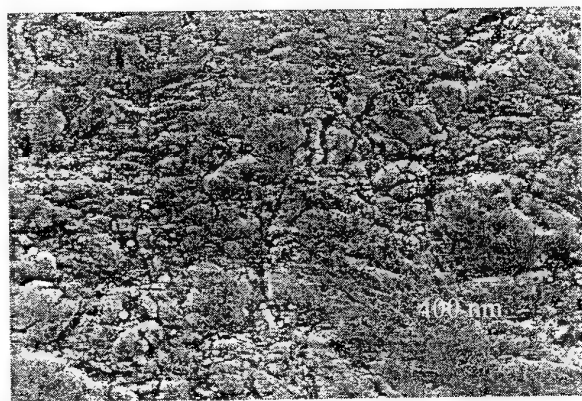


Fig. 3. SEM picture of the diamond-SiC composite (polished surface).

The amount of SiC-binder in the compact is sufficient (15-25 vol %) to isolate diamond grains from each other.

On the polished surface of the diamond-SiC compact, the layers of 50-100nm thick between the grain islands may be interpreted as a SiC phase. The thickness of these layers is consistent

with the grain size of SiC phase (20-50nm, taken from x-ray and TEM analyses) in the composite. We suggest that the presence of nanopores in the compressed nanodiamond powder is responsible for the nanostate of SiC layers. For proving this point, we infiltrated the $4\text{-}5 \mu\text{m}$ nanodiamond powder with a narrow particle size distribution and found the increase of the mean grain size of SiC in the composite material. Submicron grains of SiC were found in large "pores" among SiC nanograins of 30-50nm (Fig.4).

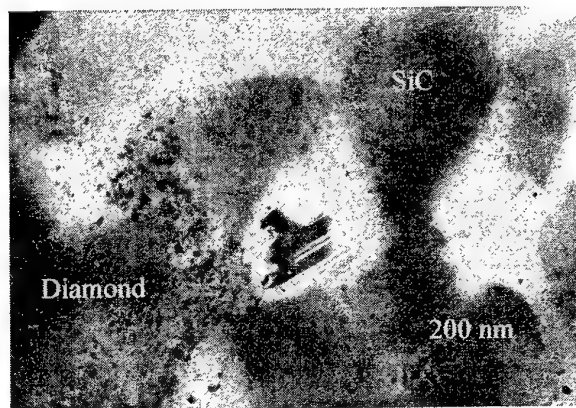


Fig. 4. TEM photograph of the nanodiamond-SiC composite.

The advantage of nanocomposites over conventional polycrystalline diamond ceramics in their application as finishing tools and dies follows from the possibility of reaching a very high wear resistance and abrasive ability of tools.

Acknowledgments

We are grateful to V.V.Brazhkin, A.G.Lyapin, A.Gavriliuk, A.Presz, and J.A.Kozubowski for their assistance in studying and discussing.

This work was supported by the Russian Foundation for Basic Research, project no. 02-03-33166.

References

- [1] O.R. Bergman and N.F. Bailey, in High Pressure Explosive Processing of Ceramics, edited by R. Graham and A.B. Sawaoka (Trans Tech, 1987) p. 67.
- [2] E.A. Ekimov, A.G. Gavriliuk, B. Palosz, et al, Appl. Phys. Lett. 77(7) 954 (2000).

LOW TEMPERATURE PLASTIC BEHAVIOR OF THE $\text{Zr}_{46.8}\text{Ti}_{8.2}\text{Cu}_{7.5}\text{Ni}_{10}\text{Be}_{27.5}$ BULK AMORPHOUS ALLOY

Tabachnikova E.D., Bengus V.Z., Natsik V.D., Macht M.⁽¹⁾, Miskuf J.⁽²⁾, Csach K.⁽²⁾

Institute for Low Temperature Physics & Engineering, Kharkov, UKRAINE

⁽¹⁾Hahn-Meitner Institut, Berlin, GERMANY

⁽²⁾Institute of Experimental Physics, Kosice, SLOVAKIA

This work is devoted to experimental study of deformation behavior and failure at 77 and 4.2 K of the $\text{Zr}_{46.8}\text{Ti}_{8.2}\text{Cu}_{7.5}\text{Ni}_{10}\text{Be}_{27.5}$ bulk metallic glass. Obtained results are considered in the framework of notions of the polycluster model of amorphous solids [1] on the atomic structure and micro mechanisms of plastic deformation.

Deformation curves at the quasistatic uniaxial compression of cylindrical (2,5 mm in diameter x 7 mm) samples of the $\text{Zr}_{46}\text{Ti}_{8}\text{Cu}_{7.5}\text{Ni}_{10}\text{Be}_{27.5}$ bulk metallic glass [2] were measured at 300, 77 K and 4.2 K with strain-rates $\dot{\epsilon}_1 \approx 2 \cdot 10^{-2} \text{ s}^{-1}$ and $\dot{\epsilon}_2 \approx 4 \cdot 10^{-4} \text{ s}^{-1}$. Fractography observations of the failure surfaces were made in the TESLA BS300 scanning electron microscope.

Values of the yield stress σ_0 and the failure stress σ_f measured at different temperatures are shown in the Table 1.

Table 1. Values of the yield stress σ_0 and the failure stress σ_f at different temperatures and strain-rates.

T, K	σ_0 , GPa		σ_f , GPa	
	$\dot{\epsilon}_1$	$\dot{\epsilon}_2$	$\dot{\epsilon}_1$	$\dot{\epsilon}_2$
300	1.7	1.58	1.91	1.79
77	2.1	-	2.5	-
4.2	2.4	-	3.0	-

It can be seen from the Table 1 that σ_0 increases under the temperature decreasing from 300 to 4.2 K. Deformation curves " σ - ϵ " demonstrate the easy glide stage, and at the room temperature deformation proceeds by a serrated flow. Mean amplitudes $\Delta\sigma$ of the serrations are of the order of 18 MPa, and corresponding plastic deformation $\Delta\epsilon$ per a load jump ΔP is estimated as

$$\Delta\epsilon = \Delta P / K \cdot l_0, \quad (1)$$

where K is the rigidity of the "sample-machine" system, l_0 is the initial length of the sample, was 0.3 %. At 77 and 4.2 K jump-like deformation was

not registered but the plastic deformation has a localized character. Local shear bands are observed on the surface of specimens at 77 and 4.2 K.

Shear band orientations at 77 and 4.2 K were approximately the same as at 300 K i. e. they were close (within 1-3 degree) to the plane of maximum shear stresses, oriented at 45 degree to the compression axis.

Ductile shear failure of the samples at 77 and 4.2 K occurred by sliding-off of one part of a sample relative to another along the plane oriented approximately at 45 degree to the compression axis as at 300 K [3, 4]. Thus, decreasing of the temperature from 300 to 4.2 K does not influence the orientation of shear bands and shear failure surfaces relative to the compression axis.

Measurements of the deformation curves " σ - ϵ " at 300 K were carried-out at two different strain-rates: $2 \cdot 10^{-2} \text{ s}^{-1}$ and $4 \cdot 10^{-4} \text{ s}^{-1}$. Magnitudes of yield stresses typical of each of these strain-rates are indicated in the Table 1. It is turned out that increasing of $\dot{\epsilon}$ from $4 \cdot 10^{-4} \text{ s}^{-1}$ to $2 \cdot 10^{-2} \text{ s}^{-1}$ increased σ_0 from 1.58 GPa to 1.70 GPa. Such a character of the strain-rate sensitivity $\Delta\sigma/\Delta\dot{\epsilon}$ at 300 K, together with the obtained temperature dependence of σ_0 , can be considered as indication on the thermally activated character of plastic deformation in the studied metallic glass.

An activation volume γ of the plastic flow was estimated assuming that the Arrhenius law

$$\dot{\epsilon} = \dot{\epsilon}_0 \exp[-(H_0 - \gamma \cdot \sigma) / kT]. \quad (2)$$

Here H_0 is the activation enthalpy, σ is a flow stress, k is the Boltzmann constant, T is the temperature. The value of γ can be calculated as

$$\gamma = kT \cdot (\Delta \ln \dot{\epsilon} / \Delta \sigma)_{T, \epsilon}. \quad (3)$$

At the yield stress σ_0 the value of γ is $1.03 \cdot 10^{-22} \text{ cm}^3$.

Electron microscopic observations of the ductile shear failure surfaces arisen by sliding-off of one part of a sample relative to another under uniaxial compression at 77 and 4.2 K revealed "vein" patterns in all studied samples "Chevrons" or other features that are characteristic of the "ductile-brittle" transition in metallic glasses under decreasing of the temperature [5] were not observed. Availability of "vein" patterns in combination with the data on the orientation of failure surfaces of samples makes possible to conclude:

- a) the failure of the $Zr_{46}Ti_8Cu_{7.5}Ni_{10}Be_{27.5}$ bulk metallic glass under decreasing of the temperature down to 4.2 K has the ductile character, as well as at 300 K;
- b) further decreasing of the testing temperature down to 4.2 K lead of a new characteristic feature of the "vein" pattern. Besides "veins" with a usual thickness there are "veins" with increased thickness at 4.2 K and the large pieces of the melted material which fell on the shear failure surfaces (during the failure) and solidified.
- c) availability of the bands of localized shear (shear steps on the surface of bulk metallic glass samples) oriented along the plane of maximum shear stresses, observing of the shear failure mode owing to sliding-off along this plane – indicate on gradual spreading of the plastic shear front in bulk metallic glasses in time. Such gradual spreading is similar to crystalline solids, where dislocation mechanism of plastic shear takes place.

Bulk metallic glasses have almost the same features of plasticity, which are typical of crystalline metallic alloys [6] (availability of the yield stress, strain-rate and temperature sensitivity, easy glide, superplasticity, creep, deformation instability and jump-like deformation, strain localization in glide bands, local adiabatic heating (up to the melting point at the low temperature catastrophic shear and failure). This allowed extending of dislocation notions to metallic glasses. As distinct from earlier considerations [7, 8], the polycluster model of metallic glasses [1] allows concretizing of the dislocation description of plastic deformation in metallic glasses.

The polycluster model of metallic glasses considers atomic structure of metallic glasses as a random aggregate of non-crystalline ordered nanoclusters (with mean dimensions of ~ 10 nm) separated by disordered intercluster boundaries. According to the polycluster model, these boundaries put up the small resistance to a plastic shear in comparison with the body of clusters. In view of large volume

density of intercluster boundaries (approximately 5 % of atoms belong to boundary layers, when clusters dimensions are ~ 10 nm), exactly the structure of these boundaries determines plastic resistance and mechanical properties of metallic glasses. The critical stress σ_p for a plastic shear along an intercluster boundary in the absence of thermal activation can be described [1] in a first approach as

$$\sigma_p = (\langle \sigma_c \rangle - \delta_c / 2) \cdot c \equiv \sigma_{oc} \cdot c, \quad (4)$$

where σ_c are local critical shear stresses in coinciding sites at the intercluster boundary; $\delta_c / 2$ is the half-width of the σ_c distribution, and $\sigma_{oc} \equiv \langle \sigma_c \rangle - \delta_c / 2$ is the smallest magnitude of σ_c . σ_p is close to σ_0 ($\sigma_p \approx \sigma_0$).

Thermal activation decreases the σ_p value due to increasing of the probability of overcoming the potential relief along intercluster boundaries [9, 10] The order of magnitude of the activation volume of the plastic flow ($1.03 \cdot 10^{-22}$ cm³) measured experimentally in our work is close to that of a lattice dislocations motion in the Peierls relief in crystals. Thus, obtained magnitude of the activation volume does not contradict to the dislocation description of the metallic glass inhomogeneous plastic deformation in the framework of the polycluster model.

REFERENCES

1. A. S. Bakai, Topics in Applied Physics, vol. 72, Glassy Metals III (eds. H. Beck and H. -J. Gunterodt) Springer, Berlin (1994) p. 209.
2. M. P. Macht, Q. Wei, N. Wanderka, I. Sieber, N. Deyneka, in Proceedings of ISMANAM-99, Drezden, Germany, Trans Tech Publications, Switzerland.
3. E. D. Tabachnikova, V. Z. Bengus, V. V. Molokanov, Materials Science Forum, vol. 225-227 (Proceedings of ISMANAM-95), Part 1 (1996) p. p. 107-112, Trans Tech Publications, Switzerland.
4. V. Z. Bengus, E. D. Tabachnikova, J. Miskuf, K. Csach, V. Ocelik, W. L. Johnson, V. V. Molokanov, Journal of Materials Science, v. 35 № 17, (September 2000) p. p. 4449-4457.
5. E. D. Tabachnikova, Fiz. Metalov and Metallovedenie, v. 64, N 6, 1987, p. 1205 (in Russian).
6. A. S. Argon, Glass Science and Technology, Vol. 5, Acad. Press, N.Y., 1980, p. 79.
7. J. C. M. Li, "Metallic Glasses" (ASM Seminar, 1976, American Society for Metals, Metals Park, Ohio, 1978) p. 224.
8. V. I. Belyavskii, V. A. Khonik, T. N. Ryabtseva, Metallofizika, v. 11, No. 3 (1989) p. 106 (in Russian).
9. A. S. Bakai, Polyclusterous amorphous solids, Energoatomizdat, Moscow, (1987) p. 117 (in Russian).
10. A. S. Bakai, Mat.Sci.Forum, v. 123 (1993) p. 145.

COPPER DOPED BISMUTH SELENIDE AS ACTIVE CATHODE MATERIAL FOR LITHIUM BATTERIES

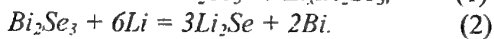
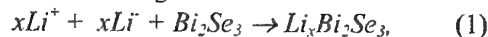
Zaslonkin A.V., Kovalyuk Z.D., Mintyanskii I.V., and Savitskii P.I.

The Frantsevich Institute of the Materials Science Problems of the National Academy of Sciences
of Ukraine, Chernivtsi Department, Chernivtsi, Ukraine

The rhombohedral crystalline structure of bismuth selenide Bi_2Se_3 is formed by a periodic arrangement of layers aligned perpendicular to the trigonal C axis. Each layer is composed of five monoatomic planes ordered according to the sequence Se-Bi-Se-Bi-Se. The chemical bonding in the layers is strong covalent-ionic one, whereas between the layers weak Van der Waals forces prevail. As it was established before, Bi_2Se_3 has competitive characteristics as an active cathode material for 1.5 V power sources with lithium anode. In this report we investigate the influence of copper on electrode properties of Bi_2Se_3 .

Single crystals of Bi_2Se_3 were grown by the Bridgman method from a stoichiometric melt of the components. Doping with 1 wt. % of copper was carried out before synthesis of the compound. The lithium batteries under investigations were of a coin-like construction and had the 2325 standard size. Cathodes for them were prepared of powdered Bi_2Se_3 and their porosity was about of 20 %. As electrolyte we used 1 M solution of lithium

tetrafluoroborate (LiBF_4) in γ -butyrolactone. As the lithium electrodes always were in plenty, the utilization coefficients obtained at room temperature for different electrodes in the three-stage discharge conditions (Fig. 1) are affected by bismuth selenide parameters. For undoped Bi_2Se_3 the values of x (in rescaling to $\text{Li}_x\text{Bi}_2\text{Se}_3$) change from 7.2 to 7.4. The X-ray analysis of final reaction products allowed to establish the presence of Bi and Li_2Se . Taking also into account the fact that Li^+ ions can be inserted into the layered matrix by the way of intercalation and in the range $0 < x \leq 1$ this process is reversible, the current formation mechanism in $\text{Li}/\text{Bi}_2\text{Se}_3$ batteries may be considered as combined "intercalation - chemical" with the following reactions:



The first of them describes the mechanism of the insertion of the cations between the layers and the second one predicts a renewal of Bi_2Se_3 to metallic bismuth.

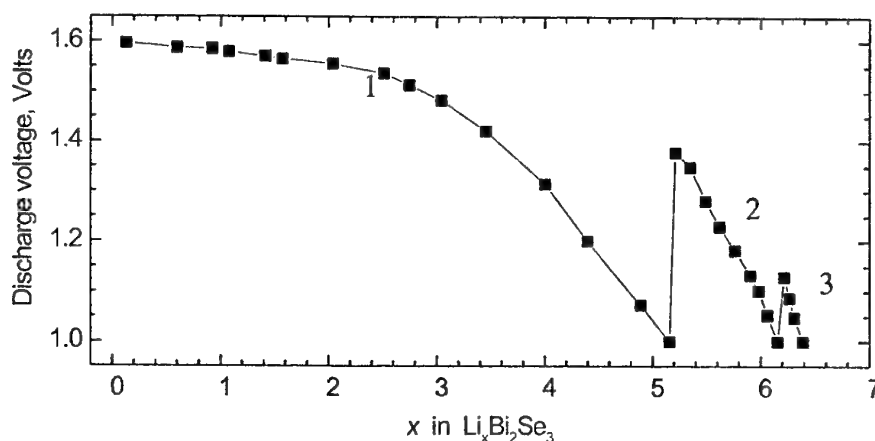


Fig. 1. Discharge curve of a battery at discharge current 1 (1), 0.3 (2), and 0.1 mA (3).

It is known that the sites appropriate for intercalated impurities are placed between the layers. To each molecular unit of Bi_2Se_3 corresponds one octahedral and two tetrahedral sites, i.e. their filling with A atoms gives $\text{A}_x\text{Bi}_2\text{Se}_3$ with $x=3$. So the decrease of the utilization coefficients for Cu-doped cathodes can be caused by the decrease of an amount of vacant sites

appropriate for filling with Li^+ ions during their intercalation. It is confirmed by the X-ray studies of the crystals performed by the methods of Bond and back slit. For Bi_2Se_3 crystals doped with 1 wt. % of Cu only an essential increase of the lattice parameters c (across to the layers) by 0.024 Å takes place, i.e. the dopant atoms are ordered in the interlayer spaces.

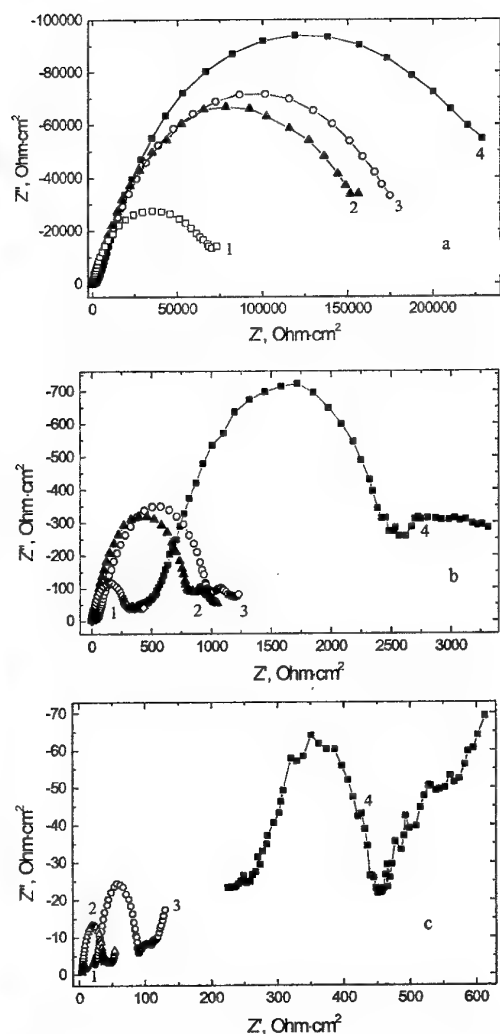


Fig.2. Impedance variations for $\text{Bi}_2\text{Se}_3<1\%\text{Cu}>$ at -40 (a), $+20$ (b), and $+60^\circ\text{C}$ (c) depending on the depth of discharge: $x=0.5$ (1); 2.6 (2); 4.03 (3), and 6.08 (4).

The self-intercalation behaviour of the copper atoms is also confirmed by the measurements of the Bi_2Se_3 conductivity components along

($\sigma_{\perp\text{C}}$) and across ($\sigma_{\parallel\text{C}}$) to the layers. For undoped bismuth selenide the anisotropy ratio is between 2 and 5, whereas for the doped compound above 200 K the conductivity components differ insignificantly and at low temperatures $\sigma_{\perp\text{C}}$ even prevails $\sigma_{\parallel\text{C}}$ by 20 to 40 %. As a result, the effective conductivity $\sigma_{\text{eff}}=(\sigma_{\perp\text{C}}^2\sigma_{\parallel\text{C}})^{1/3}$ of the active cathode material increases. The discharge capacity of 2325-sized $\text{Li}/\text{Bi}_2\text{Se}_3<1\%\text{Cu}>$ batteries is increased by 20 to 25 mA·h at an enough hard discharge condition ($I_{\text{disch}}=1$ mA).

Typical impedance spectra of a $\text{Bi}_2\text{Se}_3<1\%\text{Cu}>$ electrode in a 1 M solution of LiBF_4 in γ -butyrolactone measured at -40 , $+20$, and $+60^\circ\text{C}$ are shown in Fig. 2. At high temperatures the transition of the semicircles (the high frequency part) to the straight lines takes place in the range 0.01 to 1 Hz. A charge transfer followed by the Li^+ ions diffusion into interlayer Van der Waals spaces of bismuth selenide can explain it. The results obtained at different discharge stages were analyzed on the basis of the Randles-Ershler equivalent circuit, which includes a resistance mass-transfer correction R_{tc} , a double electrical layer capacitance C_{dl} , and an ohmic resistance R_s . As it was expected, the kinetics of the electrochemical process becomes essentially improved with increasing temperature: the resistance mass-transfer correction R_{tc} decreases and the diffusion coefficient D of Li^+ ions increases (see Table 1). The opposite change of these parameters takes place with increasing discharge depth.

Table 1. Parameters of the elements of the equivalent Randles—Ershler circuit for $\text{Bi}_2\text{Se}_3<1\%\text{Cu}>$ in 1M solution of LiBF_4 in γ - butyrolactone

x	$R_s, \text{Ohm}\cdot\text{cm}^2$			$R_{\text{tc}}, \text{Ohm}\cdot\text{cm}^2$			$C_{\text{dl}}, \mu\text{F}\cdot\text{cm}^{-2}$			$D, \text{cm}^2\cdot\text{s}^{-1}$
	-40°C	$+20^\circ\text{C}$	$+60^\circ\text{C}$	-40°C	$+20^\circ\text{C}$	$+60^\circ\text{C}$	-40°C	$+20^\circ\text{C}$	$+60^\circ\text{C}$	$+60^\circ\text{C}$
0.5	30.33	8.919	6.229	209200	858.4	28.97	12.23	11.43	11.73	$3.93\cdot 10^{-8}$
1.0	32.23	9.075	6.018	288000	1356	38.30	17.14	9.096	13.32	$1.36\cdot 10^{-8}$
1.4	36.42	11.24	7.001	353800	1597	57.19	12.97	9.748	11.00	$9.48\cdot 10^{-9}$
1.8	41.91	11.27	7.210	373700	1692	61.10	9.758	9.355	10.10	$7.27\cdot 10^{-9}$
2.2	37.85	11.99	7.736	322400	1852	79.45	14.24	8.552	9.765	$4.50\cdot 10^{-9}$
3.0	278.0	42.65	23.05	420000	2487	150.9	11.47	5.729	3.540	$7.47\cdot 10^{-10}$
4.03	481.6	133.0	70.76	520700	2828	199.4	11.83	6.097	3.456	$1.36\cdot 10^{-10}$
6.08	4054	1174	669.2	678300	6637	673.4	9.013	7.403	2.637	$5.24\cdot 10^{-12}$

PROTON INTERCALATES: OPTICAL PROPERTIES AND THERMALLY STIMULATED DEINTERCALATION OF HYDROGEN

Boledzyuk V.B., Kovalyuk Z.D., Pyrlyia M.M.

The Frantsevich Institute of the Materials Science Problems of the National Academy of Sciences
of Ukraine, Chernivtsi Department, Chernivtsi, Ukraine

The influence of hydrogen intercalation on physical properties of InSe and GaSe has essential scientific interest due to possible applications, especially for systems of accumulation and storage of hydrogen.

In this report we present the results of investigations of the transmission spectra measured in the range of the GaSe excitonic absorption. The samples for the investigations 10 to 20 μm in thick were obtained by cleaving from the ε -GaSe ingots grown by the Bridgman method.

The intercalation with hydrogen was carried out electrochemically from a 0.1 N solution of hydrogen acid by using the method of "drawing" electrical field in galvanostatic conditions [1] by means of a Π -5827 M potentiostat. At cathodic polarization of a GaSe sample the current flowing through the electrochemical cell inserts protons into bulk of layered crystals. A concentration of the inserted impurity has been determined from the amount of electricity, which was carried through the electrochemical cell, i.e. the electrical current density and duration of the intercalation are its checking parameters. The investigations of the transmission spectra were carried out for GaSe and H_xGaSe samples (at $0 < x \leq 1$) by using the installation based on IKS-31 spectrometer. Here x is the amount of the inserted protons. The incident light beam was directed along to the C axis (normally to the cleaved surfaces) of the investigated samples. A thermoregulated cryostat system YTPEKC-PTP allowed to investigate the transmission spectra in the temperature range 77 to 293 K.

Concentration dependences of the energy location (E_{exc}) of the excitonic $n=1$ maximum and half-width (ΔH) of the excitonic band measured at $T=293$ K for the proton H_xGaSe intercalates are presented in Fig. 1. These curves have non-monotonous behaviour: in the hydrogen content range $x \approx 0 - 0.4$ the magnitudes of the both parameters increase. At a further increase of x the behaviour of the $E_{\text{exc}}(x)$ and $\Delta H(x)$ curves is opposite. Fig. 2 shows the $E_{\text{exc}}(x)$ and $\Delta H(x)$ dependences measured at $T=77$ K. As one can see, the hydrogen intercalation leads to the shift of the

excitonic maximum energy location to the high-energy range and broadens the excitonic absorption band. It is worth to note that these curves are non-monotonous: E_{exc} and ΔH increase in the range $0.1 < x < 0.35$ and keep practically the same values at higher x .

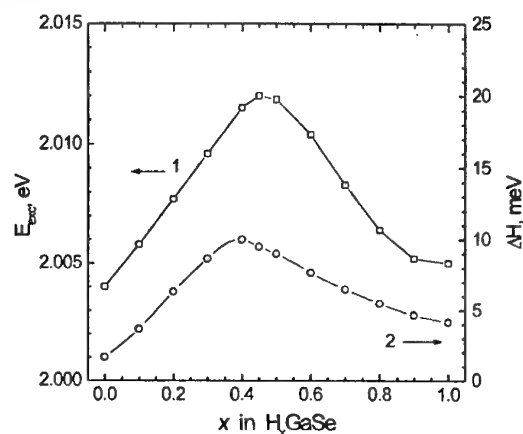


Fig. 1. Concentration dependences of the excitonic ($n=1$) maximum E_{exc} (1) and half-width ΔH of the excitonic band (2) for H_xGaSe at $T=293$ K.

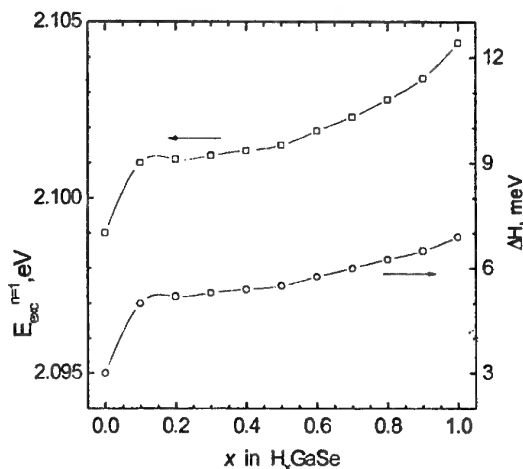


Fig.2. Concentration dependences of the excitonic ($n=1$) maximum E_{exc} (1) and half-width ΔH of the excitonic band (2) for H_xGaSe at $T=293$ K.

Starting from the temperature investigations of the transmission spectra for the "pure" and intercalated samples we have determined the temperature coefficients of the first exciton

maximum shift dE_{exc}/dT and the change of the excitonic band half-width $d\Delta H/dT$ in the temperature range 77 to 293 K. The data are listed in Table 1.

Table 1. Temperature coefficients of the parameters of excitonic absorption band

Compound	dE_{exc}/dT , eV/deg.	$d\Delta H/dT$, eV/deg.
GaSe	-4.7×10^{-4}	4.0×10^{-5}
H_x GaSe	-5.0×10^{-4}	4.5×10^{-6}

The obtained $E_{exc}(x)$ and $\Delta H(x)$ dependences for the hydrogen intercalates can be explained as a result of deformation effects on the GaSe energy band structure caused by intercalation. Proceeding from the peculiarity of the GaSe crystalline structure it is worth to point out that the contributions of interlayer and intralayer deformations to a reconstruction of the GaSe band structure vary by different way during intercalation. With increasing deformation tensions due to the increase of intercalant content, the values of elastic constants, describing the bonding between hydrogen atoms, grow slower than interlayer elastic constants [2].

For applications the reversibility of hydrogen intercalation is very important. So thermally

stimulated deintercalation of hydrogen was investigated for H_x InSe insertion compounds. It has been carried out by means of annealing of the intercalated samples at $t=100^\circ\text{C}$ for 3 to 7 h. A hydrogen deintercalation degree was established from the comparison of the exciton maximum $E_{exc}(x)$ dependence for a standard sample to those of annealed samples. It is found that for the samples H_x InSe ($0.02 \leq x \leq 1.0$) the content of reversible (deintercalated hydrogen lies between 57-78 % (see Table 2).

Table 2. Reversible hydrogen content in H_x InSe intercalates

x in H_x InSe	0.02	0.2	0.5	0.75	1.0
Reversible H_2 , %	67	54	78	67	69

References

- [1]. I.D.Kozmik, Z.D.Kovalyuk, I.I.Grigorchak, and B.P.Bakhmatyuk. Inorg. Mater. 1987, **23**, P. 754 (in Russian).
- [2]. G.L.Belenkii, E.Yu.Salaev, and R.A.Suleimanov. Usp. Fiz. Nauk, 1988, **155**, P. 89 (in Russian)

FORMATION AND CONDUCTIVITY OF OXIDES IN THE SYSTEM $\text{La}_{2-x}\text{NiO}_4$

Nedilko S., Kulichenko V., Dziuzko A.

Kiev Taras Shevchenko National University, 64 Vladimirskaya St., Kiev 01033, Ukraine

The complex oxides on the basis of lanthanum nickelates were investigated. These compounds can be described by homological series $\text{La}_{n+1}\text{Ni}_n\text{O}_{3n+1}$ ($x = 1, 2, 3$). Crystal structure of these oxides is formed by coherent grows of the layers of LaNiO_3 and La_2O_3 along c axe. $\text{La}_3\text{Ni}_2\text{O}_7$ and $\text{La}_4\text{Ni}_3\text{O}_{10}$. $\text{La}_5\text{Ni}_4\text{O}_{13}$ obtained by ceramic technology are the most stable polynickelates, according to the results of XRD investigations.

The purpose of this work was to study physical properties of cation-deficient lanthanum nickelates, such as La_2NiO_4 - $\text{La}_3\text{Ni}_2\text{O}_7$ - $\text{La}_4\text{Ni}_3\text{O}_{10}$ - LaNiO_3 .

The samples were synthesized by co-precipitation of La^{3+} and Ni^{2+} ions from aqueous solutions of metals nitrates taken at stoichiometric ratio 2:1, 1,95:1..., 0,3:1 at pH 9.

As precipitator was used 0,25 mol/l solution of K_2CO_3 which has been adding till achievement of pH \approx 9. Coprecipitated carbonates were washed out by distilled water, then H_2O -(CH_3) $_2\text{CO}$ (1:1) mixture, and then pure acetone and dried up on air. Thermal processing air-dry batch was carried out during 10 hours at 950°C.

XRD investigations of the compounds obtained have been carried out by a powder method on the x-ray diffractometre DRON-3 ($\text{CuK}\alpha$ radiation, Ni-filter). For the chemical analysis on the content of superfluous oxygen a technique of iodometric titration was used.

Based on the data of chemical analysis the Ni^{3+} content was calculated for the $\text{La}_{2-x}\text{NiO}_{4-\delta}$ system. The data are shown in the Table 1.

Electroconductivity of the samples was measured by a four-probe method on the pellets of 12x2 mm with putting In-Ga eutectic under contacts in the temperature range of 300-77K. All synthesized samples were powders of black color, which are easily dissolved in mineral acids.

It was found, that the $\text{La}_{2-x}\text{NiO}_{4-\delta}$ compounds ($0 \leq x \leq 0,4$) crystallize in tetragonal syngony with structure of K_2NiF_4 -type, s. g. I4/mmm. Increase in x results in a decrease of tetragonal unit cell parameters. The samples crystallize in rhombic syngony, s. g. Fmmm ($0,45 < x < 0,55$) as a

$\text{La}_3\text{Ni}_2\text{O}_7$ structural type with insignificant defects in cation sublattice. In an interval of $0,6 \leq x \leq 0,75$ in $\text{La}_{2-x}\text{NiO}_{4-\delta}$ system the samples of rhombic syngony with structure $\text{La}_4\text{Ni}_3\text{O}_{10}$, s.g Cmcmm are formed. XRD patterns of the $\text{La}_{1,2}\text{NiO}_3$ - $\text{La}_{1,05}\text{NiO}_{2,9}$ samples are similar on those of $\text{La}_4\text{Ni}_3\text{O}_{10}$ with an impurity NiO. Calcination at 950°C of these samples was found to result in formation of cubic perovskites structure with defects in oxygen sublattice.

Table 1. Composition of the substituted nickelates $\text{La}_{2-x}\text{NiO}_{4-\delta}$.

X	Nickelates formula
0	$\text{La}_{2,00}\text{Ni}^{2+}_{0,65}\text{Ni}^{3+}_{0,35}\text{O}_{4,17}$
0.05	$\text{La}_{1,95}\text{Ni}^{2+}_{0,64}\text{Ni}^{3+}_{0,36}\text{O}_{4,10}$
0.10	$\text{La}_{1,90}\text{Ni}^{2+}_{0,66}\text{Ni}^{3+}_{0,34}\text{O}_{4,02}$
0.15	$\text{La}_{1,85}\text{Ni}^{2+}_{0,63}\text{Ni}^{3+}_{0,37}\text{O}_{3,96}$
0.20	$\text{La}_{1,80}\text{Ni}^{2+}_{0,60}\text{Ni}^{3+}_{0,40}\text{O}_{3,90}$
0.25	$\text{La}_{1,75}\text{Ni}^{2+}_{0,58}\text{Ni}^{3+}_{0,42}\text{O}_{3,84}$
0.30	$\text{La}_{1,70}\text{Ni}^{2+}_{0,58}\text{Ni}^{3+}_{0,42}\text{O}_{3,76}$
0.35	$\text{La}_{1,65}\text{Ni}^{2+}_{0,55}\text{Ni}^{3+}_{0,45}\text{O}_{3,70}$
0.40	$\text{La}_{1,60}\text{Ni}^{2+}_{0,55}\text{Ni}^{3+}_{0,45}\text{O}_{3,63}$
0.45	$\text{La}_{1,55}\text{Ni}^{2+}_{0,48}\text{Ni}^{3+}_{0,52}\text{O}_{3,59}$
0.50	$\text{La}_{1,50}\text{Ni}^{2+}_{0,46}\text{Ni}^{3+}_{0,54}\text{O}_{3,52}$
0.55	$\text{La}_{1,45}\text{Ni}^{2+}_{0,40}\text{Ni}^{3+}_{0,60}\text{O}_{3,47}$
0.60	$\text{La}_{1,40}\text{Ni}^{2+}_{0,36}\text{Ni}^{3+}_{0,64}\text{O}_{3,42}$
0.65	$\text{La}_{1,35}\text{Ni}^{2+}_{0,38}\text{Ni}^{3+}_{0,62}\text{O}_{3,34}$
0.70	$\text{La}_{1,30}\text{Ni}^{2+}_{0,36}\text{Ni}^{3+}_{0,64}\text{O}_{3,27}$
0.75	$\text{La}_{1,25}\text{Ni}^{2+}_{0,31}\text{Ni}^{3+}_{0,69}\text{O}_{3,22}$
0.80	$\text{La}_{1,20}\text{Ni}^{2+}_{0,26}\text{Ni}^{3+}_{0,74}\text{O}_{3,17}$
0.85	$\text{La}_{1,15}\text{Ni}^{2+}_{0,21}\text{Ni}^{3+}_{0,79}\text{O}_{3,12}$
0.90	$\text{La}_{1,10}\text{Ni}^{2+}_{0,24}\text{Ni}^{3+}_{0,76}\text{O}_{3,03}$
0.95	$\text{La}_{1,05}\text{Ni}^{2+}_{0,29}\text{Ni}^{3+}_{0,71}\text{O}_{2,93}$
1.00	$\text{La}_{1,00}\text{Ni}^{2+}_{0,18}\text{Ni}^{3+}_{0,82}\text{O}_{2,91}$
1.10	$\text{La}_{0,90}\text{Ni}^{2+}_{0,18}\text{Ni}^{3+}_{0,82}\text{O}_{2,76}$
1.20	$\text{La}_{0,80}\text{Ni}^{2+}_{0,36}\text{Ni}^{3+}_{0,64}\text{O}_{2,52}$
1.25	$\text{La}_{0,75}\text{Ni}^{2+}_{0,41}\text{Ni}^{3+}_{0,59}\text{O}_{2,42}$
1.50	$\text{La}_{0,5}\text{Ni}^{2+}_{0,62}\text{Ni}^{3+}_{0,38}\text{O}_{1,94}$
1.70	$\text{La}_{0,3}\text{Ni}^{2+}_{0,76}\text{Ni}^{3+}_{0,24}\text{O}_{1,57}$

It was shown, that the average degree of nickel oxidation uniformly increases from +2.35 for $\text{La}_2\text{NiO}_{4,17}$ to +2.78 for $\text{LaNiO}_{2,89}$ and further decreases to +2.7 for $\text{La}_{0,8}\text{NiO}_{2,55}$ as a result of formation bi-phase system.

The samples with the smaller contents superfluous lattice oxygen was shown to crystallize in rhombic syngony the La/Ni ratio is

$0.75 \leq x \leq 1$. The dependence of superfluous lattice oxygen content La/Ni ratio includes three parts: $1.6 \leq \text{La}/\text{Ni} \leq 2$, where tetragonal $\text{La}_{2-x}\text{NiO}_{4-\delta}$ are formed, $1.25 \leq \text{La}/\text{Ni} \leq 1.55$, where rhombic polynickelates are formed and $0.8 \leq \text{La}/\text{Ni} \leq 1.2$ with negative values of δ' (there is an area of unstable in the given conditions of synthesis of phases with a rhombic type of $\text{La}_4\text{Ni}_3\text{O}_{10-\delta}$ and cubic perovskite lattices).

All the obtained phases can be described as $\text{La}_{n+1}\text{Ni}_n\text{O}_{3n+1+\delta}$, series, where δ is the content of superfluous lattice oxygen on n mol of ions of a nickel. The nickel degree oxidation was found to increase from +2.35 to +2.51 with growth x from 0 to 0.5. It was also shown, that $\delta = 0.17$ for $\text{La}_2\text{NiO}_{4.17}$ and $\delta = 0.03$ for $\text{La}_{1.6}\text{NiO}_{3.63}$. Thus it is possible to conclude, that the δ' value decreases with growth x , though the general contents of superfluous oxygen increases (Fig. 1).

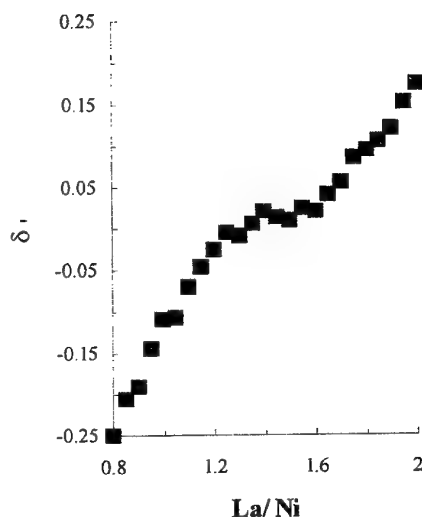


Fig.1. Dependence of the content of superfluous lattice oxygen on a ratio La/Ni.

All the $\text{La}_{2-x}\text{NiO}_{4-\delta}$ ($0 \leq x \leq 0.5$) samples was found to be characterized a semi-conducting properties.

For the samples with high La concentration ($x = 2; 1.9; 1.8$) the conductivity as a function of temperature can be described by exponential function. The activation energy of conductivity changes from 0,099eV ($x=0$) to 0,056eV ($x=0.2$). In the case of $\text{La}_{1.7}\text{NiO}_{3.76}$ and $\text{La}_{1.6}\text{NiO}_{3.63}$ samples the conductivity does not depend on temperature. The samples of $\text{La}_3\text{Ni}_2\text{O}_7$ - LaNiO_3 system were shown to demonstrate metallic type of temperature dependence of conductivity.

A part of nickel ions in lanthanum nickelates transform into trivalent state. This causes reduction of a Ni-O bond length. As a result, $d_{x^2-y^2}$ i p_{O2-} orbitales overlapping takes place with formation of a σ^* zone [1, 2]. The increase of trivalent nickel concentration leads to increase in degree of $d_{x^2-y^2}$ and p_{O2-} orbitals overlapping and decrease in gap between conductivity and valent zones

Thus it was found, that in the La_2NiO_4 - LaNiO_3 system the non-stoichiometric oxides of composition $\text{La}_{1+1/n}\text{NiO}_{3+1/n+\delta}$ are formed. It is shown, that electrokinetical processes in lanthanum nickelates essentially depend on a degree of oxidation of nickel ions. Thus, influence of the defects in cation sublattice on electroconductivity of the samples is insignificant.

Dependence between $\ln \sigma$ and $\ln(\delta)$ (δ is the content of superfluous oxygen) at 293K in system $\text{La}_{2-x}\text{NiO}_{4-\delta}$ ($0 \leq x \leq 0.4$) also has linear character (fig. 2),

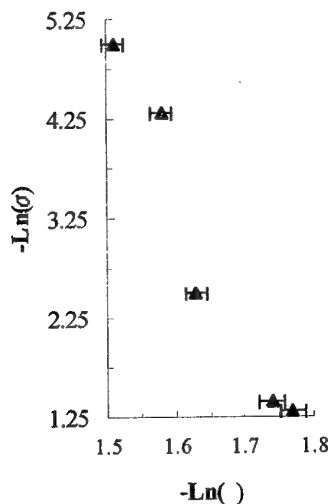


Fig.2. Dependence of the logarithm of electrical conductivity on the logarithm of average content of superfluous oxygen.

that, on seen, specifies a dominant role of -Ni-O-ayeres in electron transport, as the content of non-stoichiometric oxygen linearly is proportional to the lanthanum content.

References

1. J.B. Goodenough, P.M. Raccah, J. Appl.Phys. 36 (1965) 1031-1033.
2. J.B. Goodenough, Mater. Res. Bull. 78 (1973) 423.

EFFECT OF STRUCTURAL FEATURES OF $\text{Sm}_{1-x}\text{Ba}_x\text{Cu}_3\text{O}_y$ HIGH-TEMPERATURE SUPERCONDUCTORS ON CRITICAL TEMPERATURE

Drozd V.A., Baginsky I.L., Nedilko S.A., Nischenko M.M.⁽¹⁾, Likhtorovich S.P.⁽¹⁾

Kiev Taras Shevchenko National University, 64 Vladimirskaya St., Kiev 01033, Ukraine

⁽¹⁾G.V. Kurdyumov Institute for Metal Physics of the National Academy of Sciences of Ukraine,
36 Vernadsky Ave., Kiev 03142, Ukraine

After the effect of high-temperature superconductivity (HTSC) has been found, one of the principal problems that attract attention of researchers is that of mechanisms for appearance of superconducting state in the HTSC ceramics. Of particular importance is the following problem: how structure and chemical composition of HTSC compounds affect their superconducting properties. Solution to this problem could enable to perform purposeful and substantiated search for novel HTSC materials whose properties would be suitable for practical applications.

Using electron-positron annihilation technique, it has been found [1] that some structural feature of $\text{YBa}_2\text{Cu}_3\text{O}_7$ compound affects its superconductivity. This is inter-ion interval on each side of the CuO_2 chains along \bar{c} axis. Such interval exists in the $\text{YBa}_2\text{Cu}_3\text{O}_7$ superconducting phase only.

Our objectives were as follows: (i) to study $\text{Sm}_{1-x}\text{Ba}_x\text{Cu}_3\text{O}_y$ structure using electron-positron annihilation technique; (ii) to determine, for $\text{Sm}_{1-x}\text{Ba}_x\text{Cu}_3\text{O}_y$ cuprates, interrelation between the critical temperature T_c value and their structural characteristics, such as mean radii of oxygen ions and one-dimensional inter-ion spacing values in the crystal lattice; (iii) to verify electron-positron annihilation technique applicability for determination of oxygen ion radius; (iv) to determine sites of annihilation between positrons and electrons localized in the inter-ion space.

In this work we studied superconducting $\text{Sm}_{1-x}\text{Ba}_x\text{Cu}_3\text{O}_y$ compounds of 123 type (with $x = 0; 0.05; 0.1; 0.15$ and 0.2 , $y = 6.95 \pm 0.05$) using angular distribution of annihilation photons spectroscopy (ADAPS). We determined mean radii of oxygen ions in $\text{Sm}_{1-x}\text{Ba}_x\text{Cu}_3\text{O}_y$ structure. They lie between 0.133 and 0.137 nm depending on the substitution degree x . It was found that transformation of tetragonal symmetry into orthorhombic one (when the degree x of samarium substitution for barium is increased) results in an abrupt growth of the oxygen ion mean radius.

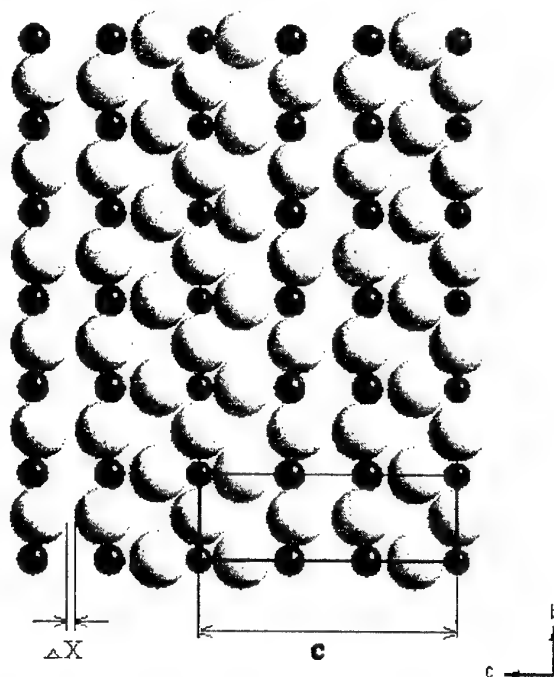


Fig.1. Geometric model for positions of copper and oxygen ions in the $[\bar{b}, \bar{c}]$ plane. ΔX is spacing between the electron shells of oxygen ions O(3).

Basing on results of x-ray diffraction studies and the values of oxygen ion radii obtained with ADAPS, we constructed a geometric model (Fig.1) for positions of copper and oxygen ions, as well as layers formed by CuO_2 chains in the $[\bar{b}, \bar{c}]$ plane (that are responsible for superconductivity). Our results evidenced that the structure studied is not close-packed along the \bar{c} axis. On each side of the close-packed groups of CuO_2 ions $\text{Cu}(2)\text{-O}(3)$ chains are located. They do not immediately contact with either close-packed CuO_2 chains or each other. Starting from this model, we calculated the ionic-covalent bond lengths and inter-ion spacing values ΔX for $\text{Sm}_{1-x}\text{Ba}_x\text{Cu}_3\text{O}_y$ structure (they are 0.03–0.04 nm). We found that spacing values affect the critical temperature value T_c in $\text{Sm}_{1-x}\text{Ba}_x\text{Cu}_3\text{O}_y$. It was shown that when ΔX values or relative number of

inter-ion intervals increase, then the critical temperature T_c grows (see Fig.2).

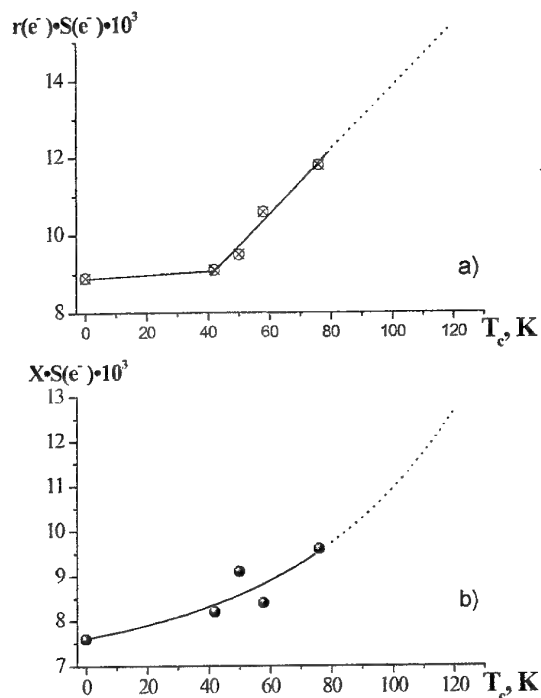


Fig.2. a) – product of the radius $r(e^-)$ of electron localization in the inter-ion space and probability $S(e^-)$ of electron-positron annihilation in the inter-ion intervals as function of T_c ; b) – product of spacing ΔX between O(3) anions and probability $S(e^-)$ as function of T_c .

The obtained ΔX values are comparable to the root-mean square shift $\langle x^2 \rangle^{1/2}$ of O^{2-} ions at thermal vibrations. The $\langle x^2 \rangle^{1/2}$ value increases with temperature; as a result, the phonon exchange along the $[\bar{c}]$ direction also increases.

This may disturb coherent movement of quasi-particles in CuO_2 chains, smear out local ion deformation (which is responsible for quasi-particle pairing) and break superconducting state when temperature T becomes over T_c .

Linear correlation dependence between the radius $r(e^-)$ of electron localization in the inter-ion space (obtained from the ADAP spectra) and spacing ΔX value was found (Fig.3). From this fact it follows that it is these intervals that are predominant sites of positron localization in the inter-ion space.

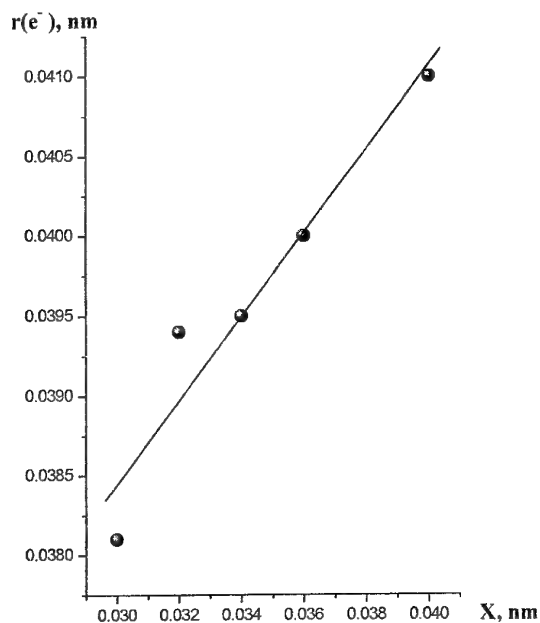


Fig.3. Correlation dependence of the radius $r(e^-)$ of electron wave function localization in the inter-ion space on spacing ΔX between the electron shells of O(3) ions.

References

1. M.M. Nischenko, S.P. Likhtorovich, A.Yu. Gerasimov // *Metallofizika i Noveishie Tekhnologii* (Metal Physics and Advanced Technologies). - 1998. - 20, No 7. - P. 3.

STRUCTURAL ANALYSIS OF NON-CRYSTALLINE POLYMER FOLLOWING EXAMPLE OF POLYVINILTRIMETHYLSILANE

Polikarpov V.M., Korolev U.M. ⁽¹⁾

Derzavin Tambov State University, International st. 33, 392000 Tambov, Russia

⁽¹⁾Topchiev Institute of Petrochemical Synthesis of Russian Academy of Sciences, Leninsky prospect 29, 117912 Moscow, Russia

It is a difficult problem to identify structure of non-crystalline system. The problem is more difficult for high-molecular polymers. The determination of experimental radial distribution function (ERDF) is one of calculation methods for structural analysis. The method is used successfully for analysis of different compounds. At the same time structural organization often can't be found on the base of another methods. The results of the calculations (made on the base of experimental radial distribution function) depend on both qualitative X-ray data and correct normalization of original experimental curve.

part of macro-chains of this polymer is packed into hexagonal lattice with $a=1,13$ nm, with conformation disordering ($c \approx 0.56$ nm). There are few diffusive maxims with lattice half – width on X-ray diffractogram of initial isotropic sample. The sample has increased structural organization than true amorphous.

For calculation used PVTMS in form of isotropic film. X – ray investigations are made by diffractometer DRON – 2. The calculations are made on the base of computer technologies.

On the base of the calculations it is established, that in initial polymer average distances among molecules are 1.18 nm and inter-chain period is about 0.53 nm. These parameters are close to analogous experimental parameters (see above). It is explained by formation of columnar mesophase during thermal treatment and stretching. Under external influences the conformation changes take place, it influences on average inter-chain periods. The conformation disordering may be explained by the supposition, that not all macro-molecular chains are changed conformationally and the changes may vary.

The obtained results were checked by decision of inverse task – modeling of diffractometrical curve on the base of the most probable conformation and obtained with help of ERDF calculated data. This calculation is made on the base of equation of Debye, considering both disperse properties of atoms and distances among atoms. As a result, error in positions of diffusive maxims doesn't exceed 7% (Fig. 1b). It proves authenticity of the results obtained with help of ERDF.

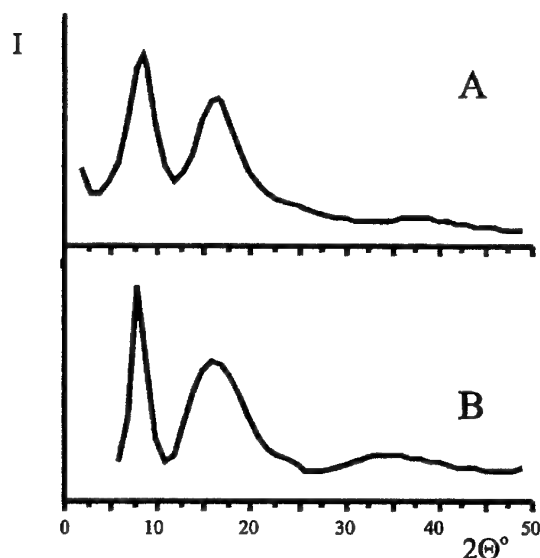


Fig.1. Experimental (a) and calculated (b) diffractogram of PVTMS at 20°C

The material used in the present work is polyvinyltrimethylsilane (PVTMS) – a well-investigated polymer. This polymer has unique structure and may be used at fabricating of gas-separated membranes. On the base of X-ray investigations, at normal conditions PVTMS has X-ray amorphous picture of diffraction (Fig. 1a). It is established, that during heating and stretching a

SYNTHESIS AND PHASE TRANSITIONS OF AMORPHOUS C_3N_4 POWDERS UNDER HIGH PRESSURE

Khabashesku V.N.^(1,2), Brinson B.⁽²⁾, Margrave J.L.⁽²⁾, Davydov V.A.⁽³⁾, Kashevarova L.S.⁽³⁾,
Rakhmanina A.V.⁽³⁾, Yakovlev E.N.⁽³⁾, Filonenko V.P.⁽³⁾

⁽¹⁾Zelinsky Institute of Organic Chemistry RAS, Moscow, Russia

⁽²⁾Rice University, Houston, TX, USA

⁽³⁾Vereschagin Institute for High Pressure Physics RAS, Troitsk, Moscow reg., Russia

Recently, the existence of potentially superhard α -, cubic and pseudocubic C_3N_4 polymorphs have been suggested on basis of calculations^{1,2}. However, all these phases are predicted to be metastable with respect to the energetically most favorable graphitic carbon nitride (g- C_3N_4), which, due to the sp^2 -bonded carbon, is expected to be a fairly soft material.³ This circumstance as well as the low thermodynamic stability with respect to the elements (C and N_2), indicated by a positive values of enthalpies of formation⁴, present the most serious challenge in the preparation of superhard C_3N_4 phases.

The synthesis of the C_3N_4 crystals with the sp^3 -bonding under high pressure appear to be very promising if the bulk quantities of stoichiometric sp^2 -bonded carbon nitride as precursor are used. To solve this problem, the convenient and inexpensive solid-state synthesis of carbo-nitride powders in gram quantities has been developed⁵⁻⁶.

This polymer material was prepared by a high-temperature polycondensation reaction using lithium nitride Li_3N as a nitridation and cross-linking agent, and a cyanuric chloride $C_3N_3Cl_3$ or its fluoro analogue $C_3N_3F_3$ as an *s*-triazine building block. The accordingly synthesized dark-brown powder shows featureless morphology with grain particle sizes exceeding 100 micrometers. The electron microprobe analysis shows that this powders are nitrogen-rich with the following varying compositions: $C_{0.34-0.38}N_{0.54-0.58}O_{0.03-0.05}Cl_{0.01-0.02}$. The elemental analysis gives an overall at. % N/C ratio of 1.33, precisely corresponding to the C_3N_4 stoichiometry. The FTIR spectra show the presence of *s*-triazine ring (bands at 1600, 986 and 805 cm^{-1}), which strongly suggests that the graphite-like sp^2 -bonded structure is most likely for the carbo-nitride powders. The solid-state (^{13}C) MAS NMR spectra exhibited two broad peaks: the larger at 168.9 ppm corresponding to the sp^2 -hybridized carbon atoms from the *s*-triazine rings and the smaller at 123.4 ppm for the *sp* carbon of the cyano group.

Modification of this process has recently led to the first preparation^{7,8} of nanoscale-size carbon nitride possessing a previously unknown spherical structure. The particle sizes in the prepared yellow powder were in the range of 1 micron to as low as 30 nm. The presence of *s*-triazine rings in the structure was established by FTIR, UV and (^{13}C) MAS NMR spectroscopy, and of pyramidalized bridging sp^3 nitrogens by XPS data. According to TEM (Fig. 1) and XRD data, the spheres are multi-walled, built by stacking curved graphitic C_3N_4 layers with the d-spacing of 3.415 Å, very close to the average intershell spacing of 3.42 Å in multiwall carbon nanotubes.

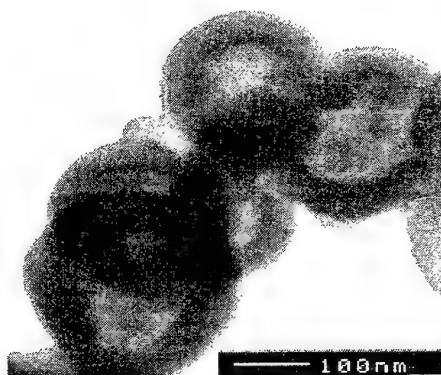


Fig1. TEM image of hollow carbon nitride spheres

Both amorphous graphitic (planar and spherical) carbon nitride powders were tested as a precursors in a series of high pressure-high temperature experiments, which were carried out in a high-pressure chamber of toroid-type. According to SEM/EDAX, micro-Raman, powder XRD and TEM/ED studies, under pressures of 8 to 10 GPa the structure of carbon nitride changes from amorphous graphitic to more ordered layered graphite-like structure with interplane d-spacing of 3.264 Å, in agreement with the predicted value of 3.29 Å for $P6m2$ g- C_3N_4 phase¹. Initial material was observed to retain the C_3N_4 stoichiometry at temperatures of about 400-500°C and release

nitrogen at higher temperatures up to 1200°C to convert into a pure carbon phase of graphite (d-spacing of 3.34 Å). These results are in agreement with the known data on high pressure investigations of carbonitrides⁹⁻¹².

The XRD data show that the sample prepared at pressure of 8.5 GPa and 500°C from spherical C₃N₄ precursor has crystallinity of about 90 %. The TEM data (Fig. 2) show the presence of well-faceted nanosize crystallites embedded in a larger size carbo-nitride phase.



Fig.2. TEM image of crystalline carbon nitride prepared at 8.5 GPa and 500 °C

The diffraction patterns, obtained for these crystallites, were indexed to the reflections expected for the cubic C₃N₄ structure. The unit cell size, calculated from experimental d-spacings both in ED and XRD, was found to be within 5.3-5.4 Å, which is in reasonable agreement with the theoretical value of 5.3973 Å^{1,2}.

These preliminary experiments helped to evaluate the pressure/temperature range where the structure transformation of graphitic carbon nitride starts to occur in the direction of crystalline cubic phase.

Based on these data, it is very likely that besides pressure and temperature, the reaction times (from milliseconds to hours) as well as a degree of openness of the system to volatile components are of primary importance for the synthesis of the *sp*³ C-bonded carbon nitride phases.

This research is partially carried out due to financial support from RFBR (Grant 02-03-32699).

1. A. Y. Liu, R. M. Wentzcovitch, *Phys. Rev. B*, 1994, 50, 10362.
2. D. M. Teter, R. J. Hemley, *Science*, 1996, 271, 53.
3. P. N. Wang, Z. Guo, X. T. Ying, J. H. Chen, X. M. Xu, F. M. Li, *Phys. Rev. B*, 1999, 59, 13347.
4. D. C. Nesting, J. V. Badding, *Chem. Mater.*, 1996, 8, 1535.
5. V. N. Khabashesku, J. L. Zimmerman, J. L. Margrave, Patent conversion filed with the US Patent and Trademark Office on July 27, 2000.
6. V. N. Khabashesku, J. L. Zimmerman, J. L. Margrave, *Chem. Mater.*, 2000, 12, 3264.
7. J. L. Zimmerman, R. Williams, V. N. Khabashesku, J. L. Margrave, *Russ. Chem. Bull.*, 2001, 2020.
8. J. L. Zimmerman, R. Williams, V. N. Khabashesku, J. L. Margrave, *NanoLett.*, 2001, 1, 731.
9. J. V. Badding, *Ann. Rev. Mater. Sci.*, 1998, 28, 631.
10. D. W. He, F. X. Zhang, X. Y. Zhang, Z. C. Qin, M. Zhang, R. P. Liu, Y. F. Xu, W. K. Wang, *J. Mater. Res.*, 1998, 13, 3458.
11. H. Montigaud, B. Tanguy, G. Demazeau, I. Alves, S. Courjault, *J. Mater. Sci.* 2000, 35, 2547.
12. H.A. Ma, X.P. Jia, L.X. Chen, P.W. Zhu, F.H. Li etc. Joint Conf. of AIRAPT-18 & HPCC-11. Beijing, China. 2001, Abstr., 279.

OXYGEN PACKING IN HIGH PRESSURE OXIDES OF W, Ta, Nb

Filonenko V.P., Zibrov I.P.⁽¹⁾

Institute for High Pressure Physics RAS, Troitsk, Moscow reg., Russia

⁽¹⁾Institute of Crystallography RAS, Moscow, Russia

For the last 10 years several new tungsten, tantalum, niobium oxides were synthesized under high pressure-high temperature conditions [1-4]. Usually, these metals in oxides have coordination numbers 7 (pentagonal bipyramid - PB) and 6 (octahedron -O). Andresen [5] has proposed structure model of α - U_3O_8 where U atoms have coordination number 7 (PB) and 6 (O) (Fig.1). Although the real structure of α - U_3O_8 consists only of PB (Loopstra model [6]) the structure of such compounds as $Nb_3O_7F(II)$ [7], $Ta_3O_7F(II)$ [8] and high pressure phases $W_3O_8(I)$ [1] and $A-Ta_2O_5$ [4] corresponds to the Andresen model.

Recently, high pressure modifications $Z-Me_2O_5$ ($Me=Nb, Ta$ [2,3]) were prepared at $P>7.5$ GPa. These phases have small monoclinic unit cell ($V\sim 137 \text{ \AA}^3$) and highest among niobium and tantalum pentoxides density. Detailed consideration of Andresen and Z phases show that they have some common elements of the structure. This work is devoted to analysis of structural features of these two structure types.

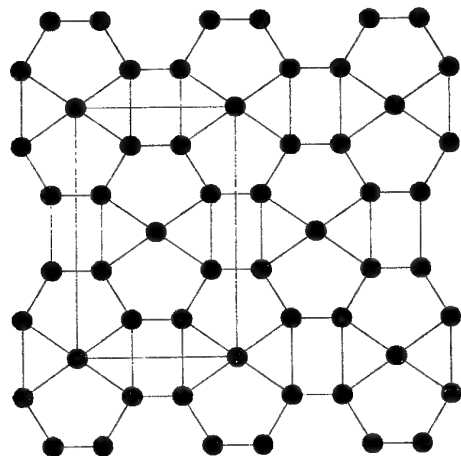


Fig.1.

The structure of $W_3O_8(I)$ (Andresen model). The unit cell in xy plane ($z=0$) is shown (filled circles correspond to oxygen atoms). Me atoms are situated in the same xy plane ($z=0$) in the centers of pentagons (PB) and rectangles (O).

Obviously, there are only two ways to realize stoichiometry Me_2O_5 in Andresen unit cell (stoichiometry Me_3O_8):

- insertion of 0.4 Ta atom per unit cell in the trigonal prisms ($z=1/2$) from the oxygen atoms (triangles on Fig.1);
- partial occupancy of the oxygen positions (15 oxygen atoms per unit cell instead 16 ones) like it occurs in the TT- Me_2O_5 ($Me=Nb, Ta$) [9] which is isostructural with α - $UO_3(\text{hex.})$ [10].

Two different starting materials were used for the synthesis of $A-Ta_2O_5$. First one was the mixture of L and H well known low and high temperature Ta_2O_5 modifications and the second one was the low hydrated amorphous tantalum hydroxide [11]. In the first case the single phase sample which X-ray pattern corresponded to $A-Ta_2O_5$ was obtained after treatment at 5.0 GPa, 1125°C for 3 min.. However, width of diffraction peaks was very high (FWHM $\sim 0.5^\circ$) what, probably, reflects high level of defects or strength in material. It was not possible to use this sample in structure refinement. In the second case the sample was treated at 6.5 GPa, 1100°C for 5 min. and had good peaks shape

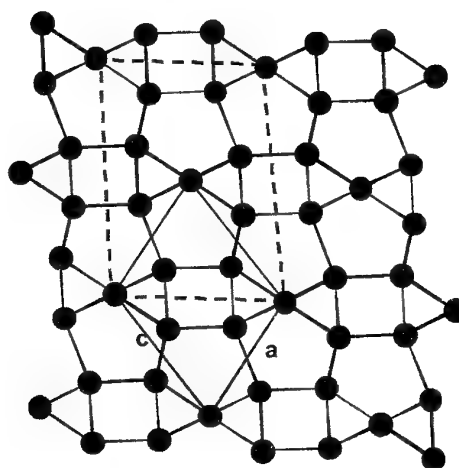


Fig.2.

The structure of $Z-Me_2O_5$. The oxygen (filled circles) plane xz is shown (the unit cell is marked by solid line). The unit cell corresponding to Andresen phase is shown by dashed line.

but contained except $A-Ta_2O_5$ approximately 10-20% of hydroxide $Ta_2O_5 \cdot 2/3 H_2O$ (the structure is

solved and will be published soon) and $\text{TT-Ta}_2\text{O}_5$. This sample was used in Rietveld refinement which show that Ta does not occupy positions in trigonal prisms of Andresen structure. It was not possible to refine occupancy of the oxygen positions because of multi-phasic sample but this mechanism looks to be more likely.

In the high pressure phase $\text{Z-Me}_2\text{O}_5$ ($\text{Me}=\text{Nb}$, Ta [2,3]) Me atoms have unusually high coordination number 8 (5 oxygen atoms in one plane, 3 atoms in another one and Me in between these planes). It easily can be seen from Fig.2 that oxygen packing is the same (with only small distortions) as in Andresen phase $\text{W}_3\text{O}_8(\text{I})$ (Fig.1). The structure of Z modification is built up from the identical oxygen planes xz (Fig.2) which are placed perpendicular to the b axis and shifted in neighbouring layers on $\frac{1}{2}a$ in x direction. The similar mechanism of phases formation is realized between α - and β - U_3O_8 : the oxygen planes xy in β - U_3O_8 [12] are the same as shown in Fig.1, but shifted in neighbouring layers on $\sim 1/3b$ in y direction. The relationship between unit cell dimensions of $\text{Z-Me}_2\text{O}_5$ and α - U_3O_8 are shown on Fig.2: the a and c axes of Z phase correspond to the half of the unit cell diagonals in xy plane of Andresen structure. The packing of the anion planes in two different structure types of $\text{Z-Me}_2\text{O}_5$ and α - U_3O_8 are very close to each other. The principle difference is only in Me atoms positions: in Z phase cations occupy positions between oxygen planes and in Andresen phase - in oxygen planes.

So, one can conclude that the oxygen packing described above is stable at high pressures even in case of formula Me_2O_5 when stoichiometry of the phase does not fit with stoichiometry of the basic unit cell.

This research was done partly due to support from RFBR (Grant 01-03-32457).

1. Sundberg M., Zakharov N.D., Zibrov I.P., Barabanenkov Yu.A., Filonenko V.P., Werner P. Acta Cryst. B49, 951, (1993).
2. Zibrov I.P., Filonenko V.P., Werner P.-E., Marinder B.-O., Sundberg M. J. of Solid State Chem. 141, 205, (1998).
3. Zibrov I.P., Filonenko V.P., Sundberg M. and Werner P.-E. Acta Cryst. B56, 659, (2000).
4. Filonenko V.P., Zibrov I.P. Inorg. Mat. 37, 9, 953, (2001).
5. Andresen A.F. Acta Cryst. 11, 612, (1958).
6. Loopstra B.O. Acta Cryst. 17, 651, (1964).
7. Wilhelmi A.S. Acta Chem. Scand. 24, 1472(1970).
8. Jahnberg L., Andersson S. Acta Chem. Scand. 21, 615, (1967).
9. H.-U. Hummel, R. Fackler, P. Remmert. Chem. Ber. 125, 55, (1992).
10. Zachariasen W.H. Acta Cryst. 1, 265, (1948).
11. Nikishina E.E., Drobot D.V., Filonenko V.P., Zibrov I.P., Lebedeva E.N. Russ. J. Inorg. Chem. 47 [1], 10, (2002).
12. Loopstra B.O. Acta Cryst. B26, 656 (1970)

COMPARATIVE ANALYSIS OF BRITTLINESS OF ANNEALED METALLIC GLASS BY BOTH MICROINDENTATION AND U – METHOD

Ushakov I.V., Feodorov V.A., Permyakova I.J.

Derzhavin Tambov State University, Tambov, Russia

INTRODUCTION

Fabrication and application of metallic glasses (MG) is of particular scientific and practical interest. The considerable attention focused on MG is motivated by the complex unique properties of these materials [1-3].

One of the negative moments in application of MG exhibits tendency to brittleness accompanying thermal treatment [4, 5]. Thus reception of an information about this question is of great significance.

MATERIALS AND EXPERIMENTAL TECHNIQUE

We studied an 82K3KhSR metallic glass of the composition (wt %) 83.7Co+3.7Fe+3.2Cr+9.4Si in the form of a ribbon 30 μm thick. Prior to experiments, samples (3×10 mm) were annealed in a furnace, in the temperature range of $T_{an}=538$ -1183K and held at a specified temperature for 10 min.

The character of deformation and fracture of the MG were investigated by *U* – method and by method of microindentation of the MG deposited on a substrate. We tested 15 samples at each temperature for statistics.

In the traditional *U* – method we estimated the deformation of bend ε at which take place brittle fracture of the MG [3]:

$$\varepsilon = h/(d-h) \quad (1)$$

where h is the thickness of the sample, d is the distance between two parallel plate of the specific designed measuring instrument at the moment of fracture.

The microindentation of the MG deposited on substrate (composite with microhardness of: 1 \approx 151 kG/mm²; 2 \approx 16 kG/mm²; 3 < 10 kG/mm², thickness of \approx 1 mm) was carried out on a PMT-3 microhardness gauge.

EXPERIMENTAL RESULTS AND DISCUSSION

a) It is found by U-method:

Dependence of the deformation of bend (Fig. 1)

At the $T_{an} < 628\text{K}$ the deformation MG proceed on the flatness of sliding. The fracture is not observed, if we bring bend to contact of ends of sample.

It is happened thanks to the plastic deformation, which display in rise of slip bands.

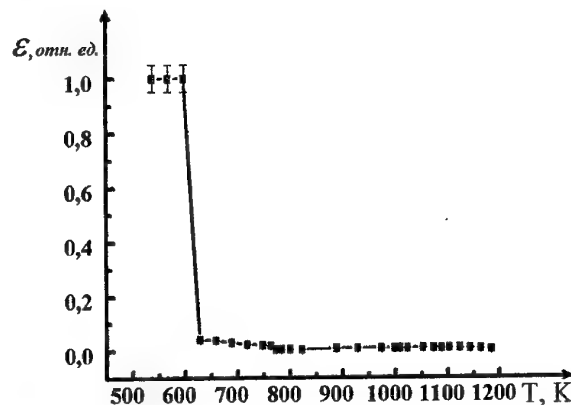


Fig. 1 Influence of thermal treatment on the deformation of fracture ε in the temperature range of $T_{an}=538$ -1183K

The visible loss plasticity starts at a $T_{an} \approx 628\text{K}$ accompanying formation main crack and leading to fracture of sample. The further reduction occurs with beginning crystallization MG. The loss plasticity lead to growth brittleness correspondingly.

At a $T_{an} \approx 823\text{K}$ conform to maximum brittleness connect with transition in a submicrocrystalline state. This temperature coincides with data of differential scanning calorimetry at which runs crystallization MG.

b) It is found by method of microindentation:

The critical temperature of annealing at which emerges of cracking formation during indentation. T_c depends for material of substrate. T_c is revealed on elastic substrate better than on the hard ones.

It is estimate that macropictures of destruction and deformation of the metallic glass after indentation depends from properties of used substrate. At the same time, the experimentally established critical temperatures, which correspond to ductile - brittle transition, are nearly for all substrates. At all substrates similar statistical regularities are obtained.

The endurance to cracking is lowered exponentially after exceeding T_c and reaches the minimal value near temperature of crystallisation (Fig. 2)

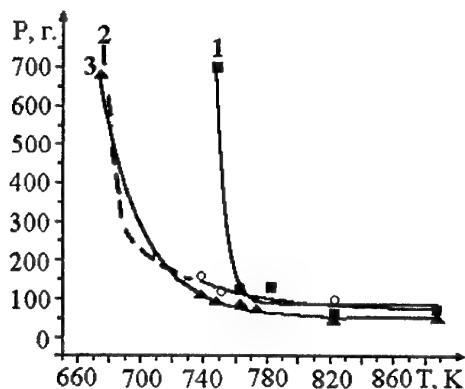


Fig. 2. Dependences of load P upon indentation on the annealing temperature T , for probability of the crack formation $W=1$: ■ – substrate № 1, ○ – substrate № 2, ▲ – substrate № 3.

Substrate № 1. $P_0=106,8\text{g} \pm 14,8\text{g}$; $A=345,2\text{g} \pm 29,5\text{g}$; $T_0=475\text{ K}$; $C=7,2 \pm 2,4\text{ K}$.

Substrate № 2. $P_0=84,8\text{g} \pm 18,9\text{g}$; $A=271,6\text{g} \pm 23,7\text{g}$; $T_0=673\text{ K}$; $C=49 \pm 35,7\text{ K}$.

Substrate № 3. $P_0=72,1\text{g} \pm 3,9\text{g}$; $A=408,8\text{g} \pm 6,6\text{g}$; $T_0=673\text{ K}$; $C=31,3 \pm 1,7\text{ K}$ [6].

Thus, the brittleness is raised exponentially after exceeding T_c and reaches the maximal value near temperature of crystallisation

correspondingly. These results tally with analogous results of U – method.

CONCLUSIONS

A change the brittleness of annealed metallic glass is investigated by traditional U – method and by method of microindentation on polymer substrates. The satisfactory concurrence of data is found. As a result, the data of U - method and data of microindentation may be united and may be used for analysis of structure and mechanical properties of metallic glass. In some case the method of microindentation is alternative method for research mechanical characteristic.

ACKNOWLEDGMENTS

This work was supported by the Grant of RFFR (project no. 01-01-00403).

REFERENCES

- 1 A. M. Glezer and B. V. Molotilov, Structure and Mechanical Properties of Amorphous Alloys (Moscow, 1992).
- 2 A. V. Likhachev and V. E. Shudegov, Organization Principles of Amorphouse Structures (St. Petersburg Gos. Univ., St. Petersburg, 1999).
- 3 K. Sudzuki, H. Fudzimori, K. Hasimoto Amorphouse alloys (Metallurgiy, Moscow, 1987)
- 4 J. Sestak // Thermochimica Acta. 1987, Vol. 110, P. 427-436
- 5 C. A. Pampillo, D. E. Polk // Mater. Sci. and Eng. 1978, Vol. 33, No 2, P. 275-280
- 6 V. A. Feodorov, I. V. Ushakov, Technical Physics. 2001 Vol. 46, No. 6, P. 673-676

RECEPTION AND RESEARCH OF PROPERTIES OF HEAT RESISTING CERAMICS ON A BASIS ZIRCONIUM DIOXIDE'S, STABILIZED OXIDES ALKALI-EARTH METALS OF METALS

Nikolenko S.V., Verchoturov A.D., Vlasova N.M.

Institute of Material Science KSC FEB RAS Russia, Khabarovsk

The further development of science and technology at its' current state is impossible without ceramic materials with high-level properties. Growth of ceramics production (annual growth increase in absolute terms – 8,7%) exceeds that of production of any other kind of materials. Recently, special attention was paid to zirconium dioxide, since some of its' properties surpass those of other materials. Usually, oxides of rare-earth and alkali-earth metals that form hard solutions with ZrO_2 are used as stabilizing additives: MgO , CaO , Y_2O_3 , etc. In recent years, combined additives of stabilizing oxides, due to the fact that twin phase ceramics has increased heat-resistance. ZrO_2 is stabilized with a combination of magnesium and calcium oxides in quantity of 16-18 mol %.

Economic factors have come to dominate the development and application of new materials, setting the technical ones aside. Industrial production of ceramics usually involves costly chemically pure ingredients and stabilizing elements. The main road to lowering the production cost of ceramics, therefore, lays through the exploration of ways of applying cheap, multi-component mineral raw materials, which include components close to those used as stabilizers in ceramics production.

The main task set forth for this study was the production of ceramic crucibles used for casting metal from baddeite mineral concentrate (96% ZrO_2) and caoline $Al_2(OH)_4Si_2O_5$ and brusite $Mg(OH)_2$ as a stabilizing additive. Another purpose was to research physics-mechanical and physics-chemical properties of the produced ceramic material. Baddeite, mineral and natural magnesium hydroxide (brusite) were used as initial components for these experiments. The charge of initial components was defined using the diagram of ZrO_2 - MgO system condition.

Phase composition of ZrO_2 -based material was analyzed in correlation with the amount of magnesium oxide additive contained in the charge: 9, 17, and 30 mol %. The mix of baddeite concentrate and magnesium oxide was blended and grinded in the planetary mill "Sand" for the dura-

tion of one hour. The produced charge was then dried and synthesized in high-temperature to produce cubic zirconium dioxide. The powder was classified and mixed with caoline in 1:1 proportion, after which it was cast to produce ceramic crucibles. Casting forms were made from $CaSO_4$ 0,5 H_2O gypsum. After the dross was cast into the form it hardened near the walls, forming the needed product. At this point excess dross was poured out of the form, while the semi-dry crucible was easily extracted and dried later on. Crucibles were dried in the SNVE-type furnace with tungsten heaters in vacuum $6,65 \times 10^{-3}$ Pa in the temperature interval of 1400-1500°C. Density of the produced sample was measured through hydrostatic weighting. DRON-3 M defractometer was used for the x-ray phase analysis of powders and polished surface of the produced samples. Shape and dimensions of particles of zirconium dioxide based powders were evaluated using JEOL JSM-30M scanning electron microscope. MBS-9 and MIM-10 optical microscopes with zoom x200 where used for the evaluation of an average size and quantity of pores on the polished surface of produced samples.

Fragility level was calculated based on Glazov-Vigdorovitch method. Total fragility mark was: $Z_p = 0 n_0 + 1 n_1 + 2 n_2 + 3 n_3 + 4 n_4 + 5 n_5$, where $n_0, n_1, n_2, n_3, n_4, n_5$ – relative amount of prints out of the total amount with that fragility mark.

Cracking resistance coefficient (K_{IC}) for the produced ceramics was calculated using an express-method based on Evans formula:

$$\frac{K_{IC} F}{HV \sqrt{b}} = 0,15 k \left(\frac{a}{b} \right)^{-3/2} \text{ where } F = \frac{HV}{\sigma_{1/2}} \approx 3 ;$$

$k=3,2$; b – half of the print's diagonal; a – b + length of the crack from the top of indenter print.

Stabilization of zirconium dioxide is carried out through transforming the originally monocline structure into a cubic one, the latter being stable at work temperatures, due to the forming of hard solutions of Zr^{4+} ion substitution by the stabilizer's ion. The correlation of ion radiuses $r_z/r_a=0,66$ in zirconium dioxide is close to the border between anions of the lattice with coordina-

tion number (c.n.) of 8 and 6. Large dimensions of zirconium cation (0,082 nm) don't allow oxygen ions to in the lattice to draw close enough to form an eight coordination. Therefore, ZrO_2 gives an unusual coordination with (c.n.)=7 and one of oxygen atoms ending up between two lattice points AB: A – eight and B – six coordination. At high temperatures, due to the heat movement of anions at lattice points, Zr-O bond elongates, causing an oxygen ion to shift from the interpoint space to position A or B realizing an eight coordination with an anion vacancy. Substitution of zirconium ions by ions of two valency metals forms one oxygen vacancy for every substituted zirconium ion or one vacancy for every two substituted ions for three valency metals. Lattice positions must increase their dimensions to allow for ZrO_2 crystallization in cubic form, this can be achieved either through the increase of an average ion radius of cations by substituting zirconium ions with ions with high radius (Ce^{4+} , Th^{4+}), or through the creation of vacancies in the oxygen sublattice, which occurs when Zr^{4+} ions are substituted by ions with lesser valency (Mg^{2+} , Y^{3+} , etc.). In practice, hard solutions in which the size of additive cation exceeds that of zirconium by 10-20% with a lower charge (Y^{3+} , Yb^{3+} , etc.) tend to be the most stable.

The influence of a brucite additive on polymorphic transformations of zirconium dioxide can be traced using the RFA data.

Polymorphic transformation in ZrO_2 -MgO begin at the temprature of 1200°C, although according to the diagram of state the cubic modification of zirconium dioxide forms only at 1500°C. The lower temperature of ZrO_2^{cubic} forming can be explained by the presence of admixtures in the raw materials used.

According to the evaluation of phase composition, based on x-ray phase analysis of smelted material with magnesium oxide containment of 30 mol %:

- 1400°C – 58%, ZrO_2 (tetragonal) – 42%;
- 1500°C – 95%, ZrO_2 (tetragonal) – 5%;
- 1600°C – 100%.

The dross casting method was used for the production of ceramic crucibles, which are generally used in dental care. High quality of forming can be achieved when using dross with high fluidity, sedimentation and aggregate stability, share of solid phase, and so on. At the same time the dross mustn't be characterized by tixotropy and dilatancy, which are related to the change of its' vis-

cosity in time. The dross's viscosity must be kept to the minimum possible level, which can ensure the necessary fluidity for the quality forming of the cast. However, high concentrations of the solid phase in the dross – 40-80% of the mass – surface activity and interaction of dispersion particles, and an inclination to form structures cause anomaly viscosity changes (structural viscosity). The flow in such systems begins only with they reach a certain shift stress. As the shift's speed increases the values of viscosity may decrease (tixotropy) or increase (dilatancy). These phenomena are especially evident if the solid phase has high dispersion. In practice, the optimal viscosity of dross is selected through experiment, changing humidity and pH of the environment. It is normally preferable to keep the viscosity at the lowest possible level. Increase of the dross's humidity leads to a significant decrease of speed at which it gains mass, time needed for it to sit in the forms, and splitting. Changes of the environment's pH have a sharp effect on the dross's viscosity. Minimal viscosity in the acidic area is noted in the range of $pH=1,5 - 2$ and alkaline – 8-9. This work uses alkaline dross with $pH=9$, giving a very stable suspension. Fragility of the material was tested on the samples of ceramics from cubic zirconium dioxide and Veskaprima gypsum. Fragility value, which shows the character of fragile destruction and speed of its' increase with the increase of stress, is a product of the total fragility mark and the value of stress derivative;

$$\gamma_p = z_p \left(\frac{dz}{dP} \right)_p = 0,2$$

This value shows that the produced ceramics is relatively fragile, $\gamma_p < 1$. Cracking resistance coefficient of the produced ceramics $K_{IC}=2,55MPa \times m^{1/2}$, microhardness $H_\mu=8,7-11,4GPa$, average size of zirconium dioxide grain – 15 micron. Medical crucibles produced using this material have survived 15 casts and were ready for future use.

The following studies have been performed in the course of the described work: polymorphic transformations in the temperature range of 1000-1700°C of brusite based zirconium dioxide; conducted research has allowed to select a stabilizing combined additive based on a natural magnesium hydroxide, which permits to decrease the temperature of the beginning of forming of cubic zirconium dioxide; partially stabilized zirconium dioxide with the following combination of components – ZrO_2 (cubic) 58%, ZrO_2 (tetragonal) 42%.

PRINCIPLES FOR CREATION OF NEW ADVANCED HIGH-STRENGTH CAST EUTECTIC ALUMINUM ALLOYS

Barabash O.M., Milman Y.V.⁽¹⁾, Korzhova N.P.⁽¹⁾, Legkaya T.N., Podrezov Y.N.⁽¹⁾,
Voskoboynik I.V.⁽¹⁾

G.V. Kurdyumov Institute of Metal Physics of NAS of Ukraine, Kiev, Ukraine

⁽¹⁾Frantsevich Institute for Problems of Materials Science of NAS of Ukraine, Kiev, Ukraine

The technical progress is impossible without creating new materials that satisfied the increased demands. It also concerns the materials produced by traditional techniques, e.g. cast aluminum alloys that in large amounts are claimed in automotive, aircraft and shipbuilding industries.

Traditionally cast aluminum alloys are eutectic ones, whose structure and phase composition is formed immediately during crystallization. Phase constituents of these alloys, possessing high thermal stability, are close to the thermodynamic equilibrium. In addition, the presence of the eutectic results in improved castability. However, the resource to improve properties of existing alloys, including high-temperature strength, which is directly bound with their melting temperature, at present, is practically exhausted. A complex alloying of these alloys, as a rule, gives rise to decreasing the volume fraction of the eutectic constituent, to widening the temperature range of melting and consequently to a loss of castability.

The present work proposes scientific principles for designing new cast aluminum alloys, based on proper theoretical and experimental developments of authors in the field of phase equilibrium of multicomponent systems [1-4]. Basing on these principles, new eutectic alloys were obtained.

To design new modern materials it is necessary to choose the base systems of alloys with high eutectic temperature, small temperature interval of melting, as well as with significant volume concentration of the second phase in the eutectic and with the phase composition that is stable with respect to additional doping.

The analysis of phase composition and properties of modern cast aluminum alloys allows to make a conclusion, that a considerable improvement of their properties (first of all the increase of the operating temperature) can be achieved by using ternary and more complicated systems, characterized by the existence of the quasi-binary phase equilibrium of aluminum solid solutions with high temperature intermetallic phases. In the multicomponent system representing real alloys, the eutectic transformation covers a considerable area of concentrations and occurs in a

range of temperatures. Potentially useful eutectic alloys should possess both the highest melting temperature and the lowest melting range. Therefore, the search for such eutectic alloys in the complex systems is a difficult and labour-consuming task.

The most perspective for designing of advanced materials are the systems, which are similar to the systems of the third type of phase diagram (the classification proposed in the work [5]). An intrinsic property of such systems is the limited mutual solubility of their components and phases, as well as steady equilibrium between the metal and the strengthening phase. A peculiarity inherent to these systems is the existence of quasi-binary sections [6], which do not coincide with the stoichiometric section "metal - strengthening phase" of the ternary diagram. The alloys settled on the quasi-binary section have in cast condition a fine eutectic structure, in which hard and more refractory intermetallic phase is combined with the more plastic matrix [2]. These requirements are satisfied in the ternary system Al-Mg-Si, where the eutectic transformation $L\Omega\alpha\text{-Al}+\text{Mg}_2\text{Si}$ does exist [3, 4, 7, 8].

A complex investigation of alloys of this system, completed with thermodynamic calculations [3], allows us to plot the fusion diagram in the aluminum angle of the ternary Al-Mg-Si system.

A distinctive feature of the ternary system Al-Mg-Si is a shift of both the quasi-binary section and the area of two-phase alloys to the magnesium rich region. This creates premises to regulate in a wide range (0.2 - 6 at. %) the magnesium content in the matrix of eutectic alloys, retaining simultaneously their phase composition and structure. In turn, it creates a possibility to develop a principally new system of alloying these alloys.

To ensure high level of physical and mechanical properties at room and elevated temperatures, different systems of coherent particles in the matrix of eutectic $\alpha\text{-Al}+\text{Mg}_2\text{Si}$ alloys can be created in the selected system of alloys. Note that such particles should not interact with eutectic colonies. This guarantees a stability

of strength of the eutectic composite at elevated temperatures. In addition, the quasi-binary eutectic transformation in alloys ensures the retaining of necessary phase composition of the material directly in crystallization process.

The proposed approach is realized in designing new cast α -Al-Mg₂Si eutectic alloys of Al-Mg-Si ternary system. Typical microstructures of these alloys before and after alloying are shown in Fig. 1. By means of additional alloying all mechanisms of hardening (composite, solid solution and precipitation) are realized. Such an approach provides a substantial increase of operational characteristics (strength, wear and corrosion resistance) of materials both at room and elevated temperatures (Fig. 2).



Fig. 1. Microstructures of eutectic (α-Al + Mg₂Si) alloys before (a) and after (b) complex alloying. The eutectic belongs to faceted-unfaceted class.

Conclusions

There is proposed a new approach to design cast aluminum alloys, based on using ternary and more complicated phase diagrams, containing eutectic quasi-binary sections of aluminium and intermetallic phases and detailed investigation of the topology of the corresponding fusion diagrams. The creation of different systems of particles,

coherent to the matrix and non-interacting with eutectic colonies, allows to improve the level of mechanical properties and to widen the temperature range of alloys usage. The complex alloying by transition and rare earth metals should not change phase composition and structure of basic alloys.

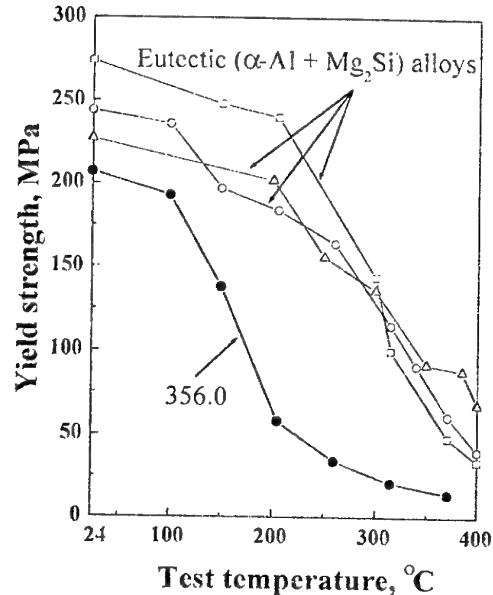


Fig. 2. Temperature dependence of the yield stress in tensile test of the multicomponent eutectic (α-Al + Mg₂Si) alloys and commercial [9] cast alloy 356.0.

References

- [1] Barabash O.M. & Legkaya T.N. Met. Phys. Adv. Tech., 1996, Vol. 15, p. 993-999.
- [2] Barabash O.M. & Legkaya T.N., J. Chim. Phys., 1997, Vol. 94, p. 1686-1693.
- [3] Barabash O.M., Sulgenko O.V. et al. J.Phase Equil., 2001, Vol. 22, 1, p. 5-11.
- [4] Barabash O.M., Milman Yu.V. et al. Functional Materials, 2001, V. 8, 1, p. 159-161.
- [5] Shurin A.K. Poroshkovaya Metallurgiya. 1973, 1, p.50-53.
- [6] Zakharov A.M. Phase Diagrams of Binary and Ternary Systems (Metallurg., Moscow 1978).
- [7] Mondolfo L.F. Aluminium Alloys: Structure and Properties (Butterworth & Co., London 1976).
- [8] Feufel H., Gödecke T. et al., Alloys Compounds, 1997, V. 247, p.31-42.
- [9] Aluminum and Aluminum Alloys (ASM International Materials Park, USA 1993).

REFRACTORY PERMEABLE THERMAL INSULATION: PRODUCTION AND APPLICATION

Gorin A.I.

Keldysh Research Center, Moscow, Russia

Dispersed layers of refractory foams or fibers, formed by carbon, ceramics or metals, find widespread adoption as high-temperature thermal insulation. Natural areas of their application are energetic and aerospace systems using high temperatures, which level has the direct impact on systems effectiveness. Thermal insulation protects metallic walls from hot gas streams on the outside and on the inside surfaces of aerospace and energetic devices respectively. Essential aspect of the similar applications is permeability of insulating layer and possibility of gas flowing inside it.

The analysis is made showing the necessity and usefulness of reducing the diameters of in-

sulation fibers. The level $5 - 7 \text{ mkm}$ was achieved experimentally. High performance parameters were obtained due to growing of the layer with enhanced density on the surface of insulating rings dividing the inner fibrous region from the main gas stream. Requirements to permeability of the surface layer are analyzed.

The experience is reported in design optimization and practical application of fibrous carbide insulating material on the inner surface of rather heavy duty canals with the working temperature – 3000 K , pressure – up to 5 MPa , and mass-flow density – above $450 \text{ kg/m}^2\text{c}$.

NEW EUTECTIC MATERIALS OF THE TERNARY SYSTEM Al-Ti-Cr BASED ON THE INTERMETALLIC $Al_3Ti_{1-x}Cr_x$

Barabash O.M., Milman Y.V.⁽¹⁾, Miracle D.B.⁽²⁾, Karpets M.V.⁽¹⁾, Korzhova N.P.⁽¹⁾,
Legkaya T.N., Mordovets N.M.⁽¹⁾, Podrezov Y.N.⁽¹⁾, Voskoboinik I.V.⁽¹⁾, Voynash V.Z.

G.V. Kurdyumov Institute of Metal Physics of NAS of Ukraine, Kiev, Ukraine

¹I.N. Frantsevich Institute for Problems of Materials Science of NAS of Ukraine, Kiev, Ukraine

²Air Force Research Laboratory, 2230 Tenth Street, Wright-Patterson AFB, OH 45433

Nowadays structure as well as physical and mechanical properties of $Al_3Ti_{1-x}Cr_x$ -based alloys having $L1_2$ crystalline structure are extensively investigated [1-3]. High melting temperature, elastic modulus, low density and increased oxidation resistance make this intermetallic to be promising as a basis for the elaboration of new high modulus heat-resistant materials. However, the cubic crystalline structure $L1_2$, forming by the addition of chromium to the intermetallic, does not ensure a sufficient enhancement of its plasticity [4-5]. There are some other ways of increasing intermetallics plasticity. For example, it can be achieved by the increase of structure dispersivity or by the creation of two-phase lamellar structure formed by alternate layers of phases having different properties [6-7].

The perfect dispersed two-phase structure, stable at high temperatures and having minimal stresses in phase boundaries can be formed also by eutectic crystallization. Such alloys have high castability and form dense ingots with minimal number of pores at crystallization.

The search of eutectic alloys in the ternary system Al-Ti-Cr containing $L1_2$ intermetallic, the examination of features of two-phase eutectic structure formation along with its effect on physical and mechanical properties of alloys were the purpose of this work.

The concentration region of existing two-phase (after crystallization) eutectic ($L1_2+\beta$) alloys was defined by using of microstructural, thermal and X-ray phase analysis it appeared to be rather wide. Both $L1_2$ and β phases have a cubic crystalline lattice. They are chromium-doped intermetallic $Al_3Ti_{1-x}Cr_x$ ($L1_2$ phase) and solid solution of titanium and aluminium in chromium (β -phase). The maximum temperature of melting completion of the univariant eutectic ($L1_2+\beta$) is 1275 °C (the melting range being 10 °C) and decreases monotonically with decreasing titanium content in the alloys. It was found that the width of the two-phase region reduces with temperature decreasing. This promotes the appearance of the third phases

($AlTiCr$ and $AlCr_2$) in the alloys after their cooling with low rates.

Structure and mechanical properties of cast alloys pertaining to the two-phase region ($L1_2+\beta$) are shown in Fig. 1.

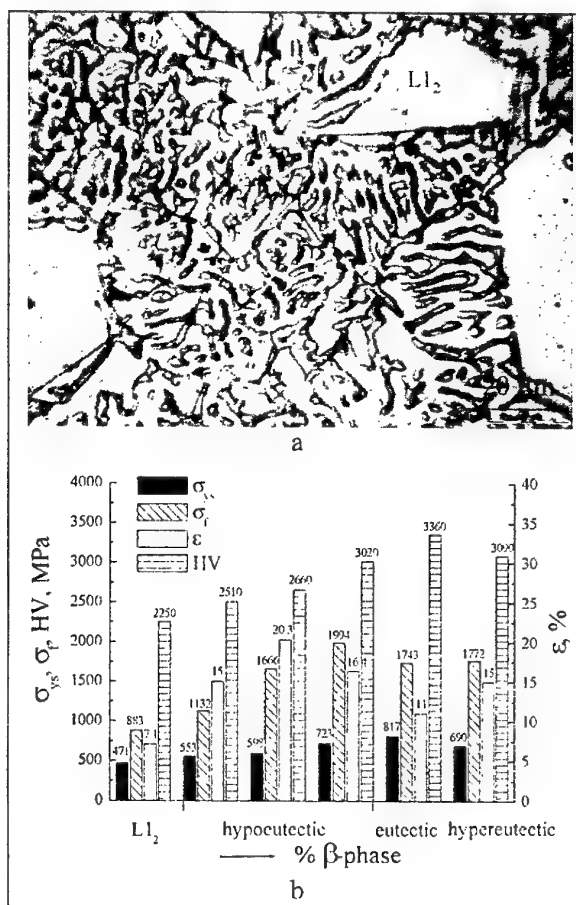


Fig. 1. Microstructure (a) and mechanical properties in compression tests (b) of as-cast eutectic ($L1_2+\beta$) alloys of the ternary Al-Ti-Cr system.

One can see that both faceted primary $L1_2$ -phase crystals and binary eutectic ($L1_2+\beta$) are present in hypoeutectic alloys. Eutectic morphology, belonging to a lamellar-rod type, is complicated: fibers and plates of the β -phase are

distributed in the $L1_2$ matrix of the alloy (Fig. 1 a). The increasing of β -phase fraction results in the change of the structure from hypoeutectic to hypereutectic.

Mechanical properties of the alloys with different volume part of eutectic were investigated in compression and bending. Room and high temperature hardness were also measured. It is established that the appearance of the eutectic in alloy structure results in the increase of its plasticity (Fig. 1 b). Thus, hypoeutectic ($L1_2+\beta$) alloys have the value of the parameter ε in compression in the range of (11-20.5) % versus 7 % for the single-phase intermetallic $L1_2$ ($Al_{63}Ti_{26}Cr_{11}$). At the same time the fracture mode is changed from totally transgranular in the $L1_2$ -structure alloy (Fig. 2 a) to cleavage with relaxation in the eutectic alloy (Fig. 2 c). The same effects were observed on the lateral surface of specimens: in the single-phase alloy there are visible cracks (Fig. 2 b) of the size comparable with the grain size; in the second alloy there appeared small cracks hampered by structural elements of the eutectic alloy (Fig. 2 d).

The change of hardness and compression strength characteristics within the hypoeutectic two-phase range has a common form: the larger is the amount of the reinforcing β -phase, the higher are these characteristics; at the same time, the concentration dependence of plasticity is non-monotonous with a maximum in the hypoeutectic range not far from the eutectic composition (Fig. 1 b).

Hot hardness of the investigated alloys depends very weakly on the temperature: over a temperature range of 20-800 °C it is not less than 3.1 GPa.

Conclusion

Thus, the elaboration of eutectic composites, containing $L1_2$ intermetallic and β -phase allows to obtain a significant increase of strength and plasticity characteristics retaining at the same time high elasticity modulus value. For instance, such eutectic alloys have a high level of mechanical properties: Young's modulus up to 190 GPa, compressive and bending strength up to 2000 MPa and 600 MPa, respectively, plasticity in compression up to 20.5 %. The eutectic character of the alloys ensures their high cast properties, while high melting temperature of the eutectic (up to 1275 °C) allows increased high temperature properties to be anticipated.

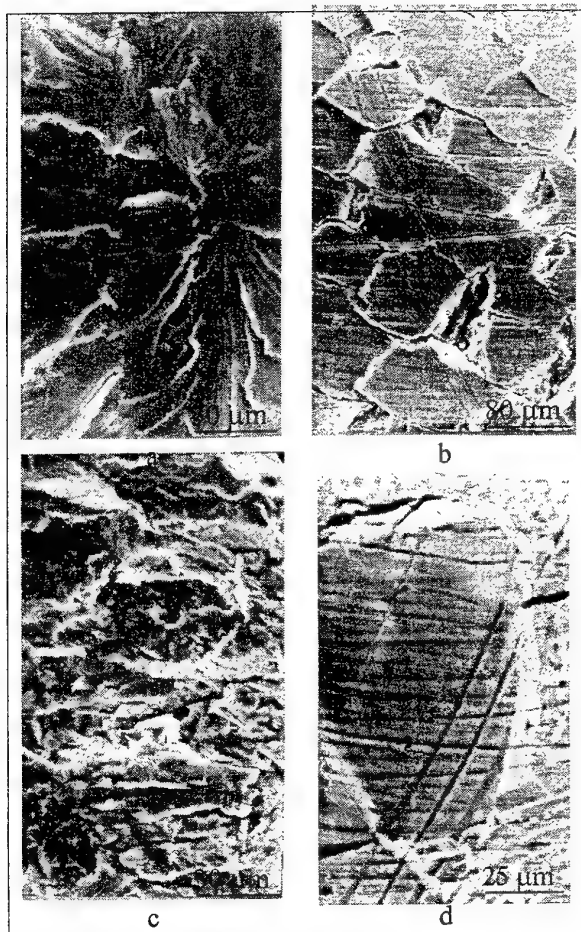


Fig. 2. Fracture (a, c) and lateral (b, d) surface of the samples after compression test: single phase alloy $L1_2$ (a, b); hypoeutectic alloy (c, d).

Acknowledgements

The work was partially financed by STCU (project P061).

References

1. Lee J.K., Park J.Y., Oh M.H., Wee D.M. *Intermetallics* 2000; 8: 407-416.
2. Jewett T.J., Ahrens B., Dahms M. *Intermetallics* 1996; 4: 543-556.
3. H. Mabuchi, H. Tsuda et al., *J. Japan of Powder Metallurgy* 1997; V.45, 3: 225-230.
4. Nic J.P., Klansky J.L., Miccola D.E. *Mat. Sci. and Eng.* 1992; A152: 132-137.
5. Milman Yu.V., Miracle D.B., Chugunova S.I. et al. *Intermetallics* 2001; 9: 839-845.
6. Zhang L.C., Palm M., Stein F., Sauthoff G. *Intermetallics* 2001; 9: 229-238.
7. Jang S.J, Woo S. *Intermetallics* 2002;10: 171-175.

HOT DEFORMATION OF HOT-RESISTANCE SILICIDE-HARDENED TITANIUM-BASED ALLOY

Kuzmenko N.N., Kulak L.D., Baglyuk G.A.

Frantsevich Institute for Problems of Materials Science of NAS of Ukraine, Kiev, Ukraine

High alloy titanium alloys are susceptible to liquation processes, which hampers essentially the possibilities of their presswork. This is due to sharp decrease of technological plasticity of the alloys, high resistance to, and narrow temperature range of, the deformation. Depending on a number and orientation of defects, being in the alloys, local stresses are increased sometimes by 5-10 times [1]. Additional source of the internal stresses is interaction between constituent phases having different plastic properties due to differences in composition and structure. Besides, low heat conductivity of titanium alloys increases nonhomogeneity of temperature field of ingot, increasing simultaneously non-homogeneity of metal flow and resulting in possibility of the surface and internal material defects formation (micro- and macro-cracks).

Therefore, in order to determine optimal thermomechanical regime of deformation, the mean values of limit deformation powers of ingots at different temperatures as well as the influence of ingot deformation power on basic structural and mechanical properties of the material should be determined.

The present work deals with tests of deformability characteristics of the alloy in conditions of free high temperature shrinkage on smooth panes. Investigation of plasticity under free shrinkage was carried out using cylindrical specimens with a diameter of 25 mm and a length of 30 mm. The specimens were obtained by plasma-arc remelting from material of the following composition: Ti-basis, Al -3,0%, Si-4,1%, Zr-5,0% (wt. %). Heating of ingots were made in electric resistance furnace up to temperatures 850-1200°C for 10 min. Ingot shrinkage was carried out using polished smooth panes slurried with mix of engine oil and graphite. The shrinkage was made during one stroke of crank press with stepped increasing power of axis deformation up to arising first cracks on forging lateral surfaces.

Investigation of dependence of maximum compression on deformation temperature has shown an increase of mean limit deformation at heating temperature increase. For example, at temperature 850°C maximum deformation power does not succeed 35%. Increase of deformation power promotes failure of specimen lateral surface.

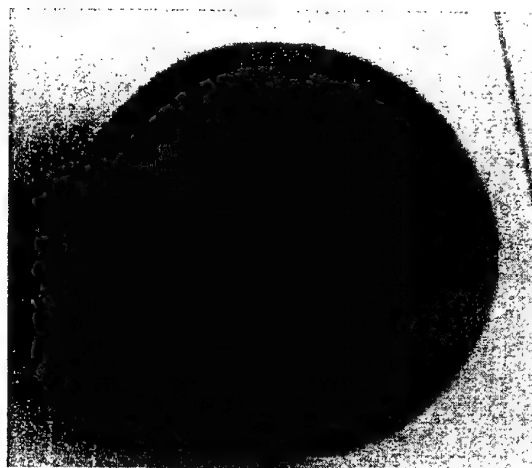


Fig.1 Specimen, having traces of lateral surface fracture ($\epsilon=50\%$, $T=900^\circ\text{C}$).

The ingots, heated to temperatures 1000-1200°C, was deformed already to deformation power more than 60% without any evidence of failure, which is a result of appropriate technological plasticity of the material in this temperature range.

Analysis of shape formation process under shrinkage shows that deformation power up to 15-20% corresponds to relatively homogeneous deformation in conditions of uniaxial compression due to weak influence of contact friction stresses. Increase of compression results in change of stress state when, along with axis compressive stresses, marked radial and tangential tensile stresses are acting. The process is accompanied by increase of deformation nonhomogeneity, resulting in tubby-shaped specimen, being typical for conditions of shrinkage with friction.

It is of very interest to obtain dependence of main mechanical properties of hot-deformed materials on ingots heating temperature and on axis deformation power. It follows from Fig...., that dependence of the material yield stress on deformation power in temperature range 850-1100°C is different essentially compared with such dependence at stamp temperature of 1200°C. At heating ingots to 850-1100°C dependence of yield stress of deformed materials on deformation power is nonmonotonous. One can see that increase of deformation power up to 30% results in increase of strength of deformed materials for all temperatures within temperature range 850-1100°C; at the same time, further increase of ε_z under shrinkage promotes marked strength decrease (Figure 1).

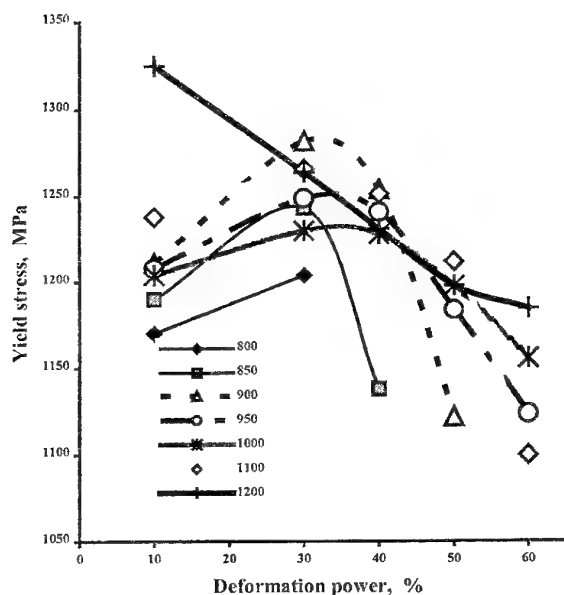


Figure 2. Temperature dependence of yield stress on deformation power in compressive tests.

Increase of material resistance to deformation at increasing ε_z on initial deformation stages is due to effect of increase of internal energy accumulated in the material. The effect arises due to enhancement of density of dislocations, being

stable at given temperature. Increase of deformation power in conditions of dynamic loading promotes annihilation of a part of defects, being formed. The process is accompanied by heat energy extraction. Therefore, deformation power increase gives rise to increase of defects density, increase of probability of the different sign defects to be met and annihilated. Then, the most fraction of crystalline disturbances disappears in the course of deformation [2], which predetermines in large extent the decrease of $\sigma_{0.2}$ under increased deformation powers.

Softening effect is also due to intensification of process of crack formation under high deformation powers. This is due to the fact that deformation conditions promotes numerous structural non-homogeneities. The effect is a sequence of many reasons. Firstly, cooling conditions result in difference of plastic flow in near-surface layers and in the bulk of deformed ingot. Essential at that is (i) the influence of both contact friction forces and various conditions of local plastic flow in different micro-volumes of the ingot, arising from high alloying, (ii) occurrence of considerable amount of eutectic component and so on.

The change of above regularity at heating to stamp temperature 1200°C seems to be due to more complete process of dynamic recrystallization in deformed material.

References

1. Lavrent'ev I.A., Petrashevich V.E. Hot pressure of precipitation-hardened metal-ceramic Ni-based alloy // Kuznechno-shtampovochnoe proizvodstvo. – 1974. – №3. – P.13-14 (in Russian).
2. Poluhin P.I., Gorelik S.S., Vorontsov V.K. Physical fundamentals of plastic deformation. – Moscow, Metallurgy, 1982. – 584 p. (in Russian)

The authors would like to acknowledge funding of this project from the US Air Force Office of Scientific Research, and the assistance of the Science and Technology Center of Ukraine.

PROPERTIES AND THE STRUCTURAL CONDITION OF COMPOSITES WC-NI WITH THE ULTRAHIGH MAINTENANCE OF THE SHEAF RECEIVED BY THE METHOD OF ELECTRON BEAM ZONED SINTERING

Bondarenko V.P., Zankevich A.B., Jurchuk N.A., Asnis E.A.⁽¹⁾, Zabolotin S.P.⁽¹⁾

Institute of superfirm materials of a NAS of Ukraine, Kiev, Ukraine

⁽¹⁾Institute of electric welding of a NAS of Ukraine, Kiev, Ukraine

Reception of qualitative products from the composites consisting of components with sharply distinguished density and ultrahigh (over 30 % a mass.) the maintenance of the sheaf, existing methods in terrestrial conditions it is problematic because of influence gravitational a liquation.

For reception of a non-porous condition of a material at sintering it is necessary to raise temperature of heating to reception of a liquid condition of a sheaf (liquid phase sintering). At occurrence of a liquid phase the product from such material, owing to absence in it of a rigid skeleton, loses the form, and in the material the liquation - non-uniform distribution of the filler and a sheaf is observed.

The researches carried out by us have shown, that at liquid phase sintering in vertical position in the furnace with rational heating samples from composites of 55 % WC + and 45 % WC+55 of % Ni (VN55) non-uniformity of distribution of components on length of a sample reaches 45 % Ni (VN45) up to 9 %, and value of hardness in the top part of a sample differs from values its bottom part in 2,6 times.

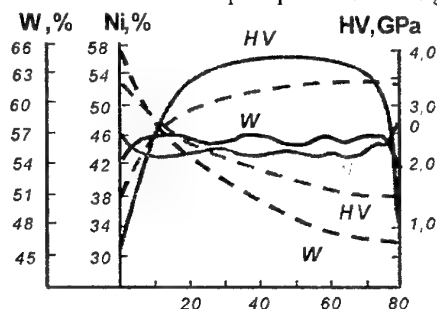
The analysis of references has shown what to exclude or reduce influence a liquation at reception of such alloys in terrestrial conditions probably at zoned sintering [1]. Due to zoned heating of products during sintering begins possible to receive a material about much smaller liquation in comparison with existing technological methods of reception of similar alloys. At zoned sintering there is an opportunity to exclude pollution of samples during sintering - them is possible sinter in non-crucible variant.

The method of electron beam zoned sintering by us received samples from composites VN45 and VN55.

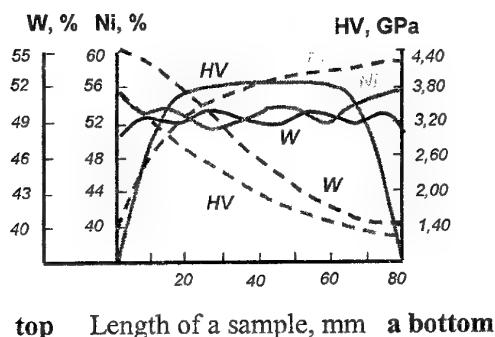
The sizes of samples were same, as well as at radiating sintering.

Zoned sintering of samples carried out in vertical position in installation of electron beam zoned sintering "Ray - 1". In samples sintered by such method the liquation also was observed. However a difference in the maintenance of components in the top and bottom parts of samples and hardness were much less. The maintenance(contents) of tungsten in samples from alloy VN45 on height equal 40 mm changed from 55,6 up to 56 % a mass., and on section of a sample (d 10 mm) percentage W changed from 55,5 up to 55,8 % a mass., i.e. maximum deviation has made 0,4 %. Value of hardness (HV) changed from 4,1 up to 4,5 GPa, the deviation is within the limits of a mistake of experiment (+0,2 GPa). In samples from alloy VN55 the maintenance of tungsten on height changed from 44,8 up to 45,2 % a mass., and on section from 45 up to 45,4 % a mass. Value of hardness changed from 2,9 up to 3,2 GPa.

On pic. 1,2, for presentation, results of distribution of nickel, tungsten and hardness on length of samples of alloys VN45 and VN55, received are combined by a method of radiating liquid phase and zoned electron beam liquid phase sintering.

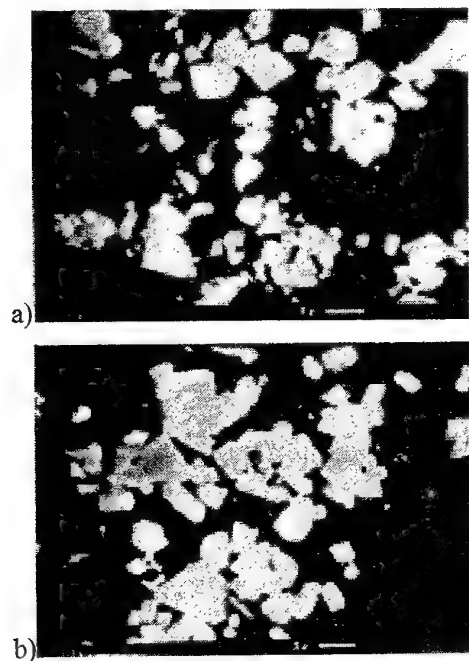


top Length of a sample, mm a bottom
Picture 1. Distribution of nickel, tungsten and hardness on length of a sample of alloy VN45
— sintered in vertical position in the furnace with radiating heating;
— electron beam zoned sintering sintered on installation.



Picture 2. Distribution of nickel, tungsten and hardness on length of a sample alloy VN55
 --- sintered in vertical position in the furnace with radiating heating;
 — electron beam zoned sintering sintered on installation.

At definition of structural characteristics of the alloys received by a method of electronic-beam zoned sintering, it is established insignificant (on the average 11 %) medium-sized growth of a grain of a carbide of tungsten, pic 3.



Picture 3 - Photos of microgrinds of composites VN45 (a) and VN55 (b), received by a method of electron beam zoned sintering on installation "RAY - 1". A white phase - WC, a black phase - Ni. (a raster electronic microscope "Cam Scan -4D", increase X3060, integration)

In initial powders of researched alloys the quantity of grains WC with the sizes from 2 up to 8 microns made 56 % of alloy VN45 and 74 % (for alloy VN55). In sintered alloys the quantity of grains WC with the sizes from 2 up to 8 microns made 60 % in alloy VN45 and 80 % in alloy VN55.

Thus, the carried out researches have allowed to establish, that a method of electron beam zoned sintering it is possible to receive more homogeneous, than at radiating liquid phase sintering. In the alloys received by such method the difference in the maintenance of making components in the top and bottom parts of samples has considerably decreased. Thus insignificant medium-sized growth of a grain of a carbide component is observed. However completely to exclude a liquation in such composites, it is obvious, possible only in conditions of microgravitation of the space flying device with use of zoned sintering.

The literature:

1. Bondarenko V.P., Halepa A.P. Zon's sintering of composite materials inclined a gravitational liquation a carbide tungsten - nickel. II international conference " Welding and related technologies - in XXI century " (November, 1998y., Kiev): -Kiev: an IEW by E.O.Paton, 1998.-C.16-17.

EFFECT OF ZIRCONIA(+CaO) CONTENT AND SINTERING TIME ON DENSIFICATION AND MECHANICAL STRENGTH OF ALUMINA- ZIRCONIA COMPOSITE

Gavriliu G., Diaconescu M., Țârdei C.

Advanced Research Institute for Electrical Engineering, Bucharest, Romania

As we know both the quality of raw materials and the processing way to the elaboration of a composite are essential for the quality of the resulted material.

For this study the ceramic matrix composite in the $Al_2O_3 - ZrO_2(+CaO)$ system was taken into consideration. First zirconia and CaO (10 mol.%) were homogenized and calcined and then this mixture (in wt.%) was homogenized and calcined together with alumina. The composition of the chosen materials is given in Table 1.

Table 1. Composition of the elaborated materials

No.	Recipe code	Composition (wt.%)	
		Alumina	Zirconia (+ 10 mol.% CaO)
1	A	100	-
2	AZC2	80	20
3	AZC4	60	40
4	AZC5	50	50
5	AZC6	40	60
6	AZC8	20	80
7	ZC	-	100

From the resulted powders were made samples by dry pressing and sintering in air at 1700 °C and different heating rate and sintering times.

The average values of the experimental results are shown in Fig.1, on bulk density, in Fig.2, on open

porosity, and in Fig.3, on bending strength, respectively.

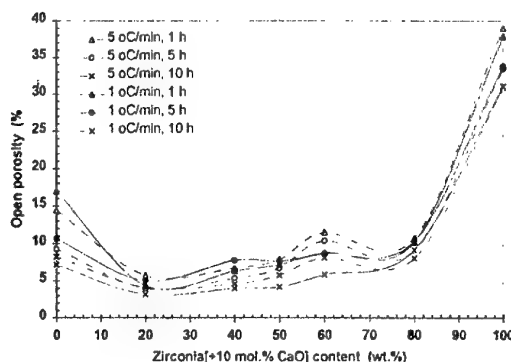


Fig.2. Effect of zirconia(+CaO) content, heating rate, and sintering time on open porosity

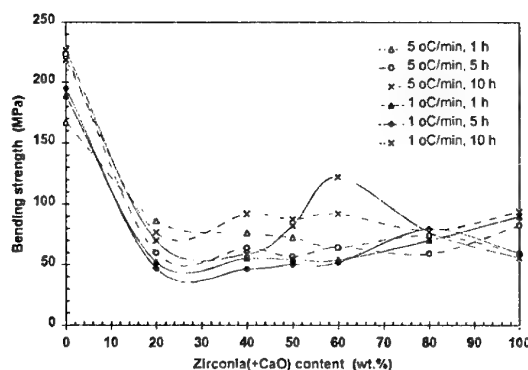


Fig.3. Effect of zirconia(+CaO) content, heating rate, and sintering time on bending strength

The experimental results are discussed and correlated.

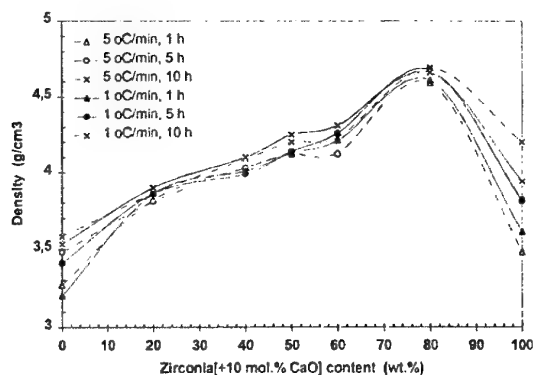


Fig.1. Effect of zirconia(+CaO) content, heating rate, and sintering time on bulk density

INFLUENCE OF NANOSTRUCTURE STATES ON MAGNETIC PROPERTIES OF FINE POWDES OF ALLOYS BASED ON CUPPER

Chuistov K.V., Efimova T.V., Zalutskiy V.P., Perekos A.E., Ruzhitskaya T.V.

G.V. Kurdyumov Institute for Metal Physics of the NASU, Kiev, Ukraine

The magnetic materials with ferromagnetic nanoparticles in paramagnetic matrix is of certain interest for studying of influence of size, form, interaction of particles on high magnetic characteristics formation. Such materials are based Cu alloys Cu-Ni-Co, Cu-Ni-Fe, which are supersaturated solid solutions (SSS) Ni, Fe, Co in Cu. Isostructure decomposition of SSS with isolation of spherical ferromagnetic particles rich in alloying elements takes place during the annealing [1].

In the present work the influence of SSS decomposition in the fine powder (FP) of $\text{Cu}_{80}\text{Ni}_{13}\text{Fe}_7$, $\text{Cu}_{80}\text{Ni}_{13}\text{Co}_7$, $\text{Cu}_{60}\text{Ni}_{30}\text{Co}_{10}$ alloys on phase-structure state and magnetic properties was investigated with methods of X-ray and magnetic analysis.

The FP was received by the method of electrospark dispergation in distilled water and alcohol. X-ray analysis was carried out on diffractometer DRON-3.0 in Fe K α radiation. The magnetic properties (magnetization I, coercivity Hc, field dependences I(H) were measured on ballistic magnetometer at room temperature and 77 K. Isothermal annealing were carried out at 873 K in atmosphere Ar during various time (from 5min to 600 min).

In initial state the small values Is are observed, and Hc and Br are absence (see table 1.1-1.3). This is connected with superparamagnetic state of fine particles[1].

Table 1.1. – Magnetic properties of material in initial state

Material	Is, kA/m	Hc,kA/m	Br, 10 ⁻⁴ Tl
$\text{Cu}_{80}\text{Ni}_{13}\text{Fe}_7$			
Massive	86	0.4	17
FD-alcohol	36	-	-
FD-water	14	-	-
$\text{Cu}_{80}\text{Ni}_{13}\text{Co}_7$			
Massive	20	-	-
FD-alcohol	24	-	-
FD-water	17	-	-
$\text{Cu}_{60}\text{Ni}_{30}\text{Co}_{10}$			
Massive	108	0.2	10
FD-alcohol	17	-	-
FD-water	17	-	-

Table 1.2. – Magnetic properties of material in annealing 873 K during 5 min

Material	Is, kA/m	Hc,kA/m	Br, 10 ⁻⁴ Tl
$\text{Cu}_{80}\text{Ni}_{13}\text{Fe}_7$			
Massive	169	1	25
FD-alcohol	129	1.5	62
FD-water	72	2.7	71
$\text{Cu}_{80}\text{Ni}_{13}\text{Co}_7$			
Massive	102	0.5	8.4
FD-alcohol	84	2	50
FD-water	35	0.6	19
$\text{Cu}_{60}\text{Ni}_{30}\text{Co}_{10}$			
Massive	172	0.6	28
FD-alcohol	52	0.7	20
FD-water	151	0.8	77

Table 1.3. – Magnetic properties of material in annealing 873 K during 300 min

Material	Is, kA/m	Hc,kA/m	Br, 10 ⁻⁴ Tl
$\text{Cu}_{80}\text{Ni}_{13}\text{Fe}_7$			
Massive	181	2.6	231
FD-alcohol	149	2	93
FD-water	87	2.6	146
$\text{Cu}_{80}\text{Ni}_{13}\text{Co}_7$			
Massive	102	48	1060
FD-alcohol	97	2.6	89
FD-water	52	2	30
$\text{Cu}_{60}\text{Ni}_{30}\text{Co}_{10}$			
Massive	173	13	679
FD-alcohol	150	6.4	207
FD-water	151	2.6	132

SSS decomposition during first 5-10 min of annealing results in sharp increasing of Is, Hc and Br both in massive alloys in FP in alcohol. After subsequent annealings Is changes negligibly, and Hc and Br are increased. The values Is depends on quantity of ferromagnetic phase while Hc and Br are defined by size, form, arrangement of dispersive particles. Sizes of magnetic phase particles -d were calculated on magnetic and data of X-ray patterns and were in interval from 4 up to 7 nm depending on fabrication conditions. As researched alloys are materials with low magnetocrystalline anisotropy ($K_1 = 5 \cdot 10^5$ Joule/m³ for Cu-Ni-Co and $K_1 = 4 \cdot 10^4$ Joule/m³ for Cu-Ni-Fe), so the critical size of nanoparticles d_{cr} was calculated on formula $d_{cr} = 2c / Is \sqrt{A/N}$ [2],

when $c = 2.95$ – constant, I_s – saturation magnetization of ferromagnetic phase, A – exchange energy parameter and $N = 4\pi/3$ – demagnetizing factor.

The particles with $d < d_{cr}$ are single domain particles. For Cu-Ni-Fe materials $d_{cr} = 23$ nm, Cu-Ni-Co $d_{cr} = 30-34$ nm. The comparison with experimental data indicates on single domain states of ferromagnetic nanoparticles of studied alloys. Isostructure (spinodal) decomposition of SSS results in certain arrangement of nanoparticles and arising of coherent intrinsic stress.

It may consider, that ferromagnetic nanoparticles are the systems of non-interacting particles on the first stages of decomposition when H_c is defined by magnetocrystalline anisotropy. For spherical particles $H_c = 2K/I_s$ and for Cu-Ni-Co $H_c = 15 \div 16$ kA/m, Cu-Ni-Fe – $H_c = 2$ kA/m. On later stage coherent intrinsic stress play essentially role,

$$H = \frac{3 \lambda_s \cdot \sigma_i}{2 I_s}, \text{ where } \lambda_s - \text{saturation}$$

magnetostriction coefficient, σ_i – intrinsic stress. For researched alloys σ_i is in interval $2 \cdot 10^9 - 10^{10}$ Pa and for all materials $H_c \approx 3 \div 30$ kA/m. It may suggest that after long times of annealing the coalescence of nanoparticles change particles form, and anisotropy of form can influence on H_c :

$$H_c = 0.5(N_1 - N_2)I_s.$$

The comparison of experimental and theoretical data indicates on essential contribution of magnetocrystalline anisotropy in coercitivity of massive and powder materials. Cooling of specimens annealed for 30-600 min from room

However, the coercitivity measured experimentally for powders is smaller than given by calculation. It is necessary to take attention to influence of dipolar interactions of particles, size factor and dispersion of magnetic energy by surface of powder particles. Probably, these reasons influence on value B_r also. B_r is always significantly smaller for powders than for massive alloys.

The received results allow to make conclusions, that fine powder, obtained in alcohol, are great similar to massive materials for all studied alloys as in character of decomposition of SSS so magnetic properties changes. In fine powder

obtained in water the great quantity of Cu, Ni, Co, Fe oxides influence on phase-structure state and properties.

Preference:

1. K.V. Chuistov, A.E. Perekos, T.V. Ruzhitskaya, T.V. Efimova, V.P. Zalutskiy, Metallofiz. Noveishie Tekhnol., **23**, No.7: pp 949-960 (2001) (in Russian).
2. S.V. Vonsovskiy. Magnetizm.-M : Nauka, 1971.
3. R. M. Bozorth. Ferromagnetism. D.Van Nostrand Company, Inc., Toronto-New York-London, 1951.

THE FORMATION OF THE SUPERHARD MATERIALS BASED ON NANODIAMOND

Senyut V.

Institute of Machine Reliability National Academy of Sciences of Belarus, Minsk, Belarus

Synthesis of the diamond under high static pressure is usually achieved within diamond stability range by the use of solvent-catalysts. Such as iron, nickel, cobalt, manganese or alloys of these metals. In this case lowering of the pressure and the temperature is connected with the compositions based on metal-catalysts, which have relative low melting point. At the same time it is necessary to note, that dispersivity and structure of the initial carbon materials also play important role at the synthesis process. There was stated earlier [1] that additions of ultradispersed diamond (UDD, nanodiamond) facilitate the transition of the graphite into diamond under high pressure including direct conversion process without metal-catalysts. In this case from one point UDD serve as a germs, from other side nanodiamond itself fulfills the role of the catalyst of the synthesis process like fullerenes [2].

Besides at present time the others areas for application of nanodiamond are well known. UDD can be used in polishing pastes, galvanic coatings, modifiers of polymers of polymers, composite materials (including superhard materials [3]) etc.

Other opportunity for application of UDD is to obtain on its base polycrystalline powders from nanodiamonds (PDD) with the size of the particles raging from 0 to 12 μm [4].

The idea of this work is to use UDD as the starting materials to obtain particles of the micron range on its base. In this work the treatment of the ultradispersed diamond with different kind of the surface at the various conditions (including vacuum and high static pressure) was conducted.

It was established that using metastable non-equilibrium system such as nanodiamond modified with non-diamond carbon it is possible to get different kinds of particles having high dispersed structure.

It is shown that synthesis of diamond occurs under high static pressure at the diamond's stability range when additions of solvent catalysts are used. Modifiers connected with the surface provide the filling of the pores during the process. At the same condition it is possible to obtain diamond particles without metal catalysts. Within graphite's stable range formation of large particles based on initial UDD also occurs.

First kind of particles represented polycrystalline powders UDD described in [4]. Such particles according to the X-ray analysis data have high dispersed structure inherent to the initial powders and possess high specific surface (Fig. 1). The size of the particles can be ranged from 0,01 μm to 100 μm and is determined by the content of no diamond carbon in the mixture (Fig. 2,3).

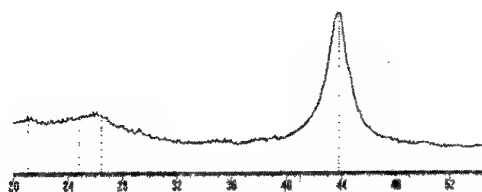


Fig. 1a. X-ray pattern of initial nanodiamond

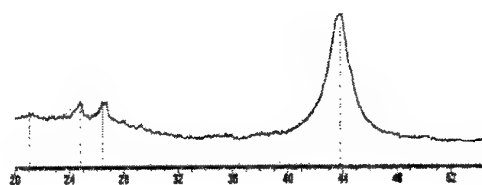
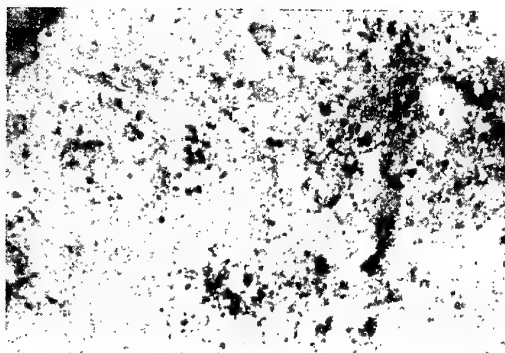


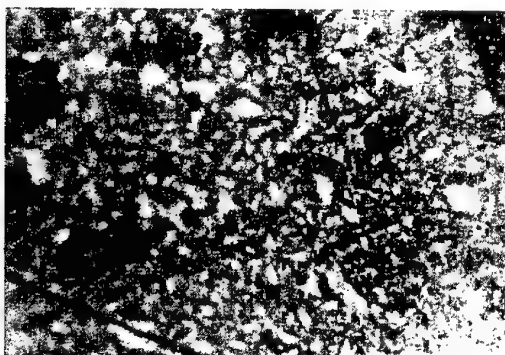
Fig. 1b. X-ray pattern of the sintered UDD-powder.

Second kind of the synthesized particles represented transparent crystals with nanostructure. (so called colloidal crystals based on UDD). The intermediate phases of carbon connected with the particles could be present or be annealed varying the temperature and the time of the treatment. The size of the particles obtained ranged from 100 μm up to 700-750 μm of some particles resulted more then m depending on the condition of the treatment. Microhardness 100 GPa. (Vickers method, load on indenter 200 g) (Fig. 4).

a) 30% mass. of non-diamond carbon.



b) 50% mass. of non-diamond carbon.



c) 65% mass. of non-diamond carbon.

Fig. 2. Image of sintered diamond particles in carbon matrix.



Fig. 3. TEM of the sintered particle based on UDD

Other advantage is high thermal stability of the obtained materials caused by low content of impurities connected with initial particles of the nanodiamond.

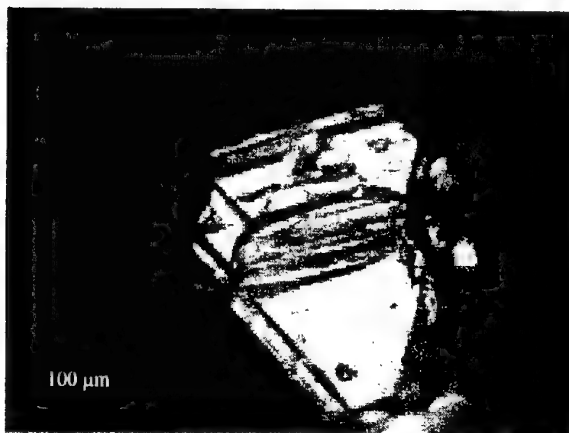


Fig. 4 Image of the crystal beset on UDD.

References.

1. V. T. Senyut, E. V. Zvonarev Interaction of ultradispersed diamond and the non-diamond forms of carbon in conditions high static pressure. Abstracts International conference "Advanced materials" Symposium A: engineering of composites: investigations, technologies and perspectives. p 264.
2. Ya. Vul, V. N. Davidenko, S. V. Kidalov, S. S. Ordanyan, V. A. Yashin. Superhard tool materials on the turn of the centuries: production, properties, applications international Science and Technology conference: 4-6 July 2001, Kiev, The Conference materials, ISM, 2001. p 61-63.
3. Zvonarev E. V. Senyut V. T. Ustinova G. P. Production of polycrystal material based on ultradispersed diamond of detonation synthesis. Powder metallurgy, Minsk, 2001, №24, p. 44-49.
4. V. Padalko. Nanodiamonds in Ukraine: synthesis, characterization and application. Superhard tool materials on the turn of the centuries: production, properties, applications international Science and Technology conference: 4-6 July 2001, Kiev, The Conference materials, ISM, 2001

NEW CERAMIC ABO_3 -MATERIALS FOR FABRICATION OF FUEL CELLS AND HEATING DEVICES COMPONENTS

Gorbunova V.A.⁽¹⁾, Gorbunov A.V., Novikov G.I.⁽¹⁾, Gamanovitch N.M.⁽¹⁾

Heat & Mass Transfer Institute - Academy of Sciences - 220072 Minsk - Belarus

Tel.: 375 017 2841223, Fax: 375 017 2322513, e-mail: ptlab_hmti@tut.by;

⁽¹⁾Belarussian State University of Technology, 220630 Minsk, Belarus

Ceramic materials based on oxides with perovskite ABO_3 -structure (e.g. doped chromites, manganites, ferrites, cobaltites of lanthanum or other rare earth metals) are widely investigated as materials for various energy conversion technologies. It is expected that the technologies based on electrochemical fuel cells and particularly on solid oxide fuel cells (SOFC) will gain an important position in future stationary electric power generation.

At last 5 years new type of air electrode of high temperature SOFC, which cost is strong lower in comparison with conventional LSM-cathodes (e.g. $La_{0.7}Sr_{0.3}MnO_3$), based on mixed lanthanide manganites (doped in A- and B-sites in ABO_3 -molecules) was developed by Westinghouse Corp (USA) et al. [1]. This work is focused on structure investigation and charge transport of such new variants of these advanced materials as $La_{0.8-x}Ln_xMnO_3$, $La_{0.8-x}Ln_xCa_{0.2}Mn_{0.94}Cr_{0.04}Ni_{0.02}O_3$ and $La_{0.6-x}Ln_xSr_{0.4}CoO_3$ (Ln = industrial mixture based on cerium group metals; $x = 0-0.8$). These compositions are mainly p-type electronic conductors with some ion conductivity (with activation energy of 0.06-0.18 eV for manganites samples) and can be effectively used for the fabrication of cathodes for SOFC (with $(0.9ZrO_2+0.1Y_2O_3)$ - and $Bi_{0.75}Y_{0.25}O_{1.5}$ -electrolytes) operated with various gas fuels at 1070-1270 K [2].

The conductivity of these lanthanide materials (prepared in ceramic form using nitrate solution precursors decomposition) was measured in air by four-probe quasi-dc method. It was found that optimal composition for SOFC (with ZrO_2 - Y_2O_3 -electrolyte) is $La_{0.4}Ln_{0.4}Ca_{0.2}Mn_{0.94}Cr_{0.04}Ni_{0.02}O_3$ (Ln - the

mixture with composition of $La_{0.32}Ce_{0.51}Nd_{0.12}Pr_{0.05}Fe_{0.005}$ or $La_{0.60}Nd_{0.19}Ce_{0.13}Pr_{0.08}Sr_{0.004}Ca_{0.002}$, which added to the precursors in form of low cost hydro-metallurgical raw materials), which has at porosity of 30-55% conductivity level (at 1000-1300 K) up to 80,0 Sm/cm. The data obtained for cobaltite series on conductivity appears that $La_{0.3}Ln_{0.3}Sr_{0.4}CoO_3$ ($Ln = La_{0.32}Ce_{0.51}Nd_{0.12}Pr_{0.05}Fe_{0.005}$) is promising material for SOFC cathode and oxygen separation membrane applications since it is low cost as well as possess semiconducting characteristics at lower temperatures and metallic conductivity at higher temperatures.

X-ray diffraction data analysis for these compositions in ceramic and thick-film ($\delta = 25-35 \mu m$) form as well as IR-spectroscopy data show that two cubic phases are mainly formed after the sintering at 1440-1520 K. It was found that first phase (up to 80-95 % of the material) is the complex oxide (e.g. composed of $(La,Nd,Pr,Ca)(Mn,Ni,Cr)O_{3-\delta}$) with perovskite structure of the loparite ($Ce_2Ti_3O_{8.7}$)-type (which was similar to that observed by Serdiuk et al.[3]) with crystal lattice constant of $a = 3.86-3.88 \text{ \AA}$; second is the phase with fluorite structure on the base of CeO_2 with crystal lattice constant of $a = 5.41-5.45 \text{ \AA}$.

Besides conventional ceramic technique based on thermal synthesis of ceramic ABO_3 -materials the advanced plasma (DC- and RF-type) processes are developed for preparation of the materials as components of SOFC and heating semiconducting devices [4]. The new spray process for the preparation of oxide powders of La-Ca-Al-Cr-O-system (which is one of the most suitable for SOFC' intercon-

nections as well as high-temperature heaters) using 200 kW triple torch electric arc plasma reactor (TTPR) [5] was recently developed in our laboratory. It can be also used for the fabrication of manganite- and chromite-based heating elements on metal and ceramic substrates operated in air. The heating film thickness varied as 20-50 μm for the plasma processing variant with nitrate solution spraying.

This work was supported by Foundation of basic researches of Belarus (grant X01-188).

REFERENCES:

- [1] Patent 5686198 USA, Kuo L. et al. (1997);
- [2] N.M. Gamanovitch, V.A. Gorbunova, G.I.

Novikov, J. Applied Chem., 2001, V.74, No2 (in Russian);

- [3] G.N. Serdiuk et al., Ukrainian Chem. J., 1998, V.64, No9 (in Russian);
- [4] R.H. Henne, M. Lang, M. Muller et al. // Heat and mass transfer under plasma conditions. - Ed. P.Fauchais (Annals of the New York Acad. Sci. - V.891). 1999, p.124;
- [5]. A.L. Mosse, A.V. Gorbunov, A. Marotta et al. // in Proc. 14th International Symposium on Plasma Chemistry, Czech Republic, Prague, 1999, V.4, p.2253.

HARD ALLOYS WITH STRUCTURAL GRADIENT FOR DRILLING TOOLS EDGES

Florea Carmen, Florea Alexandru
University of Petrosani, Romania

The excavation of mine workings in hard rocks is made through drilling-blasting technology; in the frame of this method, the holes drilling is one of the basics operations of this technology and is realised by percussive procedure.

Single edge chisel bits D.C.P., with 40mm diameter, are the most usual mining tools for holes drilling, both for coal and ores mining; its consumption has a significant weight for the cost of drilled rock ton, depending on rocks physico-mechanical properties.

With a view to reducing the costs for simple edge chisel bits, was investigate the possibility to use hard alloys with structural gradient for producing the tipped which are the edges of these tools.

Powder metallurgy is the best method for discovering and development of new

materials and especially for a large range of materials with structural gradient.

The advantages of this new technology are both economic and of the unlimited possibilities of utilisation of the processes specific for powder metallurgy for the realisation of different functional combinations.

In this context, hard sintered alloys, of WC-Co system, are used, on a wide scale, as material for mining tools edges: materials with structural gradient, from the same system, can offer a succession of spectacular solutions, for different practical imposed demands.

The encouraging results, obtained until now, allowed the estimation of specific consumptions of drilling tools, with about 15% less than currently obtained ones.

PREPARATION OF BENZENE-STABILIZED COBALT NANOPARTICLES IN HYDROGEN ATMOSPHERE

Normatov I.Sh.

Institute of Chemistry AS R. Tajikistan

The high reactivity and aggregation tendencies of metallic nanoparticles stimulate a search for effective stabilization and passivation techniques.

In this paper, we report on the preparation of benzene-stabilized cobalt magnetic nanoparticles.

The vacuum system used to prepare high-purity Co particles. The evaporator temperature was measured with a pyrometer through an optical window. The rate of Co evaporation was determined using an electronic balance vacuum-connected with the reactor. The balance was calibrated by measuring the pressure change caused by water evaporation from a special pan suspended from one of the balance arms. This method ensured absolute calibration.

Computer simulation of the motion of evaporated cobalt atoms

To study the clustering and motion of evaporated atoms we use a Monte-Carlo procedure. We consider steady -State evaporation and, accordingly. A stationary distribution of vapor species.

The probability densities for the free path length and motion direction of each particle after a collision are computed using random-number generator. After each collision, a check is made whether or not the particle has reached the reactor surface. If this has occurred, the number of deposited particles is increased by unity, and control is transferred to the beginning of the program to simulate the trajectory of the next particle.

Deposition of Cobalt particles into benzene.

When Co atoms encounter the matrix, the penetrate some depth into the layer, rapidly losing their kinetic energy. This gives rise to local

heating, favoring Co diffusion deeper into the layer.

To examine the effects of the evaporation rate and benzene-to-cobalt ratio on the size of deposited clusters, cobalt (0,08g) was deposited onto layers produced by freezing 8,25 or 80g of benzene. The deposits were examined on aJEM-1100CX electron microscopy.

Increasing the evaporator temperature at a fixed layer thickness led to partial melting of benzene, resulting in aggregation of Co particles.

Cobalt evaporation in atomic hydrogen atmosphere

It is well known that, in the process of metal evaporation, a small fraction of the atoms pass into an excited state.

It can easily be shown that, at evaporator temperatures in the range 2000-2500K, the n^*/n_0 ratio does not exceed 10^{-8} .

It is reasonable to expect that, in the presence of atomic hydrogen, metal evaporation is promoted by the recombination of hydrogen atoms on the metal surface, with a thermal effect of 434 kJ/mol.

In partially atomized hydrogen, the energy of Co evaporation was almost 3 times lower than that in vacuum.

Interaction between deposited Cobalt and benzene

Electron - microscopic examination of the Co particles deposited at the same evaporation rates demonstrates that, at high evaporation rates, the benzene layer contains coarse aggregates nonuniform in size. The main reason is that rapid evaporation increases the probability of atomic encounters.

SOLID-STATE CONSOLIDATION of WC-Co HARDMETALS. PECULIARITIES and PROSPECTS

A.V. Laptev

Institute for Materials Science Problems of UNAS, Kiev, Ukraine

Hardmetals based on tungsten carbide (WC-Co, WC-TiC-Co, WC-Ni) are produced by liquid-phase sintering technique. A promising direction among others for the amelioration of performance of these is tailoring of an ultra fine-grained structure. However, the liquid-phase sintering of ultra fine powders of WC-Co results in a considerable growth of carbide particles. In this case, their growth can not be avoided even with introduction of inhibitors if the initial size of WC particles are finer than 0.2 microns during the liquid-phase sintering [1].

Opportunity of producing of ultra fine-grained alloys at low temperature, or in solid phase, where the structure formation processes are retarded to some extent, is of interest. It is relevant to note that peculiarities and mechanisms of solid phase sintering of hard alloys are not yet studied in due manner, although attempts are made to do it lately [2,3].

Pressures as high as 1200 MPa, or the method of high-energy hot pressing permitted to obtain more knowledge in the peculiarities of densification processes of WC-Co alloys during low temperature sintering. As investigations of consolidation of specimens differing in WC particle sizes and binder contents within the 950-1350 °C range have shown, a temperature exists in this sintering region, at which a change of structure formation mechanisms likely occurs.

The study of WC-16%Co alloy densified by the sintering method at various temperatures revealed that the density variation rate significantly raised after 1200 °C, Fig. 1 [4]. This effect is hardly noticeable when high-energy pressing is used because the density of pressed

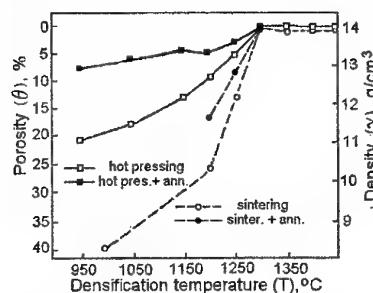


Fig.1 The density of WC-16 %Co alloy with the temperature and densification method

specimens is rather high due to the pressure applied. However, as was found during the study of porosity behavior of various specimens, the pore sizes increased with temperature despite the decrease of general porosity, while these began abruptly decrease after 1200 °C, regardless of consolidation method of hardmetal, Fig. 2 [5]. Different densification methods only produced effect on the absolute pore sizes, i.e. the pore sizes

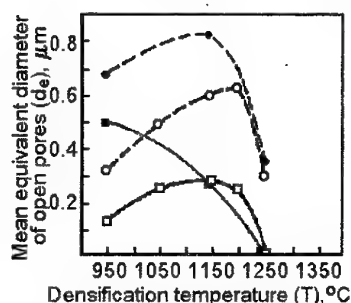


Fig. 2. The diameter of open pores vs densification temperature of WC-16% Co alloy

of WC particles have also shown the presence of an inflexion in the variation of the specimen resistivity due to the densification temperature. It was found as a result of approximation of experimental data with function $\rho = \rho_0(1-\theta)^{-m}$ and the use of log coordinates, the point of inflexion corresponded to 1200 °C being in no dependence on the specimen porosity, Fig. 3 [5]. That is, the major cause of the inflexion appearance is associated with the heating temperature of specimens.

The study yielded also fundamentally

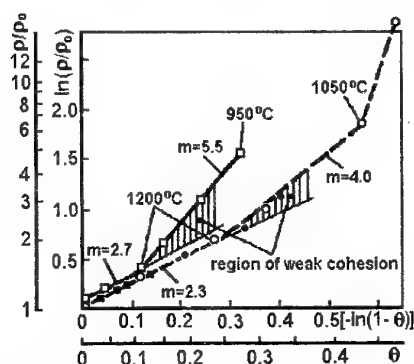


Fig. 3. The electric resistivity of WC-16% Co alloy vs porosity and temperature

valuable results consisting in the establishment of a different rate of growth for carbide particles during solid-phase sintering. The values of mean chord of carbide particles, L_{wc} as function of the pressing temperature of specimens are given in Fig. 4 [4]. As can be seen from the Figure, the growth rate of WC particles significantly increases with the specimen heating of over 1200 °C (tangent of obliquity of linear relationship, $L_{wc} = f(T)$ is four-fold greater). So, a process starts at

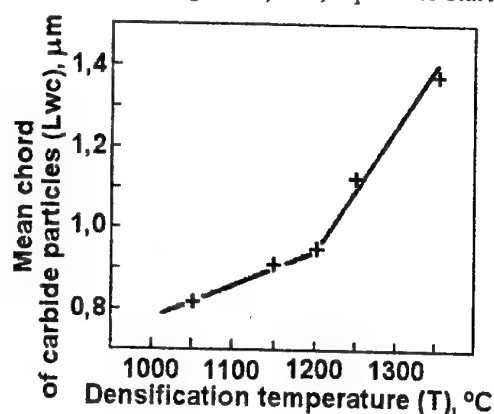


Fig. 4. The effect of the densification temperature of WC-16%Co alloy on the WC particle sizes

1200 °C which exercises a strong influence on the growth of WC particles.

Another peculiarity of the densification process was established on a rich binder hard alloy. Some drop of the density is observed during the high-energy pressing of WC-26%Co alloy at 1200 °C,

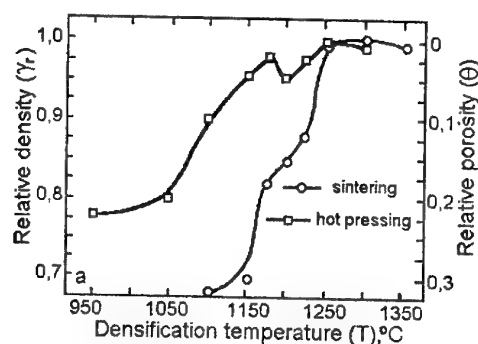


Fig. 5. The density of WC-26%Co alloy vs densification temperature

Fig. 5 [6]. On the other hand, the density increase become slower at sintering. This can be explained by the coalescence of carbide particles and formation of a rigid carbide frame at this temperature, which restrains the shrinkage in the case of sintering, while get destroyed when pores are formed in specimens in the case of pressing. It seems appropriate to note that at temperatures

higher than 1200 °C the said phenomenon is not observed.

Therefore, it was stated that the following phenomena occur at 1200 °C during the study of the solid-phase consolidation of WC-Co alloys by the methods of sintering and high-energy pressing:

- speed up of the shrinkage process for poor binder alloys and low rate of the shrinkage for more rich binder alloys,
- onset of the diminution process of pores after their earlier enlargement
- amelioration of interparticle boundaries, i.e. reduction of specific resistivity of specimens
- increase of the growth rate of carbide particles.

We can arrive at a conclusion from the above said peculiarities that the solid-phase region of sintering, which covers the temperature range between 950 and 1300 °C, is not monotonous in the terms of both the shrinkage process and the structure change (WC particle growth). This region is divided by the temperature of near 1200 °C forming two sections considerably differing in the shrinkage rates and structure forming rates. Carbide particle densification and growth rates are significantly higher within the section of solid-phase sintering over 1200 °C. Further more, low specific resistivity of specimens as prepared within this section reveals a high degree of interaction between particles.

Based on results obtained one can suppose the only reason is laid up on the basis of the phenomena discovered, i.e. the recrystallization of tungsten carbide that occurs at 1150-1200 °C in hardmetals [7].

The prospects of application solid-state consolidation technique for production ultrafine hardmetals with high mechanical properties are discussed.

References

1. Schubert W.D., Bock A., Lux B. Proc.13th Int. Plansee Seminar, Reutte, v.4 (1993) 283-305.
2. Haglund S., Agren J., Uhrenius B. Zeitschr. Metallk. v.89 (1998) N5, 316-322.
3. Missiaen S.-M., Roure S. Acta Mater. v.46(1998) N11, 3985-3993.
4. Laptev A.V., Ponomarev S.S., Ochkas L.F., Powder Metallurgy, 2000.-№ 11/12.-p.103-116.
5. Laptev A. V., Ponomarev S. S., Ochkas L. F. J. of Advanced Materials, 2001.-v.33, No.3, 42-51.
6. Laptev A.V.; Ponomarev S.S., Ochkas L.F. Proc. EURO PM'99 Conf. Adv. Hard Materials Prod., Turin, Italy, November 8-10 (1999), 205-212.
7. Gorelik S.S., Eljutin V.P., Mozzhukhin E. Izv. Vuzov, Non-Ferrous Metall. (1962) N4,143-147.

STUDY of HEAT RESISTANCE SOME INTERMETALLIDES, CONTAINING a CROMIUM

Oryshich I.V., Poryadchenko N.E., Brodnikovskij N.P., Krapivka N.A.

Institution of problems of Materials science of Ukraine, Kiev, Ukraine

Now the further elaborations of the heat proof and heat-resistant constructional materials are connected with the researches of the intermetallides. The intermetallides are used as the strengthening phases, and as the coatings, and essentially influence on the properties of the materials [1,2]. In connection with this a big attention is spared to study of the properties stability of the intermetallides in the aggressive mediums at the high temperatures.

In study [3] a heat-resistance of the intermetallide phases formed by IV group of the transitional metals (Ti, Zr, Hf) with iron group metals (Fe, Co, Ni) and copper has been learnt. It has been shown [3, 4], that there are the cases when a heat-resistance of the intermetallides is higher, than a heat-resistance of the metals, from which they were obtained.

In the present study the firmness to oxidation of intermetallides formed by metals IV (titanium, zirconium and hafnium) with chromium, possessing the highest heat-resistance among the clean metals was investigated.

The intermetallides were smelted in arc furnace with unexpended tungsten electrode and copper water-cooling bottom in medium of furbished argon. The rate of crystallization from melt of an ingot was $\sim 0,5$ %/sec. A purified chromium and iodide titanium, zirconium and hafnium used as initial raw materials. For removal of the internal stresses the intermetallides were annealed in vacuum at the temperature 800 °C for 10 hours. On data of chemical and x-ray analysis their composition is close to stoichiometric.

The tests of a heat-resistance were conducted in air. The test temperature was varied within the range 600-1200 °C for 20 hours. The specimens approximately 10 mm in diameter and 15 mm in high were used. Before the tests the specimens' surfaces are polished, cleaned by ultrasound and washed in distilled water. A microthermobalance apparatus "Derivatograph-1500" with the continuous recoding of mass change was used for determination of the oxidation kinetics. The periodic weighing of the specimens after exposure in electric furnace got the supplemental data. The

experimental results presented in this study were obtained by means of thermobalance, metallogragy and x-ray analyses.

The results of the thermogravimetric studies are shown in fig.1. Data for the oxidation rates of clean metals formative intermetallides have been also cited for comparison

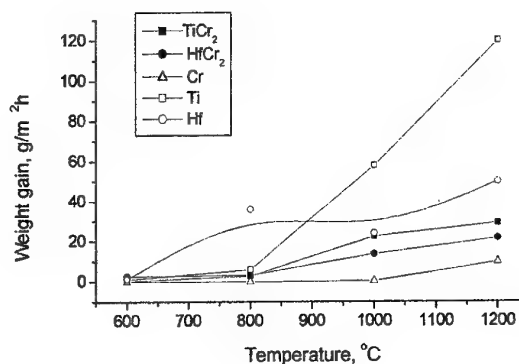


Fig. 1. Dependence of the oxidation rates against the temperature for TiCr₂, HfCr₂ intermetallides and the metals formative them.

As follow from the given results, TiCr₂ and HfCr₂ intermetallides possess relatively high level of a heat-resistance. At 600 °C an oxidation rate of HfCr₂ intermetallide exceeds an oxidation rate of TiCr₂ and Hf, and all the more chromium. TiCr₂ intermetallide is more firm to oxidation at this temperature, than clean titanium. At 800 °C the oxidation rates of TiCr₂ and HfCr₂ intermetallides become practically equal, and at higher temperature TiCr₂ is oxidized even faster, than HfCr₂. Both intermetallides are found more firm to oxidation than clean hafnium and titanium at 800 °C and above. The ZrCr₂ intermetallide is oxidized intensively at all temperatures. Moreover, as the temperature rises a heat-resistance of ZrCr₂ anxiously falls and becomes beneath such for clean zirconium. The reason of this is connected with this intermetallide is very fragile and has many cracks arised during preparing. The cracks sharply multiply the oxidation surface. As a result

of oxidation along net of the microfissures a specimen is scattered.

The phase x-ray analysis of the scale, formed on the surface of the specimens has been done. In the main, the scale consists of the oxides of the metals, formative the proper intermetallide. At low temperatures TiO_2 or HfO_2 and small maintenance of the chromium oxide form the scale. The preferable oxidation of titanium and hafnium is observed due to higher free energy of formation of their oxides on comparison with the chromium oxide. The presence of clean metals was not registered. At higher temperatures a biphasic scale is formed with large contents of the chromium oxide, and at 1200 °C a third Cr_2TiO_5 phase is formed in the scale of TiCr_2 intermetallide.

It is known, that a heat-resistance of the metals is determined by the properties of an oxide, forming on their surface [5]. An augmentation of the firmness to oxidation is reached by dint of an alloying, what provides the forming of the scale with more high protective properties. The presence of chromium in material mostly leads to rise the protective properties of forming scale due to the high protective properties of Cr_2O_3 . In our experiments the fact is tracked that the protective properties of the scale forming on TiCr_2 and HfCr_2 intermetallides are correlated of protective properties of titanium, hafnium and chromium oxides. Our data demonstrated that a presence of chromium in material in both cases raises a heat resistance. Especially this take place with growth of the temperature, when due to rise of the diffusion coefficients an essential role starts to play a diffusion of the chromium cations through the film of $\text{TiO}_2(\text{HfO}_2)$ to the external surface of the scale and an oxygen diffusion through the scale to the surface of the intermetallide [3]. This processes leads to an augmentation of quantity of the forming chromium oxide. So, a heat resistance of TiCr_2 and HfCr_2 intermetallides is in 2-4 times higher than titanium and hafnium heat resistance, but it is much lower (on 2-3 order) than a heat resistance of chromium at the temperatures 600-1000 °C. With growth of

the temperature the difference between a heat resistance of intermetallides and chromium decreases, and at 1200 °C a heat resistance of the intermetallides is less than a heat resistance of clean chromium only in 2-3 times. An augmentation of the protective properties of the scale with an augmentation of Cr_2O_3 maintenance in it is confirmed by the fact, that the specimens, for example HfCr_2 , oxidized at 1000 °C, are oxidized at the repeated heating at 600 °C in 7-8 times more slowly, than in a case without preliminary oxidation at the high temperature. And vice versa, the specimens with preliminary oxidation at 600 °C are oxidized at the temperature 1000 °C in 20-25 times faster, than without preliminary oxidation at 600 °C.

Thus, titanium and hafnium intermetallides with chromium do not possess the high level of a heat resistance at the temperatures till 1000 °C, which is much lower, than a heat resistance of clean chromium, and at more high temperatures a heat resistance of TiCr_2 and HfCr_2 is compared with such for chromium. Influence of chromium on rise of titanium and hafnium heat resistance is displayed at all explored temperatures. However, the scale with higher protective properties is formed only at the temperature above 1000 °C.

References

1. Миркин И.Л., Фантаева М. В кн.: Исследование новых жаропрочных сплавов для энергетики. М.: Машгиз.- 1961.- С. 111-178.
2. Зязев В.А., Ватолин Н.А., Гуляева Р.И., Буланов В.Я. //Металлы.- 2000, № 3.-С. 99-103.
3. Войтович Р.Ф., Головкин Э.И. //Порошковая металлургия.- 1978, № 4.- С. 61-71.
4. Гайдаренко А.Л., Спивакова Е.В., Петьков В.В. //Металлофизика.- 1973, вып. 46.- С. 100-103.
5. Томашов Н.Д. Высокотемпературное окисление. //Итоги науки и техн. ВИНТИ. Сер. Коррозия и защита металлов и сплавов.- 1991.-17.- 120с

FEATURES OF THE BEHAVIOR OF TITANIUM NITRIDE NANOPOWDERS DURING SINTERING UNDER THE CONDITIONS OF HIGH PRESSURES

Bykov A.I., Timofeeva I.I., Klochkov L.A., Ragulya A.V., and Gridneva I.V.

Frantsevich Institute for Problems of Materials Science, National Academy of Sciences of Ukraine,
Kiev, Ukraine

The formation of a nanocrystalline structure in a sintered material provides preparation of ceramic products with improved physicomachanical properties. Different processes of consolidation of nanopowders, that make it possible to prevent a significant increase in the size of starting particles and obtain a sintered polycrystal with a grain size under 100 nm, are known. Sintering under high pressures is among these. By now numerous investigations of sintering of materials by this method have been carried out. However, the currently available information does not reveal the features of the effect of quasi-hydrostatic compression under high pressures on the evolution of the substructure of grains depending on their size. In this connection, a comparison of the effects of the action of high pressures on powders with the initial particle size of about 60 μm obtained by synthesis in a furnace and plasmochemical nanopowders with a size of 70 nm.

Experiments were performed on a high-pressure unit on the base of a hydraulic press with a force of 6300 kN. A lens-type pressure chamber (PC) with a diameter of the working channel of the cell of 9 mm was used. Experiments were carried out in the pressure range 2-5 GPa at a temperature of 293 K, and in the temperature range 1273-1773 K. The sintering time was minimized in view of the necessity to preclude the effects of decreasing pressure during the sintering cycle, that are caused by the shrinkage of the material of the PC cell, and limit the process of grain growth during sintering. The total sintering time did not exceed 1.5 min. Temperature was raised linearly, and, at its maximum value, an exposure lasted for no more than 20 s. An X-ray diffraction analysis of sintered materials was performed on a DRON-3M diffractometer. Parameters of the fine structure of the material were calculated from the broadening of diffraction lines. The hardness was measured on a PMT microhardness tester. The density of sinters was determined by hydrostatic weighting.

The range of used pressures was chosen from the condition of the necessity of deforming the frame of a powder body during generation of a high pressure and in the process of sintering. It was proposed to use the Hubert-Mises condition in consideration of the deformation process under high pressures. We proceeded from the assumption that, on the free surface of a pore, the material is in the plane-strained state. For this case, the instant of deformation comes as the relationship $\sigma_{\text{mean}} \geq 2\sigma_0$ is satisfied, where σ_{mean} is the mean hydrostatic pressure produced in the working volume of the PC; σ_0 is the compression strength of the sintered material. For titanium nitride, this relationship is as follows: $\sigma_{\text{mean}} \geq 2$ GPa. Specimens of specified shape (5 mm in diameter and 4 mm in height) were sintered in the indicated pressure range.

X-ray diffraction analysis data show that splitting of the regions of coherent scattering (RCS) proceeds even at room temperature, and, in nanopowders, their size is two orders of magnitude smaller than in micropowders after action of a pressure of 3 GPa. Nevertheless, the residual microstresses of the crystal lattices of both types of powders are close in value ($\Delta a/a = (20-33) \times 10^{-4}$). As temperature and pressure are raised, the characteristics of the substructure change insignificantly. It should be noted that microstresses in nanopowders are always higher than those in micropowders. The causes of this phenomenon were considered.

It was established that the microhardness of compacts from nanopowders was 24-26 GPa and the microhardness of compacts from micropowders was not more than 20 GPa. Thus, the features of the effect of high quasi-hydrostatic pressures on titanium nitride powders with different particle sizes were determined.

THERMODYNAMIC PROPERTIES OF $\text{LaNi}_{4.5}\text{Cu}_{0.5}$ AND $\text{LaNi}_{4.5}\text{Mn}_{0.5}$ IN THE WIDE TEMPERATURE RANGE

N.P. Gorbachuk, A.A. Skrypai, V.B. Muratov, A.S. Bolgar

I.N. Francevich Institute for Problems of Materials Science, National Academy of Science of Ukraine, Krzhyzhanovsky Str., 3, 03680 Kiev, Ukraine

Binary intermetallic compound LaNi_5 is widely known due to opportunities is convertible to absorb hydrogen in significant quantities (6-7 atoms per formula unit) at temperatures close to room. However equilibrium pressure in system $\text{LaNi}_5\text{-H}_2$ makes about 3 atmospheres, that essentially reduces opportunities its practical application. Doping LaNi_5 by other transitive metals allows to operate process of hydride formation without deterioration its absorption of properties. The thermodynamics is one of the fundamental approaches by development of the theory of management hydrogenation. At the same time of items of information on thermodynamic properties of alloys on a basis LaNi_5 in the literature are absent.

The purpose of the present work was the research heat capacity and enthalpy of $\text{LaNi}_{4.5}\text{Cu}_{0.5}$ in the temperature range 64.28 – 1478 K and $\text{LaNi}_{4.5}\text{Mn}_{0.5}$ in the temperature range 59.63 – 1451 K. The intermetallides under study were produced from lanthanum, nickel, manganese and copper (99.8 %) by arc melting with tungsten non-consumable electrode in purified argon.

Heat capacity at low temperatures were measured by adiabatic calorimetry method with periodic input of heat on low temperature standard thermophysical unit [1], and enthalpy - by drop calorimetry method on high-temperature differential calorimetry [2]. The error of the heat capacity measurement not to exceed 0.4 %, and of enthalpy - 1.5 %.

The experimental data of heat capacity smoothed out by a method of sliding approximation by the cubic multimembers with weight factors [1] (fig.1).

To obtain main thermodynamic functions under standard conditions the experimental data on the low temperature heat capacity for the alloys studied were extrapolated to 0 K using equation of follows [2]:

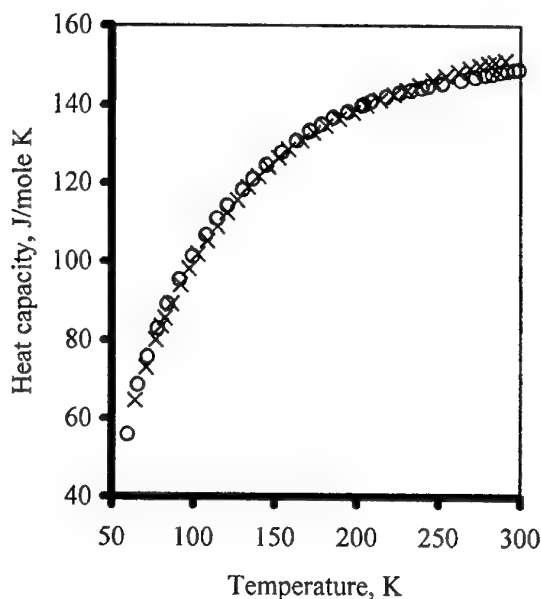
$$C_p^0(T) = \gamma \cdot T + D\left(\frac{\theta_D}{T}\right) + \sum_{i=1}^{n-1} E_i\left(\frac{\theta_{Ei}}{T}\right), \quad (1)$$

where γ is coefficient of electron heat capacity,

$D\left(\frac{\theta_D}{T}\right)$ and $E_i\left(\frac{\theta_{Ei}}{T}\right)$ is Debye and Einstein

heat capacity, respectively, n is numbers of atoms in the substance formula.

Fig.1. Smoothed data of low temperature heat capacity



× $\text{LaNi}_{4.5}\text{Cu}_{0.5}$ ○ $\text{LaNi}_{4.5}\text{Mn}_{0.5}$

The enthalpy ($\text{J}\cdot\text{mole}^{-1}$), heat capacity, entropy and Gibbs's energy ($\text{J}\cdot\text{mole}^{-1}\cdot\text{K}^{-1}$) of $\text{LaNi}_{4.5}\text{Me}_{0.5}$ ($\text{Me}=\text{Cu}, \text{Mn}$) alloys at 298.15 K were obtained: 31126 ± 159 ; $151,75 \pm 0,61$; $210,49 \pm 1,70$; $106,09 \pm 1,60$ ($\text{LaNi}_{4.5}\text{Cu}_{0.5}$); 31018 ± 155 ; $148,99 \pm 0,60$; $207,38 \pm 1,66$; $103,35 \pm 1,55$ ($\text{LaNi}_{4.5}\text{Mn}_{0.5}$).

Experimental data (fig.2) of the alloys studied enthalpy ($\text{J}\cdot\text{mole}^{-1}$) in the temperature range of 298.15 – 1478 K ($\text{LaNi}_{4.5}\text{Cu}_{0.5}$) and 298.15 – 1451 K ($\text{LaNi}_{4.5}\text{Mn}_{0.5}$) were approximation using Mayer – Kelly equation:

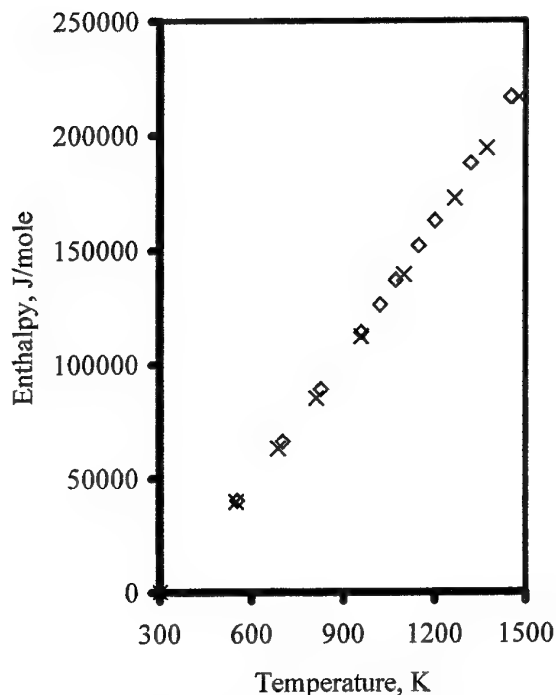
$$H^0(T) - H^0(298.15\text{K}) = A \cdot T^2 + B \cdot T + C \cdot T^{-1} + D \quad (2)$$

At confidential probably 0.95 values of enthalpy, designed on (2), are characterized by an

average relative confidential interval not to exceed 1,5 %.

Proceeding from (2) the temperature dependencies of heat capacity, entropy and Gybbs's energy ($\text{J}\cdot\text{mole}^{-1}\cdot\text{K}^{-1}$) function are as follows:

Fig.2. Experimental data for entalpy of $\text{LaNi}_{4.5}\text{Cu}_{0.5}$ and $\text{LaNi}_{4.5}\text{Mn}_{0.5}$ allows



× $\text{LaNi}_{4.5}\text{Cu}_{0.5}$ ◇ $\text{LaNi}_{4.5}\text{Mn}_{0.5}$

$$C_p^0(T) = 2 \cdot A \cdot T + B \cdot C \cdot T^{-2} \quad (3)$$

$$S^0(T) = 2 \cdot A \cdot T + B \cdot \ln T + 0,5 \cdot C \cdot T^{-2} + E \quad (4)$$

$$\Phi'(T) = A \cdot T + B \cdot \ln T - D \cdot T^{-1} - 0,5 \cdot C \cdot T^{-2} + (E - B) \quad (5)$$

Coefficients of temperature dependences (2 – 5) were calculated by the least square method using two boundary conditions, i.e. zero value of enthalpy at 298,15 K and standard value of allow heat capacity to provide agreement between high and low temperature heat capacity values. The parameters A, B, C, D, E are equal, respectively: $26,10 \cdot 10^{-3}$; 137,61; 126455; -43772,6; -598,88 ($\text{LaNi}_{4.5}\text{Cu}_{0.5}$); $29,77 \cdot 10^{-3}$; 136,96; 508709; -45187,7; -593,65 ($\text{LaNi}_{4.5}\text{Mn}_{0.5}$).

In the field of low temperatures heat capacity $\text{LaNi}_{4.5}\text{Cu}_{0.5}$ is comparable to those for LaNi_5 [3]. Heat capacity $\text{LaNi}_{4.5}\text{Mn}_{0.5}$ is higher 200 to 2-3 % below heat capacity LaNi_5 [3]. The differences of heat capacity at low temperatures are determined by insignificant shift phonon mode on fre-

quency in result of LaNi_5 doping by cooper or manganese.

At high temperatures, when phonon spectrum is completely exited, the phonon component of specific heat of researched alloys and LaNi_5 is close to meaning $3 \cdot R \cdot n$, the distinctions in meanings specific heat (3-4 %) will be determined various electronic and anharmonic by the contributions of specific heat.

REFERENCES

1. Bolgar A.S., Krykla A.I., Suodis A.P. / Low Temperature Heat Capacity of Praseodymium, Neodymium and Samarium Sesquicarbides (in Russian) // Zh. Fiz. Khim.- 1998.- 72.- p. 439-443;
2. Bolgar A.S., Gorbachuk N.P., Blinder A.V / Enthalpy of Gd_5Si_3 , Gd_5Si_4 , GdSi , $\text{GdSi}_{1.88}$ in Temperature Range 298.15 – 2200 K. Enthalpy of the Melting (in Russian) // Teplofiz. Visok. Temperatur.- 1996.- 34.- p. 541-545;
3. Gorbachuk N.P., Bolgar A.S., Skrypai A.A., Muratov V.B., Meleshevich K.A. / Thermodynamic Properties of LaNi_5 in the Wide Temperature Range // Program and Abstracts of 6th International School – Conference «Phase Diagrams in Material Science», 14 – 20 october 2001, Kiev, p. 93.

INFLUENCE OF TEMPERATURE ON FORMATION OF TRIBOTECHNICAL PROPERTIES OF REFRACTORY COMPOUNDS

Tkachenko Yu. G.

Frantsevich Institute for Problems of Materials Science, NAS of Ukraine, Kyiv

Well-founded approach to a development of new materials employing refractory compounds with a high wear resistance and low friction coefficient in a wide temperature range, first of all foresees elucidation of what processes occur in friction of refractory compounds, what mechanism of those processes and how to control them. The obtained data [1-3] on regularities of friction and wear resistance at temperatures 20-1500°C in vacuum and on the open air (Fig. 1-3), adhesion interaction in static contact, evolution of content, structure and properties of refractory compounds in a point of contact made a solid background to find out a mechanism of friction and wear resistance of those.

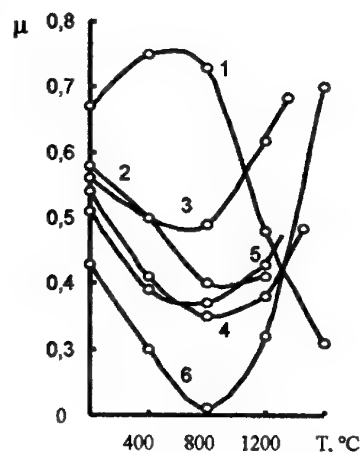


Fig. 1. Dependence of friction coefficient μ versus temperature in vacuum: 1-ZrB₂, 2-TiN, 3-MoSi₂, 4-TiB₂, 5-TiC, 6-TiC-NbC.

Tests showed a definite correlation between the obtained values of friction coefficient of metal-like carbides and borides as well as metallic components in the periodical system. Friction coefficient elevates with a growth of a number of metallic components of carbide inside the each group. Temperature when a minimum of friction coefficient is observed, also elevates with a growth of metal's number.

In case of friction of borides the dependence versus the place of metallic component in periodic system is observed in case of friction of

identical or similar structures (diborides or monoborides). The lower friction coefficient is obtained for diborides (if compare with mono-borides) and for titanium carbide and nitride of stoichiometric contents.

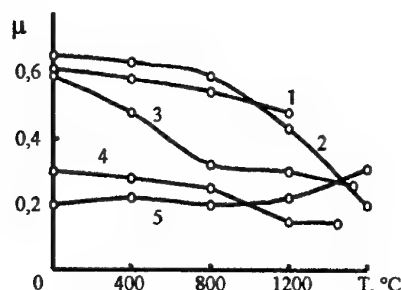


Fig. 2. Dependence of friction coefficient μ versus temperature at friction in vacuum:

1,4,5-B₄C-B₄C; 2,3-SiC-SiC

The obtained data let's to conclude that only in case of friction of refractory compounds, macro- and micro factors, including a character of interatomic interaction defined by a nature of substances involved in friction play an important role. Deformation process of near-surface region and adhesion interaction are interrelated in friction and depend upon substance nature and structure as well as tests conditions and, first of all, upon temperature and media. The data obtained while definition of "tangential adhesion", as well as status of friction surfaces certifies that friction of refractory compounds at high temperatures is associated with a development of adhesion processes in a contact zone. Growth of tangential efforts required to shift contacting unmovable samples at elevation of holding time and temperature (1200-1600°C) was observed for TiC, NbC and M₂C. These carbides have the higher friction coefficient at these temperatures than the other ones. Probably, the adhesion appears mainly at the account of formation of metallic bonds Me-Me, since when these bonds are absent (B₄C, SiC), friction coefficient varies negligibly. At temperatures $<T_{min}$ when the adhesion is not a factor to control friction process, the substances with a higher covalence rate have the less friction coefficient.

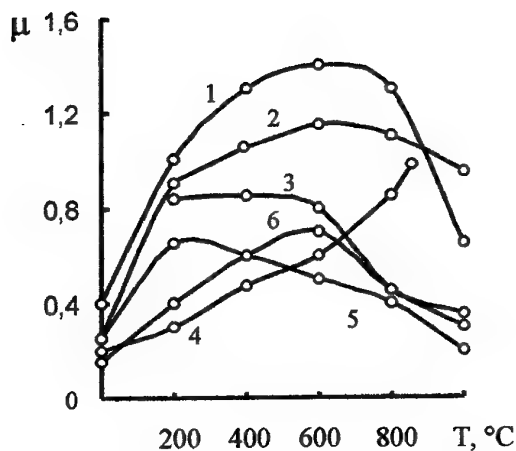


Fig. 3. Dependence of friction coefficient μ versus temperature at friction on the open air.

1-WC, 2-Mo₂B, 3-TiN, 4-ZrC, 5-Cr₃C₂, 6-TiC.

The carried out structural investigations of surface layers of metal- and non metal-like refractory compounds revealed that they possess with as mutual tendencies in deformation and structural formation in friction but a number of differences. These differences appear in deformation processes, fracture and formation of structural friction surface and pre-surface. All investigated compounds have a tendency to form pre-surface dispersion layer which is formed out of products of wear and oxidation of initial material. In case of vacuum tests this layer is made out of wear products as a result of their fragmentation and subsequent consolidation in a contact zone. However, consolidation mechanism and real structure of this kind of layer are different for TiC, AlN, B₄C and SiC. Temperature dependences of tribotechnical properties for these compounds are different also. The reason is that the higher rates of dispersion and plasticity of wear products in a contact zone provide TiC with a sintering of those at $T > 800^\circ\text{C}$. Recrystallization in a surface layer stresses also an important role of diffusion processes and their high rate in TiC. In AlN and B₄C dispersion rate of wear products in contact zone is also very high yet they do not consolidate in a solid surface layer even at 1400°C . Tracks of recrystallization were not observed in these materials and this certifies a weakness of diffusion processes. Layers of fine grain material on friction surfaces AlN and B₄C are of less strength, flocculent and are arranged in a form of islands. Unlike metal-like refractory compounds friction coefficient of non-metal-like compounds does not fall in heating. Elevation of friction coefficient

and/or its negligible alteration in heating is associated with the fact that on friction pairs AlN-AlN, B₄C-B₄C, Si₃N₄-Si₃N₄ and SiC-SiC with a growth of temperature a quantity of badly fixed dispersion particles grows up. Heating and plastic deformation of these particles, being under the forces of friction and normal loading activate adhesion of particles to each other as well as surface grains. Since the quantity of dispersion particles elevates with a temperature growth, friction coefficient grows up also. At friction of TiC-TiC in vacuum, a heating up to 800°C does not bring a formation of fine dispersion layer on a surface of friction. Friction coefficient in temperature interval $20-800^\circ\text{C}$ falls continuously. Elevation of friction coefficient for like samples TiC is observed at heating higher than $830-900^\circ\text{C}$, and at 800°C on friction surfaces fine dispersion particles - product of fracture of surface grains become visible. With elevation of total quantity of dispersion particles on friction surfaces a rate of wear grows up also.

The carried out investigations revealed that in friction the processes of plastic deformation of surface layers: AlN and SiC (20°C), B₄C (400°C) and TiC (800°C) for all refractory compounds become noticeable. Simultaneously, the processes of fracture of surface layer, dispersion of wear products and formation of dispersion layer structures - especially for TiC (in vacuum) and for AlN (open air) take place.

The obtained experimental data about tribological properties and evolution of surface layer structure expand our knowledge on friction mechanism of refractory compounds and is a solid basement practical implementation associated with a development of materials of tribotechnical purpose.

1. Tkachenko Yu. G. Friction and wear of oxygen free refractory compounds and materials on its base at high temperatures // Friction and wear, 1981. - vol.2, №5. - pp.864-876.
2. Tkachenko Yu. G., Grabchuk B.L., Bodnaruk N.I., Suchov V.V. Friction and wear of boron carbide in temperature interval $20-1500^\circ\text{C}$ // Powder Metallurgy, 1977. - №7. - pp.60-63.
3. Brytun V.F., Tkachenko Yu. G. Structure of surface layers formed in TiC and TiN in friction in vacuum // Wear and friction, 1995. - vol.16, №4. - pp.752-758.

MATERIAL SCIENCE ASPECTS OF MATERIALS FOR SPARK HARDENING

G. Bovkun, Yu. Tkachenko, A. Laptev

I. Frantsevich Institute for Problems of Materials Science, the Ukra Ukraine NAS, Kyiv, Ukraine

Attempts to govern by level of erosive properties of electrode materials exist since, while the method of spark hardening of operating details surfaces, working in conditions of intensive wear appeared and began widely to make use. Palatnik and Albinsky [1,2] attempted to work up the criterions of metals erosion resistance, originating from processes physics, taking place in materials surface layers during erosive processing. However, these attempts were not successful and adopted criterions worked only for definite range of materials and processing conditions. Interest to this question went out on measure of how metallic materials all more rarely used for hardening aims. Nevertheless it was shown, that metals erosion resistivity for invariable spark hardening processes parameters determines by complex thermophysical and mechanical properties, by their ability to suffer allotropic transformation at high temperatures, by activity of chemical interaction with elements of gas medium [3]. Herewith it is possible to find out the relation between metals erosion resistivity and subatomic links strength, which describes by the lattice rigidity factor, and peculiarities of their electronic structure [4].

For refractory compounds, distinguished by high significances of physical-mechanical properties, at all does not reveal any correlation between erosion resistivity and melting temperature, module of normal elasticity significances, but the same as for metallic materials, one can clearly see a relation between erosion resistivity and character of chemical bonding in crystal lattice [4].

Considerably more complicate is a govern task by level of erosion properties of hard metals, traditionally using for aims of metallic surfaces hardening. So, if for metals erosion resistivity rises in general case with rise of melting temperature, elasticity module, lattice rigidity factor, and erosion resistivity of refractory compounds lower on comparison with metals on 1-2 order and decreases when degree of covalent bonds in crystal lattice enhances, then the hard metals on level of erosion resistivity occupy an intermediate position. But herewith, on one, nor maintenance of metallic binder content in limits 2-100 %, nor particles dispersion of hard phase in interval 1-15 μm , noticeable influence on erosion resistivity

level of hard alloy do not render, and on other their erosion resistivity can change in 2-4 once after doping not more than 0,5 % additions, which decrease moistening of hard phase by metallic binder[5], on order reduces when alloy porosity varies in the region 0-35 %, in 3-4 once changes when changes an electrode transverse section, in once or twice rises after treating sintered alloys by current impulses 100 A, which essentially changes a level of residual stresses in electrode material.

Originating from said, one can be supposed, that a level of erosion resistivity of different materials classes determines by their destruction mechanism during spark processing, and the changes of materials erosion resistivity within the pale of set class depend on that, in what measure a complex of physical-mechanical properties or external influence affects change of destruction mechanism. So, metals and metallic alloys erode in the main in liquid and gas phase. The erosion products of metallic materials lightly fix on undercoat and transfer coefficient K (K =increase of cathode mass/erosion of cathode) and coverage continuity achieve 100 %. Refractory compounds, which have inessential on comparison with metals plasticity, erode mainly in solid phase. Refractory compounds erosion products of shrapnel form and by dimension to 0,5 mm badly fix on undercoat and even having comparatively low erosion resistivity refractory compounds assurance coverage continuity not more than 30-50 %, and significance K varies in range 2-35 %. Attached to transition to hard metals, combining high hardness of refractory compounds and metallic binder plasticity and eroding mainly in solid phase, in erosion products there are the molten, partially molten and of shrapnel form particles, but considerably lesser sizes. This determines on one high erosion resistivity of hard metals, and with other sufficiently high hardening process effectiveness. All that confirm supposition, that a materials destruction mechanism in conditions of spark processing mainly determines a level of their erosion resistivity and the effectivity of hard alloys spark hardening process. This process effectiveness can be governed only by mean of those influences, which causes change of materials destruction nature during spark processing, and as a consequence an aggregative state of anode

material erosion products. Just by this reason the effectiveness of methods of management by hard alloys erosion properties determines that, in what measure they change strength of interphase boundaries. All traditional modification methods for properties of hard metals do not allow to bring to light a relation between erosion resistivity and state of interphase boundaries unambiguously, because more frequently a few parameters, such as composition, grain size of carbide phase are variable. A method of high energy hot pressing allows essentially to change strength of interphase boundaries, while other parameters are constant. This permits to establish a correlation of hard alloys erosion resistivity with the strength of interphase boundaries. For this method a heated hard metal preform exposes to momentary action of high pressure ($>1\text{ГПа}$). For alloys, which were heated to temperatures beneath temperatures of the dense state, such action leads to notable rising of quantity and quality of interphase contacts, level of mechanical strength, conductivity, and for alloys, heated to more high temperatures - to destruction of early formed and to forming of new structure and complex of physical-mechanical properties. It is interesting, that on curves Δ_a , Δ_k , $K - f(\sigma_{tr}, K_{IC})$ the significances of erosion properties, of alloys, produced by diverse methods, subjected or not consequent heat treatment, are, practically, on the same curves (Fig1,2), and have a bend in temperatures range 1200-1250 °C. This confirms, that the processes, which take place at these temperatures, cardinally change not only level of physical-mechanical alloys properties, but also mechanism of their destruction during spark processing and anode erosion products fixing mechanism. The experimental data shows, that erosion resistivity of hard metals depends only upon their specific resistance (Fig.3), what in its turn is unambiguously determined by interphase boundaries quality. All above mentioned confirm the idea, that only destruction mechanism designates for the level of hard metal erosion resistance and we can suppose, that this conclusion is directly relevant to other materials classes.

1. Albinsky K. Research of the electrical resistance of electrodes attached to spark and electrical impulse treatment.- Lathes and tools. - №7. - 1964. - c.11
2. Палатник Л.С. X-ray photography transformations research in superficial metals layer, exposing to action of electric charges.-«Izvest. AN SSSR, series phys.». - 1951. - 15, №1. - c.80

3. Samsonov G.V., Wierchoturov A.D., Bovkun G.A. I inni.. Technologia elektroiskrowego wtapiania skladnikow stopowych.-Electronica.-1972 -№12.-c.509
4. Samsonov G.V., Wierchoturov A.D., Bovkun G.A., Sychev V.S. Spark treating of metallic surfaces. - Kiev, Naukova dumka. - 1976. - 219 with.
5. Tkachenko Yu.G., Ignatenko E.P., Bovkun G.A. et all. Dominance of anode structure on regularities of spark hardening with hard alloys.- Electronic processing of materials.-1981 -№4.- c.

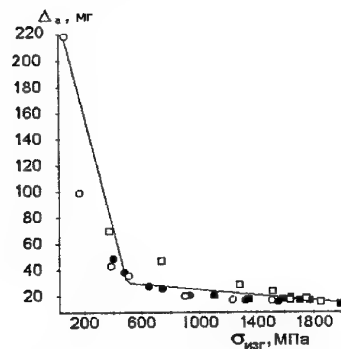


Fig. 1 Erosion resistance of WC-16%Co hard metals vs. their transverse rupture strength

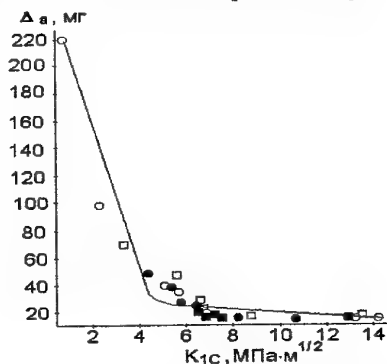


Fig.2 Erosion resistance of WC-16%Co hard metals vs. their toughness

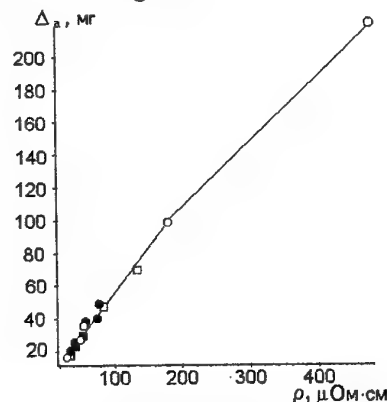


Fig.3 Erosion resistance of WC-16%Co hard metals vs. their electrical resistance

ENERGETIC CHARACTERISTICS OF FULLERENES AND FULLERENE-LIKE SUBSTANCES

Goryachev Y.M., Dekhteruk V.L., Siman M.L., Fiyalka L.L., Shvartsman O.Y.
Institute for Problems of Material Science of NAU

To property study fullerenes and fullerene-like substances it is often necessary to calculate their energetic and thermodynamic characteristics [1,2]. Such calculations were performed by means of the method of group orbitals of the linear combination of atom orbitals (Go-LCAO) [3,4].

The energetic characteristics of fullerenes and nanotubes were calculated by means of the method of group orbitals of the linear combination of atom orbitals (GO-LCAO), its many-cluster version [3, 4]. The results obtained were associated with the available related data [2, 5, 6].

On the base of the data on calculation of electronic spectra of fullerenes and different kinds of nanotubes [4], such energetic characteristics as the surface, contact and reaction energies were determined. The surface energy (σ) was determined as the difference between the atomization energy per atom and the energy of removing an atom from defectively diminishing surface of the cluster studied. To calculate this energy, the nearest bonds were substituted by the bonds in the second coordination sphere:

$$\sigma = E_{at}(1 - C / (A \cdot \epsilon^n + B)). \quad (1)$$

Here A and B – the numbers of the bonds in the first and second coordination spheres (before an atom leaving the fullerene surface), correspondingly; C – the number of the bonds in the second sphere of the neighbouring atoms; ϵ – the ratio of the interatomic distances between the central atom and the atoms in the second and first coordination spheres (for fullerenes $\epsilon = 1,73$; A = 3; B = 6; C = 15); E_{at} – the fullerenes atomization energy; $n = 2,06 + 0,005$ – empirically adjusted index. The data on the energies calculated are given in Tables 1 and 2. Here the total surface energy is reduced to the area occupied by one atom; its dimensions being eV/at.

The contact energy was determined as the energy of sticking absolutely clean surfaces of interacting bodies. In the case of fullerenes it can be displayed by lumped powders. The contact energy is caused

Table 1
Total (E_{at}), surface (σ) and contact (E_{con})
energies of fullerenes, eV/at

Type C_n Энер- гия	C_4	C_8	C_{20}	C_{60}	C_{90}	C_{240}	C_{900}
E_{at}	2,9	3,8	5,5	6,9	5,8	4,4	3,2
σ	0,06	0,08	0,11	0,138	0,116	0,088	0,064
10^{-2} $E_{конт}$	0,65	0,84	1,03	1,57	1,29	0,98	0,73

Table 2
Total (E_{at}), surface (σ) and contact (E_{con}) energies
of nanotubes with the diameter D_n , eV/at

Тип D_n Энер- гия	D_2	D_3	D_4	D_5	D_6	D_8	D_{10}
E_{at}	2,5	5,5	6,7	5,0	4,0	3,5	3,1
σ	0,05	0,11	0,134	0,100	0,08	0,07	0,060
10^{-2} $E_{конт}$	0,56	1,22	1,49	1,11	0,89	0,78	0,69

by Van der Waals forces which are inversely proportional to the distance between interacting atoms in the sixth degree. So, when the interatomic distance increases from the smallest covalent distance up to the interlayer distance (in graphite), the energy decreases by 150 times with increasing the interatomic distances by 2, 3 times:

$$E_v/E_c = (d_v/d_c)^6 \quad (2)$$

Here E_v and E_c – the energies of Van der Waals and covalent interactions, correspondingly; d_v and d_c – the corresponding interatomic distances.

Taking into account the relation (2) and the fact that the atomization energy is approximately equal to the covalent interaction energy, the contact energy can be expressed as follows:

$$E_{con} = E_{at} / (K \cdot 150) \quad (3)$$

Here K – the multiplicity of decreasing the coordination number after the passage from covalent to Van der Waals interactions (for fullerenes $K=3$). The data on the contact energy calculated for some fullerenes and nanotubes are given in Tables 1 and 2.

The data show that the contact energy of fullerenes differ not so much from that of interlayer interaction in graphite ($\sim 0,016$ eV/at). But contacting surfaces of fullerenes and nanotubes have big curvature, which explains the essential degree of looseness of nanomaterials.

The reaction energy (E_r) fullerenes with respect to certain substance determines energetic possibility for an exothermic reaction between them to occur. This energy can be calculated as the difference between the energy of bond of graphite with the corresponding substance (E_{mc}) and the average atomization energy (E_{av}) of the corresponding fullerene (or nanotube) and metal:

$$E_r = E_{mc} - E_{av};$$

$$E_{av} = \frac{1}{2}(E_{ful} + E_m) \quad (4)$$

Some of the energetic characteristics in the case of interaction of fullerenes with potassium, yttrium, titanium and iron are given in Tables 3 and 4.

Table 3

The atomization energy of metal-carbon bond,
eV/at

M	K	Y	Ti	Fe
E_i				
E_m	0,93	3,91	4,9	4,3
E_{mc}	1,38	6,78	7,12	2,88

These starting data for calculation of the fullerene reaction energy were obtained by means of the GO-LCAO method [1]. The validity of using them was testified by comparing with the corresponding experimental data, the discrepancy not exceeding $\pm 10\%$.

Table 4

The reaction fullerene-metal energy

C_n	C_1	C_4	C_8	C_{20}	C_{60}	C_{76}	C_{240}
$E_{p,i}$							
$E_{p,Y}$	4,8	2,42	2,02	1,57	1,37	1,52	2,62
$E_{p,Ti}$	4,67	2,27	1,87	1,42	1,22	1,37	2,47
$E_{p,Fe}$	0,73	-1,67	-2,07	-2,52	-2,72	-2,57	-1,51
$E_{p,K}$	0,91	-1,49	-1,89	-2,34	-2,54	-2,39	-1,29

These data show that fullerenes can react exothermally more or less reliably only with yttrium and titanium. Interaction with iron and potassium either can't occur or occur endothermally at certain changes of the system entropy.

CONCLUSION

1. A method for calculation of the surface, contact and reaction energies of fullerenes was worked out.
2. The values of these energies were calculated in homogeneous rows of fullerenes and nanotubes.
3. The characteristics calculated were shown to be associated with some physical and chemical properties of fullerenes such as sticking, defect formation and reactivity.

LITERATURE

1. Осипян Ю.Л., Кведер В.В. Фуллерены – новые вещества для современной техники. // Материаловедение. -N 1. -Киев, 1997. -С. 2 – 6.
2. Дикий В.В., Кабо Г.Я. Термодинамические свойства фуллеренов C_{60} и C_{70} . // Успехи химии. -Т. 69 вып. 2. 2000. -С. 107 – 117.
3. Горячев Ю.М., Ковенская Б.А., Самсонов Г.В. Расчет электронного спектра соединений переходных металлов методом ГО-ЛКАО. // J. Science of Sintering, Vol.10, spec. Issue, 1978, pp. 83 – 89.
4. Горячев Ю.М., Симан Н.И., Фиялка Л.И., Черногоренко А.В. К вопросу о связи электронного строения и термодинамических свойств фуллеренов. // Сб. "Электронное строение и свойства тугоплавких соединений и сплавов и их использование в материаловедении". - Киев: ИПМ НАН Укр, 2000. -С. 34 – 38.
5. Бочвар Д.А., Гальперн Е.Г. О гипотетических системах: карбододекаэдр, S- икосаэдр и карбо- S- икосаэдр. // ДАН СССР, -т 209, -№3. 1973. -С. 610 – 612.
6. Соколов В.И., Станкевич И.В. Фуллерены – новые аллотропные формы углерода: структура, электронное строение и химические свойства. // Успехи химии. -т. 62 (5). 1993. -С. 455.

WEAKENING OF POROUS TITANIUM-SILICEOUS CARBIDE Ti_3SiC_2 AT ACTIVE AND STATIC LOADING

Firstov S.A., Ivanova I.I., Pechkovsky E.P.

Institute for Problems of Materials Science, N.A.S.U., Kiev, Ukraine

By methods of a measurement of short-term and long hardness, the tests on uniaxial compression and fractography researches there are investigated regularities, features and mechanisms of processes of plastic deformation and weakening in an interval of temperatures 20-1300 °C of ternary compound – titanium-siliceous carbide Ti_3SiC_2 , obtained by a way of a solid-phase reactionary sintering with values of a porosity $\theta=0,05-0,5$. It is shown, that there are three temperature intervals of a strain, which differ by mechanisms of a course of these processes. The effects of dynamic and static weakening will increase with a diminution of a porosity, raise of temperature and magnification of a curing time under a load. By critical values of parameters of active and static modes of loading, after which reaching begins weakening and sharply plasticity is increased, are temperature 1100 °C and curing time under a load 10 minutes.

Fractography examination of a surface destroyed samples with a porosity $\theta=0,28$ had shown, that the particles-grains of ternary compound Ti_3SiC_2 have the shape of plates by thickness 1-2 microns and cross size 5-10 microns. These plates are curved, ramified, polythickness, with salients and dimples. During formation and growth such flat particles, adjoining among themselves in different places, realize contacts of a different degree of strength - from negligible touch up to mutual intergrowth with formation of bridges-necks. The presence of this structure element in porous titanium-siliceous carbide is its essential structural feature, which defines features of a plastic deformation and fracture.

The plastic deformation in this material is realized by slide of edge dislocations in basis planes with formation of pileups [1]. The overcoming of resistance of a crystal lattice and other hindrances on trajectories of a motion of edge dislocations under influence of the thermal factor (so-called crawling in adjacent slip planes) can happen at temperatures, which ensure a diffusion of atoms of a crystal lattice. As a result diffusion mechanisms of a plastic deformation come into action.

In a dense material, as follows from [1], a necessary condition of embodying of a plastic deformation is the formation of cavities, pores on

grain boundaries. In a material, investigated in at present work, already there are pores, where the moving dislocations can go out and thus to not create concentration of a stresses, i. e. the necessity for a relaxation of a stresses by power-intensive process of a delamination of grains, reference for a dense state [1], disappears.

At test for an uniaxial compression of a material with a porosity $\theta=0,28$ the absence of macroplastic strain is noticed in an interval of temperatures $T=20-600$ °C (Fig.1). Above this temperature

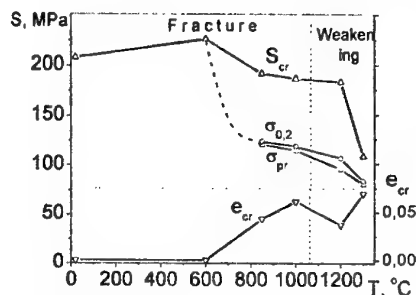


Fig. 1.

there are indications of macro plastic strain, which reaches quantity of $e=6\%$ at

$T=1000$ °C. It means, that the edge dislocations have gained an opportunity to transfer in adjacent planes by crawling, i. e. atoms of a crystal lattice (and vacancy) became to diffuse actively [2].

After reaching critical strain, at which as a result of crawling edge dislocations in adjacent planes will be formed highdisorienting cellular structure, the activity of plastic deformation is entered by one more factor of interaction of dislocations - there is an annihilation of some part of dislocations of an opposite mark in cell boundaries.

The annihilation of dislocations gives in additional slowing down of rate rise of a dislocation density. At this high strain temperature, when there are ensured raised diffusion mobility of atoms of a crystal lattice and, accordingly, intensive crawling of edge dislocations, the velocity of an annihilation of dislocations can become such considerable, that it will exceed a generation rate of new dislocations, - there will be lowering an integrated dislocation density, i. e. the dynamic weakening takes place. Accordingly, at $T \geq 1100$ °C on a strain-curve at value of critical strain at a level 5-7 %, is observed noticeable decline of a flow stress, the plasticity increases up to $e=30-40\%$.

Measurement of short-term hardness ($t = 1$ min, $P = 10$ N) in the investigated interval of temperatures

has shown (Fig. 2), that the magnitude of hardness depends on conditions of production of a porous

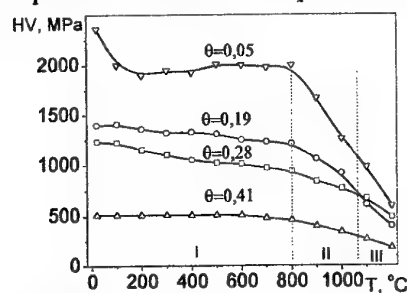


Fig. 2.

material, decreases at increasing of a porosity and sharply is reduced at exceeding $T=800\text{ }^{\circ}\text{C}$. Nevertheless the character of a temperature dependence remains constant [2].

Carried out the thermosetting analysis of temperature dependence of hardness of a material with different values of a porosity has shown, that there are three temperature intervals, which differ by values of an activation energy, i. e. by mechanisms of plastic deformation (Fig.3). Their boundaries identical to a different porosity.

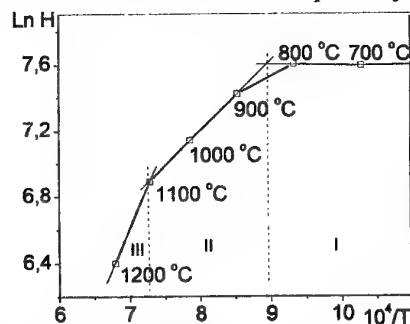


Fig. 3.

The first temperature interval is $\Delta T_1=20-800\text{ }^{\circ}\text{C}$. Here hardness practically is fixed.

In basis planes of a crystalline lattice the sliding of edge dislocations, activated by force factor happens, the contribution of thermal activation is insignificantly small. The interval of a possible strain of samples at an active strain is - from microplastic at $20\text{ }^{\circ}\text{C}$ up to $\epsilon=3\%$ at $800\text{ }^{\circ}\text{C}$.

The second temperature interval is $\Delta T_2=800-1050\text{ }^{\circ}\text{C}$. The value of an activation energy, which makes 1.1 eV , answers an energy of thermally activated formation of thresholds (footsteps) on edge dislocations by migration of vacancies in these places with consequent transition of footsteps along a line of a dislocation (diffusive-dislocation mechanism). A strain of samples reaches a value $\epsilon=6\%$.

The third temperature interval is $\Delta T_3=1050-1300\text{ }^{\circ}\text{C}$. Activation energy makes 2.6 eV , that answers of an activation energy of migration of vacancies in a titanium. Here passage (crawling over) of an edge dislocation in an adjacent plane happens by migration of vacancies, which were formed along all line of a dislocation in places of intersection with other edge dislocations, and also owing to a diffusion of titanium atoms, that is the

diffusion mechanism of plastic deformation is carried out. A common strain of samples reaches $\epsilon=30-50\%$.

Study of long-term hardness H ($t=1-60$ minutes) has shown, that the weakening process of this material in a temperature interval $800-1200\text{ }^{\circ}\text{C}$ in time t for each concrete temperature can be circumscribed by the equation of a type $H=a t^{-m}$, where a - constant, m - weakening index. It has enabled to receive a temperature dependence of a weakening index m for each concrete value of porosity of a material (Fig. 4), i. e. to express weakening effect quantitatively.

It is visible, that the magnification of a poro-

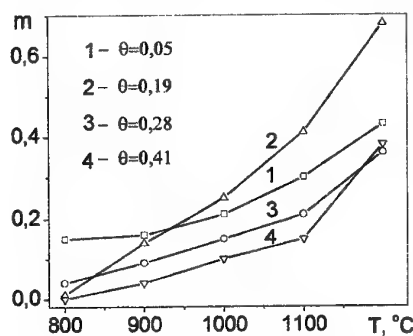


Fig. 4.

sity decelerates the weakening process of a material. With a raise of temperature the effect of a

relaxation of stresses is increased. In a temperature interval $T=800-1100\text{ }^{\circ}\text{C}$ this increasing happens practically to a steady speed, but at $T>1100\text{ }^{\circ}\text{C}$ it sharply will increase.

The thermosetting analysis of temperature dependence of hardness in an interval of temperatures $800-1200\text{ }^{\circ}\text{C}$ for each indicated curing time of indenter under a load (1, 5, 10, 20, 30, 60 min) has shown the following.

In a temperature interval $800-1050\text{ }^{\circ}\text{C}$ the intensity of weakening poorly accrues in time and does not depend on a porosity: the values of an activation energy do not exceed 1 eV , that is predominate dislocation mechanisms of plastic deformation.

In an interval of temperatures $1050-1200\text{ }^{\circ}\text{C}$ take place sharp increasing of intensity of weakening both on an absolute value, and on a velocity of its increasing, and it is exhibited in the greater degree for a material with a smaller porosity. Here magnitude of activation energy reaches values, which exceed 4 eV , - that is the diffusion mechanisms of plastic deformation are carried out.

1. Barsoum M.W. / *Prog. Solid St. Chem.* - 2000. - Vol. 28. - P. 201-281.
2. Brodnikovskyy N.P., Burka M. P, Demidik A. N, Ivanova I.I., Pechkovsky E.P., Polushko G.P., Firstov S.A. / *Intern. Conf. «Adv. Ceram. for Third Millen.»*, Kiev, 2001. - P. 115, 116.

INFLUENCE OF TRIBOSYSTEM COMPONENTS ON THE FRICTION BEHAVIOR OF Al-Cu-Fe QUASICRYSTAL

**Grinkevych K.E., Lotsko D.V., Milman Yu.V., Bykov O.I., Shurygina Z.P., Ponomarev S.S.,
Bilous A.M., Yefimov M.O.**

I.M.Frantsevych Institute for Problems of Material Science of NAS of Ukraine, Kyiv, Ukraine

Quasicrystals, Al-Cu-Fe in particular, are known as having a very low dry friction coefficient μ , but it strongly depends on characteristics of the tribo-system and friction conditions. Thus, the lowest $\mu \approx 0.05$ was obtained for sintered specimens of Al-Cu-Fe quasicrystal when using a diamond indenter, but for indenters of cemented carbide, alumina or bearing steel μ increased 3-4 times [1]. So did testing Al-Cu-Fe coating that was of rather high porosity [2]. Though quasicrystals are macroscopically brittle at room temperature, signs of microplastic deformation were found in friction tracks [1]. It was supposed that low friction of diamond indenters might be caused by the formation of graphitic surface layer [1], i.e. the form of carbon in contact layers may be of a great importance in quasicrystal friction. A very important role of carbon was noticed earlier for friction of bearing steel, where by special carbon additions to the lubricant the formation of graphite-diamond films in friction surface was observed, and μ was lowered to about 0.08 [3].

In this work we present the results of studying the friction of an Al-Cu-Fe quasicrystalline specimen with the application of various carbon additions to the lubricant. The experiment was carried out in an original tribocomplex CATC [4] developed in the IPMS.

The specimen was manufactured from powder (+63-100) μm produced by water atomization technique [5]. The content of oxygen in powder was about 1.5 %. The specimen 20 mm in diameter and 6 mm in height was compacted under a high quasihydrostatic pressure of 4 GPa at a temperature of about 700 °C. Due to temperature gradients during pressing two regions with different porosities were formed in the specimen: region A with greater porosity $\theta = 7.7\%$ and smaller average pore diameter $D = 36\ \mu\text{m}$ and region B with $\theta = 4.5\%$ and $D = 74\ \mu\text{m}$. In order to obtain a single icosahedral phase of the composition close to $\text{Al}_{63}\text{Cu}_{25}\text{Fe}_{12}$ the specimen was annealed in vacuum furnace at 700 °C for 2h. Specimen surface was mechanically polished.

Dry friction was carried out by the scheme "sphere-plane" by indenters with spherical tips

6 mm in diameter of 4 kinds: ball bearing steel ShKh-15, silinite Si_3N_4 , sintered carbides WC1 (WC - 6 %Co) and WC2 (WC - 2 %Co - 15%TiC). The indenter was moving by a reciprocating way along the track 8 mm in length with a velocity of 0.013 m/s under a load $P = 28\ \text{N}$. The wear (I) was characterized by the depth of the friction track measured in a profilometer in 20 min after starting the experiment (after 975 cycles). The friction force (F) was measured by a dynamometer in 1, 3, 5, 10, 15, and 20 min after experiment starting, and the average value was determined. Hardness was measured by a Vickers diamond indenter with a load of 2 N. Tracks were studied in Auger spectrometer JAMP-10S.

Hardness of the sample was rather non-uniform evidently due to the porosity and achieved 800 MPa. Hardness HV_i of all indenters was higher (Table 1).

Table 1. Characteristics of dry friction and friction with lubricants of Al-Cu-Fe quasicrystal

Indenter	HV_i , MPa	Region A		Region B	
		I, μm	μ	I, μm	μ
Steel	870	1.83	0.21	1.73	0.21
WC1	1720			20.9	0.49
WC2	1987	2.88	0.38		
Si_3N_4	1970	19.4	0.68	20.2	0.52
Si_3N_4 with I-20		8.83	0.111	17.83	0.086
Si_3N_4 with LP		1.83	0.065	6.67	0.05

Friction tracks consisted of smooth-faced areas 1 and of fractured areas 2 (Fig. 1).

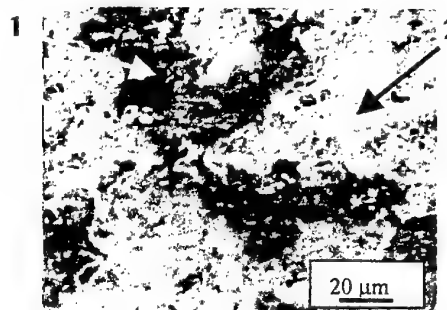


Fig. 1. Track of dry friction by Si_3N_4 , region A

The lowest value of I and μ in dry friction by steel is evidently explained by the fact that a noticeable wear of the steel indenter took place, and destroying energy was redistributed between two components of the tribocouple. Other indenters showed no signs of wearing out, and an increase of seizure could take place in these cases: thus, in works [1, 6] Al, Cu and Fe were clearly detected in the surface of WC-Co indenter, and the transfer-retransfer mechanism was proposed. As the reason for fracture the development of tensile stress close to the contact area was given. For friction by WC2 containing an admixture of TiC wear is 7 times lower than in the case of WC1 in spite of appreciably higher hardness of WC2. Evidently, it is a consequence of a known action of TiC as a hard lubricant.

The content of carbon in track surface was characterized by the ratio of Auger peaks intensities of C and Al that for dry friction after slight etching by argon ions were equal to 3.69, 4.4, 3.13 and 1.04 for four used indenters (Table 1) respectively. Note the highest level of C for the case of WC2 with small wear and the lowest level of C for Si_3N_4 with high wear. For further experiments with carbon-containing lubricants we have chosen the indenter Si_3N_4 as not facilitating carbon absorption. In Table 1 there are given the results of friction by this indenter with two kinds of lubricants: a usual industrial oil I-20 and liquid paraffin LP.

Different effects of two lubricant oils can be explained by their different surface activity. For local pressure and temperature flashes while friction a destruction of hydrocarbons with the formation of free radicals is characteristic for a majority of industrial petroleum oils [7], and for this reason they demonstrate a rather high Rebinder effect that intensifies material fracture. Liquid paraffin has alkane cycles that are very hard to destroy, and therefore it has a very small surface activity. That permitted to lower the value of μ to about 0.05. It is seen a large difference of I and μ in regions A and B. A reason could be intensifying the Rebinder effect in coarse pores of region.

Inactive liquid paraffin was chosen for studying the influence of carbon additions to the lubricant. They were: expanded graphite EG obtained by intercalation process in the form of particles with very thin lamellar "scrub" [8]; highly dispersed amorphous carbon HDAC [3]; highly dispersed diamond HDD (particle size less than 1 μm). Their influence on the friction parameters are seen from Table 2. Experiment was carried out in the region A.

Table 2. Influence of carbon additions on friction characteristics of the trybo-system quasicrystal – Si_3N_4 – liquid paraffin, region A

Characteristic	EG	HDAC	HDD
$I, \mu\text{m}$	8.1	2.72	1.99
μ	0.089	0.079	0.04

In smooth parts of friction tracks obtained with these additions the C/Al ratio in Auger spectra was 7.82, 7.28 and 17.5 respectively, and in the track without additions it was about 9. I.e. in the case of diamond addition carbon adhesion was extremely high, and other carbon additions gave no additional adhesion. The shape of carbon spectral line in all cases corresponded to amorphous state of carbon.

It is seen that the influence of carbon on friction and wear of Al-Cu-Fe quasicrystal strongly depends on its form. Thus, thin graphite lamellas in the form of a scrub instead of lubrication effect facilitated the increase of fractures in the track, and only the addition of diamond led to the formation in it of lengthy smooth areas. Moreover, only in this case small pile-ups in track edges were found in track profile that testifies to quasicrystal microplasticity. We can suppose that in this case a phase transformation to a more plastic phase took place like the case of Al-Cu-Fe indentation by diamond indenter [8]. Evidently, the mechanism of diamond effect on lowering the friction coefficient is not the graphitization, but a very strong adhesion of carbon by track surface.

This work was partially supported by STCU, project No. 1630.

1. Von Stebut J., Strobel C., Dubois J.M. // Proc. of the 5th Intern. Conf. on Quasicrystals, Avignon, 22-26 May 1995. – World Scientific: 1995. – P. 704.
2. Kang S.S., Dubois J.M., Von Stebut J. // J. Mater. Res. – 1993. – 8, No. 10. – P. 2471.
3. Bershadsky L.I., Iosebidze D.S., Kutelia E.R. // Thin Solid Films. – 1991. – 204. – P. 275.
4. Lotsko D.V., Grinkevych K.E., Yefimov N.A. // Problems of Tribology. – 1996. – 2. – P. 56.
5. Neikov O.D., Krajnikov A.V. // Mater. Sci. Forum. – 1996. – 217-222, P. 1649.
6. Sordelet D.J., Kim J.S., Besser M.F. // Proc. Mater. Res. Soc. Symp., Warrendale, PA, 1999. – 553. – P. 459.
7. Feklisova T.G., Vasiliev I.A., Sakhabutdinov A.G et al. // Trenie i Iznos. – 1982. – 3, No. 2. – P. 225.
8. Dub S.N., Milman Yu.V., Lotsko D.V., Belous A.N. // J. Mater. Sci. Lett. – 2001. – 20. – P. 1043.

THE OPTIMAL DESIGN OF IMPLANTS CONTENT AND SHAPE ON THE COMPUTER MODELLING BASE .

Mikhailov O.V., Tkachenko L.N., Shtern M.B., Dubok V.A.

Institute for Problems of Materials Sciences, Kiev, Ukraine

To implants materials the heightened demands, especially to their stiffness and strength are made. As such materials the metals and their alloys are applied. However they have deficiencies. It is poor biological compatibility and difference in implant content and mechanical characteristics from tissues of an organism. The prostheses perceive on themselves the main part of the loading applying to the construction body-implant. At the same time stresses having in the bone are the stimulus for its growth. The insufficient loading results the bone tissue resorption and shaking of the prosthesis.

The problems solution is possible in several directions. At first, this is the definition of the optimum correlation between properties of the material and his maximal biological compatibility. Secondly, it is optimization of a prostheses construction. And at last an application of new technologies of implants preparing is.

As the material of prostheses it is perspective to use the nanostructural biologically pure titanium. This material can be obtained with usage of intensive plastic deformation methods. The material has high surface strength and low elastic modulus. Biological compatibility is also highly.

Perspective direction is the application of so-called bioactive ceramic materials. Their basis is the synthetic analog of the mineral basis for the bone tissue - hydroxyapatite [1]. These materials are included after the implantation in a metabolism of the organism and allow refreshing completely structure and properties of considerable volumes lost bone tissues.

The biological compatibility can considerably be increased by coating deposition on the implant's surface. The most perspective are diamond-like carbon coatings with given structure and properties. These coating have properties similar to natural diamond. They are not only thromboresistant, but also the biologically compatible to blood cells.

The prostheses construction optimization is possible on the basis of modern computer modeling methods.

The application of integrated CAD/CAM/CAE system is perspective. Except the traditional CAD system being used for designing of the implants shape, it is necessary the special system. The special CAD system allows building three-dimensional geometrical organ model on the basis of sections obtained by a method of the computer tomography [2]. Because of the complicated geometry of these parts, modeling requires analysis preprocessors capable of handling higher order spline curves to form complex volumetric entities representing human anatomy.

The demands also are made to CAE system of a numerical modeling (the finite element method is usually used). Finite element modeling of biomedical parts presents a special challenge to stress analysts. The actual properties of materials, both alive, and lifeless nature, should be used. The nonisotropic nature of some materials used in biomedical parts requires use of orthotropic elements with differing material angles [3].

The analysis of stress-strain state of a construction allows to reveal the most dangerous areas and to found the optimum implants shape. The computer modeling allows also finding the implant material with optimal combination of properties.

The use of CAM system allows at once making the prosthesis of a necessary construction.

The application of new materials requires making technologies of preparing the materials and the implants from them. It is powder metallurgy and metal forming processes.

The use of analyzed above methods allows making implants with more high level of properties.

REFERENCES

1. Dubok V.A. Bioceramics - yesterday, today, tomorrow, *Powd. Metall. Metal Ceram.*, (translated from Russian), N 7/8, 69-87(2000)
2. <http://fam.uni-paderborn.de>
3. <http://www.srac.com/succes/medical.htm>

STRUCTURE OF THIN FILMS AND EXTREMELY GRINDED POWDERS OF FULLERENE C_{60}

Solonin Yu.M., Grayvoronskaya E.A.

Frantsevich Institute for the Problems of Materials Science NAS of Ukraine, Kyiv, Ukraine

One of the most intensively developing direction of modern physics is connected with the discovery and investigations of a new carbon allotropic form – fullerenes. The pseudospherical molecule of C_{60} about 0.7 nm in diameter possesses the structure of the regular truncated icosahedron with carbon atoms situated in the apexes of 20 hexagons and 12 pentagons. The solid form of C_{60} , fullerite, was discovered in 1991. In fullerite the C_{60} molecules are connected by Van der Waals forces and form the close-packed structures. X-ray diffraction studies of the C_{60} fullerite powder have shown that the fullerite structure is face-centered cubic (f.c.c.) with cell parameter $a = 1.416$ nm. Fullerite C_{60} thin films on a NaCl substrate at room temperature consisted of very fine grains with f.c.c. structure. These films possess the f.c.c. structure with stacking faults. At the same time it has been shown that two phases, hexagonal-close-packed (h.c.p.) and f.c.c., could coexist in fullerite thin films.

In this report the results of the C_{60} fullerite thin films structure investigation are presented [1-3]. The films were prepared by vacuum thermal evaporation and deposition on a KCl substrate. The C_{60} powder of 99% purity, free of a solvent contamination was used. The temperature of the substrates was measured by a thermocouple and was held between room temperature and 570 K. After deposition the fullerite films were coated with carbon and then separated from a substrate in distilled water and investigated in a transmission electron microscope at accelerating potential of 100 kV. The investigations revealed the dependence of a thin film structure on the substrate temperature. At room temperature fine grained films with very diffuse Debye-Scherrer rings on selected area electron diffraction (SAED) were observed. At elevated temperature grain size increased up to 0.1-0.3 μm and a well-defined diffraction pattern could be observed (Fig.1). In both cases the Debye-Scherrer rings can be indexed by a f.c.c. lattice with $a = 1.43$ nm. When the temperature of the substrate was 370-420 K the individual C_{60} particles could be observed at the first stage of a thin film formation. Two types of

C_{60} plates were observed: hexagonal or truncated triangular crystals and particles with irregular shapes like petals.

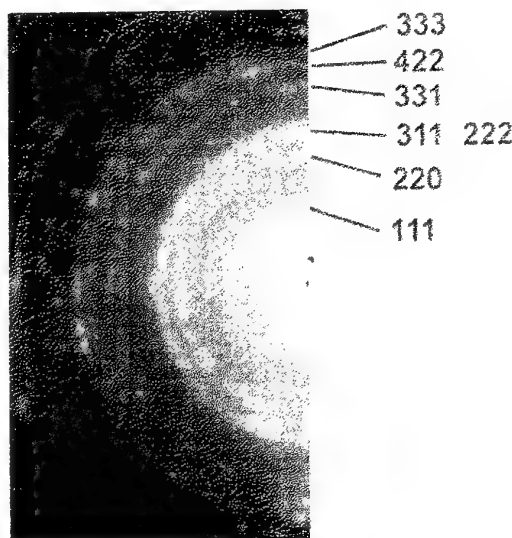


Fig.1.

Both types of the C_{60} particles are single crystals and give the point SAED according with the f.c.c. lattice. The most clear diffraction pattern was observed for the hexagonal or truncated triangular particles with marked extinction contours in form of six-pointed star. For such particles a SAED pattern corresponds to a $[111]$ zone axis confirming that the close-packed plane (111) of the f.c.c. lattice is oriented parallel to a substrate surface. The electron images of some individual fullerite particles and especially grains of continuous thin films (Fig.2) revealed the

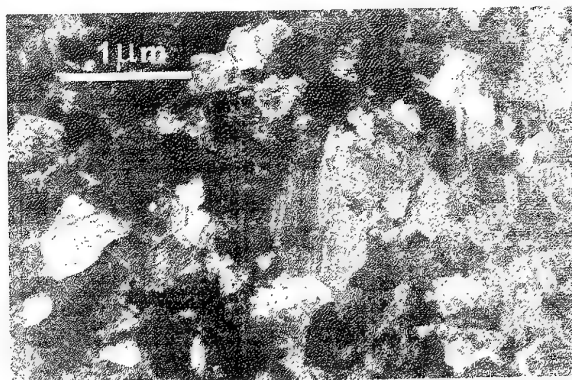


Fig.2.

stacking faults or twin boundaries. The amount of these defects increases with rise of the substrate temperature. The corresponding SAED with a $[111]$ direction perpendicular to an incident electron beam presented in Fig.3. Two types of

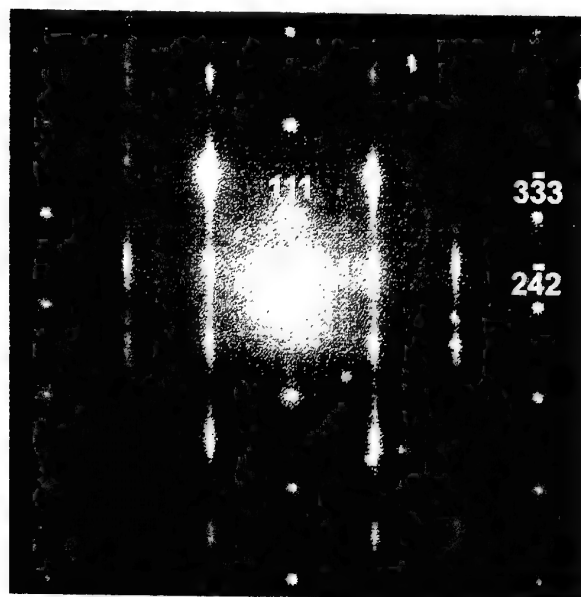


Fig.3.

reflections are observed on this pattern. The reflections with $L_0=3N$ ($L_0=h+k+l$, N -integer) such as (111) , $(\bar{4}22)$ and other in each third row oriented along $[111]$ are not changed and take correct places in a reciprocal lattice. Other reflections with

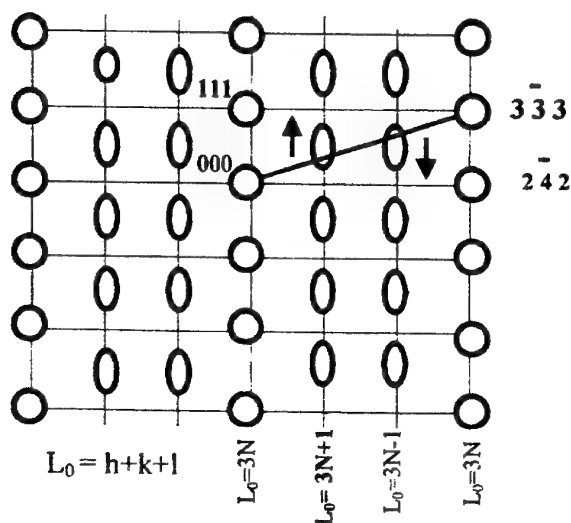


Fig.4.

$L_0=3N\pm1$ are shifted from the correct positions and are stretched along $[111]$. The shift direction depends on sign in $L_0=3N\pm1$ and is opposite for these two rows (Fig.4). The reflections with

$L_0=3N\pm1$ are stretched up to the formation of the continuous streaks or rods of intensity. Such electron diffraction picture gives evidence of the stacking fault formation in C_{60} fullerite thin films. The more detailed study of the intensity rods reveals the lot of separated spots that confirms some correlation between stacking faults. Such SAED is also typical for a mixture of different polytypes in a close-packed structure.

The change of the fullerite crystal structure during grinding in vibratory mill was investigated. The diffractograms of the fullerite powders treated in vibratory mill for different time are presented in Fig.5. For the X-ray diffractograms analyses Full

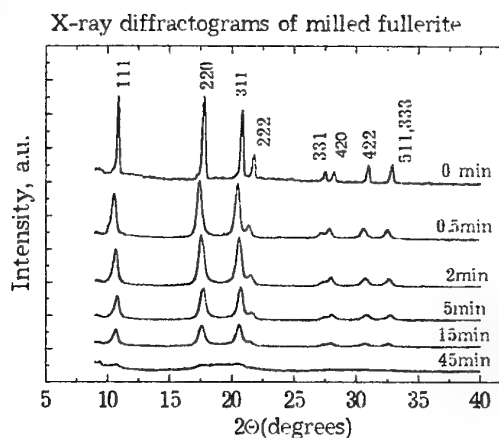


Fig.5.

Profile Rietveld method version 3.5 was used. The line profiles were described by the pseudo-Voigt function. The preliminary analyses indicated that the line broadening is connected with size effect. The best coincidence of the experimental and theoretical diffraction profiles was achieved for such structural parameters: the f.c.c. lattice ($a = 1.41$ nm) ; preferred orientation – plate like mosaic blocks with habits (113) and block size (normal to habit) decreasing from 20 nm to 2nm at grinding time increase from 0.5 to 45 min.

References

- [1]Yu.M.Solonin et al., Extended Abstracts of ICHMS'2001, ADEF-Ukraine, Kiev-2001,pp.634-635.
- [2]Yu.M.Solonin et al., ibid., pp. 690-691.
- [3]Yu.M.Solonin et al., Poroshkovaja Metallurgija. #11-12. 2001. pp. 91-99 (in Russian)

THE AFFECT OF CONCENTRATED SOLAR RADIATION INTO THE SIALON CERAMICS IN THE AIR.

Neshpor I. P., Panasiyuk A. D., Liydvinskaya T. A.

Frantsevich Institute of Sciences of Ukraine, Kiev, Ukraine

The using of solar heating is the unique possibility of both studying of influence of high temperature (more than 3000°C) into material in the air and one-sided and easy regulated inertialess character of heating. At this work the surface heating of sialon ceramics by the concentrated flow of solar radiation has been used for the investigation of high-temperature corrosion stability both pure sialon and sialon with covering. It was necessary to determine the influence of radial heating into the corrosion properties and structure conditions of ceramic based on sialon Z_2 with (Ni-Cr-Al), (Ni-Fe-Al) coverings and (TiN-TiB₂) covering through the sublayer of (Ni-Cr-Al) and (Ni-Fe-Al). Specimens were obtained by the hot pressure method and coverings were put directly before the influence of solar radiation. Different regimes of heating were used with the modifying of angle of opening of shutters and time of affect of radiation. Temperature in the zone of heating and heat flow were measured. Tested specimens were investigated by metallography, X-ray and petrography methods.

Ceramics are known to have low heat conductivity and low physical interaction with metals. By the method of wetting were chosen the composition of covering with high adhesive properties to the ceramics. This covering has both high adhesive properties and does not chemically interact with the chosen ceramics. As the materials of covering were chosen metallic alloys based on (Ni-Cr-Al) and (Ni-Fe-Al). They have high adhesive properties to (TiN-TiB₂) and to sialon ceramics.

Due to the fact that interaction occurs in the air, corrosion-proof phases can be formed as a result of high-temperature oxidation.

It was shown by the investigation that structure formed on the sialon surface is non-homogeneous across the diameter of heating spot. In the central part where the density of capacity of solar flow is higher the interaction during the process of crystallization from the melt occurs.

According to the X-ray analysis the main phases formed during the interaction amongst the material of specimen, composite coverings and oxygen are mullite Al_2SiO_5 , and solid solutions of $(Fe,Cr)_2O_3$, $(Cr,Al)_2O_3$, $NiCr_2O_4$, $FeTiO_4$. The formation of these phases in the surface level is the result of interaction between the components of the specimen, components of sublayer and coating in the condition of high-temperature interaction of concentrated solar radiation in the air. Nonevent distribution of temperature of heat flow in the zone of heating leads to the formation of crater and melting of material in the center of the spot. The formation of Al_2SiO_5 , $(Cr,Al)_2O_3$, $FeCr_2O_4$, $NiCrO_4$, $FeTiO_4$, $FeAl_2O_4$ compounds on the covered sialon surface makes for the creation of composite material with high corrosion-proof properties due to the formation of solid solutions.

The measure of microhardness of formed coating spot showed that it increases from the edge to the center. It connects with the formation in this field of strengthening phases based on solid solutions.

It was shown that formed coatings of (Ni-Cr-Al), (Ni-Fe-Al) and (TiN-TiB₂) can be recommended as high-temperature, corrosion-proof coverings for sialon ceramics.

INFLUENCE OF SILICONORGANIC ADDITIONS ON COMPOSITION MATERIALS PROPERTIES

A.G. Kostornov, I.I. Beloborodov, S.V. Sukhostavets

Frantsevich Institute for Problems of Material Science of National Academy of Science
of Ukraine, Kiev, Ukraine

Properties and cost of fillers play important role in creating compositional antifriction polymer based materials.

It is known that with the aim of the, materials price reduction their creators seek to use as a filler natural materials.

However such materials possess heightened hydrophilic wich has negative influence on materials properties.

The aim of this work is to investigate possibility of filler hydrophobisation by their treatment with siliconorganic compounds and to estimate this treatment influence on composition properties.

As fillers marshalit and trinoly (Pervozvansk and Crimean layers), wich have wide using for industrial compositions production, were used.

As binding substances epoxy and nolyether resins were used.

As hydrophoby substances polyethilenhydrosiloxane liquid GKG- 94 were used. Fillers powders treatment was performed in ball mill.

For different fillers specific surface was performed.

Modifire addition influence on physico – mechanical properties of compositions was estimated by moistureabsorbtion value and bending strength changes.

It was estimated, that additional GRG- 94 increased spesific surface of filler. At equal treatment time in ball mill increasing of specific surface was equal from 360 to 1540 cm²/g. It was shown, that 0,16 % of siliconorganic addition is optimum.

It is shown, that after GKG- 94 addition moistureabsorbtion of investigated filler decreased in 2,2 – 2,6 time. Polymer composition, wicontaine hydrophobic fillers, after 7 day standing in moisture area absorbed in 2.5 – 3 time smaller moisture. as composition without modification.

It was establish. that existence GKG- 94 in composition led to bending strength rise with modifcator content increasing.

Bending strength achieved maximum value at 0,16 % GKG- 94 contant. General increase of filled models strength was equal 22–31 %.

It is shown, that siliconorganic additions make better properties of compositional materials.

THE SEMI-DRY CERAMIC POWDER ROLLING

Radchenko A.K.

Franzevitch Institute for Problems of Materials Science NAS of Ukraine, Kiev, Ukraine

A different methods is used of fabrication the layered composite ceramic materials [1]. The direct rolling of dry ceramic powders has a series of advantages 'in comparison with such methods as a slip casting, a tape casting (a "doktor blade" method[2]). Principal advantage is that rolling it is precision, continuous, controlled process, and besides during rolling the smaller amount of the binding agents will be utilized, that diminishs contaminating a finished product. In the course of rolling it is possible to regulate a thickness and density of tapes[3]. Therefore frequently the casted tapes are densified by consequent rolling [4]. The rolling of plastic fine ceramic masses is circumscribed in operation M. Menon, I-W. Chen[5]. The opportunity of deriving by this method of stratified ceramic materials with a high level of properties was shown. The constraining factor of wide application of the direct dry ceramic powders rolling is the low green mechanical strength (adaptability to manufacture) of rolled tapes. If the tensile strength casted and dried up tapes makes 12-22 MPa, the strength of green rolled tapes at a trial on cut makes only 0,5 -0,6 MPa [6]. It is connected that in a rolled tape the porous structure is the same as in not-formed powder. The connection strength in places of contact of the binding agent is not great because of its bad adhesion in solid state at rather low temperatures. As a solution the binding agent has a heightened adhesion as to ceramic alternate particles and among themselves. Therefore semi-dry ceramic powder rolling can give good results. However this method of moulding yet is little investigated. In the work [6] was investigated a rolling tapes that include up to 9 mass. % of solvent in the binder.

In the present work the mixture of a powder Al_2O_3 grade Permalox 12 of adamant with binder (10 % a solution polyvinilbutiral in ethanol) rolled. Total amount of binder in mixture made 20 mass. %. On rolls with the diameter of 26,8 mm the tapes in width 150 mm and thickness from 0,25 up to 0,125 mm has obtained. Porosity of tapes made from 35

up to 14 % accordingly. At the further increase of a density on a tape occurred sinuosity (as during hot rolling of a lead powder). The further increase of a density results in an adhesion and damage of a tape.

1. Fabrication and area of application of the layered composite ceramic materials. /Radchenko A.K., Gogaev K.A., Yrchuk L.M., Gogotsi G.A., Orlovskaya N.A. //The theses of the reports of international conference "Advanced ceramics for third millenium". Kiev, Ukraine; November 5-9, 2001. P.89
2. Tape casting: a technique for preparing and studying new materials. Fiori C., Deportu G. Novel ceram. fabr. process. and appl. meet. basic sci. sec. inst. ceram. Cambridge, 9-11 apr. 1986- Stoke-on-Trent. 1986. P.213-225.
3. A.K.Radchenko and O.A.Katrus. Compatibility and strength of rolled strip from powders (Review)// Soviet Powder Metallurgy and Metal Ceramics, V.26, n 7 (295), July, 1987.P.523-529.
4. Hyat E.P. Electronics: tape casting, roll compaction / Am. Ceram. Soc. Bull. - 1995, - 74 - N10, - P. 56-59
5. Mohan Menon, I-Wei Chen. Bimaterial composites via colloidal rolling techniques: I, Microstructure evaluation during rolling / J. Am. Ceram. Soc., - 1999, - 82, - N12, - P.3413-3421
6. Radchenko Alexander K., Radchenko Andrey K., Starchenko V.U., Orlovskaya N.A. Investigation of the process receiving by the rolled method the layers of different composition of multilayer ceramic materials. Materials of conference " Nowe kierunki technologii i badan materialowych ". Red. naukowa J.Ranachowsri. Warszawa, 1999. P.345-349. (in Russian).

PERFORMANCES OF ELECTRODES FROM Ag AND COMPOSITION Ag-C FOR SHAPING ELECTROSPARK LAYERS

Kryachko L.A.

Frantsevich Institute for Problems of Materials Science, NAS of Ukraine, Kyiv

Objective condition of a heightening of thickness of an electrospark stratum on the cathode is the amplification of erosive destruction of the anode under an operation of electrical discharge [1]. It is known that the low erosive resistance characterizes contacts and electrodes containing in the structure graphite [2]. With allowance for this fact we carried out comparative researches of electrodes from cast silver and composition Ag-C, from a point of view of correlation of their electrical erosion with performances mass transfer at drawing electrospark coverage, and also with morphology and structure of shaped layers.

Drawing of coverage realized with the help of installations "Элитрон-12" and "Элитрон-22А" on a technique circumscribed in [3]. A plate from copper served the cathode; the anodes were manufactured as rod 3 mm.

The results of a research, reduced in a fig. 1 and 4, display, that the energetic parameters of electrospark process as a whole identically influence magnitude of an erosive wear of electrodes. So, with growth of a impulse energy W_i and its power P_i at increase of force of a working current I_w , total loss of a mass of both anodes (their erosion) $\Sigma\Delta a$ increases, though and with different intensity (fig. 1, cur. 3, 4). With increase of time of handling the linear growth of values $\Sigma\Delta a$ for silver and composition Ag-C is marked which at rather soft receipt of thermal power in the anode (installation "Элитрон-22 А" practically coincide (fig. 4, cur. 1, 4). The heightening of capacity C accumulative condensers is accompanied by increase of an impulse duration τ_i and, hence, lowering of its power P_i , therefore dependence carries falling down character (fig. 1, cur. 1,2).

From a fig. 1-4 follows, that the increase of erosion of a composite electrode in all cases entails the appropriate heightening of rate of an increase of a mass of the cathode. At the same time for cast silver their correlation carries ambiguous character. It is known that the power parameters of electrical discharge determine a ratio of a share of liquid and vapor phases in a total amount of products of erosion of a material of an electrode [4]. The quantitative performances mass transfer and microstructures researches for sections allow to

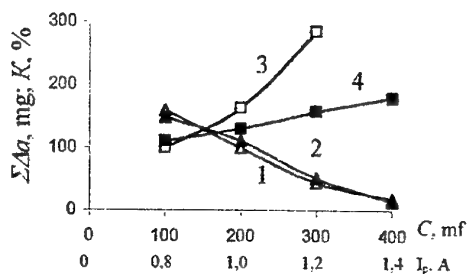


Fig. 1 - Dependence of total values of erosion of the anode $\Sigma\Delta a$ from Ag (1, 3) and composition Ag-C (2, 4) from capacity C (1, 2) and force of a current I_w (3, 4)

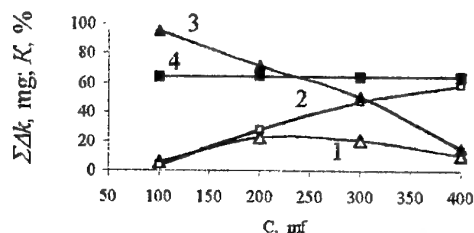


Fig. 2 - Dependence of total values of an increase of a mass of a layer $\Sigma\Delta k$ (1, 3) and coefficient of carry of a mass K (2, 4) from capacity C ($I_w = 0.8$ A) at drawing layers from Ag (1, 2) and composition Ag-C (3, 4)

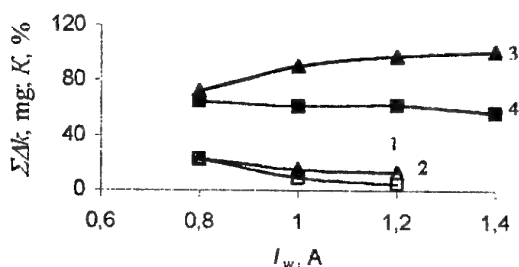


Fig. 3 - Dependence of total values of an increase of a mass of a coverage $\Sigma\Delta k$ (1, 3) and coefficient of carry of a mass K (2, 4) from force of a current I_w ($C = 200$ mf) at drawing layers from Ag (1, 2) and composition Ag-C (3, 4)

conclude, that in the carried out experiments the shaping of electrospark layers is carried out mainly at the expense of a liquid phase formed on the anode under an operation of a thermal stream due to a high thermal conductivity of silver. At the same time silver is characterized by high-pressure

vapor at heightened temperatures, that reduces in its ablation from interelectrode interval and, accordingly, to losses of a material. A consequence it is lowering an amount of substance, transported on the cathode, and also coefficient of mass transfer. Since some values W_i and P_i , with other things being equal, the share of a steam phase in a total amount of products of erosion begins to prevail, that, apparently, and reflect curves 1, 2 in a fig. 2, 3.

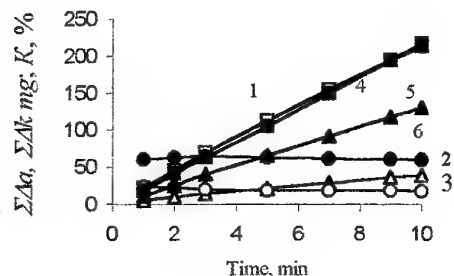


Fig. 4 - Dependence of total values of erosion of the anode $\Sigma\Delta a$ (1, 4), increase of a mass of the cathode $\Sigma\Delta k$ (2, 5) and coefficient of mass transfer K (3, 6) at drawing layers from Ag (1-3) and composition Ag-C (4-6)

Converts on itself attention that fact, that the productivity of an electrode from CM in all cases appears much above in comparison with cast silver. And only under condition of rather low energetic parameters of impulse of mass transfer performance of investigated electrodes are equalized (fig. 2). Thus, unlike silver, coefficient of mass transfer K of electrode from CM saves a rather high level and relative stability irrespective of parameters of electrospark process.

Stated reduces in the conclusion, that at erosive destruction of CM Ag-C the steam phase is shaped, in basic, for the account volatile oxides of carbon, and also disperse corpuscles of graphite formed at destruction of its conglomerates. High thermophysical characteristics of graphite promote more smooth transmission of heat to a silver matrix of CM that results in heightening of amount of silver melt in it. Thus, the presence of graphite in structure of the anode from CM provides for regulation of magnitude and power of a thermal stream acting in volume of a composite material, and losses of silver reduces during carry it on the cathode.

Despite of a burning off of graphite under an operation of discharge, its density in the put stratum can be rather significant. The absence of solubility in a system Ag-C calls its lamination, therefore the layer acquires stratified structure. The

long effect of electrical discharge on a surface stratum of the cathode reduces in accumulation of heat in its volume, softening or repeated melting of silver, that can serve the reason local flaking of a layer. A consequence it is the violation, observed in some cases, of monotone character of investigated magnitudes. However graphite is easily burned out from the put layer, therefore on a substrate there is a monolithic silver stratum of necessary thickness (fig. 5).

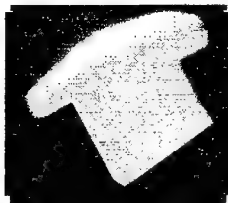


Fig. 5 - Electro-spark stratum from silver after a burning out from him(it) of graphite

In summary it is necessary to mark, that the detected regularities are shown only at the optimum contents of graphite in a composition. Its too low density in CM conducts to a heightening of erosive resistance of a material of the anode, especially at small impulse energy. The increase of density of graphite over an optimum precludes with merge melt of silver in a monolithic stratum.

REFERENCES

1. Электроискровое легирование металлических поверхностей / Г.В. Самсонов, А.Д. Верхотуров, Г.А. Бовкун, В.С. Сычев. - Киев: Наук. думка, 1976. - 219 с.
2. Малышев В.М., Румянцев Д.В. Серебро // М.: Metallurgy, 1976. - 312 с.
3. Крячко Л.А. Влияние некоторых факторов на формирование электроискровых покрытий на основе серебра, содержащих соединения кальция // Электрические контакты и электроды. - Киев: ИПМ, 1991. - С. 110-114.
4. Галинов И.В., Лубан Р.Б. Оценка величины термической эрозии на катоде и аноде при электроискровом легировании металлов // Современные проблемы физического материаловедения. - Киев: ИПМ, 1990. - С. 118-127.

ON THE POSSIBILITY OF THE $\text{Pb}(\text{Zr,Ti})\text{O}_3$ THIN FILMS PRODUCING BY THE REACTION SYNTHESIS

Andreeva A.F., Kasumov A.M., Utkin S.V., Frenkel O.A.

The Institute for Problems of Materials Science of NAS of Ukraine, Kiev, Ukraine

The ferroelectrics are widely used for different applications in the optical and acoustic electronics. There is the perspective to use thin films of ferroelectrics based on the lead zirconate-titanate $\text{Pb}(\text{Zr,Ti})\text{O}_3$ (PZT) for the infrared radiation detectors, for the memory elements, for different kinds of sensors, actuators and etc. [1-3]. However, a wide application of PZT thin films is retarded by the imperfections of their obtaining methods [4, 5].

In the CVD methods (sol-gel, spincoat) the reactive gases are released (such as I_2 , Cl_2 and the other side products), that are incompatible practically with the other technology processes in microelectronics. The laser evaporation of the PZT ceramics causes the disturbance of the condensates stoichiometry. The high frequency sputtering of PZT because of its small deposition rate produces the condensates fouled with the residual gases. The simultaneous sputtering of several oxide targets gives the irreproducible composition and properties of the PZT layers. For diffusion in the oxide films of Ti, Pb and Zr the high temperatures are required (over 1000°C). In this connections the research for more effective methods to obtain the PZT thin films is the actual problem.

The subjects of this work was to investigate a possibility of the PZT films obtaining through the reaction synthesis. The $\text{Pb}(\text{Zr,Ti})\text{O}_3$ films were formed by the annealing of the Pb-Ti-Zr solid solutions in O_2 atmosphere at the pressure of $2 \cdot 10^{-2}$ Pa in the temperature diapason $300\text{-}500^\circ\text{C}$. The thickness of deposited condensates was $0.05\text{-}0.8 \mu\text{m}$. The PZT films were obtained on the substrates of polished fused silica, a sodium chloride, and glassceramics.

For producing the MDM (metal-dielectric-metal) structures were used the glassceramics substrates with the low-resistance SnO_2 or Fe underlayer that had been put on substrates by magnetron sputtering of the corresponding targets in Ar atmosphere. As the top electrode was used the In point deposited by the vacuum evaporation. The capacitance and the dielectric loss of ferroelectric films were investigated at the frequency of 1 kHz.

The thin films structures were investigated with usage of electron diffraction method in tran-

sillumination mode. Some of the films were deposited on NaCl single crystals or on the glassceramics substrates coated with NaCl. The thick films structure was investigated on the X-ray diffractometer of DRON-4-07 type in $\text{Cu } K\alpha$ radiation.

After annealing the Pb-Ti-Zr solid solution films in O_2 atmosphere at 200°C a formation of the amorphous PZT films was observed. With the growth of the condensation temperature to 300°C the crystallization of films was occurred. There was found the formation of the perovskite type tetragonal structure for which the crystal lattice parameters were the same as those referred in literature.

There were investigated the dependencies of the structure, dielectric and optical properties of the PZT films upon their deposition conditions, thickness and the material of the bottom electrode. It was observed the correlation of coherent dispersion blocks size and ferroelectrical properties. With the growth of the coherent dispersion blocks was observed the increasing of the films dielectric constant ϵ to the several thousands.

The advantages of the reaction synthesis method for the thin $\text{Pb}(\text{Zr,Ti})\text{O}_3$ films obtaining are: the low temperatures of film formation, the opportunity to perform all stages of technology in one vacuum cycle and the possibility to modify the composition and the properties of the ferroelectric by the doping.

1. Kosec M. et al. Processing of high performance lead lanthanum zirconate titanate thick films// J. of Europ. Ceramic Soc. -1999.-19.-P. 949-954.
2. Lozinski A. et al. PLZT thick films for pyroelectric sensors// Meas. Sci. Techn.-1997.-8.-P.34-37
3. Lucat C., Menil F., Von Der Muhll R. Thick film densification for pyroelectric sensors// Meas. Sci. Technol. -1997. -8. - P. 38-41.
4. Birnie D.P., Vogt R.N., Orr M.N., Schiffko J.R. Coating uniformity and device applicability of spin coated sol-gel PZT films// Microelectronics Engineering - 1995. -29. - P. 189-192.
5. Tyunina M. Levoska J., Sternberg A. S. et al. Relaxor behavior of pulsed laser deposited ferroelectric $(\text{Pb}_{1-x}\text{La}_x)(\text{Zr}_{0.65}\text{Ti}_{0.35})\text{O}_3$ films// J. of Appl. Physics -1998. -84. -12. -P. 6800-6810.

THE USAGE PERSPECTIVES OF THE THIN FILMS OF THE RARE-EARTH METALS OXIDES

A.F. Andreeva

The Institute for Problems of Materials Science of the National Academy of Sciences of Ukraine

In this work the structure and properties of the thin films of the rare-earth metals (REM) oxides were investigated. The films were obtained by the vacuum evaporation of the metal in O_2 atmosphere with the oxides films formation on the growth surface. As the substrates were used the optical polished silica, glassceramics and the mark K-8 glass [1-2].

The films structure, their optical and electrical properties were investigated in the series of works, in particular in [3-4]. It was shown that the REM oxide films are perspective for using as the masking layers for the phototemplates, optical coatings, dielectrical layers in capacitors and in multilevel integrated circuits, etc.

The masking layers for the transparent photolithography templates had a high wear resistance. Their abrasive resistance is essentially greater than that of the chromium and iron oxides coatings, which are widely used in the last time in microelectronics. The REM oxide masking layers had the low density of defects (density of defects of size $\geq 1.5 \mu m$ was $< 0.06 cm^{-2}$). The optical density of the masking coatings at $\lambda = 430 nm$ is higher than 1.8, their thickness is 200-220 nm, the roughness of edge of picking was $\leq 0.3 \mu m$, the reflection coefficient was $< 10\%$.

The advantages of the REM oxide masking layers are: the prolongation of the service time of the photographic templates due to increase in films abrasive resistance; the increase in delivery of valid hybrid integrated circuits and other items for microelectronics; the advance in technological effectiveness and the improvement of the ecological conditions of their production; diminishing of the work intensity and the power consumage.

It is possible to produce photolithography templates of planar construction due to the phase transformations in masking layer of the praseodymium oxide. It turns out in this case that all glass surface of substrate is covered by REM oxide protecting layer that consists from the transparent and non-transparent sites according to the topology. Owing to this fact occurs the additional increase of templates wear resistance by preventing the knocking out of the glass surface and the

ability appears to use the mask layers many times, saving additionally the materials and decreasing the work expenses.

The REM oxides films are also perspective for the using in capacitors and in multilevel integrated circuits. They have the high electric resistivity $10^{15}-10^{16} \Omega \cdot cm$, the low dielectric loss $1 \cdot 10^{-4}$; the high puncture strength $10^7-10^8 V/cm$.

The high temperature and the heat flux sensors based on the REM oxides films have the following characteristics: the flux measured range is $\leq 10^8 W/cm^2$, the time constant is $< 0.1 s$, the temperature coefficient of the electric resistance at $20^\circ C$ is $0.06 - 0.08 ^\circ C^{-1}$.

REM oxides optical coatings have high transparency in wide spectral diapason $0.19-15 \mu m$, the refractive index is 1.9-2.2, the light dispersion loss of the REM oxides- SiO_2 laser mirrors is $< 0.005\%$, the threshold of the stationary irradiation strength to concentrated light flux during 120 s is greater than $2.5 kW/cm^2$.

A creation of optical coverings with increased strength to irradiation and high exploitation resource is the actual problem in development of the cavities for the power eximer lasers; in apparatuses for metals cutting and quenching, printed circuit cards production, automated cutting of different materials and other apparatuses.

The optical parameters of the REM oxides- SiO_2 mirrors are essentially better than that of the mirrors based on TiO_2-SiO_2 , ZrO_2-SiO_2 , HfO_2-SiO_2 which are currently used.

1. Heitmann W. Reactively evaporated films of rare earth oxides // *Vakuum-Technik*. -1973. -22 -№2. -P.49 - 55.
2. Андреева А.Ф. Получение и свойства пленок оксидов РЗМ // *Порошковая металлургия* - 1998. - № 1-2. -С.107 - 110.
3. Andreeva A.F. et al. Growth conditions, optical and dielectric properties of Y_2O_3 films // *Phys. stat. sol. (a)*. -1994. -145. -P.441 - 446.
4. Rainer F., Lowermilk W.H., Milan D. et al. Materials for optical coatings in the ultraviolet // *Appl. Optics*. -1985. -24, -№ 4. -P. 496-500.

THE STRUCTURE AND THE PROPERTIES OF THE THIN IRON FILMS PREPARED BY MAGNETRON SPUTTERING

Andreeva A.F., Dvoynenko O.K., Kasumov A.M., Statsenko V.M.

The Institute for Problems of Materials Science of NAS of Ukraine, Kiev, Ukraine

In this research work the iron films have been produced and some their properties were investigated.

The thin ferromagnetic films are perspective for the electronics and optics applications. Epitaxial iron films can be used for preparing the sensitive elements for optical instruments, amorphous films - for the laser thermomagnetic recording of information. At last time are interesting the multi-layer structures with alternation of the ferromagnetic and non-magnetic layers. Such heterostructures can be used for producing the magnetic integral heads in recording devices.

There are many methods for preparing the iron films: pulsed laser and electron beam evaporation in vacuum; high-frequency-, ion beam- and magnetron sputtering; electrolytic deposition and etc. The magnetron sputtering method presents more perspectives for the iron films preparing. The films produced by magnetron sputtering have the advantages: the small porosity of the condensates, the high film adhesion to the substrate, the similarity of the target and films chemical composition, the resemblance of the properties at certain thickness for the massive material and for the layers.

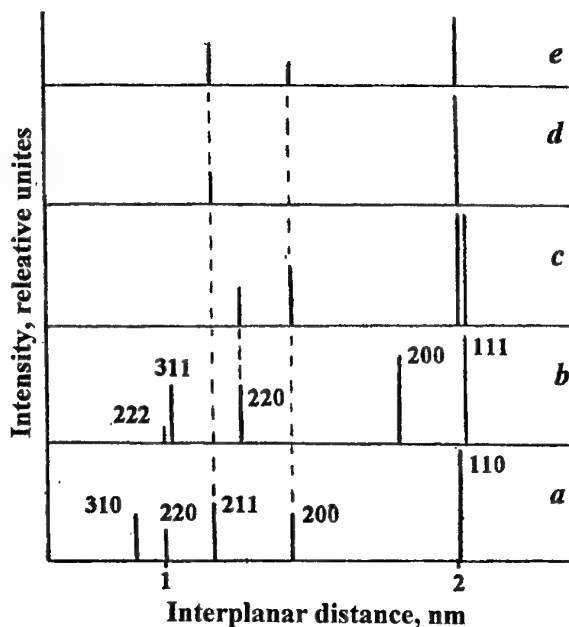
The difficulty of magnetron preparation of iron films is connected with the shunting of the magnetic field by material of the target.

In the present work the shunting was diminished by means of the special target construction.

The ultrathin iron films were amorphous. The body-centered (α) and face-centered (γ) phases were formed with increasing of film thickness to 27nm (figure). The formation of the body-centered (α) and face-centered (γ) phases of iron was observed in the case of epitaxial film growth [1-3].

With thickness increasing the γ phase was disappearing and α phase unique was observed.

Optical, magnetic and mechanical properties of iron films were investigated depending on their thickness and grain size. Their properties were compared with those of massive materials.



The diffraction picture of the iron films with different thickness: a, b - the reference data for the massive α and γ iron respectively [4]; the iron films thickness, nm: c - 27, d - 540, e - 810.

It was proposed to use the iron films as model matrixes for investigation of iron construction biocorrosion, in particular of gas mains. By using this films on glass substrates it was made possible to measure and compare the corrosion activity of different species of bacteria.

1. Detzel Th. Epitaxy and thermal behaviour of metastable metal films// Progr. Surface Sci. - 1995. - 48, № 1-4. - p. 275-286.
2. Goiglander B. et all. Epitaxial growth of Fe on Au(111): a scanning tunneling microscopy// Surface Sci. - 1991. - 225, № 3. - p. L529-L535.
3. Arnott M. et all. Growth and thermal properties of fcc iron films on Cu(100)// Surface Sci. - 1992. - 269-270. PtB. - p. 724-730.
4. X-ray powder data file. ASTM Special Technical Publication, 1975.

WEAR- AND CORROSION RESISTANT POWDER MATERIALS ON THE BASE OF TUNGSTEN-FREE HARD ALLOYS AND CARBIDE STEELS

Maslyuk V. , Napara-Volgina S.

Institute for Problems of Materials Science of NASU, Kyiv, Ukraine

One of the effective methods enhancing wear resistance of components, operating in aggressive media, is the employment of powder structural materials with special properties (including tungsten-free hard alloys and carbide steels, based on iron and stainless steels) in the process of their manufacturing.

Structure formation processes, properties and various manufacturing methods of wear- and corrosion resistant tungsten-free hard alloys, corrosion- and wear resistant powders of stainless steels of different types have been thoroughly studied and published in a number of works. [1-10]. Broadening of the fields and scope of utilization of powder materials, withstanding wear and corrosion, calls for development of new materials, being less expensive, than hard alloys and more resistant than stainless steels.

Among these materials are, in particular, carbide steels based on iron / stainless steels with chromium carbide filler alloys, as well as laminated composites with wear- and corrosion resistant operating layer.

Developing new class of carbide steels, based on stainless steels of austenite type, having chromium carbide filler alloys in amount of 20-30%, the authors investigated the influence of their composition and sintering temperature on the process of structure formation, physicomachanical properties, wear- and corrosion resistance of carbide steels.

It has been determined that elevation of sintering temperature of carbide steels based on stainless steels X18H15 and X23H18 from 1473 to 1573 enhances their bending strength in 2-3 times and reduces porosity from 20-25 down to 4-5%. Hardness of materials based on X18H15 with 20-30% Cr_3C_2 , sintered at 1573 without thermal treatment reaches 56-62 HRC, bending strength - 793-963 MPa, whereas materials on the base of X23H18 have 58-72 HRC and 603-942 MPa correspondingly. The above said materials are characterized with high wear resistance and

satisfactory corrosion resistance both: in 10% solution NaCl and 20% solution HNO_3 , conforming to 4th point of ten-point scale.

Of interest are the wear- and corrosion composites based on the stainless steels of austenite type with filler alloys Cr_3C_2 (10-30%) and MoS_2 (3-5%), we developed.

It is known that conventional stainless steels, having single-phase structure and high corrosion resistance in various media, are not assigned to the class of wear resistant materials. Introduction of the above said filler alloys into their composition fundamentally changes structure and tribological characteristics of these steels while maintains satisfactory resistance in a number of media.

The processes of structure formation in sintering of stainless steels with filler alloys Cr_3C_2 and MoS_2 have been investigated. Studied were their tribological-, corrosion- and physicomachanical properties. It has been determined that the result of interaction of chromium carbide and molybdenum disulphide with stainless steel basis of austenite type in sintering is the formation of complex hetero phase structures, which nature depends on composition and sintering temperature of materials. It has been also defined that while increasing content of carbide filler alloys from 10% up to 30% one can get hardness enhanced in 1.2 – 1.4 times along with some decrease of strength and significant increase of wear resistance.

Of significant interest are wear- and corrosion resistant layered materials. Basing on the investigations, authors carried out on powder composites, based on metal and tungsten-free hard alloys, different types of layered wear- and corrosion resistant powder materials, in particular multi-layered tungsten-free alloys of tool application and tribological materials like "composite, based on highly alloyed steel – steel". Results of experimental investigations dedicated to the property studies, manufacturing methods and layered structures of wear- and corrosion resistant

materials with operating layers out of tungsten-free hard alloys and composites, based on stainless steels, made possible to formulate principles for generation of this kind of materials. They are as follows:

1. Use of one basis (or basis of similar composition) for both operating- and bearing layers that makes possible to decrease deformations and stresses in manufacturing and operating layered powder and increase their corrosion resistance.
2. Selection of materials composition subject to their operating conditions and field of application by controlling the content of hard ceramic component (or filler alloys of other nature) in the operating layer. Content of hard component in operating layer should amount to 20-30% in case of carbide steels and to 85-95% in hard alloys, whereas in bearing layer (basis) – from zero in materials with metal basis up to 70-75 wt.% in chromium carbide alloys. As it takes place, first are assigned to the tribological materials and second – to the tool materials.

Principles for selection of structures of layered materials of different fields of application have been developed. It makes sense to manufacture tribological materials out of several layers – surface one with maximum content of hard component and sub-layer, having its lower content – aiming to generate favorable conditions for development of transitive area in sintering, and also to reduce both possibility of brittle fracture of such materials in operation, as well as deformations and level of stresses in manufacturing.

Literature cited:

1. Grigoriev V. B., Klimenko V.N. Alloys based on chromium carbide. — Kiev: Publ. AS UkSSR, . 1961.—55p.
2. Kyubarsepp Ya. Hard alloys with steel binder.— Tallinn: Valgus, 1991. — 163 p.
3. Klimenko V.N., Maslyuk V.A., Sambros Yu.V. Sintering, structure formation and properties of powder materials: system chromium carbide – iron. // Powder metallurgy. — 1986. — № 8. — p. 39—44.
4. Bondar A. A., Maslyuk V. A., Velikanova T.Ya., Grytsiv A.V. Phase equilibrium in system Cr-Ni-C and their application in development of physico-chemical principles for development of hard alloys, based on chromium carbide // Powder metallurgy — 1997. — № 5/6. — p. 13—23.
5. Napara-Volgina S.G. Powder structural materials made from stainless steels.// Powder, structural, antifriction and friction materials.-Kiev: Inst. for Problems of Materials Science AS UkSSR, 1983-p.26-33
6. Napara-Volgina S.G. Dense powder stainless steels // Powder metallurgy. - M.: SEV, 1985.-p.61-66
7. Dovydenkov V.A., Radomysel'sky I.D., Napara-Volgina S.G. Manufacturing technology and properties of sintered stainless steels for machine components // Powder metallurgy. - 1978. - №5. - p.51-62.
8. Klimenko V.N., Napara-Volgina S.G., Orlova L.N. et al. Mechanical properties of wear resistant high chromium powder materials with heterogeneous structure. // Powder metallurgy. - 1966.- № 11-12.- C.61-67.
9. A. c. 1740107 USSR. Manufacturing method of hot stamped stainless powder steels of austenite class / V. N. Klimenko, S. G. Napara-Volgina, L. N. Orlova, E.V.Venglovskaya // Discoveries. Invention. — 1992.—№ 22.
10. A. c. 1719454 USSR. Manufacturing method hot stamped stainless powder steels of austenite type / V. N. Klimenko, S. G. Napara-Volgina, L. N. Orlova, E. V. Venglovskaya // Discoveries. Inventions. — 1992.— № 10.

STUDY OF THE EFFECT OF THERMAL TREATMENT ON THE STRUCTURE AND PROPERTIES OF Ti-Al-Si-Zr SYSTEM ALLOYS

Datskevich O., Kulak L., Miracle D.⁽¹⁾, Senkov O.⁽¹⁾, Firstov S.

Frantsevich Institute for Problems of Materials Science of NAS of Ukraine, Kiev, Ukraine

⁽¹⁾Air Force Wright Laboratory, Wright-Patterson AFB, OH USA

Industrially-produced refractory titanium alloys are usually prepared by alloying them with components that form solid solutions with base metal. This mechanism of solid-solution strengthening is enough studied and its potential is being exhausted. Therefore, attractive are becoming materials, the reinforcing phase of which is formed in the process of eutectic crystallization, and due to this, the above materials feature a high thermodynamic stability. Considerable results in the area of development of such alloys have been achieved by Ukrainian scientists on the Ti-Si system through an additional alloying them with aluminum and zirconium. These alloys feature is their composition consisting of titanium matrix and reinforcing silicide phase. Solubility of silicon in β and α -phase varies with temperature, therefore the study of thermal treatment effect on the structure and properties of these alloys acquires a great significance.

Billets of Ti-2Si-3Al-5Zr, Ti-4Si-3Al-5Zr and Ti-6Si-3Al-5Zr (wt%) alloys to be used for thermal treatments were made of ingots of around 2.5 kg, which were skull-cast by arc plasma technique under helium media, with subsequent annealing at 800 °C for 1 hour.

For alloys with elevated content of silicon, the effect of high-temperature annealing between 1150 and 1300 °C was studied on their structure, hardness and plasticity. High temperature annealing produces a radical effect on the structure of alloys under investigation. A typical eutectic structure comprising α -titanium matrix, the center of which includes precipitates of silicides, β -titanium interlayers between the plates of α -titanium and eutectics, is a subject of significant changes due to transformation of eutectics and dissolving of dispersive silicides. Separate equiaxial particles are appearing instead of eutectic colonies (Fig.1).

In spite of considerable changes of the structure after high temperature annealing, alloys exhibit no significant changes of hardness with temperature

within the investigation range of 1150 to 1300 °C, holding time of between 2 and up to 8 hours.

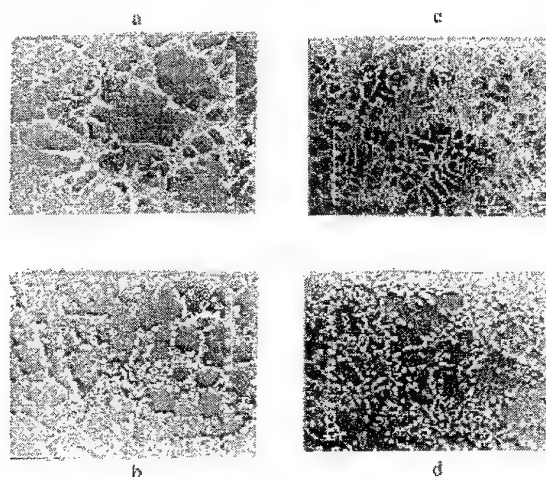


Fig.1. Microstructure of Ti-4Si-3Al-5Zr (a,b) and Ti-6Si-3Al-5Zr (c,d): a,c – as cast; b,d – annealing 1300 °C, 4 h.

The study of mechanical properties of alloys with 4 and 6 % Si after annealing at 1300 °C for 4 hours using 4-points bend test shows a tendency for their plasticity increase after annealing stage.

The effect of various low-temperature annealings ($T_{\text{anneal}} = 980$ °C) on the structure and properties of the Ti-Al-Si-Zr alloys was studied on alloys with 2.4 and 6% Si. Optical microscopy examination revealed no significant changes in the coarse structure relative to the type of annealing. Secondary silicides within the matrix showed a little increase at the expense of coalescence of more dispersive precipitates. There was no destruction of the eutectic constituent as was the case of high-temperature annealing. No change was observed in the hardness for all the alloys after various low-temperature annealings. Some trend can be observed to the appearance of microplasticity when 4-point bend tested. Comparison of microdeformation curves for the cast alloy with 4% Si after the high-temperature and low-temperature annealings (Fig.2) shows that the high-temperature annealing is more effective in the lowering of yield limit of the alloy

and its strengthening coefficient, and also in increasing of its elongation.

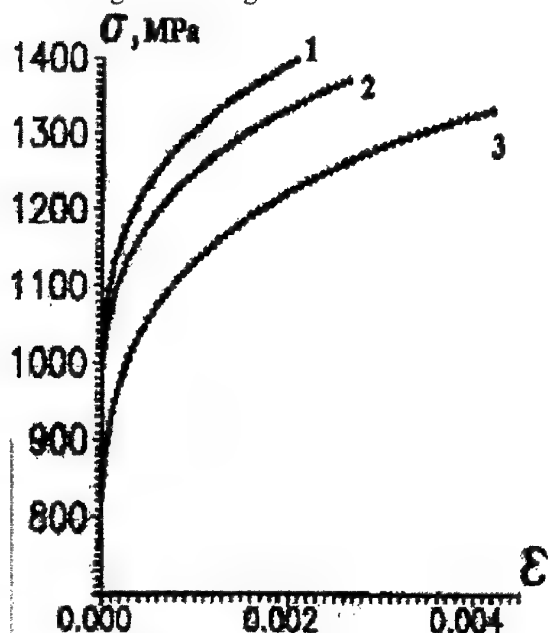


Fig. 2. Microplasticity (4-point bending) of Ti-4Si-3Al-5Zr alloy : (1- as cast, 2 – annealing 970°C 0.5h and cooling 20°C/h, 3 – annealing 1300°C, 4h).

Water quenching tests were performed within a broad temperature range: 960 °C, 1150 °C, 1200°C, 1250 °C and 1350 °C. The study of the structure of the alloy with 2 %Si after annealing teaches us that the heating for quenching resulted in the dissolving of all the silicides of the alloy and the SEM examination shows us a singly-phase acicular martensite structure having the boundaries of former β - grains. X-ray investigations prove that the structure is a single-phase one, being in the form of a silicon-oversaturated solid solution with hexagonal lattice, similar to that of α -titanium. The structures of 4 and 6 % Si alloys as annealed comprise a martensite α -titanium matrix and eutectics undergone to a coarsening of the eutectics silicides due to coalescence. There are no secondary silicides.

The hardness of the alloys with 2, 4 and 6% Si increases after quenching due to martensite transformation and the saturation of the solid solution with silicon. The higher quenching temperature, the higher is hardness (Fig.3). A considerable effect on the hardness is also produced by the quenching medium; water, oil or air. The hardness is then accordingly decreased.

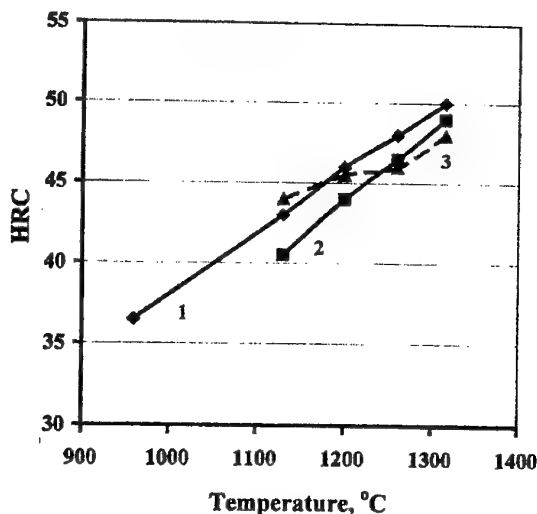


Fig. 3. Hardness of water quenched alloys: 1 - Ti-2Si-3Al-5Zr, 2 - Ti-4Si-3Al-5Zr, 3 - Ti-4Si-3Al-5Zr.

The dependence of hardness of alloys with 2,4 and 6 % Si as quenched from 1315 °C (Fig. 4) after two-hour holding presents some understandings about contributions of the dispersive (2 % Si) and skeleton (4 and 6 % Si) strengthening mechanisms. The plot suggests us that up to approximately 700 °C, dispersive strengthening is more efficient, while above 700 °C, the skeleton strengthening prevails.

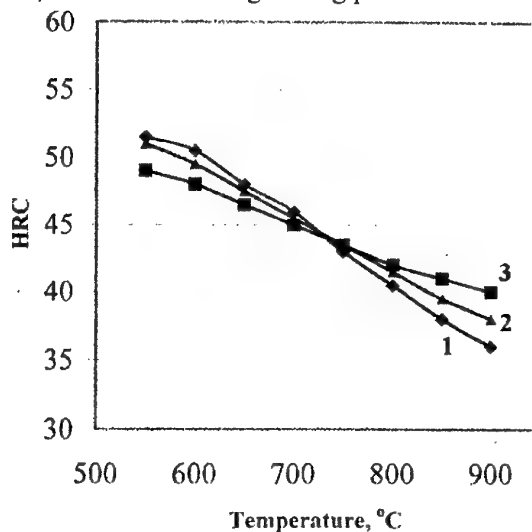


Fig. 4. Dependence of hardness on annealing temperature (water quenching from 1315 °C ; 2 hours tempering)

The authors would like to acknowledge funding of this project from the US Air Force Office of Scientific Research, and the assistance of the Science and Technology Center of Ukraine.

INVESTIGATION OF THE HEAT CAPACITY AND ENTHALPY OF Bi_2Se_3 AND Bi_2Te_3 IN THE TEMPERATURE RANGE 58 – 1012 K

N.P. Gorbachuk, A.S. Bolgar, V.R. Sidorko, L.V. Goncharuk

I.N. Francevich Institute for Problems of Materials Science, National Academy of Science of
Ukraine

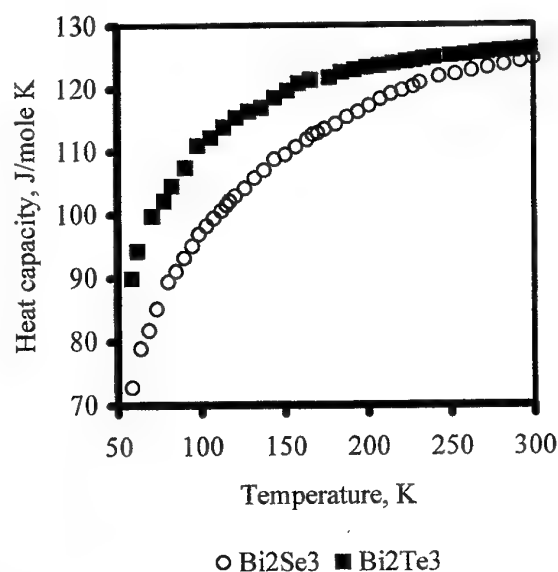
The higher of selenide and telluride of vis-
muth and the solid solution between Bi_2Se_3 and
 Bi_2Te_3 is perspective materials for the thermoe-
lectricity.

In the present work heat capacity and en-
thalpy of vismuth selenide and telluride was re-
search for solid and liquid states. The compounds
under study were produced from elements by am-
poule method.

Heat capacity at 58 – 300 K were measured
by adiabatic calorimetry method with periodic in-
put of heat on low temperature standard thermo-
physical unit [1], and enthalpy - by drop calo-
rimetry method on high-temperature differential
calorimetry [2]. The error of the heat capacity
measurement not to exceed 0,4 %, and of enthalpy
- 1,5 %.

The experimental data (fig.1) of heat cap-
acity smoothed out by a method of sliding approxi-
mation by the cubic multimembers with weight
factors [1].

Fig.1. Low - temperature heat capacity of
 Bi_2Se_3 and Bi_2Te_3



mental data on the low temperature heat capacity
for the alloys studied were extrapolated to 0 K [2].

Table 1. The enthalpy ($\text{J}\cdot\text{mole}^{-1}$), heat capacity, en-
tropy and Gibbs's energy ($\text{J}\cdot\text{mole}^{-1}\cdot\text{K}^{-1}$) of
 Bi_2Se_3 and Bi_2Te_3 at 298.15 K

Thermodynamic functions	Bi_2Se_3	Bi_2Te_3
$H^0(T)-H^0(0\text{K})$	28278 ± 142	31048 ± 156
$C_p^0(T)$	124.53 ± 0.5	126.19 ± 0.5
$S^0(T)$	215.1 ± 1.8	256.6 ± 2.1
$\Phi^0(T)$	120.3 ± 1.8	152.6 ± 2.3

Experimental data (fig.2) of the compounds
studied enthalpy ($\text{J}\cdot\text{mole}^{-1}$) in the temperature
range of 298,15 – m.p. were approximation using
Mayer – Kelly equation:

$$H^0(T)-H^0(298,15)=AT^2+BT+CT^{-1}+D \quad (2)$$

Proceeding from (2) the temperature de-
pendencies of heat capacity, entropy and Gibbs's
energy ($\text{J}\cdot\text{mole}^{-1}\cdot\text{K}^{-1}$) function are as follows:

$$C_p^0(T)=2\cdot A\cdot T+B-C\cdot T^{-2} \quad (3)$$

$$S^0(T)=2\cdot A\cdot T+B\cdot \ln T+0.5\cdot C\cdot T^{-2}+E \quad (4)$$

$$\Phi(T)=AT^2+B\ln T-DT^{-1}-0.5\cdot C\cdot T^{-2}+(E-B) \quad (5)$$

Above melting point for compounds some
enthalpy values of were obtained which were cal-
culated using linear dependence:

$$H^0(T)-H^0(298,15\text{K})=a\cdot T+b \quad (6)$$

Coefficients of temperature dependences (2 – 5)
calculated by the least square method using tow
boundary conditions, i.e. zero value of enthalpy at
298.15 K and standard value of compound heat
capacity to provide agreement between high and
low temperature heat capacity values. Using only
former boundary condition coefficients of depen-
dences (6) were found for the substances studied
(table 2).

At confidential probably 0.95 values of enthalpy,
designed on (2) and (6), are characterized by an
average relative confidential interval not to ex-

To obtain main thermodynamic functions
under standard conditions (table 1) the experi-

ceed, respectively: 1.38% and 1.72% (Bi_2Se_3), 1.32% and 1.73% (Bi_2Te_3).

Fig.2. Experimental data for enthalpy of Bi_2Se_3 and Bi_2Te_3

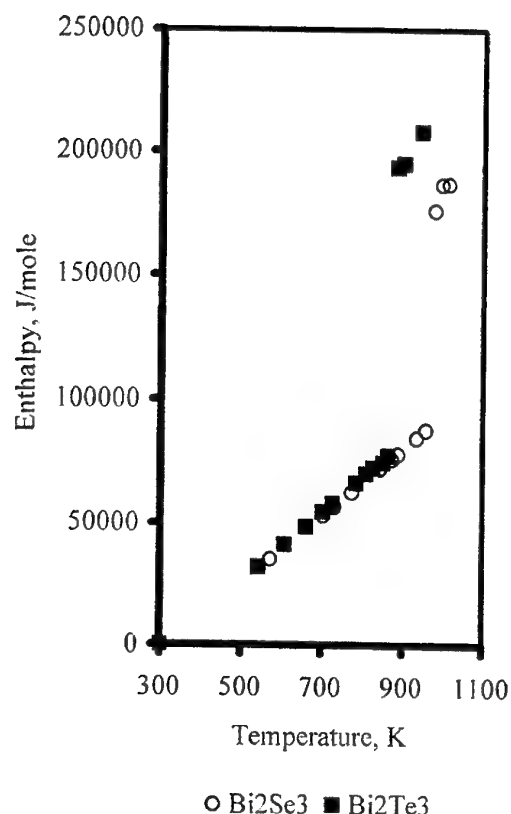


Table 2. Temperature dependences coefficients of the data enthalpy ($\text{J}\cdot\text{mole}^{-1}$), heat capacity, entropy and Gybbs's energy ($\text{J}\cdot\text{mole}^{-1}\cdot\text{K}^{-1}$) of Bi_2Se_3 and Bi_2Te_3

Coefficient	Bi_2Se_3	Bi_2Te_3
$A\cdot 10^3$	8.243	18.428
B	124.43	117.02
C	428188	161744
-D	39268	37070
-E	501.23	422.08
a	262.82	325.99
-b	78361	97193

Basing on the enthalpy temperature dependences (2,6) enthalpy and entropy of melting are determined for compounds (table 3).

Table 3. Temperatures (K), enthalpy ($\text{kJ}\cdot\text{mole}^{-1}$) and entropy ($\text{J}\cdot\text{mole}^{-1}\cdot\text{K}^{-1}$) of melting of Bi_2Se_3 and Bi_2Te_3

Characteristic	Bi_2Se_3	Bi_2Te_3
T_M	968 ± 10	874 ± 10
ΔH_M	89.3 ± 4.3	108.3 ± 4.3
ΔS_M	92.3 ± 4.5	123.9 ± 4.9

The heat capacity of Bi_2Te_3 is higher then for Bi_2Se_3 on 23 – 13 % in temperature range 58 – 300 K and 1.3 – 7.5 % in temperature range 298.15 – 850 K. At low temperatures phonon component the heat capacity compounds is determined, and average temperatures – anharmonic component.

REFERENCES

1. Bolgar A.S., Krykla A.I., Suodis A.P. / Low Temperature Heat Capacity of Praseodymium, Neodymium and Samarium Sesquicarbides (in Russian) // Zh. Fiz. Khim.- 1998.- 72.- p. 439-443;
2. Bolgar A.S, Gorbachuk N.P, Blinder A.V / Enthalpy of Gd_5Si_3 , Gd_5Si_4 , GdSi , $\text{GdSi}_{1.88}$ in Temperature Range 298.15 – 2200 K. Enthalpy of the Melting (in Russian) // Teplofiz. Visok. Temperatur.- 1996.- 34.- p. 541-545.

STRUCTURE-PHASE TRANSFORMATION IN THE CONTACT WORKING LAYER MATERIALS AND EROSION STABILITY OF THEM

Minakova R.V., Chomenko E.V., Kryachko L.A.

Institute for Problems of Materials Science, NAS of Ukraine, Kiev

Composite materials (CM) in the Me-Me systems are known as effective materials for electric contacts. Their increased properties in comparison with contacts from homogeneous materials are explained, holding on the thermal theory of arc erosion [1], by ability of the refractory component skeleton, to stay in the solid state and to reduce of the electroconductive component ejection in the vapor and liquid phases. However, in [2] it was established that the properties of a refractory skeleton and the capillary system, formed by it, are realized only during the first cycles of current commutation. Thermal effect of arc discharge and its changes cause not only material ejection, but also irreversible structural changes in the working layer of the composite contact. In this paper the results of investigation such changes in the contacts material are submitted. The tested CM contained components: W(Mo) - Cu-Ni(Co); Cu-Cr; Ag-Ni. The basic properties of investigated CMs manufacture by power metallurgy methods are included in the table.

Table. General properties of trade mark composite materials for electrical contacts

Trade mark	Composition, %	Density, $\times 10^3$ kg/m ³	Hardness HB, MPa	Electric resistance, $\mu\Omega\cdot\text{m}$
KMK-A30	Ag-70; Ni-30	9,6	550-750	0,030
KMK-A41	Ag-97; C-3	9,0	280-500	0,026
KMK-B45	W-50; Cu-46; Ni-1,5-3,5	12,0	1400	0,070
KMK-B25	W-70; Cu-26; Ni-1,5-3,5	14,0	2100	0,080
Mo-Cu50	Mo-50; Cu-50	9,37	1200	0,040
Mo-Cu30	Mo-70; Cu-30	9,6	1300	0,070
Cr-Cu50	Cu-50; Cr-50	8,12	800-1200	0,050

The bench and field tests [2] of functional properties of listed CM contacts were carried out. The representation about of the erosion features of W(Mo)-Cu CM contacts in a wide range of currents (1-100 kA) were obtained by studying of the contacts erosion performances in the opened arc, freely burning in air on the test bench.

Arc quenching chambers and automatic switching device at the enterprises - manufacturers of the switching equipment were used for the working layer structural research of the contacts from the CM in systems of Cr-Cu, Ag-Ni after field tests.

The character of the contacts wear was studied by analyses of macro- and microstructure, microhardness of the working layers, and its polished angle and perpendicular section of a working layers. The erosion products were studied with optical spectral and X-ray phase analyses.

The complex analysis of the W-Cu contacts working layer has shown the following. The effect of unit impulse with current less than 2 kA is localized on a small part of the surface decorated with peaks of the molten and cristallized Cu and extends for 20-30 μ of working layer thickness. The current growth through the gap between contacts leads to increasing of arc thermal, electric- and gas dynamic influence. The results from arc complex effect are following: working layers oxidizing; sweating of Cu-base melt; loss of mechanical strength of the tungsten base component boundaries; directed ablation of the material of working layer (including refractory component in the hard phase); thermal fatigue failure, formation of brittle crack net work; localized explosion similar failure; increase of porosity and depth of opened capillaries; increase of electric transfer coefficient and erosion rate. The further increase of current (higher of 25 kA) leads to decrease of erosion rate stabilization electric transfer coefficient, fig. 1. Increase of current leads to (besides listed structure modification) segregation of structure components, consolidation the refractory particles in the layer depleted with Cu, consequent refractory conglomerates fusion as a result of arc spots attaching on CM component. The shape and sizes of its particles are depending from influence of temperature, pressure, heating and cooling rates in the arc spots on working layer materials, fig. 2, a.

Components segregation in working layer of the Mo-Cu contacts is more expressed in comparison with those on the W-Cu contacts, especially on anode. Discharge current increase leads to formation of the multilayer heterogeneous structure. The structure changes features in the Mo-Cu contacts working layers is connected with interaction in the system Mo-Cu-O, and formation of easily fusible eutectics ($\text{MoO}_3\text{-CuMoO}_4$, $\text{Cu}_6\text{Mo}_4\text{O}_{15}\text{-Cu}_2\text{O}$), pseudo-eutectics ($\text{MoO}_3\text{-Cu}_2\text{O}$,

$\text{Cu}_6\text{Mo}_4\text{O}_{15}\text{-MoO}_3$) under influence of the discharge heat flow and oxygen of air. Volatility of MoO_3 determines its participation in the elektro transfer influences on the composition of erosion products. Interaction in the system Mo-Cu-O influences on a current threshold of the irreversible structural changes in a working layer, increases of condensed phase role in the mass transfer, fig. 1.

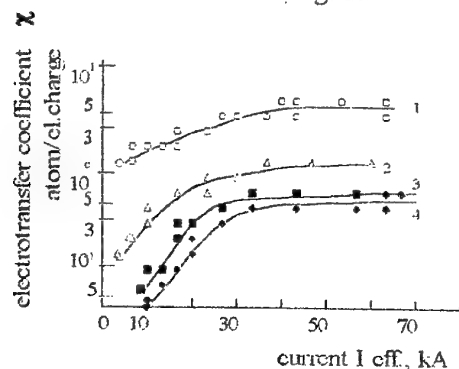


Fig. 1 - Current dependence of electrotransfer coefficient γ , for contacts from Cu (1); CM Mo-Cu50 (2); W-Cu30 (3); W-Cu50 (4)

The Cu-Cr composites last years are effectively used as vacuum switching contacts. The features of the structure irreversible changes in a working layers of Cu-Cr contacts were investigated after pre-burning of the vacuum arc-quenching chamber КДВ 21 ХД. The initial structure of Cu-Cr composite material (as well W(Mo)-Cu CM) is submitted by a low melting matrix with a particle size up to 100 microns and grains of the refractory component dispersed in it with the size up to 30 microns. After the CM contacts condition in its working layers secondary microlayered structure formation (with alternation of the non-porous and spongy, discrete microlayers) is observed. The dense microlayers are characterized by increased phase components dispersivity. All the phases have a crystalline structure. Grains of the Cr basis phase of a rounded form with diameter less than 1 micron are dispersed in the textured copper matrix. Such microdisperse and microlayered structure of working layers, microlayers boundaries have ability to relaxation of the thermal fatigue stresses, create the advantages of Cu-Cr contacts, which are implemented in practice.

Composite Ag-Ni contacts are used in a wide range of loads due to technological opportunities of creation of matrix and skeleton structures of CM with an isotropic and anisotropic refractory component. Irrespective of the anisotropy degree of Ag-Ni CM in the contacts working layer the effect of discharge thermal field courses (besides of the

silver evaporation) of components segregation with local consolidation of refractory one and macroheterogeneization of working layer structure. Fusion of agglomerates (as effect of motionless discharge spots), crystallization them at the fast cooling and the dispersion of working layer structure under consequent discharge heat effect cause of contacts functional properties increase, fig. 2, b.

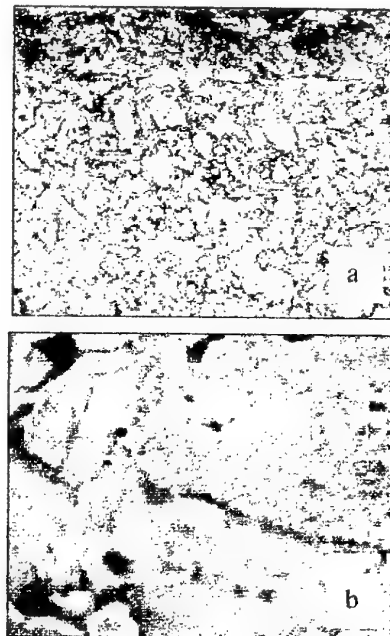


Fig. 2 - Structure changes in the working layer of contacts from CM W-Cu-Ni (a, $\times 120$) and CM Ag-Ni (b, $\times 2100$)

Carried out analysis of structure changes in the working layers of CM contacts evidences that functional properties of contacts in systems Me-Me are determined of self-organization secondary structure features in the non-equilibrium conditions of effect high temperature, pressure, rate of heating and cooling. An absence of solubility in the wide interval of temperatures as a base for Me-Me CM creation, do not responsible for assemblage of processes in the working layers, but only level information development about system Me-Me particularly in the high-temperatures bands.

REFERENCES

1. Францевич И.Н. Материалы электрических контактов // Лекции Всесоюзной школы по электрическим контактам и электродам. - Киев: ИПМ АН УССР, 1969. - Ч.1. - С.1-37.
2. Жаворонков М.А., Левченко Г.В., Минакова Р.В. и др. Структура и эрозия Мо-Си контактов // Порошковая металлургия. - 1972. - № 4. - С.72-78.

DEFORMATION AND FRACTURE OF HIGH-STRENGTH ALLOYS BASED ON Al-Zn-Mg-Cu SYSTEM

D.V.Lotsko, Yu.V.Milman, R.K.Ivashchenko, O.I.Sirko, A.V.Samelyuk, G.F.Sarzhan

I.M.Frantsevych Institute for Problems of Material Science of NAS of Ukraine, Kyiv, Ukraine

The main hardening factor in high-strength Al-Zn-Mg-Cu alloys after T6 treatment for maximum strength (aging at 120-140 °C after solid solution treatment) is the precipitation of very small (to 10 nm) particles of the metastable η' -phase [1]. Evidently, this brings peculiarities to deformation and fracture mechanisms of treated samples.

We compared the behavior while tensile test of samples with gauge diameter of 3 mm from rods of a series of high-alloyed alloys Al-10Zn-3Mg-1.2Cu (baseline alloy, wt. %) with the additions of Zr, Sc and other TM (transition metal). Rods were manufactured by hot extrusion of ingots poured to copper molds as well as of powder billets consolidated by vacuum forging. Powders were produced by the technique of high-pressure water atomization (WA-N process). In Table 1 there are given the representative alloys.

Table 1. Composition of representative cast (C) and powder (P) alloys under investigation

Alloy #	Content of element, wt. %					
	Zn	Mg	Cu	Zr	Sc	Mn
1C	10.3	2.85	1.19	0.15	-	-
2C	10.3	2.70	1.29	0.15	0.49	0.39
3C	12.0	3.30	1.20	0.13	0.49	0.38
1P	9.5	3.0	1.2	0.5	-	-
2P	9.5	3.0	1.2	0.5	0.5	-
3P	12.0	3.0	1.2	0.5	0.5	0.5

Compositions of P/M alloys are given by charge. In addition extruded rods of 99.95 Al were tested.

Tensile stress-strain curves for one-phase materials with dislocation deformation mechanism are well analyzed using Ludwik equation [2]:

$$\sigma = \sigma_s + NE^n, \quad (1)$$

where σ is current true stress at true plastic deformation E , σ_s is yield stress, N is stress hardening parameter and n is stress hardening index. Taking into account the known relations of dislocation theory $\sigma - \sigma_s = \alpha G b \rho^{1/2}$ and $E = \alpha_1 b \rho L$, where $\alpha \approx 1$, $\alpha_1 \approx 0.5$, G is shear modulus, b is Burgers vector, ρ is dislocation density, and L is

average length of dislocation free path, we obtain

$$\Delta\sigma = \sigma - \sigma_s = CE^{1/2}/L^{1/2} \quad (2)$$

with $C = \text{const}$. In metals with high stacking fault energy γ and easy cross slip for the first approximation $L = \text{const}$ and $n = 0.5$, which takes place for bcc refractory metals [3]. When γ is low, dislocations form dense pile-ups in glide planes, and L shall fall with E . Let us assume $L = \beta E^p$, then

$$n = (1 + p)/2. \quad (3)$$

For many fcc and hcp metals [3] and for W-Re alloys [4] with low γ the observed n is close to 1. For Al that has rather high γ n was lower, e.g. 0.67 [3]. In our investigation it was 0.54 (Table 2) that testifies to Al purity. In pure metals several stages with different N and sometimes n are often observed in stress-strain curves that is explained by the formation of cellular structures [3, 4].

Table 2. Strain hardening parameters of rod samples

Alloy #	n_1	N_1 , GPa	n_2	N_2 , GPa	σ_s , GPa
Al	0.54	0.07	-	-	-
1C _s	0.62	0.44	-	-	-
1C	0.56	2.18	0.13	0.24	0.81
2C	0.65	2.69	0.17	0.19	0.80
3C	0.66	2.75	0.15	0.23	0.84
1P	0.76	4.46	0.20	0.30	0.73
2P	0.71	3.98	0.21	0.28	0.79
3P	0.63	3.54	0.16	0.20	0.86

The sample 1C_s was solid solution treated, other alloy samples were T6 treated.

For Al and 1C_s samples the parameters N and n were constant for the whole curve that well obeyed Eq. (1). In 1C_s sample these parameters, especially N_1 , were appreciably higher, evidently, due to the solid solution hardening. The availability of a large amount of small particles after T6 treatment strongly changed the stress-strain curve: it became two-stage (Fig. 1), and the parameter N_1 dramatically increased that is a consequence of a

very small L (Eq. (2)). The parameter n_1 is significantly higher than 0.5 that testifies to a strong increase of dislocation density. These factors led to large values of θ (Fig. 1) in the 1st stage of deformation.

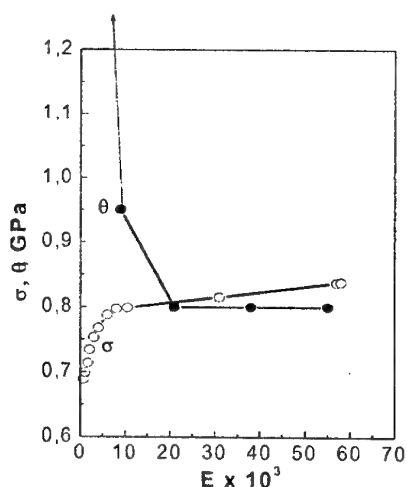


Figure 1. Stress-strain curve and strain hardening coefficient θ for the sample 1C

The stage 1 is very short ($E_1 < 0.01$), and strain hardening parameters for the stage 2 are much smaller (Table 2). The transition to the stage 2 can be associated either with cutting particles by moving dislocations or particles sweeping-out from active slip planes. Note that the stresses σ_2 of beginning the 2nd stage are close in C and P samples in spite of a rather large difference in N . Evidently, therefore the 1st stage in P samples is about 2 times shorter. Obviously, larger N in P samples is caused by their finer grain and cellular structure and oxide films in grain boundaries.

Fracture of Al sample occurred by a usual ductile fracture mechanism with the formation of a neck, when $\theta \leq \sigma$ (Considere criterion of deformation localization). In 1C_s sample an entirely different mechanism of ductile fracture was observed, when fracture occurs along the shear plane at an angle of 45° to the sample axis. This fracture is known as "void-sheeting" or "void coalescence by shear" [5]. Voids, or pores, are formed in deformation process. Void coalescence in the shear plane reduces the working shear area that localizes a further shear in this plane till sample failure. If weakening the shear plane by pores is compensated by strain hardening, deformation localization does not occur, and the sample is deformed uniformly. The localization begins, when the Considere criterion is realized.

In T6 treated samples the Considere criterion

can be realized in the 2nd stage of the stress-strain curve (see Fig. 1). It is of interest that often $\theta \approx \sigma$ in a considerable part of the stress-strain curve (Fig. 1), and thus the deformation localization does not provoke fracture immediately. As a consequence fracture may proceed in several planes favorable for crack propagation (Fig. 2a, b).

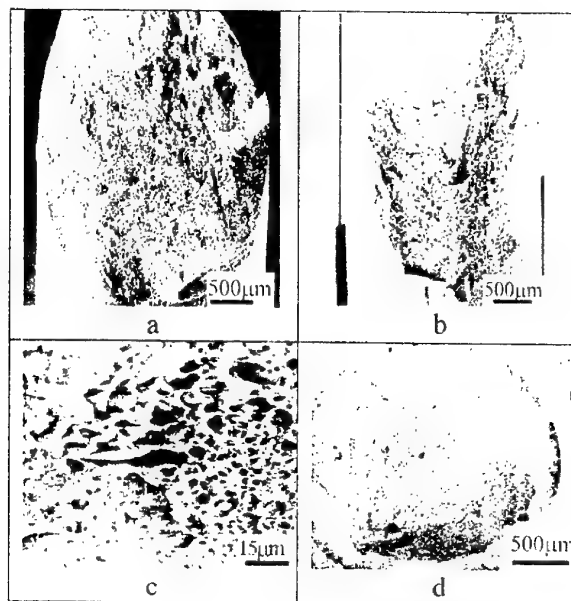


Figure 2. Fracture surfaces of tensile samples:
a, c – 1C, b – 3C, d – 3P

In fracture surface areas of dimple fracture alternated with areas of fracture along cell boundaries weakened by $MgZn_2$ precipitates (Fig. 2c). In P/M samples before the fulfillment of the Considere criterion fracture started from some faults left after powder consolidation, and since this moment fracture proceeded in the plane normal to sample axis (Fig. 2 d).

This work was partially supported by STCU, project P061.

1. Fridlyander I.N. Structural Wrought Aluminum Alloys. – Moscow: Metallurgia, 1979. – 208 p.
2. Trefilov V.I., Milman Yu.V., Firstov S.A. Physical Foundation for Strength of Refractory metals. – Kiev: Nauk. Dumka, 1975. – 315 p. (in Russian).
3. Moiseev V.F. // Metallofiz. Noveishie Tekhnol. – 2001. – 23, No. 3. – P. 387.
4. Kosachev L.S., Milman Yu.V., Rymashevski G.A. et al. // Fizika Metallov i Metallovedenie. – 1987. – 63, is. 2. – P. 366.
5. Teirlinck D., Zok F., Embury J.D., Ashby M.F. // Acta metal. – 1988. – 36, No. 5. – P. 1213.

PROPERTIES OF CERAMIC COMPOSITES BASED ON Si_3N_4 -TiN.

Lina L.Sartinska, George G.Gnesin, Irene I.Osipova

Institute for Problems of Materials Science, NAS of Ukraine, Kiev, Ukraine.

ABSTRACT

This work is devoted to obtaining and investigations of the Si_3N_4 -TiN ceramic composites without any additives and with such sintering additives as Y_2O_3 , Y_2O_3 - Al_2O_3 and Al_2O_3 , based on nanosized powders and produced by hot-pressing. The structure, phase composition, tribology, and physico-mechanical properties such as hardness, fracture toughness, strength and wear resistance have been studied as a function of the TiN content in the Si_3N_4 -TiN composite materials.

INTRODUCTION

Among other applications, Si_3N_4 materials are currently used as cutting inserts. It is known that wear of ceramic cutting tools is the totality of the adhesive, abrasive, chemical and diffusional components of the process. For better stability Si_3N_4 based materials could be used together with TiN to improve the overall chemical resistance.

The using of nanosized powders makes it possible to obtain practically porosity-free materials with high physico-mechanical properties, because of a decrease in particles size of original powders leads to intensification of the sintering process.

Thus, the aim of these investigations is to select the best composition of presented ceramics based on nanosized powders for cutting tools. For that structure, phase composition, tribological processes, physico-mechanical properties: hardness, fracture toughness, strength and wear resistance have been studied as a function of TiN content as well as additive content in the composite materials.

EXPERIMENTAL DETAILS

As the object of the investigations Si_3N_4 , TiN, Al_2O_3 obtained by plasma chemical synthesis were used.

The powder batches for hot pressing were prepared by mixing in acetone in a planetary mixer. The hot pressing was done in multicavity graphite dies at 1800-1820°C by high-frequency generator with uniaxial application of a pressure of 20 MPa and dwell times 5-20 min.

The hardness and fracture toughness was measured by using Vickers indenter with 196 N load.

The tribological processes were investigated according to the method described in literature by determining the wear resistance of ceramics in friction with a hard fixed abrasive which provided reliable information on the complex of strength characteristics of the specimen, and secondly, by evaluating its wear resistance in frictional interaction with the metal, which enabled us to establish the resistance of the ceramic material directly in frictional contact with an actual metal.

RESULTS AND DISCUSSION

It has been demonstrated that it is possible to get a high density Si_3N_4 -(30-50)wt.%TiN composite materials from nanosized powders with good physico-mechanical properties without any additives by hot-pressing (HV-16.5 GPa, K_{1c} -6.3 $\text{MPa}\cdot\text{m}^{1/2}$, strength-595 MPa). So, there is physico-chemical interaction between Si_3N_4 and TiN, because of it is impossible to produce pore-free material from nanosized powders as from Si_3N_4 and from TiN. X-ray diffraction examinations verify the given suggestion.

Alumina is an excellent sintering additive for all Si_3N_4 -TiN compositions of ceramic materials for cutting tools and gives a possibility to produce ceramic materials with improved physico-mechanical properties (HV-19 GPa, K_{1c} -8.0 $\text{MPa}\cdot\text{m}^{1/2}$, strength-800 MPa).

Y_2O_3 as sintering additive promotes compacting of a material, if the amount of TiN does not exceed 50 wt.%. Thus, Y_2O_3 is the sintering additive for Si_3N_4 and is only suitable for composites based on Si_3N_4 (TiN<50%).

The hardness of ceramics based on Si_3N_4 -TiN from nanosized powders with sintering additives is a little bit higher than hardness of dense composites without additives. If a content of TiN is higher than 50wt.%, there is decreasing in hardness, because of lower hardness of TiN in comparing with Si_3N_4 . The big porosity of hot-pressed materials based on Si_3N_4 and Si_3N_4 -(10-20 wt.%) TiN does not allow to receive a big hardness of composites.

The best values of a fracture toughness of all explored materials, are attained at the (30-50) wt.% TiN content. However, the best values of a fracture

toughness of Si_3N_4 -TiN composites without additives are lower.

The strength of materials based on Si_3N_4 -TiN grows with increasing TiN and achieves the optimum at the 30-50 wt.% TiN content. The highest values of strength were obtained in materials of Si_3N_4 -TiN- Al_2O_3 system, because of participation of Al_2O_3 in physico-chemical interaction of Si_3N_4 and TiN. The strength of materials of Si_3N_4 -TiN- Al_2O_3 - Y_2O_3 system is a little bit lower. Its values decrease with increasing of TiN content more than 60 wt. %.

The examinations of a wear resistance of hot-pressed materials with the sintering additives at turning of a hardened steel 45 have shown, that wearing does not depend on a composition of the sintering additive and is determined completely by amount 30-70 wt.% TiN, although a structures of these composites are essentially differ (Fig.1).

The material of a composition Si_3N_4 - Al_2O_3 -50wt.%TiN has demonstrated the best wear resistance at turning of a steel LIX15 due to excellent values of hardness, fracture toughness and strength. Thus, high-chromium steel is better to turn by ceramic composites based on TiN (TiN>50wt.%).

The Si_3N_4 -(50-80)wt.%TiN composites have shown a rather high wear resistance also, despite of low physical-mechanical properties, that confirms the importance of absence of adhesive interaction of explored ceramics with a work materials.

Si_3N_4 -20wt.%TiN composites demonstrate the best wear resistance in friction with abrasives, however in friction with hardened steel the best wear resistance is demonstrated by Si_3N_4 -70wt.%TiN composites. Thus, investigation of the tribological processes has demonstrated, that 50 wt.%TiN is the best content of titanium nitride in materials based on Si_3N_4 -TiN because of it makes physico-mechanical properties enough high, and the adhesive interaction is unessential.

The effect of additive content as well as TiN content in the composition of hot-pressed material on the structure and phase composition of produced ceramics has been revealed.

CONCLUSIONS

The using of nanosized powders makes it possible to expand the obtaining of the practically porosity-free ceramics of the different compositions.

Due to physico-chemical interaction between Si_3N_4 and TiN it is permitted to create high-density materials from Si_3N_4 - (30-50 wt.%) TiN with enough high physico-mechanical properties.

All ceramic composites based on Si_3N_4 - TiN in presence of Al_2O_3 addition have higher physico-mechanical properties.

It has been shown by the investigations of the tribological processes, wear resistance and the physico-mechanical properties: hardness, fracture toughness and strength, that the optimum content of titanium nitride is 50 wt.% in the materials based on Si_3N_4 -TiN. Such ceramic composite is potential materials for applications in steel machining, where the Si_3N_4 monolithic inserts severely wear.

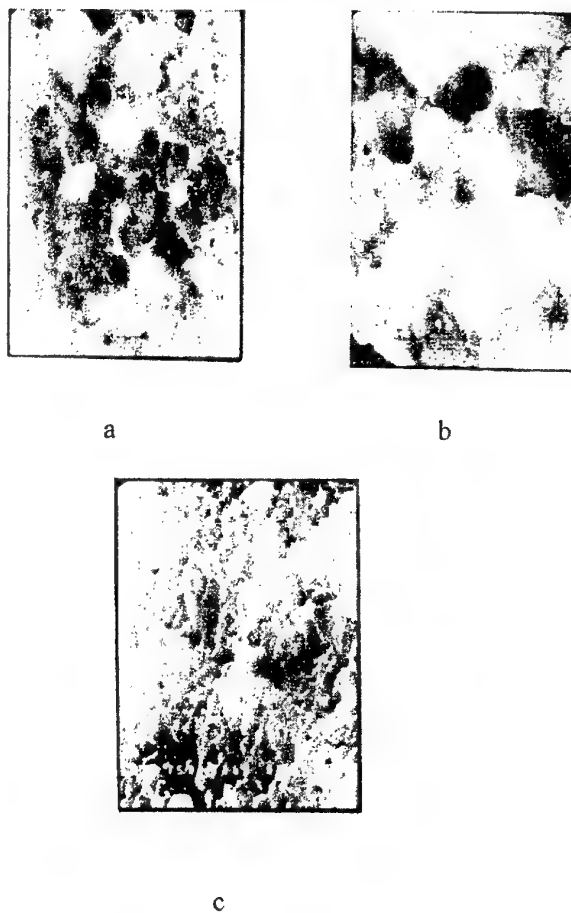


Fig.1 SEM of fracture surface of Si_3N_4 -TiN composites: a – 50 wt.% TiN, b – 80 wt.% TiN, c – 10 wt.% TiN.

THE STRUCTURE AND MECHANISM OF WEAR OF COMPOSITES ON THE BASE OF TITANIUM NITRIDE IN DRY FRICTION IN AIR

Evtushok T.M., Kostenko A.D., Grigorev O.N., Zhunkovskii G.L., Kotenko V.A., and
Shaposhnikova T.I.

Institute for Problems of Materials Science, National Academy of Sciences of Ukraine, Kiev,
Ukraine

With increases in speeds and loads, and, consequently, temperatures and strains in friction assemblies, the problem of galling becomes most urgent. Its solution lies in the field of development of composites with low adhesive activity. Refractory titanium compounds (TiB_2 , TiC , and TiN) are most attractive as a base of these composites.

Works [1-4] have actually shown that composites on the base of binary titanium-chromium boride possess a high level of physicochemical and tribologic properties and that using them as end seals and bearings had made it possible to increase significantly the wear resistance of the latter ones and reduce losses in power on friction of commercial internal combustion engines by 20-30%, as well as to decrease the oil circulation rate through a turbo-compressor [4].

New titanium nitride-based composites developed by us have shown even a higher level of tribologic properties and made it possible to pass from friction of boundary lubrication to dry friction.

Several methods of preparation of these composites were developed, and the physicochemical conditions of formation of their structure with a high wear resistance under conditions of dry friction were studied.

The influence of the ratio of components in the composites on their physicochemical properties was investigated. The ranges of the strength properties of these materials (bending strength σ from 700 to 1150 MPa, hardness HRA from 78 to 87 units) and their optimum levels that are 890-900 MPa and 83-85 units, respectively, for using in the pair with hardened steels were determined.

The tribologic characteristics of composites, namely, the friction coefficient and wear at a sliding speed from 5 to 25 m/s under a load of 1 MPa in the pair with hardened 65G steel in dry friction in air were studied (Fig. 1).

It was established that frame type

material prepared by the impregnation method have the level of tribologic properties which is twice or three times that of materials prepared by sintering.

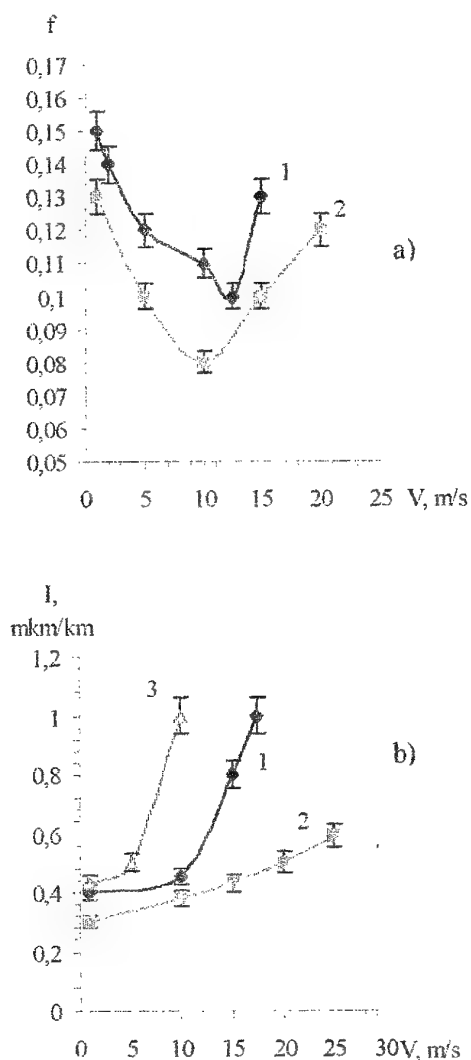


Fig. 1. Dependence of the friction coefficient (a) and wear (b) on the sliding speed under a load of 1 MPa for friction pairs:

- 1 - $[\text{TiN}-\text{Cr}_3\text{C}_2-\text{Ni}_3\text{Al}]$ - 65G steel;
- 2 - $[\text{TiN}-\text{Ni}_3\text{Al}]$ - 65G steel;
- 3 - $[\text{TiN}-(60\text{BrO}10\text{C}10-40(\text{Cu}-\text{Ni}))]$ - 65G steel.

The mechanism of wear and fracture of composites in dry friction in the indicated range of speeds and loads was investigated.

Test results show indicate that composites have a high level of tribologic properties that are almost an order of magnitude higher than those of familiar composites on the base of such refractory compounds as TiC and Cr_3C_2 .

The prepared materials can be recommended for dry friction assemblies at sliding speeds of up to 20 m/s under a load of up to 1 MPa inclusive.

REFERENCES

1. Pozdnyakov O.A., Kobzar' L.E., Minak A.F., and Evtushok T.M. Assessment of

the efficiency of bearings from nontraditional materials for a turbo-compressor// *Dvigat. Vnutr. Sgoran.*, 1990. No. 5, P. 53-63.

2. Zhunkovskii G.L., Evtushok T.M., Strashinskaya L.V., et al.// *Refractory nitrides and materials on their base: Collection of Works.* Kiev: IPM AN USSR, 1992. P. 184-190.

3. Evtushok T.M., Zhunkovskii G.L., Koval'chenko A.M., et al. *Structure and tribologic properties of cermets prepared by the impregnation method*, *Adgez. Raspl. Paika Mater.*, No. 29, 1993, P. 73-77.

4. Zhunkovskii G.L., Evtushok T.M., Mazur P.V., et al.// *Borides and Materials on its Base: Collection of Works.* Kiev: IPM AN USSR, 1994. P. 147-150.

STRUCTURE OF RAPIDLY SOLIDIFIED Al – 13 AT. % Sc ALLOY

**Yefimov M.O., Miracle D.B.⁽¹⁾, Milman Yu.V., Lotsko D.V., Slipenyuk A.N., Kuprin V.V.,
Danylenko M.I.**

I.M.Frantsevych Institute for Problems of Material Science of NAS of Ukraine, Kyiv, Ukraine

⁽¹⁾Air Force Research Laboratory, Materials and Manufacturing Directorate, Wright-Patterson, USA

Sc is an element of the IIIB group of Periodic System as well as Y and rare-earth metals (REM). Alloys of Al-REM systems are known as metallic glass forming alloys for REM content of 7-

16 at. % depending on alloying element. An amorphous structure was obtained for Al with Y, La, Ce, Pr, Nd, Sm, Gd, Tb, Dy, Ho, Er and Yb additions by rapid solidification technique in melt-spun ribbons [1]. At the same time Sc that has a similar electron structure was not studied as an addition to Al in concentration range pointed above. In rapidly solidified ribbons with Sc content to 5 at. % α -Al solid solution and Al_3Sc intermetallic were revealed, and if α -Al was stabilized by small Cr addition, ribbon hardness achieved 1600 MPa [2].

We investigated the structure of aluminum alloyed with scandium in high concentration of 13 at. %. A rapidly solidified ribbon was manufactured by the single-roller melt spinning technique. Ingot of Al – 13 at. % Sc master alloy was melted in a quartz crucible-nozzle and then poured on the side surface of a rotating copper wheel (the circumferential velocity of about 40 m/s). The obtained ribbon 4-6 mm in width contained parts of various thickness from 30 to 70 μ m. Ribbon structure was studied by means of XRD (X-ray diffraction) analysis in CuK_{α} radiation and TEM (JEM-100CX microscope). The XRD investigation of the ribbon revealed no signs of metallic glass state, but an unambiguous appearance of a quasicrystalline icosahedral phase, which is especially interesting (Fig. 1). The XRD pattern of the initial ingot (Fig. 1a) contained lines of α -Al and Al_3Sc . Normal Al_3Sc lines (n) were of rather high intensity, and superstructure lines (s) were clearly seen. XRD patterns of ribbons were different for ribbons of various thickness. Thick ribbons showed the availability of α -Al and I-phase (Fig. 1b). In Fig. 1b lines of I-phase are given with Cahn indices N/M [3]. It is seen the appearance of lines with odd N that corresponds to the face-centered quasicrystal reciprocal lattice in the 6-dimensional space. Similar lines were observed

in Al-Mn-Ce alloys, and this was interpreted as increasing the chemical order under the influence of Ce [4].

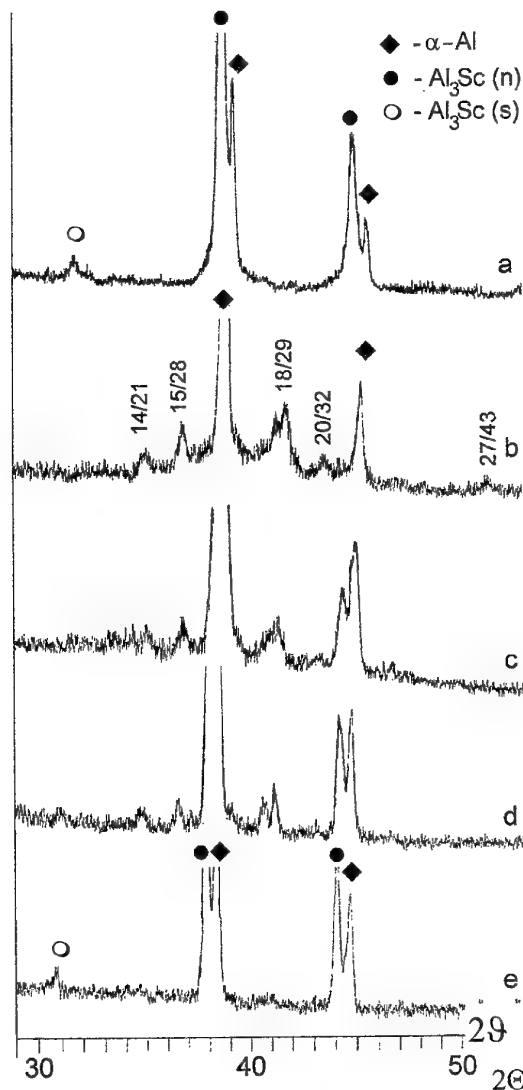
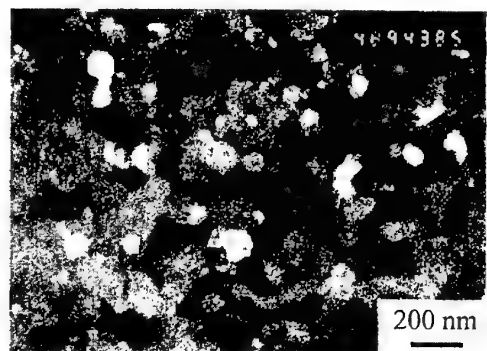


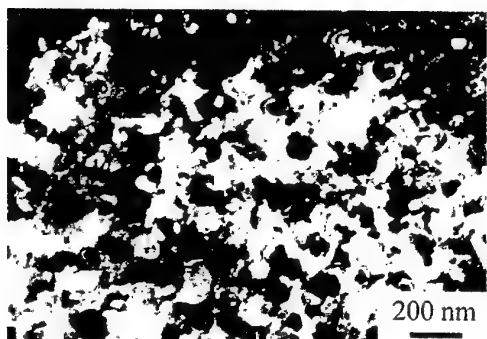
Figure 1. XRD patterns of Al-13 at. % Sc alloy:
a – initial ingot;
b – ribbon of 70 μ m in thickness, 1 day after manufacture;
c – ribbon of 30 μ m in thickness, 1 day after manufacture;
d – ribbon of 30 μ m in thickness, 45 days after manufacture;
e – ribbon of 30 μ m in thickness, 45 days after manufacture;

e - ribbon of 30 μm in thickness, 90 days after manufacture

Quasicrystalline particles in the ribbon were of 60-120 nm in size (Fig. 2a).



a



b



c

Figure 2. Quasicrystalline particles in the ribbon of 70 μm in thickness, dark field image (a), α -Al matrix in the same place, dark field image (b) and electron diffraction pattern from this area (c)

In thinner ribbons in addition to the I-phase and α -Al a rather large amount of Al_3Sc was present, and superstructural lines almost vanished (Fig. 1c). It allows to suppose at least partly disordered structure of Al_3Sc . XRD pattern of such ribbons changed with time: after 45

days since manufacture lines of I-phase became weaker and narrower, and Al_3Sc lines (n) and (s) became stronger (Fig. 1d). After staying for 90 days at room temperature I-phase lines practically vanished (Fig. 1e). XRD pattern of thick ribbons in these conditions remained unchanged. Thus, quasicrystalline phase in ribbons of about 30 μm thickness is unstable and transforms to crystalline Al_3Sc .

Fine I-phase particles give reflections in the electron diffraction pattern (EDP) in the form of rings densely sawn by fine spots (Fig. 2c). Two bright rings in Fig. 1c have indices 18/29 and 20/32. The dark field image in Fig. 1a was formed by a part of these rings. α -Al matrix in this volume is a strongly distorted single crystal (Fig. 2b), the dark field image (b) was formed by (222) Al spot reflection. With the help of our smallest selecting diaphragm (the image forming area of 480 nm in diameter) we succeeded to obtain a distinct 5-fold symmetry in EDP of a rather large I-phase particle (Fig. 3).



Figure 3. Electron diffraction pattern formed with a small selecting diaphragm from quasicrystalline particles in the edge of the foil

Hardness HV of the ribbon of 70 μm in thickness measured at a load of 0.5 N was 2082 MPa. It is close to hardness of ribbons of Al-Fe-Cr-Ti with I-phase particles of nanoscale size manufactured in our experiments.

Thus, it is first shown the formation of I-phase in rapidly solidified Al-13 at. % Sc alloy, and I-phase is stable in 70 μm ribbon (smaller cooling rate) and unstable in 35 μm ribbon.

1. Inoue A. // Progr. Mater. Sci. – 1998. – 43. – P. 365.
2. Sokolovskaya Ye.M., Kazakova Ye.F., Poddiakova Ye.I. // Neorganicheskie Materialy. – 1995. – 31, No. 11. – P. 1418.

EFFECT OF SMALL ADDITIONS OF TRANSITION METALS ON THE STRUCTURE OF Al-Zn-Mg-Zr-Sc ALLOYS

Lotsko D.V., Milman Yu.V., Yefimov M.O., Mordovets N.M., Rachek O.P., Trofimova L.M.⁽¹⁾

I.M.Frantsevych Institute for Problems of Material Science of NAS of Ukraine, Kyiv, Ukraine

(1) G.V.Kurdyumov Institute for Metal Physics of NAS of Ukraine, Kyiv, Ukraine

The Al-Zn-Mg system is the base for high-strength wrought aluminum alloys used in aerospace engineering [1]. In order to obtain hardening due to fine precipitates of the η' -phase wrought semi-products of these alloys are subjected to the thermal treatment of T6 kind consisting in quenching from 465-475 °C and aging at 120-140 °C. A very important problem in providing alloy strength is the preservation of the non-recrystallized structure after quenching. Last years it is shown that the best way for this is an additional alloying by small amounts of Sc together with Zr [1-3]. It is caused by the existence while solid solution treatment of small (to 20-30 nm in size) particles of the intermetallic $Al_3(Sc_{1-x}Zr_x)$ coherently bonded with Al matrix. Ingots of Al-Zn-Mg alloys are often subjected to a homogenizing treatment in order to eliminate the layers of residual eutectics in grain boundaries as well as to equalize the concentration of the main alloying elements in grain body. $Al_3(Sc_{1-x}Zr_x)$ particles are formed in this process too that facilitates the formation of a uniform cellular dislocation structure while following plastic working.

Alloys on Al-Zn-Mg base typically contain small additions of some other transition metals (TM). E.g., Mn, Cr, Ti are introduced mainly to increase the resistance to corrosion cracking of welds [2]. However, the information about their behavior in Al-Zn-Mg-Zr-Sc alloys is very limited. In this work we studied the influence of small additions of TM (Ti, Hf, V, Nb, Cr, Mn, Ni) on the formation of intermetallic particles of Al_3Sc type while ingot homogenization and on the tendency to recrystallization in wrought semi-products of the model alloy Al-7.1Zn-1.3Mg-0.12Zr-0.05Sc (the content of elements is given in wt. %). From equilibrium diagrams [4] we can expect a dissolving of some TM in Al_3Sc like Zr and thus intensifying the influence of Sc.

Ingots were produced in the air using an induction furnace with graphite crucible. TM were introduced into the melt by dilute master alloys manufactured in an argon-arc furnace. Ingots of 25 mm in diameter and 100 mm in length were

obtained by pouring into thick-wall copper molds. 13 alloys were investigated (Table 1).

Table 1. Alloying elements and hardness HV of as-cast alloys after homogenization annealing at 470 °C for 3 h

Alloy #	Content of the element, wt %			HV, MPa
	Zr	Sc	TM	
1	0.13	-	-	922
2	0.12	0.05	-	947
3	0.10	0.10	-	1025
4	0.11	0.15	-	1144
5	0.13	0.05	0.07Ti	1012
6	0.08	0.07	0.41Hf	961
7	0.10	0.05	0.19V	958
8	0.18	0.06	0.08Nb	966
9	0.12	0.06	0.26Cr	986
10	0.12	0.05	0.47Mn	1009
11	0.12	0.05	0.09Ni	1046
12	0.05	0.05	-	952
13	-	0.05	0.37Hf	900

Hardness was measured by Vickers pyramid with the load of 100 N.

Ingot homogenization resulted in a significant hardening. A sharp rise of hardness occurred after 15 min annealing with further deceleration. For annealing times 3-24 h hardness was almost invariable and then began to drop [3]. In ingots additionally alloyed with Ti, Ni, Mn, Cr hardness was appreciably higher than in the ingot #2 without additional alloying, but smaller than in the ingot #4 with 0.15Sc.

TEM investigation of homogenized ingots revealed in their body a large amount of small coherent particles. Most of them (type 1) were spherical particles with a characteristic two-leaves contrast of Ashby-Brown type [5] in bright field image, and in accordance to the results of EDX analysis (Table 2) they are $Al_3(Sc_{1-x}Zr_x)$ intermetallics. Note that the information for EDX analysis is taken from the volume much larger than particle size, and the data of Table 2 permit only to make conclusions about the presence of elements in the particle and about the ratio of their concentrations. Mn revealed in particles 1 in alloy

#11 is evidently in the α -Al solid solution [6].

Table 2. Content of alloying elements in coherent particles and their average size d in ingots homogenized at 470 °C for 3 h

Alloy #	Particle type	Element content, wt %			d , μm
		Zr	Sc	TM added	
2	1	2.86	2.49	-	25.6
4					10.6
5	1	0.83	0.58	-	22.5
	2	1.89	9.08	Ti<2 σ	73.0
6	1	0.04	1.75	-	41.7
	2	2.07	10.7	1.0Hf	88.8
7	1	0.63	0.14	0.06V	42.9
	2	1.74	3.13	0.06V	88.0
8	1	3.24	1.51	-	24.3
	2	1.68	1.22	<0.08Nb	70.0
9	1	0.62	1.16	-	22.8
	2	2.29	10.05	0.8Cr	55.1
10	1	1.26	1.60	0.84Mn	28.6
	2	1.03	4.63	1.16Mn	76.2
11	1	1.83	3.85	-	26.1
	2	1.44	5.49	0.17Ni	38.7

In ingots alloyed by TM there were also found about two times larger particles of the type 2 that contain the added TM (Table 2). They are also coherently bonded with the matrix (Fig. 1a) and often are faceted (Fig. 1b). Difficulties in revealing Ti are connected with the overlapping of its spectral peak with one of Sc that may lower the intensity of the Ti peak to the value smaller than the standard deviation of the experimental points 2σ . Particles of the type 2 were situated in some areas separately from particles of the type 1.

In addition alloying by TM influences the average size (Table 2) and size distribution (Fig. 2) of particles of the type 1.

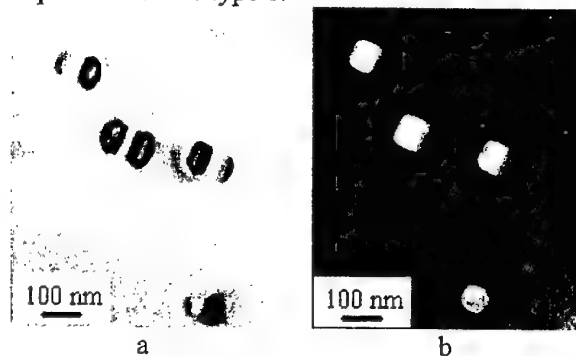


Fig. 1. Particles of the type 2 in homogenized ingots of alloy #2: bright field image (a) and dark field image (b)

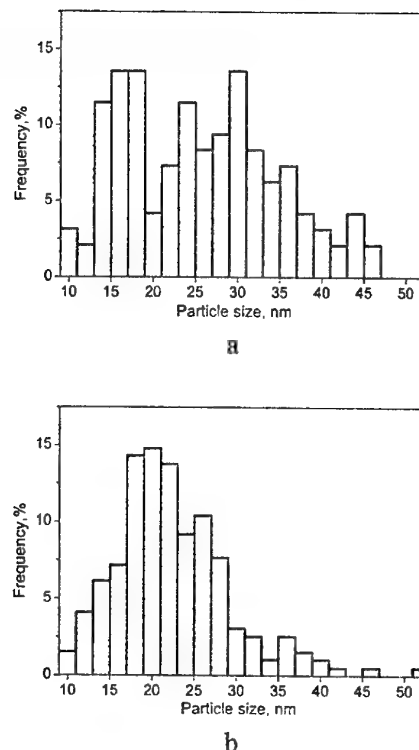


Fig. 2. Size distribution of $\text{Al}_3(\text{Sc}_{1-x}\text{Zr}_x)$ particles in homogenized ingots #2 (a) and #5 (b)

Alloying with Ti, Cr, Ni narrowed the size distribution of particles 1, alloying with Hf and V widened it. This can explain the stronger increase of hardness in homogenized ingots with Ti, Ni and Cr (Table 1).

A complete retard of recrystallization while heating to 465 °C of rods 6 mm in diameter extruded from the ingots at 350 °C was observed in alloys #4-9. For alloy #2 a partial recrystallization took place in peripheral areas of the rod.

1. Senatorova O.G., Uksusnikov A.N., Legoshina S.F. et al. // Mater. Sci. Forum. – 2000. – 331-337. – P. 1249.
2. Davydov V.G., Yelagin V.I., Zakharov V.V., Rostova T.D. // Metallovedenie I Termicheskaya Obrabotka Metallov. – 1996. – No. 8. – P. 25.
3. Lotsko D.V., Milman Yu.V., Yefimov N.A. et al. // Metallofiz. Noveishie Technol. – 1999. – 21, No. 6. – P. 9.
4. A Comprehensive Compendium of Evaluated Constitutional Data and Phase Diagrams, G.Petzow, E.Effenberg eds. - ASM Internat., USA-Germany. – 1993.
5. Ashby M.F., Brown L.M. // Phil. Mag. – 1963. – 8. – P. 1083.
6. Drits M.E., Toropova L.S., Gushchina F.L. // Metally. – 1984. - No. 4. – P. 221.

INFLUENCING OF PLASTIC DEFORMATION ON MECHANICAL BEHAVIOR OF Ti-Al-Si-Zr ALLOYS

Kuzmenko M.M., Verbylo D.G., Koval' O.Yu.

Frantsevich Institute for Problems of Materials Science of NAS of Ukraine, Kyiv, Ukraine

Elaboration of technology hot deformation of Ti-Al-Si-Zr alloys is the important task. The solution of this problem will allow creating technological physical basis for hot deformation of Ti-Al-Si-Zr eutectic alloys and regulating a complex of their mechanical properties in a direction of enhancement of plastic characteristics. The optimizations of technological conditions suppose the solution of two problems: to prepare the constructions with special shape under condition of minimum power costs, and to create an optimal structure of materials and, as a consequent, maximum mechanical property. The second problem recently attracts the special attention of scientist [1], because of it gives the possibility to receive a unique structural states. Therefore, manufacturing of new hot deformation technology of Ti-Al-Si-Zr alloys must precede the stage of systematic scientific researches, which one is founded on substantial knowledge.

The most important points of this analysis are:

1. Ranking and selection of conditions of hot deformation.
2. Analysis of process of structural evolution under different condition of hot deformation.
3. Analysis of influencing of structure on mechanical properties and mechanisms of deformation and fracture.

Materials and methods

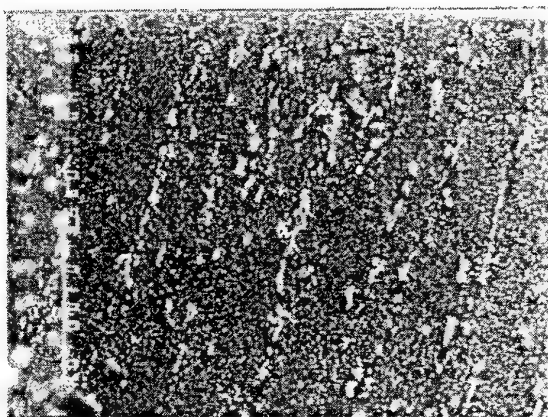
Eutectic alloys were smelted with plasma-art furnace. Cylindrical ingots have 60 mm diameter 150 mm length and the weight 2-3 kg. 40 ingots of different Ti-Al-Si-Zr alloys were obtained by this technological way. Chemical composition of these alloys is shown in the Table.

Table: Composition of alloys studied

Alloy	Chemical composition			
	Al	Si	Zr	Base
2-01	3,1	2,0	4,8	Ti
4-02	3,1	4,0	4,7	Ti
6-03	3,3	6,0	4,9	Ti

Termomechanical treatment

The ingot for forging was firstly treated by mechanically to diameter of 58 mm and length from 40 to 125 mm. The ingot was heated in gas furnace slowly from room temperature to 900°C followed by quicker heating up to 1100°C for 15 min. Pneumatic press MA-417 with an effort 750 kgs was used for forging. Investigated were structural evolution and mechanical properties of Ti-Al-Si-Zr system alloys with different silicon content (2, 4, 6%), deformed by forging up to , 90% deformation powers (Fig.1).



a



b

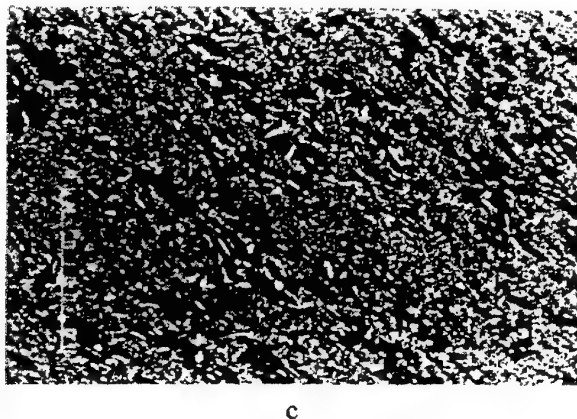


Fig. 1 Structure of deformed Ti-3Al-4Si-5Zr alloys with different silicon after deep plastic deformation with forging (a-2%Si, b-4%Si, c-6%Si).

Experimental results and discussion

Four point bending and uniaxial tension were used for investigation of influence of deformation degrees on plasticity of deformed materials. Four-point bending tests experimental data are shown in Fig.2. Experimental data demonstrate essential increasing of plasticity of samples deformed to large deformation degrees (60 and 90%) for alloys with different content of silicon. The elongation under tensile test also demonstrates the tendency of increasing with plasticity rise of deformation. The data shown in a Fig. 2 demonstrate presence of preliminary plastic deformation on bend on samples deformed by forging up to large deformation degree (90 %).

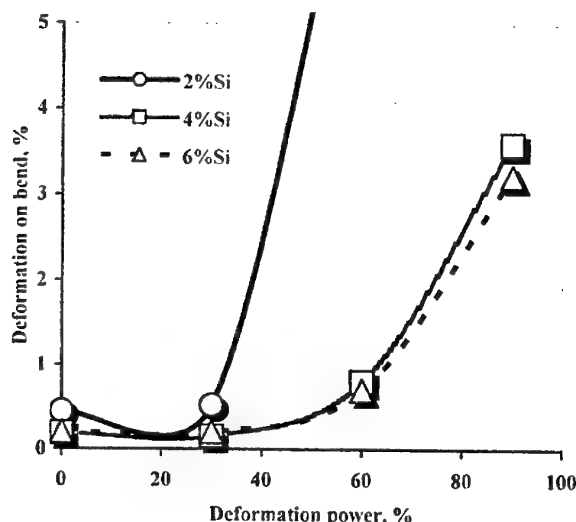


Fig. 2 Influence of preliminary plastic deformation on bend ductility of Ti-Al-Si-Zr alloys with different silicon.

Evidently, the increase of plasticity in eutectic alloys after thermo mechanical treatment is connected with fragmentation of structure, which

takes place at increase of deformation power. Results of transmission electron microscopy showed that in deformed state the grain size decrease up to 3-5 microns (as compare to 200 microns for an initial as-cast condition). As the result the size to an initial crack reduces and the value of an ultimate stress increases. The transition from cleavage to ductile fracture takes place.

It may be demonstrated the presence of micro cracks in low silicon material deformed by forging at 30% deformation. Such defects result in reduction of microdeformation stress. Investigation of microstructure in highly deformed materials demonstrates a dispersion of eutectics colonies. But the residual cracks in the high deformed materials have not been found. Healing of cracks under forging process occurs simultaneously with refinement of eutectic structure. Such structural evolution promotes to increasing of plasticity and to essential enhancement of low temperature strengthening.

Conclusions

1. On the basis of experiments the optimal interval of 1050 –1100° C for hot deformation of eutectic Ti-Al-Si-Zr system alloys is elaborated.
2. The forging up to degrees more then 60% is the optimal thermo-mechanical treatment increasing low temperature plasticity.
3. In highly deformed alloys with forging (60% and 90%) the cracks are healed during hot deformation. Simultaneously, a fragmentation of grain of eutectic structure takes place.
4. In optimal structural states deformed samples demonstrate considerable macro deformation. After forging deformation (90%) the elongation of Ti-3%Al-2%Si-5%Zr alloys reaches value 4%, in samples Ti-3%Al-4%Si-5%Zr and Ti-3%Al-6%Si-5%Zr the elongation reach accordingly 2,7 and 1,8%.
5. In material deformed by forging to low deformation power (30%) the presence of cracks was observed. It is the main reason of brittleness of low deformed alloys

Literature:

1. Firstov S.A., Vasilyev A.D., Kuzmenko M.M., Kulak L.D., Miral D., Podrezov Yu.N.. Influence of preliminary deformation on strengthening and plastic characteristics of Ti-2%Si-3%Al-5%Zr alloy. ICCE/7 International Conference on Composites Engineering Tenerife July 6-12 2001. P. 919-920.

FEATURES OF FORMING OF INTERMETALLIC COMPOUNDS IN A ZONE OF CONTACT CHROME - COATING FROM METAL OF IV GROUP.

Zykova E.V., Dubikovskiy L.F., Brodnikovskiy M.P., Sameluk A.V., Dub S.N.⁽¹⁾

I. Frantshevich Institute for Problem of Materials Science of NANU, Kiev, Ukraine

⁽¹⁾ Institute of Superhard Materials NAN of Ukraine, Kiev, Ukraine

Usage of intermetallic compounds as diffusive barrier films allows to increase the possible working temperature of many materials and alloys [1,2]. Therefore the study of kinetics of intermetallic films forming, structural features, mechanical characteristics is of interest.

In the present work the kinetics of formation of intermetallics is investigated during annealing of chromium plates with sprayed lamina of IV group metal (Ti, Zr).

For fulfillment of the work the dilute alloy of chrome BX2K was used. A film of titanium or zirconium were sprayed on plates by the size $25 \times 10 \times 1 \text{ mm}^3$ with unevenness 0,4 microns. The method of spraying was electron-beam vaporization. The installation BY-2M with vacuum $3 \times 10^{-5} \text{ Pa}$ was utilized. For deriving of high adhesion strength and needed structure of a films spraying was performed on heated substrates. The substrates temperature was 700-850 °C. Films of titanium by thickness 20-32 microns were obtained with speed of condensation $v=0,32$ and $0,54$ microns / minute. A film of zirconium by thickness 5-30 and 75 microns were obtained with speed of condensation $v=0,11$ and $0,48$ microns / minute, accordingly.

The annealings for forming intermetallic compounds were conducted in a vacuum $3 \times 10^{-3} \text{ Pa}$ in temperature range of 1100-1200 °C.

Study of a zone of reactionary diffusion was conducted on cross-cut microsections with the help of raster microscopy and X-ray microspectral analysis with Supperprobe-733, and also by indentation with Nano Indenter II and IIMT-3. X-ray phase analysis was conducted on an exterior surface of spraying films with the diffractometer ДРОН-3 in $\text{Cu-K}\alpha$ radiating.

Despite of high temperature of a substrate (up to 850 °C), formation of intermetallic phases after evaporation is not stated. The noticeable generation rate of intermetallic interlayer of TiCr_2 and ZrCr_2 is watched after annealing at

temperature 1100 °C and above. If intermetallide has formed on a cross-cut microsection at transferring through a demarcation zone between Cr and Ti (Zr) the characteristic shelf on chemical elements distribution curve obtained with help of a X-ray spectral analysis appear (fig. 1a). Nanoindentation test as well allows to determine formation of intermetallide as appearance in a diffusion zone of an interlayer with anomalously high hardness. Nanohardness of intermetallic strata are of 13,0-13,6 GPa for TiCr_2 and of 12,9 GPa for ZrCr_2 .

X-ray phase analysis has shown, that there is a formation of low temperature allotropic modification of intermetallic compounds in diffusion zone. Cubical modification of TiCr_2 and hexagonal modification of ZrCr_2 are generated.

It is established that the processes of forming of intermetallic strata at annealing of chrome with coatings from titanium and zirconium differ one from another. In case of zirconium, front of a generating interlayer of intermetallic compound is flat on both sides of stratum. The total thickness of an intermetallic compound and stayed stratum of zirconium remains practically to constant and equal original thickness of coating (fig. 1 a, b). In case of titanium, the total thickness of interlayer of intermetallic compound and stayed titanium coating exceeds original thickness of coating (fig. 1c,d). And, in the side of chrome front of growth of an intermetallic compound is flat, whereas in the side of titanium front the going around forward needles are watched. With magnification of temperature of annealing up to 1200 °C the growth of needles thickness took place.

In the table dependence of the width values of intermetallides interlayer for systems Cr-Ti, Cr-Zr on temperature and duration of annealing are given.

As follows from the table, width of a generating zone of reactionary diffusion in case of coating from zirconium is twice less, than it is for case of coating from titanium.

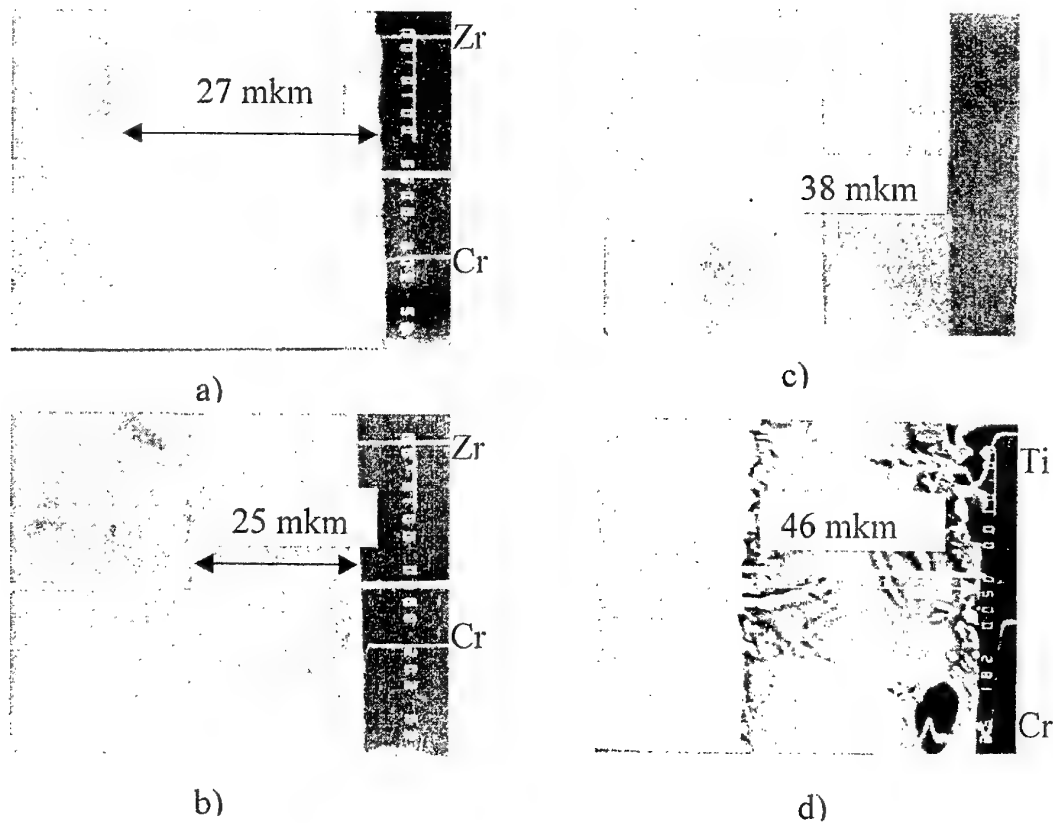


Fig. 1 Microstructure of a diffusion zone
Cr - Zr: a) After evaporation; b) after annealing 1200 °C 2 hours
Cr - Ti: c) After evaporation; d) after annealing 1100 °C 2 hours

Temperature, T, °C	Time, hour	Spraying speed, mkm/min.		
		0,11- 0,15	0,48	0,32- 0,54
		Δx , mkm		
		Zr-Cr	Zr-Cr	Ti-Cr
1100	2	-	3,3	8-10
1200	1		4	-
	2		6,8	13-15
	4		-	16
	6		10	18-20
	9		12	-

The difference of atomic radiuses of metals allows to suspect presence of distinction of partial diffusion coefficients of metals in intermetallic compounds. A variance of atomic radiuses is specially large in case of using of zirconium. However, down to self-controls during nine hours the formation of Fraenkel's pores [3] is not discovered.

At formation of an intermetallic compound volume become approximately in 3 times more than volume which was earlier occupied by zirconium atoms entering in reaction. If the thickness of a initial layer of zirconium coating is

determined with help of microphotographs, obtained mean of thickness is larger than if method of weighting and counting with assumption about of 100% dence of film is used. It means, that spraying film of zirconium has porosity and estimate gives porosity value up to 15 %. The presence of such porosity can not explain why the total thickness of an intermetallic compound and residual zirconium film remains persistence if it is not suspected that dissolution of zirconium in chrome take place.

It is possible to draw a conclusion, that selection of thickness and gravity of the spraying film allows to receive a dense stratum of the intermetallic compound without formation of Fraenkel's pores despite of diffusion coefficients difference of using metals.

Referances

1. Lazarev E.M., Kornilova Z.I. Fedorchuk N.M. Acidification of titanium alloys.- M.: Science.-1985.-138p (in Russian).
2. Modern composition materials.-M.: World - 1970.-340 p (in Russian).
3. Geguzin Ja. E. Diffusive zone.- M.: Science.- 1979.-343p. (in Russian).

RESEARCH OF DIFFUSION MOBILITY ON THE INTERFACE BETWEEN ELEMENTS OF SYSTEM Cr-Ti (Zr, Hf) AT THE TEMPERATURES 1373- 1473 K.

Pisarenko V.A., Zubets Y.E., Sameluk A.V., Dub S.N.⁽¹⁾

I.N.Frantsevich Institute for Problems of Materials Science NAS of Ukraine, Kiev, Ukraine

⁽¹⁾Institute of Superhardness of Materials NAS of Ukraine, Kiev, Ukraine

At the creation of heat resistant heat proof composite materials (CM) requires it is to know the possibility of the diffusion interaction between component of CM. CM contains strengthening and damping elements for maintenance of high strength and crack resistance, which should not lose the properties at enough high working temperatures and long times of endurance. With the purpose of preservation CM long-lived must use antidiffusion barriers for preventing interaction between individual components. This problem is very actual.

The researches of resistance intermetallides (Laves phases) Cr-Ti (Zr, Hf) system at the temperatures up to 1573 K with the purpose of their possibility the use in quality antidiffusion barriers between various alloys on a basis chromium can represent significant interest for creation CM on base of plastically chromium matrix.

The analysis of the double diagrams of a state for Cr-Ti, Cr-Zr, Cr-Hf systems has shown, that in all these systems at 30-35 at.% of a component 1Y A group the Laves phase of a Cr₂Ti (Zr, Hf) type is formed. This phase is underdone polymorph transformation from the high-temperature β -phase with a cubic lattice (A 15) in the low temperature α -phase with a hexagonal lattice (A 14).

The BT1-0 titanium foil by thickness 60 microns was used for research of system Cr-Ti pair. It was placed between two plates of the BX-2K delute chromium alloy by thickness of 1 mm, and then it was spent the diffusive welding at the temperatures 1123 or 1273 K in vacuum 10^{-2} Pa, specific pressure 25 MPa for 20 minutes under loading.

For research of system Cr-Zr a high quality (iodide) zirconium foil by thickness 70 microns was used, and for Cr-Hf pair the specimens of high quality (iodide) hafnium thinning up to 1000 microns by a mechanical way was used. For Cr-Zr system the temperature of diffusion welding was 1273 and 1323 K, vacuum 10^{-2} Pa, the for 20 minutes at specific pressure 25

MPa, and for Cr-Hf system specific pressure was increased up to 70 MPa.

The annealing was spent in vacuum 10^{-2} Pa at the temperatures 1373 and 1473 K for 2, 5, and 10 hours.

The structural researches was spent with the help of scanning electronic microscopy "Superprobe -733", which allows also to carry out local x-ray spectral analysis in a researched zone. The diameter of a probe was 3,0-4,0 microns.

It has been established, that the diffusive zone is formed during the annealing at the temperatures 1373-1473 K by initial components, which is represented a layer of intermetallide. The intermediate condition of a type "eutectics + α -phase" is not formed. The rate of intermetallide layer growth in Cr-Ti system is larger in 3-4 times, than this in Cr-Zr system (fig.1). There was the inconvenient take place at the metallographical research of Cr-Hf system connected with the division of the samples on two half during its preparation of the specimens after annealing.

The measurements of microhardness have shown, that the microhardness, for example, of TiCr₂ phase is $14,6 \pm 0,6$ GPa and almost in 6 times surpasses microhardness of the delute alloying BX-2K alloy. This implies, that the intermetallide layers can be used as strengthening layers in CM.

The researches have show, that diffusion is accompanied by the intensive formation of the pores (pores Frenkel). Probably besides formation of the pores the effect of Kirkendal may take place and, since the growth of diffusion layer goes in both parties, but mainly in the chromium side because of the large difference of the self-diffusion coefficient of chromium and metals of 1Y A group. The accounts of self-diffusion coefficient because of strong pore formation can have the large error in the party of their increase, since the effective surface actually is significant less than calculated and changes with decrease of the duration annealing. If to take into account this error, it is possible to assert, that coefficient mutual diffusive will be much larger. The microsteps are

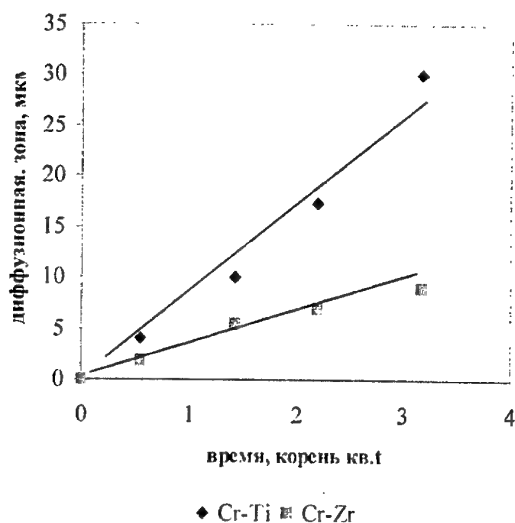


Fig.1. Change of width of the diffusion zone for Cr-Ti, Cr-Zr systems after annealing at the temperature 1373 K in vacuum against the time.

found out inside pore (fig.2), that can testify about dislocation-vacancy transfer of substance during the mutual diffusion. Thus it is possible to assume, that in the diffusion pairs the supersaturation by point defects is supported by a difference of counter flows of atoms at the expense of various diffusion coefficient of the researched component. The occurrence of the microsteps in pore is caused by that the forming surface is simultaneously drain of vacancies and dislocations, which is drive to a forming surface from volume of a diffusion zone.

Summary.

1. At the research of the diffusive mobility on the boundary of division in Cr-Ti (Zr, Hf) systems received by diffusion welding of researched components with the subsequent

annealing at the temperatures 1373-1473 K it is established, that diffusive zone is formed on the interface between components. The spent x-ray spectral analysis is determined, that the zone consists of Cr_2Ti (Zr, Hf) intermetallide.

2. The process of diffusion interaction is accompanied the intensive pores formation on the interface between components, and, with increase of the temperature and time the quantity pores is increased.

3. The experiments have shown, that the interlayers using for formation of intermetallide in the Cr-Me^{IV} system as diffusion barrier, should not exceed 5-10 microns, since at the more large thickness the pores is formed intensively on boundary of the diffusion zone, which can result to scaling intermetallide from strengthening or damping layers in the composite materials.

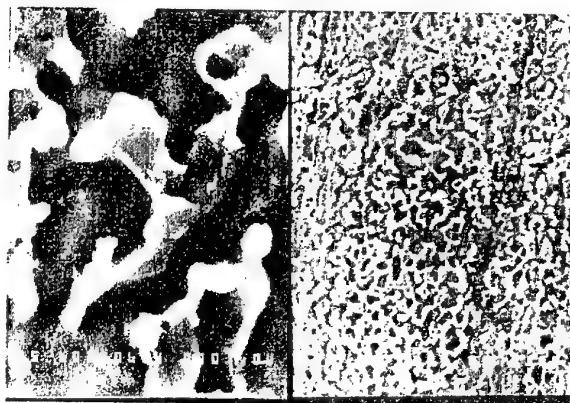


Fig.2. Photomicrographs of the pores, which formed on the interface in Cr-Hf system the after the annealing in vacuum at 1473 K for 2 hours:

a) x6000; b) x1000.

EFFECT OF CRYSTALLIZATION ON DEFORMATION OF ZrTiCuNi METALLIC GLASS INVESTIGATED BY NANOINDENTATION TECHNIQUE

Dub S.N.⁽¹⁾, Slipenyuk A.N., Milman Yu.V., Danylenko N.I.

I.M.Frantsevych Institute for Problems of Material Science of NAS of Ukraine, Kyiv, Ukraine

⁽¹⁾ Institute for Superhard Materials of NAS of Ukraine, Kyiv, Ukraine

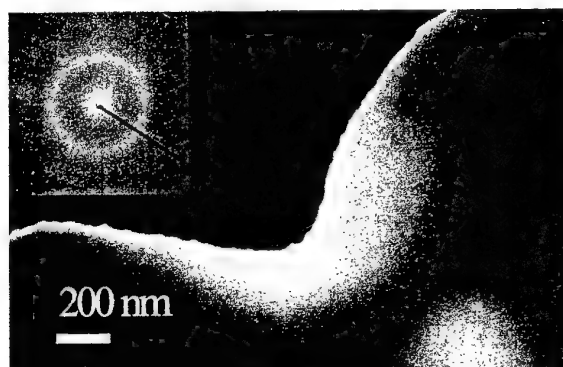
Amorphous metallic alloys were discovered more than 40 years ago. In spite of this fact they are still of interest for the scientists all over the world. First of all it is connected with their unique properties. Formerly amorphous metals were used mainly as functional materials (soft magnetic ones for instance) due to small thickness of amorphous objects. Recently discovered systems of the alloys with low critical cooling rate make possible manufacturing of bulk amorphous articles [1]. This allows using amorphous metals as a construction material, and hence investigation of mechanical properties of these materials becomes more and more actual.

The investigation presented here was performed with $Zr_{50}Ti_{16.5}Cu_{15}Ni_{18.5}$ bulk metallic glass forming alloy. The alloy was produced in the form of a thick ribbon using single roller melt spinning technique. The mechanical properties of the material were studied by an original method of cyclic nanoindentation (Nano Indenter-II device) with registration the load – penetration depth (h) curve. This method together with special data processing allows determining hardness, Young's modulus and other mechanical characteristics of the material under investigation [2]. Vacuum annealing in the temperature range of 125 – 525 °C was used for changing the alloy structure. Transmission electron microscopy and differential scanning calorimetry methods were used for investigation the structure of the annealed samples.

In accordance to the DSC data no structure transformation occurred on annealing at 125 and 225 °C, and hardness of the material did not change. Annealing at the temperature of 325 °C led to an insignificant structure modification resulted in some hardness growth. Increasing of the annealing temperature up to 425 °C allowed to obtain a mixed amorphous-crystalline state (annealing time 7.5 min) as well as nano-grained crystalline state. More coarse-grained crystalline samples were formed after annealing at 525 °C.

Mechanical behavior of amorphous (as-received), mixed amorphous-crystalline and fully crystalline specimens was studied (Fig.1). It was

shown that the process of plastic flow upon indentation is significantly different for various structural states. The transition from pure elastic loading to plastic deformation is very sharp for amorphous (as-received) sample (Fig. 2), and its further plastic flow is realized highly unevenly.



as-received



425 °C, 7.5 min



525 °C, 4 hours

Figure 1

In the case of completely crystalline alloy (annealing at 525 °C during 4 h) the transition from elastic to plastic deformation occurred uniformly and smoothly. The mixed state is intermediate with respect to mechanical behavior. Jumps are also present in the curve, but are not so strongly marked.

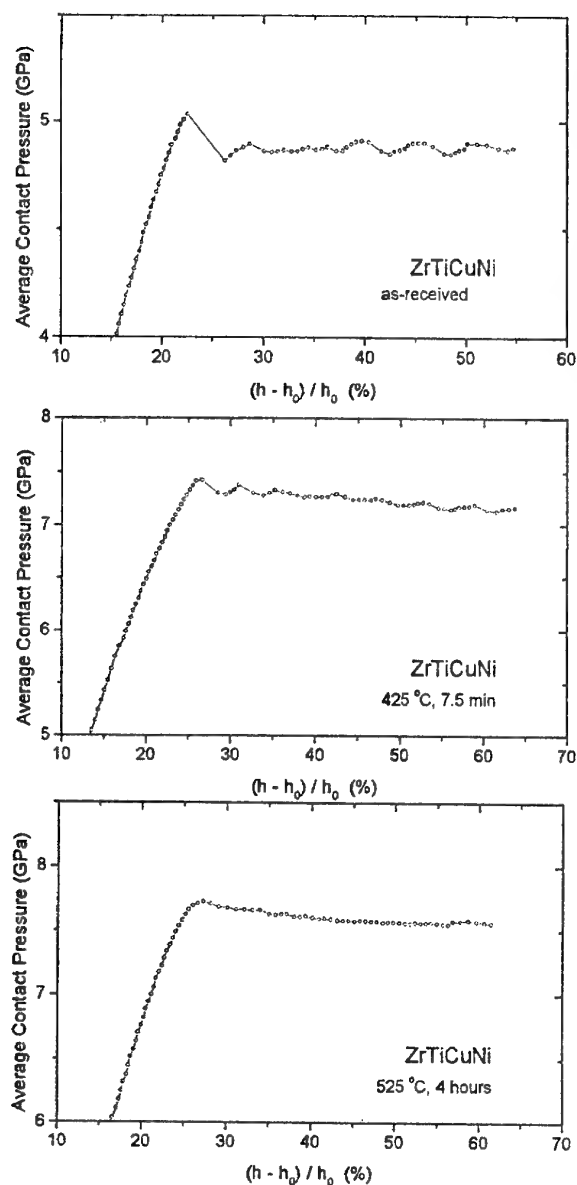


Figure 2

Non-uniform deformation of the amorphous sample during indentation is apparently connected with heterogeneous plastic flow of an amorphous alloy at room temperature. Owing to the absence of deformation strengthening the plastic flow occurs and leads to significant one-shot deformation. The view of the indentation on the surface of the amorphous alloy is given in Fig. 3. Separate portions of the material extruded

from under indenter are visible. Indentation structure confirms the non-homogeneous character of plastic flow under indenter. One may suppose that each layer formation is accompanied by sharp average contact pressure release visible in the curve.

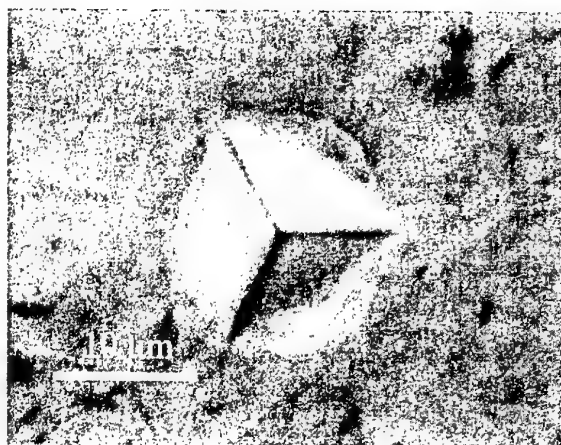


Figure 3

In mixed state the crystalline phase particles act as an effective barrier to suppress the shear deformation of the amorphous matrix. As a result deformation occurs at higher average contact pressure. Plastic flow becomes less localized, and jumps in the curve are not so strongly marked.

Homogeneous plastic flow takes place in fully crystalline sample, and plastic deformation at loading occurs uniformly and smoothly.

This work was partially funded by STCU (project 1997).

1. Inoue A. // Acta mater. – 2000. – 48. – p. 279 – 306.
2. Dub S.N. // In: MRS Symp. Proc. Vol. 505, MRS, Pittsburgh. – 1998. – p. 223 – 228.

STRUCTURE AND PROPERTIES of THE WC+8 mass % Ni CEMENTED CARBIDE FABRICATED BY PRESSURE FREE SINTERING AND IMPULSE HOT PRESSING IN VACUUM

Kovalchenko M.S., Yurchuk M.O.⁽¹⁾

I.N. Frantsevich Institute for Problems of Materials Science, the Ukraine NAS, Kyiv, Ukraine

⁽¹⁾V.M. Bakul Institute of Superhard Materials, the Ukraine NAS, Kyiv, Ukraine

The quantitative indexes of microstructure in WC+15 mass % cemented carbide fabricated by sintering in hydrogen, in vacuum as well as by hot pressing in vacuum are considered as a result of stereological study of microstructure. It is shown that sintering conditions essentially influence on the structure and mechanical properties of the cemented carbide above.

A commercial powder mixture with the content (in mass) of 8.4 % Ni, 5.9 % total carbon, 0 % free carbon, 0.07 % Fe, 0.19 % O₂, and 0.02 % N₂ is used. The mean tungsten carbide grain size in the mixture is 1.71 μm .

The sintering of specimens in hydrogen is carried out in an experimental two-zone muffle furnace with graphite heater. For vacuum sintering a laboratory vacuum furnace is used. The hot pressing of preforms in vacuum is carried out in laboratory impact machine with vacuum chamber.

Structural studies carried out on a section with three photos for each specimen. The photos are made with the use of electron microscopes "Super-Probe 733" and T-20. A total area of specimen in study amounts to 1300 μm^2 . The quantitative characteristics of structures are determined by a method of intersecting lines [1]. Processing of the structure photos by 35 intersecting lines provides an estimate accuracy of 2.5 % for the volume fraction of carbide phase, 3.5 % for the phase-boundary surface, 4–5 % for the contact surface of carbide grains, and 2 % for the representative size of tungsten carbide particles.

The mechanical properties of cemented carbides are determined by accepted methods. For determination of a density, the method of hydrostatic weighing is used.

The Vickers hardness (HV) of cemented carbide is determined in a unit TK according to an indentation diagonal length forming as a result of impression of a diamond pyramid with the corner at a top of 136°.

The transverse rupture strength (TRS) of specimens is examined in tension test machine P-5 by three-point bending with a distance between

fulcrums of 30 ± 0.5 mm. A loading tool rate is 5 mm/min. The compression strength (σ_{com}) cemented carbide is examined in a hydraulic press of the P-50 model. The working elements of test implement are made of the WC+2 mass % Co cemented carbide.

The cemented carbide fracture toughness (K_{Ic}) is determined by the method of transverse rupture stress testing on the specimens with incision. The latter is made in spark-cutting machine by brass wire with the diameter of 0.1 mm. The length and width of incision are equal 2 mm and 0.155 mm respectively.

The impact strength (KC) of the specimens is determined in impact-testing machine of the type of 04 according to the energy of the specimen fracture.

The determination of Young's elastic modulus (E) is made by the dynamic resonance method.

The materials specific electrical resistance is measured by a potential-metric method with the help of automatic potentiometer B7-16.

A number of the property determinations is fluctuated from four to six in respect to such properties as transverse rupture, compression and impact strength as well as fracture toughness. For determinations of density, hardness, electrical resistance, and elastic modulus, a number of determinations are fluctuated from six to eight.

The data of stereological examinations for the cemented carbide structure as well as determinations of their physical and mechanical properties are cited in the Table.

The structural examinations show, that contact surface between carbide grains $S_{\text{V wc-wc}}$ in cemented carbides fabricated by hot impulse pressing in vacuum is decreased in the mean by 24% in comparison with the same surface of the cemented carbide specimens fabricated by vacuum sintering, and by 30% in comparison with the carbide contact surface of the same cemented carbide fabricated by sintering in hydrogen atmosphere. The mean representative thickness of nickel interlayer in hot pressed cemented carbide is

II. PERSPECTIVE MATERIALS OF FUNCTIONAL AND STRUCTURAL PURPOSES: POSSIBILITIES OF OBTAINING NEW LEVEL OF PROPERTIES

decreased by 14 % and 29 % in comparison with the same sintered one in vacuum and hydrogen atmosphere respectively. Also the decrease in a degree of tungsten carbide grains contacts C_{WC-WC} by 37 % and 49% as well as a number of contacts per a tungsten carbide grain N_k by 33 % and 51 % in the same comparison take place.

The conditions of hot impulse pressing, when applied pressures reach up to 1200–1300 MPa, lead to lowering in specific phase-boundary surface $S_{V_{WC-Ni}}$ by 8 % and 12 % in comparison with the phase surface of the same cemented carbide sintered in vacuum and hydrogen atmosphere respectively.

Temperature reduction by 120 °C during hot impulse pressing in comparison with pressure free sintering temperature diminishes the tungsten

carbide grain growth. The mean carbide grain size of 1.71 μm is elevated to 1.90 μm , that is 11 %, during hot impulse pressing whereas the grain growth amounts to 22 % (from 1.71 μm up to 2.20 μm) during vacuum sintering and 40 % (from 1.71 μm up to 2.40 μm) during sintering in hydrogen atmosphere.

Hence, a rise in the level of physical-mechanical properties of the cemented carbide, fabricated by hot impulse pressing in vacuum, one can be accounted for improvement of its structure.

Reference

[1] Chernyavskiy K.S.: Stereology in metal science, Metallurgiya, Moscow, 1977.

Table. Stereologic characteristics of structure and physical-mechanical properties for the WC+8 % Ni cemented carbide fabricated by pressure free sintering in hydrogen atmosphere and vacuum as well as by hot impulse pressing in vacuum

Fabricating method	Pressure free sintering		Hot impulse pressing in vacuum
	in hydrogen atmosphere	in vacuum	
Volume fraction of carbide phase V_{WC} , %	85 ± 2	86.0 ± 0.9	87.0 ± 1.9
Specific contact surface of carbide grains $S_{V_{WC-WC}}$, $\mu m^2 / \mu m^3$	1.70 ± 0.08	1.59 ± 0.06	1.20 ± 0.05
Specific phase-boundary surface $S_{V_{WC-Ni}}$, $\mu m^2 / \mu m^3$	1.45 ± 0.05	1.51 ± 0.05	1.63 ± 0.05
Mean representative size of tungsten carbide grains	2.40 ± 0.04	2.20 ± 0.04	1.90 ± 0.03
Mean representative thickness of nickel interlayer τ_{Ni} , μm	0.77 ± 0.05	0.63 ± 0.05	0.54 ± 0.04
Tungsten carbide grains contiguity C_{WC-WC} , %	44.0 ± 1.2	35.0 ± 1.2	22 ± 1
Number of contacts per one grain N_k	3.7 ± 0.1	2.7 ± 0.1	1.8 ± 0.1
Density γ , g/cm ³	14.6 ± 0.3	14.7 ± 0.3	14.8 ± 0.3
Hardness HV, GPa	12.1 ± 0.6	14.1 ± 0.6	15.5 ± 0.6
Specific electric resistance ρ , $\mu\Omega \cdot cm$	22.1 ± 0.9	18.8 ± 0.8	17.5 ± 0.7
Young's elastic modulus E, GPa	620 ± 20	595 ± 20	620 ± 20
Transverse rupture strength TRS, GPa	1.4 ± 0.2	1.6 ± 0.2	2.1 ± 0.2
Compression strength σ_{com} , GPa	2.8 ± 0.5	2.9 ± 0.2	3.5 ± 0.2
Impact strength KC, kJ/m ²	35 ± 3	28 ± 3	40 ± 3
Fracture toughness K_{Ic} , MPa·m ^{1/2}	9.0 ± 0.7	10.0 ± 0.6	12.0 ± 0.6

RESEARCH OF IMPACT OF TECHNOLOGY OF RECEIVING FRAGILE MATERIALS ON THEIR STRENGTH UNDER UNI-BIAXIAL PRESSURE

G. Okhrimenko⁽²⁾, L. Dubikowsky

Institute for Problems of Materials named of Frantsevich of National Academy of Science

⁽²⁾ Institute for Problems of Strength Science NAS of Ukraine, Kiev, Ukraine

Introduction and production of problem. Non-controlled mining of metal constructional materials and their frequently thoughtless using (for example for military purposes) make threat of human society being now and in not far future on the Earth.

On this reason developing and incalcation of new non-metal materials with constructional assignment is a very important trend scientists's activity. The purpose of the present research is experimental valuation of fragile nonmetallic materials strengths under condition of uniaxial and biaxial pressure depending of their production technology.

Short bulletin about typical technologies of production materials. Investigated materials are conventionally divided into 5 groups depending on the peculiarities of their typical production technology. Glasses and glassceramics obtained from molten working mass in electric furnace are considered to the first group. The representatives of above mentioned group are quartz glass QU, technical glass S-57, on which basis the technical glassceramic STL-10 was obtained. The necessary forms and sizes of crude mass is formed from the fusion moulding into fixed forms or the align casting is used.

Raw material of the necessary forms and sizes are formed from the melt by the casting into fixed forms, pressing or the circular casting is used.

The second typical technology forecasts mechanical fragmentation of the specified chemical and mineral composition crude mass in the circular mills up to medium size elements of 38 mcm, the next moistening (H_2O up to 16 %) or preparing ceramic slurry (H_2O up to 32 %). The working mass is formed from the raw mass or it is casted into gypsum forms and is dried on the air or in electrical furnace and than is baked at the temperatures of 1100 – 1200 °C. The objects of the present research are electrotechnical porcelain (EP) and solid chemically resistant formed porcelains (SCRFP), and solid chemical resistant casted porcelains (SCRCP).

The next group of metal-ceramic materials is obtained by the technology, which is called powder one. Specially prepared powders of certain chemical composition are mixed and pressed with form heating at the same time. Than raw material is

baked in electrical furnaces at high temperatures. Glass carbon GC-2000, ferrite 30S47, titanium carbides (TC) and carbide of boron (CB) SM-1 are produced in such way. The technology of monocrystal growing is provided from the certain chemical composition melting at the given temperature. As the sample we can take monocrystallic silicon (MS) S3. Material keral K-0 was obtained by the technology of reaction exudation of ceramic material with silicon oxide content up to 65 % in fluid aluminum.

Test procedure. The samples were manufactured with the help of diamond instrument by the group method. The high of microasperity was $R_a \leq 0,63$ mcm on sides. Cylindrical samples of $\text{III}10 \times 30$ mm were tasted under uniaxial pressure conditions. Plates of $5 \times 22 \times 22$ mm were tasted under biaxial pressure conditions. Quotient of the main pressures σ_2 та σ_3 is signed as k and was equal 0; 0,25; 0,50; 0,75 and 1,00 [1, 2]. Pressure was made on the erecting work for biaxial pressure of fragile materials with lager growing speed as to the absolute magnitude of pressure σ_3 from 20 to 30 MPa/c. The accuracy of tests is proved by the polarized – optical method and by the method of moire fringe [1].

Results of the tests, discussion and conclusions. The experimental data that characterize strength of examined materials under uni- and biaxial pressure conditions are showed in the tables 1 and 2 accordingly. Sample coefficient of variation and the size of sampling are indicated as v and n_0 correspondently. Coefficient γ_T is equal to the attitude of σ_C to the analogous magnitude of glass S-57. From the tab. 1 we can see that representatives of metal-ceramic materials TC PM and CB SM-1 obtained with the help of powder technology have the largest σ_C among the examined materials. The next place (according to maximal σ_C) belongs to monocrystallic materials. The third place belongs to MC S3 which is the material produced by the monocrystal growing technology. Further in the tab. 1 in the order of the biggest strength we can see the representatives of technical constructional

II. PERSPECTIVE MATERIALS OF FUNCTIONAL AND STRUCTURAL PURPOSES: POSSIBILITIES OF OBTAINING NEW LEVEL OF PROPERTIES

ceramic (SCRCP, SCRFP, EP) and keral. The peculiarity of tasted materials is that their σ_c is within 535 (SCRCP) and 5410 (BC SM-1) and

Table 1. Experimental magnitude of strenghs σ_c examined materials under condition of uniaxial presure [3]

M*	σ_c , MPa	ν , %	n_o , piece	γ_T
Materials obtained from the crude mass melting				
1	1800	6,8	8	1,00
2	2700	6,0	267	1,50
3	3200	6,5	28	1,77
Materials obtained from the raw mass or casted from ceramic slurry				
4	535	4,7	70	0,30
5	736	12,6	18	0,41
6	998	8,8	20	0,55
Materials obtained by the powder technology				
7	940	9,9	31	0,52
8	980	8,9	15	0,54
9	3330**	13,6	10	1,85
10	5410**	8,7	10	3,00
Material obtained by the technology of monocrystal growing				
11	2145	9,7	4	1,19
Technology of reaction exudation				
12	890***	7,0	5	0,49
Constructional steels [1]				
13	240	6,2	896	0,13
*) Materials : 1. Glass S-57. 2. Glassceramic STL-10 (from the glass S-57). 3. Optical glass KU. 4. FTHSL. 5. SCRPF. 6. EF. 7. 30S47. 8. GC-2000. 9. TC PM. 10. CB SM-1. 11. MS S3. 12. Keral K-0. 13. Steel St.3				
** 3,5x5x18 mm mm samples are used				
*** 9,5x9,5x25 mm samples are used				

Table 2. Experimental magnitude of strenghs σ_3 (МПа) of examined materials under condition of biaxial presure [1,2]

M*	Quotient of the main presures k				
	0	0,25	0,50	0,75	1,00
Materials obtained from melting working mass					
13	1870	2060	2060	2045	1940
14	2184	2182	2014	1958	1787
2	2310	2670	2560	-	2730
Materials obtained from crude mass or casted from ceramic slurry					
4	513	677	696	663	610
5	791	966	928	928	947
6	998	1020	1011	866	818
*) Materials : 13. Plate glass. 14. Glass 13v.					

exceed the respective magnitude of steel St.3 in 2,2 – 22,5 times. This is a convincing evidence of obtaining constructional materials availability according to the analyzed technologies.

The important characteristic of the similar materials is their reliability in the exploitation of goods. For the examination of the materials conditionally the sample coefficient of variation ν is such magnitude, which has the value from 4.7 (SCRCP) to 13,6 % (TC PM) according to the table 1. It is appreciably that this value is equal 6.2 % for steel St. 3. Thus the technical level of the examined materials is such that allows to produce new constructional non-metallic and metal-ceramic materials with reliability that is not less then it is in traditional metals and alloys.

The selection of technology for producing new material will be determined by the technological requirements to the concrete good and technical possibility of obtaining raw material of proper sizes and characteristics. This can be illustrated by the tabl.2 data. As boundary state of casing of cylindrical ($k=0,5$) and shape ($k=1,00$) forms, that work under external hydrostatic pressure, is conditioned by strength under biaxial pressure, so plain glass, silicon STL-10, SCRCP and SCRFP under above mentioned quotient of the main pressures have the strength not less than under uniaxial pressure. On this reason this materials can be used for producing mentioned goods with diameter up to 700 and length up to 1800 mm [1,2]. The casings of the same forms also can be produced from glass 13v and EF, but at the same time we should take into account the ractual reducing of strenth when $k=1,00$ concerning to σ_c is conditioned by the kind of pressure state. The results of materials tasting produced in accordance with examined technologies indicate that the very important aim is improvement of their state with the purpose of preparing and manufacturing of new materials which would be characterized the higher magnitude of strength and reliability with comparison of the indicated in table 1 and 2.

Literature

1. Конструкционная прочность стекол и ситаллов/Г.С.Писаренко, К.К.Амельянович, Ю.И. Козуб и др. - Киев: Наук. думка, 1979.
2. Прочные оболочки из силикатных материалов/Г.С.Писаренко, К.Амельянович, Ю.И.Козуб и др. - Киев: Наук. думка, 1989.
3. Охрименко Г.М. Характеристики прочности и упругости силикатных и керамических материалов//АН УССР. Ин-т пробл. прочности. - Препр. - Киев, 1992. - 46 с.

THE INFLUENCE OF METALL-LUBRICANT ON COPPER BASIS ON THE STRUCTURE AND TRIBOTHCHNICAL CHARACTERISTICS OF THE COMPOSITE ANTI-FRICTIONAL MATERIAL THAT WORKS IN THE VACUUM

A.G. Kostornov, O.I.Ficshich, Y. Simeonova ⁽¹⁾, T.M. Chevychelova, A.D. Kostenko

Frantsevich Institute of material science problems, National Academy of Science, Kiev, Ukraine

⁽¹⁾ Space Reaearch Institute, Bulgaria Academy of Sciences, Sofia, Bulgaria

The influence of the quantity of the metallic lubrication on the structure and tribological properties of compositional anti-frictional materials has been researched on the alloys with copper base. The alloys were got by two methods: by casting and hot pressing.

The estimation of the workability of the alloys under research in the air was conducted on the machine of friction MT-62M according to the scheme shaft-bush in the pair with hardened steel 45 with constant load 200 VGF and variable speeds of sliding - 6, 8, 10, 12 m/s. The characteristics got ware confronted with their initial structural condition.

The cast bronze is coarse-grained; the impurities of the lubricant in it are uneven. The sintered bronze is more small-grained; the impurities of the lubricant in it are even and fill all the space at the boarders of the grains of the solid solution.

As the research showed the tribological properties of the sintered bronze, independent on the quantity of metallic lubrication, in all cases are higher then in cast bronze, that is well in accord with the structure of material.

The formation of the pellicle is lightened; the surface of friction is plain.

In case of the friction of the cast bronze at the temperature increase there is softening, melting of the lead that leads to the violation of the cohesion of the grains and decrease of the carrying ability of the cast bronze.

Besides, it is ascertained that bronze that contains about 18-21% of metallic friction obtains the best complex of frictional properties.

Therefore, it is determined that the increase of tribo-technical properties of compositional anti-frictional materials while injecting the alloy on the lead basis as a metallic lubricant can be reached if the following conditions are fulfilled:

1. The content of the metallic lubricant should be in the range of 18-21%
2. The metallic lubricant must be evenly spread as rather small impurities between the grains of the solid solution.
3. Bronze should be got on the technology of hot pressing that provides the getting of the structure with which the alloy, having high mechanical properties, is able to form the secondary structures, that decrease the work of friction

Hence, managing the content and technological process, it is possible to get the structure providing good anti-frictional properties.

MICROSTRUCTURAL MODIFICATION OF AS-CAST HYPOEUTECTIC Ti-Al-Si-Zr ALLOYS BY MICROALLOYING WITH ADDITIONAL ELEMENTS

Gornaya I., Kulak L., Miracle D.⁽¹⁾, Senkov O.⁽²⁾, Firstov S.

Frantcevykh Institute for Problems of Materials Science of NAS of Ukraine, Kyiv, Ukraine

⁽¹⁾Air Force Wright Laboratory, Materials and Manufacturing Directorate, Wright-Patterson AFB, OH USA

⁽²⁾UES, Inc., 4401 Dayton-Xenia Rd, Dayton, OH 45432, USA

As-cast eutectic alloys of a Ti-Al-Si-Zr system are attractive structural materials for elevated temperature applications due to their high oxidation and wear resistance and high temperature strength [1-2]; however, they are macroscopically brittle at room temperature (RT). Microstructure modification is one of the common ways to increase ductility of as-cast alloys [3.]. In hypoeutectic Ti-Al-Si-Zr alloys such microstructural modification should result in refinement of beta-Ti dendrites and eutectic colonies. In the current work such modifying elements as B, La, Y, Ce, Sc, Ga, and Bi were used to refine microstructure of an as-cast Ti-3Al-6Si-5Zr (wt.%) alloy. Optical and scanning electron microscopy methods were used to study microstructure, and Vickers hardness, bending and tensile tests were used to evaluate mechanical properties.

Selection of the modifying elements was based on the literature data and on the analysis of equilibrium diagrams of binary systems in the Ti-rich part [4-5]. From the selected elements, B, La, Ce, Sc, and Ga are known to be α - stabilizers, and Bi is a β -stabilizer [6].

The hypoeutectic Ti-3Al-6Si-5Zr alloy in as-cast condition is mainly composed of β -transformed dendrites (α -Ti or α' martensite + secondary Ti_5Si_3) and eutectic colonies (α -Ti + Ti_5Si_3) (Fig. 1 a,b). Small additions of B, Y, La, Ce, Sc, Ga or Bi refines primary dendrites and eutectic colonies, including eutectic silicides. For example, gradual refinement of the β -dendrites and eutectic silicides was observed when the amounts of Sc increased from 0.04 to 0.25%, and the modifying effect of 0.2 wt.% Sc is shown in Fig. 1(c,d). An addition of Bi (from 0.04 to 0.2 %) to the basic alloy refined both β -dendrites and eutectic silicides

Computation analysis of SEM images using Furie and Vivelett transformation [7] allowed to determine the prior beta dendrite spacing to be 22-26 μm in the alloy without modifying elements. An addition of 0.05% B or 0.08% Sc decreased

the dendrite spacing to 11 μm or 15 μm , respectively. The effect of La and Bi on refinement was between these two edges. Thus boron is more effective modifying element than the other elements.

Vickers hardness measurements showed a small increase in hardness after addition of 0.05% B. On the other hand, small additions of Y, La, Ce, or Ga led to a decrease in the Vickers hardness. The latter may be connected with a decrease in the oxygen content in the α -Ti solid solution due to formation of the rare earth metals (REM) oxides, because these elements have higher affinity for oxygen than titanium.

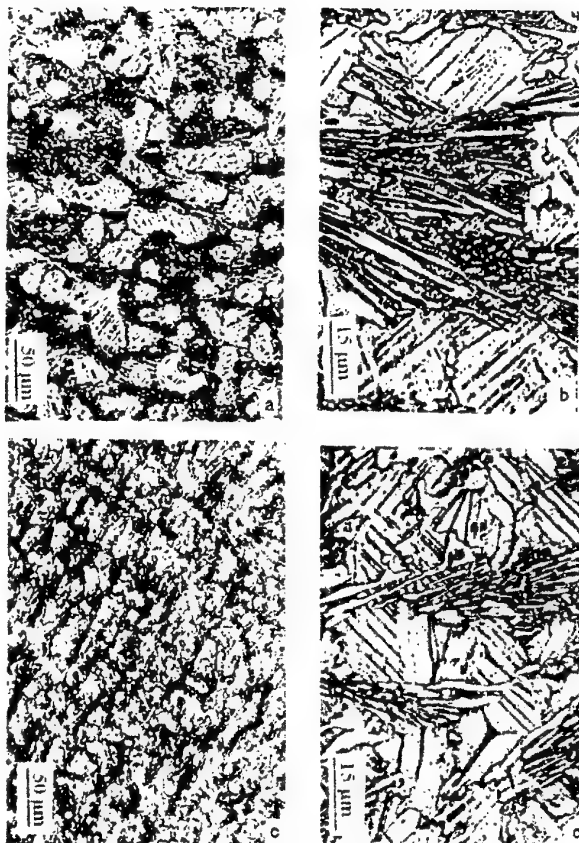


Figure 1. Microstructure of as-cast Ti-3Al-6Si-5Zr alloy: (a, b) non-modified and (c, d) with an addition of 0.2 wt. %Sc.

The effect of modifying elements on room temperature (RT) plasticity of the as-cast Ti-3Al-6Si-5Zr alloy was studied using 3-point and 4-point bending tests. Typical stress-strain curves are shown in Fig. 2. Modifying of hypoeutectic Ti-3Al-6Si-5Zr alloy with small additions of Y, La, Ce, Bi, Sc, Ga was found to increase RT bending plasticity. For example, the plasticity almost doubled after alloys with 0.08% Bi or 0.08% Sc. An addition of 0.05 %B and 0.08 % Y decreased the bending plasticity.

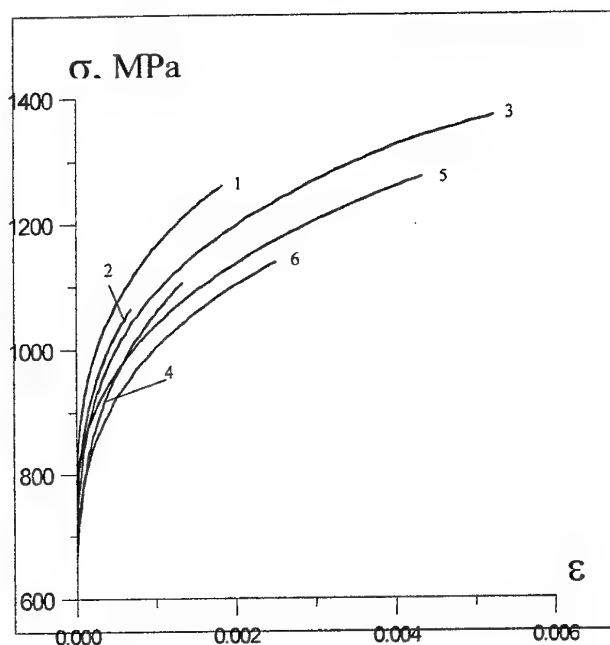


Figure 2. Stress-strain curves under 4-point bending of as-cast Ti-3Al-6Si-5Zr alloy: (1) with no modifying elements; and (2-6) with an addition of (2) 0.05B, (3) 0.08Bi, (4) 0.08 Y, (5) 0.08 Sc, and (6) 0.08La.

Tensile tests carried out in the temperature range of 600-800°C showed that additions of Y, La, or Sc in the amounts of 0.08% did not affect the high temperature strength, while an addition of 0.05% B increased the strength and an addition of 0.08% Bi decreased it. In this temperature range, the non modified alloy showed a rather high tensile ductility that increased from about 1% at 600°C to

24 % at 800°C. Additions of Y, La, Sc, or B led to a decrease in the temperature effect on ductility and an overall decrease in ductility while an addition of 0.08% Bi led to an increase in ductility in this temperature range. It is concluded that an optimization of the amount and combination of the modifying alloying elements is required to achieve better refinement of the microstructure and better property combinations of the as-cast alloy.

Acknowledgements

The authors would like to acknowledge funding of this project from the US Air Force Office of Scientific Research, and an assistance of the Science and Technology Center of Ukraine.

References:

1. S.Firstov. Titanium-matrix composites in comparison with ceramic ones. In: *Advanced Multilayered and Fibre-Reinforced Composites*, Ed. by Y.M. Haddad, Nato ASI Series 3, High Technology, V.43, 1998,p.175-186.
2. S.A. Firstov, Yu.N. Taran, V.I. Masur et al. *Noval metal-ceramic materials based on titanium. Metal i litje Ukrainy*, 1999, N11-12, p.42-46 (In Russian).
- 3.. Maltzev M.V. *Modification of metals and alloys structure*. - Moscow.-Metallurgy. - 1975. - 304 P. (In Russian)
4. Masalski T.V., Subramanian P.R., Okamoto H., Kasperak I. (Eds.) *Binary Alloy Phase Diagrams*. 2nd ed., V.I.-Ohio: ASM Int.materials Pard.-1990.
5. *Phase Diagrams of Binary Metallic Systems V.1,V.3*.-Moscow.-Metallurgy.-1999. (In Russian)
6. Molchanova E.K. *Atlas of Phase Diagrams of Titanium*.-Moscow.- Tehnika.-1964.--385 P. (In Russian).
7. Minakov N.V., Krasikova I.N., Kartuzov V.V.et al. Estimation of structure parameters of as-cast hypoeutectic type alloys by methods of computer transformation of image. *Electron microscopy and strength of materials. Proceedings of IPMS NANU*, 2001. P. 113-118 (In Russian).

ACID RESISTANT CERAMICS ON THE BASE OF SLAG WASTES OF THE METALLURGY INDUSTRY AND WALL BRICK WASTES

Vlasova M.⁽¹⁾, Kakazey M.⁽¹⁾, Gonzales-Rodriguez J.G.⁽¹⁾, Dominguez G.⁽¹⁾, Tomila T.⁽²⁾,
Kilimnik A.A.⁽³⁾

⁽¹⁾ The Autonomous University of State of Morelos, Cuernavaca, Mexico

⁽²⁾ The Institute for Problems of Materials Science, National Academy of Sciences of Ukraine,
Kiev, Ukraine

⁽³⁾ The State Technical University of Construction and Architecture, Kiev, Ukraine

Large volumes of slag wastes of the metallurgy industry and wastes of the wall brick production call for the development of technologies providing processing of this type of silicate materials into ceramics with new properties. It has been shown [1-5] that oxide and nonoxide ceramics possessing a complex of new properties can be prepared on the base of slags different in composition.

The high-energy grinding of a slag with the composition (mass %) 52.00 SiO₂, 6.5 Al₂O₃, 11.49 FeO, 21.81 CaO, 6.48 MgO initiates the formation of binding properties in the given disperse system. An analogous treatment of brickbats also results in the same effect. By using different conditions of grinding of individual components and their mixtures, different slag/brickbats ratio, by introducing brickbats as a filler with different particle sizes, one can prepare building ceramics with a complex of new properties (Fig. 1)

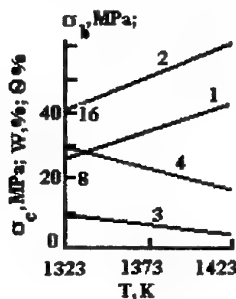


Fig. 1. Changes in the physico-mechanical characteristics of bricks prepared from the mixture 60 mass % slag + 40 mass % brickbats.
1 – bending strength, 2 – resistance to compression, 3 – water absorption, 4 – porosity.



Fig. 2. IR-spectra of the slag (1), slag ground in water for 300 s (2), and bricks (3).

IR spectroscopy is the most sensitive and informative method of investigation of initial stages of formation of hydrated calcium silicates, responsible for the formation of binding properties of a disperse system, and of the increase of their content. From absorption bands at $\nu \sim 3420$, 1620, and 1440 cm⁻¹ (Fig. 2) one can control the conditions of grinding of individual components and their mixture and choose the required water/solid ratio (Fig. 3).

In the stage of preparation of the unfired ceramics, the conditions of thermal-vapor treatment are controlled well from the change of the appearance and intensity of the IR absorption bands of hydrated calcium silicate.

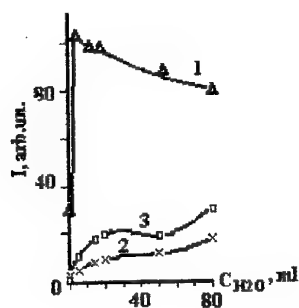


Fig. 3. Variation of the intensity of IR-absorption bands after grinding slag with different water content.

1 - $\nu \sim 1000 \text{ cm}^{-1}$, 2 - 3420 cm^{-1} , 3 - 1440 cm^{-1} .

In the preparation of the fired ceramics on the base of slag containing iron oxides, the hedenbergite phase forms. It favors the formation of the acid resistance properties of a ceramic tile (Fig. 4).

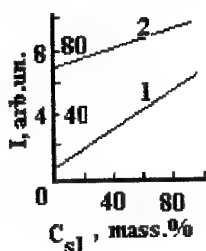


Fig. 4. Changes in the content of the hedenbergite phase (1) and the acid resistance (2) in bricks obtained at 1373 K, 1 h. from slag-brickbats mixtures.

On base of the mixture slag (8-30 mass %)-clay (40-72 mass %)-brickbats (10-40 mass %) ceramic specimens with the following characteristics were obtained: $\sigma_{\text{com}} \sim 43\text{-}50 \text{ MPa}$, $\sigma_{\text{bend}} \sim 16\text{-}18 \text{ MPa}$, water absorption of 3-4 %, thermal expansion coefficient of $(6,8\text{-}7,0) \cdot 10^{-6} \text{ K}^{-1}$, modulus of elasticity of $(3\text{-}2,9) \cdot 10^4 \text{ MPa}$, thermal shock resistance equal to 8-9 cycles at $T \sim 1400\text{-}1430 \text{ K}$, resistance to acid attack of 97-98%.

The studies carried out showed that the indicated operating parameters made it possible to obtain an acid resistant ceramic material with good physicomachanical characteristics on the base of slag-brickbats and slag-brickbats-clay mixtures.

REFERENCES

1. Vlasova M.V., Kilimnik A.A., Golubnichi A.V., Tomila T.V., Matsera V.E. Properties of ceramics on base of clay-slag mixtures of ferronickel process. / *Ceramica Acta* (1997) v. 9, No. 2/3, p.19-35.
2. Vlasova M.V., Kilimnik A.A., Golubnichi A.H., Tomila T.V. Crushing of granulated ferronickel cinder for acid proof ceramic production. / *Ecotechnologies and Preservation of Resources* (1998) No. 2, p.39-43.
3. Vlasova M.V., Lavrenko V.A., Dyubova L.D., Tomila T.V., Isaeva L.P., Smimov V.P. Investigation of the fine-dispersion silicon nitride and oxynitride powders manufactured by titanium-magnesium production waste nitriding. / *J. Materials Synthesis and Processing* (1999) v.7, No. 3, p.151-157.
4. Vlasova M.V., Lavrenko V.A., Dyubova L.D., Tomila T.V., Isaeva L.P., Podchernyaeva I.A. Formation of ultrafine silicon carbide from waste of titanium-magnesium production / *Ceramica Acta* (2000) 12, No. 3, p.68-78.
5. Vlasova M.V., Lavrenko V.A., Dyubova L.D., Gonzales-Rodrigues J.G., Kakasey M.G. Nitriding of Ferrosilicon Powders/ *J. Materials Synthesis and Processing* (2001) v.9, No. 3, p.111-117.

SIMPLEST SYNTHESIS OF FULLERENES USING ECONOMIC ARC DISCHARGE POWER SOURCE

Chujko A.A., Dymenko V.V.*, Kasumov M.M.,

Malashenkov S.P., Ogenko V.M., Paton B.E. *

Institute for Surface Chemistry of the NAS of Ukraine, Kyiv, Ukraine

* E.O.Paton Electric Welding Institute of the NAS of Ukraine, Kyiv, Ukraine

The method of synthesis of fullerenes, well-known since 1990 [1], i.e. the arc discharge using graphite electrodes in an inert gas atmosphere, is still the most productive and widely applied in the art. This method is employed to produce fullerene-containing carbon black in the discharge. Fullerenes are separated from carbon black by means solvents and filters. Liquid chromatography is used for separation of fullerenes. Out of the above operations, the arc discharge one is considered to be the most power-consuming process, making up the major part of the cost of a synthesized material and, therefore, the main limiting factor [2].

1. *Calculations.* Parameter S , defined as a ratio of mass of synthesized fullerenes, M , to power Q consumed for the synthesis process, may serve as an objective parameter for estimation of power efficiency of the discharge, i.e

$$S = M/Q, \quad (1)$$

where values M and Q are determined as follows:

$$M = a_{es} \cdot \alpha \cdot q \cdot t, \quad (2)$$

$$Q = W \cdot t, \quad (3)$$

where: a_{es} is the coefficient of transformation of the electrode material into the fullerene-containing carbon black [relative units, < 1]; α is the content of fullerenes in carbon

black [relative units, < 1];

q is the electrode erosion [g/s];

t is the fullerene synthesis process duration [s];

W is the arc discharge power [kW].

The calculations were made using equalities (1-4), experimental results [3] and data on different fullerene synthesis methods taken from review [2]. Our calculations show that the highest value of parameter S is achieved in the He arc discharge: $S \approx 0,8 \text{ g/kW} \cdot \text{h}$

(5)
With such a value of parameter S fullerenes synthesized in the arc would have been advantageous as compared with conventional materials in a number of important area [2], such as pharmaceuticals and diamonds synthesis. ...However, an objective calculation of costs of synthesis considerably diminishes optimism. Power losses for ballast resistance used to provide

stability of the discharge decrease the value of parameter S in 1.5-4.0 times. These losses are minimum if the arc is powered from a source with a steeply drooping characteristic. A welding transformer has the most economic operation among other power sources with a steeply drooping characteristic.

2. *Description of an experimental installation.* 2.1. For the investigations we developed a source for synthesis of fullerenes, based on the arc discharge. Graphite electrodes for the discharge were made with a geometry similar to electrodes for the HF-discharge described in [4]: rod with a diameter of 6 mm and conical aperture in a disc with a minimum diameter of 5 mm. The possibility is provided for feeding the rod type electrode as it burns down.

The next unit is a space for drift and collection of the synthesis product, attached to the discharge chamber. In our source it is a quartz cylinder 50 mm in diameter and 500 mm long. The cylinder is covered by a lid with an orifice. In initial measurements the quartz cylinder was replaced by a copper one 100 mm long.

The discharge chamber, components to which the discharge electrodes were secured, and walls of the drift space were cooled with water. For this the quartz cylinder was fitted with a system of copper tubes. Locations of attachment of the components were sealed with fluoroplastic. Seals protect cavities from ingress of the atmospheric air in the case of an excessive pressure in the cavity, as compared with the atmospheric one. Auxiliary gas Ar and working gas He were fed to the cavity of the source through a buffer volume at the location of the rod electrode attachment. The gas supply lines were equipped with pressure regulators and rotameters.

An experimentally selected orifice was made in the drift tube lid to ensure a controlled gas flow from the point of introduction and over the entire volume of the fullerene source.

2.2. To power the arc, our source uses a commercial frequency transformer with a regulated dispersion flow, i.e. the TDM-317 U2

II. PERSPECTIVE MATERIALS OF FUNCTIONAL AND STRUCTURAL PURPOSES: POSSIBILITIES OF OBTAINING welding rectifier with the USGM NEW LEVEL OF PROPERTIES

stabilizer. The stabilizer comprises the a.c. source, capacitor and thyristorized switch with an electronic control unit [5, 6], connected in series. Connection of the USGM arc stabilizer to the transformer makes the power source versatile and equivalent to the rectifier.

With such a connection of the transformer and USGM, the arc is initially ignited by a contact method. Upon ignition, at the moments of transition of the mains voltage through zero the arc is maintained by a voltage pulse with an amplitude of 200-500 V and duration of 10^{-5} s, formed by USGD. With the discharge ignited, the electrodes are drawn apart and installed at a distance optimal for the working conditions.

3. *Experiment.* 3.1. Prior to ignition of the discharge, the atmospheric air in the fullerene source cavity was replaced by purging with Ar and then, immediately before the discharge, with He. The arc was reliably ignited by bringing the electrodes in contact, and was burning until the electrodes were drawn apart to a distance of 3-7 mm. The tests were conducted for 0.5-5.0 min at a current of 60-200 A, the He gas flow rate amounting to 20 l/min. Bright glow of the discharge electrodes prevented observation of a clearly defined plasma jet, such as that observed in the HF-discharge [4].

With the discharge ignited, the working gas carries the products of plasma-chemical reactions out of the electrode materials. The product is deposited on the water-cooled drift space walls. The amount of the material produced was monitored visually by formation of a deposit on the quartz cylinder walls. Density and length of the deposit along the length of the quartz cylinder increased with an increase in the discharge current and the working gas flow rate. It was noted that a deposit of a small thickness might have a different color, i.e. from purely black to black and brown.

3.2. Oscillograms of current and voltage of the arc with the graphite electrodes are similar to those of the welding arcs using conventional materials: a clearly defined ignition peak at a change of polarity at the arc, rising to a half sine wave length, and then a constant voltage (plateau) for half a period.

Spikes are formed on the half period plateaus of the oscillograms some time after ignition of the graphite electrode arc, as opposed to the conventional arc, at a discharge current of about 100 A and higher. The spikes in the oscillograms correspond to wandering of the cathode spot [7] along a contour of the graphite electrode. This results in elongation and shortening of the arc and, therefore, decrease and increase in the arc voltage by a value of the spike.

The high power density at the cathode spot (about 10^7 W/cm²) and, accordingly, the high concentration of plasma in the plasma column adjoining the spot, as well as their chaotic wandering over the cone surface, are the effective sources of particles C, C* and C+. Formation and the probability complete formation of fullerenes of them are determined by temperature, concentration of carbon vapor and working gas flow rate.

4. *Investigation of the synthesized material.* Carbon black deposited on the walls of the quartz cylinder and copper tubes was removed mechanically and immersed into benzene. The presence of fullerenes in this solvent showed up as a marked coloring of the solution. It is in this way that the discharge conditions necessary for synthesis of fullerenes were established. These conditions correspond to formation of a brown tint of a deposit on the quartz cylinder walls.

The fullerene-containing carbon black was also treated in xilol. A solution produced in this case had a less marked coloring. Evaporation of the solvent resulted in crystals characteristic of fullerene associates, that formed on the surface [1].

To obtain the IR-spectrum, several successively evaporated layers of the concentrated benzene solution of fullerene were deposited on the KBr-glass and KRS-5. The IR-spectrum differing from the known ones [1, 8] was obtained on our sample. This is associated with the presence of a mixture of fullerenes in our sample.

Peculiar feature of the discharge is a deposit buildup on a conical orifice and, in some cases, on the rod electrode.

- [1]. W.Krätschmer, Lowell D.Lamb, K.Fostiropoulos & Donald R.Huffman. Nature.- 1990.- 347.- № 6291.- P.- 354. [2]. A.A.Bogdanov, D.Draiger, G.A.Dyuzhev // Zhurnal Tekhnicheskoy Fiziki. - 2000.- 70.- №5.- P. 1. [3]. D.Afanasyev, I.Blinov, A.Bogdanov, G.Dyuzhev, V.Karagaev, A.Kruglikov // Zhurnal Tekhnicheskoy Fiziki.-1994.- 64.- №10.- P. 76. [4]. G.N.Churilov. Pribory i Tekhnika Eksperimenta - 2000.-№1.- P.5. [5]. B.E.Paton, V.A.Zavadsky // Avtomaticheskaya Svarka. -1956. - №3. - P.26-35. [6]. I.I.Zaruba, V.V.Dymenko, V.V.Bolotko // Avtomaticheskaya Svarka. -1989. - №10. - P.46-52.[7]. I.G.Kesaev. Cathode processes of the electric arc.- Nauka Publ. House.- 1968. [8]. A.P.Shpak, Yu.A.Kunitsky, V.L.Karbovsky. Cluster and nano-structural materials.- V.1.- Kyiv: Akademperiodika, 2001.- P.206.

PECULIARITIES OF PLASTIC DEFORMATION OF WC SINGLE CRYSTAL

Yu.V. Milman¹, S. Luyckx², S.I. Chugunova¹, I.V. Goncharova¹, S.N. Dub³

¹ Frantsevich Institute for Problems in Materials Science, NAS of Ukraine, Kyiv

² University of Witwatersrand, South Africa

³ Bakul Institute of Superhard materials, NAS of Ukraine, Kyiv

Being a unique refractory compound, tungsten carbide combines a high hardness (~20 GPa) and high Young's modulus (~720 GPa). Thanks to this set of properties tungsten carbide possesses the plasticity characteristic δ_H [1, 2] higher than other refractory compounds.

For WC $\delta_H \approx 0.82$, meanwhile δ_H is noticeably lower (0.3-0.6) for other as well as carbides, borides and nitrides. Just this combination of mechanical properties of tungsten carbide stipulates its effective implementation as the main component for hard alloys WC-Co.

While an employment of the composite WC-Co as a cutting or drilling tool, an intensive heating is observed. Accounting for this, a present effort involves an investigation of the temperature dependence of hardness and plasticity characteristic δ_H for WC single crystal and hard alloys.

Single crystals WC (0001) obtained by Takahashi technique [3] and hard alloys WC-6%Co and WC-15%Co were investigated. Grain size of WC in hard alloys was of about 1.17 μm .

Microhardness of WC single crystal was measured in a temperature interval of 20-900°C, in vacuum with the load on the indenter of 5 N and hardness of WC-Co composites was measured with the load of 60 N (Fig.1). The temperature dependence of δ_H was compared with one for hard alloys and other refractory compounds (Fig.2).

As it can be seen from Fig.1, the temperature dependence for of WC hardness has a form characteristic other covalent materials, namely a linear dependence $HV(T)$ at low temperatures and exponential one at elevated temperatures. Activation energy for dislocations movement defined from the temperature dependence of hardness [4] turn to be $U \approx 1.8$ eV, and this approximately corresponds to the activation energy for dislocations movement in covalent crystals and other refractory compounds [4]. For hard alloys WC-Co the temperature dependence of hardness is of other type. HV weakly depends on the temperature in a broad temperature range of 20-600°C.

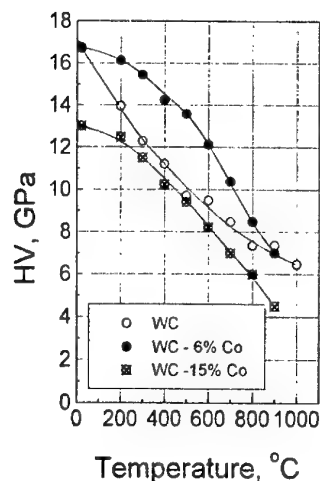


Fig.1. Temperature dependence of hardness WC single crystal and hard alloys

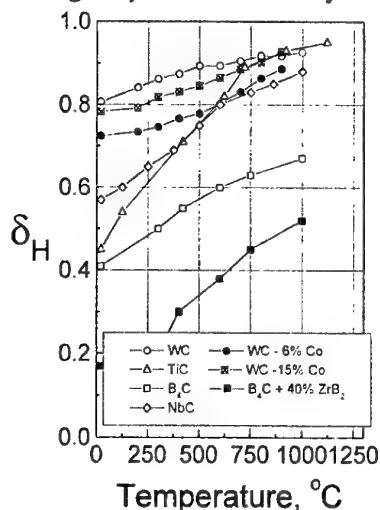


Fig.2. Temperature dependence of plasticity characteristic δ_H for WC single crystal, hard alloys WC-Co and a number of refractory compounds

This is governed by a peculiarity of deformation mechanism for composites WC-Co with a low WC grain size d and even smaller thickness of cobalt layers (ℓ). For each component of alloy (WC and Co) the Hall-Petch relation $\sigma_s = \sigma_0 + K_y d^{-1/2}$ is true for yield stress (and hardness). The value of the second term of this is high because the value d (and especially of ℓ) is low and depends weakly on temperature up to 600°C [5]. That is why, in a broad temperature

range of 20-800°C hardness of WC-6%Co alloy turns to be even higher than hardness of WC single crystal. One more tangible distinction in hardness of WC and WC-Co alloys is different type of the dependence of hardness versus load. For WC single crystal dramatic drop of hardness with the growth of load is observed since the free path length grows up with the growth of indenter print size (Fig.3). At the same time for WC-Co alloy the free path length is defined by the size of structural elements, and hardness depends on the load very weakly.

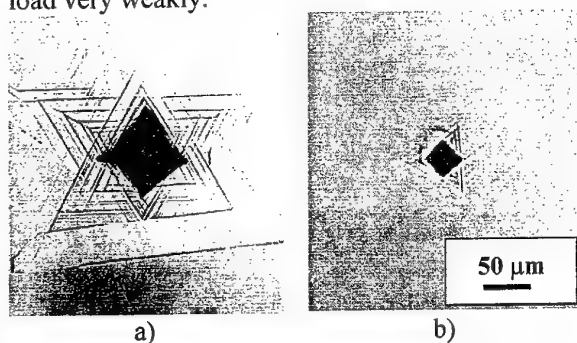


Fig.3. Prints and slip lines for WC single crystal at different load on the indenter P:
a) P = 50 N; b) P = 10 N

The plasticity characteristic of tungsten carbide δ_H is still lower than the critical value 0.9, and therefore while standard tension and bending tests, tungsten carbide shall behave as brittle [1]. Apart from that, a small size of WC samples did not permit to carry out mechanical tests. Therefore to define the mechanical properties of WC various techniques of indentation [4] were employed. The values of δ_H for WC and TiC are almost similar only if the temperature is higher than 700°C.

A comparison of hardness of WC single crystal with hardness of WC grain in hard alloy performed by nano-indentation technique revealed that tungsten carbide in hard alloy VK20KS with a grain size of 12-15 μm has the lower hardness and Young's modulus (Tabl.).

Hardness and Young modulus at a load of 60 mN

Material	E, GPa	H, GPa
WC (0001)	758±19	31.5±1.0
Tungsten carbide grain in alloy VK20KS	512±53	20.7±2.7

The mechanical properties of WC (0001) and WC grain in WC-Co hard alloy were studied also in interrupted depth-sensing nanoindentation experiments (loading – reloading technique).

The curve of elastic-plastic loading obtained by interrupted nanoindentation consists of two portions. First portion is the elastic loading of the

initial indent (Fig.4). The slope of the elastic portion of the deformation curve is in proportion to Young's modulus. Second portion characterizes the resistance to the plastic deformation at a point loading. Such a deformation curve does not depend on the depth of the initial indent and characterizes the mechanical behavior of materials under the point loading conditions. The last point in the deformation curve is the hardness at 90 mN load measured using Oliver and Pharr approach [6]. The difference of deformation at point loading from that at uniaxial tension lies in the fact that the plastic deformation of material in indent is constant and load independent. It depends on the indenter shape and for Berkovich indenter is equal to 9.7%.

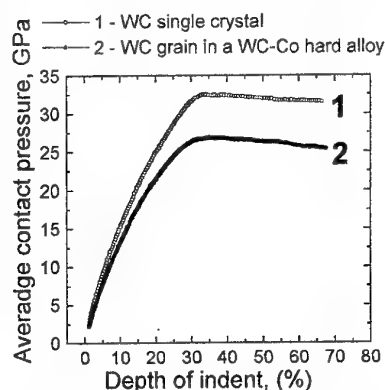


Fig. 4. Curves of elastic-plastic loading obtained for WC single crystal and WC grain in WC-Co hard alloy (VK20KS) by reloading of the initial indent

Fig.4 confirms the ideas that deformation of WC grain in hard alloy occurs at a lowered stress and the value of Young's modulus is lower than for WC single crystal.

Acknowledgements. Authors acknowledge STCU for partial financial support of this effort under the project #1997.

References:

1. Yu.V.Milman, B.A.Galanov, S.I.Chugunova. *Acta Mater and Met.* **41**, 9, 1993, 2523-2532.
2. Yu.V.Milman. In: *Advanced Materials Science: 21st Century*, ed: Cambridge International Science Publishing, 1998, 638-659.
3. T.Takahashi, E.J.Freise. *Phil Mag.* **12**, 1, 1965.
4. Yu.V.Milman. In: *Materials Science of Carbides, Nitrides and Borides*, eds.: Y.G.Gogotsi and R.A.Andrievski, Kluwer Academic Publishers, 1999, 323-336.
5. Yu.V.Milman, S.Chugunova, V.Goncharuck, S.Luyckx, I.T.Northrop. *J.Refractory Metals & Hard Materials* **15**, 1997, 97-101.
6. W.C. Oliver and G.M. Pharr. *J. Mater. Res.*, **7**, 1992, 1564.

STRUCTURE AND PROPERTIES OF AL-8%FE-3.4%CR ALLOY PREPARED FROM RAPIDLY SOLIDIFIED MELT FLAKES

Gornaya I., Kusmenko N., Kulak L., Miracle D.⁽¹⁾, Sarzhan G., Senkov O.⁽¹⁾, Firstov S.

Frantsevich Institute for Problems of Materials Science of NAS of Ukraine, Kiev, Ukraine

⁽¹⁾Force Wright Laboratory, Materials and Manufacturing Directorate, Wright-Patterson AFB, OH USA

Higher mechanical properties of aluminum alloys are attainable through the use of processing routes, which provide high solidification rates during the melt crystallization resulting in anomalous oversaturated solid solutions and new metastable phases that favorably influence then the material properties.

The Al-8Fe-3.4Cr (wt. %) alloy was prepared by the melt atomization technique upon the surface of a rotating copper disc under the atmosphere of an inert gas. The alloy was solidified at around 10^6 °C/sec during crystallization. This technology allowed formation of rapidly solidified flakes, which were cold pressed. After the billets were vacuum compacted the density of specimens was 98 %. The vacuum forging was followed by hot extrusion.

Light metallography, transmission electron microscopy (TEM) and X-ray phase analysis were used to study the alloy structure.

A TEM examination of the structure of rapidly solidified flakes revealed quasicrystals being in the form of roundish particles having a specific (black-gray) contrast. They measure from around 60 to 120 nm. Coarser quasicrystals of around 500 nm are sometimes encountered. The inner structure of quasicrystals can be clearly seen in the dark field (Fig. 1b).

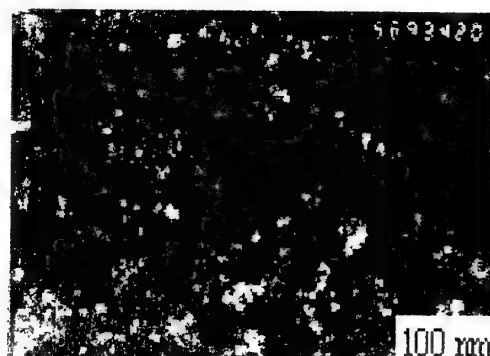
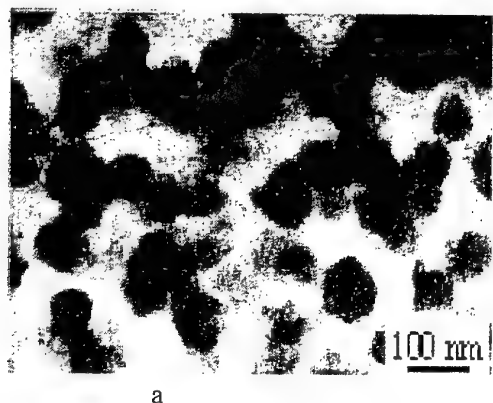


Fig.1. Structure of flakes from alloy Al-8Fe-3.4Cr, TEM investigation: a-bright field images, b-dark field image with using a part of the intense rings in the EDR.

The electron-diffraction pattern as taken from the major portion of the foil, along with aluminum reflections, contains also 5 uninterrupted rings characteristic for the Al-Fe-Cr system (Fig.2a). The electron-diffraction pattern taken directly from the quasicrystals is a dotted one with the 5-order axis of symmetry, characteristic for quasicrystals (Fig. 2b).



Fig.2. Electron diffraction pattern of aluminum alloy containing quasicrystals prepared from a-major portion of the foil; b-directly from quasicrystals.

The X-ray phase analysis supported formation of quasicrystal structures in the rapidly solidified flakes of aluminum alloy (Fig.3, where arrows show extra maximums associated with the presence of quasicrystals).

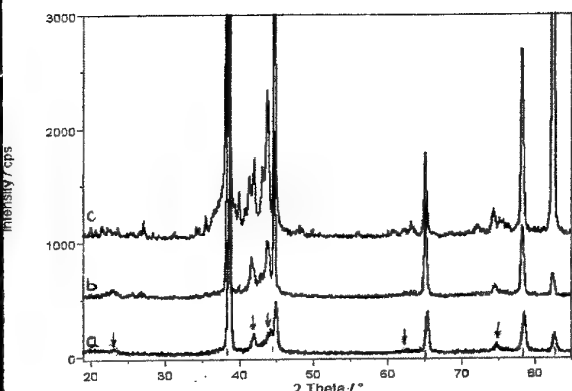


Fig.3. X-ray phase analysis Al-Fe-Cr alloy: a- rapidly solidified flakes; b- forged billet; c- extruded rod.

At his intermediate stage of compacting, i.e. forging under vacuum, boundaries between separate flakes is retained. The alloy then retains its quasicrystalline structure. Therefore, the quasicrystals are available in the structure both as separate particles and in the form of a chain of precipitates along the boundaries of sub grained structure of aluminum matrix (Fig.4).



Fig.4. TEM investigation: dark field image with using reflections from the quasicrystalline phase.

The hot extrusion is followed by a deeper processing of the whole bulk of the metal under deformation. The degree of working is then around 94 %, thus leading to a complete disappearance of the boundary between the separate flakes (Fig.5). This is accompanied with a decrease of the quasicrystalline constituent, and the $Al_{13}(Cr,Fe)_2$ intermetallic compounds appear (Fig.6).

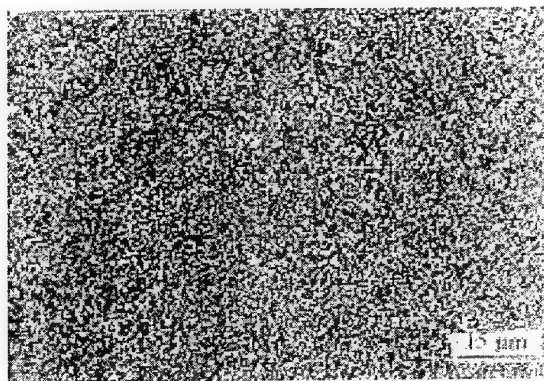


Fig.5. Microstructure of the extruded rod from the alloy Al-Fe-Cr.



Fig.6. Structure of the alloy (TEM) after hydraulic extrusion.

Such a heterogeneous structure with a relatively uniform distribution of dispersive intermetallic compounds and quasicrystals (Fig.6) is found to demonstrate high mechanical properties in the compacted state in the temperature interval of 20-300 °C (Table).

Table. Tensile mechanical properties of Al-Fe- Cr alloy

Temperature, °C	$\sigma_{0.2}$, MPa	σ_U , MPa	δ , %
20	332	410	2,9
190	242	303	5,2
300	218	250	8,1

The authors would like to acknowledge funding of this project from the US Air Force Office of Scientific Research, and the assistance of the Science and Technology Center of Ukraine.

DISTRIBUTION OF MANGANESE IONS AND ITS INFLUENCE ON THE PROPERTIES OF PTCR CERAMICS BASED ON BARIUM TITANATE

V'yunov O., Kovalenko L., Belous A.

V.I. Vernadskii Institute of General and Inorganic chemistry, Kyiv, Ukraine

Positive temperature coefficient of resistance (PTCR) occurs in ceramic materials based on doped barium titanate $(\text{Ba,Y})\text{TiO}_3$ above the temperature of phase transition. Rise of potential barriers at grain boundaries is one of formation conditions of such effect. Therefore PTCR ceramics are purposefully synthesized under conditions when semiconducting grains and high-resistance grain boundaries are formed. This is achieved, in particular, when a small amount of yttrium ions is introduced in barium site and grain boundaries oxidize under sintering in air. In this case materials are characterized by small resistance change in PTCR temperature range and considerable varistor effect (decrease resistance under external electric voltages). This limits the application of such materials in devices operating under high electric voltages. Introduction of acceptor dopants (in particular manganese ions) in synthesized materials is known to improve the above electric characteristics due to change in resistance of grain boundaries [1]. Manganese dopants influence on PTCR effect because redox reactions in manganese oxide take place in the same temperature range in which partial transition $\text{Ti}^{4+} \leftrightarrow \text{Ti}^{3+}$ occurs in ceramics [2]. However distribution of manganese dopants in polycrystalline materials is studied insufficiently. These data would allow one to explain and to control purposefully the properties of PTCR ceramics.

Therefore the aim of this work was to study the distribution of manganese ions and its influence on properties of grains, outer grain layers and grain boundaries of PTCR ceramics.

Analysis of results of studying complex impedance (Z^*) and complex electric modulus (M^*) in wide frequency range at room temperature showed that regardless of yttrium content $(\text{Ba,Y})\text{TiO}_3$ ceramics include electrically different regions: grain, outer grain layer and grain boundaries. However electric properties of grain and outer grain layer at room temperature are difficult to distinguish in high-conductivity samples because of small difference in resistance.

PTCR ceramics based on $(\text{Ba,Y})\text{TiO}_3$ were synthesized by solid state reaction technique using extra-pure initial reagent. For uniform

distribution of acceptor dopants in ceramics manganese has been precipitated from solutions. Electrophysical properties of materials were studied in a wide frequency and temperature range.

Analysis of temperature dependencies of resistance of grain, outer grain layer and grain boundaries of PTCR ceramic based on $(\text{Ba,Y})\text{TiO}_3$ shows that the temperature dependence of resistance of grain and outer grain layer has similar value and character and does not have anomalies. Consequently, PTCR effect in $(\text{Ba,Y})\text{TiO}_3$ ceramics without manganese dopants occurs due to change in electric properties of grain boundaries.

It has been found that increase of manganese content of $(\text{Ba,Y})\text{TiO}_3$ ceramics increases the resistance of grain boundaries, but practically does not change the resistance of grain (Fig. 1). This occurs because manganese in the concentration range investigated does not incorporate in crystalline lattice of PTCR barium titanate and, therefore, does not compensate excess charge in titanium site. A difference in resistance value between grain and outer grain layer of PTCR ceramics becomes pronounced with temperature increase.

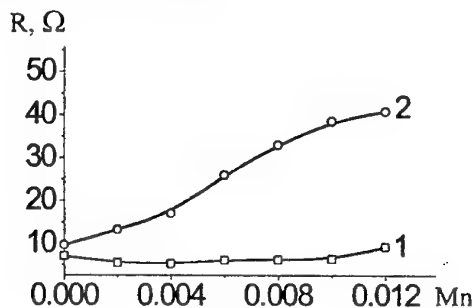


Fig. 1. Resistance of grain (1) and total resistance of outer grain layer and grain boundary (2) of PTCR ceramics as a function of manganese content (mol. %). $T_{\text{meas.}} = 20^\circ\text{C}$.

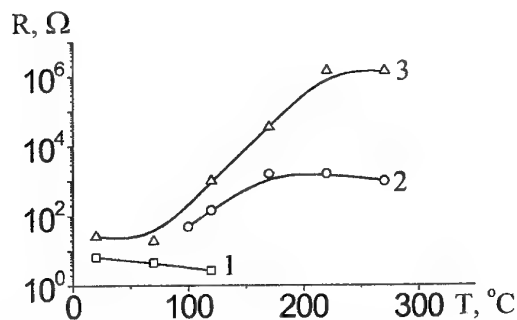


Fig. 2. Resistance of grain (1), outer grain layer (2) and grain boundary (3) of PTCR ceramics based on $(\text{Ba,Y})\text{TiO}_3 + 0.006 \text{ mol.\% Mn}$ as a function of temperature.

Analysis of temperature dependencies of resistance of grain, outer grain layer and grain boundaries of PTCR ceramic with manganese dopants shows that resistance of outer grain layer changes with temperature like resistance of grain (Fig. 2). Resistance of grain boundaries of PTCR barium titanate increases with manganese content.

The results obtained showed that increase of resistance change value of $(\text{Ba,Y})\text{TiO}_3$ PTCR ceramics with manganese dopants occurs due to change of electrophysical properties of outer grain layers and grain boundaries.

Earlier it was shown that the amount of varistor effect in $(\text{Ba,Y})\text{TiO}_3$ ceramics correlates with average grain size, *viz.* in fine-grained ceramics varistor effect is weaker [3]. Our research showed that introduction of manganese in ceramics $(\text{Ba,Y})\text{TiO}_3$ is accompanied with considerable decrease (improvement) of varistor effect, but average grain size of ceramics practically does not change. Varistor effect depends on a number of factors, including oxidation degree of grain boundaries [4]. Therefore one can suppose that varistor effect in PTCR barium titanate decreases on manganese introduction due to the formation of high-resistance outer layer.

In order to clear out the origin of increase of resistance change value of PTCR ceramics with increasing manganese content, the potential barrier at grain boundaries has been calculated using equation from Heywang' model [5]. Results of calculation show that the potential barrier increases with manganese content of ceramics (Fig. 3). This leads to increase of resistance change value in PTCR range. Value obtained for potential barrier at grain boundaries of PTCR barium titanate agreed with literature data [6]. Therefore manganese dopants in PTCR barium titanate form high-resistance outer

grain layer and increase the potential barrier at grain boundaries.

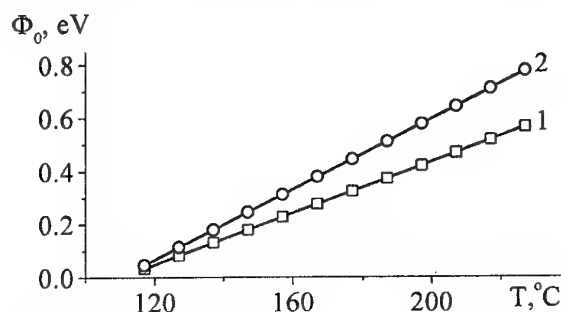


Fig. 3. Potential barrier (Φ_0) at grain boundaries of PTCR barium titanate ceramic $(\text{Ba}_{0.996}\text{Y}_{0.004})\text{TiO}_3 + \text{mol.\% Mn}$ at different manganese content: =0 (1); 0.012 (2).

Thus investigations of PTCR ceramics based on barium titanate in wide frequency and temperature ranges allow us to conclude that manganese content slightly affects the resistance of grains. The manganese ions are mainly at grain boundaries and in outer grain layers, and act as acceptors. This essentially improves properties of PTCR materials, *viz.* resistance change value increases and varistor effect decreases.

References

1. Yanchevskii O.Z., V'yunov O.I., Belous A.G. and Vasiliev A.D. *Effect of Nature of Mn-containing Dopants on Properties of Semiconducting Barium Titanate* // Digest. Electron Microscopy and Materials Strength. Kyiv. - 1997. - P.106-113.
2. Kostikov Yu.D., Leikina B.B. *Effect of Transition 3d-metal Oxides on PTCR Properties of Ceramic Based on Semiconducting Barium Titanate* // Inorganic Materials. 1990. V. 26. No 4. P. 884-886.
3. Belous A.G., Kolodiaynyi T.V., Yanchevskii O.Z. *On Varistor Effect in PTCR Ceramics Based on Semiconducting Barium Titanate* // Ukrainian Chemical Journal. 1995. V. 61. No 8. P. 86-89.
4. Pavlov A.N., Raevskii I.P. *Varistor Effect in Semiconducting Ferroelectric Ceramics* // J. Tech. physics. 1997. V. 67. No 12. P. 21-25.
5. Heywang W. *Semiconducting Barium Titanate* // J. Mater. Sci. 1971. № 6. P. 1214-1226.
6. Hari N., Padmini P., Kutty T. *Complex Impedance Analyses of $n\text{-BaTiO}_3$ Ceramics Showing Positive Temperature Coefficient of Resistance* // J. Mater. Sci. 1997. V. 8. P. 15-22.

CARBIDE STEELS OF METASTABLE AUSTENITE STRUCTURE

Latypov .G.

Powder Material Research Centre, Perm, Russia

The creation of wear-resistant materials with high mechanical properties and low cost is necessary for machine-building, automobile, oil, paper and pulp and other industries. Carbide steels (ferrotics) surpass other industrial alloys in wear- and thermostability at a minimum friction coefficient [1,2]. The ferrotics usually consist 20-70 % vol. titanium carbide [3], therefore to their preparation the same operations as in technology of hard alloys are applied. A final sintering are conducted in a protective atmosphere at temperature 1350-1450 °C. The attempts are undertaken to reduction the cost of carbide steels through mechanical activity with consequent sintering at the presence of a solution phase [4]. In this case sintering temperature can be reduced up to 1260 °C, but other deficiencies of technology are conserved and the viscosity of materials remains not high. The applying Gatfild steel (Г13) as flow bundle does not decide problem of improvement of indexes of viscosity [5], because the Gatfild steel has phase transformations only at a high scale of deformation.

The combination of heightened mechanical properties of structural steels and wear-resistant best tool steel can be reached at ferrotics with metastable matrix by a lower die based on nickel steels [6].

The purpose of present work is study of relation between structure, phase transformations and properties low-alloy powder carbide steels of metastable austenite structure.

Samples are received from polycomponent mix materials containing 4-9 % of a nickels and hardened by a solid phase TiC (3-10 %); extruded at pressure 600 MPa in the steel folded pressure casting dies, sintered in an atmosphere of

hydrogen at temperature 1200°C. The heat treatment plugged a hardening from temperature 780-950°C and low-temperature tempering 180°C, 2 h.

In work a capability of improvement of the mechanical and tribotechnical characteristics sintering carbide steels with low fraction of a solid phase by means of phase deformation transition is demonstrated experimentally. At the equal contents of a carbide phase the best mechanical and tribotechnical characteristics are reached for low alloyed steels.

Reference.

1. Кипарисов С.С., Левинский Ю.В., Петров А.П. Карбид титана: получение, свойства, применение. М.: Металлургия, 1987. 216с.
2. Гуревич Ю.Г., Нарва В.К., Фра-ге Н.Р. Карбидостали. М.: Металлургия, 1988. 144с.
3. Баглюк Г.А., Позняк Л.А. Порошковые износостойкие материалы на основе железа. 1. Материалы, полученные спеканием и пропиткой // Порошковая металлургия. 2001. №1/2. С.44-53.
4. Влияние механоактивации порошкообразных компонентов на технологию и свойства карбидосталей / Нарва В.К., Егорычев К.Н., Курбаткина В.В. и др. // Известия высших учебных заведений. Цветная металлургия. 1999. №1. С. 64-66.
5. Яблокова О.В., Кульков С.Н. Исследование влияния структурно-неустойчивой связки на свойства карбидостали // Перспективные материалы. 1997. №5. С. 65-68.
6. Масленников Н.Н., Латыпов М.Г., Шацов А.А. Карбидостали с повышенной трещиностойкостью // Митом. 1993 №8. С. 20-23.

FORMATION OF FULLERENES DURING SINTERING OF POWDER STEELS

Antsiferov V.N., Grevnov L.M.

Research Center of Powder Materials Science, Perm, Russia

It is known [1], that formation of metalfullerite occurs during sintering of powder steel based on P10 carbonyl iron powder, containing 15 % nickel, 5 % TiC and 10 % SiO₂. The metalfullerite has been face-centered cubic lattice with 14.4 ± 0.1 Å. Lattice period.

It is interesting to elucidate the influence of kind and quantity of alloying elements on synthesis of fullerenes.

It has been investigated the possibility of fullerenes synthesis in 1 % powder steels, alloyed with nickel, copper, silicon, during low-temperature sintering.

Concentrations of alloying elements were changed within 5 to 20 %. Powder steels were prepared based on ПДЖП 3.200.28 iron powder. Part of the samples having 15 % nickel content was prepared based on P10 carbonyl iron and ОЧ 6-2 iron. Samples were pressed at 400 MPa and sintered in vacuum at 850°C for 5 hours.

It has been established by x-ray diffraction analysis that synthesis of fullerenes occurs at all investigated steels. Metalfullerite based on fullerite C₆₀ with 14.3 Å face-centered cubic lattice period was formed in P10 iron steel with 15 % nickel content. The synthesis goes more actively in surface layers of the samples. It is testified by 4.27; 4.14; 3.34 and 2.54 Å diffraction lines. The most strong line is 3.34 Å.

The synthesis goes less actively in steel with the same nickel content (15 %), but on the bases of ОЧ 6-2 iron. Fullerenes are found only in a surface layer of the investigated sample. There is one 3.34 Å diffraction line of average intensity on the x-ray diffraction pattern.

Synthesis of fullerenes occurs actively in steels based ПДЖП 3.200.28 iron powder, especially at 15 % nickel content. X-ray diffraction patterns of this steel sample show the most intensive lines of a metalfullerite with the 14.3 Å lattice period. On a surface it is 3.36 Å and 3.65 Å lines, and in a core – 3.56 Å and 3.35 Å.

So, the synthesis of a fullerenes occurs most actively in P10 and ПДЖП 3.200.28 iron steel alloyed with 15 % of nickel. The metalfullerite with the 14.3 Å lattice period is formed in this process.

The investigation of steels alloyed with silicon has shown that synthesis of fullerenes occurs too. This process occurs most actively in steel containing 5 % of silicon. The 2.48 Å line is stated on x-ray diffraction pattern of a surface, and 3.575 Å and 3.34 Å lines – on x-ray diffraction pattern of a core. All lines have been average intensity. The intensity of lines decreases with an increase of silicon content.

The formation of metalfullerite with the 14.3 Å lattice period occurs also in a copper steels. There is 3.36 Å line on the x-ray diffraction patterns of surface, and 3.575 Å and 3.36 Å – in a core. The influence of copper on synthesis of fullerenes is weak in comparison with influence of nickel and silicon. Never the less the metalfullerite diffraction lines of 15 % copper steel are more intensively in comparison with ther copper steels.

So, nickel, copper and silicon promote the synthesis of fullerenes in powder steels.

References

1. В.Н. Анциферов, В.Г. Гилев., С.А. Оглезнева, А.А. Шацов. Низкотемпературный твердофазный синтез металлофуллеритов // Перспективные материалы. 2000. № 1. С. 11-15.

LIQUID-PHASE SINTERED SILICON CARBIDE BASED ON COMMERCIAL POWDERS

Antsiferov V.N., Gilev V.G.

Research center of powder materials science, Perm, Russia

The solid-phase sintering of SiC is sufficiently complete when using submicron powders without impurities [1]. For liquid-phase sintering of SiC-90%, Al_2O_3 -6%, Y_2O_3 -4% composition compared to solid-phase sintering, lower temperatures of sintering, 1875-1900 °C are required, and the produced materials have higher density and mechanical properties. Liquid-phase sintered SiC has the best combination of hardness and fracture toughness compared to materials based on silicon nitride. For liquid-phase sintering of SiC the requirements on purity of powders are reduced, therefore, despite of use of expensive Y_2O_3 additive, total SiC production cost is lower than with SiC solid-phase sintering [2]. Necessity of silicon oxide impurity minimization is marked in paper [3]. Absence of SiO_2 (except for small impurities) guarantees the decreased viscosity of melt and its high wetting ability of a SiC surface.

Cheap and available commercial SiC powders, as a rule, are coarse. The most simple method of producing the disperse and active powders is the crushing in various mills. Essential complication preventing the milling in ball crushers is crushed iron, therefore the usage of mills lined with hard alloy is of interest.

In the present work the milling process and feasibility of liquid-phase sintering of commercial silicon carbide powder produced by Volgograd abrasive factory were investigated.

Kinetics of crushing and structural changes were investigated when grinding a silicon carbide commercial powder in a ball mill lined with hard alloy. Grinding parts of hard alloy were made as 10 mm diameter short length cylinders with rounded endings. Volume of a mill is 0.78 cub.dm at 100 mm diameter. Degree of filling is approximately 0.45. Speed of rotation is 29 rev/min. Ratio of a balls mass to a SiC powder mass is $m_b/m_p = 20$, 10. Ratio between a mill diameter and rotation speed provides a roll-over mode. A dry grinding was performed.

Kinetics of powders crushing is well described by known exponential function:

$$S = S_m - (S_m - S_0) \exp(-Ct),$$

Where, S_m , S and S_0 - maximal, current and initial values of a specific surface, accordingly; C - grinding constant; t - duration of crushing.

When grinding duration increases, filling and shake down densities appreciably decrease in the first hours, and then they decrease insignificant according to kinetics slowdown at last stages of crushing. In this process, after 40 to 50 grinding hours the small growth of these characteristics is observed, apparently, owing to a hard alloy grinding.

X-ray structure analysis has shown that in a investigated powder at initial condition there are 6H, 15R, 4H alpha-SiC polytypes, and this is a typical composition for silicon carbide commercial powders [1]. Already after 5 hour grinding, WC line appears on X-ray diffraction patterns diagram, which intensity grows with increase of grinding time. At initial condition in a powder there is a silicon impurity, lines intensity of which decreases after long grinding. The influence of grinding is expressed in reduction of intensity of 0.239 nm line of 15R polytype in a X-ray diffraction patterns diagram, which considerably decreases already after 5 hours of dwell and almost absolutely disappears after 20 hours.

Oxide additives raise a trend of powders to agglomerations. Increase of a specific surface is stabilized at 3-4 m^2/g level, and further grinding does not result in S_{specific} . When testing of benzyl alcohol as a grinding medium it was achieved $S_{\text{specific}} = 7.5-8.6 \text{ m}^2/\text{g}$ for 96 to 120 hours of grinding. It is necessary to note, that on walls of cups the powder is more rough, than suspension volume. When grinding the mixes in ethanol a more disperse condition of a mix up to $S_{\text{specific}} = 10 \text{ m}^2/\text{g}$ has been achieved for the same grinding time, however when grinding in benzyl alcohol a maximum density of materials after sintering is reached, Tab. 1.

In microstructure of sintered samples, except for a grey background of a silicon carbide matrix, the inclusions of more light phase, apparently, WSi_2 phase are observed, significant quantity of which is indicated by X-ray structure analysis, fig.1. (1)

Table 1
Results of liquid-phase sintering of SiC-6%Al₂O₃-4%Y₂O₃ mixture ground in benzyl alcohol for 96 hours

T°C	Charge	Δm, %	ρ, g/cm ³	Water absorption
1950	Fresh	8.5	3.3	0.43
1930	Used	10.2	2.9	0.85
1940	Mix of fresh and used	10.5	3.3	5.2
1880	Fresh	13.0	3.26	0.4
1950	Fresh	11.0	3.28	0.7

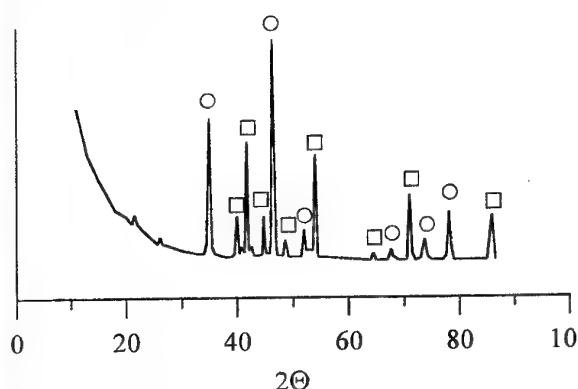
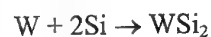
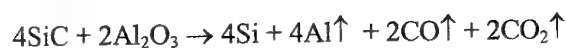
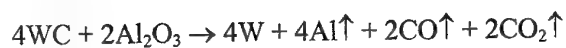


Fig. 1. X-ray diffraction patterns of a material sintered from SiC powder ground in ball hard alloy mill with the oxide additives.

○-WSi₂, □-SiC(6H)

Phase composition of sintered materials consists basically of 6H phase, cubic SiC is not present. WSi₂ formation probably occurs under the following scheme: tungsten and silicon carbides recover oxides.

Aluminium, thus can be absorbed by carbide and escape.



Design density of initial mix (γ_k) is 3.29 g/cm³. When using powders ground in benzyl spirit the density after sintering reaches 3.4 g/cm³ that is connected with WC grinding from a hard alloy and subsequent formation of tungsten silicide from it. WSi₂ phase has 9.8 g/cm³ density and 2160 °C

melting temperature. Estimation on water absorption gives 0.4 % value of open porosity.

The liquid-phase SiC sintering in mixes such as SiC-CaO-SiO₂ is tested to produce the porous substrates of ceramic membranes. SiO₂ addition promotes a shrinkage minimization during sintering up to 2-3 % level that allows to receive strong substrates with the 4-6 microns pore size and gas permeability up to 0.09 μm².

References

1. G.G.Gnesin. Silicon Carbide Materials. M.: Metallurgy, 1977, p.216.
2. Kerber A., Velken S.V. Liquid phase sintered silicon carbide: productions, properties, and possible applications // Fourth Euro Ceramics. 1995 V.2.P.177-184.
3. S.S.Ordaryan, N.Y.Artsutanov, N.Y.Chuov. Activated sintering of ceramics on SiC basis // Refractory products and technical ceramics. 2000, No.11, C.8-11.
4. V.N.Antsiferov, V.G.Gilev. Liquid-phase sintering of ceramics on the basis of a silicon carbide with the oxide additives // Experimental methods in physics of structurally non-uniform medium. EMP 2001. Composite and powder metal materials: Transactions of Second International Scientific conf. Barnaul. Published by Altay University, 2001.c.7-12.

WEAR - RESISTANT POWDER MATERIALS WITH METASTABLE AUSTENITE STRUCTURE

Antsiferov V.N., Smyshlyaeva T.V.⁽¹⁾

Powder Material Research Centre, Perm,

⁽¹⁾Institute of Technical Chemistry, Ural Department of Russian Academy of Science, Perm

In extreme operation conditions, self-organizing materials are used, in particular, steels with a Metastable Austenite Structure (MAS). Improvement of the MAS characteristics during operation occurs mainly due to energy accumulation of external mechanical actions (loading, friction) on phase deformation transformation (γ - α'), and the gain of properties is proportional to the volume of transformation.

The volume of γ - α' transformations, except for the external factors - value and loading speed - is determined by steel chemical structure and uniformity of element distribution, which, in turn, depends on conditions of sintering and heat treatment.

Powder chromium-nickel MASs combine a high level of abrasive resistance with low production cost due to standard manufacturing process.

The best parameters of abrasive resistance and wear resistance are received for carbide steels with a metastable matrix.

The purpose of work is a study of alloying element distribution influence on structure and phase composition of hardened powder steels of metastable structure, and determination of relation between abrasive resistance and structure characteristics.

Infiltrated powder steels of the following compositions: 1-4% Cr; 0.6-2.5% Ni; 1.5.%C; Fe - the base, and carbide steel (2 % Cr; 1 % Ni; 1.5. % C; 5 % of a TiC; Fe - the base) were investigated.

Powder steels were produced by sintering in dried hydrogen, and the sintering was combined with a copper infiltration.

The heat treatment was a hardening from 850, 900, 950 and 1050 °C.

Samples of steels were tested on abrasive resistance.

The study of material structure was performed by metallographic and microdurometrical methods.

Changes in a surface layer of steels after tests were recorded according to the data of X-ray analysis, and Cr, Ni and Cu concentration in metallographic phases and element distribution concentration were determined by a method of Microradiography Spectral Analysis (MRSA).

The heterogeneity of alloys was measured by a concentration variation factor, v .

Structure of steel-copper pseudoalloys after self-cooling with the furnace (average cooling rate of 10 °C / min) is austenite - martensite, with sites of a perlite and rough cementite grid pattern on grain borders; the basic structural components of the treated steels are austenite and martensite.

Metallographic, microdurometrical and MRSA studies of a chromium-nickel steel - copper (1-4 % Cr; 0.6-2.5 % Ni) pseudoalloys have shown that under conditions of slow cooling high-carbon steels have a perlite structure at concentration up to 1.4 % Cr and 0.2 % Ni; the concentration of alloying elements in austenite areas has made more than 2 % chrome and 0.8 % nickel.

The sites with intermediate concentrations of alloying elements have been identified as areas with metastable austenite phase.

In this case the average concentration of copper in austenite reaches 4 %, and in perlite does not exceed 2 % (wt.).

Based on several histogram investigation, the correlation has been found for 1.3-2.3 % chrome concentration interval of W_1 sample and volume of γ - α' phase transformation on a friction surface at abrasive wear.

The microstructure of HIA-ЖГp1.5X2H + 5 % TiC carbide steel represents an austenite-martensite matrix.

The carbide phases in the material are mainly on the borders of grains and are represented by alloyed cementite (up to 7.7 % Cr) of 900-1100 HV_{0.05} microhardness and titanium carbide with microhardness more than 2000 HV_{0.05}.

As a hardening temperature increases the chrome concentration in a matrix grows from 1.9 % up to 2.6 %, and factor of chrome concentration variation decreases down to 0.17 after a high-temperature hardening (1050°C).

With growth of heating temperature for a hardening the amount of a residual austenite in samples of a carbide steel grows from 49 % (hardening from 850 °C) up to 83 % (see the table), and hardness of materials is reduced from 460 down to 210 HB.

II. PERSPECTIVE MATERIALS OF FUNCTIONAL AND STRUCTURAL PURPOSES: POSSIBILITIES OF OBTAINING NEW LEVEL OF PROPERTIES

Table: Intensity of abrasive wear I_A , results of X-ray analysis and statistical MRSA of) carbide steel ПA-ЖГp1.5X2H +5%TiC infiltrated with copper.

Temperature of a hardening. °C	I_A mg/min	V_γ	ϕ , %	W_i , %	C_{Cr} , % (wt.)	v_{Ni}	v_{Cr}
850	3.6	49	38	32	1.7	0.27	0.41
900	3.2	82	53	58	1.9	0.27	0.40
950	0.8	82.5	69	<75	2.4	0.26	0.33
1050	2.6	80	0	<20	2.6	0.17	0.27

Designations: V_γ - austenite volume in a material; v - factor of a concentration variation; ϕ - volume of a phase transformation

The data on an abrasive wear and volume of austenite phase in a material before the tests and volume of γ - α' phase transformation on a friction surface after the tests are shown in the table above.

The abrasive resistance of carbide steels is non-linear and depends on hardening temperature.

The wear intensity of carbide steels has made approximately 3 mg/min, except for samples hardened from 950 °C.

As can be seen from the table, for the given samples the least wear (0.8 mg/min) has been achieved at maximal volume of transformation, ϕ = 69 %.

The increase of wear intensity and absence of phase deformation transformation after a hardening from 1050 °C relates to changing the chrome distribution in a matrix.

As 70 % of points on analyzed metallographic sample had the chrome contents of more than 2.3 %, the maximum of distribution was displaced into area of the increased chrome concentration.

In a supposed interval of austenite instability an W_i frequency density amounts to 20 %.

Comparison of frequency density W_i (%) in an concentration interval of a "metastable austenite" (chrome 1.3 - 2.3 %) with volume of phase transformation, ϕ (see the table), has shown their agreement within the limits of measurement errors

So, the chrome distribution in a material allows to evaluate the volume of potential phase transformations.

Based on the results of the phase analysis and measurements of hardened layer microhardness the fracture energy of a transformation induced plasticity (TRIP) steel at friction on an abrasive has been evaluated.

The linear dependence of a steel relative abrasive resistance on "metastable austenite - deformation martensite" transformation volume has been established.

Thus, for chromium-nickel steels the concentration interval has been determined, in which the austenite is unstable at a loading and friction.

The amount of a metastable austenite can be predicted using the statistical data microradiographic spectral analysis.

CONCERNING DENTAL COATINGS ON TITANIUM SURFACE

Kulmetyeva V.B., Porozova S.E., Belyaeva O.V.⁽¹⁾

Powder Material Research Centre, Perm, Russia

⁽¹⁾Regional Clinical Dentistry, Perm, Russia

Process of population aging, common for all industrially developed countries, and also, injury growth, connected, in particular, with increase of quantity of vehicles and permanent local armed conflicts, put forward as one of paramount tasks of medical service a problem of "man's repair" including partial or complete replacement of some body parts. Use of donor organs (including those supposedly produced by cloning), except for medical difficulties, is connected with complex socio-ethical aspects, from which only artificial materials are free. The manufacturing the artificial implants has resulted in appearance of the whole branch in material engineering, namely, development of bioinert and bioactive ceramics, polymers, metals and alloys.

Efforts of many researchers are focused on creation of substitutes for hard tissues: bones and teeth. Their partial or complete replacement is used for a long time, however, aspiration of medical personnel and patients to the maximal convenience, durability, low cost and natural origin results in necessity of permanent development of new materials. So, the data on "washing away" of some elements, for example, nickel and chrome during long-term running in organism, stimulated wider use in medical practice of non-toxic materials, such as titanium [1, 2].

Problem of titanium appearance and biocompatibility improvement is solved by application of ceramic or composite polymeric coatings. Indispensable condition of a high-quality coating is a strong bonding of the coating layer with metal. Layer, which is directly put on metal, is only usually required to provide a good binding both with titanium, and a layer which is carrying out a decorative function. The most evident option is an application of gluing composition as a bonding layer.

Photopolymers are widely used today in modern stomatological materials. The firm "Ivoclar" (Germany) developed a composite polymeric material with ceramic filler - Targis ceromer. The bond of ceromer with metal is provided with a Targis-Link special liquid, which is put on sandblasted and steam passivated metal, and then precured at illumination. After that the

subsequent layers (each presolidified) are applied. Final solidification is performed in special box [3].

Taking into account absence of thermal treatment, it is reasonable to suppose photopolymers suitable for decoration of any metals. In a Powder Material Research Centre the bond resistance of Targis ceromer with "Cellite H" TU' 9391-008-11329825-97 nickel-chrome alloy has been investigated. Test samples were made in Denture Branch of Perm Regional Clinical Dentistry. The tests were performed with Instron-11.95 rupture-test machine by a method of a three-point bend according to GOST P 51736-2001 "Metalloceramics stomatological for dentures: specifications, testing methods". According to the GOST requirements a bond resistance of ceramics with an alloy should be not less than 25 MPa. Cermet is considered to have passed the test, if not less than 4 samples of 6 samples meet the above specified requirement. The average bond resistance of Targis ceromer with an alloy was 24.6 ± 2.8 MPa, and only 3 samples from a test set had a bond resistance above 25 MPa. Thus, in this case, bond resistance with metal of simple glue bonding without thermal treatment is not sufficient.

Ducera Dental-Gesellschaft mbH (Germany) has developed Duceratin for application on titanium dentures, and this ceramic mass is bonded with metal by bonding layer formed during thermal treatment in vacuum at 830 °C [4]. Investigations performed in Powder Material Research Centre to define a competitiveness of the Centre's engineering, have shown that the binding layer represents just a crystal substance. Decoding of the data with ASTM File [5] has allowed to clearly identify this substance as tetragonal InSbO_4 (ASTM card №. 15-552). Usually InSbO_4 is applied in semi-conductor engineering [6, 7]. The idea of application of semi-conductor heteroepitaxial structures in denture stomatology is interesting and could be very fruitful. However, in this case use of a non-toxic titanium with decorative layers containing indium and antimony instead of a "toxic" nickel - chrome alloys is controversial.

When using a traditional method of coating the metal by thermal processing of applied charge the bond resistance of a ceramic layer with

a titanium depends on oxide film thickness on a surface, rate of heating and cooling, difference in thermal factors of linear expansion and etc. The features of titanium oxidation strongly limit a range of applied temperatures at which the layer strongly bonded to metal is formed [8]. The application of vacuum during thermal treatment almost does not influence oxidation of titanium layer, contacting with a ceramic coating, as the ceramic melt is rich with oxygen.

Powder Material Research Centre in cooperation with Perm State Medical Academy has developed the methods of proprietary BT1-00 charge composition application on titanium [9]. It has been shown that the methods of surface preparation usually used in denture practice are insufficient for high-quality bonding layer, which in this case represents a whole with oxidized metal layer. It has been established that the following sequence of operations is optimum: sandblasting, surface degreasing in an acetone, phosphatizing [10]. When phosphatizing a deep passivation of surface occurs allowing to considerably slow down or completely prevent an oxidation of internal surfaces of titanium coronas during thermal treatment. The calcination modes for a bonding layer and subsequent layers have been determined [11].

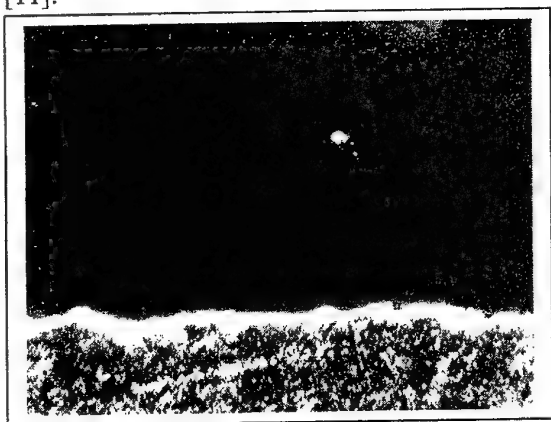


Fig. 1. Microstructure of an oxide layer on a surface of BT1-00 titanium, magnifying by 500.

The bond resistance of a ceramic layer with titanium, measured according to GOST P 51736-2001, has made 35.2 ± 3.2 MPa that meets the

specified requirements. Fig. 1 shows the surface of a titanium covered with stomatological ceramics in 2 layers. Oxide layer has 3 micron thickness and uniformly covers a surface of metal.

References

1. Medvedev E.F. Ceramic and glass-ceramic materials for bone implants // Glass and ceramics. 1993, № 2. P.18-20.
2. Vlasov A.S., Ludanova O.V. Biocompatible glass-ceramic coatings for titanium alloys // Glass and ceramics. 1995, № 4. P.22-24.
3. TARGIS. Arbeitsweisung / Ivoclar.
4. DUCERATIN.Titankeramik: Arbeitsweisung / Ducera Dental GmbH.
5. Diffraction Data File ASTM. Philadelphia, 1969. Inorganic Index to the Powder Diffraction File ASTM.
6. Milvidsky M.G. Semi-conductor materials in modern electronics. M.: Science, 1986. 144 p.
7. Chemistry Encyclopedia: In 5 volumes: vol. 4. / Editors: N.S. Zefirov (chief editor) et all. M.: Large Russian Encyclopedia, 1995.693 p.
8. Zvikker U. Titanium and its alloys. M.: Metallurgy, 1979. 512 p.
9. Russia Federation Patent № 2132672. Composition for manufacturing of cermet dentures / E.V. Suvorina, V.N. Antsiferov, S.E. Porozova, et all. PSMA, PMRC. Published: July 10, 99, Invention Bulletin № 19.
10. Kulmetyeva V.B., Porozova S.E., Suvorina E.V. Treatment of titanium surface before application of stomatological enamel coatings // Chemistry of Solid Body and Functional Materials. Symposium of report theses of Russian Scientific Conf.. Ekaterinburg, 2000. P. 203.
11. Kulmetyeva V.B., Porozova S.E., Suvorina E.V. Optimization of heat treatment conditions of glass-ceramic enamel on titanium // Materials and coatings at extreme conditions: Researches, application, ecologically pure technologies and product recycling: Theses of the reports of International Conference. Sept.18-22, 2000 , Katsiveli, Crimea, Ukraine. Katsiveli, 2000. P.151.

COMPUTER-AIDED DESIGN OF COMPOSITION AND STRUCTURE OF WC-Co CEMENTED CARBIDES – CANDIDATES FOR SOLID-PHASE HIGH-PRESSURE APPARATUSES

Novikov N.V., Shestakov S.I.

V.N. Bakul Institute for Superhard Materials of the National Academy of Sciences of Ukraine,
Kiev, Ukraine

A key feature of materials produced by modern PM methods is an essential dependence of their static and fatigue strengths on the scale factor as well as on the mode and nonuniformity of stressed-strained state of these materials. In addition, the majority of these materials, e.g. structural ceramics, WC-Co cemented carbides exhibit a distinct dependence of their properties on the composition and structure. We have found that the computer-aided modeling of stressed-strained and limiting states of commercial high-pressure apparatuses (HPA) not allowing for the above factors yields overestimated values of the strength and life. Therefore, it cannot provide the basis for the optimization of the HPA design and operation conditions.

To allow for these factors, we have modified our previously developed criteria for static and fatigue strengths of alloys used in HPA [1].

Generally, a criterion for the static strength of WC-Co cemented carbides that are sensitive to scale factor and structure parameters can be written

$$\sigma_{eq} = F[\bar{\sigma}, A_i(V_r, v_{Co}, \bar{d}_{WC})] \leq 1, \quad i = 1, 2, \dots, n \quad (1)$$

as

Here σ_{eq} are the equivalent stresses related to tensile strength of the cemented carbide that are calculated in terms of one of the known criteria for the strength of structure-inhomogeneous materials; F is a — function; $\bar{\sigma}$ is the tensor of stresses at the combined stressed state of the material; A_i are the material tensile, compression, torsional etc. strengths (for anisotropic materials, they are different in different directions). In expression (1) the A_i constants depends not only on the reduced volume V_r (scale factor), but also on the Co mass content v_{Co} and mean value of a WC grain \bar{d}_{WC} . The $A_i(V_r)$ was taken according to Weibull theory

$$A_i(V_r) = K_i / (V_r^{1/m_i}), \quad m_i > 0,$$

where K_i are the constants, m_i are the parameters of homogeneity of the material defined according

to [1]. With due account of the dependence of the material homogeneity parameters on the stressed state mode, the value of the reduced volume was

$$V_r = \int_V [\sigma_{eq}(\bar{r}) / \sigma_{eqmax}]^{m(\bar{n})} dV,$$

calculated by $\bar{n} = \bar{\sigma} / |\bar{\sigma}|$

where unit vector \bar{n} is the radius vector of points of the V material volume, σ_{eqmax} is the maximum equivalent stress in the V volume.

The equivalent stresses were FEM calculated using Pisarenko-Lebedev criterion, which most adequately describes the limiting state of the materials under consideration [2].

To evaluate the fatigue strength of the structural elements, we have established a criterion, which fits to that of static strength (1) and takes into account various modes of resistance of structure-inhomogeneous materials to fracture when changing the stressed state mode during non-symmetric cyclic loading. The criterion has been established on the assumption that in stress space in each point of the V volume, the cyclic loading proceeds along the section of the line that is limited by ends of vectors corresponding to two stressed state modes of the material. As applied to commercial HPA, the above modes of the stressed-strained state correspond to operating and unloading conditions.

The basic relations that allow one to evaluate the number of cycles of loading of HPA cemented carbide elements up to their fracture.

A basic advantage of the suggested criteria, e.g., as compared to those based on the hypothesis for a "weak" link, is their non-locality, i.e. the dependence of structural element strength and durability on the distribution of the stress tensor components, which vary cyclically over the region under study.

Using the suggested procedure implemented in a set of programs, the problem has been solved of optimization of the composition and structure of the cemented carbide matrix of a cylindrical HPA (an analogy to the Belt-type apparatus) for diamond synthesis.

We \bar{d}_{wc} have studied WC-Co cemented carbides with the ranging from 1.4 to 4.1 μm and cobalt content from 4.5 to 37.5 wt%.

Our calculations have shown that to increase the service life of commercial HPA of the above type by a factor of 1.5-1.7, the cemented carbide should have the following characteristics: a cobalt content of about 8.5 wt%, grit size of 1.8-2.0 μm with the ratio between the tensile and compressive stresses of no less than 0.24.

A series of numerical experiments has been conducted on evaluation of the efficiency of liquid cobalt imbibition of cylindrical HPA carbide matrixes following the procedure developed at the ISM of the National Academy of Sciences of Ukraine [3].

Our calculations have allowed us to obtain the optimal geometric parameters of the imbibition regions, in which the Co-concentration varies

from 24 (on the working and lateral surfaces of the matrix) to 10 (in the main bulk product) wt% [4]. It has been found that the formation of a gradient structure of this kind in a matrix allows the matrix service life to be increased in average by 30-50% due to the increase in the resistance to fracture of the cemented carbide in the region of the maximal tensile stresses.

1. N.V. Novikov, V.I. Levitas, S.I. Shestakov. Numerical modeling of strength and durability of constructions with regard for scale effect. Communication 1. Substantiation of strength and durability criteria// *Prochnost Materialov*, no. 5, pp. 37-43, 1991.

2. N.V. Novikov, M.G. Loshak, S.I. Shestakov. The use of the Pisarenko-Lebedev criterion in the calculation of strength of high-pressure apparatus for synthesis of superhard materials. *Ibid.*, no. 5. Pp. 27-35, 2001.

3. A.F. Lisovsky. Migration of Metal Melts in Sintered Composite Bodies [in Russian], Kiev, Naukova Dumka, 1984, 256 p.

4. S.I. Shestakov and A.F. Lisovsky. Formation of gradient structure in high-pressure apparatus for diamond synthesis// *Superhard Materials*, vol. 23, no. 5, pp. 3-6, 2001.

THE IMPROVEMENT IN THE EFFICIENCY OF THE USE OF ENGINEERING CERAMICS FOR IMPACT-RESISTANT BARRIERS

Shestakov S.I., Maystrenko A.L., Kulich V.G.

V.Bakul Institute for Superhard Materials of the National Academy of Sciences of Ukraine, Kiev,
Ukraine

One of the main problems in the development of multilayer impact-resistant protective barriers (IRB) is the choice of a basic material, which when being fractured, is able to be the efficient sink for the kinetic energy of a firing pin. At impact velocities that are characterized by the pin kinetic energy of above 2.5 kJ, this requirement is best met by structural ceramics based on boron or silicon carbides. At present the assessment of the efficiency of ceramics-based IRB and the search for an IRB optimal design are performed mainly by ballistic tests. However, because of a great number of types of the impact interaction between pins and barriers and in view of the changed economical conditions, ballistic tests have become a very expensive test method. In the present paper we suggest a new engineering approach to the assessment of the ballistic limit to multilayer barriers that is based on the finite-element simulation of the barrier deformation and fracture at the initial instant a pin strikes a barrier. In our opinion this approach allows ballistic tests to be considerably reduced and in some cases avoided.

According to the developed procedure, the determination of the ballistic limits to ceramics-based combined armor elements implies three main stages:

- the determination of the impulsive force and contact pressure distribution over the IRB surface taking into account large plastic deformations of a steel firing pin and the peculiarities of its contact interaction with the barrier;

- the finite-element simulation of the stressed-strained and limiting states of an IRB at various impact angles and velocities, including those that are close the ballistic limit;

- the determination of the ballistic limit (the lowest ballistic velocity of a firing pin, at which it still can break through the barrier) by calculating of the IRB reduced radius and mass involved in the impact.

It has been found that in the case of the normal impact ($\alpha=0$), the radius, R_b , of the barrier involved in the impact is found as a boundary, beyond which axial stresses are $\sigma_y < 10\% \max \sigma_y$.

For impact angles of $\alpha \neq 0$, we have taken as a criterion for R_b the radius of the compressed

nucleus that is adjacent to the impact zone and whose size is found from distribution of the major principal stresses σ_1 . By comparison between the σ_1 and σ_y stress fields for a normal impact, we have found the $\sigma_1/\max \sigma_1$ ratio that defines the boundary of the compressed nucleus for all the impact angles, α . If impact velocities are close to ballistic limit, the inertial forces are comparable with the strength characteristics of the IRB material. In this case, knowing the impact force and assuming that the IRB materials are elastoplastic, one can assess their limiting state and the compressed nucleus size based on the nonlocal strength criterion we have suggested earlier.

The efficiency of the approach we suggested and realized in the form of a PC software package has been verified by solving a number of test and applied problems on breaking through combined multilayer armor elements used as various protective systems.

For different impact angles and velocities, including those that are close to the ballistic limit, we have related the ultimate ballistic velocity to the properties of the pin material and the barrier thickness. It has been shown that the increase of the pin hardness by a factor of 3 decreases the ballistic limit by 15 % and at high impact velocities and a high thickness of a barrier, firing pins of materials with higher mechanical characteristics are of a higher breaking ability. At sufficiently low velocities of an impact with thin ceramic plates, firing pins of high-strength steels and cemented carbides exhibit the highest breaking ability.

Examples illustrating the potentialities of the suggested approach are results of the solutions of the problem on optimization of the composition of a multilayer IRB, which is based on a 9-mm thick large silicon carbide plate that is produced by slip casting at the V.Bakul Institute for Superhard Materials of the National Academy of Sciences of Ukraine. With a limited thickness of the entire armor sandwich, the ratio between thicknesses of the facing material (kevlar) layers at the face and back sides of the ceramic plate should be no less than 1:14 in order to prevent the firing pin with a kinetic energy of about 3.5 kJ from breaking through the IRB.

ON PHASE COMPOSITION OF ALUMINUM SURFACE TREATED IN THE ELECTROLYTIC PLASMA

Fedorenkova L.

Dnepropetrovsk National University, Ukraine

Result of treatment of aluminum and its alloys in electrolytic plasma is diffusive layer on aluminum surface with qualitative change characteristics. There are wear resistant, corrosion stability, heat resistance, increased specific resistance [1, 2]. The coating having such properties has a phase composition differing from aluminum matrix. In this work a phase composition of diffusive layer has been investigated.

The treatment samples microstructure was determined by etch in 0,5% HF solution and metallographic analyses on microscope "Neophot-21" and PMT -3.

Phase composition identification was carried out by method of X-ray structure analysis on diffractometer DRON - 2 in iron and copper radiation.

Structure and composition investigation of surface zone of sample was carried out by microradiostructure analyses on scanning electron microscope "Link analytical".

Results obtained by metallographic analyses of surface aluminum and its alloys after treatment are microstructure changing: white layer with thickness 30 - 80 μ .

Microhardness of layer change in depth of metal from $1107 \pm 115 \text{ kg/mm}^2$ to $643 \pm 96 \text{ kg/mm}^2$ depend on saturation regime and composition of aluminum alloys. Microhardness of sample matrix was an increase in 3-4 times.

The phase of $\alpha\text{-AlB}_{12}$, $\alpha\text{-AlB}_{10}$, $\beta\text{-AlB}_{12}$, $\text{C}_4\text{AlB}_{24}$, $\gamma\text{-AlB}_{12}$, $\text{Al}_8\text{B}_4\text{C}_4$, Al_4H_2 , $\text{Al}(\text{BH}_4)_3$ was determined in result of X-ray structure analysis. The diffraction maximums have been moved towards big angle of deflection. Besides, the extension of diffraction maximums is observed, that indicate on existence of amorphous structure in the surface layer.

Results of microradiostructure analyses have been presented on fig. 1.

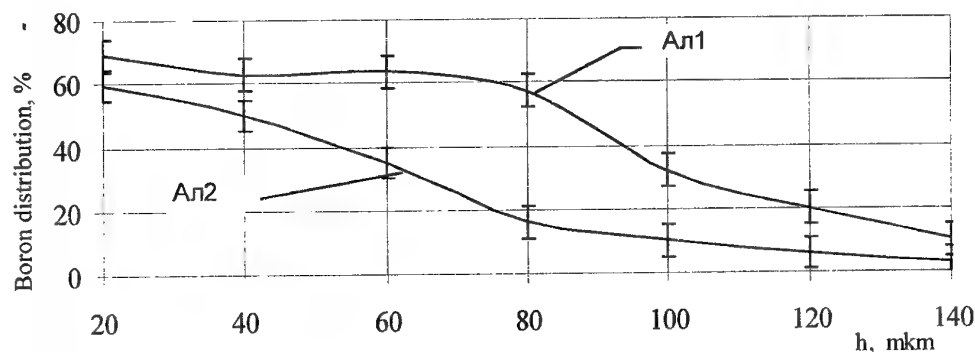


Fig. 1. Boron distribution in depth of aluminum alloys samples Al1 and Al2.

Chemical, physical, mechanical properties of borides aluminum are the same well-known substance as boron carbide, silicon carbide and alumina. Its form the unique material class combined a physical-chemical properties of refractory crystals with characteristic properties of amorphous semi-conductors. Therefore, boron modification and

high- boron combination with complicated structure was named a quasi-amorphous semi-conductors [3].

According to X-ray structure analysis dates the diffusive layer consists from several borid aluminum modifications. Some of there are high - boron combinations ($\alpha\text{-AlB}_{12}$, $\alpha\text{-AlB}_{10}$, $\beta\text{-AlB}_{12}$, $\text{C}_4\text{AlB}_{24}$, $\gamma\text{-AlB}_{12}$) and low-

boron combinations ($\text{Al}_8\text{B}_4\text{C}_4$, Al_4H_2 , $\text{Al}(\text{BH}_4)_3$). This is conditioned by specificity of metal surface treatment in electrolytic plasma. Boron atoms diffusion in metal under condition of treatment in electrolytic plasma has some peculiarities. Saturation operation can realize in several mass transfer mechanisms. This saturation process is characterized by surface local heating. The local temperature may be $10^3 - 10^4$ K. Under the action such temperatures an ion implantation is realized and as a result a boron, hydrogen and aluminum atom mixtures are formed in metal without limitations determined by solubility and chemical activity [4].

Simultaneously with implantation the reaction diffusion of interstitial element in metal substantially along grain boundaries, dislocations as well as bulk of boundaries but a lesser degree take place. Maximum boron penetration range in metal is 150μ . However, according to sectioning method the borid aluminum formation realize in the range of coating thickness determined by etching and metallographic analyses. This thickness is $50 - 80 \mu$. The fig. 1 shows that boron concentration allowing the formation of borids to alloy Al2 reach into 60μ and to alloy Al1 – to 80μ . The boron penetration thickness depends on chemical composition of aluminum alloy. Thus, presence of silicon (10-13%) in alloy Al1 promote boron penetration in metal at greater distance than to alloy Al2

where silicon is absent. With increase of silicon will be formed most likely, borids $\alpha\text{-AlB}_{12}$, and at reduction - $\gamma\text{-AlB}_{12}$. Chromium content in alloy promotes formation such as phase $\alpha\text{-AlB}_{10}$, $\text{B}_{12}\text{C}_2\text{Al}$. For alloys containing Mg - $\alpha\text{-AlB}_{10}$, $\text{AlB}_3\text{H}_{12}$, $\text{Al}(\text{BH}_4)_3$, $\beta\text{-AlB}_{12}$. Thus, the appearance of a phase $\beta\text{-AlB}_{12}$ and phases containing hydrogen is characteristically for coverings on alloys containing Mg.

So, forming and composition of diffusive layer on the aluminum surface depend on many factors. As a result its action the diffusive layer with heterogeneous composition and qualitatively differing of metal matrix is formed.

1. Ясногородский И.З. Нагрев металлов и сплавов в электролите. - М.: Машгиз, 1949. - 128 с.
2. Fedorenkova L., Spiridonova I., Investigation of the saturation with boron of aluminum and its alloys in aqueous solution of electrolyte. // Вісник ДДУ Фізика. Радіоелектроніка. - 1998. - №3. - С. 35-38.
3. Samsonov G.V., Neronov V.A., Lamikhov L.K. The conditions, structure, and some properties of phases in the Al - B system // J. Less Common Metals. - 1979. -67. - №12. - P. 291-296.
4. Котельников О.И. Сюрпризы плазмы. - Киев, 1980. - 154 с.

DEVELOPMENT OF SCIENTIFIC APPROACHES OF DERIVING OF COMPOSITE METAL MATERIALS BY A METHOD AT EXPLOSIVE ALLOYING

Sitalo V.G., Usherenko S.M.⁽¹⁾, Gubenko S.I.⁽²⁾, Bunchuk J.P.

Yuzhnoye State Design Office, Dnepropetrovsk, Ukraine

⁽¹⁾ Institute of pulse processes, Minsk, Byelorussia

⁽²⁾ National metallurgical academy of Ukraine, Dnepropetrovsk, Ukraine

The method volumetric alloying of metal materials is carried out at super-deep penetration of high-speed dispersed particles as a result of explosive influence. Such processing allows obtaining composite materials with a high level of physical-mechanical and operational properties. It is revealed a number of the interesting abnormal phenomena proceeding at explosive alloying.

The problem of the present research included studying structural changes in metal materials (steels E3, 08X18H10T, P6M5, 60G, Armco-iron, titanium, molybdenum), connected with development of hardening.

The comparative analysis of a microstructure of a matrix of materials with volume-centered cubic lattice, face-centered cubic lattice and GP-lattices has shown, that law of super-deep penetration the disperse particles accelerated by energy of explosion, at them are similar and include movement and braking of particles, formation and shutting down channels for ways of their moving, and also occurrence of non-uniform fields of pressure, accumulation of high density of defects and occurrence complex dissipative substructures indicating about relaxation processes of strain character at which local plastic deformation is carried out. In result there is a self-organizing of cooperating defects of a crystal structure which is accompanied by formation of a non-uniform high-energy substructure of a material. For the relaxation processes proceeding in researched materials, realization near to particles and trajectories of their movement of essential plastic shifts and the turns peculiar to strongly deformed condition when there are collective forms of movements in ensembles of strongly interacted dispositions is general. Thus in the areas covered fragmented or cellular structure, are shown large-scale heterogeneity of the crystal-lattice orientations causing significant off-orientation. Near to channels and channel zones high-energy no equilibrium substructures with high charging density of a disposition, extensive long-distance pressure both big continuous and discrete off-orientation are formed.

Distinction in character of the relaxation processes proceeding in a metal matrix near to particles and trajectories of their movement is caused, first of all, by type of a crystal lattice and different energy of defect of packing, is abnormal the big mobility regional a component dislocation loops in metals with volume-centered cubic lattice and primary sliding of a disposition on to octahedral systems in metals with face-centered cubic lattice, distinction of the form and behavior of dislocation loops and different behavior of twin dispositions in metals with volume-centered and face-centered cubic lattices. If deformation of shear-rotary type in the investigated materials similarly with formation fragmented and cellular structures, a zone with system of crossed dispositions and, at last, with their chaotic distribution distinction in processes of twinning and formations of defects of packing is observed. In Armco-iron and molybdenum, on the one hand, and in steel 08X18H10T, on the other hand, mechanisms of twinning and formations of defects of packing that has caused distinction of morphology of doubles and different result from process of formation of defects of packing (a pre-twinning condition in metals with volume-centered cubic lattice and formation of a new phase ϵ -martensite in metals with face-centered cubic lattice) essentially differed. Distinction was shown and in behavior of a disposition and borders of grains (their abnormal splitting in metals with volume-centered cubic lattice and traditional in metals with face-centered cubic lattice).

Moving particles, testing resistance on the part of a matrix, reduce the speed, are decelerated and stop. In places of their braking arise the long-distance fields of pressure inducing relaxation processes which have a wave nature. Shock waves raise pulses of impact. Waves of pressure generated by these processes, being imposed, form superposition of pulses. Relaxation processes near to particles are carried out by consecutive dumps of pressure as a result of emission from borders of a particle - matrix of defects (dispositions and disclinations). Presence testifies to occurrence long-distance fields of pressure close decelerated

particles spider-like extinction loops of wave type which character testifies about them elastic - plastic origination. In all cases of a field are shielded by a field of the disposition, arising around of particles. Extinction loops have arisen as a result of localization of swirl deformation in a place of braking of particles. This fixed condition of the plastic deformation proceeding at impact with very high speed and resulting in occurrence around of particles of long-distance fields of pressure of elastic - plastic character.

With the purpose of studying character of change long-distance fields of pressure close decelerated particles measured tensors a bend - torsion of the crystal lattice, caused by presence in structure various disposition - disclination formations. Fields of pressure near to particles derivate a significant bend $\partial\varphi/\partial x$ nuclear planes which may be connected to components of plastic bend - torsion H , tensor β of superfluous density of a disposition and radius R of curvature of a lattice.

Researchers also influence of a mode of processing change of density of a metal target. Change of density of stability for each concrete case. In case of consecutive loading of a material occur self-adjustments of its structural elements, including formation of map of distributions of density. It allows explaining registered experimental gallop of concentration of an entered powder after triple processing. Apparently, the basic responsibility for it is carried with the following structural elements: channel structures, zones of "amorphization" and deformations, doubles of border of grains, zones of local change of density. Obviously, it explains increasing influences of process explosive alloying at increase of an alloying degree and structural heterogeneity of an initial matrix. Change of structure and properties of steel P6M5, under equal conditions of processing, always much above, than at Armco-iron and carbonaceous steels.

In metal materials process of hardening by disperse particles dispersed by energy of explosion, is multiple-factor and consists in reinforcing by channels and channel zones, amorphization and μ -alloying, dispersive hardening by particles, deformation hardening as a result of local plastic acts of relaxation type, and phase hardening if in a material will carry out phase transformations. Character of the last in many respects is defined by type of a crystal lattice of a matrix. Each of the listed factors is local and brings the contribution to hardening a material at explosive alloying, and their actions according to a principle of additivity are summarized

$$\sigma = \sigma_{взр} + \sigma_{арм} + \sigma_{амор} + \sigma_{лег} + \sigma_{дисп} + \sigma_{деф} + \sigma_{д} + \sigma_{фаз}$$

Where

$\sigma_{взр}$	Deformation hardening of all volume of the processed material, achievable by explosive influence
$\sigma_{арм}$	Reinforcement making hardenings by channels and channel zones
$\sigma_{амор}$	Hardening subsurface zones of channels in result of amorphization
$\sigma_{лег}$	Hardening subsurface zones of channels by μ -alloying at partial dissociation of moving particles
$\sigma_{дисп}$	Dispersive hardening by particles dependent on their sizes and a volume fraction
$\sigma_{деф}$	The deformation hardening of local zones consisting of pressure, created by fragmented ($\sigma_{фраг}$), cellular structure ($\sigma_{яч}$) and area with the raised density of dispositions ($\sigma_{дисп}$) near to particles: $\sigma_{деф} = \sigma_{фраг} + \sigma_{яч} + \sigma_{дисп}$
$\sigma_{д}$	Long-distance fields of pressure
$\sigma_{фаз}$	Phase hardening if in a material phase transformations proceed

Thus, explosive alloying metal materials allows making purposeful change on depth of a defective substructure. Kinetic redistributions of defects it is defined by a mode of processing and an initial structure of a material. Evolution of a defective substructure occurs at different structural levels: nuclear (redistribution of dot defects, formation of vacancy clusters, shutting down of vacancy disks, crawling of dispositions, local amorphization, μ -alloying of matrixes), mesoscopic (formation of high-energy dissipative substructures with high charging density of a disposition, doubles and defects of packing, splitting of a disposition, formation(education) of non-uniform loading fields with big continuous and discrete off-orientations), microscopic (formation of channels and channel zones, penetration of particles, formation ϵ -martensite, splitting of borders of grains, occurrence of zones of the located deformation). Relaxation processes and the phase transformations proceeding in metal materials at explosive alloying, have a wave nature.

COMPOSITES WITH ACTIVE COMPONENTS, IMMOBILIZED IN FILLER'S CRYSTALLINE LATTICE: THE NEW CONCEPT MATERIALS FOR ZONE OF FRICTION

Paschenko E., Shilo A., Kukharenko S., Klimenko N.

V.N.Bakul Institute for Superhard Materials of the National Academy of Sciences of
Ukraine, Kiev, Ukraine

The raise of functionalities of materials working in conditions of zone of friction or abrasive cutting requires development of the new approaches to shaping their structure. The basic landmarks, which specialists engaged in desidning of such materials hold on to, remain invariable: decrease of contact forces and temperatures, and also prevention of various undesirable structural transformations in contacting surface layers. Traditional methods of a solution of these problems are the introduction in structure of composites of solid lubricants and use of various cooling technological mediums. However, possibility of reception of qualitatively new solutions on the basis of these two approaches to the present time practically is exhausted. First of them is essentially restricted to a decrease of wear resistance (and generally - bearing strength) of composites with magnification of the volumetric content of solid lubricants. The second approach nor is universal, as can not guarantee a protection of contacting surfaces at those levels of loadings and relative velocities, which quite often are required by modern engineering.

Under our judgement, the creation of materials, which would be substantially free from the above mentioned restrictions, can be connected to a solution of a problem of formation in contact zone of active gas mediums, capable essentially influence a condition of contacting surfaces [1, 2]. The components of such mediums, being adsorbed on a surface of a solid in dynamic contact zone, are capable to result in a significant decrease of forces of interatomic interaction in thin superficial stratum of treated materials [3]. It opens wide prospects of control of a dissipation of an energy in zone of friction, defining longevity and structural perfection of contacting surface. With reference to processes of abrasive cutting it means a possibility of redistribution of energy expended on formation of imperfections of a treated surface, and it abrasive disintegration, for the benefit of the latter.

The activity of the mentioned gas mediums can be stipulated first of all by content in them of electronic-excited molecules and submolecular

particles - radical - ions and free radicals [4]. Thus the greatest efficiency of their use can be reached in conditions, when by their radiant appears itself abrasive or antifrictional material. First of all it concerns materials on the basis of organic polymers.

From our point of view, there are two directions of creation of polymeric composites with a high emission of active gas mediums in zone of friction. First of them is connected to shaping of such structure of a polymeric grid, which would ensure a necessary level of a radical emission at the expense of yields of the destruction. Other approach is based on introduction in a polymeric matrix of such substances, which are capable to be radiants of active components (in particular, free radicals) in contact zone.

In this case necessary condition is immobilization of entered substances on any carrier, as many from them can be unstable in conditions of deriving of a composite. Thus the adsorption on a surface of ultra-disperse powders is not the best yield, as the introduction of submicronic particles covered with adsorbed stratum of fluid components can essentially decrease composite's strength. Our attention was attracted with natural stratified minerals with weak connections between separate stratum of atoms and, in particular, clay minerals [5]. These substances, which typical representative is montmorillonite, are capable to accumulate in the structure, at the expense of magnification of interlayer distances, significant amounts of water or, in defined conditions, organic substances.

Such intercalation happens in two stages. First of them - adsorptive - consists in an adsorption of an active component by a surface and interlayer gaps of a crystalline lattice of a mineral. On the second stage - osmotic - the significant absorption of an active component by interlayer space accompanying with magnification of interlayer distances happens. This process, apparently, can be governed by preliminary

modifying of a mineral - carrier by various exchange cations.

Such mode of immobilization of active components has essential advantages on a comparison from their adsorptive fixing on a surface of particles of a filler. At first, will increase durability of deduction of the used organic compound in conditions of manufacture of composite supposing heat treatment. Secondly, the stay in interlayer space of a crystalline lattice of a clay mineral promotes a modification of properties of organic molecules. The lengths of bonds, angles between them and all gang of allowed conformations vary. Owing to redistribution of an electronic denseness in absorbed molecules becomes possible their destruction in interlayer space of a crystalline lattice of a mineral - carrier, with consequent excretion of free radicals in dynamic contact zone. Interlayering space appears in this case as a microreactor permitting to control process of destruction of an absorbed organic compound. Thus the excretion of active components in zone of friction or abrasive cutting becomes not connected with obligatory loose of strength of a superficial stratum of a composite, as in its basis lays resersible change of parameters of a crystalline lattice of a filler, instead of destruction of its particles.

The full realization of the given approach to deriving polymeric composite materials intended for work in zone of friction and abrasive cutting will allow to increase considerably a degree of activity of gas mediums created by aggregates in

contact with machined surface. It opens a possibility of development of composites, in which filler, except for function of providing for of physical-mechanical performances of a material, will appear as an accumulator and radiant of active components, capable to improve conditions and effects of operation of antifrictional and abrasive composites.

References

1. Шило А.Е., Пашченко Е.А. Оксидополимерные материалы матричного типа. – Киев: Наукова думка, 1989. – 168 с.
2. Pashchenko E., Shilo A. Development of quantitative model for destruction of polymers in friction zone // 4 th IUMRS international conference. Symposium D, Tokyo, 1997
3. Нестеренко Б.А., Ляпин В.Г. Фазовые переходы на свободных гранях и межфазных границах в полупроводниках. – Киев : Наукова думка, 1990. – 152 с.
4. Мясников И.А. Влияние поверхностных структурных превращений твердых тел на гетерогенные физико-химические процессы // Физическая химия. Современные проблемы. – М. : Химия, 1984. – С. 212-247.
5. Кухаренко С.А. Использование глинистых минералов при изготовлении инструмента из сверхтвердых материалов // Физико-химия формирования абразивсодержащих материалов инструментального назначения. – Киев: ИСМ АН УССР, 1988. – С. 46-54.

IMPULSE THERMOSTABILITY OF COMPOSITE MATERIALS ON POLYMERIC BINDING

Paschenko E., Silchenko Ya., Chernenko A.

V.N.Bakul Institute for Superhard Materials of the National Academy of Sciences of
Ukraine, Kiev, Ukraine

Composites on the basis of polymeric bonds are the basic type of materials of the diamond tools, which are used for machining metals and cermet, and on finishing operations - also for machining a glass, natural stone and other building materials. Manufacture and the consumption of such tools in the world continues to grow, and, according to the prognoses, such tendency will be kept in the future.

The most important elements of any directed research gains in the field of development of materials are scientifically justified criterions, on which the functional properties of composites will be improved.

The researches, which were carried out last time in a department of physico-chemistry of diamond-containing composite materials of ISM, create necessary preconditions for designing of qualitatively new criterions of refinement of polymeric-abrasive composites. This preliminary backlog contains detailed representations about a character of thermal loadings, to which is exposed polymeric component of materials in zone of cutting.

According to our conceptions, average temperature in zone of cutting can not be used for performance of conditions, in which the destruction of a polymeric grid during work happens. The real process develops under action of short temperature impulses ($700 - 1000^{\circ}\text{C}$), considerably exceeding boundary of static thermostability of organic polymers. Actually polymeric composite (is exacter, thin working stratum) is maintained in conditions, when the energy of thermal oscillations of its basic structural units (segments of macromolecules) can be compared to durability of the appropriate chemical bonds of a polymeric grid. As during work of the tool the continuous renewal of such working stratum happens, it is possible to state, that all volume of polymeric composite all phase of its resistance contacts to a treated material extremely in such "thermally superintense" condition.

The high intensity of temperature impulses initiating processes in polymeric composites in a contact zone means key difference of contact destruction from destruction at static heat input.

However time component, namely - the duration of impulses of heat, plays the not less important role. The processes of destruction of polymers have a relaxation nature, that is the plurality of the elementary acts of relative transition of segments (or other kinetic unites) of polymeric grid resulting in to tearing up of bonds, is characterized by the particular spectrum of relaxation times.

In real conditions of operation of polymer-abrasive composites the characteristic duration of thermal impulse resulting in destruction of a polymeric grid, is close or less characteristic interval of time necessary for a relaxation of segments of macromolecules. Therefore majority of traditional views about a behaviour of polymers under thermomechanical stress becomes in this situation inapplicable. Actually, studying a behaviour of polymers in contact zone, we deal with a special state of substance, namely: substance, which has achieved temperature considerably exceeding a limit of its thermostability, but yet not had time to react to it by the relevant structural modifications. Such condition is possible to name "superintense".

Obviously, duration of such phase, when the polymeric grid in real contact with countersurface already has received powerful temperature impulse, but has not reacted on its with catastrophic destruction in contact microvolume, is a determinative, which defines a character of work of the tool.

The behaviour of polymeric materials in a similar situation is almost not explored. It concerns as peculiarities of a structural condition of the "superintense" polymeric grids, and modes of physico-chemical influence on this condition, and also correlation between duration of preservation "superintense" state of polymer, and working performances of the composite, made on its basis. The duration of such phase can be considered as performance of thermostability of polymer under an operation of short high-temperature impulses or, shorter, impulse thermostability. Impulse thermostability of the bond can be used as qualitatively new criterion promising essential refinement of the diamond tool on a polymeric basis.

The quantitative definition of magnitude of impulse thermostability of a material requires use of methods of mass-spectrometry and thermal analysis and is based on existence of correlation between micromechanical performances of destructing layer of polymer and magnitude of loss of a mass in process of destruction. We offer to determine this index as time, for which the sample loses 50% of initial microhardness (other micromechanical performances) at temperature corresponding maximum velocity of loss of a mass of a sample. For various investigated compositions this magnitude changes from the shares of second about several seconds.

According to our conception, the important physico-chemical performance of a polymeric grid which is in charge of magnitude of its impulse thermostability is the distribution of free volume between kinetic unites forming a structure of polymer. The common regularity, found out by us, consists in sharp magnification of magnitude impulse thermostability at a diminution of a breadth of the above mentioned distribution of free volume. The molecular mechanism underlying this appearance is connected, apparently, with known, but poorly claimed at description of solids reactions "effect of a cell". In this case this effect is exhibited that the radical fragments formed at a rupture of chemical bond of polymer under an operation of powerful short thermal impulse have no time to move from each other on a large enough distance, and with high probability recombine. In an outcome instead of avalanche increase of volumetric concentration of ruptures the system of "blinking" connections is formed, that allows to keep a high level of micromechanical performances of superficial stratum of composite. The gradual accumulation of ruptures of a polymeric grid happens in this case too. Thus each "implemented" rupture raises probability of ruptures of the next bonds, as submits additional free space for separation of next formed radical

pairs. A role of a breadth of a distribution function of free volume to segments of a polymeric grid from here is quite obvious: the diminution of a share of segments, for which the magnitude of accessible free volume exceeds most probable, constrains self-accelerating process of accumulation of ruptures.

In conditions of destruction under an operation of short high-temperature impulses the real accumulation of ruptures of connections happens on those sites of a chain, on which the radical fragments are formed not in singlet, but in triplet condition. Probability in this case is great that the final fragment will come off a grid as triplet free radical, which is not inclined to a recombination. Such radical particles rather easily reach a treated surface and, are adsorbed on it, essentially facilitate process of abrasive cutting.

Total of fugitive yields of destruction, evolved by a polymeric composite in zone of friction, at magnification of an impulse thermostability of a material, sharply decreases. However both the share, and absolute amount of hitting in zone of friction triplet radicals rendering the greatest action on a treated surface appears the more, the more is index of impulse thermostability of composite.

Thus, the perfecting of polymeric-abrasive composites basing on a criterion of impulse thermostability, allows to pursue collaterally two contradicting each other purposes: to raise wear resistance of a material and to reduce contact forces and temperatures, explicating in process of abrasive cutting.

On the basis of polymeric composites with heightened impulse thermostability we design wide range of tools with usage of diamonds, cubic boron nitride and usual abrasives. Such tools now is successfully used by different customers in Ukraine, Czechia, Hungary, Germany for grinding and finish machining of hardened steels, hard alloys, ceramic materials, natural stone.

GLASS-COMPOSITE ABRASIVE-CONTAINING MATERIALS OF TOOL ASSIGNMENT

Shilo A., Bondarev E., Kukharenko S.

V.N.Bakul Institute for Superhard Materials of the National Academy of Sciences of
Ukraine, Kiev, Ukraine

The need of an industry of the developed countries in abrasive tools from superhard materials (SHM) continuously increases. For last 10-20 years manufacture of abrasive SHM tools on ceramic bonds, for example, in the countries of Europe, has increased in 3-5 times. A defined complex of properties approached to demanded, can have the composite materials on glass bond.

The properties of glass materials on basis of two systems are investigated: sodium-boron-silicate and lead-zinc-borate, which can be a basis of abrasive tools on ceramic bonds. The complex of properties describing glass as binding for SHM is investigated. It includes temperature of sintering and flowing, chemical activity, wear resistance, wetting ability and adhesion of a melt of a glass in relation to SHM and fillers, durability of deduction of SHM in glass matrix, crystallizing ability, kinetics of sintering of glass powders and composites, thermal conductions, mechanical and other properties.

To provide for a demanded level of interaction of components of composites and their high aggregate stability in heterogeneous melts of systems "glass - filler" the physico-chemical and technological aspects of interphase adhesion appearances were investigated.

The regulation of properties of CBN- and diamond-containing composites by means of a modification of structure of glass bonds is realized at the expense of use of glasses of various chemical structure or modifying them by oxides, use of fillers of various functional assigning, and also application of different modes of manufacture of composites.

In systems "glass - SHM - filler" the materials possessing new properties at the expense of use of adhesion-active to SHM and fillers of glasses, described by the increased ability to moisten and to keep grains of SHM, and also distinguished from known by high wear resistance and antifrictional properties are obtained.

For reaching the given properties of glass-composite binding materials a traditional process of sintering in a free condition, high-speed low-temperature process of thermoplastic pressing and "solution" technology are used.

The diamond tool on ceramic bonds has found a use on finishing operations of machining of steel products and unmetal materials, and tool from CBN - at grinding and honing of hardened steel.

Ceramic bonds are applied to manufacture of the following types of the diamond tool:

- The grinding instrument for sharpening the cutting instrument from hard-facing alloys together with a steel;
- Short-grained bars for finishing dimensional treatment of bearing rollers from hardened steels;
- Blocks - bars for a finish machining of steel nicks of gear-wheels of hydraulic pumps both bent shafts of tractor and automobile drives;
- Elastic wheels for draft and fair grinding of non-metallic materials (glass, ceramics, self-colour stones).

The instrument from CBN has recommended itself on operations of draft and fair sharpening, and also operational development with refrigeration and without it of hardened intractable steels. Such instrument effectively works at outside and interior grinding, and also honing of quenched steel articles(workpieces). The instrument ensures grinding steels with productivity 600 mm³/minute and more.

The serviceability of the instrument from CBN on ceramic bonds is tested at treatment of cutting tools from steels P6M5, P9K5, P9M4K8, P12Φ3K10M3 and others at the machine-building plants of Ukraine and other countries of CIS, and also Poland, Bulgaria and China.

INFLUENCE OF VARIABLE MAGNETIC FIELD ON FORMATION OF SOLID SOLUTION DURING MECHANICAL ACTIVATION OF FURE Cu, Ni AND Fe POWDER MIX

Prokopenko G.I., Mordyuk B.N., Efimova T.V., Perekos A.E., Ruzhitskaya T.V.

G.V. Kurdyumov Institute for Metal Physics of the NASU, Kiev, Ukraine

Last years the methods based on intensive mechanical influence on a material are used more often for creation of materials with the new or improved characteristics. First of all are methods of mechanical treatment in ball mills and intensive plastic deformation under high pressure.

At present time, the methods of combination influence on a material are developed in Institute for Metal Physics of the NAS of Ukraine. For example, the ultrasonic vibrations are induced in the working chamber at ball mill crushing. It was shown, that such combined treatment results in essential increasing of speed of different solid-phase reactions in materials and allows to reduce time of treatment considerably. In present work the attempt is made to study influence ball mill crushing with additional influence of the ultrasonic vibrations and variable magnetic field on regularity of formation of solid solution Cu-Ni-Fe from elementary powders.

Ultrasonic treatment of powder mixtures permits to conduct a mechanical alloying due to activation of diffusion and mass-transfer processes and solid phase reactions. Using of ultrasonic vibrations leads to considerable decreasing of treatment time to obtain the necessary result in compare with conventional mechanical alloying in planetary ball mills.

In the present paper the ultrasonic treatment was carried out in the ultrasonic mill designed in the Institute for Metal Physics that consists of ultrasonic generator (1kWt, 20kHz) and magnetostrictive transducer. The vibration amplitude of step-like ultrasonic born tip was 10 mm. Treatment of 80%Cu13%Ni7%Fe powder mixture was conducted in container made from high carbon steel with steel balls filled by ethanol with and without magnetic field (3,5 kA/m).

X-ray analysis was carried out on diffractometer DRON-3.0 with using $K\alpha$ of radiation Fe. The field dependences of magnetization were studied on ballistic magnetometer at room temperature. Isothermal annealing of samples was carried out at temperature 873 K in an atmosphere Ar during various time (till 30 hours).

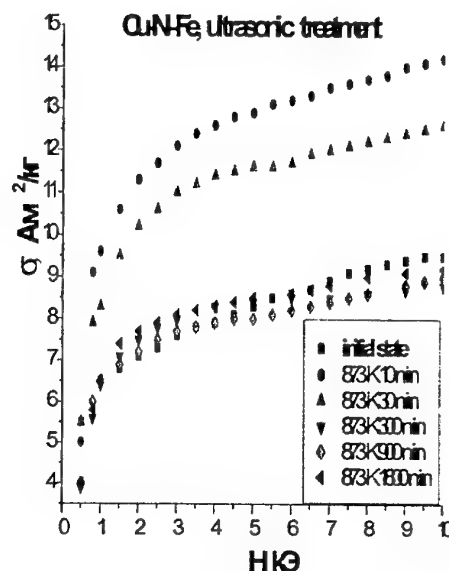


Fig.1. Field dependences of specific magnetization in a powder mixture Cu, Ni and Fe in a initial state and after ultrasonic treatment with following annealing at 873 K during different time.

Fig.1 demonstrates the field dependences of specific magnetization in a powder mixture subjected combined treatment (ball mill crushing + ultrasonic treatment) for 12 hours and annealed at 873 K during various time. It is shown, that at small times of annealing magnetization is increase sharply, and then at subsequent increase of annealing time magnetization decreases gradually, while magnetization of massif alloy CuNiFe with analogy composition increase in all annealing time intervals and achieves saturation. The comparison with the corresponding dependences for a massive alloy Cu-Ni-Fe allows to make the following conclusions. There is a significant acceleration of decomposition process at small time of annealing, that can be caused with high density of crystal structure defects in a mixture and its energy high saturation. It is more difficulty to explain reduction of magnetization at later stages of decomposition. Probably, it is connected with that intensive mechanical treatment results to formation of unequilibrium phase-structural state

in a powder. In such conditions the appearance of large quantity of a new phase germs on defects of a crystal structure is possible. And germ sizes can be less critical at approaching of system to more equilibrium condition. As a result of magnetic phase germs dissolution corresponding reduction of magnetization will take place.

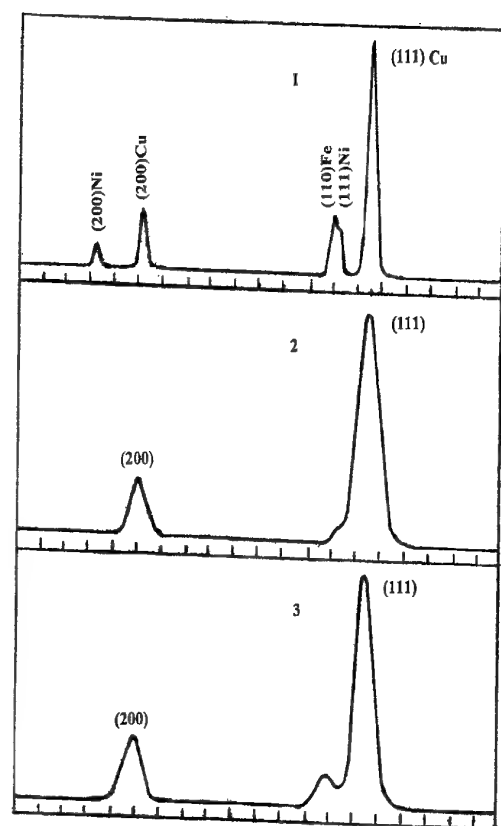


Fig.2. Fragments of X-ray patterns of coarse-grained powder mixtures Cu, Ni and Fe: 1- initial state, 2-after ultrasonic treatment in alcohol during 7 h in magnetic field, 3 – selfsame without magnetic field

Fig. 2 shown x-ray pattern of powder mixtures Cu, Ni and Fe in an initial condition (x-ray pattern 1) and after ultrasonic treatment in a ball mill at the presence of a variable magnetic field (x-ray pattern 2) and without field (x-ray pattern 3). Comparison of these x-ray patterns with x-ray patterns of an initial mixture of elementary powders shows, that the combined machining results in reduction of intensity of lines Ni and Fe, broadening of all lines and their mutual approachement. It indicates on formation of solid solution of atoms Ni and Fe in copper and increasing of defects density in a composite

powder. If mechanical treatment of initial elementary powders is carried out at the presence of a magnetic field, the process solution formation passes more quickly. The comparison x-ray pattern 2 and 3 on fig. 2 demonstrate it. It may explain the specified effect using idea of the authors of work [1, 2] about reduction of activation energy of atoms Ni and Fe diffusion at the presence of a magnetic field.

The results, received in present work, allow to make a conclusion about significant acceleration of process solution formation in powder mixture Cu, Ni and Fe, subjected to the combined treatment in a ball mill with introduction of ultrasonic vibrations in the working chamber and using of a variable magnetic field.

Reference:

1. D.V.Mironov, A.V. Pokoev, V. F. Mazanko, *Metallofiz.*, **20**, No. 6: 62 (1998) (in Russian)
2. D.V.Mironov, A.V. Pokoev, V. F. Mazanko, *Metallofiz.*, **20**, No.7: 18 (1998) (in Russian)

PECULIARITIES OF THE STRUCTURE OF QUASICRYSTALLINE Al-Cu-Fe COATINGS, PRODUCED BY EBPVD

Ustinov A.I.^(1,2), Movchan B.A.⁽¹⁾, Polischuk S.S.⁽²⁾

⁽¹⁾International Center of Electron Beam Technologies of E. O. Paton Electric Welding Institute,
Kyiv 03150, Ukraine

⁽²⁾G.V.Kurdumov Institute for Metal Physics, Kyiv 03142, Ukraine

A set of unique properties, inherent to materials with a quasicrystalline structure, primarily such as relatively high hardness (about 7 GPa), low coefficient of friction, low heat conductivity, semi-conductor dependence of conductivity on temperature, etc. [1] open up new perspectives in improvement of the performance of parts, made of these materials or creation of a new class of coatings, based on quasicrystals. The latter seems to be the most promising. In this connection, technologies of producing quasicrystalline coatings, using the methods of plasma spraying [2] and electron beam deposition [3] were proposed. On the other hand, several studies report a low quality of the coatings produced by this process, because of high porosity and the presence of oxide inclusions [4].

More perfect quasi-crystalline coatings are formed by electron beam deposition. The proposed method, however, is a two-stage one and envisages formation of a microlaminate condensate in the first stage, consisting of layers of pure components, and in the second - a long-term heat treatment of the microlaminate condensate in vacuum, making the process much more complicated [3]. In addition, coatings produced by this procedure are thin.

In order to form thick quasicrystalline coatings with a perfect microstructure, we developed a one-stage technology, based on high-speed electron beam evaporation of an ingot of the specified composition with subsequent vapour condensation on the substrate. It was established, that at substrate temperature above a certain critical temperature the EBPVD method can produce thick (up to 100 μm) Al-Cu-Fe coatings with a quasicrystalline structure, formed directly by vapour condensation on the substrate.

Evaporation of ingots (of 70 mm diameter) was performed from water-cooled copper crucibles in the vacuum chamber using powerful electron beam guns. The deposition rate was varied in the range from 8 up to 200 nm/s by changing the electron beam gun power.

X-ray diffraction analysis of the coatings formed at vapour condensation on stainless steel

substrates at the temperature of 400 – 800 °C, showed that their phase composition changes essentially, when the substrate temperature (T_s) rises above 520 °C (Fig. 1). The coating structure is crystalline below the above-mentioned temperature, and quasicrystalline above it. Deviation of condensate composition from the composition of $\text{Al}_{62.5}\text{Cu}_{25}\text{Fe}_{12.5}$ was accompanied by an increase in the volume fraction of the cubic phase. Coating microhardness remained constant across the thickness and was 8.5 to 9.5 GPa.

X-ray analysis of the structure of condensates, produced under different conditions, demonstrated, that in a number of cases changes were observed in the relations of the quasicrystalline phase intensity peaks. Considering the nature of the produced condensate microstructure, in study [5] it was supposed that such a phenomenon may be related to the presence of the texture.

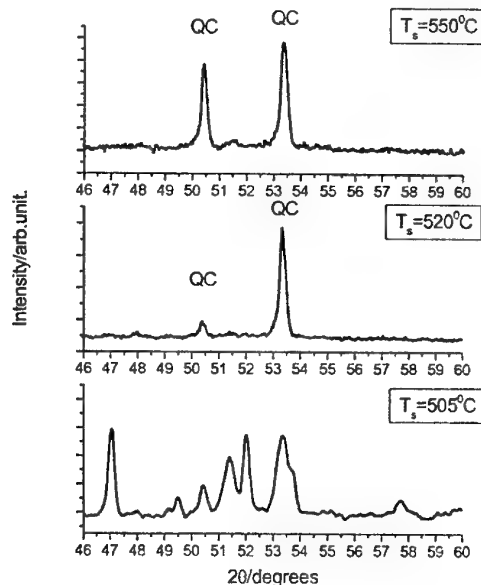


Fig. 1. Fragments of X-ray diffraction patterns for $\text{Al}_{62.5}\text{-Cu}_{25}\text{-Fe}_{12.5}$ coatings produced at substrate temperatures of 505, 520 and 550 °C. Co- $\text{K}\alpha$.

Texture formation in quasicrystalline materials was observed for the first time in Al-Mn and Al-Li-Cu based alloys produced by melt spinning [6]. In this case an axial texture of the icosahedral phase was found along the 5-fold axis direction. This work presents the results of the X-ray diffraction analysis of the texture using pole figures (PF) of quasicrystalline coatings produced by electron beam deposition in vacuum.

Analysis of the coating microstructure with SEM and X-ray analysis indicate that the all coatings are characterized by the presence predominantly of two phase. Namely, coating matrix corresponds to quasicrystalline phase, while inclusions - to the cubic B2 phase. Cubic phase inclusions have a columnar structure. The volume fraction of the crystalline component is the greater, the more significant is the deviation of the local composition from the optimal one.

Tabl. 1.

Texture type	i-phase texture	Cubic phase texture	Coating composition
I	$\langle 2f \rangle$	$\langle 111 \rangle$	$\text{Al}_{61.2}\text{Cu}_{26.6}\text{Fe}_{12.1}$
II	$\langle 2f \rangle + \langle 5f \rangle$	$\langle 111 \rangle$	$\text{Al}_{58.5}\text{Cu}_{26}\text{Fe}_{15.5}$
		$\langle 113 \rangle$	$\text{Al}_{57.2}\text{Cu}_{28.4}\text{Fe}_{14.4}$
III	Weak texture	Weak texture	$\text{Al}_{61.0}\text{Cu}_{26.2}\text{Fe}_{12.7}$

The study of the texture of both icosahedral and cubic phases with a texture diffractometer indicate that the distribution of pole density is non-uniform for the all condensates. Axial textures of both icosahedral and B2-cubic phase were observed. The type of the axial texture of quasicrystalline component correlates with the texture type of the crystalline phase. By the nature of their distribution, the studied samples can be divided into three groups, presented in Tabl. 1.

It is known, that in a number of cases the crystalline and icosahedral phases coexist, while being in certain orientation relationships [7-9]. The

found relations between the directions of the axial texture of the cubic and icosahedral phases correlate with such orientation relations [7, 9]. The following orientation relation between the icosahedral and the cubic phases was the most often observed: $i2//[111]$.

Our results and their analysis suggest that the axial texture of the quasicrystalline phase is the consequence of individual grains of the icosahedral phase nucleating on the crystalline phase, and being oriented in keeping with the orientation relations between these phases. The differences between the obtained orientations can be associated with the presence of additional crystalline phases (for instance, monoclinic) in some cases, as well as with the kinetic factors during deposition.

Thus, it was found that the method of high-speed electron beam evaporation enables producing thick coatings on a quasi-crystalline base, in which the structural parameters can be varied in a broad range, changing the ratio of the quasicrystalline and crystalline components, their texture, characteristic grain size, roughness, etc.

1. J.-M. Dubois, Mater. Sci. Eng., A294-296, 1 (2000).
2. M.F. Besser and T. Eisenhammer, MRS Bulletin/November 1997.
3. T. Grenet, F. Giroud, C. Loubet, J.L. Joulaud and M.Capitan, Materials Science and Engineering A294-296 (2000), p.838.
4. D. J. Sordelet, S. D. Widener, Y. Tang, M. F. Besser, Mater. Sci. Eng., A294-296, 834 (2000).
5. A. I. Ustinov, B. A. Movchan, S. S. Polischuk, Metallofiz. I Noveish. Technolog., to be published.
6. T. Sugawara, K. Edagawa, K. Oda, F. Seki, K. Ito, H. Ino, K. Kimura and S. Takeuchi, Scr. Metall. 23, 711 (1989).
7. C. Beeli, T. Ishimasa and H.-U. Nissen: Phil. Mag. B. 57, 599 (1988).
8. Z. Shen et al.: Phys. Rev. B. 58, 9961 (1998).
9. Z. Zhang, Y. C. Feng, D. B. Williams and K. H. Kuo: Phil. Mag. B 67, 237 (1993).

MECHANICAL AND THERMAL-PHYSICAL PROPERTIES OF DISPERSIBLE HARDENED MATERIALS ON THE BASIS OF POWDER COPPER

Kolmogorov G.L., Mokretzov A.S., Gorokhov V.U., Ulrikh T.A.

Perm State Technical University, Perm, Russia

Possibilities of modern engineering, using copper alloys hardened by traditional alloying methods, are limited by their comparatively low high-temperature strength.

Dispersible hardened composite materials (DHCM) on the basis of powder copper of a system Cu-Ti-C-O have a favorable combination of thermal-physical and mechanical properties in the wide temperatures range. Introducing of dispersible parts in small concentration into the copper matrix provides increases of the temperature threshold of recrystallization under conservation of high electric conductivity and technological plasticity of a material.

Hot extrusion of briquetted blanks improves thermal stability and high-temperature strength of the aggregates, and also provides increased wear resistance, what makes them attractive by using as electrodes for resistance welding, current conducting tips for wire welding,

and also for pieces operating in conditions of increased temperatures and mechanical wear.

The paper contains methods and results of experimental research of mechanical properties of the aggregates of KM-4 mark (system Cu-Al-Ti-C-O). Nowadays there is a complete technology of production of material KM-5 of the system Cu-Ti-C-O, having several distinctions from KM-4. Choice of the systems' elements is based on the use of the effect of dispersible hardening by means of the uniform distribution of hard phase's parts in metal matrix preventing the dislocations movement.

Fig. 1 illustrates dependence of strength limit σ_B and relative lengthening δ of material being investigated under one-axis tension in the temperatures' interval 200 - 800°. Standard cylindrical samples were made of the pressed rods with a stretching coefficient $\lambda = 19,3$.

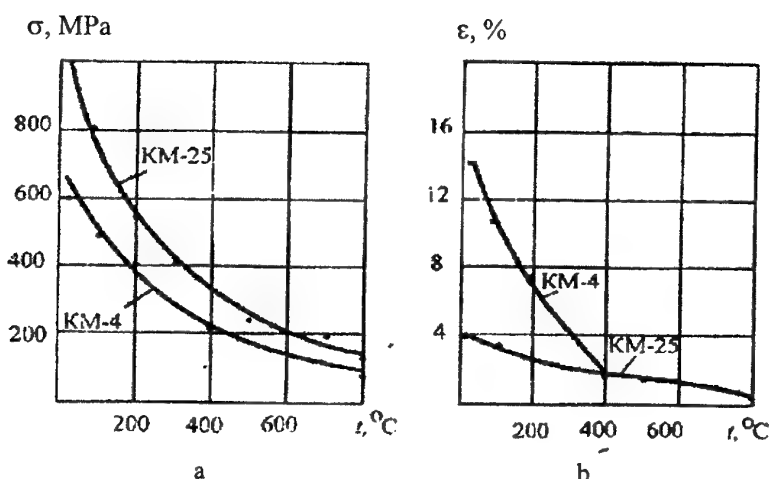


Fig. 1. Dependence of a strength limit (a) and relative lengthening (b) on the temperature of tests.

Material KM-25 at a room temperature in conditions of one-axis stretching has rather significant strength under low plasticity

($\delta = 4\%$), which decreases up to 80% together with a temperature growth (at the temperature 800°).

However, experimental result have shown that behavior of a material changes under the pressure. The strength level is rather high, but plasticity increases together with a temperature growth up to 15%. Origination of cracks along generator on the lateral area preceded the failure process.

Plastic properties of KM-4 with low values of deformation resistance are more sensitive to the temperature changes, in the interval 20 - 400° relative lengthening reduces more then to 6 times.

It should noted that KM-4 and KM-25 keep carrier ability rather long time, since they have a descending branch in the diagram (Fig. 2).

Complex investigation of mechanical properties of the aggregates is complemented by results of experimental research of thermal and physical characteristics. Result of experimental research allowed to define coefficients of the heat capacity, heat conductivity and temperature coefficient of linear extension.

Experiments have shown that dispersible hardened materials have more complicated dependence of heat capacity (Fig. 3). Coefficient of linear extension KM-4 $\alpha = 1,75 \cdot 10^{-5}$ 1/K for $T=295$, is more than for cooper (for cooper $\alpha = 1,6 \cdot 10^{-5}$ 1/K for $T=273$ K).

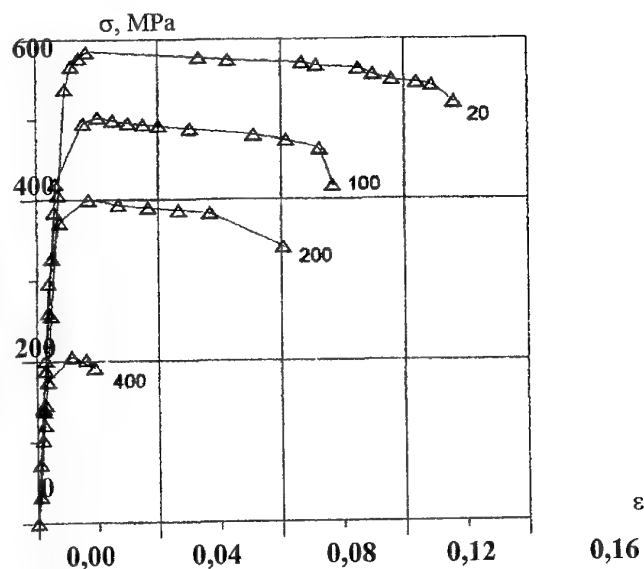


Fig. 2. Tension curves KM-4. Figures of curves correspond to the temperatures, C°

Comparing obtained results it is possible to say that given materials have comparatively low heat conductivity coefficient, heat coefficient KM-4 is 10 times less than heat conductivity of copper. It is explained by microscopic porosity of sintered materials.

Thus, thermal-physical and mechanical characteristics have been defined. It will allow more effective realization of thermal calculations under solution of applied tasks for analysis of thermomechanical indexes of resistance welding, and also justified choice of power-force parameters of blanks production from (DHCM) and their further working.

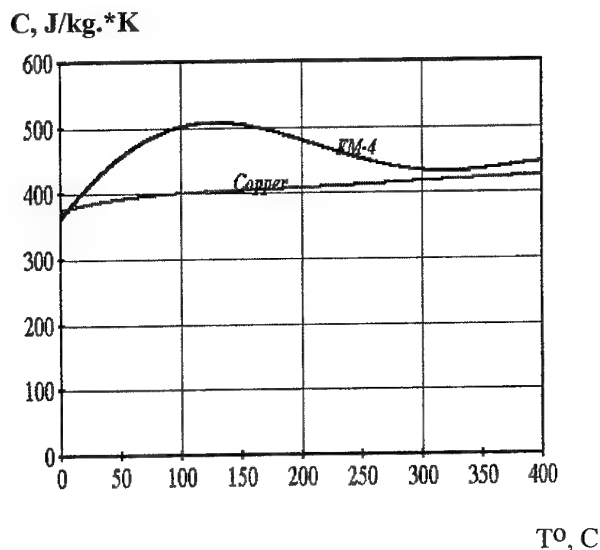


Fig. 3. Temperature dependence of copper heat capacity and KM-4.

SOME FEATURES OF THE MECHANICAL ALLOYING IN THE SYSTEMS Cu-Bi AND Fe-Bi

Grigorieva T.F., Barinova A.P., Lyakhov N.Z.

Institute of Solid State Chemistry and Mechanochemistry SB RAS, Novosibirsk, Russia

Mechanical treatment of metals in the presence of liquid metal phase (Hg, Ga) is known to cause sharp worsening of strength properties; thus, dispersing work (especially for plastic materials) decreases several hundred times [1]. Spreading of liquid metal occurs along the boundaries of grains and structural defects formed during plastic deformation [2], which prevents secondary aggregation (recovery process) in plastic metals.

In high-energy mills of the planetary type, unusually high grinding rates are observed for copper, nickel, iron, silver not only in the presence of liquid mercury and gallium but also with higher melting metals, for example indium, tin, bismuth. Taking into account the data obtained by Gerasimov and Gusev [3] who demonstrated that the major part of power input in the activators of this type is consumed for the heating of the balls, especially at the initial step of mechanical alloying, one can assume that In, Sn and Bi melt; activation of higher melting metals (Cu, Ni, Fe, Ag) occurs in the presence of liquid metal phase. In order to avoid the influence of the formation of solid solutions and intermediate intermetallic compounds, the Cu-Bi and Fe-Bi pairs were selected for the investigation of dispersing process in the liquid metal - solid metal systems. Enthalpies of mixing in these systems, calculated according to Miedema, are +1.1 and +7.1 kJ/mol, respectively, at bismuth concentration of 10 at.%. According to the equilibrium diagrams of state, no mutual solubility of metals occurs in these systems at any temperature. Substantial differences in atomic radii (more than 30 %) allow one to reveal even the inclusion of small amounts of bismuth into copper or iron lattice, and to state the formation of non-equilibrium solid solution, which would be evident from the positions of diffraction reflections. X-ray diffraction investigation of the products of mechanical alloying in the Cu-Bi system showed the decrease of the intensities of basic reflections of bismuth with increasing time of mechanical treatment, copper reflections exhibiting no shift. Under the activation conditions involved in our studies, bismuth reflections disappear practically completely within 10 minutes; copper diffraction patterns broaden substantially without changing their position.

Somewhat longer time of mechanical alloying is required for the Fe-Bi system than for the Cu-Bi system to achieve complete disappearance of the diffraction reflections of bismuth.

So, the decrease of the intensity of diffraction reflections from bismuth during MA occurs in both systems without the formation of any metastable intermetallic phases or non-equilibrium solid solutions. Moreover, the disappearance of bismuth-related reflections is not accompanied by the formation of amorphous halo in X-ray diffraction patterns; electron diffraction does not reveal bismuth reflections in these samples, too. According to the data of chemical analysis, bismuth content of these samples immediately after MA is 9.8 mass.% in mixture with copper, 9.6 mass.% in mixture with iron, bismuth content of the initial mixture being 10 mass.% Bi. Such a behaviour of bismuth, along with the data on wettability of copper and iron surface with bismuth, allows assuming rather reasonably that bismuth is transformed into the liquid (liquid-like) state during MA; spreading over the newly formed surfaces of the solid component it gets adsorbed on them. Coherent lengths, estimated from X-ray data, are estimated to be ~ 30 nm for copper and ~ 20 nm for iron. It should be noted that according to high-resolution electron microscopic data even smaller block size is observed for the Cu-Bi system, though these blocks do not have clear boundaries.

References.

1. Likhtman V.I., Shchukin E.D., Rebinder P.A. Physicochemical mechanics of metals. Moscow, Publishers of the Academy of Sciences of USSR, 1962, 303 p (in Russian).
2. Summ B.D., Goryunov Yu.V. Physicochemical foundations of wetting and spreading. Moscow, Khimia, 1976, 232 p. (in Russian).
3. Gerasimov K.B., Gusev A.A., Kolpakov V.V., Ivanov E.Yu. Sib.Chem.Journal, 1990, issue 3, p. 140-145 (in Russian).

MULTILAYER COMPOSITE STEEL FOR MODERN MACHINE-BUILDING

Kondratenko V.M., Stovpchenko A.P.⁽¹⁾, Knohin V.N.⁽²⁾, Kazakov S.S.⁽²⁾

Iron and Steel Institute of National Academy of Science, Dnepropetrovsk, Ukraine

⁽¹⁾National metallurgical Academy of Ukraine, Dnepropetrovsk, Ukraine

⁽²⁾OJS "Electrometallurgical Steel Works "Dneprospsstal" after A.N.Kuzmin", Zaporozhie, Ukraine

Introduction

The improving of technical characteristics, the providing world's standards quality of metal goods and the using of resource- and energy-saving, environmentally friendly technologies of their manufacture are the necessary conditions for native machine-building competitiveness.

Currently the high-speed development of energy generating, nuclear, chemical industries and machine making sector and also the increased industrial and civil construction scales dictate the need in new materials to be developed which will provide high levels of working reliability, service life, reduced metal consumption of metal structures to be used both under normal and extreme conditions.

So, in solving the above mentioned problems the alloy steels are of great importance. Notwithstanding the tendency of reducing the share of iron-based alloys in overall volume of structure materials according to the experts' forecasts in the nearest future it is expected the increase in share of alloy steels in world metal production.

However, in many cases the use of alloying elements is not economical and efficient because they are rather expensive. Because the workability and service life of number of metal products are determined first of all by their working layer. Therefore, in the most cases there is no need in alloying through the full volume of the metal part/product.

Cast metal composite features and advantages

One of the alternative solutions of the problem of saving the expensive alloying materials and of decreasing the cost price of metal products shall be the production of the composites. Now the producers of metal structures begin to use the composites filled with reinforcing fibers, coated with coating layers, or as passed the precipitation hardening. The most widely practiced are casting

methods and technologies for creation of coatings of layer composites/materials production.

Under proposed methods and materials of cast composite creation the saving of alloying elements is to be obtained by means of difference between its contents in layers. The preset complex of properties of the composite is to be ensured by means of changes in chemical composition and microstructure of layers and also by high strength and defect-free border formed between the metal layers in liquid state.

The changes in casting schedule can permit the wide range variation of layer thickness and composition which offers the flexibility of the technology proposed.

The prospects of the method to be proposed are in the real possibility of making differential alloying of interior and surface layers which ensures the considerable saving of alloying elements/materials.

The advantages of the method to be proposed as to compare with the other technologies are as follows:

- easy realization and reliable obtaining of high mechanical and working properties of rolled products (high strength, wear resistance, etc.);
- acceptability under actual industrial conditions of metal production without any additional capital investments;
- mobility and flexibility of the process.

Authors developed the number of prospective multilayer composite materials and effective metallurgical technologies that permit to produce the high qualitative rolled metal.

The proposed materials advantages are as follows:

- possibility of creation of new class of cast layer materials (sheets and shapes, rolled reinforcing bars etc.) with different chemical compounds;
- differential approach to alloying the layers;
- possibility to control the rolled metal product properties via variations in layer composition and thickness.

Multilayer steels for exhaust systems of automobiles

The techniques of multilayer sheets manufacture named "liquid sandwich" ensures to create various materials with different chemical compound, in that number with using chromium alloyed ferrite steels:

Alloy number	Chemical elements contents*, wt %				
	C	Mn	Si	Cr	Ti
1	0.08	0.34	0.45	17.8	0.75
	0.08	0.54	0.41	13.7	0.67
2	0.08	0.61	0.58	18.1	0.57
	0.12	0.64	0.48	12.0	0.34

This technique permits to receive multilayer sheets with the improved complex of properties and expands area of ferrite steels using for exhaust systems of automobiles.

Increase of the complex of properties of details and units of exhaust systems of automobiles from multilayer sheets both the rather low technological and operational expenses are the factors, which promote expansion of area of chromium alloyed ferrite steels use.

The multilayer steels have the transition boundaries from surface layers to inner. It width varies from 5 to 15 microns and has a smooth changing of the chemical elements content - iron, chromium, titanium and characterises by lack of spills that is one of main advantages of developed method as compared other known techniques of composite manufacture.

The smaller concentration of chromium and its carbides and also lot of iron in inner layer resulted to increasing of composite plastic properties in whole. Mechanical properties of cold rolled multilayer sheets are followed:

Alloy number	Sheet thickness (mm)	Surface layer thickness (mm)	TS (MPa)	YP (Mpa)	A ₅ (%)
1	1.2	0.141	465	320	47
1	1.2	0.223	470	340	43
1	1.2	0.249	470	335	42
2	1.0	0.150	560	366	34

The sheet with such properties ensures the large reliability of work of articles in aggressive mediums and at dynamic loads, for example of coaches for transportation of chemically active substances, in motor - vehicle construction industry etc. Multilayer sheets from chromium alloyed ferrite steels is able to connect by spot welding and pressure contact welding and by shielded arc

welding with using of consumable and permanent electrodes.

Multilayer steels for cultivators

The home cultivators evoke the claim from customers stipulated for low reliability and wear resistance of rolled metal. Such situation caused to increasing the costs of working the land and agricultural products. The mastering of high strength and wear resistant kind of rolled metal permit to reduce the fuel consumption, constructions specific weight, forced standing idle and service life of agricultural machines and implements.

The base technological scheme of composite ingot pouring for three layer steel manufacture with solid insert was developed for condition of metallurgical works Dneprospetsstahl and Zaporozhstahl. The main parameters of composite ingot component geometry and pouring in the mould with central flat solid insert, regimes of heating and deformation of ingots were carried out by authors.

The composite ingot with solid insert with necessary volume of solid insert was manufactured in laboratory. The high carbon steel 60 was melted in Tamman furnace in magnesium crucible. The solid insert from low carbon steel 10 was immersed into crucible and after 1-3 minutes keeping of ingot at the 1873 K temperature the crucible was took out till full cooling.

The effectiveness of lubricant for weldability increasing of solid insert with melt was under study: graphite mixture (up to 30 % of graphite), coal varnishes with flake amorphous graphite addition, bitumen varnish and synthetic mixtures of eutectic alloys of borax and boric anhydride. All studied mixtures promote to creation of connection between layers (first due to prevent of surface oxidation and spatter adhesion), but the graphite mixtures and bitumen varnish were the best.

The inner inserts of ingot had ferrite microstructure (grain size 6-7) with features inherent to deformed metal. The microstructure of surface layers steel 60 was dendrite type created by close of two opposite directed fronts of crystallization. All laboratory ingots had satisfactory metallurgical quality.

Conclusion

Conducted researches and developed technical decision and technological schemes for multilayer sheet steel manufacture in conditions of home metallurgical works allow to recommend the expansion of such class of steels manufacture.

* numerator - the surface layer; denominator - the inner layer;

METALLURGICAL METHOD FOR ADVANCED COMPOSITE WELDING WIRE MANUFACTURE

Stovpchenko A.P., Panin V.N.⁽¹⁾, Polyakov V.A.⁽²⁾

National metallurgical Academy of Ukraine, Dnepropetrovsk, Ukraine

⁽¹⁾ Engineering-technical center "Prometej", Chekhov, Moscow region, Russia

⁽²⁾ Iron and Steel Institute of National Academy of Science, Dnepropetrovsk, Ukraine

Introduction

The article produces and summarizes some results of theoretical and experimental investigations and a practical solution of an important problem of creation principles of design and developing a cost-effective, highly efficient technology for metallurgical production and processing of composite steel ingots for making advanced welding wire grades [1-4].

Main reason for composite wire designing and results of researches

Special designs have been developed for ingots with composite inserts varying in design and containing components that stabilize the welding process and enhance the metallurgical treatment of the metal bath. The composite insert may have a sectional design enabling introduction of several materials.

Based on the uniform approach to the welding wire as the key component of and the major feeding medium for the metal bath, rational ways have been found to ensure appropriate effects of the various additives introduced into the composite insert for purposes of microalloying, deoxidizing and fluxing on welding process and composition and properties of welds.

Merits of eliminating the microalloying additions and carbon in the steel bulk and concentrating them in the composite insert, thus preventing any reactions in the process of making the ingot, are substantiated physico-chemically. Thermodynamic calculations have confirmed that, in the welding temperature range, carbon undergoes oxidation first, so that good conditions are established for interactions of the microalloying elements with impurities in the metal and/or for alloying reactions [5,6].

Physical modeling has revealed features of melt flow and solid growth in the presence of a central macro-size chill during solidification of a composite ingot [7].

A method of analysis has been developed and mathematical modeling carried out for

solidification of a composite ingot having an axially symmetric central insert filled with powdered materials [8] whose thermal properties have been determined experimentally.

The model adequacy has been supported by close agreement between measured and numerically calculated values of frozen-on layer thickness on composite insert.

Table 1. Frozen-on layer thickness in real composite metal and calculated by numerical simulation.

I iller	External \varnothing of CI*, mm	Frozen-on layer thick- ness**, mm	Error, %
EE astera loy	100/100	95/92	3,2
	102/105	115/111	3,5
	108/110	120/113	5,8
r erro- lloy	102/105	115/85	26
	108/110	120/109	9,2
	110/110	115/109	5,2

Forming of composite sections has been studied at the various stages of working ingots to thin wire. Both metallic and nonmetallic filler powders in the composite insert are shown to flow congruently with the ingot bulk metal.

An extensive program of research into making and working composite ingots varying in their compositions and applications has been carried out. The composite inserts under study contained a great variety of powders, namely microalloying additions, such as rare earth metals, zirconium, titanium, molybdenum etc.; fluxing and oxide mixes; and partial or complete sets of alloying additives for the respective wire grades:

Figure 1 presents the fragment of microstructure of zone of layer connection in commercial composite square billet 80 mm with REE filler in composite insert.

* Numerator – real CI dimension and denominator – value preset in calculation

** Numerator – real dimension, denominator – calculated value.

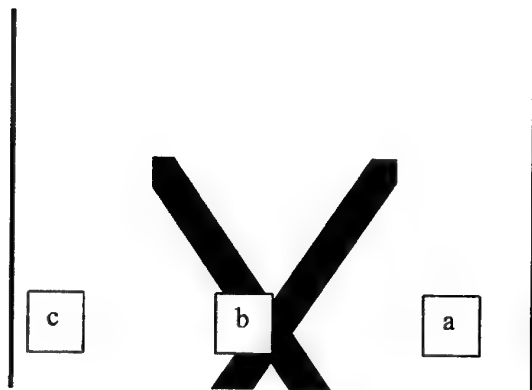


Figure 1. Microstructure (100x) of zone of layers connection in commercial composite square billet 80 mm (a – REE masteralloys, b – insert's shell, c – frozen-on layer).

Feasibility of making composite welding wire based on various types of steel as well as nickel alloys has been investigated.

Aside from plain and low-alloy steels and, more specifically, the Sv-08G2 and Sv-08 grades as the candidates for a unified matrix, the studies involved high-alloy and stainless steels. Successful tests have been performed for making and processing of composite ingots with composite insert fillers of diverse powders, both metallic, like ferroalloys and metals, and nonmetallic, e.g. various oxides and carbon. The great potential of the composite method for introduction of numerous additives into steel ingots is demonstrated, thus enabling development of advanced composite welding wire grades of a variety of compositions for diversified applications, using the ingot bulk steel. The basic considerations affecting expediency, rational engineering and cost effectiveness have been determined together with production engineering limitations relating to composite insert geometry and filler materials.

Technical feasibility of industrial production of heavy composite ingots involving the Sv-08G2S or Sv-08GS steel as the unified matrix together with rare earth ferroalloys and zirconium as microalloying additions has been validated. This approach offers great flexibility allowing manufacture of small lots of diverse wire grades exclusively through variation of insert filler composition.

In a program of qualification tests of REM-added composite wire, compliance of the resultant welds to EN and DIN requirements has been confirmed alongside with improvements over

conventional wire grades currently in use in the European Union.

The high productivity of composite ingot processing and conservation of ferroalloys by their introduction into an isolating composite insert, jointly with enhanced levels of properties, make the composite welding wire a promising and competitive material in the markets of the European Union and the Commonwealth of Independent States.

References

1. Stovpchenko A.P., Panin V.N., Steel, 8, 2000, p. 63-66.
2. Zigalo I., Stovpchenko A., Pavlenko Yu., Gristchenko Yu., Proc. of Conf. "Welding Science & Technology", Tatranska Lomnitca Matliare (Slovakia), 1997.
3. Stovpchenko A., Panin V., Polyakov V., Proc. of the Int. Congress "Machinebuilding technology MT-01", Sofia (Bulgary), 2001.
4. Stovpchenko A., Zigalo I. Proc. of the ASM International European Conference on Welding and Joining Science and Technology, Madrid (Spain).- 1997.-p.407-415.
5. Stovpchenko A.P., Panin V.N., Proc. of the Int. metallurgy and materials congress (24-28 may 2000), Istanbul (Turkey): ITF-CME, 2000.-v.2.-p.1223-1230.
6. Stovpchenko A.P., Yakovlev Yu. N., Theory and practice of metallurgy, 1999, 6, p.18-20
7. Stovpchenko A., Titova T., La Revue de Metallurgie (SF2M-JA99), 1999 (Numero hors serie), p.136.
8. Pavluchenkov I., Stovpchenko A., Minaeva V., Samokhvalov S., La Revue de Metallurgie (SF2M-JA99), 1999 (Numero hors serie), p.138.
9. S. Brodskij, I. Pavluchenkov, A. Stovpchenko, S. Samochvalov, S. Kazakov //Simulation, Designing and Control of Foundry Processes.-Krakow, Aachen, Sofia: Institut Odlewnictwa Krakow-1999.-p.85-90.- ISBN 83-911283-1-8.

ELECTRICAL CONDUCTIVITY OF POLYMERIC FILMS FILLED WITH NI-CARBON FIBRES

Shpilevskaya L.E., Safonova A.M.

Institute of general and inorganic chemistry NAS of Belarus, Minsk, Belarus

It is known, that the use of carbon fibres for filling of the polymers has a lot of advantages in comparison with powdery (dispersible) fillers. The essential lack of dispersible fillers which are used for creation of polymeric electro-conductive coats is what for achievement of high values of electric conductivity of polymer it is necessary to introduce in it plenty of filler. That essentially increases the weight of the compositional coat and makes worse its physical-mechanical properties. The introduction of carbon fibres in to the polymeric films permits to lower considerably electrical resistance of polymers at small degrees of filling. It enables to keep positive properties of the polymer (hardness, elasticity and etc.). However the resistance values of obtained compositional films are much higher, than at the use of metal dispersible fillers.

In IGIC of NAS of Belarus the ways of reception of metal-carbon fibres containing the particles of metal (Ni, Co, Fe) in the structure of fibre are developed and their properties are investigated [1, 2]. The use of these fibres for filling of the polymers permits to combine the positive properties of carbon and metal fillers.

At this work the influence of the additions of Ni-carbon fibres (Ni-CF) on electrical conductivity of polymeric films on the basis of polystyrene (PS), polyvinylchloride (PVC), polymethylmethacrylate (PMMA) and latex films of butadienstyrene (BS) was investigated. It is shown, that the threshold of electrical conductivity of poly-

mers filled with Ni-CF comes at smaller degrees of filling than at the case of the use of high dispersible carbon (HDC) or carbon fibres without nickel (CF). And the achievable value of specific electrical resistance (ρ_v) is on some orders below and is equal to $(5\div7)\cdot 10^{-3}$ Ohm·m (table 1).

It is established, that the increase of average length of Ni-carbon fibres (l_{av}) used for filling reduces essentially the value of specific electrical resistance of received compositional films, this especially has an effect at small degrees of filling. So, the use of Ni-CF with $l_{av} = 3$ mm enables to obtain the compositional films on the basis of PS and BS-latex with low $\rho_v - (3\div6)\cdot 10^{-2}$ Ohm·m even at small degrees (5 mas. %) of film filling. At the degree of filling 17 mas. % and the change of fibre length from 0,1 up to 3 mm ρ_v changes on 5 orders (from $2\cdot 10^2$ up to $7,5\cdot 10^{-3}$ Ohm·m for PMMA films and from $6\cdot 10^3$ up to $3\cdot 10^{-2}$ Ohm·m for PVC films), that allows to receive the compositional films with different conductivity at one degree of filling. The kind of polymer also influences on the value of obtained resistance (table 2). It is established, that the threshold of conductivity in the filled films of PS and BS-latex comes earlier than in the films on the basis of PVC and PMMA in all investigated interval of fibre length (0,1 - 3 mm). The investigated compositional films on the basis of PS, PMMA and BS-latex achieve the lowest meanings of $\rho_v - (7,5\pm 1,5)\cdot 10^{-3}$ Ohm·m already at 17 mas. % of filling, and on the basis of PVC - only after 33 mas. % of filling.

Table 1.

Specific electrical resistance (Ohm·m) of compositional films
on the basis of polystyrene with different carbon fillers

The content of filler, mass. %	HDC	CF, $l_{av} = 0,5$ mm	Ni-CF, $l_{av} = 0,5$ mm
5	10^4	$1,7\cdot 10^1$	$1,6\cdot 10^{-1}$
10	10^4	$4,0\cdot 10^0$	$2,2\cdot 10^{-2}$
17	10^3	$9,2\cdot 10^{-1}$	$7,5\cdot 10^{-3}$
23	$2,0\cdot 10^2$	$2,3\cdot 10^{-1}$	$7,5\cdot 10^{-3}$
28	Not moulded	$1,0\cdot 10^{-1}$	$7,5\cdot 10^{-3}$
33	Not moulded	$1,0\cdot 10^{-1}$	$7,5\cdot 10^{-3}$
50	Not moulded	$1,0\cdot 10^{-1}$	$7,5\cdot 10^{-3}$

Table 2.

Specific electrical resistance (Ohm·m) of compositional films
on the basis of some polymers filled with Ni-carbon fibres of different length

The content of filler, mass. %	PS		BS-latex		PMMA		PVC	
	average fiber length, mm		average fiber length, mm		average fiber length, mm		average fiber length, mm	
	0,5	3,0	0,5	3,0	0,5	3,0	0,5	3,0
5	$1,6 \cdot 10^{-1}$	$3,0 \cdot 10^{-2}$	$4,5 \cdot 10^{-2}$	$6,6 \cdot 10^{-2}$	10^4	10^4	$6,0 \cdot 10^3$	$1,0 \cdot 10^{-1}$
10	$2,2 \cdot 10^{-2}$	$2,0 \cdot 10^{-2}$	$1,4 \cdot 10^{-2}$	$4,5 \cdot 10^{-2}$	$4,0 \cdot 10^0$	$3,5 \cdot 10^{-1}$	$5,0 \cdot 10^{-1}$	$4,0 \cdot 10^{-2}$
17	$7,5 \cdot 10^{-3}$	$7,5 \cdot 10^{-3}$	$8,1 \cdot 10^{-3}$	$3,8 \cdot 10^{-2}$	$2,6 \cdot 10^{-1}$	$6,0 \cdot 10^{-3}$	$4,0 \cdot 10^{-2}$	$3,0 \cdot 10^{-2}$
23	$7,5 \cdot 10^{-3}$	$7,5 \cdot 10^{-3}$	$8,1 \cdot 10^{-3}$	Not moulded	$2,0 \cdot 10^{-2}$	$5,5 \cdot 10^{-3}$	$1,0 \cdot 10^{-2}$	$1,0 \cdot 10^{-2}$
28	$7,5 \cdot 10^{-3}$	$7,5 \cdot 10^{-3}$	Not moulded	Not moulded	$1,0 \cdot 10^{-2}$	$5,5 \cdot 10^{-3}$	$1,0 \cdot 10^{-2}$	$1,0 \cdot 10^{-2}$
33	$7,5 \cdot 10^{-3}$	Not moulded	Not moulded	Not moulded	$5,5 \cdot 10^{-3}$	Not moulded	$7,5 \cdot 10^{-3}$	Not moulded

At this work the temperature influence on the changing of electrical conductivity of the filled films of PS and PVC was investigated. It is shown, that ρ_v of these films begins to change at temperatures close to glass transition of polymer. The temperature dependence of electrical resistance of the specified films decreases as the degree of filling and average length of fibrous filler increase. At the certain meanings of the filling degree and the fibre length of filler it is possible to receive the compositional films with the constant value of electrical resistance in an interval 20 - 120 °C.

The main feature of received Ni-carbon fibres is their magnetic sensitivity caused by the presence at their structure of metal nickel, having magnetic properties. In this connection at this work the orientation of fibres in filler under the action of the stationary magnetic field was carried out during the process of film casting. It is shown,

that the use at such action of a mix of carbon fibres with magnetic (Ni-CF) and nonmagnetic (CF) properties allows to receive the polymeric films with anisotropic electrical conductivity, which value depends on the ratio of magnetic and nonmagnetic fibres in the carbon filler, the degree of filling and the length of fibres.

The developed compositional polymeric films with Ni-carbon fibres can be interesting as the screens absorbing or reflecting the electromagnetic radiation.

Literature

1. Ермоленко И.Н., Люблинер И.П., Гулько Н.В. Элементосодержащие угольные волокнистые материалы. Мн., 1982.
2. Сафонова А.М., Ермоленко И.Н., Апанасенко В.И. и др. //Журн. Прикл. химии. 1991. Т. 64, № 11. С. 2447 - 2451.

SOLDERING OF MELT-TEXTURED YBCO USING Tm123 POWDER

**Prikhna T.A.⁽¹⁾, Gawalek W.⁽²⁾, Moshchil V.E.⁽¹⁾, Sergienko N.V.⁽¹⁾, Surzhenko A.B.⁽²⁾,
Sverdun V.B.⁽¹⁾, Litzkendorf D.⁽²⁾, Kordyuk A.A.⁽³⁾, Melnikov V.S.⁽⁴⁾, Dub S.N.⁽¹⁾,
Alexandrova L.I.⁽¹⁾**

⁽¹⁾Institute for Superhard Materials, Kiev Ukraine

⁽²⁾Institut für Physikalische Hochtechnologie, Jena, Germany

⁽³⁾Institute of Metal Physics, Kiev, Ukraine

⁽⁴⁾Institute of Geochemistry, Mineralogy and Ore-Formation, Kiev, Ukraine

The widespread use of HTS bulk materials is restricted by the absence of technologies that allow the manufacturing of high-quality large and complex-shaped parts. The quality of MT-YBCO (melt-textured $\text{YBa}_2\text{Cu}_3\text{O}_{7-\delta}$ -based mono- or several-domain ceramics with non-superconductive Y_2BaCuO_5 inclusions) that is at present the most promising bulk material for practical application is defined by the maximum of magnetic energy, which can be trapped in the material. The current load, that is the product of critical current density and diameter of superconducting current loop, in turn, defines the magnetic energy. The diameter of superconducting current loop is limited by the magnetic domain size, which is depending of the crystal growth conditions during the melt texturing process. The material quality is decreasing from the seed (in the center) to the sample edge. At present the size limit for a high quality material is about 50 - 60 mm.

Using $\text{TmBa}_2\text{Cu}_3\text{O}_{7-\delta}$ (Tm123) powder as a solder we can obtain junctions between bulk superconductive parts of MT-YBCO. The best junctions were practically invisible under the polarizing microscope and under SEM (SEI image). Analyzing by SEM the COMPO (Composition) image we found out that Tm is present in a 50 μm width layer along the seam. The critical current density (j_c) through the junction estimated by vibrating sample magnetometer and using field mapping was the same as through the MT-YBCO material. The mechanical properties of junctions, i.e. microhardness and banding stress were of the same level as those of bulk material.

In order to estimate the (j_c) through the soldered seam, we have drilled rings (8x4 mm in diameters and 4 mm in height) from single-domain MT-YBCO blocks. Then these rings have been cut into two pieces along the diameters (the width of

cut was about 0.7 mm) and soldered using a Tm123 powder under the 3-4 kg/cm^2 pressure at 990-1010 °C with following oxygenation in a separate process. The j_c in the soldered rings estimated from the loops of magnetization using a vibrating sample magnetometer (Fig.1) was even higher than that of the uncut single-domain rings. The calculated j_c value through the best-soldered seam in 0 T field at 77 K was $j_c=34 \text{ kA/cm}^2$. The observed increasing of j_c through the soldered ring by a factor of 1.5 as compared to the j_c through the initial (uncut) ring can be explained by the fact that during the oxygenation that followed the soldering process the superconductive properties of the MT-YBCO material have been increased as well. The increase in j_c through the soldered ring have been observed up to the 2.5 T field, while in the higher fields some decrease of j_c took place.

The results of field-mapping using Hall sensors gave us the undoubted proofs that the high quality junction have been obtained and are shown in Fig.2.

When we estimated the bending strength of the seam the breaking occurred mainly through the joined material, but not through the place of soldering. This is the evidence of the high mechanical properties of the junction.

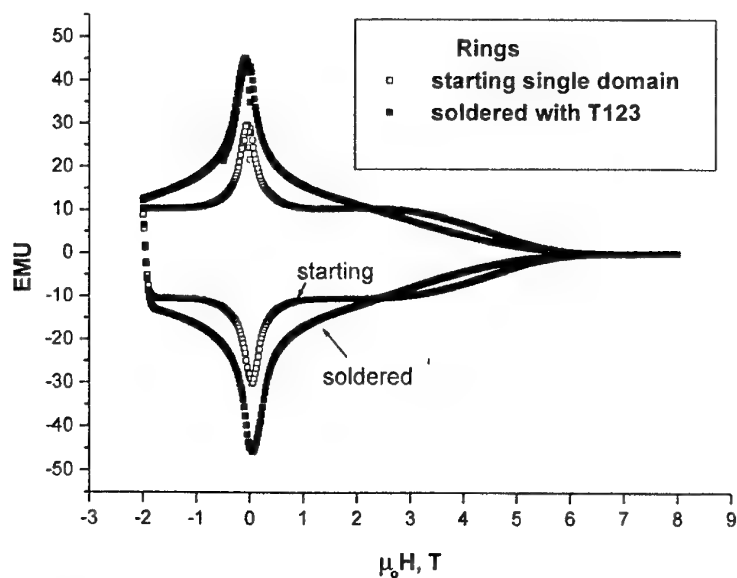


Fig.1 Magnetization loops of single domain (starting) and soldered (with Tm123 powder) MT-YBCO rings obtained by vibrating sample magnetometer.

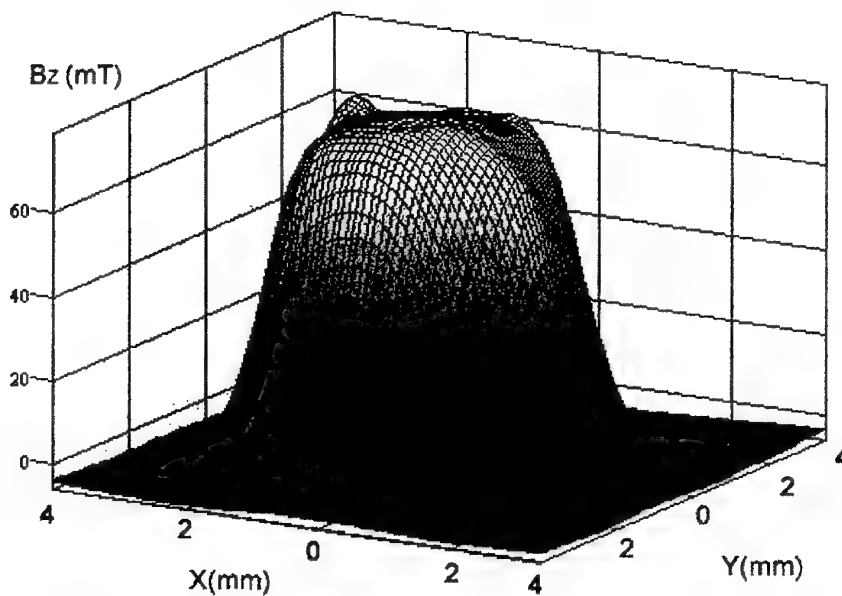


Fig.2 Trapped-field map for the MT-YBCO ring soldered with Tm123.

QUANTUM CHEMICAL SIMULATION OF NEW HYBRID NANOSTRUCTURES: SMALLER FULLERENES C_{20} AND C_{28} ENCAPSULATED INTO BORON-NITROGEN NANOTUBES

Ivanovskaya V.V., Sofronov A.A., Enyashin A.N., Makurin Yu.N., Ivanovskii A.L.⁽¹⁾

Ural State Technical University, Ekaterinburg, Russia

⁽¹⁾Institute of Solid State Chemistry, Ural Branch of the Russian Academy of Sciences,
Ekaterinburg, Russia

The prospects of further application of nanotubes (NT) are closely related with the development of methods of targeted modification of their properties. In this respect, creation of the so-called hybrid nanotubular structures formed by a combination of two (or several) different nanoobjects opens up interesting possibilities.

The first representatives of such structures are the so-called *peapods* consisting of C_{60} fullerenes intercalated inside one- or two-layered carbon nanotubes ($C_{60}@C$ -NT) [1, 2]. They can also be considered as unique composites combining two allotropic forms of carbon of different dimensions (1D+0D): quasi-one-dimensional (1D) – nanotubes and null-dimensional (0D) – fullerenes. We have proposed new 'hybrid' nanostructures involving III-VI group TMs, viz. one-dimensional crystals ($1D-M_8C_{12}@NT$) consisting of linear chains of metallocarboedrenes located inside nanotubes. We studied their electronic properties using $1D-M_8C_{12}@(12,0)C$, BN-NTs, (M-Sc, Ti, V) as an example. [3, 4].

It was found that carbon peapods could contain fullerenes of different dimensions ranging from C_{36} to C_{120} . However major attention until recently was focused on synthesis methods and properties of peapods with participation of "classical" fullerenes C_{60} . We suggest that also the minimum-size fullerenes C_{20} and C_{28} may be potential molecules-intercalants in smaller-diameter NTs. The electronic structure peculiarities of the outer shells of those molecules, in particular the presence of unsaturated "external" bonds, may bring about their spontaneous one-dimensional polymerization with the formation of a variety of new C_{20} - and C_{28} -based nanostructures (dimers, trimers, various extended "nanocapsules" etc.) inside the tube (a peculiar kind of reactor).

In the present work we performed quantum chemical calculations of the electronic structure

and chemical bonding in hypothetical hybrid nanosystems containing the above-mentioned smaller fullerenes C_{20} and C_{28} intercalated into one-layer non-chiral zigzag (n,0) boron-nitrogen nanotubes. The choice of BN-NTs was determined by the circumstance that their electronic properties (in particular, the value of dielectric gap ΔE_g) are rather stable with respect to the structural parameters of the tubes (diameter, chirality), which is significant for the application of BN-NTs in nanoelectronics. (C_{20}, C_{28})@(n,0)BN-NTs were simulated using the unit cells (Fig. 1) chosen for the following reasons. In the majority of synthesized carbon peapods, the distances between C_{60} and NT walls are close to the so-called Van der Waals gap (interlayer distance in graphite or hexagonal BN), as well as to the distances between fullerenes in molecular fullerite crystals or between adjoining coaxial cylinders in multi-layer NTs. Therefore the first objects ($C_{20}@(13,0)BN$ -NT) were modeled by a 124-atomic cell, in which fullerene-NT distances and distances between fullerenes approximated that value (0.311 nm). Another characteristic distance is covalent C-C (B-N) bond length in layers of graphite-like phases or between neighboring atoms in fullerenes or NT walls, which is ~ 0.142 nm. Hybrid nanostructures with the corresponding fullerene-NT and fullerene-fullerene distances were described by 92- and 108-atomic cells. In all the calculations, fullerene and NT structures were assumed unchanged. The calculations were performed using the tight-binding band method with matrix element parameterization according to EHT.

The electronic properties and interatomic bonds in those nanostructures were analyzed as a function of (1) fullerene type, (2) distances between fullerenes in the chain and between fullerenes and NT walls. As an example, the electronic spectrum density of states is shown in Fig. 2. for the C_{20} -chain, 'pure' (9,0)BN-NT, adsorption system $C_{20}+(9,0)BN$ -NT and for $C_{20}@(9,0)BN$ -NT. The

electronic characteristics of the hybrid nanostructures were compared with those of (1) "isolated" fullerenes and nanotubes and (2) $(C_{20}, C_{28})+NT$ systems simulating the adsorption of fullerenes on the tube surface as an initial stage of $(C_{20}, C_{28})@NT$ formation.

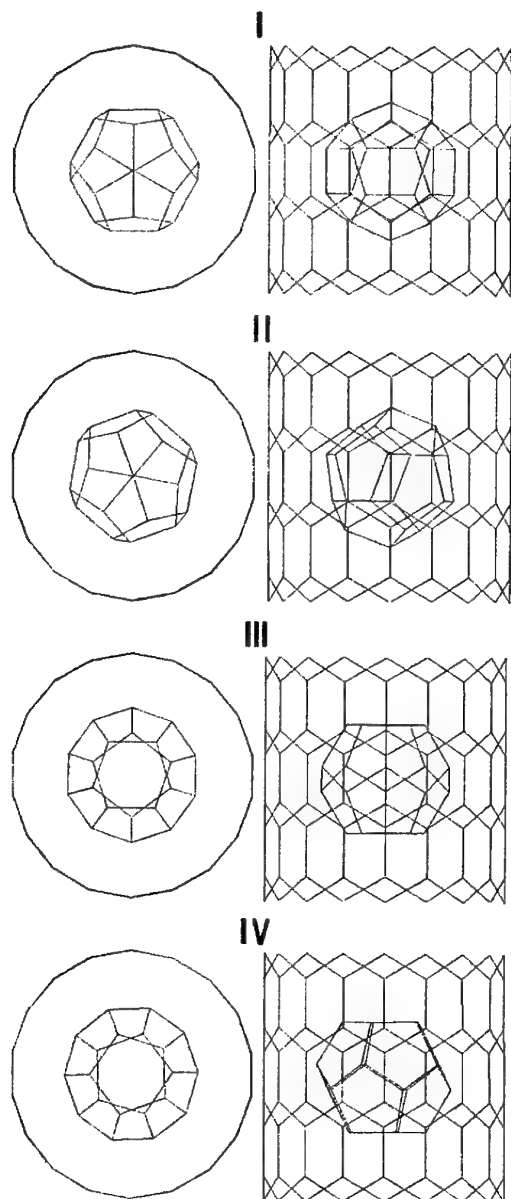


Fig.1. Unit cells of $C_{20}@(9,0)BN-NT$ and their configurations (I-IV).

In conclusion it may be said that the electronic properties of the considered peapods can be efficiently controlled by varying the chemical composition of intercalated cell nanoclusters. In this connection peapods containing familiar endohedral complexes based on the smaller fullerene C_{28} , viz. endofullerenes $M@C_{28}$ ($M = Sc, Ti, Zr, Hf$), become interesting objects for further investigations. We suggest that the

intercalation of those endocomplexes inside NTs may provide possibilities for creating unique nanotubular materials with participation of III-V group d -metal atoms. The calculations of model $M@C_{28}@(n,0)C, BN-NT$ nanostructures are currently under way.

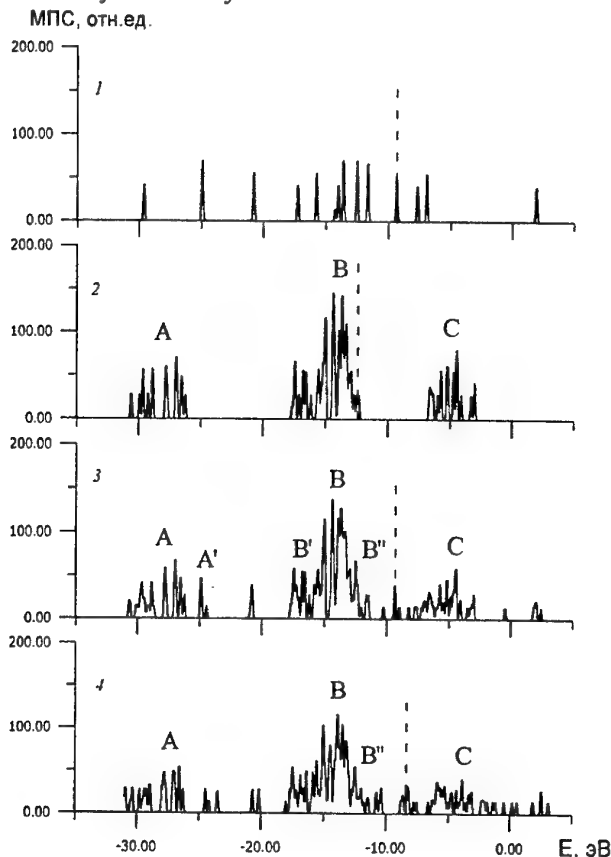


Fig.2. Density of states of C_{20} -chain, 'pure' $(9,0)BN-NT$, adsorption system $C_{20}+(9,0)BN-NT$ and $C_{20}@(9,0)BN-NT$.

References

- [1] Smith B.W., Monthieux M., Luzzi D.E. // Nature. 1998. Vol. 396. N. 6709. P. 323-324
- [2] Smith B.W., Luzzi D.E. // Chem. Phys. Letters. 2000. Vol. 321. № 1-2. P. 169-174.
- [3] Sofronov A.A., Ivanovskaya V.V., Makurin Yu.N., Ivanovskii A.L. // Chem. Phys. Letters. 2002. Vol. 351. № 1-2. P. 35-41.
- [4] V. V. Ivanovskaya, A. A. Sofronov, Yu. N. Makurin, A. L. Ivanovskii // J. Mol. Struct.(TEOCHEM)-in press

This work was supported by the Russian
Foundation for Basic Research,
grant 01 - 03 - 32513

HEAT RESISTANT AND HEAT- AND WEAR-RESISTANT DISPERSION STRENGTHENED COMPOSIT MATERIALS ON A COPPER POWDER BASE OF DISCOM® TRADE MARK FOR VALVE GUIDES AND VALVE SEATS FOR DIESEL AND PETROL ENGINES

Shalunov E.P., Orlov S.A.⁽¹⁾, Slavoljubov V.S.⁽²⁾

Scientific and Technological Company TECHMA Ltd, Cheboksary, Russia

⁽¹⁾JSC Zavolzhsky Engine Plant, Zavolzhje, Russia

⁽²⁾JSC DIESELPROM, Cheboksary, Russia

The mechanism of gas distribution is one of the most crucial organs of an engine, since it ensures a strictly defined sequence and given duration of processes lasting of an admission intake of fuel and issue of products of its combustion (gases) in a duty cycle of an engine.

The following figure illustrates the typical construction of the gas distribution mechanism with inlet valve 1 and exhaust valve 2 used in automobile, tractor and other types of engines.

powerful high-speed engines. The temperature on height of a valve guide in a direction from the head of the valve is reduced, but its maximum value can reach 700°C.

At a reciprocation of the valve the guide is exposed to a mechanical wear, and the seat besides undergoes crushing powerful shock loads.

It is necessary to add, that these parts work under the conditions of a hostile environment – gases driven at the speed of 400...600 m/s, heated up to 730...1200°C.

The above-stated working conditions of valve guides and valve seats require the application of heat resistance and heat and wear-resistant materials for their manufacture, which also should endure effect of the hostile environment. These materials are supposed to cause the valve itself minimal wear at that.

Due to the fact that all standard bronzes and brasses available have a lower recrystallization temperature, than the heating temperature of valve guides and valve seats, they can not work steadily in engines, especially under high-speed and augmented operating conditions.

To meet these requirements there were developed two new Oxide and Carbide Dispersion Strengthened composit materials on a copper powder base (OCDS-Copper) of DISCOM® Trade Mark: C 0/94 (for valve guides) and C 3/03 (for valve seats) by TECHMA Co., Ltd.

Material C 0/94 of Cu - Al - C - O system in a final state represents a copper matrix, in which ultra-dispersible (0,03 ... 0,04 μm) particles of γ - Al₂O₃ and residual carbon are evenly distributed.

Material C 3/03 of Cu - Al - Ti - C - O system in a final state represents a copper matrix, in which ultra dispersible (0,02...0,03 μm) particles of γ - Al₂O₃ and TiC, and also residual carbon are evenly distributed. The materials have subgrain structure, that testifies to absence of a recrystallization of alloyed copper at hot (870...900°C) extrusion of its granules into a bar or a tube.

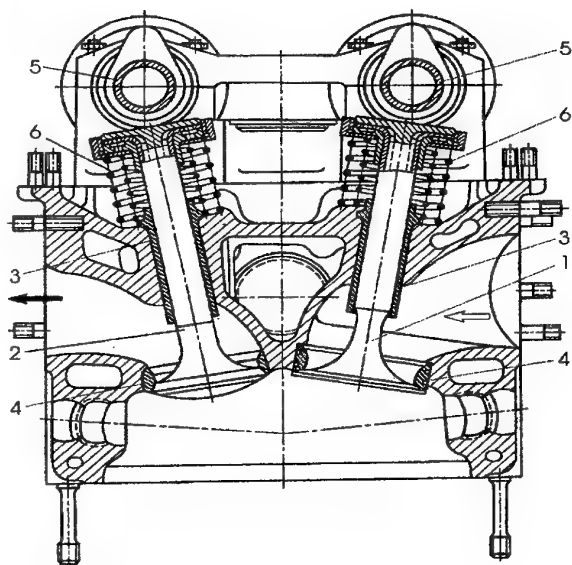


Fig. Drive of two rows of valves by two distributing shafts: 1 – an inlet valve; 2 – an exhaust valve; 3 – valve guides; 4 – valve seats; 5 – distributing shafts; 6 – springs.

Major parts of the gas distribution mechanism are also their valve guides 3 and seats 4 apart from the valves themselves. The temperature of a seat in a zone of its contact with the head of the valve can make up over 900 °C in

II. PERSPECTIVE MATERIALS OF FUNCTIONAL AND STRUCTURAL PURPOSES: POSSIBILITIES OF OBTAINING NEW LEVEL OF PROPERTIES

The above materials have the following basic physical and mechanical properties stated in the table.

Table

Technical characteristics	Type of OCDS-Copper	
	C 0/94	C 3/03
1	2	3
Melting temperature, °C	1080	1080
Recrystallization temperature, °C	1000	1000
Factor of linear thermal spreading, $\times 10^6$ 1/°C:		
- at 20...100°C	17,0	15,0
- at 100...200°C	18,8	19,1
- at 200...300°C	22,5	22,6
- at 300...400°C	24,7	25,4
- at 400...500°C	23,8	21,7
- at 500...600°C	22,4	22,6
- at 600...700°C	22,6	23,7
- at 20...300°C	19,6	19,3
Brinell hardness HB 5/750/30	230	258
Ultimate tensile strength, MPa:		
- at 25°C	770	931
- at 200°C	328	562
Relative elongation, %:		
- at 25°C	2,0	2,3
- at 200°C	2,5	7,3
A ultimate strength at compression, MPa:		
- in a longitudinal direction	1022	1092
- in a transversal direction	1062	1117
Relative settling up to a compression fracture, %:		
- in a longitudinal direction	30	24
- in a transversal direction	28	15
The module of normal elasticity, GPa	110	92
Shear modulus, GPa	39,6	43,0
Ultimate cut strength, Mpa	529	563

The above features of materials structure and also presence in them of ultra-dispersible free carbon in an amount 0,69...0,73 % mass. with the

above-stated physical and mechanical properties combined have ensured to these materials good operation properties at that.

So, at operation of valve guides made of OCDS-Copper DISCOM® C 0/94 together with exhaust valves having ion-nitrogen rods, the average weight wear of these guides is in 2,6 times lower, than that of valve guides made of gray iron Gh1051, used in FIAT engines. The wear of the valves themselves became 2,75 times less.

The wear-resistance factor of valve guides made of OCDS-Copper DISCOM® C 0/94 exceeds the wear-resistance factor of guides made of 'bronze CuNi2Si F65 DIN 17666, used in engines produced by MOTOREN - und TURBIENEN UNION Friedrichshafen G.m.b.H. and PORSCHE AG in 17 times.

The wear-resistance factor of the interface between a guide made of OCDS-Copper C 0/94 and valve manufactured of a valve steel and chromium-plated, is 21 times higher, than this parameter for a similar pair, in which the guide is manufactured of the specified bronze.

The materials of DISCOM® Trade Mark are made according to Specifications TU 1479-001-13092819-99, registered by State Standard of Russia under No. 001871, using the technique mechanical and chemical activation of the original powder mixture in attritors and consequent hot extrusion of the granulate obtained.

These materials are manufactured as hot extruded rods and tubes, from which blank parts (with a hole or without it) for valve guides with diameter from 11 up to 20 mm and valve seats with an external diameter from 30 up to 45 mm are made by means of machining.

The consumers of the specified production are JSC Zavolzhsky Engine Plant, where it is used in 16-valve diesel and petrol engines of a new generation, JSC DIESELPROM, which uses it to complete German powerful diesel engines 8V396EC4 made by MTU, and also car manufacturing works in Tolyatti (JSC AvtoVAZ), car manufacturing works in Ulyanovsk (JSC UAZ), car manufacturing works in Nizhni Novgorod (JSC GAZ), which have been using valve guides and valve seats made of these materials to complete their high-speed augmented engines of sports automobiles.

Providing its own machining facilities equipped with high-performance CNC machine tools, TECHMA Co., Ltd is able to supply not only workpieces for valve guides and valve seats, but also ready-made valve guides and valve seats to motor-building enterprises.

FEATURES OF MICROSTRUCTURE FORMATION AND MECHANICAL PROPERTIES OF Ti-B AS-CAST ALLOYS

Bankovskiy O., Beha N., Kulak L., Miracle D.⁽¹⁾, Senkov O.⁽¹⁾, Firstov S.

Frantsevich Institute for Problems of Materials Science of NAS of Ukraine, Kiev, Ukraine

⁽¹⁾Air Force Wright Laboratory, Wright-Patterson AFB, OH USA

As analysis of compositions and properties of best titanium alloys shows, the potential of their solid-solution strengthening is practically exhausted [1]. Oxide or carbide strengthening is among the mostly frequent types of traditional dispersion strengthening of metals by intercalation phases (oxides, carbides, nitrides, borides). However, for titanium, the oxide (and nitride) strengthening is not efficient because of high solubility of oxygen (and nitrogen) in titanium that causes a drastic brittleness of alloys. On the other hand, boron and carbon are low-soluble in titanium (<0.05 %B, 0.5 % C) and form eutectics that comprises α -solid solution and particles of refractory boride, TiB_2 or carbide, TiC [2]. Under such conditions, according to existing understandings, boride and carbide strengthening may have potential for improving the refractoriness of titanium alloys [3]. Examples of successful application of boride strengthening of powder material, XDTiAl are known, as well as the carbide-boride strengthening of Ti-6Al-4V cast alloy [5].

This work has as objective the study of microstructure and mechanical characteristics of Ti-B cast alloys needed to evaluate their potential when development of new refractory titanium alloys.

The Ti-B alloys under investigation were cast by the vacuum arc melting. The alloys were iodide titanium and cast TiB_2 . Ingot weighed 80 to 100 g, of 80 mm in length and 15 mm in diameter. Mechanical characteristics were measured in tensile tests at room temperature. The working portion of specimen was $L_0=15$ mm, diameter of 3 mm. Refractory testing was made by one of accelerated methods, i.e. long-term hardness (value of hardness after 1 hour of holding under loading) [3].

The structure of alloys was investigated by methods of optical metallography and X-ray analysis. The structure of alloys was found to consist of α -solid solution and acicular

precipitates of TiB boride. Sizes of boride particles were naturally enlarged with higher boron concentration, reaching 0.3 to 0.5 mm in the after-eutectic composition (3.5 wt %B).

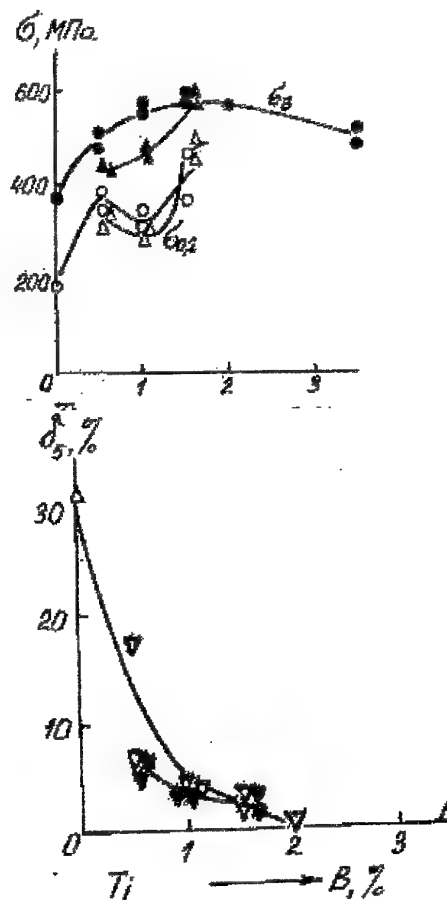


Fig. 1. Mechanical characteristics of Ti-B cast alloys in their initial (● ○ ▼) and annealed (▲ △ ▽) states.

The Ti-B cast alloys were tensile-tested both in original state and in so called «equilibrating» vacuum annealing at 800 °C for 2 hours. The alloy strength ($\sigma_{B1} \sigma_{0.1}$) is seen (Fig. 1) to increase in monotone way with higher boron concentrations and exhibits maximum values at 1 to 2 %B, which is suggested to be an optimum

combination of such two factors as sizes of boride particle and their weight content. A decrease in the alloy strength with $> 2\%$ B can be suggested by an excessive coarsening of boride phases.

An unexpected result was obtained when measuring the plasticity of the Ti-B alloy while increasing the boron concentration. Elongation (δ_5) rapidly lowers reaching zero value at -2% B. X-ray analysis of lattice parameters (Fig.2) shows that α -solid solutions of alloys are boron-oversaturated. This is undoubtedly associated with a higher cooling rate of small ingots. The content of oxygen in ingots is within 0.019 and 0.03 %. The vacuum annealing results practically in a complete recovery of titanium lattice parameters. It can be suggested that the solid solution is somewhat self-purifies due to active diffusion during annealing.

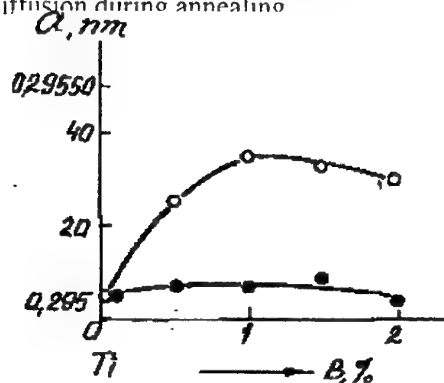


Fig.2. Lattice parameters variations of as-cast Ti-B alloys in initial (○) and annealed (●) states.

However, as can be seen from Fig. 1, this self-purification of the solid solution of boron does not improve mechanical properties of alloys, moreover, deteriorates them to some extent. This deterioration may result from the surface oxidation of specimens during vacuum annealing.

The presence of solid refractory boron phase in alloys ameliorates the Ti-B alloy refractoriness. As Fig 3 shows, the most significant increase of the refractoriness occurs at the $>1\%$ boron concentration.

Therefore, the boron strengthening is a promising way in the improvement of high-temperature (up to 800°C) strength of titanium alloys. The optimum content of boron in cast alloys is 1 to 2 %. The TiB alloys feature their brittleness at

room temperature. Further investigations are needed to solve the problem.

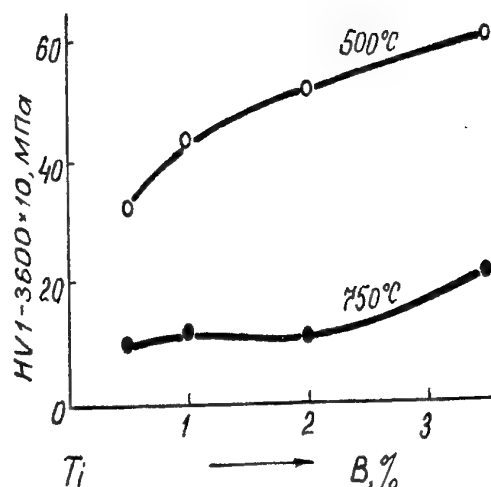


Fig. 3. Long-term hardness of Ti-B cast alloys.

References:

1. Solonina O.P., Glazunov S.G. Refractory alloys. - M: Metallurgia - 1976, 447 p. (In Russian)
2. Molchanova E.K. Chart of phase diagrams of titanium alloys. - M: Mashinostroyeniye, - 1964, 389 p. (In Russian).
3. Zakharov M.V., Zakharov A.M. Refractory alloys - M: Metallurgia. - 1972, 384 p.
4. Discontinuously Technology Titanium 92. Science and Technology. Edited by F/H/ Froes and I. Caplan. The Minerals, Metals, Materials Society, 1993. V.1.15-24 pp.
5. Yoltan C.F. and Moll I.H. Evaluation of a Discontinuously Reinforced Ti-6Al-4V Composite. Titanium 95. Science and Technology. V. 2.2755-2761 p.

The authors would like to acknowledge funding of this project from the US Air Force Office of Scientific Research, and the assistance of the Science and Technology Center of Ukraine.

ADVANCED NANOSTRUCTURED MATERIALS BASED InN FILMS: PREPARATION, PROPERTIES AND POTENTIAL APPLICATION

Goryachev Yu. M., Malakhov V.Ya., Rud B.M.

I. Frantsevich Institute for Problems of Materials Science, NAS, Kiev, Ukraine

Group III-nitrides like AlN, GaN and InN are a new generation of wide band semiconductors with unique physical and chemical properties suitable for using in high-power and high-temperature microelectronics and photonics (e.g. bright light emitting diodes, laser diodes, UV detectors and high efficiency solar cells). The development of low temperature growth methods has resulted in remarkable improvements in the structural, electrical and optical properties of these compounds. As well known, that in the nitride series InN film material is a most preferable candidate for potential applications in photovoltaic, photochromic and sensor devices. Thus, some fabrication details, plus basic structural and optical properties of low temperature plasma enhanced reactively sputtered (LTPERS) InN nanostructured layers are reported. RHEED and AFM studies of the natural surface morphology of InN polycrystalline films were performed. Optical absorption and reflectance spectra of InN textured films were taken to reproduce accurately dielectric function as well as to determine optical effective mass of electrons and the direct band gap energy (2.03 eV). Some TO (485 cm^{-1}) and LO (585 cm^{-1}) phonon features of indium nitride polycrystalline films in the NIR and Raman spectra are observed and discussed. The attractive possibilities of InN layers as top coatings of InN/Si tandem heterojunctions for potential application in PV devices including high efficiency solar cells are confirmed.

Over the last ten years, physical properties of InN thin films obtained by different methods have been studied in numerous works [1-8] including ones of the author. However, optical and electrical parameters, such as dielectric and optical constants, energy gap, effective mass of carriers as well as phonon wavenumbers await for further more accurate definition. A lack of single crystal samples explains the situation regarding the above data. No structural or thermal properties of InN have been studied for epitaxial films on lattice-matched substrates. For this reason, the paper presents original structural and optical data obtained for InN polycrystalline nanostructured films synthesized previously and recently by LTPERS [6-8]. It also offers to use the potential

possibilities of InN/Si heterojunctions in PV devices, including high efficiency solar cells.

Inasmuch as a dissociation temperature of InN films is about 650°C [2], therefore the low temperature growth technique is required. In our case, LTPERS equipment to synthesize InN thin films was used. Intensive Ti-wire evaporation, applied as getter, was carried out during all time of deposition process to reduce oxygen contamination inside of the reactor and in the growing films as well. High quality smooth surfaced Si, quartz, fluorite and compound ceramics were used as substrates. During film growth, the substrate temperature was about 350°C , due to intensive ion bombardment of the top electrode (anode) during sputtering process. Film thickness varied in the range 100-2000 nm. To determine the chemical composition of the sputtered InN films Auger spectrometer (JAMP-10) was used. The surface morphology and the microstructure of a cross-section of the films were investigated using Philips SEM5V scanning electron microscope plus standard atomic force microscope (AFM) equipment. The crystalline structure parameters of the sputtered films were determined using an X-ray diffractometer (DRON-3) employing $\text{Cu}(\text{K}\alpha)$ radiation, and also by means of the electronograph EG-100a. Reflectance and transmittance measurements in visible and NIR regions ($25000\text{--}200\text{ cm}^{-1}$) were carried out using a Bruker IFS-66 Fourier transform spectrometer (FTIR) and Carl Zeiss M40 grating spectrometer, respectively. A Raman spectrometer Dilor XY equipped with microscope, was used to study the phonon spectra of the nitride films.

X-ray diffraction patterns of α -InN (wurtzite) layers deposited on ceramic substrates demonstrate a very strong diffraction peak corresponding to the InN (002) plane. This suggests a textured crystalline structure of deposited layers, where the c axis is perpendicular to the plane of substrate. The same result was obtained from study of the AFM image of InN layer on ceramics (Fig. 1). These results plus an Auger-investigation, show that no outsider phases except InN one were presented in the films. Some off-stoichiometric In/N ratio, with an abundance

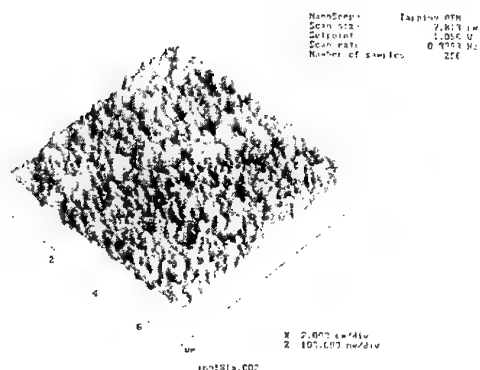


Figure 1. AFM image of InN layer on ceramics.

of In inside nitride films was caused by nitrogen vacancies. They were revealed in the films that, probably, leading to amorphous indium oxide partially forming (bound oxygen). Moreover, other inactive oxygen molecules are incorporated in voids between the InN grains.

Further transmittance and reflectance spectra in visible range were taken to determine the band gap energy of InN thin films on CaF_2 (fluorite) substrates. In this procedure the gap energy was derived from absorption coefficient spectrum of InN layer and yielded $E_g \approx 2.03$ eV which is very close to earlier value [6]. Moreover, the PDS method was used to explore some peculiarities in the free carriers absorption spectra for InN polycrystalline films deposited on different substrates. In order to obtain the necessary information about phonon features of InN films as well as to determine precisely some optical parameters the Drude-Lorentz formalism was used for dielectric function modeling procedure to reflectance spectra from both InN films surface and bare fluorite substrate. Final result shown a good agreement between experimental data and the calculated curve [7]. Also, in our opinion, the reflectance peaks at 485 and 590 cm^{-1} , respectively, are connected with TO and LO vibration modes of indium nitride [3-5]. An identical result was obtained from a study of Raman spectra for InN textured films (>1 μm thickness) on ceramics. The broadening of the peak at 485 cm^{-1} in the Raman spectra of nitride layer is very close to that observed in the reflectance spectra. However, because of the imperfect crystalline structure of our samples, we can observe only two optical phonon modes: $E_1(\text{TO})$ at 480 cm^{-1} and $A_1(\text{LO})$ at 585 cm^{-1} . For this reason, it was also difficult to find the main LO phonon mode at 694 cm^{-1} , as predicted by Osamura *et al.* [4].

In order to estimate potential possibilities of InN film material for solar cell fabrication, some theoretical and practical considerations were used. To achieve an optimum power conversion efficiency η for solar cells based on an InN n-layer (emitter) and p-Si (base), large $\alpha(E)$, minority carrier lifetime τ , diffusion length L (at least $\alpha L > 3$ for front side illumination) and surface recombination velocity S have to be combined. This can be achieved under compromise condition of optimum band gaps E_g (~ 1.0 and 2.0 eV) for an efficient tandem system consisting of several stacked single cells between a large I_{sc} or V_{oc} [1].

Summarizing, an appropriate solar cell base material should exhibit a proper energy gap and a strong absorption ($\alpha_{\text{InN}} > 10^4 \text{ cm}^{-1}$) adjusted to the solar spectrum, a dopability by carriers featuring high mobilities and long lifetimes. Another important advantage of an InN/Si heterojunction in future solar cells is a protective function including protection from radiation using the absorptive InN layer as a top coating. The existing problem of heteroepitaxy of InN films on Si will be resolved by research into an appropriate buffer layer (e.g. AlN thin layer) on InN-Si interface, to match the lattice periods and improve of the heterojunction operating parameters (fig.2). The fabrication of high quality heterojunctions based InN/Si is also of great importance for manufacturing of high efficiency solar cells.

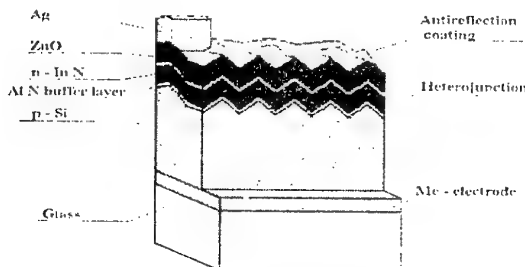


Figure 2. Layer structure of an InN/Si solar cell

References

1. Yamamoto A. *et al.*, *Sol. Energy Mater. & Sol. cells.* **35** (1994) 53-60.
2. Ambacher O., *J. Phys. D Appl. Phys.* **31** (1998) 2653.
3. Tansley T., Egan R., Horrigan E., *Thin Solid Films.* **164** (1988) 441-448.
4. Osamura K., Naka S., Murakami Y., *J. Appl. Phys.* **46**. (1975) 3432-3437.
5. Kwon H., Lee Y., *Appl. Phys. Lett.* **69** (1996) 937.
6. Tyagai V., Malakhov V. *et al.*, *J. Sov. phys.Semicond.. (USA)*, **11** (1977) 1257-1261.
7. Malakhov V., *Proc. of Euromat'99*, **9** (1999) 75-79.
8. Malakhov V., *Proc. of TATF'2000*, Extended Abstr. Booklet (2000) 351-353.

WEAR-RESISTANT W-C AND Cr-Ti-C PARTICULATE COMPOSITES

Spiridonova I., Sukhova O., Butenko V.
Dnipropetrovs'k National University, Ukraine

In engineering and metallurgical industries, machine parts often work in conditions where intensive abrasive wear occurs.

Over the past years, a lot of studies concerning various composites have been done. It has been shown that composites of metal matrix reinforced with particulate made of tungsten and chromium-titanium carbides have specific resistance to wear. However, the control of the interfaces has become more critical as its effect on the wear resistance of the composites has been revealed. It has been established that some metal matrices (e.g. copper-base alloys) are too weak to support the carbides. Besides, the reaction between matrix and particles should be controlled by the proper selection of composite constituents for achieving high performance.

In this abstract, a new Fe-B-C eutectic matrix reinforced with W-3.5C or Cr-20Ti-10C particles has been studied for use in place of the traditional copper-base matrices.

The metal matrix composites were fabricated by infiltrating the particulate by Fe-B-C eutectic alloy at 1130°C to 1200°C for 30 to 60 mins. The used particulate had irregular shape and was about 0.5 to 2.0 mm in size. Optical and scanning electron microscopy and X-ray microanalysis were employed to investigate the specimens.

Wear tests were carried out using a tester in which specimens were fixed with certain angles. Quartz sand particles impacted specimens at an angle of 45°. For each period the measured erodent quantity was 6 kg. Not less than four tests of 35 mins each were run in ambient air (60-pct humidity, room temperature). Specimens were tested against the composite material composed of the W-3.5C reinforcement and Cu-20Ni-20Mn binder.

The microstructures of the composite materials under investigation consist of reinforcing particles distributed uniformly in the iron-base matrix. The volume percentage of the particulate in the composites reaches 55 pct to 65 pct.

The W-3.5C reinforcing particles are distributed in the α -Fe₃(C,B) eutectic matrix alloyed with tungsten. A shell consisting of the WC and Fe₃W₃C carbides is observed around each particle (fig. 1, a).

When raising the temperature and prolonging the holding time during infiltration up to 1170°C

and 60 mins, respectively, new microconstituents appear near the particle/matrix interface (fig 1, b). They have two-phase non-uniform structure which is a result of a solid state transformation. Morphology, microhardness ($H\mu=2.7\pm0.5$ GPa), and mean chemical composition allow to identify this phase as austenite alloyed with tungsten.

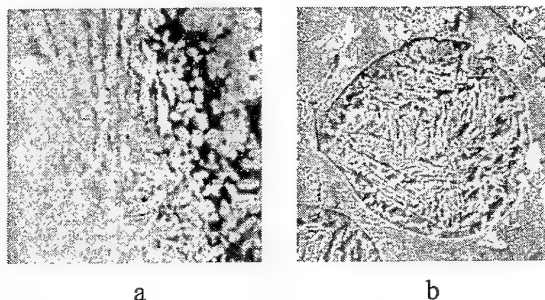


Fig.1 Microstructure of W-3.5C particulate composites infiltrated: a – at 1150°C for 30 mins, x 800; b - at 1200°C for 45 mins, x 800

The Cr-20Ti-10C carbide exhibits two-phase structure consisting of dark primary crystals of $(Ti_{0.5}Cr_{0.5})_3C$ and light crystals of $(Cr_{0.95}Ti_{0.05})_7C_3$ (fig.2, a). After infiltration by Fe-B-C eutectic alloy the structure of the composites displays the formation of interfacial zones between the carbide and the matrix which vary in width from 50 μ m to 250 μ m. The interfacial zones produced as a result of the contact interaction consist of $(Cr,Ti)_7C_3$ and $(Ti,Cr)_3C$ embedded in the α -Fe₃(C,B) eutectic alloyed with Cr and Ti (fig. 2, b). The microhardness of the eutectics is 8.5 GPa.

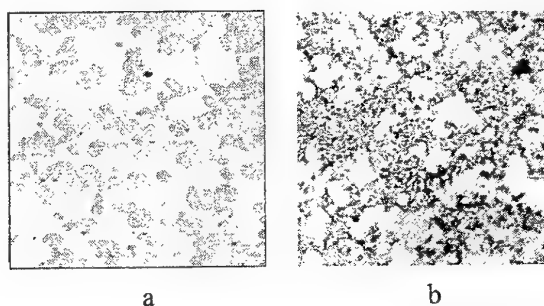


Fig. 2 Microstructure of Cr-20Ti-10C and interfacial zone Cr-20Ti-10C/Fe-B-C, x200

At higher infiltrating temperatures and longer holding times the formation of $(Cr,Ti)_7C_3$ can be accelerated. The width of the interfacial zones increases.

II. PERSPECTIVE MATERIALS OF FUNCTIONAL AND STRUCTURAL PURPOSES: POSSIBILITIES OF OBTAINING NEW LEVEL OF PROPERTIES

The results of determination of wear resistance of the investigated composite materials are given in Table.

Table
Coefficients of relative wear resistance (ϵ) of the composites with Fe-B-C eutectic binder

Infiltration parameters		ϵ , units	
		Particulate	
T, °C	t, mins	W-C	Cr-Ti-C
1130	40	1.45±0.32	0.78±0.54
1150	30	1.47±0.22	0.89±0.36
1150	40	1.51±0.43	1.03±0.46
1150	50	2.00±0.17	0.97±0.21
1150	60	1.94±0.28	0.98±0.12
1150	90	1.86±0.14	0.85±0.26
1160	40	2.03±0.51	1.12±0.16
1170	60	1.92±0.47	0.90±0.41
1190	60	1.73±0.72	0.82±0.22
1200	60	1.61±0.58	0.75±0.04

First, coefficient of relative wear resistance (ϵ) increases with increasing temperature and duration of infiltration, and, then, decrease. Maximum wear resistance show the composites infiltrated at 1150 °C to 1160°C during 40 to 50 minutes.

While infiltrating at proper temperature and holding time, the reinforcing particles are soundly anchored in the matrix and show only slight brittle fracture behavior and resistance to cracking and chipping off of small pieces by the erosive media. Rates of the particulate erosion are substantially lower than those for other specimens.

Based on the above results, it is possible to conclude that during infiltration the reinforcing particles dissolves in the Fe-B-C molten alloy. The crystals of W_2C observed in the structure of W-3.5C particulate dissolve in the first place. It appears that the accompanying dissolution of tungsten and carbon in the Fe-B-C eutectic alloy leads to the formation of the Fe_3W_3C crystals when solidified. Therefore, the shell of Fe_3W_3C alloyed with boron in which the WC carbides are distributed is observed around the reinforcing particles. On cooling, intensive solid state diffusion processes take place, and, that is why, some iron traces are revealed in the center of the tungsten carbide particles.

At higher infiltration temperatures and longer holding times the above described processes cause the alteration of the initial eutectic composition of the Fe-B-C alloy. It changes to hypoeutectic one, which leads to the formation of the primary aus-

tenite crystals upon solidification. Then, the α - $Fe_3(C,B)$ eutectic alloyed with tungsten supplied from the reinforcing particles crystallizes. The austenite crystals more easily form on the surface of the Fe_3W_3C carbides. Therefore, a lot of them are observed near the particle-matrix interfaces. While cooling, the austenite crystals decompose to the microconstituents of a sorbite kind that are alloyed with tungsten and inherit the morphology of the primary austenite crystals.

The origin of the formation of interfacial zones between Cr-20Ti-10C and Fe-B-C alloys is probably related to the partial dissolution of the low-melting-temperature phase identified as Cr_7C_3 alloyed with titanium from the particulate into molten matrix. Due to the loss of carbon, Cr_7C_3 carbide decomposes to the lower $Cr_{23}C_6$ carbide, which contributes to the rapid dissolution of the phase. The high-melting-temperature ternary $(Ti,Cr)_3C$ phase remains unchanged during all the processes of contact interaction, and, therefore, it is present in the form of dark inclusions in the α - $Fe_3(C,B)$ eutectic structure. The dissolution of the ternary phase is hampered not only by relatively high melting temperature of the phase, but also by an increase in the melting temperature of the surrounding eutectic alloyed with titanium.

The suggested mechanisms seem to explain the increase in the width of the interfacial zones due to the intensification of the diffusion of components from the particulate into the matrix.

At lower temperature and shorter holding time the reaction occurring between the matrix and the carbide particles is not enough to provide the necessary amount of the particles components alloying the matrix. Accordingly, its hardness lowers somewhat. And, the matrix fails to support the carbide particles and they fall out.

After infiltration at temperature of 1170°C to 1200°C and holding time longer than 50 mins, the width of the interfacial zones increases significantly, and, in some cases, in the structure appear detrimental phases (e.g. the austenite crystals). Wear proceeds severely in the boundaries around the particulate where these crystals are distributed. It weakens matrix/particle interface and causes faster destruction of the composites.

Maximum wear resistance show the composite materials infiltrated at 1150°C to 1160°C during 40 to 50 mins. They combine the proper structure of the matrix and strong particulate/matrix interface, which allow them to work well in severe service conditions. The investigated composite materials can be used to strengthen wearing parts of metallurgical, machine-building, etc. equipment.

THE INFLUENCE OF LITHIUM- AND ALUMINUM-CONTAINING ADDITIVES ON THE PROCESSES OF PHASE FORMATION DURING THE SILICON NITRIDE-BASED MATERIAL SINTERING

Grigoriev O.N., * Rogozinskaya A.A., Klochkov L.A., Krushinskaya L.A., Dubovik T.V.,
Zyatkevich N.S.

Frantsevich Institute for Problems of Materials Science of NAS Ukraine, Kyiv, Ukraine

As can be seen from publications, Li-containing ingredients and aluminum nitride additives shall be useful for increasing resistance of Si_3N_4 -based materials to lithium melts, enhancement of ion conductivity, and as opportunity of using them as solid electrolytes [1-3]. Therefore, a need arouse to investigate the

powder; $\alpha\text{-Si}_3\text{N}_4$ - 20 % Li_2CO_3 - 10 and 20 % AlN or Al -powder. As it was expected while using the Al -powder as additive to Si_3N_4 , the Al -powder would be nitrated and passed into the AlN -phase.

The pressed compacts were sintered in nitrogen medium at 1700, 1800 and 2000 K in a fill of BN powder. Diffractometer of DRON-3M

Table 1. The phase-formation process in materials based on $\alpha\text{-Si}_3\text{N}_4$ with Li- and Al-containing additives during the sintering

N	Material composition, mas. %	Sintering temperature, K		
		1700	1800	2000
1	$\alpha\text{-Si}_3\text{N}_4\text{-10AlN}$	-	$\alpha\text{-Si}_3\text{N}_4$, $\beta\text{-Si}_3\text{N}_4$, AlN	-
2	$\alpha\text{-Si}_3\text{N}_4\text{-20 AlN}$	-	$\alpha\text{-Si}_3\text{N}_4$, $\beta\text{-Si}_3\text{N}_4$, AlN	-
3	$\alpha\text{-Si}_3\text{N}_4\text{-10Al}$ - powder	-	$\alpha\text{-Si}_3\text{N}_4$, $\beta\text{-Si}_3\text{N}_4$, AlN , AlSiO_2	-
4	$\alpha\text{-Si}_3\text{N}_4\text{-20Al}$ - powder	-	$\alpha\text{-Si}_3\text{N}_4$, $\beta\text{-Si}_3\text{N}_4$, AlN , AlSiO_2	-
5	$\alpha\text{-Si}_3\text{N}_4\text{-20Li}_2\text{CO}_3\text{-}$ 10AlN	$\alpha\text{-Si}_3\text{N}_4$, $\beta\text{-Si}_3\text{N}_4$, AlN , LiSi_2N_3 , Li_2SiO_3	$\alpha\text{-Si}_3\text{N}_4$, $\beta\text{-Si}_3\text{N}_4$, AlN , SiAlON , LiAlSiO_4 , Li_5SiN_3	$\alpha\text{-Si}_3\text{N}_4$, $\beta\text{-Si}_3\text{N}_4$, AlN , LiAlSiO_4 , Li_5SiN_3
6	$\alpha\text{-Si}_3\text{N}_4\text{-20Li}_2\text{CO}_3\text{-}$ 20AlN	$\alpha\text{-Si}_3\text{N}_4$, $\beta\text{-Si}_3\text{N}_4$, AlN , LiSi_2N_3 , Li_2SiO_3	AlN , SiAlON , LiSi_2N_3 , LiAlSiO_4 , LiAl_5O_8	$\alpha\text{-Si}_3\text{N}_4$, $\beta\text{-Si}_3\text{N}_4$, AlN , LiAlSiO_4 , Li_5SiN_3
7	$\alpha\text{-Si}_3\text{N}_4\text{-20Li}_2\text{CO}_3\text{-}$ 10 Al-powder	$\alpha\text{-Si}_3\text{N}_4$, $\beta\text{-Si}_3\text{N}_4$, AlN , LiAlSiO_2 , $\text{LiAlSi}_2\text{O}_3$	$\alpha\text{-Si}_3\text{N}_4$, $\beta\text{-Si}_3\text{N}_4$, AlN , SiAlON , LiAlSiO_4	$\alpha\text{-Si}_3\text{N}_4$, $\beta\text{-Si}_3\text{N}_4$, AlN , LiAlSiO_2 , $\text{LiAlSi}_2\text{O}_3$
8	$\alpha\text{-Si}_3\text{N}_4\text{-20Li}_2\text{CO}_3\text{-}$ 20 Al-powder	$\alpha\text{-Si}_3\text{N}_4$, $\beta\text{-Si}_3\text{N}_4$, AlN , LiAlSiO_2 , $\text{LiAlSi}_2\text{O}_3$	SiAlON , LiAlSiO_4 , AlN , LiSi_2N_3	$\alpha\text{-Si}_3\text{N}_4$, $\beta\text{-Si}_3\text{N}_4$, AlN , LiAlSiO_2 , $\text{LiAlSi}_2\text{O}_3$

influence of lithium and aluminum-containing additives on the processes of phase formation during the sintering of silicon nitride-based materials.

Eight different mixtures based on $\alpha\text{-Si}_3\text{N}_4$ (in wt%) were prepared to study the processes of structure formation while adding Li_2CO_3 and AlN or Al powder: $\alpha\text{-Si}_3\text{N}_4$ - 10 and 20 % AlN or Al -

type was used to perform X-ray phase analysis in $\text{CuK}\alpha$ -radiation. The results of study are given in Table 1.

As it was stated when analyzing binary systems sintered at 1800 K, higher are amounts of Al-containing additives, stronger are the AlN -pattern lines. On the other hand, the Al powder-derived AlN -lines are faint and blurred, thus

* grigorev@ipms.kiev.ua

suggesting an imperfection of this structure lattice.

The data concludes that the phase-formation process of the triple system under study is dependent on the temperature of sintering, amount and composition of additives (AlN or Al-powder). Rising amounts of Al-containing additives contribute the intensity of lines of developing phases, and the increase of lattice parameters α -

characteristics of α -Si₃N₄- based material in contrast to the Al-powder addition, which «loosen» the material during its sintering, and at higher temperature in particular.

The parameters of α -Si₃N₄ lattice were computed within the compositions studied. The lattice parameters variation of silicon nitride can be observed in triple systems at the 1800 and

Table 2. The variation of α -Si₃N₄ crystal lattice parameters during the sintering of Si₃N₄ -Li₂CO₃-AlN (Al-powder) system materials

Material composition, mas. %.	Sintering temperature, K	Crystal lattice parameters of α -Si ₃ N ₄ , Å		
		a	c	a/c
Initial α -Si ₃ N ₄	-	7,756	5,615	0,724
α -Si ₃ N ₄ -20Li ₂ CO ₃ -10AlN	1800	7,881	5,695	0,723
α -Si ₃ N ₄ -20Li ₂ CO ₃ -10 Al-powder	1800	7,885	5,684	0,721
α -Si ₃ N ₄ -20Li ₂ CO ₃ -10 AlN	2000	7,889	5,725	0,726
α -Si ₃ N ₄ -20Li ₂ CO ₃ -10 AlN	2000	7,903	5,748	0,727
α -Si ₃ N ₄ -20Li ₂ CO ₃ -10 Al- powder	2000	7,880	5,716	0,725
α -Si ₃ N ₄ -20Li ₂ CO ₃ -10 Al- powder	2000	7,884	5,710	0,724

Si₃N₄ and β -Si₃N₄. Addition of Al-powder at the 1700 and 2000 K sintering temperatures produces no change of phase composition, but the intensity of lines of aluminum-lithium silicates is considerably weaker, and lattice parameters of α -Si₃N₄ and β -Si₃N₄ are greater at 2000 K. The AlN additives produced a difference between the specimen compositions as prepared at 1700 and 2000 K: blurry lines of new triple phases (Li₃SiN₃ and LiAlSiO₄) have appeared at 2000 K. The most interesting processes occur at 1800 K. A noticeable effect on the phase composition is exerted by a quantity increase of AlN and Al-powder additions, measuring from 10 to 20 %. The 20 % addition causes disappearance of the Si₃N₄ phase and well developed phases of sialon and double nitride (LiSi₂N₃) appear. Adding of 10 % maintain the α -Si₃N₄ and β -Si₃N₄ structures with increased lattice parameters unchanged and a distinct LiAlSiO₄ phase and less distinct sialon phase are appearing. It should be noted as a whole, addition of AlN produces a significant influence on the strength and hardness

2000 K sintering temperatures due to interstitial lithium in its crystal lattice. Data is given in Table 2.

So, regulation of the sintering temperature, composition and amount of lithium- and aluminum-containing additives may be provided materials based on Si₃N₄ with desired phase compositions and respective properties.

REFERENCES

1. Pilipchuk M.A., Kedrinskiy I.A., Moroz S.V. et al. Corrosion resistance of nitrides of aluminum and silicon / Refractory nitride (Proceed.) - K. Naukova dumka, 1983. P.118-121 (In Russian).
2. Samsonov G.V., Dubovik T.V., Trunov G.V. et al. Resistance of some non-oxygen materials to lithium and barium attack / Ibid. -P.110-112 (In Russian).
3. Non-metal refractory compounds / T.Ya. Kosolapova, T.V.Andreyeva, T.S.Batrnitskaya et al. Moskow: Metallurgiya. 1985. - 224 p.

THE INFLUENCE OF VIBRO-MILLING ON THE PROPERTIES OF AlN-BN SYSTEM MATERIALS

Kovalchenko M.S.,* Dubovik T.V., Rogozinskaya A.A., Panashenko V.M., Zyatkevitch N.S.

Frantsevich Institute for Problems of Materials Science of NAS Ukraine, Kyiv, Ukraine

There are publications covering the formation of AlN-BN system materials during sintering using initial mixtures such as Al-BN, AlN-B or $AlB_{1/2}$ powder [1]. This paper describes an attempt to design composite materials made of nitrides of Al and B through the direct use of AlN and BN initial powders.

It is known that the process of BN sintering activation requires initial powders having disordered microstructures or reaction sintering agents, while the aluminum nitride needs an enlarged reacting surface, and faulted structure of initial powders achieved by mechanical milling [1, 2]. The high-defect states of ground powders of aluminum and boron nitrides are expected to create conditions useful for their joint sintering.

Due to the above said, this paper is aimed at the research of the influence of initial vibro-ground powders of various grain size and defect degree on the processes of densification during sintering, and physical-mechanical properties of AlN-BN system composite materials.

As initial powders, AlN and BN powders were used having the 3.0-4.5 and 11.5-12.0 m^2/g specific areas, respectively. Each powder was ground in the vibrating mill of M-10 type for 1, 2, 4 and 8 hours.

As it was stated, an increase of grinding time from 1 to 8 hours resulted in a proportional increase of AlN specific area from 5.3 up to 7.5 m^2/g , while the BN powders remain at the initial level between 11.5 and 12.0 m^2/g . AlN as a brittle material is easily subjected to grinding, whereas BN is hardly-ground material due to its crystalline structure as the powder «spread» over the mill walls and nodulizes. It would be rational to perform the boron nitride vibro-milling jointly with a brittle powder, which shall serve as a «filler» and an additional grinding agent.

As X-ray analysis has shown, the initial powder of AlN had a distinct wurtzite structure with lattice parameter of: $a=3.110$ Å, $c=4.978$ Å. The powder remains its structure within one hour after the vibro-milling, and low angles produce $\alpha-Al_2O_3$ -phase patterns. After 2, 4 and 8 hours of vibro-milling, the thin crystalline structure of the AlN powder changes, i.e. coherent dissipation areas become shorter, and microdistortions occur, that increase with the grinding duration. This is exhibited through a blurring and enlarging on X-ray pattern lines, hkl (101) and (302). The BN powder has a hexagonal structure with the lattice parameters of $A=2.504$ Å, $c=6.668$ Å. This hexagonal powder structure remains unchanged for one hour. After 2 to 8 hours, the structure approaches to an amorphous state, and line blurring can be observed at low angles while high angles showing a rather fusing with the background.

Further investigations used powders of AlN and BN having the 5.3-7.5 and 12.0 m^2/g specific areas, respectively.

To select a material of desired composition in the AlN-BN system, a lot of mixtures of boron nitride (12.0 m^2/g) were prepared added with 10-90 wt% of AlN (5.3 m^2/g) and the 10 % step involved. Different pressing and sintering regimes for aluminum nitride were used to produce specimens of the AlN-BN system useful for measuring compressing strength and resistivity at 293 and 1270 K. The peak values of these parameters were used to determine the optimum composition for the 50 AlN and 50 BN (wt%) composite material.

The processing conditions for making materials of the AlN-BN system were studied using an optimum composition under the pressures of 100, 200 and 300 MPa and temperature of sintering of 2070, 2170 and 2270 K. The optimum processing conditions (pressure of 200 MPa and sintering temperature of 2170 K) were determined using the

* mscoval@ipms.kiev.ua

electric resistance values and compression strength values.

The grain size influence of initial powders on the densification process at pressing, thermal-mechanical properties and electric resistance was measured on a sintered material of optimum composition. Powders of aluminum and boron nitrides with the 5.3-7.5 and 12 m²/g specific areas, respectively, were used. In fact, AlN powder grain size influence on composite material properties was studied. Tables 1 and 2 give data of study.

As can be seen from Tables 1 and 2, the higher specific area of AlN powder, the higher are the

$c=6.659-6.660$ Å. The values as obtained correlate with those in publications [1]. Further more, aluminum pattern lines have also been observed, low-angle reflections had faint lines of the α -Al₂O₃ phase.

The chemical analysis data concludes that the AlN power grain size has any substantial effect upon the material composition. All the specimens correspond to the following compositions (in wt%): 17.1-17.4 B; 34.5-34.8 Al; 35.2-35.5 N; 0.3-0.7 B₂O₃; 3.2-3.5 C; and 0.5-0.6 Fe. The material based on AlN or BN is easy machinable.

The physical-mechanical properties of the material as designed open opportunities for the use of

Table 1. Thermal-mechanical properties of the AlN-BN-based material of optimum composition when using AlN powders differing in specific areas

Surface area AlN powders, m ² /g	Properties of specimens as ground			
	Density, g/cm ³	Mechanical strength $\sigma_{сж.}$, MPa	Thermal resistance, numbers of cycles 2170-293 K	Thermal expansion coefficient, $\times 10^{-6}$, grad ⁻¹ , at 293-1270 K
5.3	2.17	90.1	144	0.77-4.2
5.8	2.29	98.6	163	0.77-4.4
6.7	2.44	105.4	175	0.7-4.0
7.5	2.50	108.8	171	0.77-4.3

Table 2. Temperature dependence of electrical resistivity (Ohm·cm) of the AlN-BN-base material having optimum composition when using AlN-powders differing in specific areas

Temperature, K	Electric resistivity, Ohm·cm*			
473	$2 \cdot 10^{12}$ (5.3)	$1.9 \cdot 10^{10}$ (5.8)	$4.9 \cdot 10^{10}$ (6.7)	$5 \cdot 10^{11}$ (7.5)
673	$1 \cdot 10^{11}$ (5.3)	$1.6 \cdot 10^{10}$ (5.8)	$6 \cdot 10^{10}$ (6.7)	$2 \cdot 10^{10}$ (7.5)
873	$2 \cdot 10^9$ (5.3)	$3.5 \cdot 10^9$ (5.8)	$1.1 \cdot 10^9$ (6.7)	$8 \cdot 10^8$ (7.5)
1073	$3 \cdot 10^7$ (5.3)	$6 \cdot 10^7$ (5.8)	$5.6 \cdot 10^7$ (6.7)	$2 \cdot 10^7$ (7.5)
1273	$5 \cdot 10^6$ (5.3)	$6 \cdot 10^6$ (5.8)	$8 \cdot 10^6$ (6.7)	$3 \cdot 10^6$ (7.5)
1473	$6 \cdot 10^5$ (5.3)	$1 \cdot 10^6$ (5.8)	$9 \cdot 10^5$ (6.7)	$2 \cdot 10^5$ (7.5)

*The parenthesis contain specific area values for AlN powder in m²/g.

values of density, mechanical strength and thermal resistance of the material. On the other hand, coefficient of thermal expansion and electric resistivity of the material are independent of the AlN powder grain size.

As X-ray phase analysis revealed, all the specimens under study, irrespective of the AlN grain size, had two phases - AlN and BN with lattice parameters as follows: AlN - $a=3.110-3.115$ Å, $c=4.978-4.982$ Å; BN - $a=2.501-2.504$ Å,

vibro-milling for creating ceramics on the base of nitrides of aluminum and boron, directly using initial powders of AlN and BN.

REFERENCES

1. Non-metal refractory compounds/T.Ya.Kosolapova, T.V.Andreyeva, T.S.Batrnitskaya et al. Moskow: Metalurgiya. 1985. - 224 p.
2. Poluboyarinov D.N., Kuznetsova I.G., Sadkovsky E.P. et al. On influence disordered crystal lattice of BN on its sintering // Ogneupory. - 1971. - N 2. - p. 27-32.

INTERACTION OF PULSED PLASMA WITH SURFACE LAYERS; PROCESSES OF IMPLANTATION AND MASS TRANSFER

Tyurin Y.N., Pogrebnjak A.D.⁽¹⁾, Kshnjakin V.S.⁽¹⁾, Kolisnichenko O.V.

Paton Institute of Electric Welding, Kiev, Ukraine

⁽¹⁾Institute of Surface Modification, Sumy, Ukraine

The performed experiments demonstrated that treatment of the tool surfaces by a pulsed plasma containing doping elements is accompanied by a total complex of various effects (shock, heat, electromagnetic, deformation ones). The implantation of elements into a plasma is realized with the help of an evaporated metallic electrode and gas (a propane-butane mixture, a nitrogen, an oxygen). In such a way, on the basis of the performed experiments, we concluded that in the process of pulsed plasma treatment, a tool surface is initially subjected to an elastic-deformation effect of a shock wave and a pulsed plasma jet, then it is subjected to an action of an electric current. The amplitude current value reaches 4 kA. As a result, a pulsed magnetic field of to 2000 Oe intensity is formed. Practically simultaneously combustion products of combustible gases cover the surface for 3 to 5 μ s together with an accelerated and heated (and/or melted) doping material from a destroyed electrode. Interaction of the metal containing plasma jet with the tool surface is realized for 2 to 5 $\times 10^{-3}$ s, which conditions its short time heating. A combined gas dynamical and electromagnetic action on the metal surface provides mixing of the doping material with the substrate and induces an accelerated crystallization of the surface layer. Metallography investigations showed that as a result of pulsed-plasma treatment of tools on iron base, a micro-crystal doped layer of 60 to 120 μ m thickness was formed on their surfaces (Fig.1). The main component is iron. After 10 pulses a limiting Mo concentration is about 8 at.%. The maximum is positioned at about 7 μ m depth from the surface.

The layer hardness reached 16 Gpa. The presence of visible defects in the layer depends on the plasma composition and number of treating pulsed. The layer Fig.2 shows the data on the measured concentration of elements over the depth in α -Fe after pulsed plasma treatment.

The Figure shows that the thin surface layer of α -Fe is saturated by an oxygen, a nitrogen and a carbon, and their concentration quickly decreases with depth. Mo concentration in the

near surface layer of to 10 μ m thickness is 4.7 at.% and increases with depth to 7.8 at.%.

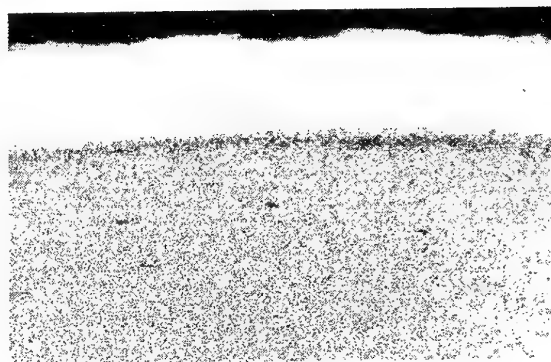


Fig.1. The structure of the modified layer after treatment, 5 pulses.

One should note that the carbon concentration increases non-essentially with increasing number of pulses, whereas that of the oxygen reaches 40 at.% even after 15 pulses.

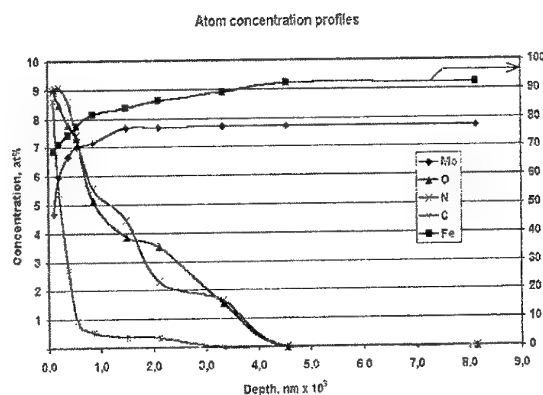
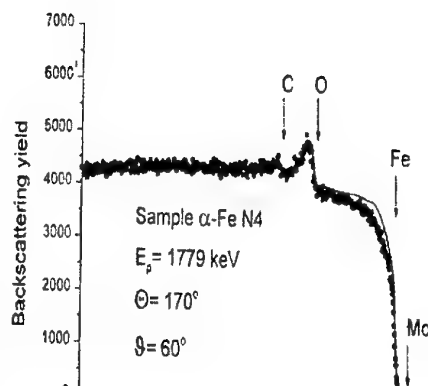
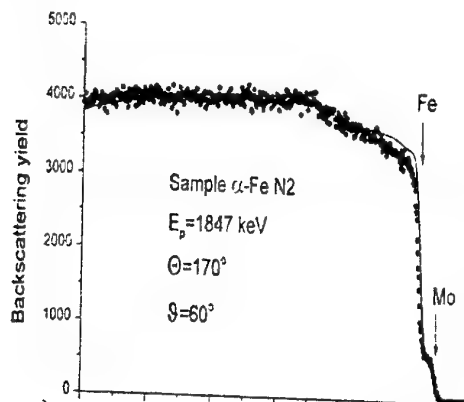
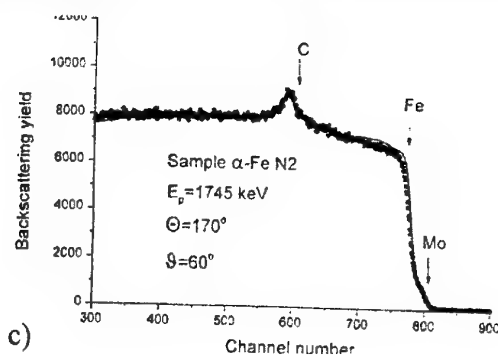


Fig.2. The concentration profiles of elements vs the depth in α -Fe after plasma jet treatment during 15 pulses.

The molybdenum concentration in the implanted α -Fe increased to its maximum and falls within the interval 4 to 20 pulses. Its maximum concentration is 8at.%, which is reached after 10 pulses of a high-rate pulsed jet.

Fig.3 (a,b,c) presents the energy spectra of Rutherford back scattering of ions (a), which were obtained for α -Fe after its treatment by the plasma jet, and the spectrum of an elastic resonance on protons within 1745 keV (b,c), which was obtained for the same sample.

The boundary of the kinetic Fe and Mo factor, which peak is at the right side, is well pronounced and seen. The formation of a small step evidences that near the surface, in the layer



FORMATION OF COMPOSITE METAL MATERIALS IN CONDITIONS OF SHOCK-WAVE LOADING

Usherenko S.M., Zel'dovich V.I.⁽¹⁾, Homskaja I.V.⁽¹⁾, Ovchinnikov V.I., Koval O.I.

Research Institute of Impulse Processes, Minsk, Belarus

⁽¹⁾Institute of Metal Physics, Ekaterenburg, Russia

The essence of superdeep penetration effect is the fact that microparticles of a various nature (metals, carbides, nitrides etc.) under certain loading conditions are capable to penetrate into metal barrier on the distances exceeding the size of particles in 100-1000 times. Conditions of realization of superdeep penetration are the following: the size of particles is up to 500 microns, speed- 0,5-2,5 km/sec, time of influence $100-400 \cdot 10^{-2}$ sec [1]. Dispersal of particles is executed by the explosive accelerator. The stream of particles at impact with the barrier raises shock waves in it. Outstripping action of shock waves creates in a material of a barrier of a condition necessary for superdeep penetration a small share of the dispersed particles ($\approx 1\%$). Particles of the sizes up to 70 microns penetrate into a processable material on depth of several tens millimeters.

The purpose of the work consists of research of the microstructural changes caused by influence of a stream of high-speed particles and definition of efficiency of superdeep penetration for metals and alloys with various physical and mechanical properties. Density of formed channel formations and their average diameter were accepted as the criterion of efficiency shock-wave penetration.

As a material of metal barrier were chosen: alloys of system Fe - Ni (H6, 10H6, 20H6, 45H24, H32), steel 10, steel 40, aluminum, titan, copper. The choice of metals for research was made counting the difference of their physical characteristics. In particular, for iron - nickel alloys existence of dynamic phase transition (polymorph transformation) is experimentally known and there are no experimental data about its presence in copper and aluminum. By modeling performances about cause of the superdeep penetration and the factors that influence this process, phase transition plays the important role.

The material of particle is powder SiC of fraction 63-70 microns.

Particles those are moving in material form channels of superdeep penetration. The

microstructure of the processed samples is characterized by high density of channels: 10^2-10^4 mm².

The amount of channel formations in regular intervals decreases by depth of the sample. It was found that the sizes of penetrated particles 1-2 times less than initial particles of the powder. In samples of the all researched materials superficial saturation of walls of channels by elements of brought particles was found.

Action of shock waves is accompanied by high-speed deformation and formation of phases of high pressure. In alloys H6, 10H6, 20H6 traces $\alpha \rightarrow \varepsilon \rightarrow \alpha$ transformations, in alloys 45H24 and H32 - $\alpha \rightarrow \gamma$ transformation are found out. It means that the size of background pressure in separate sites of samples reaches 8-12 GPa [2]. It is found that phase transformations proceed non-uniform on all the volume of samples. Zones of realization of phase transitions are zones of channel formations.

It is proved, that on efficiency of realization of superdeep penetration process essential influence on the density of a material of a barrier, microhardness, concentration of carbon in steel render, frequency rate of processing.

With the increase of microhardness and concentration of carbon the density of registered channel formations is reduced. Under identical conditions penetration general defectiveness of samples from

Steel 10 exceeds a similar parameter for samples from steel 40 in 1,1 times. It is probably because of that in constructional steel with ferrite - perlite structure at the application of loading deformation begins to develop in ferrite, and perlite colonies are "barriers" for such deformation [3].

The increase of density of the target material results the reduction of average diameter of registered channel formations. Comparison of the average changes of channel structure of steel,

copper, and aluminum, titan showed that the maximal changes are observed in aluminum. By observance of identical conditions of penetration average diameter of the channel in aluminum exceeds this parameter in steel 40 in 2 times, and their density in 3,4 times.

It is established, that in considered modeling materials after penetration of stream of particles the size of grain decreases in 1,2 - 2,9 times. Increase of dispositions density in constructional steel in 17-30 times is found on variant of processing.

It is found that in the barrier from steel 40 by transition from unitary penetration to triple one

the average total density of registered defects increases in 2 times, the average size of defect in 1,5 times.

Based on the results of the researches that were done the analytical technique of parameter's definition the dynamic phase transitions, stated in work is offered experimentally.

Literature:

1. Dynamic reorganization of structure of materials// S.M. Usherenko /Minsk, 2000, 188p.
2. V.I. Zeldovich, S.M. Usherenko //FMM, 2001. Vol. 91, №6, p. 72-79

SURFACE ALLOYING OF METALS BY IMPULSED HETEROGENEOUS PLASMA JETS

Budovskikh E.A., Martusevich E.V.

Siberian State Industrial University, Novokuznetsk, Russia

The development of manufacture expands area of the requirements to materials concerning their mechanical properties. The increase last with use of traditional kinds of thermochemical treatment in line of cases appears economically unprofitable. Therefore last years the new technologies of hardening develop which, as well as thermochemical treatment, are based that mechanical strength of details is guaranteed at the expense of application low-alloy steels, whereas the special properties of a surface with according to the service requirements are provided with continuous or local formation of alloying microlayers on it or spraying of coatings.

Perspective way of obtaining of a complex of necessary properties on surface layers of materials determined by purpose of a product, is the influence by pulse heterogeneous plasma formed at electrical explosion of conductors. Idea of method consists in melting of surface layers, saturation by their products of explosion and subsequent self-hardening. The comparative analysis of the available references shows the large potential opportunities of development in this direction. The wide choice of materials of exploding conductors causes wide opportunities of application of a method. For one pulse of treatment it is possible alloying of surface layers by the area up to 5... 10 cm² and thickness up to 20... 40 μm.

The application of electrical explosion and phenomena, accompanying it in various technologies of treatment of materials now has resulted in creation of the appropriate equipment distinguished by simplicity of a design, low cost, high reliability and ecological safety.

Peculiarities of structure and phase formation and the service properties of layers modified by alloying are reflect the basic features of treatment: a) its pulse and high-intence character (time of a pulse of influence is made about 10⁻⁴ s, absorbed intensity 10⁵... 10⁶ W/cm²); b) heterogeneous structure of jets formed during electrical explosion, which includes high-enthalphing gas-plasma front and rather slow particles of rear; c) gas-dynamic pressure (order 10⁶ ...10⁷ Pa) on a surface during influence.

The carried out researches on carburizing have allowed to determine the basic regularities of pulsed

electroexplosive alloying, and also structure and phase features of the modified layers state. The pulse character of process and gas-dynamic pressure on a surface is caused with high cross gradients of temperature and speed of melting motion, the opportunity of overheat it is higher than temperature of boiling at normal pressure. A consequence it is the development of hydrodynamical instabilities and convective processes of mass- and heat transfer. Convective mass transport causes the appreciable contribution (up to several percents on weight) in a degree of alloying by gas-plasma components of a jets and promotes penetration in liquid of the condensed particles of products explosion. The action of dynamic pressure on surface melting determines also threshold modes of treatment bringing to ejection.

The features of crystallization, microstructure, phase formation and service properties of the modified layers are investigated. In particular, the microhardness and wear resistance in conditions of dry friction of sliding of carburizing layers of titanium and iron was increased in comparison with base in some times.

Advantage electroexplosive alloying is that as an exploding conductor anyone can be used any electroconductive material. It is known, that the high service properties have the surfaces, hardened, for example, intermetallic compounds. Taking into account these results of traditional thermochemical treatment as one of opportunities studied alloying of titanium base by electroexplosion of aluminium and nickel foils.

The layers with a high degree of alloying (about tens percents on weight), caused by the basic contribution of the condensed particles of products of explosion were received. Thus convective motion the levelling distribution of the alloying element on depth, was determined also by processes cavitation, e.g. melt boiling because of sharp decrease of pressure in drops of products of explosion at impact with a surface, and their mechanical interaction with the melt also.

The carried out researches on samples of alloys BT20 and BT6C have shown, that speed of oxidation at temperatures 700... 900°C after alumizing decreased

II. PERSPECTIVE MATERIALS OF FUNCTIONAL AND STRUCTURAL PURPOSES: POSSIBILITIES OF OBTAINING NEW LEVEL OF PROPERTIES

in 2 and 4 times accordingly. It allows increase the temperature of operation of details from alloys on 50 and 100 °C or time of operation up to an allowable degree of oxidation on 3 and 6 hours accordingly.

It is necessary to emphasize, that carburizing layers in comparison with layers received at traditional thermochemical treatment, are represented thin. Therefore selection of the appropriate nomenclature of details is necessary for application of a method. In a case aluminizing the modified surfaces are comparable to layers received methods of thermochemical treatment. Therefore area of application of the electroexplosive metallization can be wider, than carburizing process.

A series of tests on electroexplosive surface hardening of concrete details was carried out also. In particular, the considered method is convenient for treatment internal surfaces of details. Accompanying carburizing the process of formation of a layer of firm greasing as a graphite covering is the positive factor, if the hardening will be carried out with the purpose of increase the wear resistance. Therefore for improvement of the tribotechnical characteristics of friction pair "titanium-titanium" in the valve of the steam-turbine engine carried out graphitizing of an internal cylindrical surface of its case. The treatment consist in coating of a dividing layer of graphite on a surface without melting of a base. The treatment through of internal surfaces of rotary cartridges of the blades of steam-turbine engine made of the alloy BT9, both by electroexplosion of the coal-graphite fibres and aluminium foils, resulted in formation of the alloying layers with microhardness twice above initial. For increase of stability to fretting-corrosion of a detail of injector of the steam-turbine engine made from austenitic cast iron carried out treatment through with melting of its internal cylindrical surface by electroexplosion of coal-graphite fibres. The treatment resulted in formation hardened and steady against annealing layer, smoothing out of an initial relief of a surface and formation on it of a layer of small dispersion graphite strongly connected to a base.

The results of development received on faculty of physics SibSIU, in area electroexplosive alloying are published in a series of articles and are protected by patents. Their analysis and estimation of a prospective economic efficiency of application electroexplosive alloying allows to recommend it for practical use.

Till now all executed works in this area used action any of one component in addition entered into structure of a surface layer, thus the optimum

structure was created by the certain choice of parameters of pulsed plasma treatment and conditions of course of uniform technological operation including heating of a hardened surface, saturation of a melting layer by products of explosion of a conductor and subsequent self-hardening, with which the process of treatment was finished.

For the decision again of arising practical tasks connected, for example, with aspiration to increase of working temperatures, sold speeds of movement and transmitted pressure in mobile interfaces of machines at simultaneous decrease of weight on unit of capacity, and, in this connection, with frequently arising necessity of maintenance not it is necessary to find one any of property, but complex combination simultaneously of several properties (for example, resistance to oxidation and wear resistance), new methods of hardenings based first of all on the basis of complication of phase constitution and structure of surface layers. According to it the ways of the further development of scientific, working and practical approbation of methods electroexplosive alloying are planned also:

- a) creation of a hardened layers by simultaneous or consecutive introduction of two or several components in constitution of a surface;
- b) the creation of the modified layers with use of the combined methods of hardening combining, for example, electroexplosive alloying and subsequent heat treatment, at which their new structure is formed by a diffusion way. The thermochemical treatment which is carried out in such a way, has that advantage before traditional methods, that the stage of additional heat treatment will be carried out at less temperature and (or) with much smaller holding in time.

The offered methods of development of methods electroexplosive alloying offers to an opportunity of significant increase or obtaining of new necessary properties of surface layers and also combination of different properties in one layer.

HIGH-TEMPERATURE ANTIFRICTIONAL COMPOSITES

Shevchuk U.F., Roik T.A.⁽¹⁾

Institute for Problems of Material Science NAS of Ukraine, Kyiv, Ukraine

⁽¹⁾State Scientific and Technical Center of Artillery-Rifle Arms, Kyiv, Ukraine

Now for equipping the friction units of chain conveyers for transportation the metal blanks to heating furnaces, autoclaves trucks for transportation materials to autoclaves operating at the temperatures up to 300 °C, for friction units of machines for continuous casting of steel etc. operating at the temperatures up to 500 °C, and also for friction units of gas turbine aggregates operating at the temperatures up to 700-800 °C on air the bearings of babbits, sintered materials on the base of iron, bronzes, cast iron, cast nickel alloys etc. are applied.

For reasons of high wear rate (250-400 mcm) of these materials at the increased temperatures (up to 200 °C - on the base of bronzes, up to 500 °C - on the base of iron and cast iron, up to 650 °C - on the base of cast nickel alloys) operating resource of such friction units is considerably limited [1].

In the present message research results of three types of materials designed for operation at increased temperatures are presented:

1. On the base of iron - powder composites produced of "ИХХ15СГ" steel powder-wastes for operation at the temperatures up to 350 °C.

2. On the base of iron - powder composites manufactured of "P6M5K5" steel powder-wastes for operation at the temperatures up to 550 °C.

3. Composites on the base of powder high-alloy nickel alloy "ЭП975" for operation at the temperatures up to 900 °C.

As new antifrictional materials are intended for operation at the increased temperatures (350-900 °C), when a liquid grease is already inoperated in the capacity of solid lubricant CaF₂ was added in all cases [2].

The materials with using "ИХХ15СГ" and "P6M5K5" steels powder-wastes [3] were produced by pressing and sintering at the temperatures 1100-1150 °C, and composites on the base of powder alloy "ЭП975" were manufactured by method of gas-static pressing at 1210 °C with postheat treatment.

The physic mechanical and antifrictional properties of new composites (tab.1 and tab.2) have been researched.

Table 1

Physic mechanical properties of materials

№	Structure, % mas.	σ_b , MPa	a_k , J/m ²	HB, MPa
1.	ИХХ15СГ + 5 CaF ₂	420-460	570-590	680-720
2.	P6M5K5 + 5 CaF ₂	480-500	660-720	750-850
3.	ЭП975 + 6 CaF ₂	550-600	550-600	2500-2600
4.	Бр.ОГр.10-6	140-160	50-70	420-460
5.	ЖГр.3М15	290-410	80-94	700-800
6.	Ni+(18-45)Fe+(5-10)(MoB ₂ +ZrB ₂)+5(CaF ₂ or BaF ₂)	240-300	350-520	850-950

Table 2

Antifrictional properties of materials

№	Structure, % mas.	Temperature, °C	Coefficient of friction	Intensity of wear process, mcm/km	Ultimate load, MPa
1.	ИХХ15СГ + 5 CaF ₂	350	0,13	28	7,0
2.	P6M5K5 + 5 CaF ₂	550	0,12	25	8,5
3.	ЭП975 + 6 CaF ₂	900	0,26	30	7,0
4.	Бр.ОГр.10-6	200	0,28-0,4	520	2,0
5.	ЖГр.3М15	400	0,29	470	3,0
6.	Ni+(18-45)Fe+(5-10)(MoB ₂ +ZrB ₂)+5(CaF ₂ or BaF ₂)	500	0,31	130	1,5

The analysis of results submitted in tab.1, 2 shows that all three types of new materials (1-3 positions) have higher physic mechanical,

antifrictional characteristics and able to operate at the higher temperatures in comparison with applied alloys (4-6 positions) now at the similar conditions [1].

The friction coefficients as a function of loads at the external heating friction pairs up to 350, 550 and 900 °C accordingly are presented on fig.1.

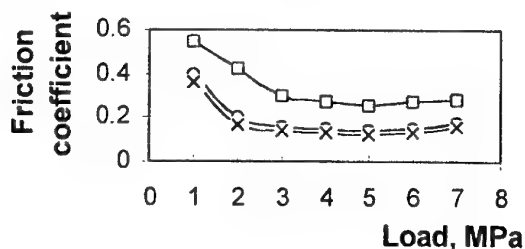


Fig.1. Friction coefficients as function of loads of new composites at the operating temperatures. o - $\text{IIX15CF}+5\%\text{CaF}_2$ - 350 °C. x - $\text{R6M5K5}+5\%\text{CaF}_2$ - 550 °C. - $\text{EP975}+6\%\text{CaF}_2$ - 900 °C

The fig.1 shows that a general rule is decrease of friction coefficients at increase of loads. In the interval of loads 3-6 MPa friction coefficients of all composites are stabilized and minimized [2]. This fact could be explained that at the increasing of loads and temperatures in friction zone the oxidation processes are promoted on the friction

surfaces. This causes to formation the antiscoring films of heterophase compositions, due to these reasons adhesive and deformative components of friction coefficient are decreased.

The presented research results offer to recommend the new composites for using in friction units of machines and mechanisms operating at the temperatures up to 350, 550 and 900 °C accordingly. Besides using the readily accessible powder-wastes of "IIX15CF" and "P6M5K5" steels containing useful alloy elements lays the foundations for design of resource-saving technologies and offers partly to solve an ecological problem.

1. Fedorchenko I.M., Pugina L.I. Composite sintered antifrictional materials. - Kiev: Naukova dumka, 1980, 403 p.

2. Shevchuk U.F., Roik T.A. Powder antifrictional materials for operating at increased temperatures //Powder metallurgy.-2001.-№1-2.-P.53-58.

3. Roik T.A., Shevchuk U.F. Powder bearing material on the base of iron for increased temperatures. Patent of Ukraine №32854, Bul. №1, 2001.

COMPOSITE MATERIALS FOR EROSION-CORROSION APPLICATIONS

Ilyuschenko A.Ph, Belyaev A.V., Talako T.L., Formanek B.⁽¹⁾
Powder Metallurgy Research Institute with Pilot Plant, Minsk, Belarus
⁽¹⁾Silesian University of Technology, Katowice, Poland

It is well known that materials science plays a key and enabling role in Science and Industry. Materials chiefly determine the efficiency, economy, environmental acceptability and safety in energy conversion systems. Materials to be used in power units have to withstand to the combined effect of wear and high-temperature corrosion. The problem is complicated by the fact that damage mechanisms for these two processes are distinctly different, resulting in the different and sometime opposite materials properties required. Only composite structure is evidently to be optimal to provide the high level and stability of the material performance. Composites based on IV-VI group metal carbides are promising materials to answer the energy needs requirements. In this work composite powder materials based on double chromium and titanium carbides with nickel-chromium binder produced using self-propagating high-temperature synthesis (SHS) are investigated. The idea of creating such a composition is based on the attempt to combine excellent wear resistance and extremely high hardness of titanium carbide and high corrosion resistance of chromium carbide.

Surface engineering attempting to create at the surface both corrosion- and wear-resistant protective layer is obviously the most economical way to reduce the material wastage in power units. In spite of the wide range of available technologies for the processing protective coatings, very few of them are suitable for application in energy conversion and utilization systems. Diffusion coatings are, for the most part, either too thin or not hard enough. Casehardened coatings are not sufficiently corrosion resistant and lose their effectiveness at higher temperatures. Recently, hypersonic velocity oxygen fuel (HVOF) thermal spray process showed the excellent coating properties (regarding their porosity, hardness, bond strength, density and roughness). Due to its lower flame temperature and the shorter dwell time of the particle in the flame as compared to the electric arc and plasma processes, the HVOF is particularly suitable for the deposition of carbide coatings without their decomposition. That is why our investigations were concentrated on the HVOF coatings from the synthesized powders.

SHS yields the fine-grained product with the composite structure. X-ray analysis identifies three phases: chromium carbide, titanium carbide and based on gamma-nickel solid solution.

The ability of a material to resist rapid degradation in aggressive environments normally depends upon its potential to form and maintain a protective surface oxide scale. Of the possible oxides, Cr_2O_3 is found to be the most protective. In our case oxidation kinetics is strongly dependent on the content of chromium forming its proper carbide and dissolved in titanium carbide.

Table 1 represents oxidation resistance of the SHS composite powder 25wt.% (Ni20Cr) - 75wt.% ($\text{TiC-Cr}_3\text{C}_2$) depending on the carbide phase composition. To control the content of chromium dissolved in double carbide solid solution, titanium carbide lattice parameter measurements are presented. (chromium is known to occupy titanium sites in TiC decreasing its lattice parameter). It is clear from the table that, for all the compositions but 10wt.% Cr_3C_2 , dissolving of chromium in TiC results in increasing its oxidation resistance. Such an effect of low chromium content can be explicated in terms of titanium carbide lattice defect concentrations. It has been reported that when chromium content in titanium carbide is less than 3 atomic %, the higher concentration of vacancies on carbon sites is observed. The oxygen atoms under oxidation conditions can easily occupy these vacancies. For the composition with 30wt.% Cr_3C_2 , in spite of significantly lower weight gain, oxidation kinetic is still controlled by titanium oxides formation that does not exhibit high protective ability. Protective layer is formed at titanium - chromium carbide ratio 30:70 (composition 6). The material oxidation behavior is practically similar to the composite with pure chromium carbide. Interestingly, that when synthesis conditions assist chromium to form its proper carbide, leading to the lower Cr content in titanium-chromium solid solution, oxidation resistance of the composition drops again (compare line 5 and 6, Table 1).

HVOF process enables the coatings of high quality to be obtained. Their porosity does not exceed 2%.

Table 1. Weigh gain of the SHS powders 75%(Cr₃C₂-TiC)-25% Ni20Cr during oxidation in air

N	Carbide phase composition, wt. %	TiC lattice parameter, nm	Weigh gain, mg/g at temperature (°C)					
			300	400	450	500	550	600
1	100TiC	0.4345	33	36	38	63	73	362
2	10Cr3C2-90TiC	0.432	53	48	49	78	127	130
3	20Cr3C2-80TiC	0.4315	0	3	7	39	131	139
4	30Cr3C2-70TiC	0.4290	0	2	6	71	78	79
5	70Cr3C2-30TiC	0.4320	0	4	12	26	40	100
6	70Cr3C2-30TiC	0.4280	0	4	10	14	15	13
7	100Cr3C2	-	0	0	3	5	10	9

Mechanical properties of the coatings as compared with that of HVOF coatings from conventionally used WC-17%Co and 25NiCr-75Cr₃C₂ powders are summarized in Table 2. In spite of the best mechanical properties of WC-Co coating their thermal cycling lifetime was rather poor because of the low coefficient of thermal expansion - $(6-6,5) \cdot 10^{-6} / K$). High sensitivity to thermal stresses results in cracking and spallation

of the coatings at the elevated temperature erosion tests.

HVOF coatings from the synthesized powders at the comparable mechanical properties demonstrated an extremely high thermal cycling lifetime: 8-10 fold higher than for the conventional materials. Fine-grained structure and high cohesion strength of the composite materials formed during SHS are likely to provide for their excellent performance.

Table 2. Properties of HVOF coatings

N	Material Composition, wt. %	Hardness, HRC	Bond Strength, as-sprayed, MPa	Bond Strength, cycled, MPa	Lifetime, cycles
1	83WC-17Co	57.2	>60	>48	6
2	75Cr ₃ C ₂ -25Ni20Cr	52	50	58	8
3	75(70Cr ₃ C ₂ -30TiC)-25Ni20Cr	56.6	40	-	61

Elevated temperature erosion tests did not reveal any signs of the material corrosion. The main mechanism of the surface degradation is mechanical wear caused by the impacting particles.

Over 30 tests were carried out in different ashes. The ashes were divided into three groups according their erosivity relative to AISI 1018 Steel, normally used as a standard material for the erosion-corrosion tests: ashes with high erosivity (AISI 1018 Steel wastage at test condition is 100-300 mkm), moderate (50-100 mkm) and low one (less than 50 mkm). Coatings from the synthesized materials showed the best performance for the all ashes and test conditions. In contrast to the 1018 Steel exhibiting typical ductile erosion behavior with maximum material wastage at impact angle 30°, HVOF coatings are characterized by the brittle erosion behavior typical for cermets. However, material wastage mechanisms for the coatings based on double chromium-titanium and single chromium carbides are quite different. Cr₃C₂-NiCr

coatings exhibit the maximum erosion rate at 45°. Such a behavior is usually observed when erosion runs via brittle failure resulted from the carbide grains fragmentation. Cracking and chipping of the fractured pieces of the coatings taking place during testing accord well with this point. (Cr₃C₂-TiC)-NiCr coatings exhibit the highest erosion rate at impact angle 90°. However, in spite of the higher hardness, there is no evidence of the lateral cracking formation in these coatings. Surface morphology of the erosion grooves is indicative of ductile wear mechanism.

Thus, when adjusting carbide phase composition and chromium content in titanium carbide solid solution, one can control the oxidation kinetic and wear resistance of the composition. Fine-grained structure and high cohesion strength of the materials developed provide for the excellent elevated temperature erosion performance in a wide range of test conditions.

CERAMIC COMPOSITE MATERIALS FOR MICRO-ELECTRODES PRODUCED

Sudnik L.V., Ananitch G.V.⁽¹⁾, Gorelik P.N.⁽¹⁾

Powder Metallurgy Research Institute with Pilot Plant, Minsk, Republic of Belarus

⁽¹⁾ Concern "Planar", Minsk, Republic of Belarus

Introduction: At present stage of development of national economy in Republic of Belarus ensuring the quality of the produced production is one of the priority directions. Concept of quality includes many components i.e. designing, engineering, technological fulfillment and metrology securing. Rejects on any stage of this chain eliminates efforts of preliminary and following components. Achievement of high quality of products is of special importance for electronics and instrument engineering.

Materials based on aluminum oxide have a large application in industry, and also in producing micro-electrodes which are widely used for ultrasonic welding. Compositions containing 75÷100% of aluminum oxide are used more often. Their properties and their changes in necessary direction are obtained by inducting of a small quantity of additions. To lower the sintering temperature it is often inducted a glass phase, which forms during adding a certain quantity of natural minerals, pure chemical substances, synthesized before compounds or welded glass to the initial mixture.

The aim of this work is the creation of compositions which can provide a high serviceability of the products like micro-electrodes. Production technology - Injection Moulding.

Materials and investigation methods.

Investigated materials: powder compositions, including aluminum, magnesium and silicon oxides. Initial powders were first activated in attritor with horizontal axis of rotation with application of surface-active substances.

Estimation of adhesion properties between mixture components was carried out according to wetting edge angle and to the adhesion work defined by the «laying drop» method.

The fractography, structure investigations and X-ray phase, micro-X-ray spectral analysis were carried out.

Experimental investigation. Composite materials properties depend on compound, on configuration and components injection methods. In the literature there are some fragmentary information about selection of glass additions for

compositions on the base of aluminum oxide. In general this information concerns coating on huge dimension products and describes the manners of pyrolysis attack of substances, which pass into glassy state within heating; melting of glass powders, produced by precipitation, jet spraying, cathode sputtering and some others.

In this work we use the methods of glass ceramic coating directly on the initial powder. The glass ceramic component compound is chosen according to the conditions which provide high adhesion activity to Al_2O_3 and is sprayed on the powder activated before. The ready mixture represents an aggregate from 2-10 grains of aluminum oxide, coated with glass component and joined by the bridge from it. This mixture is used for producing of dross for heat moulding.

When developing compositions there were analyzed ways of achieving the maximum value of surface energy of the main material (corundum) particles and minimizing the energy of intercrystal boundaries.

Decrease of intercrystal energy takes place as a result of changing the structure of boundary layers when leveling the asymmetry of contacting particles field of forces, what contributes to the formation of intercrystal structure with high density of strong contact directions. Considered is a process of cracks propagation in the corundum material during slow loading and shown is that the maximally achieved bending strength would be 540 MPa (max $\delta_{bending}$ for pure corundum 750 MPa) in the presence of additives. The material strength may be lower that the calculated one, because of increasing the boundary energy on some value depending on the crystals orientation and their syngony revealing themselves mostly with increasing of the crystals

size. On the basis of the made calculations it is determined that to ensure the needed physical-mechanical characteristics the charge of the source material in the form of small crystal particles (having around shape with low anisotropy) should be used.

Carried out are investigations of microadditives effect, regulating surface tension of a liquid phase during sintering and a surface

energy in the place of hard and liquid phase contact. Shown is a necessity of using microadditives Cr_2O_3 , ZrO_2 and SiO_2 for realization of high strength and technological indicators as well for microelectrodes used in wits of ultrasound welding, therewith a macrostructure of the material may be a flame one the general density being high.

Cr_2O_3 adding in the amount 7-15 mass.% enables to increase the bending strength on 12-15%. This increase is achieved due to origination of a hard solution in Al_2O_3 - Cr_2O_3 system, what contributes to the increase of the surface energy of destructing matrix grains of aluminum oxide.

SiO_2 microadditives are added to regulate surface tension of the liquid phase originating during sintering, resulting in increase of compressing capillary pressures among aluminum oxide particles and therefore in direct increase of the material density.

It is determined that glass component must correspond to the diagram of MgO - Al_2O_3 - SiO_2 and its compound must correspond to the domain of the primary crystallization of moulitte. The compounds of glass generation composition and

parameters of the composition microstructure on the base of aluminum oxide are given in the table.

X-ray phase analysis shows, that all investigated samples, sintered at the temperature to 1400°C , contain cordierite ($d=3.027$; 3.198 ; 3.379 ; 1.688 nm) and spinel ($d=2.085$; 2.008 nm), which is homogeneously distributed in the matrix from α - Al_2O_3 . At the final sintering in the temperatures interval $1500\div 1550^\circ\text{C}$, electrode structure consists of α - Al_2O_3 with spinel equally distributed.

For completion research works and for production of small and medium lots of micro-electrodes we were using a table casting tool developed at PMRI with PP, which enables carry out injection moulding with maximum injection volume of 63 cm^3 , pressure up to 100 kg/cm^2 , maximum height of casting form - 120 mm and injection head heating temperature - $70 - 300^\circ\text{C}$. Small overall dimensions in working state are $500\times 240\times 500\text{ mm}$ and in packed condition $500\times 240\times 100\text{ mm}$ and mass less than 10 kg allow to make casting process in a small working room.

The table: compound and properties of investigated compositions

Composition	Compound of glass component			Grain size, mkm	Density, g/cm^3	Porosity, %
	Al_2O_3	SiO_2	MgO			
$\text{Al}_2\text{O}_3 + 7,0\% \text{ CTK}$	40.8	44.7	14.5	>10	3.5	>5
$\text{Al}_2\text{O}_3 + 7,0\% \text{ CTK}$	45	40	15	>10	3.2	>5
$\text{Al}_2\text{O}_3 + 7,0\% \text{ CTK}$	63.5	27.9	7.6	>10	3.2	>5
$\text{Al}_2\text{O}_3 + 5,0\% \text{ CTK}$	40.8	44.7	14.5	6.1	3.78	$2\div 3$
$\text{Al}_2\text{O}_3 + 5,0\% \text{ CTK}$	45	40	15	5.5	3.76	$2\div 4$
$\text{Al}_2\text{O}_3 + 5,0\% \text{ CTK}$	63.5	27.9	7.6	5.8	3.7	$2\div 3,5$
$\text{Al}_2\text{O}_3 + 2,5\% \text{ CTK}$	40.8	44.7	14.5	7.0	3.4	>5
$\text{Al}_2\text{O}_3 + 2,5\% \text{ CTK}$	45	40	15	6.5	3.4	>5
$\text{Al}_2\text{O}_3 + 2,5\% \text{ CTK}$	63.5	27.9	7.6	6.1	3.4	>5

Analyzing the above mentioned we should notice that stable aluminum-oxide ceramics structure, high resistance of electrodes are provided with the developed methods of preparing the mixture that help $\gamma \rightarrow \alpha$ phase transfer in Al_2O_3 , melting and interaction of glass components with the matrix, which wets corundum crystals and are equally distributed within the whole volume.

The using of developed adhesion-active bundles in the compound of temporary binder enabled to produce the material with good

physical properties: density $\sim 3.78\text{ g/m}^3$; bending strength $\sim 380\text{ MPa}$; the loss tangent of a dielectric $\sim 3.5\cdot 10^{-4}$; dielectric permeability 9.4 (at the frequency of 10^6 Hz).

The complementary positive result of this work is prolongation of service life of casting forms, as using of mixture with glass components coatings enables to reduce friction coefficient of corundum particles with the walls of casting form.

STRUCTURE AND MECHANICAL PROPERTIES OF Ti-Si-X *IN-SITU* COMPOSITES

Firstov S., Koval' O., Kulak L., Kuzmenko M., Miracle D.⁽¹⁾, Podrezov Yu., Vasylyev O.

Frantsevych Institute for Problems of Materials Science of NAS of Ukraine, Kyiv, Ukraine

⁽¹⁾ Air Force Wright Laboratory, Materials and Manufacturing Directorate, Wright-Patterson AFB, OH USA

Novel titanium-based *in-situ* composites are attractive materials for a wide range of applications because of their high specific strength and stiffness, and good fracture-related properties. Mechanical behavior of these materials depends strongly both on the composition and microstructure of the matrix and on the type, size and volume fraction of the reinforcing phase.

It was found that these composites have multiphase structure, and the reinforcing phase is formed inside the matrix during eutectic solidification and solid state decomposition of a high-temperature phase (Fig. 1). *In-situ* processes can create a range of reinforcement morphologies, from discontinuous to continuous, and at least ten structural constituents can be distinguished in the Ti-based *in-situ* composites. These are polycrystalline (prior β -grains 1) matrix with small α' -martensitic lamellas 2 inside these grains, intergranular eutectic layers 3 consisting of soft intergranular matrix 4 and eutectic silicide skeleton of bars as parts of like-palm lives eutectic silicides 5, secondary small intragranular silicides 6 resulting from solid solution decomposition, precipitation-free zones 7 surrounding initial grains, and a few interfaces like between prior β -grains and intergranular eutectic layers 8, between matrix and silicides, β -interlayer phase between α' -martensitic lamellas etc. These structural constituents determine overall mechanical properties of material and result in non-homogenous deformation.

As to the fracture mechanisms SEM fractography reveals some their spectrum showing except cleavage ductile and brittle intergranular fracture as well as ductile pores coalescence arising near silicides at high temperatures. Fracture surfaces reveal that intergranular regions consisted of brittle rod-like silicide particles, which are embedded in a soft ductile matrix undergoing hundreds of percents of local strain before final macroscopic failure occurred. Increasing temperature higher 600°C promotes laminating grains. The fracture behavior of deeply deformed alloys is quite different from the as-cast ones. First of all, owing to more homogenous structure sites of crack starts

shifted from inner areas of samples on their surface. Fracture mechanisms became mostly intragranular revealing microfragmented cleavage and pores coalescence.

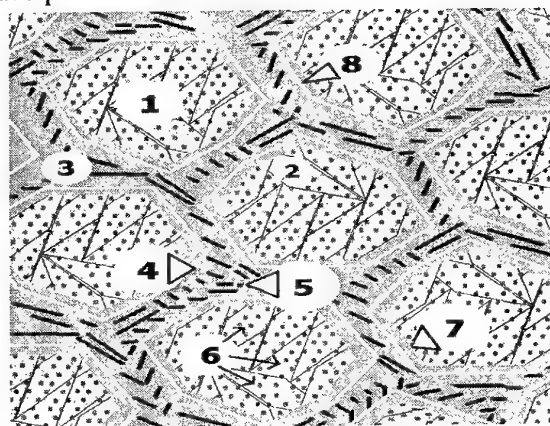


Figure 1. Schematic view of structure of as-cast Ti-3Al-2Si-5Zr *in-situ* composite.

Explanation of pointers is in the text.

The temperature dependency of mechanical properties of these *in-situ* composites is close by its shape to brittle materials (Fig. 2) revealing rather big scatter of data in areas of low and high temperatures arising from dependence on chemical composition and small scattering in area of middle temperatures between 150-500°C where plastic yield may be observed revealing non-dependence on chemical composition.

Plastic deformation for 90 % strengthens material to such an extent that some of structural constituents like interface between prior β -grains and intergranular eutectic layers are not proved themselves in mechanical behavior. Structure homogenized with hot plastic deformation leads to equalizing strength of all the structural constituents on the level of α' -lamellae body resulting, in its turn, in practical eliminating intergranular fracture as a class of micromechanisms.

The temperature dependencies of ultimate tensile strength and elongation of the Ti-3Al-5Zr *in-situ* composite containing 2, 4 and 6 wt. % silicon in as-cast and deformed for 90 % conditions are shown in Fig. 2 demonstrating typical brittle-to-ductile behavior. The upper limit of the brittle-to-

ductile transition is around 600 °C in all the cases. It is seen that both strength and elongation increased significantly after forging with 90 % strain in all the cases. These experiments clearly evidence that deformed for 90 % material with 2 wt. % of silicon may show 4 % of elongation; material with 4 and 6 wt. % of silicon may show 2.7 and 1.8 % elongation respectively. Naturally, plasticity of alloy with 2 % Si is higher than in composites with 4 and 6 wt. % Si. Room temperature strength is increased for around 200 MPa with a deep plastic deformation.

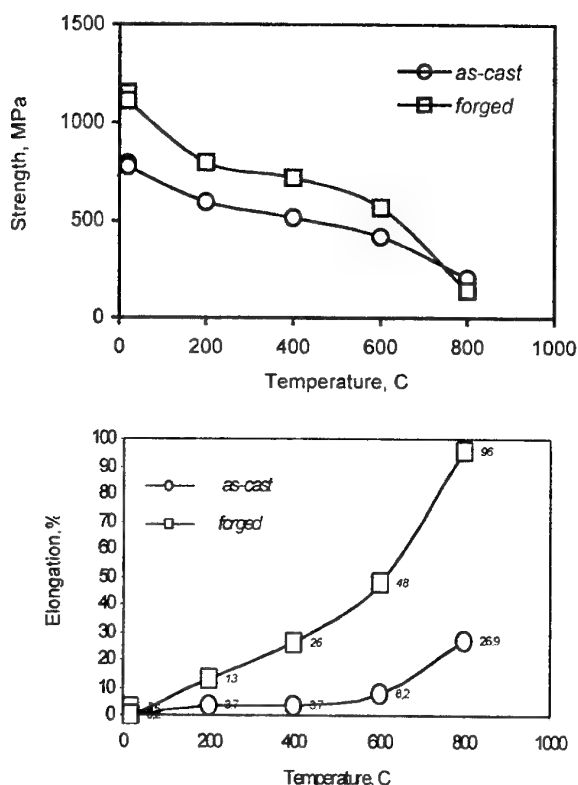


Figure 2. Temperature dependencies of strength (a) and elongation (b) of the alloy with 2 wt. Si in as-cast and forged (90% strain) conditions.

Fig. 2 shows that plastic deformation is radical mean to increase plasticity. And the reason, as structural data shows, is purification of titanium matrix from silicon via intensified decomposition of its solid solution in titanium with precipitation of secondary silicides inside of prior β -grains when number of secondary silicides became obviously more. They become coarser too. It is seen that namely +2Si alloy comes stronger under influence of plastic deformation resulting in plasticity (elongation) growth up to 4 %. Hot plastic deformation is some activating mechanism

purifying titanium lattice easier than simple heat treatment. It is necessary to note that high temperature plastic deformation leads to arising in structure new the $(\text{Ti,Zr})_2\text{Si}$ silicide. Fig. 3 shows the dependence of room temperature plasticity (elongation) of Ti-3Al-5Zr in situ composite in dependence on silicon content.

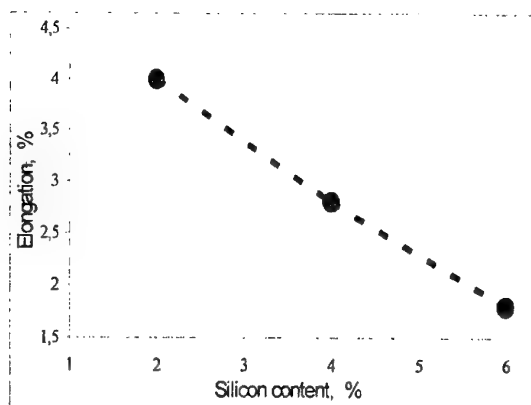


Figure 3. Room temperature plasticity (elongation at uniaxial tension) of forged for 90 % Ti-3Al-5Zr vs. silicon content in it.

Ti in situ composites studied demonstrate typical brittle-to-ductile behavior caused by temperature. The transition of as-cast states in a ductile state is realized in a wide temperature interval occupying a few hundreds of degrees centigrade. As to its upper temperature limit it is in a range of 600 °C where plasticity has a significant growth. Fractography confirms this conclusion because cleavage does not take place more there. As to the lower temperature limit it is significantly below room temperature because in spite of near zero plasticity fractography points out a significant part of samples, which fails with ductile pore coalescence, evidencing the high plastic potential of materials. Deformed states have probably wider brittle-to-ductile transition. As to its upper temperature limit it is a little below position of as-cast states. As to the lower limit it must be significantly lower than in as-cast states because part of cleavage in fracture is very small. At this it is clear that alloy containing lower silicon content has lower temperature limit.

The authors would like to acknowledge funding of this project from the US Air Force Office of Scientific Research and the assistance of the Science and Technology Center of Ukraine.

OXIDE CERAMIC MATERIALS ON THE BASIS OF COMPOSITIONS WITH LOW THERMAL EXPANSION

Pavlikov V.N., Garmash E.P., Tkachenko V.D., Pleskach I.V., Maroresku I.I.

Frantsevich's Institute of Problems of Materials Science, NAS of Ukraine, Kiev, Ukraine

The friable ceramic materials differ by stability at action of sign-variable cyclic loadings caused by heat drops. The specified feature is defined mainly by value of their temperature-expansion coefficients ($TKLE$). To number of oxidic phases with low sensitivity to changes of temperature, and naturally, low $TKLE$, concern synthetic cordierite ($2Al_2O_3 \cdot 2MgO \cdot 5SiO_2$), aluminium titanate (Al_2TiO_5), mullite ($3Al_2O_3 \cdot 2SiO_2$), silicates of lithium etc. In this connection the making on their basis of high spalling-resistant ceramics and products for use in extreme requirements represents scientific and practical interest.

In the present work the results of complex examinations on development physicochemical requirements of cordierite aluminium titanate synthesis with the maximal content of the basic phase ≥ 98 vol. % are submitted. The phase changes in activated by various expedients natural minerals as pyrophyllite, talc and kaolinite by processing by acids, explosion and electric discharge in water are investigated. Cordierite and aluminium titanate synthesis was carried out by a method of solid-phase sintering in a temperature band $1000-1400^\circ C$ (I) and melting of the relevant oxides intermixtures with the subsequent sharp quenching of a melt. The process of production of melted fine-grained aluminium titanate and cordierite with a proportional distribution of the stabilizing additives is designed.

For compositions synthesis by crystallization from a melt the oxides intermixtures fusion was carried out in a "cool" crucible on high frequency system such as "Crystal - 401", in a graphite crucible with a high frequency heating. At melting of oxides intermixtures of compositions, explored in work, the theoretical allocation of builders at a nuclear level was reached, that essentially facilitated their chemical interaction. For by one of possible mechanisms of a crystalline phase formation is the structural ordering at transferring in an equilibrium state according to stoichiometry and

new formation structure type. The melts, homogenised by the specified method, poured out in water. Granulates, produced as a glass, fine-crystalline (1-2 microns) cordierite and aluminium titanate have used for carrying out of examinations at development of test compositions of thermally sound ceramics.

The field of investigated compositions of threefold system $MgO-Al_2O_3-SiO_2$ is shown in figure 1. It covers compositions, boundary with stoichiometric, which settle down on triangulation lines. The specified lines join a point adequate cordierite composition with points on the sides of a concentration triangle, which correspond to mullite, enstatite, forsterite, silicon dioxide compositions.

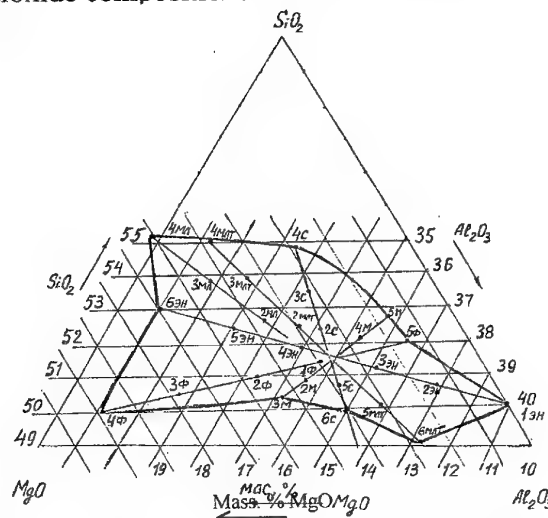


Fig. 1. Field of investigated compositions of threefold system $MgO-Al_2O_3-SiO_2$.

The phase composition of glass ceramics, and also temperature and character of their crystallization is investigated. The $TKLE$ values of ceramic samples, made by glasses sintering are spotted. On the

basis of these data the field of compositions of threefold system with minimum TKLE quantities in limits $0,9-1,2 \cdot 10^{-6} \text{ }^{\circ}\text{C}^{-1}$ is established and submitted in figure 2.

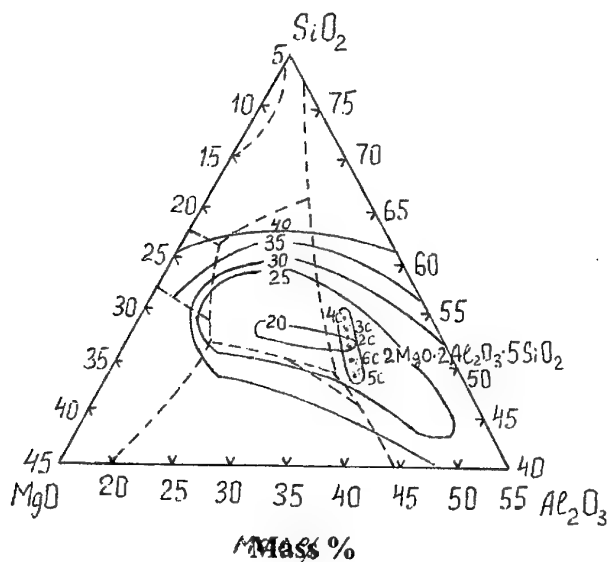


Fig.2. Compositions with minimal TKLE values.

The formation of fluoride replaced kaolinite, pyrophyllite and talc analogs, distinguished by higher, in comparison with starting minerals, dehydroxylation temperatures established at chemical treatment of laminated silicates by concentrated fluorhydric acid (5-20 mass. %). In all cases the chemical treatment mineral component of fusion mixture for cordierite synthesis produced negative effects: the formed fluorides reduced temperature of cordierite synthesis (on 200-250 $^{\circ}\text{C}$), but caused samples deforming. The additives of sulfuric and nitric acids (up to 20 mass. %) result in partial destruction of minerals and to a decrease of the volumetric cordierite content.

At processing by explosion and electrohydraulic crushing of silicates a decrease on 50-70 $^{\circ}\text{C}$ of cordierite sintering point and occurrence of attendant phases (enstatite, mullite, glass) is achieved.

On the basis of the obtained data the deduction about an essential role of heritable structure of minerals at solid-phase cordierite synthesis is made. Any fracture of this structure intensifies sintering and the sealing of a material, but impedes reorganization of nuclear groupings at cordierite phase formation.

At introduction in composition of starting charges of the dispersible mullite, spinel, enstatite established, that their activity during cordierite synthesis is incremented in a direction from spinel to enstatite and mullite. The formation of thermodynamically stable binary compositions previous to cordierite synthesis is undesirable, as at their presence for solid-phase reactions terminating the temperatures about 1400 $^{\circ}\text{C}$ and above are necessary.

The developed compositions of charges and expedients of their preliminary preparation allow to lower temperature began of cordierite synthesis up to 1000 $^{\circ}\text{C}$ and to finish it at temperature 1360 $^{\circ}\text{C}$.

The thermally sound ceramic materials with boosted strengthening properties on the aluminium titanate basis, dense and porous gas-permeable cordierite ceramics are developed. The materials are tested in as filters for molten metals with temperature of embedment 800-1600 $^{\circ}\text{C}$, carriers of catalytic agents and sooty filters for clearing the exhaust gases of automobiles.

MECHANICAL BEHAVIOR OF LaCoO_3 PEROVSKITES FOR SOLID OXIDE FUEL CELL CATHODES

Gogotsi G. A., Orlovskaya N.⁽¹⁾, Einarsrud M.-A.⁽²⁾

Institute for Problems of Strength, Kiev, Ukraine

⁽¹⁾Drexel University, Philadelphia, USA

⁽²⁾Norwegian University of Science and Technology, Trondheim, Norway

Lanthanum cobaltite perovskites are promising materials for manufacturing solid oxide (ceramics) fuel cell cathodes and membranes of air-oxygen separation plants. However, their mechanical behavior, practically controlling the performance of these materials under full-scale conditions, has scarcely been studied. In this connection corresponding investigations were conducted.

The materials under study (Table 1) were produced by cold isostatic pressing followed by sintering [1].

Table 1

Ceramics	Density (g/cm ³)	Porosity (%)	Grains (μm)
LaCoO_3	6,077	16,6	2-3
$\text{La}_{0.8}\text{Ca}_{0.2}\text{CoO}_3$	6,695	0,15	1-2
$\text{La}_{0.8}\text{Sr}_{0.2}\text{CoO}_3$	6,274	9,5	2-3

Load – deflection diagrams (Fig. 1) recorded upon four-point bending demonstrated that these ceramics were reliability brittle inelastically deformed materials (brittleness measure χ by Gogotsi was taken as an inelasticity property) displaying residual strains.

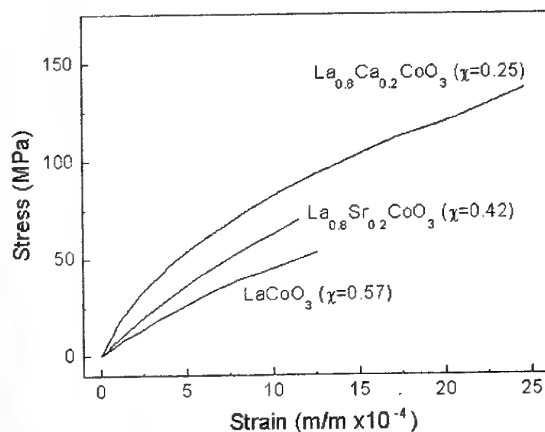


Fig. 1. Stress-strain curves for LaCoO_3 perovskites at room temperature

In contrast to other ceramics, the inelasticity of perovskites is associated with possible twinning connected with ferroelastic domain switching. Therefore, the analysis of these data was also based on investigation results for zirconia materials having a typical domain structure

With an increase in test temperatures the inelasticity of these ceramics was first decreased (the brittleness measure χ was increased), then it increased (the brittleness measure χ was decreased), as this was earlier obtained for inelastic ceramics exhibiting microfractures under loading (Fig. 2).

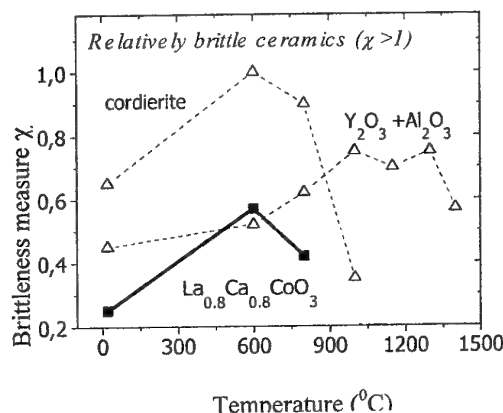


Fig. 2. Temperature dependences of the brittleness measure χ .

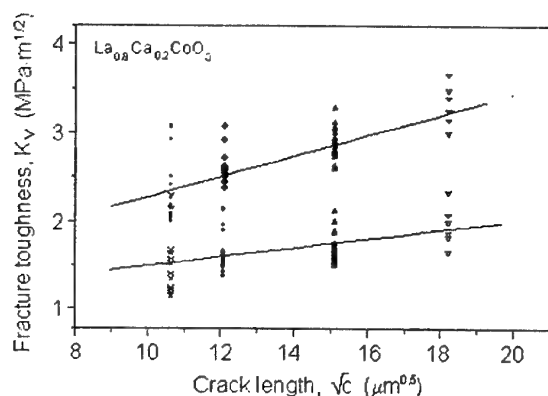
It is not inconceivable that this effect is associated with Mott transition (insulator-metal transition) affecting the strength and deformability of perovskites. However, for final conclusion, additional studies would be necessary.

Vickers fracture toughness tests demonstrated its increase with an increase in a crack length (indentation load). Figure 3 depicts calculation data corresponding to the formation of the median cracks (1), which were observed in our case (Fig. 4), and Pamqvist cracks, which are most often

observed in the tests of conventional ceramics. The data show that LaCoO_3 perovskites and other inelastically deformed ceramics, display fracture described by the R-curve. However, in our case, it is probably connected with ferroelastic domain switching in the area of crack propagation.

Fig. 3. Variation of K_v values as a function of the mean length of a crack near Vickers impression angles (100 N load): Lawn and Marshall (1) and Niihara et al. (2) calculations.

As is seen in Fig. 4, the crack near the impression angles are less expended on the specimen surface than in its depth. Such an observation call into question the validity of K_v calculation by

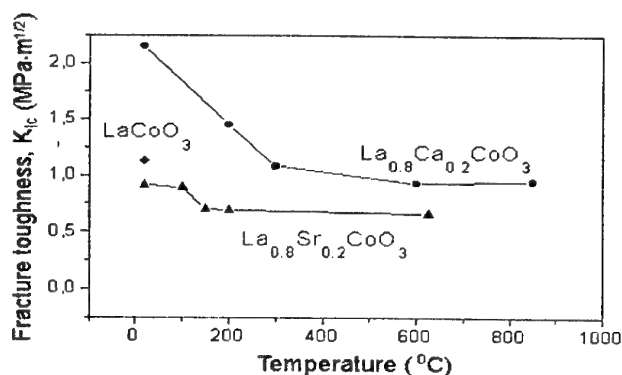


commonly accepted equations.

Fig. 4. Photos of the Vickers impression zone on a $\text{La}_{0.8}\text{Ca}_{0.2}\text{CoO}_3$ specimen: surface (a) and grinding of surface layer (b).

Fracture toughness was also determined (Fig.5) upon bending of specimens with a 5-8 μm V-notch radius (SEVNB method [2]). At the same time, its dependence on phase transformations and other effects controlling the fracture toughness of these materials was revealed.

Much attention was also given to studying the relations of the load on a conical microindenter and its displacement in the materials, fracture surfaces of specimens (in many cases, twins were found), strength in uniaxial compression, etc.



References

1. Kleveland K., Orlovskaja N., Moe A.-M., M.-A. Einnastrud, Breder K., Gogotsi G. Non-elastic behavior of LaCoO_3 -based ceramics, J.Am.Cer.Soc. 2001, v. 84, No 9, pp.2029-2033.
2. Gogotsi G. A., Fracture Toughness Studies on Ceramics and Ceramic Particulate Composites at Different Temperatures // Fracture Resistance Testing of Monolithic and Composite Brittle Materials, ASTM STP 1409, J. A. Salem, G. D. Quinn, and M. G. Jenkins, Eds., American Society of Testing and Materials, 2002, pp. 199-213.

OPTIMISATION OF STRUCTURE OF ALLOYS OF THE SYSTEM CU-AL-NI-ME HAVING MARTENSITE TRANSFORMATION FOR WORK IN CONDITIONS OF SLIDING FRICTION

O.A.Shcheretsky, V.G.Novytsky, V.L.Lakhnenko, V.S.Shumikhin, V.P.Havryliuk

Physico-technological Institute of Metals and Alloys of NASU

Modern machine-building development tendencies are direct connected with tribology, development and improvement of tribo-materials. Amongst all diversity of tribo-materials the copper-based alloys are of special interest as the most in daily use for pillow of sliding.

Lately capacity of majority of machines and equipment was considerable increased, that has caused to increasing of loading on friction units.

In order to increase wear resistances of units undergoing the most violent wear numerous methods of reinforcing of initial surface of contacted sections such as manifold types of surface plastically deformation, chemical-heat-treatment, coating by chemical (CVD) and physical (PVD) methods, etc. are used.

These methods are often effective within little interval of technological and working details parameters, that is why for elevation of reliability and longevity of friction units complex using of internal structural reserves of materials becomes the extra topical.

In this connection employing of materials in metastable condition with high level of their structure unequilibrium for friction units is perspective. Such materials have ability to dissipation of friction power due to structure and phase transformations, that precludes accumulation of critical stresses after which destruction of material arises.

The object of investigation is one of such materials, alloys having martensite transformation of system Cu-Al-Ni-Me. Their initial structure can be changed in wide interval, depending on alloying and regimes of heat-treatment.

For fulfilment of investigation specimens were molten in inductive furnace in atmosphere of argon. Using alloying and special heat-treatment, alloys with different parameters of martensite transformations were obtained.

Alloys were tested in conditions of dry friction under scheme block-on-ring. Specific loading was 1.77 MPa and sliding velocity was changed within interval 0.75-3 m/c.

The specimens were examined with optical microscope and by X-ray structural method.

Obtained result permits to establish the correlation between wear resistance studied Cu-Al-Ni-Me-alloys and their structure and to show, that their wear resistance can be 5-20 time more then wide used standard bronze have which[fig.1].

Predominating effects proper to alloys with martensite transformation having the largest influence to wear resistance have been determined.

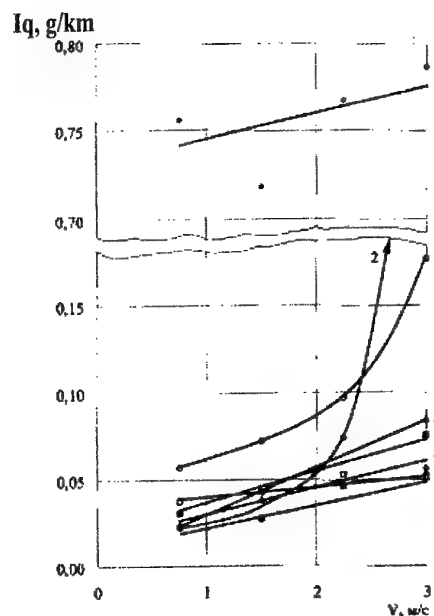


Fig.1 Influence of the sliding speed on the intensity wear-and-tear:

1. Bronze (Cu - 5%Sn - 5%Zn - 5%Pb);
2. Cu-Al-Ni ($\alpha + \gamma_2$) - phases;
3. Bronze (Cu - 9%Al - 4%Fe);
4. Cu-Al-Ni (γ' -phase);
5. Cu-Al-Ni (monocrystal β_1' - phase);
6. Cu-Al-Ni (monocrystal β - phase);
7. Cu-Al-Ni (β_1' - phase);
8. Cu-Al-Ni (β_1 - phase);

IMPULSE THERMOSTABILITY OF COMPOSITE MATERIALS ON POLYMERIC BINDING

Paschenko E., Silchenko Ya., Chernenko A.

V.N.Bakul Institute for Superhard Materials of the National Academy of Sciences of
Ukraine, Kiev, Ukraine

Composites on the basis of polymeric bonds are the basic type of materials of the diamond tools, which are used for machining metals and cermet, and on finishing operations - also for machining a glass, natural stone and other building materials. Manufacture and the consumption of such tools in the world continues to grow, and, according to the prognoses, such tendency will be kept in the future.

The most important elements of any directed research gains in the field of development of materials are scientifically justified criterions, on which the functional properties of composites will be improved.

The researches, which were carried out last time in a department of physico-chemistry of diamond-containing composite materials of ISM, create necessary preconditions for designing of qualitatively new criterions of refinement of polymeric-abrasive composites. This preliminary backlog contains detailed representations about a character of thermal loadings, to which is exposed polymeric component of materials in zone of cutting.

According to our conceptions, average temperature in zone of cutting can not be used for performance of conditions, in which the destruction of a polymeric grid during work happens. The real process develops under action of short temperature impulses ($700 - 1000^{\circ}\text{C}$), considerably exceeding boundary of static thermostability of organic polymers. Actually polymeric composite (is exacter, thin working stratum) is maintained in conditions, when the energy of thermal oscillations of its basic structural units (segments of macromolecules) can be compared to durability of the appropriate chemical bonds of a polymeric grid. As during work of the tool the continuous renewal of such working stratum happens, it is possible to state, that all volume of polymeric composite all phase of its resistance contacts to a treated material extremely in such "thermally superintense" condition.

The high intensity of temperature impulses initiating processes in polymeric composites in a contact zone means key difference of contact destruction from destruction at static heat input. However time component, namely - the duration of impulses of heat, plays the not less important role. The processes of destruction of polymers have a relaxation nature, that is the plurality of the elementary acts of relative transition of segments (or other kinetic unites) of polymeric grid resulting in to tearing up of bonds, is characterized by the particular spectrum of relaxation times.

In real conditions of operation of polymer-abrasive composites the characteristic duration of thermal impulse resulting in destruction of a polymeric grid, is close or less characteristic interval of time necessary for a relaxation of segments of macromolecules. Therefore majority of traditional views about a behaviour of polymers under thermomechanical stress becomes in this situation inapplicable. Actually, studying a behaviour of polymers in contact zone, we deal with a special state of substance, namely: substance, which has achieved temperature considerably exceeding a limit of it thermostability, but yet not had time to react to it by the relevant structural modifications. Such condition is possible to name "superintense".

Obviously, duration of such phase, when the polymeric grid in real contact with countersurface already has received powerful temperature impulse, but has not reacted on its with catastrophic destruction in contact microvolume, is a determinative, which defines a character of work of the tool.

The behaviour of polymeric materials in a similar situation is almost not explored. It concerns as peculiarities of a structural condition of the "superintense" polymeric grids, and modes of physico-chemical influence on this condition, and also correlation between duration of preservation "superintense" state of polymer, and working performances of the composite, made on its basis. The duration of such phase can be considered as performance of thermostability of polymer under

an operation of short high-temperature impulses or, shorter, impulse thermostability. Impulse thermostability of the bond can be used as qualitatively new criterion promising essential refinement of the diamond tool on a polymeric basis.

The quantitative definition of magnitude of impulse thermostability of a material requires use of methods of mass-spectrometry and thermal analysis and is based on existence of correlation between micromechanical performances of destructing layer of polymer and magnitude of loss of a mass in process of destruction. We offer to determine this index as time, for which the sample loses 50% of initial microhardness (other micromechanical performances) at temperature corresponding maximum velocity of loss of a mass of a sample. For various investigated compositions this magnitude changes from the shares of second about several seconds.

According to our conception, the important physico-chemical performance of a polymeric grid which is in charge of magnitude of its impulse thermostability is the distribution of free volume between kinetic unites forming a structure of polymer. The common regularity, found out by us, consists in sharp magnification of magnitude impulse thermostability at a diminution of a breadth of the above mentioned distribution of free volume. The molecular mechanism underlying this appearance is connected, apparently, with known, but poorly claimed at description of solids reactions "effect of a cell". In this case this effect is exhibited that the radical fragments formed at a rupture of chemical bond of polymer under an operation of powerful short thermal impulse have no time to move from each other on a large enough distance, and with high probability recombine. In an outcome instead of avalanche increase of volumetric concentration of ruptures the system of "blinking" connections is formed, that allows to keep a high level of micromechanical performances of superficial stratum of composite. The gradual accumulation of ruptures of a polymeric grid happens in this case too. Thus each "implemented" rupture raises probability of ruptures of the next bonds, as submits additional free space for separation of next formed radical pairs. A role of a breadth of a distribution function of free volume to segments of a polymeric grid from here is quite obvious: the diminution of a share of segments, for which the magnitude of accessible free volume exceeds most probable,

constrains self-accelerating process of accumulation of ruptures.

In conditions of destruction under an operation of short high-temperature impulses the real accumulation of ruptures of connections happens on those sites of a chain, on which the radical fragments are formed not in singlet, but in triplet condition. Probability in this case is great that the final fragment will come off a grid as triplet free radical, which is not inclined to a recombination. Such radical particles rather easily reach a treated surface and, are adsorbed on it, essentially facilitate process of abrasive cutting.

Total of fugitive yields of destruction, evolved by a polymeric composite in zone of friction, at magnification of an impulse thermostability of a material, sharply decreases. However both the share, and absolute amount of hitting in zone of friction triplet radicals rendering the greatest action on a treated surface appears the more, the more is index of impulse thermostability of composite.

Thus, the perfecting of polymeric-abrasive composites basing on a criterion of impulse thermostability, allows to pursue collaterally two contradicting each other purposes: to raise wear resistance of a material and to reduce contact forces and temperatures, explicatings in process of abrasive cutting.

On the basis of polymeric composites with heightened impulse thermostability we design wide range of tools with usage of diamonds, cubic boron nitride and usual abrasives. Such tools now is successfully used by different customers in Ukraine, Czechia, Hungary, Germany for grinding and finish machining of hardened steels, hard alloys, ceramic materials, natural stone.

THE DEVELOPMENT OF THE STRUCTURAL-PHYSICAL BASES OF STRENGTH AND PLASTICITY OF LAMINATED MATERIALS AND HYBRID COMPOSITIONS ON THEIR BASIS

Kolomiets A.T., Firstov S.A., Rogul T.G., Usakov E.I.

Institute of Material Sciences of the National Academy of Sciences of Ukraine, Kiev, Ukraine

The actuality of this problem is adjusted by absence of technological and construction materials that have small specific gravity, enough level of corrosion, radiation and heat resistance in the same time at temperature $T \geq 1273$ K by the terms of high pressing and temperature hopping.

Have been learned the destruction limit of the stratified composite field Cr-V system by the theoretic and experimental foundation structure-dimension hardness, sensitivity, plasticity and viscosity and a possibility to regulate this parameters by the way of modification layer thickness have been established.

It is shown that when the δ_i layer thickness (λ) is smaller then $10 \mu\text{k}$, soundness and crack durability of composite field grows. These absolute values of shown characteristics can become 3 and more times bigger than for the basic chromium alloy.

The experimental values of hardness limit of the Cr-V composite field can be approximated by equations:

$$\sigma_{0.2K} = \sigma_{0.2V} + \frac{\alpha \cdot G_{(Cr+V)} \cdot b_{(Cr+V)}}{\lambda}$$

$$\sigma_{0.2K} = \left(\sigma_{0.2Cr} + \frac{\alpha_1 \cdot G_{Cr} \cdot b_{Cr}}{\sqrt{h_{Cr}}} \right) \cdot f + \left(\sigma_{0.2V} + \frac{\alpha_2 \cdot G_V \cdot b_V}{\sqrt{h_V}} \right) \cdot (1-f)$$

Where $\alpha=35$ - non-dimensional coefficient, $\alpha_1=17 \mu\text{k}^{-1/2}$, $\alpha_2=35 \mu\text{k}^{-1/2}$.

It have been investigated the impaction of structure-dimension parameter to the thermocyclic afterflow and long time durability in stratified composite field Cr-V. It has been established that the reduction of δ_i layer thickness with constant

volume consistence of components results to increase of soundness and decrease the speed of thermocyclic afterflow in the temperature interval 293-1373 K.

The speed of thermocyclic afterflow, as it proved, can be shown as equal:

$$\dot{\xi} = B \cdot \sigma^\beta$$

Where B, β - constant coefficients, σ - pressure in the cycle.

There is an exponential dependence between the stress and number of thermal cycles before fracture in the temperature and time limit under study:

$$N_p = A \cdot e^{-\alpha \cdot \sigma}$$

where A, α - constants.

In practice, the authors prove the prospects of the idea of creation of high-temperature high-strength materials of a new generation by using layered polymatrices hardened by high-modulus fibers as a base. The object of research is polymatrix composite material, the basis of which consists of Cr-V layers and in addition is hardened by fibers of alloys of tungsten.

It have been investigated mechanical features of first made composites (Cr-V) - BP-5, (G-V) - BP-20, and shown that these materials with a volume part of fibers 20% have hardness 1215 MPa with relative lengthening up to 7%. Hundred hour hardness at temperature 1273 K is more than 120 MPa.

DEPOSITION OF a-C:H FILMS ON NON-CONDUCTING SUBSTRATES BY TWO DIFFERENT PACVD TECHNIQUES

Varshavskaya I.G., Bukhovets V.L., Ravi N.⁽¹⁾

Institute of Physical Chemistry of Russian Academy of Sciences, Moscow, Russia

⁽¹⁾International Advanced Research Center for Powder Metallurgy and New Materials,
Hyderabad, India

a-C:H films have been obtained in hydrocarbon rf glow discharge implemented in two different ways, namely, three-electrode (or two discharge) and two-electrode (or single discharge) modes. PET and glass were used as substrate material.

In the case of the two-discharge mode the first discharge with a frequency of 50 Hz was used for activation of the gas medium in the positive column of glow discharge. The second discharge with a frequency of 250 kHz, characterized by the density of the deposition current, was used to control the ion flux to the deposition surface. A cylindrical quartz reactor 6 cm in diameter was used in the experiments. Internal electrodes of the hollow cathode type were placed on the edges of the reactor. Glow discharge was ignited between the two electrodes. The third electrode with a 150 cm² area was placed outside on the reactor wall and the high frequency field was fed to this electrode. The substrate to be coated by DLC film was placed inside the reactor just over the third electrode. The high- and low- frequency voltage sources were connected through a system of filters, which made it possible to determine independently the activation and deposition currents. Methane or cyclohexane/argon mixture were used as a precursor gases. Dependence of film deposition rate, film microhardness and absorption coefficient upon gas pressure, gas flow rate and deposition current density was studied. a-C:H films deposition rate is proportional to a precursor gas mass flow rate whereas it has a maximum at a certain deposition current density. Dependence of film microhardness on the precursor gas mass flow rate as well as on the deposition current density has the pronounced peak. The stimulation coefficient was introduced, which was the ratio of two fluxes falling onto the deposition

surface, namely, the ion flux and the precursor gas molecules flux. In the case of the single-discharge mode a-C:H films were deposited in a rf glow discharge sustained by a hydrocarbon gas. The deposition system was very asymmetric: small central powered electrode and large grounded screen electrode. 250 rf power was coupled to the central electrode which served as a substrate holder. The powered electrode was subjected to a negative dc self-bias, which was due to the higher mobility of electrons as compared to ions in rf regime.

Voltage-current characteristics at dc and rf regimes both for skinned and masked electrode in methane, argon and air have been taken. Dependence of bias voltage on the discharge parameters such as amplitude voltage, current density, gas pressure has been determined which is: $V_B \sim j \times V^{0.5} \times P^{-0.5}$. Both the active and reactive components of discharge impedance as well as the rf current lag relative to rf voltage have been found.

Mass gain as a function of deposition time was studied. It is linear for both types of substrates and its value for PET and glass differ slightly. Dependence of a-C:H films deposition rate upon both methane pressure and bias voltage have been examined. Deposition rate has a weak dependence on the methane pressure whereas it is linear with the bias voltage and does not depend on a substrate thickness up to its certain value, because impedance of the discharge is far greater than that of the substrate.

Molybdenum substrates were exposed in the air rf discharge at various values of bias voltage in order to determine ion energy in accordance with the depth of ion penetration which has been measured by EPMA.

MICROSTRUCTURAL FEATURES AND MECHANICAL PROPERTIES OF Ti-Si AS-CAST ALLOYS

Bankovskiy O., Beha N., Vasylyev O. Kulak L, Miracle D.⁽¹⁾, Senkov O.⁽¹⁾, Firstov S.

Frantsevich Institute for Problems of Materials Science of NAS of Ukraine, Kiev, Ukraine

⁽¹⁾Air Force Wright Laboratory, Wright-Patterson AFB, OH USA

An advantage of silicon as an alloying element for titanium alloys is in the possibility for dispersive strengthening by Ti_5Si_3 silicide particles of solid and refractory phase. Due to the eutectic transformation that occurs at 8.5 wt.% Si, as-cast Ti-Si alloys with the concentration of Si above ~3% are natural composites, with very promising high temperature and wear resistance property [1]. Therefore, analysis of relationships between composition, microstructure and mechanical properties in the Ti-Si alloy system is a crucial scientific challenge. There have been only few papers on Ti-Si alloys with high concentrations of Si published so far [1-3]. Directionally crystallized Ti- Ti_5Si_3 eutectics [2] and the effect of some modifying elements on microstructure of the eutectic alloys have been investigated.

The present work studies the microstructure and mechanical properties of Ti-Si cast alloys within a composition range from zero to 8.5 wt% Si. The alloys were prepared from iodide titanium and ion-crystalline silicon using vacuum-arc melting. The cast ingots were 15 mm in diameter and 80mm in length. Tensile tests were conducted on specimens with the gauge of 3 mm diameter and 37 mm long. Creep resistance was measured as long-term hardness after 1-hour indentation with 9.8 N load [4].

Tensile properties depended on the alloy composition and the morphology of reinforcing silicide phase. Tensile strength (σ_B) increased from ~300 MPa to 700 MPa when the silicon concentration increased from 0 to 2%, Figure 1, probably, due to an increase in the silicon content in the HCP α phase and precipitation of secondary Ti_5Si_3 particles. Indeed, optical microscopy revealed no primary Ti_5Si_3 silicide particles, while TEM analysis found fine precipitates of secondary silicides, mainly at dislocations.

An abrupt decrease in strength that occurred in the range of 2-3 %Si was probably a result of formation of a new constituent, i.e. eutectic,

Figure 1(a). A subsequent rapid increase in strength at higher concentrations of Si can be related to an increase in the volume fraction of the eutectic.

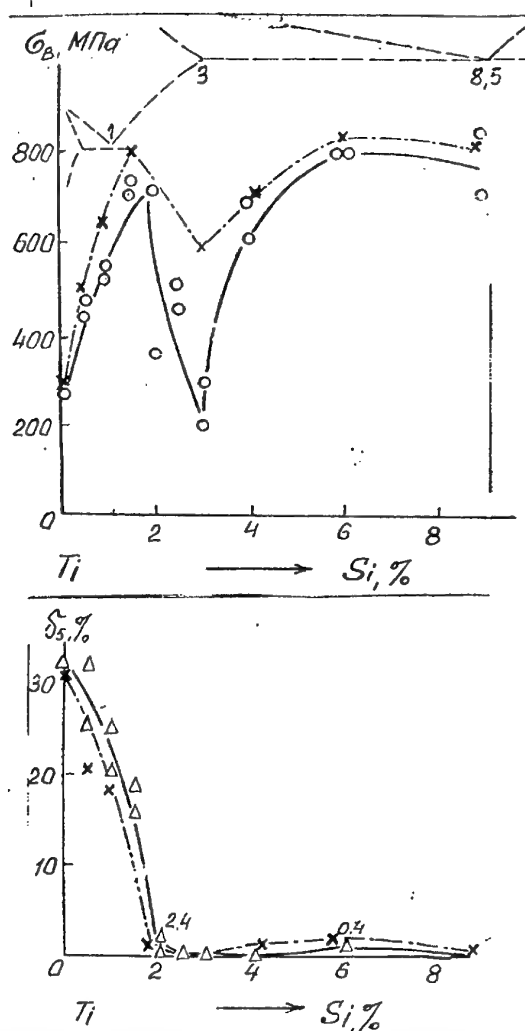


Fig. 1. Dependence of tensile strength (a) and elongation (b) on Si content in Ti-Si cast alloys: o, Δ are results of the current work, x is data from [3].

Elongation decreased rapidly from ~30% to almost 0% when concentration of Si increased from 0 to 3%, Figure 1(b). During further increase in the Si content, elongation increased slightly to 0.4% at 6% Si and then decreased again to 0% at 8.5% Si. X-ray study showed that

the lattice parameters of the α phase decrease when the concentration of silicon increased from 0 to 4% (Fig. 2). During further increase in the Si concentration, the lattice parameters increase slightly and then remain unchanged in the range of 6 – 8.5% Si. Such a behavior in the lattice parameters may indicate that the concentration of Si in the α phase increases continuously the concentration range of 0-4% Si, and probably Si is in a supersaturated solid solution. Indeed, according to the phase diagram, maximum equilibrium solubility of Si in the α phase is less than 1%; therefore, at concentrations of Si in the alloy exceeding this limit, the lattice parameters of this phase decrease only if supersaturated solid solution is formed. An increasing volume fraction of the eutectic in the range of 4-8% Si lead to a decrease in the concentration of Si in the α solid solution. It can be seen from Figure 2 that the concentration of Si in the solid solution decreases to a value corresponding solubility of Si in the Ti-2%Si alloy.

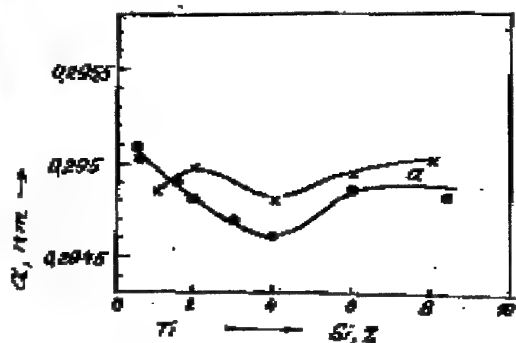


Fig. 2. Lattice parameter variation of Ti-Si as-cast alloys (●) and after annealing at 800 °C, 2 hours, vacuum 10^{-5} Torr (x).

The effect of Si on creep resistance is shown in Figure 3. At 500°C, the creep resistance has maxima at 2% Si and 6% Si and a minimum at ~3.5% Si. At 700°C, the minimum is observed at 4% Si; the creep resistance increases continuously at Si concentrations above 4%.

Vacuum annealing at 800°C for 2 hours led to an increase in the lattice parameters of the α -solid solution, indicating a decrease in the concentration of Si in this phase after annealing.

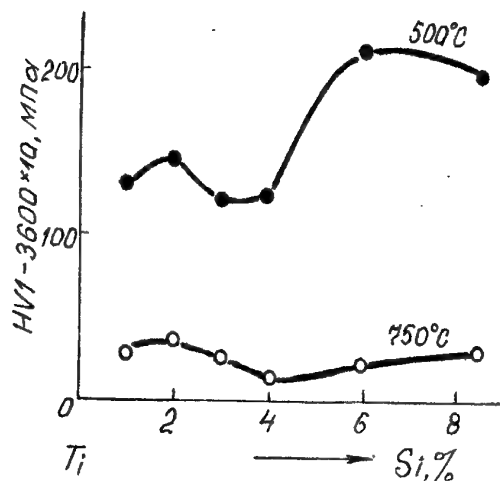


Fig. 3. Long term hardness of as-cast Ti-Si alloy.

Conclusions:

1. In Ti-Si as-cast alloys their α -solid solution is oversaturated with silicon at real rates of cooling. The degree of over saturation is around 0.1 to 0.2 of the total content of silicon in the alloy. The vacuum annealing at 800 °C provides a lowering of silicon concentration nearly to an equilibrium value.
2. In spite of the embrittling influence of silicon on titanium, the most significant interest for the development of as-cast refractory alloys of titanium can be in compositions containing up to 2 % of Si, and pre-eutectic ones containing 4 to 6 % of Si. Plasticity of alloys can be improved through the use macro and micro alloying, or plastic deformation (hot pressing, forging etc.).

Acknowledgement

The authors would like to acknowledge funding of this project from the US Air Force Office of Scientific Research and the assistance of the Science and Technology Center of Ukraine.

References

1. Hrihorovich V.K. Refractoriness and phase diagrams - M. Metallurgia, 1969 - 323 p. (In Russian).
2. Crossman F.W., Yue A.S. Unidirectionally solidified Ti-TiB and Ti-Ti₅Si₃ Eutectic Composites - Met. Trans.1971. Vol.2, p 1545.
3. R.Sana.,T.Nandy and R.Misra. Microstructural changes induced by ternary additions in a hypoeutectic titanium - silicon alloy. J. of Material Science, 26 (1991), p. 2637-2644.
4. Zakharov M.Y., Zakharov Q. M. Refractory alloys.- M., Metallurgia. 1972, 384 p. (In Russian)

PROCESSES OF PHASE FORMATION IN SPARK COATINGS WITH UTILIZATION OF ELECTRODES ON BASE OF INTERMETALLIDES, NITRIDES AND CARBIDES

Paustovsky A.V., Alfintseva R.A., Kirilenko S.N., Kurinnaya T.V., Gubin Yu.V.,
Novikova V.I.

I.N.Franthovich Institute for problems of Materials Science of NAS of Ukraine, Kiev,
Ukraine

Fundamental essence of spark treatment consist in utilization of spark charge in gases medium. This process consist in anode material erosion and deposition of this products to catode. Pulse and temperature loadings and material transport leads to formation of layer with complicate composition and structure.

Choice of alloying electrode material based on accounting of phase formation process in alloyed layer and residual stresses formation process in the coatings.

Electrode materials which were investigated in this work belong to two groups on nitride base:

1. on nitrides and intermetallides base with plastic bunch on nickel base
2. on WC and TiC carbides base with metal bunch of cobalt.

Eutectic alloys of Ni-Cr-Al system concern to first group. Main advantage of this alloys is low melting temperature and formation of thin conglomerate structure by spark treatment process.

As anodes for spark alloying (SA), the most characteristic alloys were chosen, namely, A1 which is a binary Ni-Cr alloy of eutectic composition according to the phase diagram. A2 which is ternary Ni-Cr-Al eutectic alloy, A5 which is ternary Ni-Cr-Al alloy located in the quasibinary Cr-Ni-Al section and A6 which is a Ni-Cr-Al-Y alloy analogous to the second eutectic composition and is alloyed by 2 mass % of yttrium.

SA was carried out on an EFI-46A equipment under the following conditions: a specific treatment time of 10 min/cm²; an oscilation frequency of a vibrator of 100 Hz; a short circuit current of 1.5 A.

Electrodes for SA were made by two methods, namely, high-energy hot pressing in vacuum (HEHP) and melting in arc furnace with a nonconsumable tungsten electrode in a protective atmosphere.

It has been shown that, in cast alloy 1A, biphas eutectic structure, consisting of Ni-based γ -solid solution and Cr-based α -solid solution, is observed. An analogous phase composition is observed in hot-pressed alloy 1A.

In cast and hot-pressed alloys 4A and 6A, a triphase structure consisting of an α , γ and β (Ni-Al) phase is observed.

In cast alloy 6A, the intermetallic phase Ni₃Y, located along boundaries of eutectic colonies, was detected. In hot-pressed alloy 6A, the oxide phase Y₂O₃ was identficated.

The X-ray studies of spark coatings showed the presence of intermetallic phases containing iron and the metals of anode. In the coating from alloy 1A (Ni-Cr), the intermetallic compounds NiAl, CrAl and FeNi, as well as carbides FeC and complex δ -NiO·Al₂O₃ type oxides were detected. In the coatings from cast alloy 6A (Ni-Cr-Al-Y), a phase containg yttrium in the form of anoxide or an intermetallic component was not detected by radiographic analysis. In the case of SA by hot-pressed alloy 6A, the intermetallic phases NiAl, CrAl, FeNi, Al₃Y and NiAlY were identifed in the coating.

Wear resistance tests of the coatings were performed in MT-68 test unit on 5×10.5×15 mm specimens in dry friction in air with 65G steel conterbody.

In the tests the friction coefficient f and the intensity of wear of a specimen I (mm/km) were determined.

The test conditions were as follows: a slip speed $V=10$ m/s, a load of 5 kg. Friction coefficient is equal 0.26-0.30 for coatings which deposited by melted electrodes and electrodes obtained by HEHP method. More wear-resistance have 5A alloy. Significance of wear 9.3 mkm/km is commensurable with $I=10$ mkm/km wear of BK-34 alloy.

Electrode materials on titanium nitride base with nickel bunch utilize for receiving spark coatings with high oxidation resistance in aggressive medium. Phase composition of spark coatings include Ti_2Ni , $TiNi$, $TiNiO_3$, Ni_2O_3 intermetallides and Ti-Ni-Fe hard solutions. Particles TiO_2 and NiO present in erosion products. It is determined that optimal tribotechnical and mechanical characteristics have composition with (15-20)%mass. of plastic bunch on nickel base.

One of significant lacks of spark treatment is limit depth of coating. This depth depend on mechanical properties of coating material sufficiently. Process of tight-melting materials plotting to steel leads to cavitation mixation of this material with surface material. On condition of utilization of tungsten carbide alloys for receiving wear-resistance coatings in surface layer formed composition material with ferrum content commensurable with tungsten carbide content. Bunch of coating composite is steel with

significant concentration of WC and Co. Chrome addition 4%mass. to steel leads to increasing of steel ferrite strength. Chrome addition to WC-Co electrode material leads to such result. This addition allow to increase deposition of strengthened material on surface up to 40-60%. Hardness of coating increased to 3-4 GPa in this conditions.

Residual stress distribution in spark coatings is significant factor on choice of alloyed electrodes on tight-melted carbides base. Investigation of this characteristics were worked out in coatings obtained on steel by spark treatment of hard alloy with content (15%TiC+6%Co, rest WC).

X-ray phase analysis of this coating showed presence of W_2C , TiC carbides and pure tungsten. This investigations showed formation of tensile residual stresses 150 MPa in TiC carbide phase. Residual stresses with 200 and 110 MPa magnitude accordingly formed in products of tungsten carbide desintegration. This products consist in W_2C and W mixation.

Austenite layer has not residual stresses practically. This austenite layer leads to relaxation of residual stresses on "surface-coating" boundary. This phenomenon is significant on high energy regimes of spark treatment. Plastic austenite layer can play buffer role between the base and fragile components of coating on micro percussive mechanical loadings in exploitation process of details with wear-resistance materials.

PECULIARITIES OF MECHANICAL ACTIVATION OF TITANIUM IN THE PRESENCE OF WATER AND ALCOHOL

Kharlamov A.I., Antonova M.M., Bobet J.L.⁽¹⁾, Khomko T.V., Ushkalov L.N.,

Fomenko V.V.⁽²⁾, Kosourukov P.A.

Institute for Problems of materials Science, Kiev, Ukraine

⁽¹⁾Institute of Condensed Matter Chemistry at Bordeaux, France

⁽²⁾National University of Food Technologies, Kiev, Ukraine

High-capacity metals in respect to hydrogen require the certain treatment before the first sorption of hydrogen. Especially when we deal with such high-active metals, as Be, Al, Mg and Ti. After direct contact with hydrogen, they do not tend to form hydrides without being previously activated. However, these very elements and their alloys form hydrides characterized the highest content of hydrogen.

In our work the method of mechanochemical treatment of metals and alloys for activation materials before sorption of hydrogen was used. Titanium was chosen as an model object because of its high capacity and modest cost of metal itself.

Mechanochemical treatment was carried out in a high-rate planetary mill with metallic drums and metallic balls. Water and alcohol were used as dispergation media. Weights of titanium loaded were 6, 10, and 20 g. X-ray patterns were taken using DRON-3M ($\text{CuK}\alpha$) X-ray diffractometer. Hydrogenation of Ti powders was performed directly after the treatment in a mill on Sivers't's type device. Absorption of hydrogen was measured regarding the change of pressure in a closed system with volume about 65 cm^3 . Initial pressure 0.1 M Pa was fixed to the normal in constant intervals (5 min.) with following noticing of hydrogen absorbed. Dehydriding was carried out in vacuum 13 Pa. Temperature at which hydrogen started to evolve and its amount were noticed as well.

Analysis of X-ray spectra showed that under the mechanical activation during 20 min. the peak corresponding to TiH_x hydride phase ($2\theta \approx 86^\circ$) is present in X-ray patterns (fig.1). On the other hand, peaks corresponding to titanium oxide formation are absent. Further increase of the treatment duration results in lowering of this peak and after 40 min. of activation in a mill one can observe transformation of Ti powder in the X-ray amorphous state occurred due to significant

dispergation, which could be attributed to formation of "fragile" TiH_x phase.

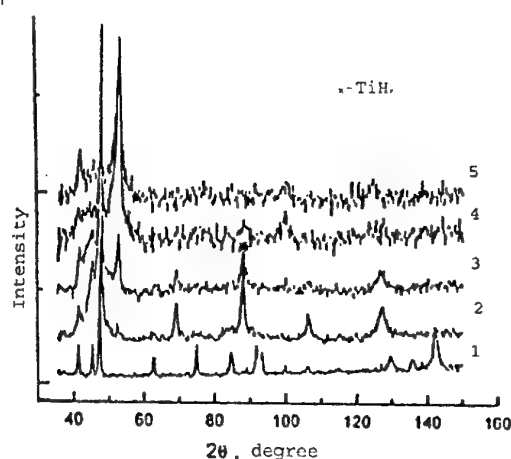


Fig.1 X-ray patterns of titanium powder. 1-initial Ti, 2, 3, 4 and 5-treated in water during 20, 30, 40 and 80 min., respectively.

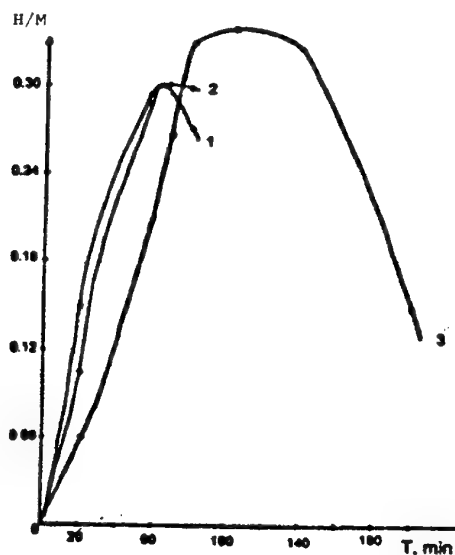


Fig. 2 Dependence of hydrogen content in the hydride phase on duration of Ti milling in water. Weight of titanium loaded in a drum: 1-6 g., 2-10 g., and 3-20 g.

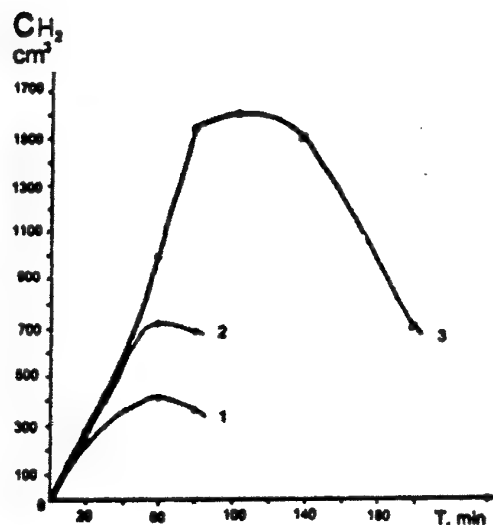


Fig. 3 Dependence of total content of hydrogen in a hydride material on duration of milling. Weight of titanium loaded in a drum: 1-6 g., 2-10 g., and 3-20 g.

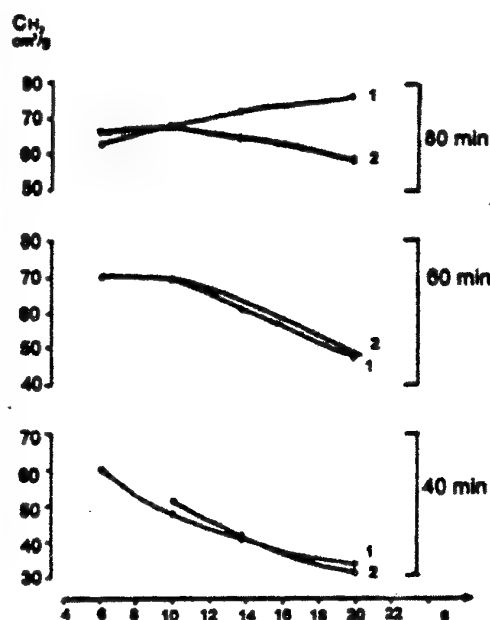


Fig. 4 Influence of the mechanical treatment medium on concentration of hydrogen in a hydride material. 1- water, 2-alcohol.

It was found out that hydrogen concentration in the hydride phase is higher when weight of loaded in a drum titanium powder is lower (fig.2). Total

content of hydrogen in the whole weight loaded in a drum is higher when mass of powder is higher (fig.3). It is worth noticing that formation of the hydride phase occurs when, as dispergation medium was also used alcohol. It was shown that amount of hydrogen evolved insignificantly depends on medium of the treatment up to 80 min. of activation. After the treatment exceeds that time, it was noticed that for 10 and 20 g. loaded titanium powder we have more hydrogen evolved in water than alcohol (fig.4). The process of mechanical activation of titanium powder was also accompanied by grinding of iron from metallic drums and balls (fig.5). It was shown that the highest amount of iron has been ground when 20g. of titanium powder was treated in a mill.

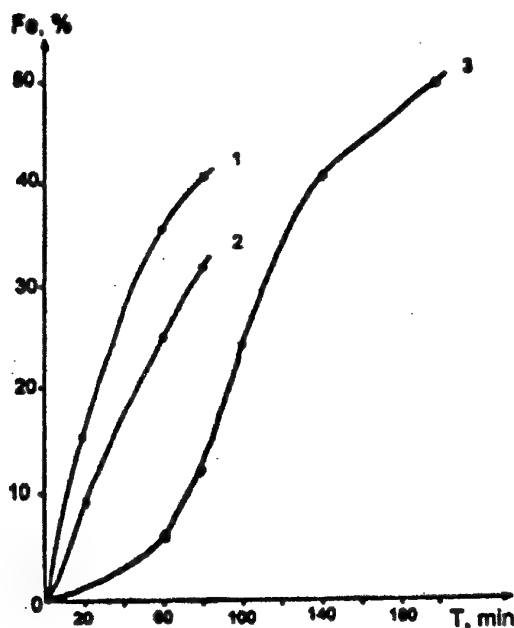


Fig. 5 Dependence of Fe content in titanium powder on milling duration and amount of Ti powder. Weight of titanium loaded in a drum: 1-6 g., 2-10 g., and 3-20 g.

Thus, mechanochemical treatment of titanium powder results in both the activation of titanium powder itself and, what is more interesting, formation of titanium hydride phase TiH_x. Moreover, the formation of titanium hydride occurs under treatment of the powder in water as well as alcohol. Therefore, mechanochemical activation is a promising method for development of new and improvement of existing as hydride materials as methods of their obtaining.

MECHANOCHEMICAL TREATMENT AS AN EFFICIENT MEAN TO MODIFY SUBSTANCE TEXTURE

Kharlamov A.I., Ushkalov L.N., Bobet J.L.(1), Gubareni N.I., Bondarenko M.E., Shipovskiy V. Yu.

Institute for Problems of Materials Science, Kiev, Ukraine.

(1)Institute de la Matière Condensée de Bordeaux, Pessac, France.

It is well known that reactivity of solids strongly depends on their surface properties. Generally, the properties vary with the conditions of the synthesis, which determine the texture, particle size, specific surface area, type of crystal face exposed and the number of active sites. One of the most promising methods to modify these parameters is the mechanochemical treatment (MCT).

In this report results of investigations of structure and state of oxide systems after MCT in different media are presented. Powders of V_2O_5 , MoO_3 which are catalysts of many important industrial processes were used as initial reagents.

Mechanochemical treatment was carried out by means of a high-energy planetary ball mill in media such as water, ethanol and in air with the duration of milling varying. Specific surface area was measured using the nitrogen desorption method by means of "Gasohrom-1" device. X-ray patterns of powders were obtained by means of "Dron-1M" ($CuK\alpha$) device. The surface composition was investigated employing VG ESCA-3 ($AlK\alpha$) spectrometer (XES method) and IR-spectroscopy. Morphology of samples was observed by tunnel electron microscopy (TEM). From data performed in Table. 1 one can see that along with dispergation of oxide powders considerable modification of samples texture takes place. It worth noticing that the extent of

Table 1. Relative intensities of characteristic peaks in dependence on the duration and medium of dispergation and specific surface areas of: a - V_2O_5 , b - MoO_3 .

a) <u>Treatment in ethanol</u> <u>Treatment in water</u> <u>Dry milling</u>									
Time, min	SSA, m ² /g	XRD		SSA, m ² /g	XRD		SSA, m ² /g	XRD	
		I_{010}/I_{110}	I_{010}/I_{400}		I_{010}/I_{110}	I_{010}/I_{400}		I_{010}/I_{110}	I_{010}/I_{400}
0	3,80	1,33	1,59	3,80	1,33	1,59	3,80	1,33	1,59
2	5,80	2,17	2,04	5,20	0,91	1,90	5,40	1,05	2,08
5	5,80	2,63	2,38	-	-	-	-	-	-
10	6,20	3,33	3,13	10,50	0,78	1,77	11,6	0,69	1,28
20	8,0	4,00	3,70	-	-	-	-	-	-
25	-	4,13	3,78	-	-	-	-	-	-
30	8,80	4,33	3,85	1,60	0,52	1,50	-	-	-
40	-	-	-	-	0,22	1,25	-	0,78	0,88

b) <u>Treatment in ethanol</u> <u>Treatment in water</u> <u>Dry milling</u>											
Time, min	SSA, m ² /g	XRD			SSA, m ² /g	XRD			XRD		
		I_{040}/I_{021}	I_{040}/I_{060}	I_{040}/I_{020}		I_{040}/I_{021}	I_{040}/I_{060}	I_{040}/I_{020}	I_{040}/I_{021}	I_{040}/I_{060}	I_{040}/I_{020}
0	0,64	4,32	1,45	1,46	0,64	4,32	1,45	1,46	4,32	1,45	1,46
10	-	2,46	2,24	1,21	-	7,48	1,56	1,43	0,34	1,43	1,10
15	2,80	0,78	2,20	1,27	4,20	-	-	-	-	-	-
30	4,62	-	-	-	5,10	2,08	1,50	1,59	0,23	1,00	1,10
50	3,20	1,02	2,10	1,02	2,64	0,82	2,33	1,40	-	-	-
60	-	-	-	-	-	-	-	-	0,31	1,30	0,66

SSA- specific surface area; I- intensity of X-ray peaks.

texturing depends much not only on the duration of treatment but also medium of dispegeation. Study of XES spectra revealed that besides the modification of oxides texture there are considerable changes in composition of their surface. After 5 min. of MCT, low-energy peaks responding to vanadium ions in reduced state (V^{4+}) are observed. Mechanical treatment of MoO_3 in water results in partial amorphisation of samples and emergence of weak reflexes which characterize $MoO_{2.8}$ phase. But, unlike remarkable modification of texture of oxide systems, no any significant difference in relative intensities of characteristic peaks in Si_3N_4 and TiC X-ray patterns in comparence with those of initial powders was noticed (Fig. 1a,b,d,e). However, considering X-ray patterns of Si_3N_4 sintered it is clearly seen that relation of intensities of main peaks are noticeably different than that of powderous Si_3N_4 (Fig. 1a,c). The influence of temperature on texture the most obviously can be seen studing X-ray patterns of $VOHPO_4$ and $(VO)_2P_2O_7$ systems which are high-temperature (above $400^{\circ}C$) catalysts of partial carbon-hydrogen oxidation (Fig. 2). What is the most exciting that, when heated, $VOHPO_4$ is not only textured but also morphology of its

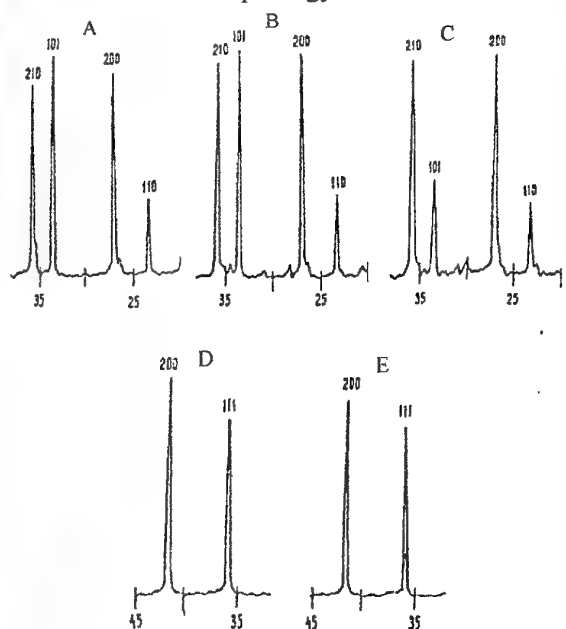


Fig. 1. X-ray patterns: a-initial Si_3N_4 powder, b-mechanotreated during 48 hours, c-sintered Si_3N_4 powder, d- initial TiC powder, e- TiC mechanotreated during 48 hours.

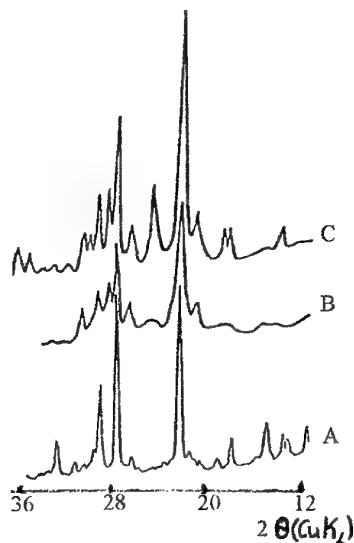


Fig. 2. X-ray patterns of pyrophosphate vanadyl: a-initial powder, b-mechanotreated in air during 30 min., c-oxidized in air.

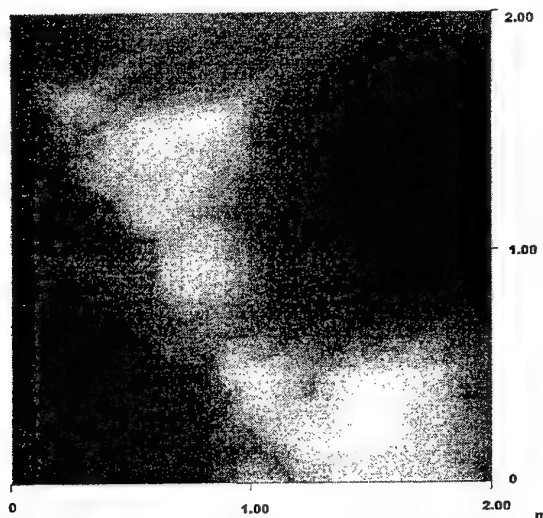


Fig. 3. TEM image of $VOHPO_4 \cdot 0.5 H_2O$ treated in vacuum at $400^{\circ}C$.

particles transforms into the laminar structure (Fig. 3).

Thus, in this paper it can be concluded that MCT of oxide systems results in significant modification of as samples texture as composition of their surface. It was also shown that state of powders mechanically treated depends not only on nature of samples (oxides or nitrides) but also medium of their disprgation. Moreover, it was also shown that thermal treatment affects texture of samples much as well.

ЗАКОНОМЕРНОСТИ ФОРМИРОВАНИЯ СТРУКТУРЫ И СВОЙСТВ В ДИСПЕРСНО-УПРОЧНЕННЫХ КОМПОЗИЦИОННЫХ МАТЕРИАЛАХ НА ОСНОВЕ МЕДИ

Плеханов К.А., Данилов Н.В., Мкртычев Ю.Г.
АО "Уралэлектромедь", г. Верхняя Пышма, Россия

Для исследования были использованы материалы следующих систем: Cu-Al-C, Cu-Ti-Al-C, Cu-Ti-C. Исходными компонентами служили порошки меди ПМС-1, алюминия ПП-1Л, титана ТПП-6 и графита ГК-1. Дисперсно-упрочненный композиционный материал был получен методом механического легирования в шаровой мельнице – атриторе, с последующим брикетированием и горячим прессованием в прутки. Коэффициент вытяжки составил 25.

Структурное состояние материалов изучали методами микродюрометрии, металлографии и электронной микроскопии. Как показали исследования, после операции механического легирования, образующиеся гранулы имеют мелкозернистую структуру с размером зерна менее 5 мкм и равномерно распределенные в объеме медной матрицы оксиды. Размер обнаруженных оксидов составляет порядка 0,1 мкм. Кроме того, наряду с дисперсными оксидами в структуре гранул присутствуют более крупные частицы склонные к выкрашиванию размером до 30 мкм – оксиды меди. Структура готового материала идентична структуре гранул. Микродюраметрический анализ показал, что в процессе горячего прессования происходит снижение начальной микротвердости гранул на величину порядка 200...300 МПа, но в тоже время заметного роста зерна не происходит. Следует отметить, что данные результаты несколько отличаются от ранее полученных, когда считалось, что в процессе нагрева под экструзию происходит "дозревание" материала, что приводит к росту твердости. То же подтверждают исследования гранул ДУКМ после кратковременных отжигов в интервале температур горячего прессования. Таким образом можно предположить, что механизм упрочнения полностью реализуется в процессе механического легирования в атриторе. При этом образуются мелкодисперсные оксиды, сдерживающие разупрочнение при температурах до 800°C и выше. Следует отметить, что при нагреве до таких температур в воздушной атмосфере происходит интенсивное окалинообразование на

поверхности медных материалов. Присутствие фазы упрочнителя в виде оксидов позволяет сохранить достаточно высокую электропроводность материала, которая достигает 50% от электропроводности меди марки М1, что позволяет использовать данные материалы в сварочной технике. Промышленные испытания и серийные поставки наконечников для автоматов и полуавтоматов дуговой сварки, изготовленных из указанных материалов, показали практически во всех случаях преимущество в стойкости по сравнению с применяемыми из БрХ и БрХЦр.

ФОРМУВАННЯ НАНОСТРУКТУРИ АМОРФНИХ ПЛІВОК $\text{As}_x\text{Se}_{100-x}$ і $\text{Ge}_x\text{Sb}_{100-x}$ В УМОВАХ ДИСКРЕТНОГО ТЕРМІЧНОГО НАПИЛЕННЯ

Дубровська Г., Колінько С., Ковтуненко В.

Черкаський державний технологічний університет, Черкаси, Україна

Наведено результати електронно-мікроскопічних досліджень наноструктури аморфних тонких плівок систем As-Se і Ge-Sb. Встановлена залежність ступеня мікронеоднорідності конденсатів від їх хімічного складу та технологічних умов напилення. Відзначається залежність наноструктури досліджених плівок від енергії адсорбованих частинок і складу парової фази.

Тонкі плівки для електронно-мікроскопічних досліджень отримували на вакуумних постах ВУП-4 і ВУП-5. В якості вихідних матеріалів використовували прокалібрований по розмірах (200-300 мкм) порошок стекловидної системи As-Se відповідних складів, або суміш порошків германію і сурми, змішаних у необхідних пропорціях, для системи Ge-Sb. Порошок за допомогою спеціального дозатора, яким оснащена технологічна установка, подавався у танталовий випаровувач. Температура випаровувача T_v дорівнювала 770 К і 870 К при напиленні плівок системи As-Se і 1470 К - при отриманні плівок системи Ge-Sb. Температура випаровувача контролювалася платино-платинородієвою термопарою. Тиск залишкової атмосфери підковпачного об'єму в процесі напилення підтримувався на рівні $6 \cdot 10^{-3}$ Па. Плівки конденсувалися на свіжі сколи по площині (001) монокристалів NaCl і KCl, які знаходилися при кімнатній температурі. Структурні дослідження отриманих зразків проводили на електронних мікроскопах EM-200 і EMB-100Б при прискорюючій напрузі 75 кВ. Для кожного хімічного складу плівок цикл напилення і досліджень проводився не менше двох разів.

Наноструктурна неоднорідність досліджених нами плівок проявляється на електронно-мікроскопічних знімках у відмінностях абсорбційного контрасту для ділянок плівок з різною густиною. В основному, ділянки з більшою густиною є окремими утвореннями округлої форми розмірами 10-30 нм, оточені ділянками з меншою густиною у вигляді "каналів"

шириною 5-20 нм. При аналізі наноструктури конденсатів, нами в якості критерію ступеня їх мікронеоднорідності використовувався контраст K на мікрознімках, між локальними ділянками з максимальною і мінімальною густиною зразків. Контраст розраховували по формулі:

$$K = \frac{D_{\max} - D_{\min}}{D_{\max} + D_{\min}},$$

де D_{\max} , D_{\min} - покази мікрофотометра для ділянок фотопластинки з різною ступінню почорніння. Абсолютна похибка визначення K не перевищувала $\Delta K = 0.04$.

Аморфні плівки $\text{As}_x\text{Se}_{100-x}$ з точки зору формування наноструктури, можна умовно поділити на дві групи. Конденсати складів з $x < 30$ ат. % мають структуру з низькою ступінню мікронеоднорідності ($K = 0-0.1$) і слабкою залежністю наноструктури від технологічних умов напилення. По особливому себе ведуть тонкі плівки в області $x \leq 10$ ат. %. Для них характерна дуже низька механічна міцність і вони чутливі до дії електронного променя мікроскопа. При опроміненні таких зразків, безпосередньо в процесі електронно-мікроскопічних досліджень, їх ступінь мікронеоднорідності суттєво збільшується від $K = 0.05$ до $K = 0.5$. При цьому основні зміни відбуваються на протязі перших 3-4 хвилин з початку опромінення.

Шари складів $30 \text{ ат. \%} < x < 60 \text{ ат. \%}$ мають наноструктуру з високою ступінню мікронеоднорідності, яка сильно залежить від технологічних умов напилення. Найвищу ступінь мікронеоднорідності з K близьким до одиниці мають плівки $\text{As}_{38}\text{Se}_{62}$, отримані при $T_v = 770$ К. Для конденсатів, хімічний склад яких знаходиться в області $x = 50$ ат. %, характерна чутливість наноструктури до опромінення електронним пучком мікроскопа. Ступінь мікронеоднорідності плівок при цьому зменшується від $K = 0.6$ до $K = 0.2$.

При використанні вище зазначених технологічних параметрів нами отримані аморфні конденсати $\text{Ge}_x\text{Sb}_{100-x}$ в усьому

діапазоні хімічних складів ($0\text{ат.}\% \leq x \leq 100\text{ат.}\%$). Враховуючи ступінь неоднорідності наноструктури напилених плівок, їх також можна розділити на дві групи.

Плівки з $40\text{ат.}\% \leq x \leq 100\text{ат.}\%$ мають практично однорідну наноструктуру з $K=0-0.05$, яка не змінюється в процесі дослідження і старіння. Виняток складають лише зразки із складом в околі $\text{Ge}_{60}\text{Sb}_{40}$, наноструктура яких при опроміненні ставала мікронеоднорідною з $K=0.3-0.4$ і розмірами неоднорідностей 8-10

нм. Для наноструктури тонких плівок $\text{Ge}_x\text{Sb}_{100-x}$ з $0\text{ат.}\% \leq x < 40\text{ат.}\%$ характерна слаба мікронеоднорідність з $K=0.2-0.3$. Крім цього, плівки в околі складу $x=15$ ат.% були дуже пористі з середнім розміром пор $\sim 15-20$ нм. Особливістю наноструктури аморфних плівок сурми є наявність великої кількості округлих включень з білим "темним" контрастом розміром ~ 20 нм і середньою відстанню між ними ~ 30 нм.

КЛЕЕВЫЕ МАТЕРИАЛЫ ДЛЯ КОНВЕЙЕРНОЙ СБОРКИ

д.т.н. Г.В. Малышева

МГТУ им. Н.Э. Баумана, Москва, Россия

Применение клеевых материалов позволяет повышать надежность и экологичность автотранспортных средств, упрощать конструкцию, экономить материалы и трудовые затраты. Однако, несмотря на все многочисленные преимущества клеевых технологий, их широкое внедрение сдерживается их не технологичностью и, в первую очередь, длительностью процесса отверждения.

Проблема внедрения клеев и герметиков в конвейерную сборку связана с тем, что все работы по склеиванию должны быть увязаны с тактом сборки, который на автозаводах изменяется в пределах минут, тогда как длительность процесса отверждения клеев составляет часы или даже сутки. Следовательно, чтобы встроить клеевую технологию в поточное производство, нужны специальные участки с накопителями, для которых требуются свободные площади и в итоге себестоимость машин от применения клеев не только не снижается, а, наоборот, повышается.

К клеям нового поколения (в литературе их называют основой техники XXI века) относятся адгезивы, которые обеспечивают склеиваемым конструкциям высокие деформационно-прочностные характеристики, при этом скорость их отверждения не превышает нескольких минут. Именно эти материалы отвечают требованиям конвейерной сборки.

К ним относятся:

- клеи ультрафиолетового отверждения;
- акриловые клеи;
- анаэробные герметики ускоренного отверждения.

Основное отличие клеев ультрафиолетового (УФ) отверждения от любых других адгезивных материалов заключается в операции отверждения, которая происходит только после облучения клеевого шва ультрафиолетовыми лучами. В состав клеев УФ отверждения входят специальные добавки - фото инициаторы, которые при обычных условиях в химическую реакцию не вступают. При экспозиции клеевого шва УФ лучами в течение нескольких секунд фото инициаторы расщепляются и ини-

цируют полимеризацию, которая происходит с очень высокой скоростью и процесс полного отверждения клея может закончиться в течение нескольких секунд. Все операции по нанесению клея и монтажу собираемого агрегата выполняются в обычном режиме, т.к. клей остается до начала облучения, в неотвержденном состоянии.

При УФ полимеризации может происходить:

- полная полимеризация (если УФ облучается вся площадь клеевого соединения). Полная УФ полимеризация возможна только при склеивании прозрачных для УФ материалов (это силикатные стекла и некоторые виды пластмасс). При сборке автотранспортных средств по такой технологии приклеивают зеркала заднего вида к лобовому стеклу (клеи марок *Квант-401* ТУ 6-01-2-731-84 и *фотоклей* ТУ 224230-008-51049574-00)).

- частичная полимеризация (если облучается часть клеевого шва). При таком способе отверждения происходит мгновенная поверхностная полимеризация только той части клеевого шва, на которую воздействовали УФ лучи. При частичной УФ полимеризации клеевое соединение в течение нескольких секунд достигает до 30 – 70% прочности от максимально возможной. Полностью процесс полимеризации заканчивается по обычному для данного клея механизму. Это позволяет не увеличивать длительность сборочных операций и проводить поточную сборку в заданном режиме. При сборке автотранспортных средств по такой технологии собирают резьбовые и цилиндрические соединения (клеи марки *Анатерм 50-УФ* ТУ 6-02-41-90).

Ведущим лидером среди разработчиков и производителей клеев УФ отверждения является корпорация Локтайт. Она выпускает более сотни марок клеев и герметиков УФ отверждения, которые применяются при сборке двигателя, трансмиссии, подвески и рулевого управления для: герметизации неподвижных плоских стыков (*Локтайт 5088, 5091* и др.); склеивании разнородных материалов (*Локтайт 322; 366; 3103; 3166; 3920* и др.); в качестве заливочных компаундов (*Локтайт 394; 3608* и др.) и пр.

Акриловые клеи (марок *Анатерм-103* ТУ 6-01-1300-85, *Анатерм-106* ТУ 6-02-29-90, *Анатерм-110* ТУ 6-02-238-92, *Анатерм-111* и *112* ТУ 2257-274-00208947-96, *Локтайт 330* и др.) предназначены для склеивания и герметизации плоских и гладких цилиндрических соединений. Применяются для склеивания металла, стекла, керамики и пластмасс.

Анаэробные герметики ускоренного отверждения (марок *Анатерм-114* ТУ 2257-301-00208947-98, *Анагерм-101* ТУ 225761-010-51049574-01, *Локтайт 262* и др.) применяются при сборке резьбовых соединений. Их использование существенно улучшает качество резьбового соединения. Первоначально, при нанесении, они фактически выполняют функцию смазки, компенсируют погрешности резьбы, приводя к снижению коэффициента трения. После отверждения за счет стопорящего эффекта, они обеспечивают резьбовому соединению стабильность силы затяжки при длительных вибрационных нагрузках.

Использование акриловых клеев и анаэробных герметиков ускоренного отверждения при сборке автотранспортных средств позволило:

- исключить фреттинг-коррозию;
- повысить качество соединения;
- повысить ремонтпригодность машин за счет сокращения номенклатуры стопорных элементов;
- уменьшить число крепежных элементов и тем самым упростить конструкцию.

При сборке автотранспортных средств анаэробные герметики ускоренного отверждения используют для крепления шпилек в блоке цилиндров двигателя внутреннего сгорания, шпилек картера двигателя, крышки картера главной передачи и дифференциалов, распределительной шестерни, карбюратора к коллектору, корзины сцепления к маховику, для фиксации шаровой рукоятки рычага переключения передач, для стопорения болтов крепления защитных кожухов дисковых тормозов, взамен шаровых соединений на трубопроводах, для стопорения регулировочных винтов уже после их регулировки (без разборки) и т.д.

Нормы расхода данных клеевых материалов существенно меньше, чем

нормы расхода при использовании других клеев. Например,

- 1 мл клея полностью покрывает площадь 400 см² при толщине слоя 0,025 мм;

- при диаметре адгезивного шва в 2 мм, что бы получить клеевой шов длиной 320 мм, требуется всего 1 мл клея;

- количество капель в 1 грамме составляет 25 – 35 и при стопорении ста штук резьбовых соединений, например М10, расход клея не превышает 4,8 г;

- при склеивании ста штук цилиндрических соединений при зазоре 0,1 мм, расход клея составляет всего 1,6 г.

В России анаэробные материалы ускоренного отверждения, акриловые клеи и клеи УФ отверждения разрабатывают и производят НИИ Полимеров им. В. А. Каргина г. Дзержинск Нижегородской обл. (серии *Анатерм* и *Унигерм*) и производственно-коммерческая фирма «Техно-Базис» г. Москва (серии *Анагерм* и фотоклей).

В настоящее время производство клеев и герметиков ускоренного отверждения освоили многие фирмы, ведущими из которых являются: ф. Loctite (США), Three Bond. (Япония), Industrial Lubricants (Швейцария), Imperial Chemical Industries (Великобритания).

SECTION IV.
CHARACTERIZATION
OF MATERIALS
PROPERTIES

"SELF-REGULATION" OF HEATING AND ABLATION AT HEAT DESTRUCTION OF MATERIAL

Frolov G.A.

Institute for Problems of Materials Science of National Academy of Science of Ukraine

Ultimate quantity of heat, which the material may swallow up by increase of the heat storage, reached at the moment of equality for thicknesses of heated and the removed layers [1]. In other words, any isotherm of temperature field terminates "run-off" from driving ablation surface in that moment when it occurs at depth, equal thickness of the removed layer. Further all isotherms of temperature field which are above considered isotherm, will move with the speed equal stationary ablation rate of material.

As this law is observed at any value of material gasification factor it is possible to conclusion, that speed of ablation is not depended on heat flow which determines balance of heat on material surface in stationary regime, but it is depended on the value of heat flow determining rate of surface heating before the beginning of its destruction.

The experimental data received at the tests of asbestos-reinforced laminate specimens in flows of air and nitrogen plasma, and also in conditions of radiation heating show, that ablation speed of this material strongly depends on destruction surface mechanism. At the same thermal effect in various heating conditions it differs by almost three times. At the same time total thickness of charring and removed layers up to establishment of stationary regime remained identical for all three versions of heating [2].

At the same initial surface heating rate of alloyed quartz glass ceramics in jets of combustion products of gas-dynamic bench and air plasma (enthalpy of 4700 and 12300 kJ/kg, accordingly) were received identical of ablation velocities. Thus heat flows for stationary regime differs by 5 times, and gasification factor - by 8 times [3]. As against of asbestos-reinforced laminate the ablation speed of alloyed quartz glass ceramics does not depend on heating kind. Heating rate before the beginning of surface destruction determines of ablation speed and heating of this material to the same extent.

Determining influence of the heat flow brought to material surface before the beginning of its destruction, allows to explain constancy of thickness of charring layer determined at the tests of asbestos-reinforced laminate specimens in conditions of identical mechanism of surface destruction. It was shown, that stationary value of thick-

ness of charring layer remains identical in spite of the fact that stationary values of ablation speeds may differ more, than on the order. In this case increase of moving speed of charring isotherm at increase of heating rate in the initial moment proportionally increases a filtration speed of gaseous products of decomposition binder and, thus, increases time of establishment of stationary ablation speed in comparison with its value at absence of filtration through the charring layer. As considered processes are interconnected, such "self-regulation" results to charring depth at the identical ablation mechanism does not depend on surface speed of destruction and keep its the constant value.

Temperature fields in specimens of alloyed quartz glass ceramics determining influence of heating rate of surface before the beginning of its destruction was studied. It is established that duration of non-stationary regime of heating and ablation depends, apparently, on heat conduction of material only until near destructed surface of material energy which is equal $\sim 1000 \text{ kJ/m}^2$ will not be absorbed. Further the heat flow heating internal layers does not depend any more on heat conduction of material and it is determined only by ablation rate of surface, i.e. in accordance with the formula

$$-\left(\lambda \frac{\partial T}{\partial y}\right)_w = \rho \bar{V}_\infty c_p (T_w - T_0) = \rho \bar{V}_\infty H(T_w)$$

Here ρ, c_p, λ are density, thermal capacity and heat conduction of a material, accordingly; T_0 is temperature non-heating material; \bar{V}_∞ is stationary speed of ablation; $H(T_w)$ is heat storage of material at temperature T_w .

Fig.1 demonstrated that near destructed surface of material at non-stationary regime "zone" with the special mechanism of heat accumulation is formed. There law of Fourier in this period of heating does not work.

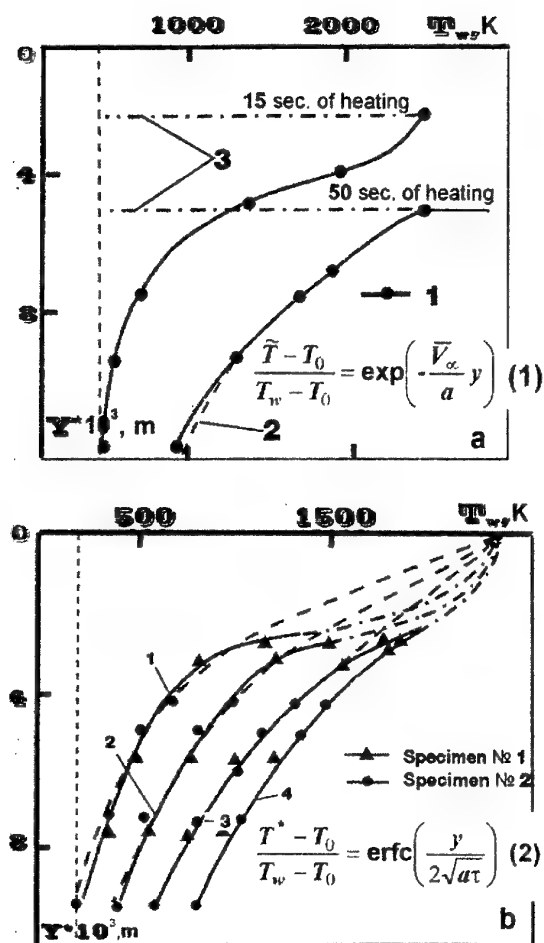


Fig.1. Experimental temperature profiles in a specimen of alloyed quartz glass ceramics at $\bar{V}_\infty = 0.11 \cdot 10^{-3}$ m/sec (a) and at surface melting without ablation (b): a) 1 – experimental data; 2 – calculation on formula (1); 3 – position of heated surface ($q_c = 7260$ kW/m²); b) 1-4 – 10, 20, 40, 60 sec of heating duration; points and solid lines are experimental data, dotted lines – calculation by formula (2), chain lines – forecasted temperature profile nearby of heated surface. a – temperature conductivity, T^* – temperature of considered isotherm.

At research of temperature fields in specimens without an ablation from surface (fig.1, b) also was established similar “zone” near melting surface.

The received results allow to draw following conclusions:

– “zone” with anomalous conditions of absorption and heat transfer renders significant influence on non-stationary heating and an ablation only materials with low heat conduction, including ablating heat-protective coatings;

– as at increase of heat conduction of material influence of “zone” on a temperature field strongly decreases, at calculation of heating, for example metals and alloys, this influence can be neglected even at high temperatures;

– satisfactory coincidence of experimental temperature fields with calculation ones the formula (2) up to $\theta^* = (T^* - T_0)/(T_w - T_0) \approx 0.4$ gives the basis to make the estimation of heating at a melting of solids without removal of a melt from surface in accordance with laws of “classic” automodel regime; thus the requirement of fast achievement of constant temperature of a heated up surface is completely optionally as enough to know, under what law the surface temperature changes.

It is concluded that heating and ablation of material is set by a heat flow before the beginning of a melting (destruction) of a surface and does not depend on what quantity of a material further will be removed in liquid or gaseous state and therefore the most economic installations for cutting, melting and coatings are the installations ensuring high-speed gas flows (large factors of heat exchange) with the gas temperature not strongly exceeding temperature of a melting processed material.

Reference

1. Frolov G.A., Polezhaev J.V., Pasichny V.V. Influence of internal and surface processes of absorption of heat on heating and destruction of materials // *Inj.-Phis. J.*-1987.-Vol.53, №4.- P. 533-540.
2. Frolov G.A., Polezhaev J.V., Pasichny V.V. at all Investigation of parameters of heat-protective materials in condition of non-stationary heating// *Inj.-Phis. J.*-1981. - Vol.40, №4. – P. 608-614.
3. Frolov G.A. Influence of heating kind on speed of materials destruction // *Inj.-Phis. J.* - 1986.-Vol.50, №4. – P. 629 – 635.

NANOMANIPULATION, NANOLITHOGRAPHY AND NANOASSEMBLING BY PROBE MICROSCOPY. REVIEW

Pokropivny A. V., Pokropivny V. V., Skorokhod V. V.

Institute for Problems of Materials Science of NAS of Ukraine, Kiev, Ukraine

Tendency for miniaturization of microdevices, microelectromechanical systems (MEMS) and integrated circuits (IC) have led during the 1980s to change paradigm in industry - instead of traditional assembly of microdevices from individual units the shaping and assembly must occur simultaneously and incrementally. In place of casting, molding, stamping, milling, turning and other mechanical processes the chemical and physical vapor deposition, sputtering, masking, etching, photolithography, oxidation, diffusion, doping, etc. For this reason a watchmaking industry has faded and automatical electronic industry become to be thrived.

However it also have reaches growth limit - nanoelectronics comes in place of microelectronics. Therefore we are on the threshold of approaching a new paradigm combined both of them with R.Feynman idea, namely, automatic computer-aid atom-by-atom and layer by layer assembling. Manufacturing of nanoelectromechanical systems (NEMS), ultra-low-scale IC (ULSIC) and biochip of one or two orders of smaller magnitude requires a fundamental research of physico-chemical processes of the contact phenomena at atomic and molecular levels, a development of nanomanipulators on the base of atomic-force, tunneling and other types of probe microscopes, and a creation of novel nanotechnologies for treatment of nanostructures. This is a global problem of international importance, and Ukraine with its powerful materials science potential may occupy in it appropriate niche.

State-of-the-art is shortly outlined of the forth main components of the problem, namely: physico-chemical background of the nanomanipulation, nanolithography and nanoassembling processes, with use of the scanning probe microscopes (SPM).

Different kinds of SPM are used as nanomanipulators and nanomodifiers, namely: the scanning tunneling microscope (STM), atomic force microscope (AFM), near-field scanning optical microscope (NSOM), scanning electrochemical microscopes (SECM), etc. For all of them common elements are scanning, feedback mechanism and means of

recording. Novel industrial SPMs combine modes of STM, AFM, NSOM, etc. in the single device. Cantilever is a common feature of such SPMs. The AFM records interatomic forces and the STM records tunnel currents between the apex of the tip and atoms in the sample as the tip is scanned over the surface of the sample. A general view of AFM is shown in the fig. 1a.

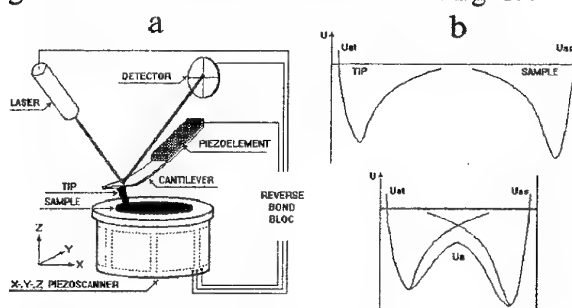


Fig.1. a - Scheme of AFM. b - Diagram of interatomic tip-sample interactions.

The demonstrated ability of the SPMs to image and modify surfaces with atomic resolution suggests opportunities for their use in generating nanostructures and nanodevices. AFM have been used: 1) to scratch nanostructure in soft materials, 2) to expose thin films of resist, 3) to induce and enhance oxidation of H-terminated surfaces, 4) to change the headgroups or packing density of organic monolayers (monitoring surface reactions), 5) to "write" patterns, 6) to manipulate clusters, etc. STM have been used: 1) to alter the structure or order of organic monolayers, 2) to oxidize H-terminated surfaces, 3) to induce phase transition in a solid material, 4) to manipulate atoms or molecules, 5) to create and characterize of individual molecular bonds, etc. NSOM and SECM have been used to expose photoresist films and to deposit metals, respectively.

By a theoretical background of problems under investigation is a correct calculation of integrated interatomic interactions of the probe with the sample, a general view of which is shown in fig.1b. When the tip to sample distance is large, the atom-sample interactions do not overlap significantly. When distance is shortened, the sum of sample and tip potentials exhibits a double well with a

small activation barrier. Then the atom can transfer from the tip to the sample as well as from the sample to the tip.

Two types of forces are the most important for the modification of surfaces: the contact forces and the electrostatic forces. In this point of view several types of the tip influence on the surface nanostructures are shown in fig.2., namely: 1) vertical and horizontal transfer, 2) the method of field-induced surface diffusion; 3) mechanical surface modification, etc.

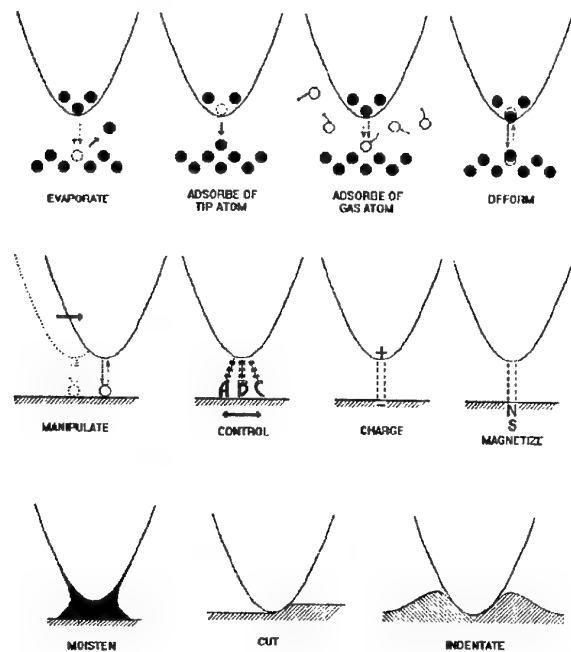


Fig.2. Types of the tip influence on the surface.

Experimental results of manipulation and surface modification are presented. Nanostructures can be built by means of the next methods: 1) atom by atom assembling with use of ultra-high vacuum STM; 2) manipulation of adsorbed clusters, fullerenes or nanotubes by contact or non-contact AFM; 3) induced transfer of tip materials on the surface; 4) fabrication of nanostructures by the SPM-nanolithography. Some examples are shown in fig.3.

In the horizontal sliding method, the probing tip is placed above an adsorbed atom. The tip is carefully lowered to increase the interaction between tip atoms and the adsorbed atom. After this, the tip is slowly moved in a direction parallel to the surface to a desired position. When the atom is dragged to that position, the tip is lifted (fig.3a).

The method of manipulation of nanoparticles is based on continuous scanning of a line and simultaneous acquisition of the vibration amplitude of the cantilever.

The method of deposition of a clusters on the surface is based on the follows. Tip approach due to an additional voltage pulse leads to the deposition of a cluster, provided that this approach is close enough (fig.3c).

The SPM-lithography scheme is field induced anodization of H-passivated surfaces in air, which uses a proximal probe tip negatively biased against the surface (fig.3b).

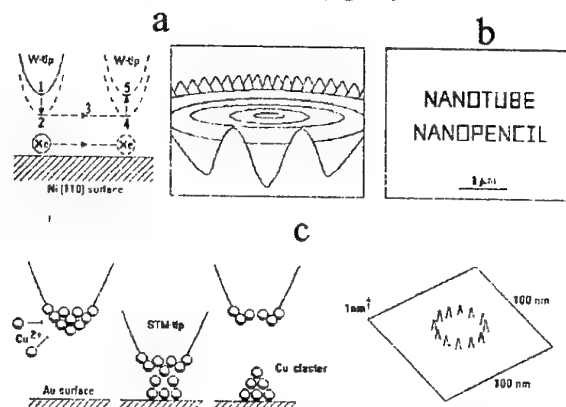


Fig.3. a - Schematic illustration of the sliding process and STM-image of generated atomic "quantum corral". b - AFM-image of silicon-oxide lines fabricated with use of a nanotube tip as a pencil. c - Schematic diagram of the mechanism of material transfer from the tip to the sample and generated structure.

Development of methods for automatic nanoassembling of nanostructures are considered. The SPM-based nanoassembling may one day enable us to create artificially designed material structures with new properties, or to create new molecules, or to construct new devices on the atomic scale. Examples of such future devices are the fullerene based amplifier (fig.4) and nanotube based transistor.

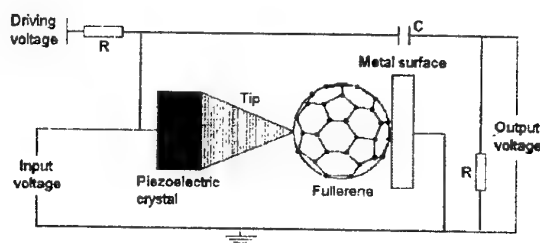


Fig.4. Scheme of fullerene based amplifier.

The described extraordinary and revealing studies allow us to hope that the probe microscopes will come the routine instruments of the nanoworld in the nearest future. Such confidence lies in the fact that SPMs have a wide range of possibilities, a compactness, and relatively low prices.

DISLOCATION SUBSTRUCTURES EVOLUTION DURING FATIGUE TESTS OF AUSTENITIC STEEL

Konovalov S.V., Kovalenko V.V., Sosnin O.V., Tsellermaer V.V., Gorlova S.N., Gromov V.E., Kozlov E.V.⁽¹⁾

Siberian State University of Industry, Novokuznetsk, Russia

⁽¹⁾Tomsk State University of Architecture and Construction, Tomsk, Russia

The problem of fatigue fracture of steels and alloys is important despite a young history of investigations.

As the fracture is the final stage of substructures evolution; the knowledge of accumulation mechanism of destruction and change of dislocation substructures and phase composition especially acquires the special importance.

In this work such a problem was being solved for austenitic steel 45G17Yu3 (0,45% C, 17% Mn, 2,74% Al) undergone the fatigue tests before fracture.

The intermediate stage of loading of $N = 7 \cdot 10^4$ cycles, corresponding to appearance of sub- and microcracks, was chosen, where, side by side, with initial and fractured samples the dislocation substructure was being analysed.

The inner structure of steel in initial state is characterized by different types of dislocation substructure which are classified below in accordance with: the substructure of dislocation chaos, nonoriented – down net- shaped dislocation substructure, oriented – down net-shaped dislocation substructure with torn geometrically necessary low-angular boundaries and fragmented dislocation substructure. Besides, there are the grains of microsizes with a small number of dislocations in steel. Their share in grained ensemble of steel is 0,25-0,30.

The grains of steel apart from types of dislocation substructure being in them contain a large number of bending extinctional contours that indicates the elastic-plastic bend of material. In this connection each grain as a whole in many cases is undergone the bend-torsion, i.e. the reason of inner far-acting fields of stresses is to a large extent the incompatibility of the deformation of neighbouring grains and of their groups, than intergrained dislocation substructure.

The quantitative analysis of steel dislocation substructure in its initial state showed that the largest density of dislocations spreaded along the volume is fixed by net-shaped substructure; the maximum level of curvature-torsion of the crystalline lattice is in fragmented substructure. Here, in fragmented substructure the elastic constituent of material curvature-torsion is maximum. Therefore,

the fragmented dislocation substructure of research steel is the most stressed structural constituent of initial material.

The fatigue tests of steel ($N=7 \cdot 10^4$ cycles) brings to the evolution of dislocation structure – substructure of dislocation chaos is transformed into net-shaped dislocation substructure. The volume fraction of fragmented substructure in this particular time is not changed. The deformation of steel is accompanied by an increase of scalar density of the dislocations from $1,3 \cdot 10^{10}$ to $1,8 \cdot 10^{10} \text{ cm}^{-2}$ in net-shaped substructure and from $0,5 \cdot 10^{10}$ to $1,1 \cdot 10^{10} \text{ cm}^{-2}$ – in fragmented one. The increase of scalar density of dislocations in net-shaped – substructure is accompanied by the formation of weakly-orientied-down strips. These strips are the anisotropic fragments containing inside of themselves the dislocation structure.

The test of steel for fatigue is accompanied by essential increase of curvature-torsion amplitude of the crystalline lattice in fields with net-shaped dislocation substructure. The cyclic deforming of steel fields with fragmented substructure is accompanied by some other processes despite that the scalar density of dislocations located inside of fragments essentially grows (more than in two times), the curvature-torsion of crystalline lattice of these fields material is decreased. This, obviously, testifies about the relaxation of elastic-plastic stresses saved in steel at thermomechanical treatment, in the process of further loading in conditions of change of deforming method.

The studies of steel layer adjoining to the surface of fraction revealed the presence of all three types of dislocation substructure enumerated above. The relative content of these types of substructures is as follows: dislocation chaos occupies ~0,18 volume of foil, net-shaped structure ~0,42 and fragmented structure ~0,40. The average parameters of grains sizes are: $D=7,4 \text{ mcm}$ – the width and $L=1,38 \text{ mcm}$ – the length of grains.

Comparing these data with the results obtained during studies of the structure of initial state one can note that the evolution of steel dislocation substructure, preceding its fracture, occurred in

such a way. The structure of dislocation chaos in initial state, during the process of fatigue tests at some stage disappears fully about which the results of material at intermediate stage of loading testify. However, to the moment of fatigue fracture of the sample the meaningful value of material volume occupied by the structure of dislocation chaos ($P_0=0,18$) is fixed in it. Obviously, that it is a dislocation substructure formed as a result of cyclic loadings of steel, namely. The grains of dynamic recrystallization being in steel in initial state and, as will be shown below, arising during the process of fatigue can be the places of the formation of this substructure.

Net-shaped dislocation substructure, formed in initial state of steel, during the process of cycling is steadily developed occupying at intermediate stage of loading 0,5 volume of foil cut out of zone with maximum amplitude of action. This increase of a relative content of material with net-shaped substructure is connected with the corresponding transformation of the structure of dislocation chaos into net-shaped one and, with the development during the process of fatigue tests of dislocation substructure in grains being in initial material, practically free from dislocations. Some decrease of material fraction occupied by net-shaped dislocation substructure, found during study of zone of steel fracture, obviously, is connected with its reconstruction into a fragmented dislocation substructure. Consequently, cycling of steel 45G17Yu3 is accompanied by the following scheme of transformation of the dislocation substructure: dislocation chaos \Rightarrow net-shaped+ ϵ -martensite \Rightarrow fragmented+ ϵ -martensite substructure.

The fragmented dislocation substructure in initial steel, being dominating after thermomechanical treatment of steel by rolling during the process of steel tests for fatigue gradually loses its positions despite the fact that the transition of net-shaped substructure into fragmented one is fixed.

The steel fracture during these tests is accompanied by the formation in zone of the fracture of dislocation substructure, the average scalar dislocations density of which is equal to initial one. In this time the density of dislocations in structure of dislocation chaos is quite lower, in net-shaped it is practically equal and in fragmented one, it is slightly higher of the corresponding sizes characterizing the initial state. The change of scalar density of the dislocations during the process of loading has non-monotonous character. The analysis of intermediate state being formed at $N_1 \sim 0,7N$ fract., revealed the meaningful increase of disloca-

tions density and in net-shaped – and in fragmented substructures too. One can suppose that one of the reasons of such a character of the evolution of scalar density dislocations size is the state of dislocation substructure formed as a result of preliminary thermomechanical treatment of steel. Obviously, this character of substructure change has no universal character and with another way of preliminary treatment of material it will be another one.

The analysis of the amplitude evolution of curvature-torsion of steel crystalline lattice during the process of cyclic loading shows that both in average on material and in each of substructures separately, the amplitude of stresses fields being formed in structure of steel in zone of fracture greatly (in 1,5-5 times) increases this characteristics of initial state. At the same time at intermediate stage of loading the change of amplitude of curvature-torsion of the material crystalline lattice is small. Such a character of this parameter change of steel dislocation substructure can be connected with the peculiarities of dislocation substructure reconstruction, preliminarily created in steel during hot rolling. Obviously it indicates the critical moment in substructure evolution, after which the material irreversibly prepares to fracture.

In initial state the small number of ϵ -martensite crystals already have been in steel located along the boundaries of grains. In intermediate stage of test (at $N=7 \cdot 10^4$ cycles) their number are not practically changed, however in zone of fracture the volume fraction of ϵ -martensite crystals in zone of fracture is being formed in many cases in net-shaped dislocation substructure and quite rarely – in chaotic one. In fragments ϵ -martensite has not been found. Such a behavior of material confirms the critical character of substructure state in the vicinity of point $N=7 \cdot 10^4$.

The performed electronic-microscopic diffraction studies of steel 45G17Yu3, fractured as a result of cyclic fatigue tests showed that one of the possible mechanisms of fracture is martensite $\gamma \rightarrow \epsilon$ transformation with the further formation of high-unbalanced interphase boundaries of microcracks division. In these interphase boundaries later on microcracks are nucleated, being developed into manifold cracks. In its turn, the far-acting fields of stresses localized in net-shaped dislocation substructure is the reason of martensite $\gamma \rightarrow \epsilon$ transformation. The incompatibility of deformation of neighboring grains and their groups and also γ - and ϵ -phases are the sources of far-acting fields of stresses fields generally.

EVOLUTION OF DISLOCATION SUBSTRUCTURE STAINLESS AUSTENITE STEEL DURING ELECTROSTIMULATED LOW-CYCLE FATIGUE

Kovalenko V.V., Sosnin O.V., Gromov V.E., Konovalov S.V., Efimova I.E., Tsellermaer V.V.,
Ivanov Yu.F.⁽¹⁾, Kozlov E.V.⁽¹⁾

Siberian State University of Industry, Novokuznetsk, Russia

⁽¹⁾Tomsk State University of Architecture and Construction, Tomsk, Russia

The purpose of this work was the study of evolution of the dislocation substructure and phase composition of stainless austenite steel 08Cr18Ni10Ti ($C \leq 0,1\%$, $Cr \approx 18\%$, $Ni \approx 10\%$, $Ti \approx 1\%$) during usual and electrostimulated low-cycles fatigue.

Fatigue test have been carried out according to scheme of out of zero bend on samples from austenite steel 08Cr18Ni10Ti with loading frequency of 8Hz and amplitude of 80 MPa. Here, this sample withstood 12000-14000 cycles of loading. The measurement of ultrasound propagation velocity by means of IST-12 device was carried out in parallel with fatigue tests.

The experiments made allowed to state that the dependence of ultrasound velocity (V) from the number of loading cycles (N) has the sign of three-stage curve. Earlier it was stated that the abrupt drop of ultrasound V during fatigue tests is connected with appearance of fatigue microcracks that signals about approach of final stage of sample process-fracture. In our experiments the samples were undergone by the action of current one-polar impulses of 80Hz frequency, 8kA amplitude during 20 seconds when the third stage of dependence $V(N)$ began. These parameters were chosen by experimental way in order to provide the developing of electroplastic effect and not to warm up the material above 200°C. Current impulses were created by specially developed thyristor generator of powerful one-polar current impulses with regulated parameters.

Measurements of subgrained steel structure, behaviour of the second phases were being carried by methods of metallography of etched lap, scanning electron microscopy and electron diffraction microscopy. Images of thin structure of materials were used for classification of structure according to morphological signs; definition of sizes, volumetric portion and places of localization of the second phases and depositions; scalar $\langle \rho \rangle$ and excess $\rho \pm$ density of dislocations; amplitudes of curvature-torsion of crystalline lattice χ and moment-stresses τ .

The structure and phase composition of samples in initial, loaded and electrostimulated states have been analyzed in sections placed at a distance of 0,1; 1,2 mm from the surface of fracture, and also directly in zone of fracture.

Electron-microscopic researches of thin foils have shown that the inner-grained structure of steel being investigated is characterized by the following set of dislocation substructures: dislocation chaos, nets and fragments. The basis is the chaotic dislocation substructure, having $\sim 0,8$ volume of material. Fragmented substructure in inside of fragments contains either chaotically spreaded dislocations or nets. In many cases the dislocations are decorated by particles of the second phases. At the same time with this, the carbide particles are placed in boundaries of fragments and boundaries of grains.

The studies of dislocation substructure showed that in the process of fatigue tests in a region of material siding with the surface of fracture, the celled and fragmented substructures are formed. The volumetric portion of fragmented substructure is 0,55, with the value of dislocations density in it as $1 \cdot 10^{10} \text{ cm}^{-2}$. The volumetric portion of celled substructure is 0,45, and $\rho = 1,7 \cdot 10^{10} \text{ cm}^{-2}$. The average density of dislocations in a sample is $2 \cdot 10^{10} \text{ cm}^{-2}$. One can also note that the celled substructure is formed at initial stage of tests. With the increase of cycles number the cell substructure is converted into fragmented one. The density of free dislocations in fragmented substructure appears to be lower as the part of dislocation is spent on the formation of subboundaries.

As a rule, there are the boundaries of division in finished dislocation substructures, to which two mentioned above denote. In this case these are the boundaries of cells and fragments. According to them the nucleation microcracks can be formed and spreaded especially on disoriented boundaries of fragments. Therefore the probability of microcracks nucleation in it is great.

The interphase boundaries γ - ϵ are another dangerous places of microcracks nucleation. In

particular according to them the microcracks are largely developed. The microdiffraction analysis of steel has revealed the presence of ϵ -martensite in zone of sample fracture. It is clearly seen, that the maximum quantity of ϵ -martensite is in some removal (~ 100 mcm) from the surface fracture. It is necessary to note that the martensite transformation occurring in the process of deformation, strengthens the steel, increasing at the same time its brittleness with it. Suppressing γ - ϵ transformation, from the other hand, plastifies the material.

The quantitative analysis of samples structure showed that the parameters characterizing the state of dislocation substructure are changed in a correlation manner. The area located at a distance of ~ 100 mcm from the fracture surface is of special analysis. In this zone the microcracks have almost been un observed already, but the rest parameters achieve the maximum values. One can state that in zone of fracture and in site of material being from it at a distance of ~ 100 mcm, the fatigue processes are developed exclusively in different way. If in zone of fracture the active microcracks create the large far-acting fields of stresses and make a large contribution to a value of plastic deformation, at a distance of ~ 100 mcm the contribution of microcracks to the deformation is not large, but the dislocation sliding and the development of deformed $\gamma \rightarrow \epsilon$ transformation prevail. In a sample a cell-nets and band dislocation substructures and also ϵ -martensite are formed. It is not excluded that the band dislocation substructure is itself the parts of anisotropic fragments occurring at initial stages of deformation. They are present at a distance of 1,2 mm from the surface of fracture, i.e. in areas with low density of dislocations and without crystals of ϵ -martensite.

In electrostimulated sample during the process of fatigue tests the structures are formed being qualitatively different from unstimulated sample. The cell-substructure in small quantities ($P_v=0,15$) and especially the cell-net one ($P_v=0,85$) are present. Despite the large difference of substructures the average density of dislocations is $\sim 2 \cdot 10^{10} \text{ cm}^{-2}$. So, in case of electrostimulation the character of substructure construction has a quite low finished character in comparison with unstimulated sample.

In finished dislocation substructures there are the boundaries of division. According to them the nucleated microcracks can be formed and spreaded especially along disoriented boundaries of fragments. There are no such boundaries of division in cell-net structure. Therefore the probability of microcracks nucleation in it, respectively, in

electrostimulated sample, as a whole, is near the zero. The interphase γ/ϵ boundaries are the other dangerous place of microcracks nucleation. The microcracks in electrostimulated sample are largely developed namely according to them. In both cases the change of ϵ -martensite content with the growth of distance up to the surface of fracture, is similar to: maximum number of ϵ -martensite being in some removal from the surface fracture. From given results it also follows that the electrostimulation due to the development of the second sliding suppresses the process $\gamma \rightarrow \epsilon$ of martensite transformation. As in electrostimulated material the ϵ -martensite is in small quantities and at the background of cell-net dislocation substructure, it is quite obviously, that the stability to nucleation of microcracks must be higher on qualitative level during analysis of the type of substructure which is being formed.

The treatment by impulse electric current by techniques chosen in this work decreases the probability of ϵ -martensite crystals appearance during fatigue loading in two times.

The quantitative analysis of samples structure showed that the parameters, characterizing the state of dislocation substructure in electrostimulated sample are changed very much similar to unstimulated sample, slightly being differed quantitatively. The most essential differences in behaviour of initial and electrostimulated samples are in regions of material a joining with the fracture surface. Namely, the electrostimulated sample is destroyed under higher values of scalar density of the dislocations and density of bent extinctial contours, under smaller number of microcracks and smaller size of curvature-torsion of the crystalline lattice in comparison with initial sample.

Thus the effect of electrostimulation has a multifactor character and is the suppression of martensite of deformation transformation; the development of second sliding; the decrease of amplitude of internal fields of stresses, the development of defect structure because of transformation deformation and recovery. The final results of all the processes is the abrupt decrease of density of possible places of microcracks nucleation in electrostimulated austenite steel, the large decrease of sensitivity to concentrators of stresses, the essential difficulty of microcracks development and its sufficient plastification in conditions of fatigue loading. The totality of these processes make difficult the nucleation and the development of microcracks moving the fracture to the high number of loading cycles.

NEW METHODS AND MACHINE FOR TRIBOLOGICAL TESTS OF MATERIALS

Shipitsa N.A., Zharin A.L., Saroka D.I.

Powder Metallurgy Research Institute, Minsk, Belarus

One of the main tasks for investigators is development of new methods for quicker and more precise determination of serviceability range for materials and friction assemblies in laboratory conditions. This mostly depends on shortening period for design and industrial introduction of new machines and equipment.

We have proposed a new approach to determination of serviceability range based on control of friction surface condition according to electron work function [1]. New methods and devices have been developed enabling to control condition of a fine material surface layer during friction process according to registering changes in electron work function.

Method for assessment of material serviceability - the essence of the method is determination of critical loading of transformation from normal wearing to catastrophic one.

Multiple investigations of dependency between sliding surface work function and loading have showed that character of dependencies between friction surface work function and normal loading is similar and has three typical areas (fig. 1). Growth of work function is observed in area 1 with increase of normal loading. Then change of a curvature trend takes place and work function reduces in area 2. With the following increase of loading, value of the electron work function stops reducing in area 3 and even increases in some cases. Electron work function reduces sharply during seizure and at the same time volume temperature and friction torque grows in the same way. As you can see in figure 1, friction torque and surface temperature grow monotonously within the mentioned range of loadings and have no extremes correlating to the electron work function behavior. Thus, changes in surface material layer can be registered according to the character of electron work function, which can't be observed according to outer friction parameters (friction torque and volume temperature).

The investigations carried out according to independent methods and also simulation to determine factors contributing changes in electron work function presented in figure 1 enabled us to interpret distribution of dependencies in thin superficial of materials. According to this dependency area 1, probably, corresponds to the area of elastic deformations, i.e. surface layer deformations without significant increase in dislocation concentration. Area 2 corresponds to the area of prevailing plastic deformations, but these processes, from the point of view of dislocation density, are not yet saturated, as reduction of electron work function and increase of loading take place in this area. Area 3 also corresponds to the area of prevailing plastic processes, but in this case dislocation processes have saturating character, i.e. process of dynamic equilibrium between dislocations multiplication and processes of their coalescence with formation of micro-pores and micro-cracks take place.

The investigations have showed that transformation loading from area 2 to area 3 can be an objective criterion for evaluation of materials serviceability for friction assemblies and, as it was shown, it can be used for evaluation serviceability of a wide range of materials.

The method can be used practically in all friction machines equipped with a device for measuring electron work function.

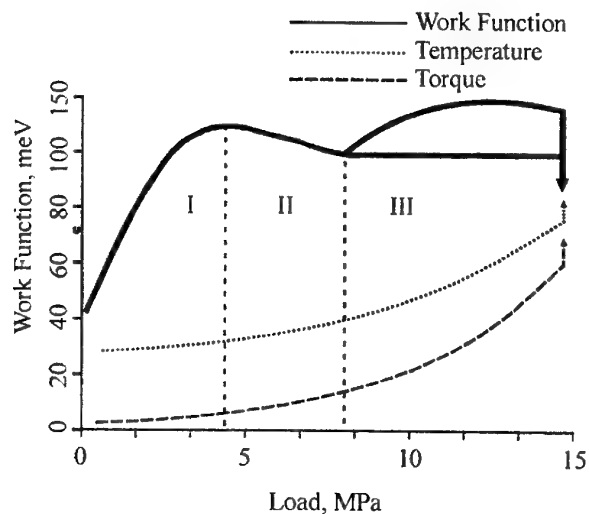


Fig. 1. Bronze rubbing surface electron work function, torque and surface temperature vs. normal load curves.

Quantity estimation of material friction fatigue parameters.

The investigations have showed that in area 3 (zone of severe wear) materials have suffered periodical changes in friction surface electron work function. The investigations of periodical changes in friction surface electron work function have showed that they were caused by fatigue destruction of material surface layer [2]. Changes in friction surface electron work function within one period suffer the whole cycle of fatigue destruction, i.e. accumulation of material crystal lattice defects, hardening of a surface layer, formation and distribution, destruction of friction surface.

To analyze periodical changes algorithm and software for statistic processing of results achieved during tests based on discrete Furier transform was developed, which enabled to calculate spectral function of friction surface electron work function according to a number of runs of a counter-body along the sample. In this case, specific spectral density has the meaning of friction surface destruction probability function during some certain number of loading cycles and it can be the function of distribution density [2], and the number of loading cycles, corresponding to the spectrum maximum, will determine a statistically average number of cycles before destruction of a friction surface, i.e. cycle durability [2]. The investigations based on the developed method have showed that according to periodical changes in friction

surface electron work function it is possible to plot a curve analog to the fatigue curve during volume loading (Voller curve) (Fig. 2). Thus, it is possible to determine fatigue curve parameters and a number of probability characteristics (surface layer destruction probability during a certain number of loading cycles or within a set range of cycles, confidence interval of cycle durability, etc.), enabling to get a better characteristics of materials for tribotechnical application.

The method can also be realized practically on any friction machine equipped with a device for measuring electron work function.

Thus, the described methods for continuous non-destructive control of friction surface electron work function enables to investigate materials behavior during dry and edge friction modes and it can be used while development of properties of tribotechnical materials.

To realize this method a number of measuring devices have been developed which can be mounted on most types of friction machines.

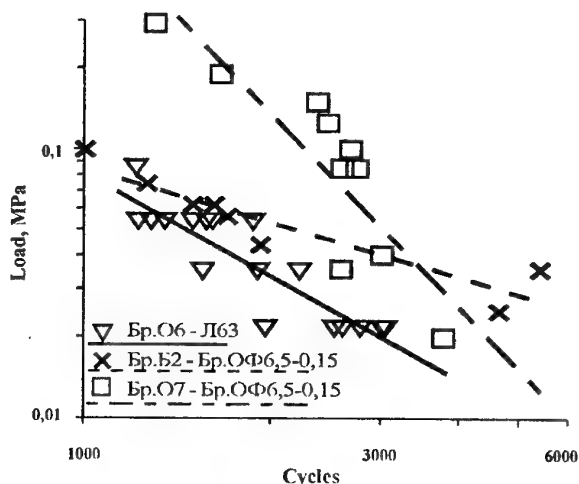


Fig. 2. Curve similar to the curve of fatigue and wear per cycle vs. spectral pick layout of periodic changes of rubbing surface work function in logarithmic axes.

References.

1. Патент РБ №2434 «Способ оценки работоспособности пар трения» // В.А.Генкин, А.Л.Жарин, С.С.Кресик, Е.И.Фишбейн, Н.А.Шипица.
2. Жарин А.Л., Шипица Н. А., Сарока Д.И. Определение характеристик усталостного разрушения материалов при трении скольжения.// Трение и износ. 2001. Т. 22. №4,5,6.

ACCOUNT OF ACOUSTIC EMISSION FEATURES AT STRENGTH DIAGNOSTICS OF POLYMERIC COMPOSITE MATERIALS

Mileshkin M., Biblik I.

A. Podgorny Institute for Mechanical Engineering Problems of the National Academy of Science of Ukraine, Kharkov, Ukraine

The polymeric composite materials (PCM) represent the most perspective class of constructional materials, most widespread from which are the glass-, Kevlar- and carbon-fibre reinforced plastics. A material and product from PCM are created simultaneously. For PCM the scatter of mechanical properties is still great, therefore it is necessary to develop the methods of strength diagnostics of products.

For PCM the presence of three mechanical conditions – elastic deformation, viscoelastic deformation and state of fracture – is characteristic. It is obviously, that the limiting state on bearing ability (strength) of PCM will be determined by state of fracture.

The method of acoustic emission (AE) is widely applied to definition of dynamics of change of fracture state of PCM. However at that it is necessary to take into account such features as anisotropy of acoustic wave propagation in products from PCM; strong attenuation of signals in PCM; presence of "Kaiser's effect"; complexity of selection of identical AE sensors (transducers) and their identical installation on a product etc.

With regard to that the problem of division of possible types of fracture of PCM by parameters of AE till now is not solved, earlier [1] the representations about conducting types of fracture of PCM, determining on various stages of loading character of AE activity change were entered.

In Fig. 1 the change of AE activity is schematically shown at loading of cylindrical shells from PCM by internal pressure. On portion of curve AB the formation of cracks in ring and spiral layers in parallel to fibres is conducting type of fracture, and on portion of curve CD – conducting type are the breaks of fibres. The presence of two conducting types of fracture requires stricter account of the fracture mechanism at realization of strength diagnostics of products from PCM.

The additional researches with application of computer modeling have shown [2], that character of

dependence of AE, shown in Fig. 1, in general is typical for PCM at biaxial loading. Point is that for all PCM the limiting deformations of layers in parallel and across fibres essentially differ (for example, for glass- and Kevlar-fibre reinforced plastics these values are usually equal 4,0 % and 1,0 %, for carbon-fibre reinforced plastics – 1,0 % and 0,3 %). It means, that at deformation, equal 0,25 % from limiting deformation in reinforcement direction of one layers, in layers, for which this deformation is cross, all fibre-matrix boundaries practically will be destroyed and strength of these layers will be essentially reduced, as well as strength of the whole of product.

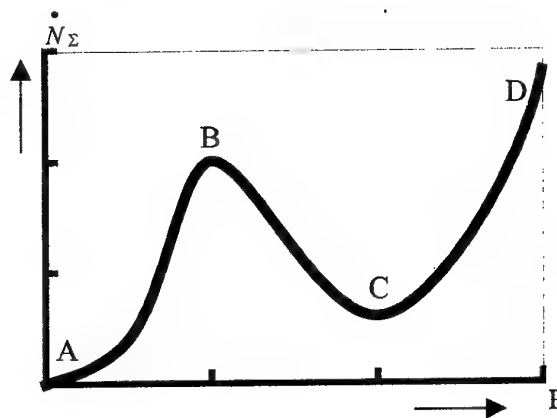


Fig. 1. The schematic change of AE activity during loading of shells from PCM

Let's consider now some features of amplitude distribution of AE signals at test of PCM. Amplitude and amplitude distribution of AE signals are the important information parameters connected with energy of AE sources. However before the present time there are no precisely enough valid models of occurrence of AE signals with various amplitude and their connection with concrete sources. In this connection in the report approach to the analysis of amplitude distribution from position of definition of kinetic energy of microbreaks of various nature is considered.

At the same time at numerous tests of various samples and products from PCM was established:

- the AE curves, registered on channels with various level of amplitude discrimination, have similar character. It relate to dependence, given in Fig. 1 also;

- the amplitude spectrum is wide enough, especially at the test of large dimension products;

- at the test of products in conditions of measurement of AE activity the saturation of channels with low level of amplitude discrimination is characteristic. It is connected with high values of AE activity (so, in cylindrical shells with bottoms the saturation of low amplitude channels always occurred near point B (see Fig. 1);

- using registration of the AE count rate is undesirable, as complete saturation of channels does not occur, but the registered parameters become incorrect.

Thus, the amplitude of AE signals at strength diagnostics of PCM is of quasi "consultative", but extremely great importance, as it is the indicator of reliability of AE measurements results.

For strength diagnostics of PCM the various AE-criteria can be used [1], and the account of fracture mechanism is obligatory.

In our opinion, the relative AE-criterion K_N [3], which is determined at the transition from active loading to period of constant load and represents the relation of number of AE pulses, registered during first three seconds during a load hold to number of AE pulses, registered during three seconds at the approach to the point of load hold, is most perspective.

At the test of samples and products from PCM the opportunity of application of criterion K_N for strength diagnostics was established as 100 %, if correct test is probable. At the same time it turned out that the relative AE-criterion expands opportunities of AE-diagnostics by cardinal way, as there is an opportunity to carry out it at all stages of life cycle of products after any uncontrollable influences, while all other known criteria allow to carry out diagnostics only at first loading, that is connected with Kaiser's effect.

An application of special design-experiment method [4] has allowed some accurate definition of AE nature during the period of constant load of PCM. Computer modeling was carried out for clarification of contribution of viscoelasticity and

stress redistribution in zone of microbreaks in elastic aftereffect of PCM. At that one AE pulse has been associated with one fractured structural element of model of material (Fig. 2). The results of modeling allow to conclude, that stress concentration in zone of microbreaks is given decisive contribution in AE, and viscoelasticity of matrix in zone of stress concentration only reduces slightly the process of their redistribution.

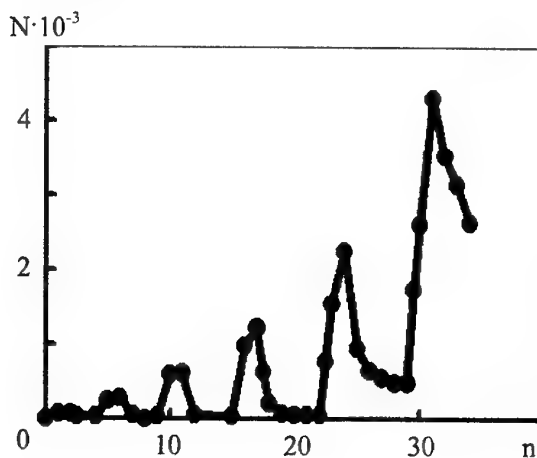


Fig. 2. Change of number of the fractured structural elements (N) during the step loading of PCM

References

1. Милешкин М.Б., Библик И.В. Физические основы акустико-эмиссионной диагностики прочности изделий из полимерных композиционных материалов. - Труды МНТК «Современные приборы, материалы и технологии для технической диагностики и неразрушающего контроля промышленного оборудования», Харьков, 1998. - С. 111 - 118.
2. Mileshekin M.B., Biblik I.V. Diagnostics for strength of fibre-epoxy composite material wares using computer modeling of fracture processes // Proceedings 2nd Jnt. Conf. «Computer Methods and Inverse Problems in Nondestructive Testing and Diagnostics», Minsk, 1998. - P. 123 - 129.
3. Милешкин М.Б., Музыка Е.И., Библик И.В. Способ определения прочности изделий / А.с. № 1295271, БИ №9, 1987.
4. Спосіб неруйнівного визначення міцності виробів з шаруватих полімерних композиційних матеріалів. Деклараційний патент на винахід №28636 А, Україна, G01N3/00. М.Б. Мілешкін, І.В. Біблік.- Опубл. 29.12.99, бюл. 8, бюл. 5-II.

DIAGNOSTICS of FATIGUE DESTRUCTION of MAGISTRAL PIPELINES

Ovchinnikov I.N., Ermishkin V.A., Lepeshkin Y.D.

Bauman Moscow state technical university, Moscow, Russia

Institute of metallurgy RAN, Moscow, Russia

The developed approach to the analysis of fatigue damaging of metal structures with long terms of operation bases on the two experimental facts. Their reliability was established by means of statistical thermoactivative analysis of outcomes of experiments on a fatigue of a number of constructional materials in laboratory conditions [1,2].

1) The fatigue curves, irrespective to a mode of tests (monoharmonic loads, polyharmonics or with a random spectrum) may be circumscribed by the equation of a kind:

$$\sigma = \sigma_w + A / \lg t_r \quad (1)$$

Where σ - averaged on time of measurement amplitude of the applied tension, σ_w - the constant of a material, having a sense of a physical limit of a fatigue, A-factor for want of time-dependent part of a resistance to fatigue destruction, t_r - time of life of a sample.

2) For want of by constant of a velocity of vibration loading the deformation of a flat sample in a place of contact with the capacity gauge of a special construction is changed in time on monotone dependence with a maximal appropriate to time of test about 0,8 t_r . This fact can be interpreted as manifestation of two stage character of fatigue damaging: on the first, most long, stage the origin of fatigue micro cracks on a surface of the examinee of a sample happens, and on the second - the distribution of the located magistral crack generated to an extremity of the first stage begins. Thus, there are basis to consider, that the critical degree of fatigue damaging, appropriate to the beginning of distribution of a magistral crack, makes about 0,8 t_r .

The transformation of the equation (1) allows reducing it in to a kind:

$$t_r = e^{2,303 A / (\sigma - \sigma_w)} \quad (2)$$

Following the approach of Kachanov [3], we shall enter function φ of damaging, satisfying to the conditions:

$$\varphi(0) = 1, \varphi(t_r) = 0 \quad (3)$$

The elementary kind of damaging function, satisfying to the conditions (3) may be represented as $\varphi(t) = t/t_r$. Finally we has

$$\varphi(t) = t e^{-2,303 A / (\sigma - \sigma_w)} \quad (4)$$

The formula (4) describes the kinetics of fatigue damaging of a material of a sample down to liftoff moment of a magistral crack. The experimental check of the offered approach for deriving settlement evaluations of a damaging degree of a material for want of various levels of tension for specific time of test both polyharmonics and casual modes was conducted.

The algorithm was obtained, on which it is possible to calculate a kinetic curve of damaging both at the stage of origin of micro cracks, and at the stage of shaping and distribution of a magistral crack..

The established regularities of fatigue damaging allow:

1) To select the heaviest modes of cyclical loading causing an accelerated degradation of a sample material and loss of a resistances to destruction;

2) On known characteristics of the local tensioned state we can determine lines of equal damaging of a material on length of the pipeline;

3) We can evaluate kinetics of development of magistral cracks in function of the tensioned state and from here to define residual resource (safe life) of local parts of the pipeline.

THE LITERATURE

1. S.K.Arutunov, K.S. Kolesnikov, I.N. Ovchinnikov. Regularities of fatigue destruction for want of random vibration loading. Mashinovedenie 1.1985.p.81-86.
2. V.A. Ermishkin, I.N. Ovchinnikov. The application of the thermoactivative analysis for forecasting a curve of fatigue. Sb. trudov "Energodiagnostica and condition monitoring". v. 4, part2. M.:ERCGP, 1999, p.84-94.
3. L.M. Kachanov. A fundamentals of a mechanics of destruction. M.: Nauka.1974. 311p.

EXOEMISSION DIAGNOSIS OF SURFACE LAYERS ON CONSTRUCTION MATERIALS

Skilko A.M.

Ukrainian Engineering Pedagogical Academy, Kharkov, Ukraine

In last time it was appeared large numbers of the papers devoted to research and diagnosis of the surface on solid state objects with attraction of charge particle exoemission method (EE) and its variety among them are photo- and thermostimulation exoelectron emissions (PSEE, TSEE), afteremission of electrons (AEE), phphotothermostimulated exoelectron emission (PTSEE) and exoemission video image. EE method allows to register such changes of the subminiobjects (microcracks and other defects) which are registered other methods with difficulties. Moreover the exoemission methods give information both in the form of the image and the quantitative form.

Our development of EE method and its modifications and carrying out of fundamental researches of electron properties and physicochemical ones of surfaces for great series of metals, semiconductors and dielectrics, which have been carried out from 1980 at close collaboration with industrial factories and sectorial institutes, were aimed also at practical use of scientific and methodical achievements.

In given work in correspondence with simple model described earlier on experimental examples it is shown analytical possibilities of method for study physical and chemical properties of materials and also practical use of them. It should be noted that potential employment of EE is practically in any technological problem where it is important to know the variation kinetics of surface condition or interface under and after distinct external effects.

Concrete examples researches of the processes taking place in metals at plastic deformation, estimation of corrosion resistance of protective films on metals, phase identification in superconductor and oxide films, estimation of oxide films thickness, determination of skin diffusion coefficient et al. have been mentioned.

The applicability of EE method for studies of physical and chemical properties of materials is shown experimentally.

1. Studies of oxide layers.

Metals (Ni, Cr) and their alloys, when heat-treated, form oxide layers of varying thickness on their surfaces and these oxide layers can be identified by TSEE method. TSEE curves show distinct difference for the alloys with and without the oxide layer. The curve with a peak at 400 – 450 K is characteristic of the oxide layer with a high density of defects whose levels in the band gap are located at the depth of several tenths of eV. The proposed enables to measure layer thickness of 0.001 to 1 μm whatever the substate material is.

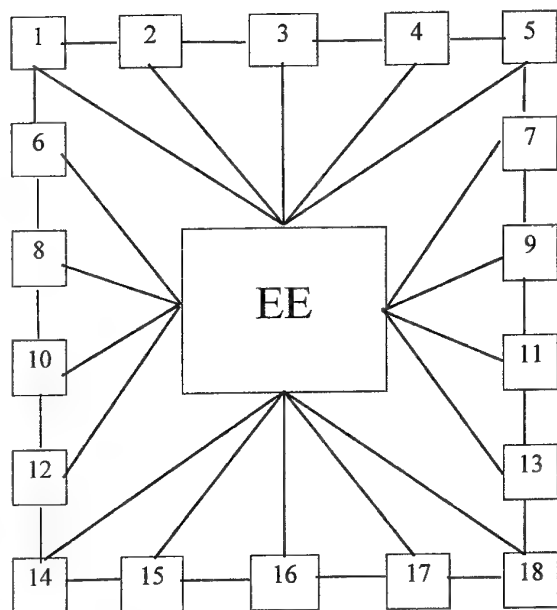
2. TSEE method for estimation of the protective covering corrosion resistance is based on the experimentally established time dependence of the oxidation rate with the subsequent determination of the oxidation constant which reflects the rate of forming a new medium on the material surface. The relation obtained for the oxidation constant — surface charge density dependence is in reasonable agreement with the results published elsewhere. The method was tested on Ni specimens oxygen at 840 K.

3. TSEE method is proposed to study selective oxidation processes in Cr-Ni steels. It was found that the exosum for Cr-Ni steels may have both falling and rising region, depending on Cr content -- similar to a well - Known dependence of the oxidation rate on the chemically more active metal content in noble metals. Actual Cr content corresponding to the exosum maximum was estimated. The obtained value of 15% corresponds to the minimum critical concentration of the additive agent to start the selective oxidation process.

4. TSEE – based technique is developed to determine the surface diffusion coefficient (D). From the experimental results the following relation was derived: $\ln D = f(1/T)$, where T is temperature. This relation is used to determine D, and using the tg of the curve slope it is also possible to determine the activation energy for Cu and Ni diffusion on Mo surfaces.

5. Phase identification in superconductor structures (Y-Ba-Cu-O ceramics). EE method can be used to assess of the proportion of the impurity phases to the superconductive phase in superconductor structures.

Principal use areas of the EE method are represented on diagram.



13. Exoemission spectrometer;
14. Energy analyzer;
15. EA flaw detector;
16. Contact potential difference meter;
17. Meter of electron work function by Anderson method;
18. Conjugation unit to computer.

In spite of the certain progress achieved in the research and the practical use of the EE phenomenon, many questions remain uncertain concerning mechanism of the phenomenon. Theoretical models based on sounding are practically absent. The character and yield depth and energy distributions are obscure. Although it was stressed repeatedly necessity on strict control of surround medium and realization of measurements on certificate samples, many works are fulfilled as before in vacuum at $10^{-3} \div 10^{-4}$ Pa without control of residual gas composite. Absence of basic understanding of the EE phenomenon prevents more extensive use of them.

Fig. Using areas of exoemission spectroscopy

1. Analysis and effect control of various types of treatments on the state of solid state objects surface;
2. Detection of starting stages of materials surface layer failure under mechanical and corroding effects;
3. Control of the conditions at protective films forming;
4. Control of purity and defects of semiconductors surface in various stages of manufacture of microelectronics products (photovoltaic converter of solar energy, Shottke diodes, sensors for various appointments et al.);
5. Control of thickness of metal oxides (Al- Al_2O_3 , Ni-NiO, Nb-Nb $_2\text{O}_5$);
6. Control of materials porosity (oxide-nickel electrodes);
7. Estimation of corrosion resistance of welded joints;
8. Control of surface of materials working in conditions of contact and cyclical loads;
9. Undestroying control method of oxide aggregates (polymer materials);
10. Research of absorption processes and desorption processes;
11. Research of radiation defects, radiation absorption processes and radiation catalysis processes, heterogeneous radiolysis et al.;
12. Exodosimetry;

FEATURES OF RESEARCHING STRUCTURE AND COMPOSITION OF THE THIN GLASSY FILMS PREPARED BY THE SOL-GEL METHOD

Shilova O.A., Moshnikov V.A.⁽¹⁾, Maximov A.I.⁽²⁾, Rumyantseva A.I.⁽²⁾, Koscheev S.V.⁽²⁾, Bubnov Yu.Z.⁽³⁾, Zhabrev V.A.

Institute of Silicate Chemistry of Russian Academy of Sciences, St. Petersburg, Russia

⁽¹⁾Saint-Petersburg State Electrotechnical University, St. Petersburg, Russia

⁽²⁾«Avangard-Microsensor» Co, St. Petersburg, Russia

Thin glassy films obtained by sol-gel technology are successfully used in a cycle of manufacturing of semi-conductor devices as the sources of diffusion, catalytic coatings, passivating films, insulating, getter and planarization layers [1-4].

Thickness of films routinely is made from 30 up to 250nm and may change depending on composition of film-forming sols and coating conditions. These films deposit on semi-conductor single-crystal and polycrystalline materials, as a rule, with the help of a centrifuge. Therefore often these films are named "spin-on glass" films.

The films routinely form from alkoxide-derived sols. One of mostly used precursors is tetraethoxysilane (TEOS). The different dopants are involved into the sols to impart to the film necessary properties. Usually nitrates of metals are used as dopant precursors. The sol-gel method allows involving a wide number of the dopants into the sols and films. There are elements traditional in semi-conductor technology B, P, Sb as well as Tl, As, rare earth elements e.t.c., which involving into the films and semi-conductor by other methods is impossible or connects with significant difficulties. The method is rather simple, allows refusing application of highly toxic substances.

The spin-on glass films are an interesting, but rather uneasy subject of inquiry. Here complex of research techniques to study the composition and structure of these films will be considered, as well as the problems, which solution has scientific and practical interest, are formulated.

The TEOS-derived sols are spontaneous and self-organizing systems. Their viscosity grows eventually and they turn into a gel. Therefore it is extremely important to define life time of the sols to achieve reproduced preparing the uniform, homogeneous films. Informative in this respect there was an ellipsometry utilized by us for these purposes [5]. Spread in values of film thickness and refractive index is sharply increased for the unusable sols and may be criterion of their quality. To define the dopant concentration in the sols and in the films to within 30 % the method of

emission spectral analysis is rather effective [6]. To realize the element analysis of film composition it is possible also the using methods of electron probe microanalysis [7]. A valuable information source concerning to the film chemical composition are the infrared, auger and photoelectronic spectrums [5,8]. At the same time the film obtained routinely are identify as amorphous at use high-angle X-ray scattering [5]. The methods of researching film surface morphology play the important role because in semi-conductor technology the great value is attached such parameters as uniformity, transparence and homogeneous of films. Here the ellipsometry also may be used successfully, e.g. to estimate the parameters of film porosity [9]. The last is very important for catalytic coatings. The most informative in this respect are different methods of optical and electronic microscopy (as transmission and scanning). As the spin-on glass films are fractal objects, one can obtain the helpful information by means of the appropriate researches at different scale levels [10-12].

A modern method of researching structure of materials is atomic force microscopy probe. More often it is used with reference to traditional ceramic materials. However the using to research the surface morphology of the spin-on glass films also rather informative [13]. The images obtained by this method allow showing the structure modification caused by involving polymer additives into the sols (see figure 1 and 2).

Here we are going to illustrate with concrete examples use of the above-mentioned methods of researching the structure and composition of the spin-on glass films doped by B, Pt etc.

The special attention will be given to consider the opportunities of atomic force microscopy probe to estimate the porosity and homogeneity of these films.

Perspective approaches to define the valency and a charge of different dopants distributed inside a silica matrix will be examined. Similar researches represent practical interest for the catalytic dopants Pt, Pd and Mn.

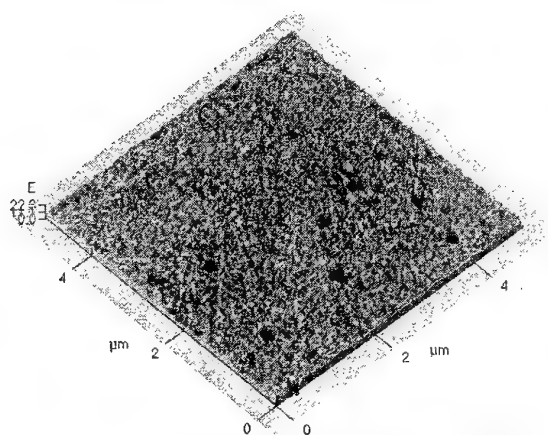


Fig. 1 Surface morphology of the borosilicate film deposited from the TEOS- and H_3BO_3 -derived sol.

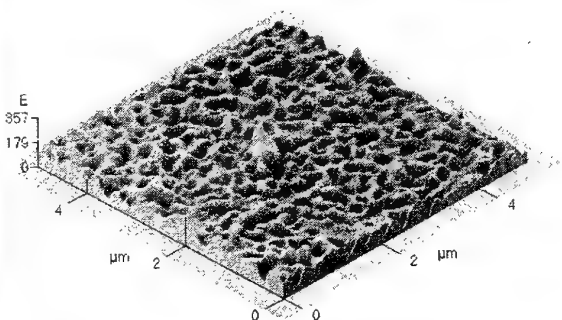


Fig. 2 Surface morphology of the borosilicate film deposited from the TEOS- and H_3BO_3 -derived sol with a polymer additive.

Thus, the studying such objects as the spin-on glass film is possible only using the whole complex of the modern research methods, first of all, spectroscopic and microscopic.

References

1. A.I. Borisenko, V.V. Novikov, N.E. Prikhidko, I.M. Mitnikova, Chepik L.Ph., Thin Inorganic Films in Microelectronics, Leningrad: Nauka, 1972, 114p (in Russian).
2. Glass and ceramics XXI. Prospects for Development, editing by Shevchenko V.Ya., Zhabrev V.A., Konakov V.G., Shults M.M., St.Petersburg: Yanus, 2001, 303p (in Russian).
3. A. Martucci, N. Bassiri, M. Guglielmi, L. Armelao, S. Gross, J.C. Pivin, Proceeding of 11th International Workshop on Glasses, Ceramics, Hybrids and Nanocomposites from Gels», Padova, Italy, 2001. – Journal of Sol-Gel Sci. & Techn., 2002 (in press).
4. O.A. Shilova, Yu.Z. Bubnov, S.V. Hashkovsky, Questions of Chemistry and Chemical Technology (Science-Engineering Journal of Ukrainian State Chemical Technological University), **1**, 2001, P.75 (in Russian).
5. O.A. Shilova and S.V. Hashkovsky, Materials. Technologies. Instruments (Journal of National Academy of Science of Belarus), **6**, 2, 2001, P.64 (in Russian).
6. Borisenko A.I., Chepik L.Ph., Shilova O.A., Menshikova E.M., Glubokaya E.V., Questions of Radio Electronics. Technology, Manufacture, Equipment (Scientific and Technical Collection of the Radioindustry Department of USSR), **3**, 1984, P.111 (in Russian).
7. Chepik L.Ph., Shilova O.A., Hashkovsky S.V., Troshina E.P., Proceeding of XVII Meeting on Temperaturestable Functional Coatings, St. Peresburg, V. 2, 1997, P.94 (in Russian).
8. Shilova O.A. Mitnikova I.M., Pyanova L.N., Khaeirusova L.I., Yakovlev A.S., Questions of Radio Electronics. Technology, Manufacture, Equipment (Scientific and Technical Collection of the Radioindustry Department of USSR), **2**, 1982, P.15 (in Russian).
9. O. A. Shilova, L.Ph. Chepik, Yu.Z. Bubnov, Journal of Applied Chemistry, **68**, 10, 1995, P.1608 (in Russian).
10. C.F. Brinker, G.W. Scherer, Sol-Gel Science. The Physics and Chemistry of Sol-Gel Processing, San Diego: Academic Press, Inc. 1990, 908p.
11. Krakovsky I., Urakawa H., Kajiwarra K., Kohjiya S, J. Non-Cryst. Solids, 1998, **231**, P.31.
12. O. Shilova, Proceeding of Second International Conference "Organic Hybrids II. Science, Technology & Applications", 2002, Surrey University, PRA, UK (in press).
13. Maximov A.I., Moshnikov V.A., Rumyantseva A.I., Proceeding of XVIII Meeting on Temperaturestable Functional Coatings, Part 2, Tula, 2001, V.2, P.222 (in Russian).

FRACTURE INDENTATION PHENOMENON: APPLICATION FOR CERTIFICATION AND CONTROL OF CERAMIC COATINGS

Byakova A.V.

National Technical University of Ukraine "Kiev Polytechnic Institute", Kiev, Ukraine

Introduction

Wide scope for determining the mechanical properties of coatings has become true due to effective development of the theory and practice of the indentation technique. One of the important applications of this technique to certification of ceramic coatings is that related to the Direct Crack Measurement (DCM) method [1,2], which has no limitations to the specimen size and based on the relation between the indentation cracks and the K_{Ic} criterion. Nonetheless, direct application of this method to the subject matter is complicated problem because of coating non-uniformity and the presence of an initial field of residual stresses. Therefore, the characteristic features of the indentation fracture phenomenon typical for ceramic coatings and its application for their certification is reviewed in present report.

Results and Discussion

The indentation 'star pattern' typical for small material pieces was observed only with tests in coating surface, which is isotropic in structure and stress distribution. This 'star pattern' is characterised by equal dimensions of the cracks occurred in the directions prescribed by the indentation diagonals (Fig. 1a). However, with tests in coating cross section the substantial anisotropy of the fracture resistance was revealed. Both the probability of the cracking process and crack dimensions in the directions prescribed by the indentation diagonals were found to be different (Fig.1 b-e).

Two different cases were pointed out and classified when applying the DCM method on fine-grained and coarse-grained coatings for which the dimensions of cracked indentations were found to be correspondingly greater or less than those of crystallites.

It was shown [2] in fine-grained coatings (Fig.1) that a field of the indentation stresses σ^e , which is usually symmetrical referring to sections of the

indentation diagonals, was ordered on the distortion. Effective stress σ^e of normal cleavage, which is defined by the superimposition of the σ^r stress on the σ^c stress, occurs in the section of the indentation diagonal arranged perpendicular to coating surface. With this residual stresses such as tension/compression correspondingly expands or suppresses the distance of crack propagation. Compared to this above no effect of the σ^r stress on crack paths in the direction prescribed by the indentation diagonal arranged parallel to coating surface was found experimentally. It is notable, that when the indentation diagonals are arranged arbitrary in respect to the σ^r stress, the paths of the cracks deviate from the directions prescribed by the indentation diagonals and form with them some angle θ_c (Fig.1 d). Under this condition crack path is controlled by the effective stress σ^e , which contains two different components: normal cleavage (mode I) and transversal shear (mode II).

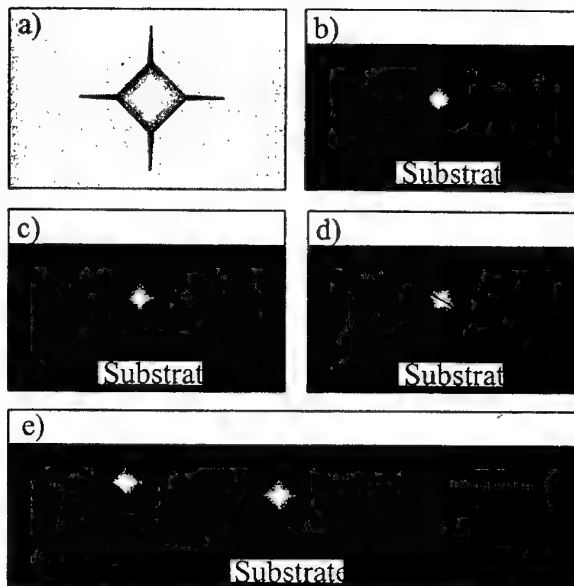


Figure 1. Schematic presentation of the indentation fracture phenomenon occurred in (a) surface and (b-e) cross-section of ceramic coatings, which are affected by residual stresses of (b) tension and (c-d) compression; (e) crack systems observed under 'edge effect'.

In tests with coarse-grained coatings, indentation crack paths did not deviate from the directions prescribed by the indentation diagonals since no effect of the σ^r stresses on measurement results was found [2]. Under this condition the experimental results probably reflect the fracture resistance of the each grain similar to that of single crystal. Thus, the fracture anisotropy found in coarse columnar crystallites was considered to occur because of micro-scale structural stresses σ^s arisen due to grain shape anisotropy.

Indications were obtained that the dimensional factor, which is associated with the phenomenon called by the 'edge effect', dictates the upper limit of the permitted loads. If no precautions were made the 'edge effect' results in increasing the dimensions of the cracks paths, which deviate from the indentation diagonals and comes across coating interfaces. (Fig.1e).

The study of the indentation fracture phenomenon has gained dominant feature for certification of ceramic coatings as it incorporates number of unique advantages. First of all, it was suggested to define the overall fracture toughness of non-uniform ceramic coatings as a collections of the fracture criteria presented in the form of a function $K_{Ic}(y, \varphi)$, where y is a distance from the coating surface and φ is coordinate angle between the direction of crack propagation and the surface, which with tests in fine-grained coatings may take only the values 0 and $\pi/2$.

Secondly, correlation test method procedures were developed when applying the DCM method on coatings. The representative results obtained by the modified DCM method complying with guidance of these test method procedures are given in Table.

Table. Fracture Toughness of Coating

Coating composition	Thickness, μm	y , μm	φ , deg	$K_{Ic}(y, \varphi)$, $\text{MPa} \cdot \text{m}^{1/2}$
V_2C	15	0	$\pi/2$	3.9
Cr_{23}C_6	3	8	0	1.6
		26	0	3.0
Cr_7C_3	18	26	$\pi/2$	4.8

It is notable that both the $K_{Ic}(y, \pi/2)$ value, which is influenced by both structural parameters and residual stresses simultaneously, and the $K_{Ic}(y, 0)$ value, which is independent of residual stresses,

could be determined as shown in Fig.2. Thus, this modified method makes it possible to record the structural zone and direction (see Table), which are the most dangerous in refer to catastrophic fracture under operative loading.

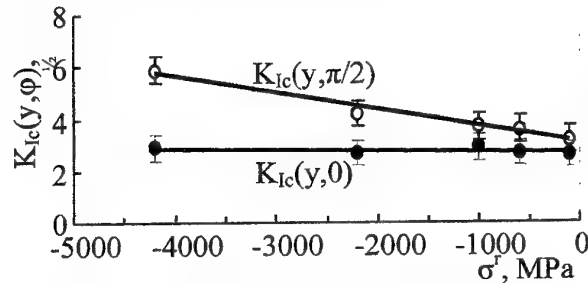


Fig.2. A summary of the data for the fracture toughness criteria determined in VC-coating consisted of fine ($\sim 1\mu\text{m}$) equiaxial grains vs. the value of residual stresses σ^r .

Concluding Remarks

The results, which were obtained in both scientific and industrial applications [3], showed that by the use of the modified DCM method undoubted benefits could be derived additionally for effective coating development and design purposes. In particular, the modified DCM method was found to be quite informative in examination of preferable micro mechanism of coating fracture as well as fracture anisotropy occurred in response to structural anisotropy as well as that caused by an initial field of residual stresses. Furthermore, the characteristic features of the indentation fracture phenomenon studied in coatings hold the key to development of the test method procedures capable for determining the intrinsic stresses shared on components distinctive to macro-scale residual stresses and to micro-scale structural ones.

References

1. G. Evans, E. A. Charles. Fracture toughness determination by indentation// J. Am. Ceram. Soc. - 1976. - 59, No7/8. - 371-372.
2. A.V. Byakova, V.G. Gorbach. Fracture toughness and evaluation of coating strength with an initial residual stress field// Strength of materials. - 1994. - 26, No1. - 40 - 47.
3. A.V. Byakova. Structural aspects of strength and methods to increasing of serviceability of carbide coatings// Powder Metallurgy and Metal Ceramics. - 2000. - 30, No1/2. - 85-91.

ELECTRONIC STRUCTURE OF METASTABLE AND NONSTOICHIOMETRIC PHASES BASED ON TUNGSTEN AND MOLYBDENUM TRIOXIDES

Khvzhun O.Yu., Solonin Yu.M., Graivoronskaya E.A.

Institute for Problems of Materials Science, National Academy of Sciences of Ukraine,
Kyiv, Ukraine

Reduction of monoclinic tungsten and molybdenum trioxides leads to formation of the so-called Magnéli phases belonging to the homologous series M_nO_{3n-1} and M_nO_{3n-2} ($M = Mo, W$) having ordered $\{102\}$ and $\{103\}$ crystallographic shear planes, respectively [1]. The Magnéli phases consist of largely unchanged slabs of either tungsten or molybdenum trioxides joined along the mentioned planes. Crystal structures of WO_3 , MoO_3 and M_nO_{3n-1} oxides belong to the pseudocubic ReO_3 -type, i.e., can be represented as constructed from $[M-O_6]$ octahedra linked by corner sharing and their arrangement results in a simple cubic symmetry [1,2]. Nevertheless, the structures are less symmetrical than ReO_3 because of distortions of the $[M-O_6]$ octahedra [1]. In addition to low-temperature MO_3 reduction, the Magnéli phases may be also prepared in equilibrium conditions from the corresponding components.

The new hexagonal form of tungsten trioxide, $h-WO_3$, has been synthesized by Gerand et al. [3] by dehydration due to dry heating of $WO_3 \cdot 1/3 \cdot H_2O$ hydrate. Since then $h-WO_3$ has been intensively investigated especially as an intercalating host for obtaining hexagonal tungsten bronzes M_xWO_3 and a promising material for positive electrodes of rechargeable lithium batteries [4]. As shown in Ref. 5, $h-WO_3$ could be prepared using the low-temperature selective reduction of copper tungstate, $CuWO_4$, with following Cu separation by dissolving in HNO_3 : the hexagonal hydrogen tungsten bronze $H_{0.24}WO_3$ was observed as an intermediate phase [6]. The oxidation of the bronze in air resulted in formation of $h-WO_3$ with cell parameters $a=0.7276$ nm and $c=0.7800$ nm, which are close to those obtained by Gerand et al. [3].

On the initial stage of reduction of $h-WO_3$ the nonstoichiometric $h-WO_{2.8}$ phase was synthesized very recently [7]. The X-ray powder diffraction analysis and subsequent refinement

using the Rietveld Full Profile Matching & Integrated Intensities Refinement of X-Ray and/or Neutron Data Programs (FullProf Version 3.5 Dec97-LLB-JRC) indicated that the crystal structure of the $h-WO_{2.8}$ phase is ascribed to the UO_3 -structure type with lattice parameters $a=0.3625$ nm and $c=0.3780$ nm [7]. Figure 1 shows arrangement of the metal atoms in the (001) plane of the $h-WO_{2.8}$ phase and, for comparison, of the hexagonal form of tungsten trioxide.

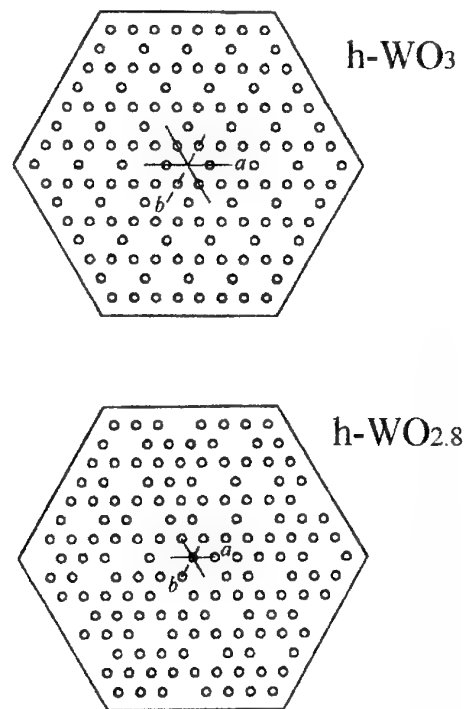


Fig.1. Arrangement of the metal atoms in the (001) plane of $h-WO_3$ (top panel) and $h-WO_{2.8}$ (bottom panel).

Electronic structure of two hexagonal tungsten oxides, $h-WO_3$ and $h-WO_{3-x}$, was studied

using the X-ray photoelectron spectroscopy (XPS) method. XPS valence-band and core-level spectra were derived using an ES-2401 spectrometer. The Mg K α ($E=1253.6$ eV) excitation was used as the source of X-ray radiation.

In tungsten oxides the X-ray Mg K $\alpha_{3,4}$ satellite excitation of W 4f $_{7/2,5/2}$ electrons overlaps the structure of the XPS valence-band spectra owing to photoemission from the O 2s-like states located in the energy region near 22.5 eV binding energies (BEs) with respect to the Fermi energy, E_F . In the present work the Mg K α satellite excitation of the W 4f $_{7/2,5/2}$ core-level spectra were subtracted using the method [8]. As an example, Fig.2 shows the XPS spectra of the studied compound without any corrections (solid curve 1) and after the subtraction (dashed curve 2) of the XPS W 4f core-level spectra excited by the radiation of the Mg K α' , α_{3-6} satellites. The present XPS results indicate that the peak intensity of the XPS valence-band spectra decreases somewhat when going from h-WO $_3$ to h-WO $_{2.8}$.

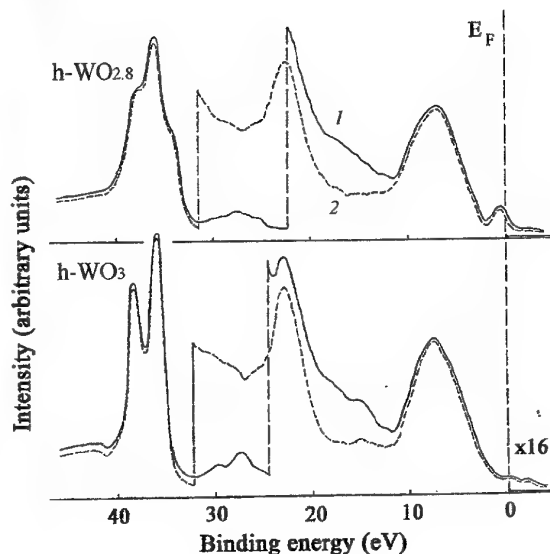


Fig.2. XPS spectra of hexagonal WO $_{2.8}$ (top panel) and WO $_3$ (bottom panel): (1) without any correction and (2) after the subtraction of the W 4f $_{7/2,5/2}$ spectra excited by the radiation of the Mg K α' , α_{3-6} satellites [7].

The relative intensities of the O 2s-like sub-band decreases in the sequence h-WO $_3 \rightarrow$ h-WO $_{2.8}$. This can be explained by the decrease of the oxygen content in the mentioned sequence of compounds. The broad structures representing the XPS O 2s-like sub-band do not allow us to detect

any tendency of a shift of the sub-band maximum when going from h-WO $_3$ to h-WO $_{2.8}$: BEs of the sub-band maxima remain constant (within the experimental error).

As shown in Fig.2, the XPS W 4f core-level spectrum of h-WO $_{2.8}$ shows that the surface of this compound is covered by a thin film of WO $_3$. We could not eliminate this thin layer of tungsten trioxide on the surface of the h-WO $_{2.8}$ compound using cleaning of the surface by a diamond file. A similar situation was observed earlier when studying nonstoichiometric tungsten oxides with the structure belonging to the monoclinic group: the three-peak structure of the W 4f spectra is characteristic for the WO $_x$ compounds, where $2 \leq x < 3$ [9]. As can be seen from Fig.2, the XPS valence-band spectra of the nonstoichiometric h-WO $_{2.8}$ compound show a creation of an additional sub-band at E_F . The sub-band is absent on the XPS valence-band spectrum of h-WO $_3$ (as well as of the m-WO $_3$ compound [9]). According to the results of Ref. [9], the above near-Fermi sub-band of the monoclinic WO $_{x<3}$ compounds is created due to the W 5d- and W 6s-like states taking part in the formation of the shortened W-W bonds in the nonstoichiometric monoclinic tungsten oxides. It is believed that, this is also true for the nonstoichiometric h-WO $_{2.8}$ compound studied. Half-widths of the XPS W 4f and O 1s core-level spectra increase somewhat in the sequence h-WO $_3 \rightarrow$ h-WO $_{2.8}$.

The analogous studies were carried out for molybdenum oxides.

- [1] H.J. Goldschmidt, *Interstitial Alloys*, London, Butterworths, 1967.
- [2] M. Sundberg, R.J.D. Tilley, *J. Solid State Chem.*, **11** (1974) 150.
- [3] B. Gerand, G. Nowogrocki, J. Guenot, M. Figlarz, *J. Solid State Chem.*, **29** (1979) 429.
- [4] W. Han, M. Hibino, T. Kudo, *Bull. Chem. Soc. Jpn.*, **71** (1998) 933.
- [5] Yu.M. Solonin, Yu.G. Privalov, *Dokl. AN UkrSSR, Ser. B*, No.1 (1985) 46, in Russian.
- [6] O.Yu. Khyzhun, Yu.M. Solonin, *Rep. NASU*, No. 7 (2000) 82.
- [7] Yu.M. Solonin, O.Yu. Khyzhun, E.A. Graivoronskaya, *Crystal Growth & Design*, **1** (2001) 473.
- [8] O.Yu. Khyzhun, *J. Alloys Compd.*, **259** (1997) 47.
- [9] O.Yu. Khyzhun, *J. Alloys Compd.*, **305** (2000) 1.

SCANNING TUNNELING SPECTROSCOPY: A NANOMETER RESOLUTION PROBE OF ELECTRONIC PROPERTIES

Rodichev D., Sacks W., Klein J., Cren T., Giubileo F.⁽¹⁾, Bobba F.⁽¹⁾, Lamy R.

Groupe de Physique des Solides, C.N.R.S., Universités Paris 6 et 7, Paris, France

⁽¹⁾Physics Department, University of Salerno, Salerno, Italy

First implemented in 1982 by Binnig et Rohrer the Scanning Tunneling Microscopy (STM) revolutionized the world of the research. Relatively easy to construct, the STM allows a very high resolution in real space, and atomic or molecular arrangements are routinely observed. Since its discovery the STM has become a widely-used technique in many research fields: surface science physics, chemistry, biology, medicine etc. In all these areas the STM is mostly used to produce high-resolution images of studied surfaces. At the same time one should not forget that the principle of an STM is based on the quantum tunneling of electrons across a junction formed by the sample surface and a sharp metallic tip. Due to such a particular geometry, the electric current (tunneling current) flows only in an extremely small area of the sample, just under the tip apex. Thus, the STM tip situated somewhere above the sample surface may be considered as a local tunneling junction.

The tunneling spectroscopy is known for many years as a powerful method giving a direct insight in the electronic properties of materials. The planar junction tunneling is widely used to study the electronic structure of metals and semiconductors. It was particularly successful in the discovery of the energy gap in conventional superconductors (superconducting gap).

In the STM geometry the tunneling junction is local and the tunneling spectroscopy finds its new dimension – the electronic structure may be studied on the nanometer scale, thus allowing the mapping of the electronic states in spatially inhomogeneous materials. The Scanning Tunneling Spectroscopy (STS) combines the STM imaging and the tunneling spectroscopy which is performed locally in each point of an topographic STM image, taken simultaneously. Although the STS technique is much harder to realize, it gives complete information about the spatial distribution of the density of electronic states (DOS) with record spatial and energy resolutions.

In this work we report a new high-speed scanning tunneling spectroscopy experiment, which led us to perform a full mapping of the quasiparticle DOS in high-T_c superconductors as well as in a recently discovered superconductor MgB₂ [1]. In this material, a very high critical temperature T_C ≈ 39K, well above the values reported for all other conventional superconductors, and quite simple binary structure, make it a good candidate for future technological applications. That is why, this discovery stimulates a great effort of the research.

In the case of high-T_C materials the measurements carried out at 5K show a complex spatial pattern of important variations of the LDOS in both Bi_{2-x}Pb_xSr₂CaCu₂O₈₊ and in YBa₂Cu₃O₇₋ (single crystals and thin films) on the nanometer scale [2]. In these materials the superconducting areas, characterized by a well-pronounced superconducting gap (regions *A* in fig.1), are co-existing with of a peak-less gap structure which we called low temperature pseudogap (LTPG) regions *B* in fig.1).

Within the large superconducting regions, the spectra reveal strong peak/dip/hump signatures, identical to the pristine Bi_{2-x}Pb_xSr₂CaCu₂O₈₊ case (these peak/dip/hump spectral features are the subject of interest in many research groups right now). On the contrary, in very small superconducting regions this fine structure is attenuated. We relate the peak/dip/hump features to the scale of the phase coherence [4], whereas the regions with LTPG are associated with a coherence-less state. Our STS study suggests that the local loss of superconducting phase coherence is a natural consequence of in both intrinsic (doping induced impurities) and extrinsic (substitution) disorder in quasi- 2D cuprates.

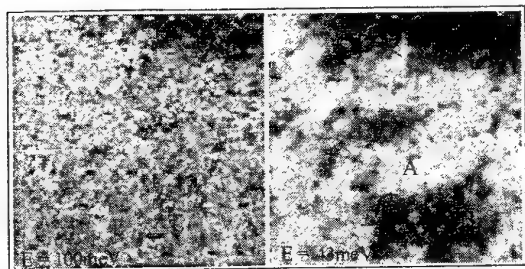


Fig.1 Spatial variations of the DOS in $\text{Bi}_{2-x}\text{Pb}_x\text{Sr}_2\text{CaCu}_2\text{O}_{8+}$. Left image: DOS at 100meV above the Fermi level, well beyond the superconducting gap energy. The state density is perfectly homogeneous over the scanned area. Right image: DOS map at the bias voltage $V=43\text{mV}$ corresponding to the energy of the superconducting gap of the material. Two kinds of regions are visible: i) superconducting areas (bright regions A) and, ii) non-superconducting areas (dark regions B).

Both maps correspond exactly to the same area of $150\text{nm} \times 150\text{nm}$ on the sample surface.

In the case of new superconductor MgB_2 , due to the STS we acquire a huge number of tunneling spectra (more than 10^6) allowing a significant statistics. The measurements were performed on MgB_2 powder, which was glued to the sample holder by silver paint. Mechanically etched Pt/Ir wires were used as STM tips. The local tunnelling spectra have a very particular shape in some locations, as shown in fig.2a. They show a relatively small gap $<4\text{mV}$ with almost no excitations near the Fermi energy (the tunneling DOS is practically zero at zero bias). The gap is followed by two pairs of quasiparticle peaks, that are seen in both occupied and empty states sides [5].

Such a DOS shape can be understood considering the contribution of two distinct gaps, with the magnitudes of 3.9mV and 7.5mV , i.e. well below and well above the BCS limit (fig. 2b).

Our finding gives no evidence for any important gap anisotropy. Instead, it suggests that MgB_2 is a multiple gap superconductor in the clean limit, becoming the single gap superconductor in the dirty limit [6].

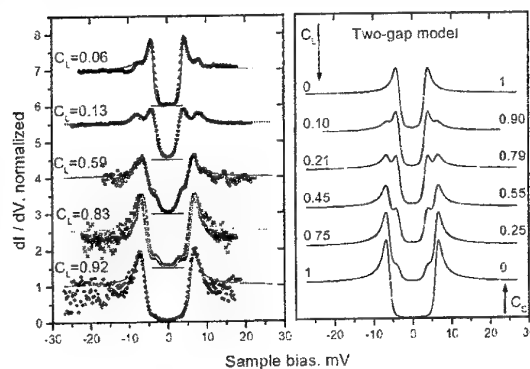


Fig.2. Two-gap superconductivity in MgB_2 .

Left panel: Superconducting DOS observed in different locations of the same granular sample. In all cases, the superconducting gap is clearly observed near the Fermi energy (almost no states at zero tunneling voltage). Two pairs of quasiparticle peaks are evident on each side of the Fermi energy instead of only one predicted theoretically for conventional superconductivity. The experimental data (points) are perfectly fitted by a weighted sum of two superconducting state densities (theoretically predicted by BCS) with two corresponding superconducting gap energies (lines).

Right panel: Numerically generated superconducting DOS, considering two quasi-independent superconducting gaps in the same material in the directional tunneling regime.

The details of the experimental set-up allowing such a fine STS at low temperature on conducting materials are discussed.

1. J. Nagamatsu *et al.*, Nature **410**, 63 (2001).
2. T. Cren *et al.* Europhys. Lett., 54(1), 84-90 (2001)
3. T. Cren *et al.* Phys. Rev. Lett., 84, 1 (2000)
4. T. Cren *et al.* Europhys. Lett., 52(2), 203-209 (2000)
5. F. Giubileo *et al.* cond-mat/0105146 (Europhys. Lett.(2002), in press)
6. F. Giubileo *et al.* Phys. Rev. Lett. 87(17), 177008 (2001)

FURTHER ADVANCE IN USAGE OF THE COMPOSITE PIEZOELECTRIC VIBRATOR METHOD: NONDESTRUCTIVE ACOUSTIC SPECTROSCOPY OF MATERIALS AT HIGHER HARMONICS

Smirnov S.N., Natsik V.D., Pal-Val P.P.

B. Verkin Institute for Low Temperature Physics and Engineering, National Academy of Sciences of Ukraine, Lenin Ave. 47, 61103 Kharkov, Ukraine

Resonance ultrasonic methods (in particular, the method of a two-component composite piezoelectric vibrator) are widely used in the modern materials science for experimental study of the effects stipulated by local structural rearrangements of a different nature. The main advantages of the resonance methods are their high sensitivity and high selectivity relative to the measured experimentally values. In particular, the composite vibrator technique is rather efficient tool for the acoustic spectroscopy of crystals in the frequency range from $5 \cdot 10^4$ Hz to $2 \cdot 10^6$ Hz. This method allows studying thermally activated structural processes in solids with the broad enough spectra of the relaxation times. Activation parameters of such processes may be obtained by the well-known method of a change of the oscillation frequency of the composite vibrator. To provide nondestructive character of the acoustical spectroscopy, the main problem is to retain the defect structure of samples unchanged. It is especially important when studying the low-energy structural rearrangements with the activation energies about 10^{-2} eV and lower which determine a number of physical properties of solids at low and very low temperatures.

In practice, the oscillation frequency change is realized traditionally by successive testing of a sample with the help of several piezoelectric transducers with different basic resonant frequencies. However, such procedure has the essential disadvantages restricting area of its application. Each piezoelectric transducer must be repeatedly adjusted in length to a sample under investigation. Alongside with other required technological manipulations with the sample, these repeated adjustments may also cause serious mechanical damages of the sample and thus to result in unchecked irreversible changes in the defect structure of samples. At the low-temperature measurements there appears an additional risk factor: each cycle of measurement may be accompanied by the hardly predictable

structural changes due to the action of the thermoelastic stresses arising at temperature cycling. For the reasons mentioned above, the procedure of successive usage of several piezoelectric transducers is of little use, for example, for analysis of relaxation processes in the functional materials with a low yield strength because of high sensitivity of the parameters of their defect structure to small external influences.

As the alternative way of the oscillation frequency change in the experiment, free from the restrictions listed above, the excitation of the composite vibrator at higher harmonics may serve. It should be noted, however, that a correct algorithm of processing of the obtained experimental data when using such a procedure, is not designed till now. This circumstance essentially restricts application of the excitation of the composite vibrator at higher harmonics as a non-destructive method of material testing.

Earlier we have suggested a theory of the forced longitudinal vibrations in the two-component composite vibrator of a rod type with a piezoelectric transducer [1]. We have not used the approach of a thin rod and therefore the theory may be used for the description of oscillations at the basic and several higher harmonics as well. The theory is based on the general relations of the dynamic of the linear hereditary elastic continuum. When deriving the vibrator characteristics, the dissipative properties of the vibrator are correctly taken into consideration. The problem of the influence of dissipative losses on the spectrum of the resonant frequencies is also studied in detail and an expression for the electrical impedance of the vibrator is obtained. When deriving the expression for the electrical impedance, any essential restrictions on geometrical parameters of the vibrator and the type of the frequency variance of the complex elastic moduli, the electric permittivity and piezoelectric coefficients are not superimposed. Resonance properties of the piezo-crystal and the composite vibrator as a whole are

discussed in detail and the relations of several lowest resonant frequencies and the resonance values of the pure electric resistance with the elastic and dissipative parameters of the components of the vibrator are obtained and carefully analyzed. Results of the analysis are presented as the formulas and the algorithms suitable for practical usage. On this basis, the algorithm of determination of the logarithmic decrement of oscillations and the complex modulus of a passive component of the vibrator (i.e., of the sample) including preliminary testing of a piezo-crystal is offered.

In the present communication, the further development of the method of the two-component composite vibrator for a nondestructive ultrasonic spectroscopy of solids is suggested. On the basis of the theory developed in paper [1], a new algorithm of deriving of the frequency dependences of internal friction in materials from the experimental data obtained by the method of consecutive excitation of the composite piezoelectric vibrator on higher harmonics is offered. Sets of the experimental values of the vibrator resonant frequencies and values of the pure electric resistance at these frequencies are taken as the basic values for the calculations.

The algorithm includes simultaneous processing of the ensemble of the experimental parameters obtained at several harmonics and consists of two stages. At the first stage, preliminary testing of the piezo-crystal in a selected frequency range is carried out and the values of the electromechanical coefficients and the parameters describing propagation and attenuation of the acoustic wave in the piezoelectric transducer are determined. Preliminary testing of the piezo-crystals enhances essentially performance capabilities of the developed procedure and allows to select an optimal type of the transducer for carrying out the concrete acoustic investigations.

For elastic waves in a passive component of the vibrator (i.e., in the studied sample), it is possible to introduce the dispersion relation as a power series relative to the complex propagation coefficient k :

$$\omega^2 = E k^2 (1 + \theta_1 k^2 + \theta_2 k^4).$$

Here ω is the angular frequency of oscillations, $E = E' + iE''$ - the complex Young's modulus for the longitudinal strain along the

sample axis, and θ_i - some coefficients dependent on the material parameters of the sample (the elastic compliance tensors, the electric permittivity and piezoelectric coefficients) that must be determined from the experiment.

The second part of algorithm suggested is a self-consistent procedure of obtaining of parameters θ_i . Then, with the help of coefficients θ_i , the components of the complex Young's modulus are determined, and also the absorption coefficients and the logarithmic decrements of oscillations of the passive component of the vibrator (i.e., of the sample) are evaluated for each resonant frequency.

A package of application programs for the acoustical experiment management, mathematical processing and record of the information obtained in the experiment is developed by authors. The programs allow to implement the suggested algorithms both in testing of the piezoelectric transducers and in deriving the dissipative and elastic characteristics of the investigated materials with the help of a personal computer in the real-time mode.

The suggested algorithm and the programs were approved by us during the low-temperature acoustical experiment and interpretation of the obtained experimental data when studying in the range 2 - 20 K the temperature dependences of ultrasonic properties of the alkali-haloid single crystals CsI widely used in the modern science and technique as scintillators in the ionizing-radiation detectors. With the help of the algorithm offered, the activation parameters of the discovered low-energy relaxation processes with the characteristic activation energies about 10^{-3} - 10^{-2} eV were correctly determined [2, 3].

References

1. V.D. Natsik, P.P. Pal-Val and S.N. Smirnov. *Acoustical Physics* **44**, 553 (1998).
2. S.N. Smirnov, V.D. Natsik and P.P. Pal-Val. *Low Temp. Phys.* **24**, 904 (1998).
3. V.D. Natsik, S.N. Smirnov and P.P. Pal-Val. *Czech. J. Phys.* **49**, 1091 (1999).

ACOUSTIC MATERIALS SCIENCE TODAY

Bezimyanniy Y.G.

I.N.Franseich Institute for Problems of Materials Science of NAS of Ukraine, Kiev,
Ukraine

Effective application of any material to solve the concrete consumers' problem suggests that this material has certain operating characteristics. Technical progress constantly specifies the stringent requirements to these characteristics what stimulated application of materials with new and more unique properties. [1]

Life of material may be divided into three main stages: development, production and operation. For effective practical application of material a number of problems need to be resolved at each stage.

So, development of new materials is related to the optimum technology for their production. The technology must provide formation of the given properties. Here we should mark out three problems: development of the technology itself that is a combination of some operations; its refinement and the change of characteristics desired; analysis of possibilities for the newly developed material and certification of its properties.

Development of materials with concrete properties according to the certain technology is important at the production stage. Here we can mark out two main problems: production of material by means of the chain of the certain technological operations developed and testing the products. Testing sets up correspondence of the products to the certificate data.

Provision of reliable operation of the material is important at the third stage. Here the main problem is testing how the material can retain its operating characteristics.

These problems may be resolved by different ways. Application of acoustic methods of action on materials (ultrasound technologies), measurements, control and testing allows us to achieve the best and sometimes only possible results [2-7]. Classification of acoustic methods applications in materials science is shown in Fig.1. Examples of acoustic methods of action, research and testing applied to solve different problems are considered.

The advent of new materials having specific properties and the present achievements in science and technology give rise to the development of acoustic methods. The more complex material is, the more difficult its development and production

are. The qualified evaluation of its properties is a complicated problem. These problems need to be resolved by means of more highly organized technological processes, complex methods for research and testing. At present there are hundreds of acoustic methods that differ by their physical essentials, power, frequency band, parameters used etc. The choice of the acoustic method is related to the type of the problem resolved, features of the technological process and (or) the structure of material. Classification of acoustic methods applied in materials science is shown in Fig.2. Physical essentiality of above methods is considered.

We do not always succeed in applying the already known acoustic method to solve the materials science problems especially related to the materials with a complex structure. Methodology for development of the acoustic method satisfying the solution of the problem formulated is described. [8]

References

- [1] Современное материаловедение XXI век. Отв. Ред. И.К.Походня. Киев, Наук. думка, 1998.
- [2] Й. Крауткремер, Г.Крауткремер: Ультразвуковой контроль материалов, Москва, Металлургия, 1991.
- [3] Неразрушающий контроль. В 5 кн. Кн. 2. Ермолов И.Н., Алёшин Н.П., Потапов А.И. Акустические методы контроля. Москва, Высш. шк., 1991.
- [4] Ультразвук. Маленькая энциклопедия. Под ред. И.П.Голяминой. Москва, Сов. энциклопедия, 1979.
- [5] Агранат Б.А., Дубровин М.Н., Хавский Н.Н., Эскин Г.И. Основы физики и техники ультразвука. Москва, Высш. шк., 1987.
- [6] Абрамов О.В., Хорбенко И.Г., Швекла Ш. Ультразвуковая обработка материалов. Москва, Машиностроение, 1984.
- [7] Марков А.И. Ультразвуковая обработка материалов. Москва, Машиностроение, 1980.
- [8] Безымянный Ю.Г.: Возможности акустических методов при контроле структуры и физико-механических свойств пористых материалов. Порошк. металлургия, 5-6, 2001.

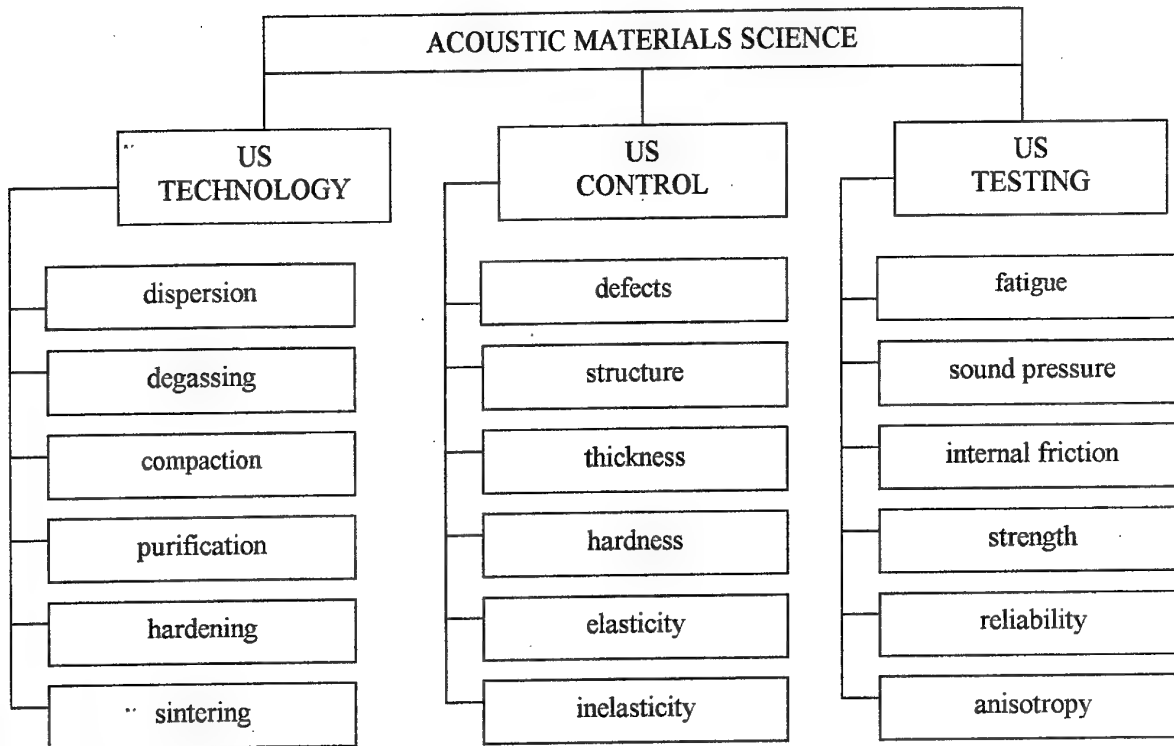


Fig. 1. Application of acoustics in materials science

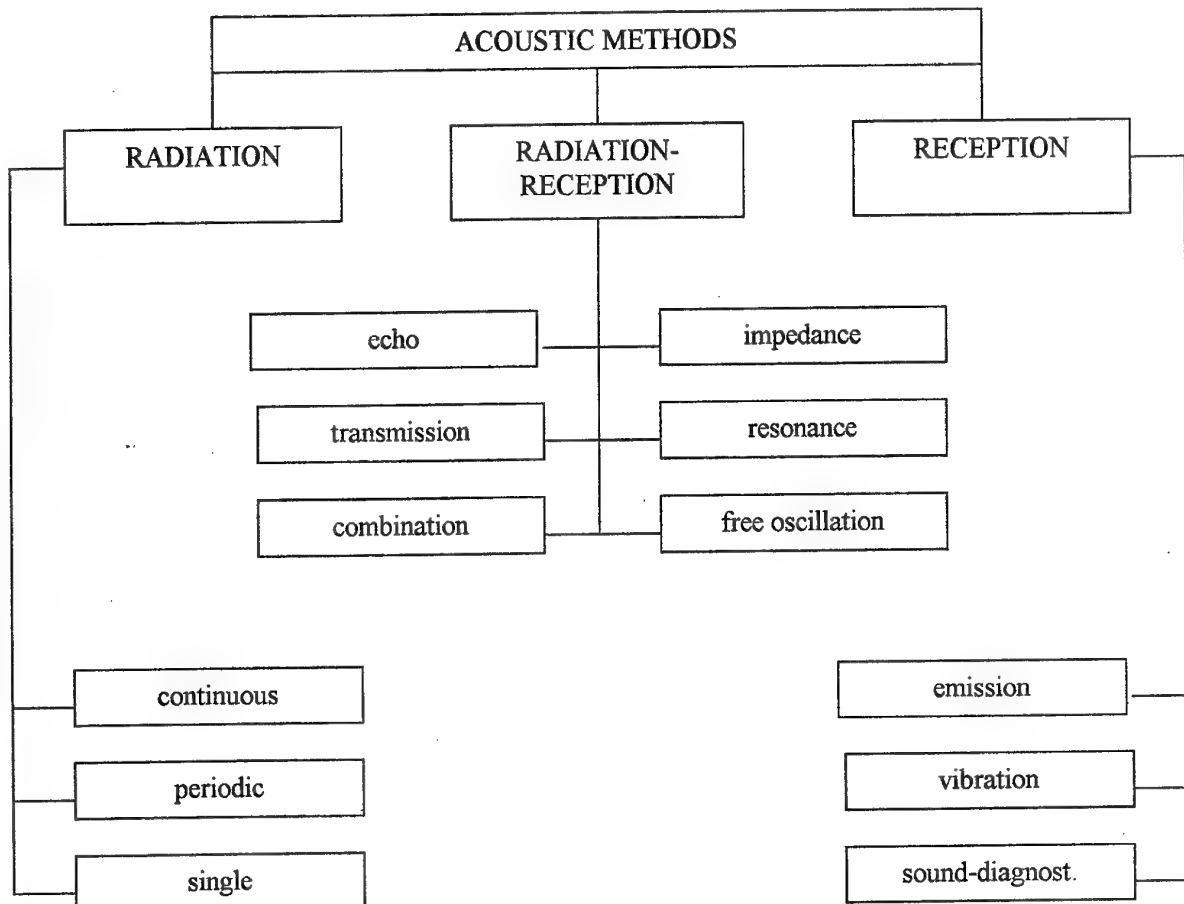


Fig. 2. Classification of acoustic methods applied in materials science

HIGH-TEMPERATURE RAMAN SPECTROSCOPY OF DEFECT STRUCTURE IN COMPOSITE OXIDE PHASES

Koviazina S.A., Pereliaeva L.A., Leonidova O.N., Leonidov I.A., Strekalovsky V.N.⁽¹⁾

Institute of Solid State Chemistry, Ural division Russian Academy of Science, Ekaterinburg, Russia

⁽¹⁾Institute of Hightemperature Electrochemistry, Ural division Russian Academy of Science, Ekaterinburg, Russia

The high-temperature studies «in situ» are of considerable interest both in synthesis and in study of properties in different materials. Methods of vibrational spectroscopy are fruitful for study of crystalline structure dynamics as these methods are possessed of high sensitivity to short-range order. IR and Raman spectroscopies allow to investigate local structure distortions in response to doping of the compounds and to fix an appearance of new phases fragments in phase transitions.

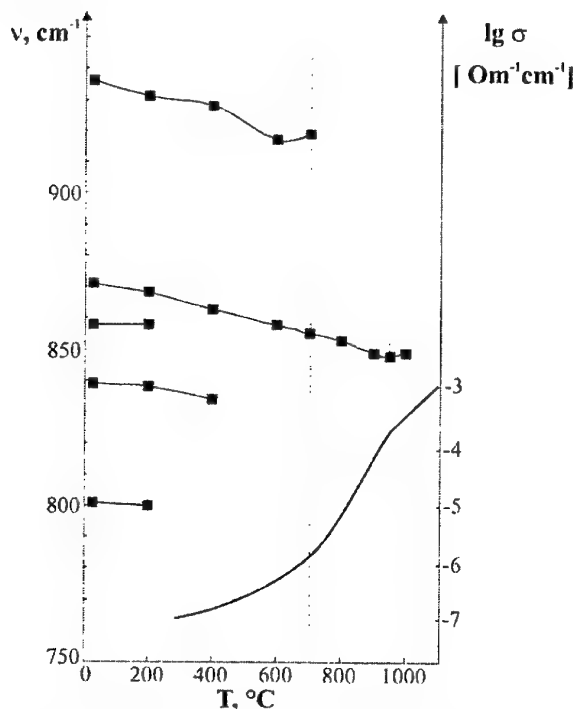


Fig. The temperature influence on the position of Raman bands and calcium conductivity in $\text{Ca}_{2.64}\text{Nd}_{0.24}(\text{VO}_4)_2$.

The investigation of structure disorder of phases with variable compositions $\text{Ca}_{3-x}\text{Nd}_{2x/3}(\text{AO}_4)_2$, where $A = \text{P}, \text{V}$ and $0 \leq x \leq 3/7$ by means of Raman spectroscopy at high temperatures is performed in this work.

Raman spectra were collected with Renishaw-1000 spectrometer in backscattering geometry with CCD signal detection. Raman scattering was excited by the Ar^+ laser at a wavelength 514.5 nm.

High-temperature experiments were carried out with a LINKAM TMS-1500 heating stage up to 1000 $^{\circ}\text{C}$.

The observed Raman bands in $\text{Ca}_3(\text{VO}_4)_2$ are distributed only in two wavenumber regions corresponding to the V-O stretching modes (950 - 750 cm^{-1}), O - V - O bending modes mixed with the translational and rotational modes of VO_4 - groups as well as Ca^{2+} cation displacements (450 - 50 cm^{-1}). The Raman bands in β - $\text{Ca}_3(\text{PO}_4)_2$ are distributed in five distinct 170 - 305 cm^{-1} , 405 - 483 cm^{-1} , 547 - 631 cm^{-1} , 946 - 970 cm^{-1} , 1005 - 1091 cm^{-1} wavenumber ranges, corresponding to the lattice modes ν_2 , ν_4 , ν_1 and ν_3 internal modes of the PO_4^{3-} ions, respectively.

The Raman spectra of phases with variable compositions are similar to spectra of $\text{Ca}_3(\text{VO}_4)_2$ and $\text{Ca}_3(\text{PO}_4)_2$ at ambient temperature, as Raman band shifts are insignificant. There are band broadening, considerable wavenumber shifts, decreasing peak intensities and smearing of all spectrum with temperature increase. The considerable changes in spectra for orthovanadate and phases with variable compositions based on it are fixed at 200 $^{\circ}\text{C}$, while corresponding changes in spectra for phases based on orthophosphate appear at higher temperatures. At cooling up to ambient temperature spectra return to the initial form.

Observed changes in Raman spectra in the temperature range 20 - 1000 $^{\circ}\text{C}$ we connect with reversible phase transition, accompanied by the redistribution of structural vacancies on different calcium positions. The sharp increasing of calcium conductivity at temperature near phase transition (Fig.), when new β' - phase fragments appear correlates with changes in Raman spectra. New β' - phase was detected by mean of Raman spectroscopy at 600 $^{\circ}\text{C}$ for phases with variable compositions $\text{Ca}_{3-x}\text{Nd}_{2x/3}(\text{PO}_4)_2$ with large neodymium content. This result is in good agreement with the results obtained by means of the thermal analysis and the measurements of cation conductivity.

The influence of the structure disorder on calcium mobility is also considered in this work.

APPLICATION OF GLOW DISCHARGE MASS SPECTROMETRY FOR ANALYSIS OF ADVANCED MATERIALS

Kurochkin V.D.

Institute for Problems of Material Science, NAS of Ukraine, Kyiv, Ukraine

Glow discharge mass-spectrometry ranks among the most advanced methods of modern analytical chemistry. This method allows to measure concentrations of all elements and isotopes of the periodic table without preliminary treatment in concentration range from tenth percents to sub-ppb level ($< 10^{-7}\%$). At the start of the analytical process sample introduction has great influence on system performance. Such methods as atom-absorption analysis (AAA), emission spectral analysis with inductively coupled plasma (ESA-ICP) require preliminary treatment of samples (dissolution, concentration) and have many limitations for certain elements.. The principal restriction of traditional methods is lack of information on isotopic composition of a sample. Such information is very important in geology, monitoring of environmental pollution, analysis of isotopic enriched elements.

GDMS is now well accepted as good technique for depth profiling study. It has a distinct advantage, since it is capable of penetrating to micron depths, quickly, over a relatively large surface area, averaging out the often considerable variations in detailed composition of the surface.

The main problem of the GD-MS are molecular ions (MI), known as source of spectral interferences. Glow discharge in argon produces a great number of ionic compounds of argon ions with other argon isotopes, gases - H, O, N, C, components of the sample and molecules formed from sample components. The number of possible combinations runs into the thousands. Despite high resolution of modern instruments (5000 - 10000 at 50% of a peak intensity) these polyatomic ions may be insufficiently resolved from the isotope investigated. Molecular interferences are the primary source of incorrect analysis.

The analysis of detrimental impurities in materials used as implants must be safe against analytical errors. Surgeon's implants with impurities exceeding the limit of tolerance may be harmful to the health. Similar heavy demands

imposes also the trace analysis of drinking water.

The problem of molecular interferences is always in focus of attention of design engineers and scientists - users of GDMS instruments. The most sophisticated software of manufacturing company calculates only the mass of ion. The main reason of inefficiency of modern methods is lack of theoretical methods for calculation of molecular ion concentrations in the glow discharge plasma.

A stride forward could be done on a basis of fundamental investigations of processes in GD plasma. The main subject of this paper is result of investigations of mechanism of ion-molecular reactions between discharge gas and particles of sputtered cathode, investigation of stability of molecular ions and their dependence of discharge parameters.

Concentrations of cluster ions of the form ArX^+ and simple ions were studied as functions of direct current glow discharge parameters. Mass - spectrometric measurements were carried out at constant voltage, pressure and constant discharge current when varying other two parameters. Typical curves for constant voltage are given in the fig.1

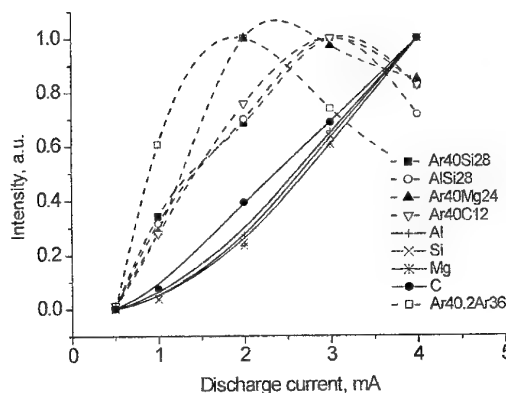
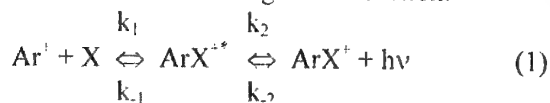


Fig.1. Normalized integrated currents of single charged ions as functions of discharge current (pressure) at constant voltage 1 kV.

Results obtained show that formation of molecular ions proceeds through the stage of

intermediate excited ionic cluster. This cluster goes into the product by monomolecular reaction with radiation according to the reaction:



Elimination of MI and excited clusters occurs mainly in collision-induced dissociation by argon atoms. This mechanism explains practically stable concentrations of MI at constant voltage for currents above 1.5-2 mA and respectively increased pressures whereas concentrations of reagents increase. Normalized to the matrix current concentrations of molecular interferences may be reduced in an order of magnitude using increased current and pressure. This dependence may be used as an indicator pointing out on MI and improving detection limit in GDMS analysis of samples with complex matrices.

These investigations were used for mathematical simulation of mass-spectra [1, 2]. In the Fig. 2 and 3 are shown calculated and measured spectra in analysis of cobalt alloy used as surgeon implant.

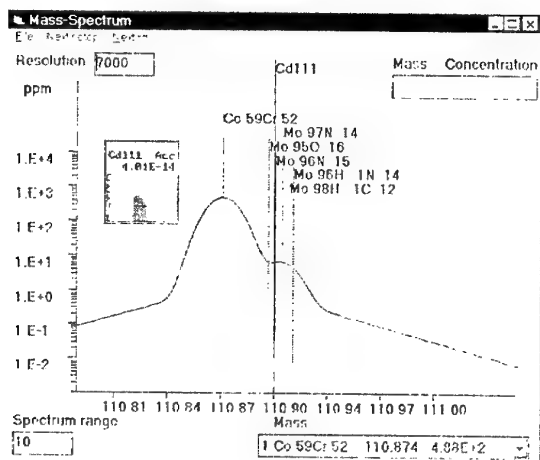


Fig.2. Calculated and measured mass-spectra in determination of Cd at analysis of Co-alloy.

Comparison calculated and measured spectra indicates that mathematical model gives good qualitative and quantitative information in the area of spectra studied. Calculations show that isotope Cd111 allows to reach detection limit of about 10 ppm (concentration of N = 3000 ppm). It is restricted mainly by molecular ion $^{97}\text{Mo}^{14}\text{N}^+$ and wing of a line $^{59}\text{Co}^{52}\text{Cr}^+$. Use of isotope Cd113 allows to improve detection limit down to 1 ppm.

Molecular interference of $^{97}\text{Mo}^{16}\text{O}^+$ is the reason of this restriction.

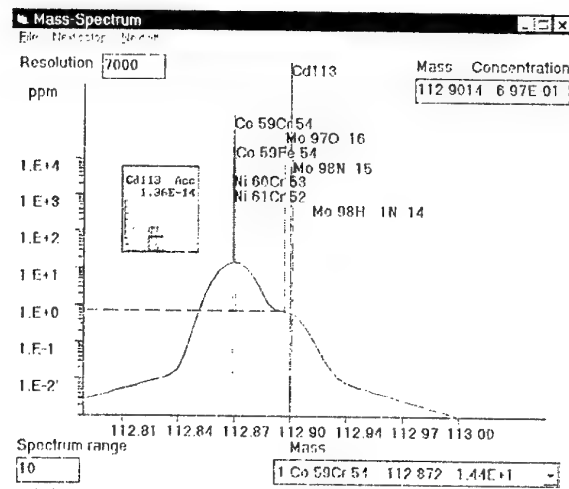


Fig.3. Calculated and measured mass-spectra in determination of Cd at analysis of Co-alloy.

As an example in the table are given calculations for other isotopes of Cd.

Isotope	Detection limit [*] , ppm (10 ⁻⁴ %)	Interferences
Cd110	< 0.3	Mo96N14
Cd111	<0.3	Mo97N14
Cd112	<0.3	Mo98N14
Cd113	0.7	Mo97O16
Cd114	0.6	Mo100N114
Cd116	7.0	(Ar40) ₂ Ar36

- at concentrations of N and O about 100 ppm
- Similar calculations were performed in analysis of hydrogen storage materials, new types of aluminum alloys, titanium alloys, refractory steels and others. The combination of high resolution mass-spectrometer with glow discharge plasma is also effective in the studying of ion-molecular reactions involving carbon atoms [3]. Results demonstrate ability of the method to improve correctness of analysis and point out the way to minimize influence of molecular interferences in GDMS.

REFERENCES

1. Kurochkin, V.D. // Anal.Comm. -1996. - 33. - P.381 - 384.
2. Курочкин В.Д. //Укр. хім.журн. -1999. -65. №3. -С. 57-63.
3. Kurochkin V.D., Kravchenko L.P. // VII Intern. Conf. "Hydrogen Materials Science and Chemistry of Metal Hydrides".-2001, Alushta, Crimea, Ukraine, P. 642-643.

HIGH-TEMPERATURE X-RADIOGRAPHY IN PHYSICAL METALLURGY

Belots'ky O. V., Yurkova O.I.

National Technical University of Ukraine "Kiev Polytechnic Institute",
03056, 37 Prospect Peremohy, Kiev, Ukraine

The study of diffusion and phase transformations is the theoretical base of physical metallurgy. X-ray diffraction analysis gives the very objective information about the changes, which take place during this processes. However, X-ray analysis of research subjects is making at room temperature. Kinetics of phase changes at high temperature remains uncontrolled under such conditions.

High-temperature X-ray diffraction analysis extends the information about diffusion and phase transformations and gives a possibility to control the material structure formation at different stages of heat treatment. During many years we conduct the investigations in this direction. This investigations show the prospects in store of application and development of such research method.

We employed a special technique of high-temperature X-radiography [1] for studying the diffusion processes and phase transformation, which take place right at the temperature of heat or thermochemical treatment.

The nitrogen solubility in polycrystalline and single crystal made of iron alloys was investigated with the help of this method. The sequence of changes of interference patterns were recorded in Fe-Ti polycrystalline objects at 698K (Fig.1). This changes showed the increasing of α solid solution lattice parameter. That is connected with the rising of nitrogen solubility in α phase.

The scales of changes of nitrogen solubility depending on titanium content are presented at Fig.2.

The nature of nitrogen solubility changes was studied on iron-silicon single crystals [2]. Radial blurring of all the spots in Laue diffraction pattern (Fig. 3) is a consequence of the increase in nitrogen solubility. The presence of the additional interference bands of asterism is a result of the precipitation from a solid solution of a nitride phases.

High-temperature X-radiography was used to research the features of joint influence of nitrogen and carbon on the sequence of phase

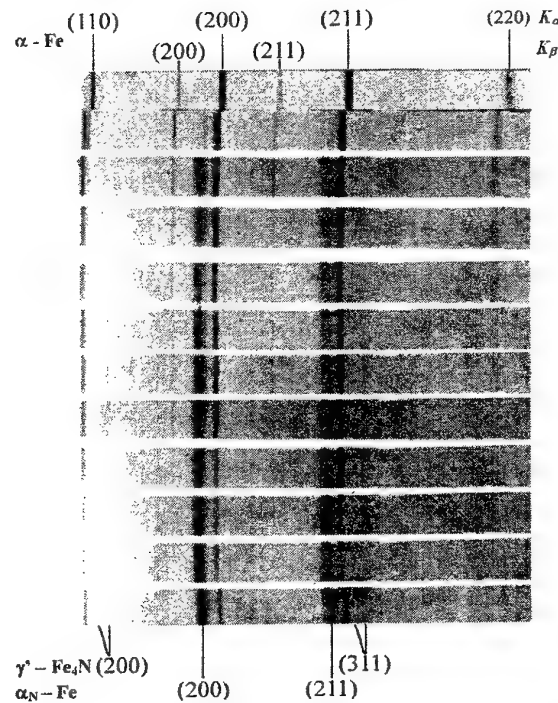


Figure 1. High-temperature X-radiographic pattern of the surface of Fe+1.96%Ti alloy. Nitriding at 698K for 2 h.

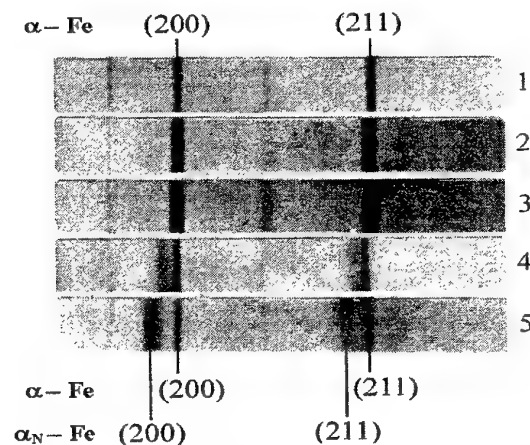


Figure 2. High-temperature X-radiographic pattern of Fe-Ti alloys, nitriding at 698K for 2 h: 1 - Fe; 2 - 0,35; 3 - 0,6; 4 - 0,95; 5 - 1,96% Ti.

formation (solid solutions, carbide, nitride, carbonitride phases) in the course of saturation of steel 18XГТ (Fig. 4) [3].

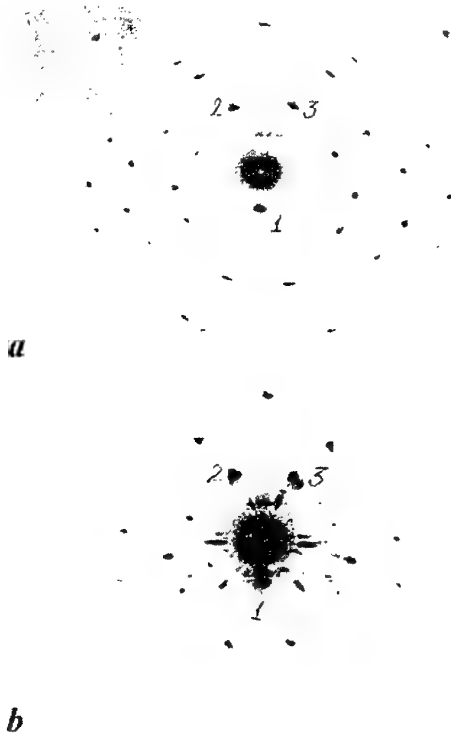


Figure 3. Laue diffraction patterns of the transformer steel single crystals (Fe+3.08% Si by mass): a – initial state prior to nitriding; b – high-temperature X-ray photograph: nitriding at 823K for 3 h.

The temperature intervals of $\alpha \rightarrow \beta$ phase transformation of cobalt depending on the time of ultrasonic treatment were determined with the help of high-temperature radiography [4].

Wide information about chemical elements redistribution in the process of isothermal decomposition of a supercooled austenite in steels and highly strong spheroidal graphite cast iron is accumulated by this research method. Decomposition of the high-nitrogen austenite was investigated in the 823-473K range, directly at the transformation temperature. X-ray diffraction patterns were recorded every 5 min, at the end of nitriding and during isothermal holding at the transformation temperature [5]. A temperature range within which structures providing a high strength diffusion layer form during austenite decomposition was established.

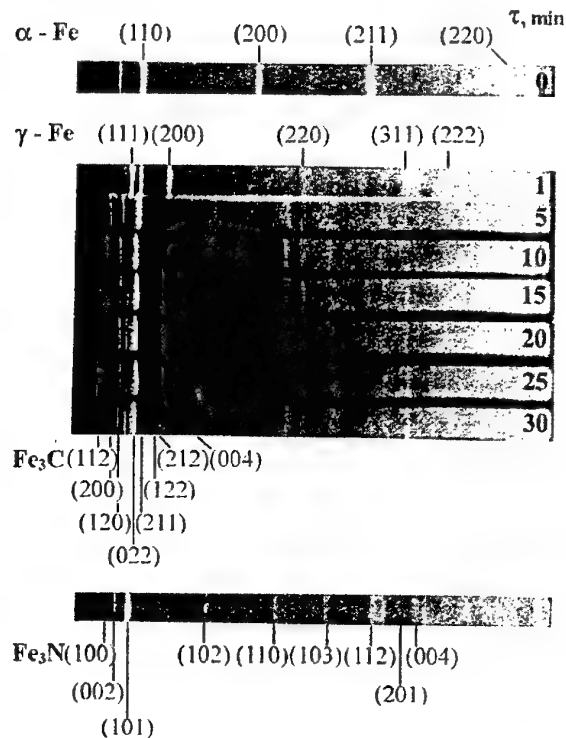


Figure 4. High-temperature X-radiographic pattern of the surface of steel 18XГТ. Saturation by nitrogen and carbon at 1143K for 0,5 h, air

References

1. A.V.Belots'ky, Prybory dlya Issledovaniya Fizicheskikh Svoystv Materialov (The Instruments for Studying Physical Properties of Materials) (Kiev: Naukova Dumka: 1974), p.35 (in Russian).
2. O.V. Belots'ky, A.M.Pavlovs'ka, Crystal-Chemical and Structure Alterations in Iron-Silicon Substitutional Solid Solutions Under Diffusive Saturation with Nitrogen, Met. Phys. Adv. Tech., 2001, Vol.19, pp.883-890.
3. O.V. Belots'ky, O.A. Pleshkanovs'ka, The Phase and Structural Transformations During the Co-Operative Diffusion of Nitrogen and Carbon in Steel, Met. Phys. Adv. Tech., 1999, Vol. 18, pp.187-192.
4. A.V.Belots'ky, V.N.Vinnichenko, I.M.Muha, Ul'trozvukovoe Uprochnenie Metallov (Ultrasonic Strengthening of Metals), Kiev: "Technica", 1989, 168p.
5. A.V.Belots'ky, A.I. Yurkova, The Formation and Decomposition of High-Nitrogen Austenite at Controlled Heating and Cooling Rates, Met. Phys. Adv. Tech., 1996, Vol.16, pp.43-49.

STM STUDY OF THE SURFACE MICROSTRUCTURE OF MAGNETIC GRANULAR THIN FILMS.

Yu. I. Gorobetz, V. I. Silantiev, G. V. Bondarkova, A. F. Kravets

Institute for Magnetism, NAS of Ukraine, 36-b Vernadsky blvd., 03142 Kyiv, Ukraine

The scanning tunneling microscopy (STM) study of the surface microstructure of the magnetic granular thin films has been carried out. Two types of the magnetic granular films have been investigated: ferromagnetic-nonmagnetic metal CoFe-Ag, Co-Ag, Co-Cu granular films and ferromagnetic metal-insulator CoFe-HfO₂ and CoFe-Al₂O₃ granular films. Giant magnetoresistance was found in both types of films below the magnetic metal percolation threshold. It has different electron transport mechanism: spin-dependent scattering of conduction electrons on the grain boundaries in the case of metal granular films and spin-dependent tunneling of electrons between the metallic particles in the case of metal-insulator (cermet) granular films. The necessary conditions of the existence of giant magnetoresistance (super-paramagnetic state of the system, nanoscale sizes of metallic granules, small interparticle distances) depends strongly on the microstructure of the granular films.

The specimens in the wide range of compositions have been prepared by electron beam co-evaporation of magnetic and nonmagnetic components from the two independent sources in a vacuum 10^{-4} Pa. The films have been deposited at ambient temperature onto glassceramic substrates. The thickness of the deposited films was about 500 nm.

The structure of the film surface was studied by combined device of SELMI manufacture: scanning tunneling (STM) and scanning electron (SEM) microscopes. STM was built in the chamber of the scanning electron microscope. They were operated at room temperature in a vacuum $5 \cdot 10^{-4}$ Pa. STM topographic images have been obtained in the constant current mode with using a tungsten tip.

Figure 1(a,b) shows STM topographic images of (CoFe)₆₈(HfO₂)₃₂ granular film with different magnification. These pictures are typical for the surface structure of both cermet and metal granular thin films. The nearly round granules of nanoscale sizes are not homogeneously distributed on the surface but combine more large clusters, which become one of the cause of the roughness of the granular film surface. The other cause of

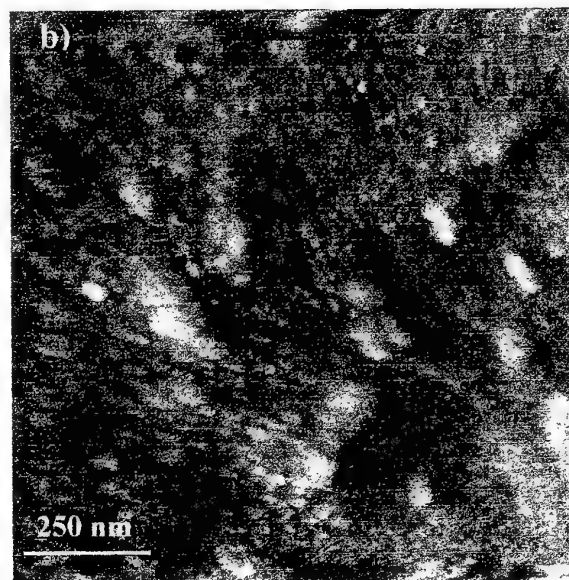
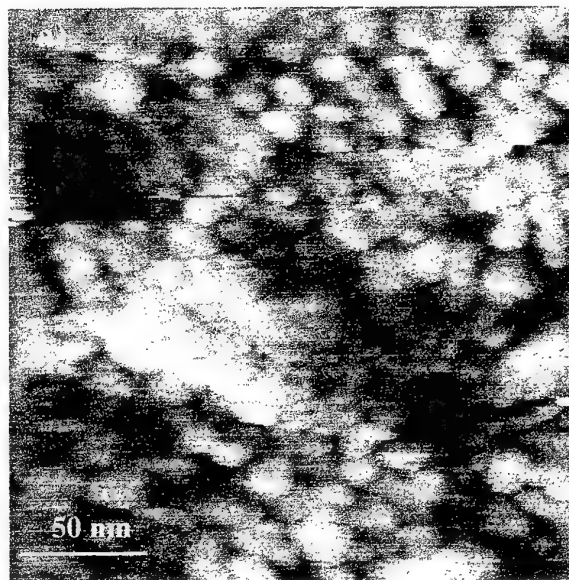


Fig.1. STM topographic images of (CoFe)₆₈(HfO₂)₃₂ granular film

the surface roughness is the surface condition of glassceramic substrates. Figure 2 represents the granular film surface by scanning electron microscope. It is quite possible that each granule is a single crystal randomly oriented on the surface. Then the clusters of granules are probably the polycrystalline grains of each component of the granular film.

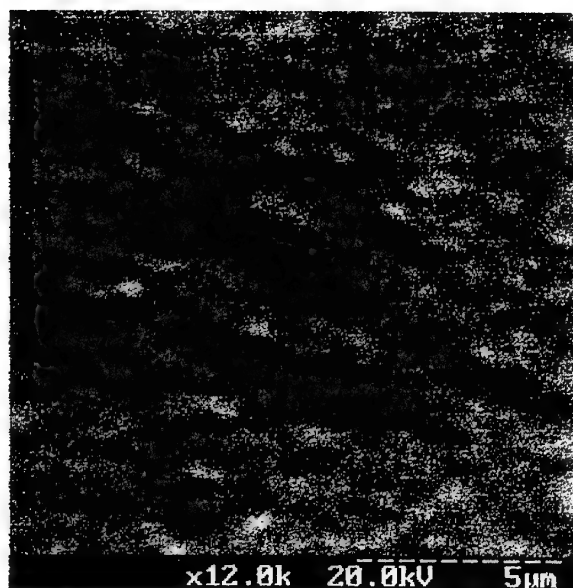


Fig.2. SEM micrograph of CoCu granular thin film.

Figure 3 shows STM topographic image of $(\text{CoFe})_{30}(\text{HfO}_2)_{70}$ granular film. The image is not clear in comparison with STM images of $(\text{CoFe})_{68}(\text{HfO}_2)_{32}$ granular film because of the low content of the metal phase. But one can perfectly see the bright spots of the round shape on the dark background, which we associate with the metallic CoFe granules dispersed in the amorphous matrix of HfO_2 . The previous high resolution transmission electron microscopy (HRTEM) investigations [1] of metal-nonmetal granular thin films confirm this assumption.

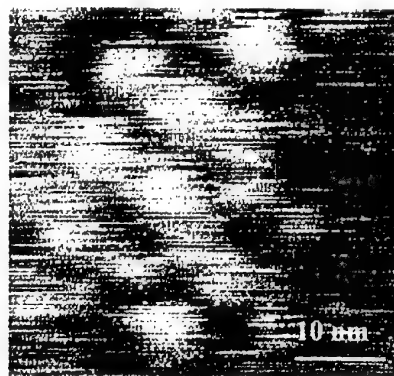


Fig.3. STM topographic image of $(\text{CoFe})_{30}(\text{HfO}_2)_{70}$ granular film.

So, STM topographic images of the cermet and metal granular thin films exhibit the similar structure of the surfaces. Although the diameters of granules for different films vary in the range of $2 \div 8$ nm, the tendency for granules to coalesce and form more large combinations, so-called clusters, is typical for each case. These clusters having dimensions of $20 \div 50$ nm cause to surface roughness of the granular films. So, the structure of the film surface is not the homogeneous distribution of the granules on the substrate, but more complicated structure of cluster-upon-cluster.

[1] Gorobetz Yu.I., Silantiev V.I., Bondarkova G.V., Kravets A.F., Mater. Sci. Forum, Vol.373-376, 2001, p.221-223.

EVOLVING HETEROGENEOUS DISTRIBUTION AND ANISOTROPY OF FACTUALITY OF SURFACE ROUGHNESS IN SINGLE CRYSTAL FOILS UNDER CONSTRAINED CYCLICAL TENSION

Gordienko Yu.G., Zasimchuk E.E.

G.V.Kurdymov Institute for Metal Physics of NAS of Ukraine, Kyiv, Ukraine

Our previous work has shown that single-crystal metal foils attached to metals under cyclic tension develop surface relief patterns, multi-scale characteristics (information, correlation and capacity fractal dimension) of which correlate with the number of loading cycles. Now we carried out the quantitative analysis of foils, which were attached to the samples of non-uniform aircraft alloys. We investigated the welded samples with different zones: parent metal, thermo-mechanically affected zone (TMAZ), weld/TMAZ transition zone, weld. We analyzed the structural heterogeneity by optical methods and the properties of different zones-by microhardness and X-ray methods and statistics of information dimension in 2D cross-sections perpendicular to foil surface. The value of hardness is nearly equal at the equal distances from weld if distance $S > 10\text{mm}$. One can see complex hardness changes along the welded plate. These changes correlate with macrostructure of welded joint. The maximum hardness value is in parent metal; in weld it slightly higher in comparison to surrounding regions but less of parent metal. There are two 'soft' zones on the both directions from the weld but the hardness value in these directions is different. The reason of structure and properties heterogeneity is connected with complex phase and chemical composition of aircraft aluminum alloy. The data, obtained during our investigation, allow us to imagine a priori the most probable map of strain localization sites. It can be very useful for determination of the places where sensors can be located. The qualitative and quantitative information about deformation relief was extracted from modernized optical data. We used the automated method on the basis of stereo microscope with the CCD camera attached to personal computer by video adapter and frame-grabber card. We created automatically a panoramic view by means of specially designed software and used the fractal analysis of deformation relief with implementation of automation procedures.

During our work we used two types of illumination:

1 - directional illumination;

2 - diffuse ring illumination. At the intervals of loading the specimens were scanned by microscope with creation of many single snapshots of sensor surface. To get the whole set of snapshots for diffuse ring illumination (directed illumination) it takes $200 \div 300$ ($100 \div 200$) iterations of precise shifting and manual focusing at each image capturing point. The minimal average overlapping of snapshots of neighboring regions assumed to be 15%, but for better performance on the next stage (panoramic view creation) we used overlapping up to 30%. We preferred to use information dimension because it gives the richest and most useful information. We carried out some tests on the objects with well-known fractal dimension and information dimension was the most precise method among other box-counting methods. But a simple method of measuring the correlation of one multiscale characteristic (information dimension) with the number of loading cycles, is not adequate for real specimens with heterogeneous strain map. Therefore we develop two new methods for visualisation of this heterogeneity by means of this methods:

— equidimensional contour maps for statistical comparison of relative changes of structural self-similarity over the whole foil surface and for search of persistent strain localisation sites;

— pole dimensional figures that allow us to bring to light anisotropic features of foil surface and characterise persistent strain localisation sites.

For higher numbers of cycles the evolution of direct illumination images can be characterised by splitting of the information dimension in two different values. These tend to appear earlier for higher levels of stress amplitude and are assumed to be a consequence of the appearance of a network of crossing ridges on the foil. Clearly this could be a valuable investigative tool in the introduction of new structural concepts, materials or processes.

We can conclude that by naked eye all sensors in all zones demonstrate the same behavior, namely, permanent increase surface relief with the same

features: black-and-white initial contrast bands; elongated hills, crossing system of hills, 'blisters'. But if we construct equidimensional maps for sensors in different zones and compare them, then we can note that some of them (parent metal and heat-affected zone) have homogeneous distribution of maximal dimension contour, and in other (weld and transition zones) — heterogeneous distribution. This heterogeneity consists in irregular shape, appearance and growth of asymmetry, splitting of initially linked contour in several islands (like dumb-bell). In addition to this heterogeneity changes with the number of cycles and has the more pronounced nature on the late stages of testing before fracture. This observation relates to small solitary sensors that are supposed to cover one of the zones aforementioned.

As to large sensors (on narrow-weld and flank sides) they have some different behavior which is caused by obvious cumulative influence of several zones. This method allows not only to find strain localization places, but also to envisage its dynamics. It should be noted that large sensors which can fully cover the possible place of stress localization are necessary for this purpose. In addition to this we develop the new technology of polar dimensional plots that allow us to bring to light not only anisotropic features of sensor

surface, but also catch increase of angular distortions and asymmetry of polar dimensional plots caused by persistent strain localization. We tried to measure and compare angular dependencies for two parts of large foil in significantly different zones with a priori known various strain levels, create histograms, found peaks and precisely define their positions. On initial stage of fatigue loading we observed only one peak and peak splitting phenomenon appear for the higher numbers of cycles. These double peaks tend to appear earlier for higher levels of stress amplitude and are assumed to be a consequence of the pronounced appearance of a network of 2 systems of crossing erections. Then we create polar plot of the peak values and areas under Gaussian fit and obtain the pole figures. In the low strain zone these polar figures are symmetric as to the axis of tension. It is obvious that 8-like polar figure for relative area values of information dimension histograms reflect the anisotropic nature of foil surface relief. But in the high strain zone this symmetry is broken (it is symmetric only in relation to center of coordinates). We assume this phenomenon can be used for determination of zones with large distortions of symmetry of sensor relief caused by strain localization in underlying specimen.

STATISTICAL ANALYSIS OF PLASTIC INSTABILITY: UNIVERSAL SCALING

Lebyodkin M.A., Dunin-Barkowskii L.R., Lebedkina T.A.

Institute of Solid State Physics, RAS, Chernogolovka, Russia

The dislocation ensemble represents an example of a non-linear dissipative system far from equilibrium. The dynamics of such systems obeys universal laws. In particular, dynamical processes are characterized by self-organization at different scales in space and/or time [1]. Recently a series of works appeared, in which the plastic flow of solids was investigated in terms of self-organization (see review [2]). The analysis of a complex evolution of the deforming stress under conditions of jump-like deformation (plastic instability) attracts great attention since in this case the collective processes in the dislocation ensemble manifest themselves at the macroscopic level of deformation curves [3]. Moreover, the microscopic nature of plastic instability may be different that provides an opportunity of studying its universal and unique features.

Using methods of statistical, dynamical and multifractal analysis, complex correlations of plastic processes were found in several works (e.g., [4-6]) under conditions of discontinuous deformation associated with dynamical interaction between dislocations and solute atoms – the Portevin - Le Chatelier (PLC) effect [7]. Dynamical chaos [8] was proved for low strain rates, which changes to self-organized critical (SOC) dynamics [9] upon an increase in the strain rate. The transition between these two regimes is accompanied by a specific alteration of statistical distributions of amplitudes and durations of stress jumps. In [10] a qualitatively similar trend in the effect of strain rate on statistics was reported for another kind of plastic instability, namely, the low-temperature discontinuous deformation, in which a coupling between the local strain and the strain-induced heat plays an important role [11].

In the present work statistical properties of plastic flow governed by the PLC effect and low-temperature mechanism of plastic instability were investigated. The effects of strain rate and initial microstructure of crystals on distributions of parameters of stress jumps were studied upon deformation of polycrystalline samples of an Al-2.5at.%Mg (PLC effect) and Cu-12at.%Be-0.2at.%Co (low-temperature catastrophic glide) alloys.

The specimens of Al-Mg ($30.5 \times 1.5 \text{ mm}^3$; straining at $T = 300 \text{ K}$) and Cu-Be (wire 30 mm

long by 0.5 mm in diameter; $T = 4.2 \text{ K}$) were deformed by tension with a constant strain rate in an interval covering more than three orders of magnitude ($\sim 2 \cdot 10^{-6}$ – $1.4 \cdot 10^{-2} \text{ s}^{-1}$). The samples were used in both as-delivered (strain-hardened) state and after annealing (Al-Mg: 320° – 460°C ; Cu-Be: 800°C) with quenching in water.

The statistical analysis of deformation curves at various strain rates provided similar results for both kinds of plastic instability. Relatively regular deformation curves with a pronounced scale of stress drops are observed at low values of the strain rate. Correspondingly, the histograms of the distribution of stress-jump parameters acquire a bell-like shape. When the strain rate is increased, the distributions become asymmetrical: the maximum position shifts towards the axis of ordinates (the probability of small stress jumps is increased). Finally, in the strain-rate range above 10^{-4} – 10^{-3} s^{-1} the histograms are described by monotonically descending curves.

The transition to monotonic curves takes place earlier with respect to strain rate in the case of annealed samples as compared to as-delivered ones. Since the depression of the characteristic scale of stress jumps is apparently due to an increasing heterogeneity of strain in the crystal, the annealing effect can be related to a decrease in the spatial coupling between local strains. The investigation of the PLC effect [4-6] led to a conclusion about plastic relaxation of the spatial-coupling strength. The data obtained testify that such a conclusion is also valid in the case of low-temperature discontinuous deformation, although the nature of the spatial coupling may be different. Elastic stresses caused by incompatibility of plastic strains are the dominant coupling mechanism in the PLC instability, whereas processes of heat release and propagation play an essential role in the low-temperature instability. The conclusion is also confirmed by the earlier (with regard to strain rate) transition in Al-Mg than in Cu-Be. Indeed, the grain size is smaller in the latter case ($\sim 10 \text{ }\mu\text{m}$ in Cu-Be samples, as compared to 50 – $500 \text{ }\mu\text{m}$ in Al-Mg, depending on the annealing regime). Thus, the plastic-relaxation conditions are less favorable in Cu-Be.

The distribution density functions of stress-drop amplitudes δ and durations τ , obtained from the monotonic histograms at high strain rates, can be approximately described by power-law dependences: $n_\delta \sim \delta^{-x}$, $n_\tau \sim \tau^{-y}$ (the only exception concerns unannealed Cu-Be samples, although the qualitative trend in histograms is the same). Herewith, a scaling relation $\delta \sim \tau^h$ exists between the amplitudes and durations, and the scaling exponents, typically taking on the values between 1 and 1.5, are related to each other as $y = h(x - 1) + 1$. The power-law statistics, indicating the absence of characteristic scales in the dynamical system, is generally considered as an evidence of a SOC state [12]. Besides, taking into account the numerical values of the scaling exponents, an additional proof of this conclusion stems from observation of the power-law dependence $S(f) \sim f^{-2}$ for low-frequency parts of power spectra of deformation curves [12].

The scale invariance is usually associated with a universal behavior, so that the scaling exponents only depend on a small number of fundamental factors, such as the effective dimensionality (number of degrees of freedom) and symmetry of the system. Thus, one can try to justify the universality observed. The non-linear material equations are believed to be similar for the PLC and low-temperature instabilities and stem from an N-shaped function of stress sensitivity to strain rate [7, 11]. It is known that the temporal instability of plastic flow is coupled with spatial instability - localization of strain in deformation bands [3, 7]. The development of deformation bands across the specimen occurs much faster than the plastic activity is transferred in the axial direction. Thus, the situation seems to be confined to a single dimension. One should note that the spatial coupling is different in the cases under discussion. Indeed, it is generally observed that the PLC bands may be stationary or propagative, depending on specific conditions [7], whereas multiple localized bands occur upon low-temperature instability [3]. Nevertheless, recent studies indicate a propagative regime in low-temperature deformation with high strain rate, as well [13]. Therefore, one can suppose that the difference in the nature of spatial coupling must not be an essential factor for dynamics of strain localization at high strain rate. A possible approach for understanding the observed types of dynamics was suggested for the PLC effect [4-6]. It consists of considering the interplay of relevant time and

length scales and their variations with the loading rate and microstructure. In essence, the homogenization of strain heterogeneity in a crystal is less efficient at high strain rates. Thus the critical conditions for a plastic burst are always locally satisfied, as expected in a SOC system. This leads to a recurrence of partial plastic-relaxation events and the absence of a characteristic scale of plastic bursts.

In conclusion, a similar behavior of plastic instabilities is observed in the whole range of strain rates, despite the difference in the nature of spatial coupling between elements of a heterogeneously deforming crystal. The effect of the initial microstructure of specimens is also similar. This indicates the existence of universal laws governing dynamical processes upon unstable plastic flow. The occurrence of a SOC state characterized by scale invariance is proved for a range of high strain rates.

The work was partly supported by the Russian Foundation for Basic Research (grants nos. 00-15-96703, 01-02-16461, 01-02-16476, 02-02-06352), and INTAS (YSF 01/1-47).

1. G.Nikolis, I.Prigogine, *Self-organization in Non-Equilibrium Systems*, N.Y., J. Wiley (1977).
2. G.A.Malygin, *Usp. Fiz. Nauk*, **169**, 979 (1999).
3. O.V. Klyavin, *Physics of Crystal Plasticity at Helium Temperatures*, Moscow: Nauka (1987).
4. M.A. Lebyodkin, L.R. Dunin-Barkowskii, *JETP*, **86**(5), 993 (1998).
5. M.Lebyodkin, L.Dunin-Barkowskii, Y.Br chet, Y.Estrin, L.Kubin, *Acta Mater.*, **48**, 2529 (2000).
6. M.S.Bharathi, M.Lebyodkin, G.Ananthakrishna, C.Fressengeas, L.P.Kubin, *PRL*, **87**, 165508 (2001).
7. L.P.Kubin, Y.Estrin, in: *Continuum Models for Materials with Microstructure*, Ed. by H.-B. M hlhaus, N.Y., J. Wiley & Sons, 395 (1995).
8. D.Ruelle, F.Takens, *Comm. Math. Phys.*, **20**, 167 (1971).
9. P. Bak, C. Tang, K. Wiesenfeld, *Phys. Rev. A*, **38**(1), 364 (1988).
10. M.Lebyodkin, L.Dunin-Barkovskii, V.Bobrov, V.Gr ger, *Scripta metal. mater.*, **33**, 5, 773 (1995).
11. G.A.Malygin, *Fiz. metal. i metalloved.*, **40**, 1, 21 (1975).
12. J.Kert sz, L.B.Kiss, *J. of Physics A*, **23**, L433 (1990).
13. Z.Troyanov , V.Gr ger, J.Stelzhammer, G.Bischof, *Mat. Sci. Eng.*, **A234-236**, 449 (1997).

A NEW METHOD OF THE ANALYSIS OF RELAXATION RESONANCES: BROADENING AND SHIFT CAUSED BY RANDOM DISPERSION OF THE PARAMETERS OF THE ELEMENTARY RELAXATORS

Natsik V.D., Semerenko Yu.A.

B. Verkin Institute for Low Temperature Physics and Engineering, National Academy of Sciences of Ukraine, Lenin Ave. 47, 61103 Kharkov, Ukraine

The equilibrium state of a solids which is disturbed by external fields is spontaneously restoring, however this relaxation process lags behind the time of the change of the parameter describing this external effect. The duration of this process in the elementary cases is characterized by a relaxation time τ , and in more common case by set (spectrum) of relaxation times. The excitation can be implemented by mechanical stress, magnetic or electrical fields and the relaxation is named accordingly mechanical (acoustic), magnetic or dielectric.

The dynamic experiments (methods of dynamic spectroscopy) using harmonic effects of small amplitude with period of the order τ are convenient in information acquisition about physical mechanisms of relaxation. In these experiments the external effect $\alpha = \alpha_0 e^{i\omega t}$ with amplitude α_0 and circle frequency ω is operated on the investigated body and the response of the body $\beta_0 = \beta_0(\omega)$ is detected: here $\beta_0 = \beta_0(\omega)$ is an amplitude of the response, and $\varphi = \varphi(\omega)$ is a phase shift of the response from external effect. The response linearity and its periodicity with effect frequency ω is provided by rather small amplitude α_0 . Relation $\beta/\alpha = M^*(\omega) = M_1(\omega) - iM_2(\omega)$ is named as a complex susceptibility of a material. For oscillations of a concrete physical type $M_1(\omega)$ is the dynamic elasticity modulus, dynamic magnetic or dielectric susceptibility. The relation $M_2(\omega)/M_1(\omega) = \tan \varphi(\omega)$ determines the energy dissipation of corresponding oscillatory process caused by relaxation.

Acceptable model for the description of dynamic excitation of the majority of real materials is the standard linear body, for which as the macroscopic characteristics of relaxation it is convenient to use defect of a susceptibility (defect of a modulus) $\Delta M(\omega)/M_\infty$ and decrement $\delta(\omega)$ or inverse Q-

factor (internal friction) $Q^{-1}(\omega)$:

$$\frac{\Delta M(\omega)}{M_\infty} = \frac{M_\infty - M_1(\omega)}{M_\infty} = \frac{\Delta_r}{1 + \omega^2 \tau^2}, \quad (1a)$$

$$Q^{-1}(\omega) = \frac{\delta(\omega)}{\pi} = \frac{M_2(\omega)}{M_\infty} = \Delta_r \frac{\omega \tau}{1 + \omega^2 \tau^2} \quad (1b)$$

where M_∞ - susceptibility before relaxation, Δ_r - "power" of the relaxations.

In many cases the processes of relaxation at a microscopic level are caused by elementary thermo-activated changes of structure and the time of relaxation is described by the Arrhenius relation:

$$\tau(T) = \tau_0 \exp(U_0/kT) \quad (2)$$

where τ_0 and U_0 - is accordingly the attempt period and the activation energy of elementary relaxator, k - the Boltzmann constant, T - the temperature. Studying of such processes by dynamic methods at fixed value of the frequency ω on temperature dependences Q^{-1} and $\Delta M/M_\infty$. Debye peak of relaxation and appropriate to the peak broad "step" localized near the temperature $T_p^{(0)}(\omega) = -U_0/k \ln \omega \tau_0$ with width $T_h^{(0)}(\omega) = 2U_0/k (\ln \omega \tau_0)^2$ have been observed.

The basic problem of dynamic spectroscopy is detection of such resonances and their analysis for determination of parameters of elementary relaxators τ_0 and U_0 .

The real materials, as a rule, have random distributed structural imperfections (defects) arising during the synthesis of samples and various processing of them. The experience shows, that the change of defective structure of the material can change both temperature of localization $T_p \neq T_p^{(0)}$, and widths $T_h \neq T_h^{(0)}$ of relaxation resonances. The interpretation of such changes is one of important and discussed for a long time questions of the dynamic relaxation theory. In Refs. [1-3] it was shown, that for number of low-temperature acoustic relaxation resonances the influence of

structural defects can be described taking into account the statistical dispersion of local values of activation energy U from its initial value U_0 if we select correctly distribution function $P(U)$. Undoubtedly, that the similar interpretation is effective also for spectra of dielectric and magnetic relaxation in materials with defects.

It has been detected during experimental study of the various types of dynamic relaxation that the change of the defective structure of the materials results in shift of temperature T_p of the resonances both in the side of high (+) and in the side of low (-) temperatures. By this is meant that the structural changes increasing dispersion of activation energy from an initial value U_0 can enrich both high-energy ($\bar{U} > U_0$) and low-energy ($\bar{U} < U_0$) states of relaxators. Both of these cases can be described by probability density of the quasi-Gaussian type accordingly $P^{(+)}(U)$ and $P^{(-)}(U)$ with a small variance $D \ll U_0$:

$$P^{(+)}(U) = \frac{U}{U_0 \sqrt{2\pi D}} \exp\left(-\left[\frac{U-U_0}{\sqrt{2D}}\right]^2\right), \quad (3a)$$

$$P^{(-)}(U) = \frac{U}{U_0 \sqrt{2\pi D}} \left(2 - \frac{U}{U_0}\right)^4 \exp\left(-\left[\frac{U-U_0}{\sqrt{2D}}\right]^2\right) \quad (3b)$$

With a statistical distribution of activation energy it is necessary to consider average functions of a response $\Delta \bar{M}/M_\infty = \mu_1(T, \omega, \tau_0, U_0, D)$ and $\bar{Q}^{-1} = \mu_2(T, \omega, \tau_0, U_0, D)$ with the probability density (3) containing four parameters: (ω , τ_0 , U_0 , D) instead of a Debye temperature spectrum of relaxation (1).

Let us consider the average characteristic of the defect of a susceptibility μ_1 and the average characteristic of the absorption μ_2 using a dimensionless temperature $\theta = T/T_p^{(0)}$, a dimensionless inverse frequency $\Omega = 1/\omega\tau_0$ and a dimensionless characteristic variance $d = \sqrt{2D}/kT_p^{(0)}$:

$$\mu_1^{(+)} = \frac{\Delta_r \Omega^2 \theta^2}{\sqrt{\pi d \ln \Omega}} \int_1^\infty dx \cdot f(x, \theta, \Omega, d), \quad (4a)$$

$$\mu_2^{(+)} = \frac{\Delta_r \Omega^2 \theta^2}{\sqrt{\pi d \ln \Omega}} \int_1^\infty \frac{dx}{x} \cdot f(x, \theta, \Omega, d), \quad (4b)$$

$$\mu_1^{(-)} = \frac{\Delta_r \Omega^2 \theta^2}{\sqrt{\pi d \ln \Omega}} \int_1^\infty dx \left(2 - \frac{\theta \ln x}{\ln \Omega}\right)^4 f(x, \theta, \Omega, d), \quad (4c)$$

$$\mu_2^{(-)} = \frac{\Delta_r \Omega^2 \theta^2}{\sqrt{\pi d \ln \Omega}} \int_1^\infty \frac{dx}{x} \left(2 - \frac{\theta \ln x}{\ln \Omega}\right)^4 f(x, \theta, \Omega, d); \quad (4d)$$

$$f(x, \theta, \Omega, d) = \frac{\ln x}{\Omega^2 + x^2} \exp\left(-\left[\frac{\theta \ln x - \ln \Omega}{d}\right]^2\right).$$

A numerical analysis of expressions (4) make it possible to connect temperature T_p and characteristics of the absorption peak form with parameters of elementary relaxators τ_0 , U_0 and D in materials with defects. It was found that the ratio of the derivatives with temperature of the functions $\mu_2^{(+,-)}(\theta, \Omega, d)$ in the inflection points has the identical value

$$K = -\max\left[\frac{\partial \mu_2^{(+,-)}}{\partial \theta}\right] / \min\left[\frac{\partial \mu_2^{(+,-)}}{\partial \theta}\right],$$

which has an extremely strong dependence on the Ω , but is practically independent of the dispersion parameter d and admits the analytical approximation:

$$K(\Omega) = 1 + 10/(\ln \Omega)^{\sqrt{2}}. \quad (5)$$

Using this formula we can obtain the parameter τ_0 from the analysis of only form of the peak, not resorting to experiments with change of the frequency ω . The relations which make it possible to determine values of the initial activation energy U_0 and its variance U_0 using the experimental values of Ω and the measurements of the temperature T_h and width of the peak T_h , have the following form:

$$U_0^{(+,-)} = \left(\frac{k(\ln \Omega)^3}{(\ln \Omega)^2 \pm 2}\right) \cdot \left(T_p \pm \frac{2T_h}{\ln \Omega} + \sqrt{T_p^2 \pm \frac{4T_p T_h}{\ln \Omega} + 2T_h^2}\right), \quad (6a)$$

$$D^{(+,-)} = \frac{k(\ln \Omega)^2}{\sqrt{2}((\ln \Omega)^2 \pm 2)} \cdot \left(-T_p + T_h \ln \Omega - \sqrt{T_p^2 \pm \frac{4T_p T_h}{\ln \Omega} + 4T_h^2}\right). \quad (6b)$$

References

- V.D. Natsik, P.P. Pal-Val, L.N. Pal-Val, and Yu.A. Semerenko, Low Temp. Phys. **25**, 558 (1999)
- V.D. Natsik, P.P. Pal-Val, L.N. Pal-Val, and Yu.A. Semerenko, Low Temp. Phys. **26**, 522 (2000)
- V.D. Natsik, P.P. Pal-Val, L.N. Pal-Val, and Yu.A. Semerenko, Low Temp. Phys. **27**, 404 (2001)

THERMAL CONDUCTIVITY RESEARCH OF POWDER AND SUPERHARD MATERIALS BY SOLVING OF HEAT CONDUCTION INVERSE PROBLEMS

Isayev K.B.

Francevich Institute for Problems of Materials Sciences NAS of Ukraine, Kyiv, Ukraine

The development of a science and engineering has required significant volume for knowledge of thermophysical properties of substances and materials. Without them it is impossible to execute practically any designer or technological development, especially in conditions of large gradients of temperatures. One from the major characteristics in this plan is the thermal conductivity (TC), which is a fundamental characteristic of substances and materials. It determines carry of a heat in a material, and thus the character of a temperature field in products from it.

It is possible to divide all existing methods of thermal conductivity determination, conditionally into two groups. The traditional methods of research TC [1], such as stationary method, various pulse methods, methods of monotone heating etc concern to the first group. From all realized methods we select two: a stationary method and method of pulse laser heating. In modern researches of materials they are used today more, than other methods. The first method is more exact and it allows immediately determine the thermal conductivity of materials. However its realization requires a lot of time, with help of this method it is impossible to determine thermal conductivity of materials, in which at heating the various physical chemical processes take place, it does not allow to investigate influence of heating rate to thermal conductivity etc. The pulse laser method (for example, method of temperature waves, installation of the corporation "Murata", Japan) research thermal physical characteristics of materials requires for its realization a sample with a small sizes, this method cannot be used for research powder and high-porous materials. The marked methods require creation expensive and frequently complicated equipment, though their mathematical apparatus is rather simple, especially for a stationary method.

The methods for determination TC, based on an experimental temperature field (generally one-dimensional) in samples of a researched material

and methods for solving of heat conduction inverse problems (HCIP) concern to the second group of methods.

The first group of methods for research TC of materials practically is absent in Ukraine. As to the second group, it is necessary to mark, that in Kiev and Kharkov there are scientific schools, in which the various methods of solving HCIP are developed. However, only some of them were used for research thermophysical properties of materials. Usually their authors limit oneself to demonstration of the methods capabilities on model temperature fields.

In this activity the engineering (methodology) of thermal conductivity research for various materials (ETCR) is offered. It consists of several stages. The first stage consists of a design development (or its adaptation) and manufacturing of heatreiver (sample with temperature sensors) from a researched material. Further there is a stage of its tests in conditions of one-sided heating. As a result of these tests are the experimental temperature fields in samples of a researched material. As a result of solving HCIP we obtain temperature dependence of this material thermal conductivity in frameworks of mathematical model initial selected.

The experimental information (temperature fields in samples of researched materials), additional information (data about specific heat and density of a material, distance of thermocouples from heating surface of heatreiver etc) and also the results of the solving IPHC come in a database. All this information is used for the analysis of different factors influence on thermophysical properties of a material, and also for correction of mathematical model of heat and mass transfer in a researched material in case of need.

In the given activity the designs of heatreceivers (HR) for powder and superhard materials are adduced. For powder materials [2,3] the researched powder is covered in a thin-walled tube, which thermal conductivity either is closed to thermal conductivity of a researched material, or it is more

then that one. One end (not heated) of this tube is closed by the piston, which allows to change volume of a powder. In a tube on a diametrical plane four slots (up to a half of diameter) are made, in which the thermocouples are stacked. Also other way of thermocouples seal is possible. Instead of a slot in a thin-walled tube two apertures are drilled till its diameter, into which the thermocouple is inserted.

After filling of a tube by a powder it heated end is covered by poultry netting (for example, nichrome). This net executes some functions. It passes gaseous products, which is extracted at heating of a researched powder by the concentrated radiation (for example, solar), equalizes temperature of a heated surface, and also it can serve as the heater at passing under it an electric current. A lateral area of a thin-walled tube are heat-insulated. For powders, which at heating do not extract gaseous products, instead of a net "cork" of a material with high thermal conductivity (copper) is used.

In a design HR for a superhard materials (hexanite-R, polycrystalline diamond etc) its sample consists of four disks [3,4]. On one flat surface of each disk on diameter with the help of the laser the flutes by depth 0.2-0.3mm and width 0.2mm are made. In these flutes the thermocouples BP5/20 (diameter of electrodes is 0.1mm and they are coated with a dioxide of a yttrium). The thermocouple in a flute is pressed with help of a copper powder. After seal of thermocouples the disks of an investigated material stick together by high-temperature glue. The copper disk is pasted to the first disk of an investigated material. Further, the pasted together sample covers by two layers of silica filament. The prepared thus sample places into the copper bush (tube), which are heat-insulated. The copper disk serves for equalization of a heat flow going to a sample, and the copper bush prevents outflow of heat from a lateral area of a sample of an investigated material and precludes the violation of one-dimensional temperature field in it.

The connection of superhard material disks was conducted with the help of glue, that after tests the disks could easily be carved out from each other and to use further for production of a cutting tool. In spite of the fact that the thermal conductivity of glue is much lower than this characteristic of a superhard material, however because glue interlayer has small depth its thermal resistance

insignificant and does not influence on result of determination TC.

For obtaining temperature fields in heatreceivers, described above, any heater ensuring one-dimensional heating of all surface of butt end HR can be used as a source of a heat. It can be a melt of metal, concentrated solar radiation, different high-temperature jets etc.

The experimental temperature fields in samples of investigated materials are the base information for determination of theirs TC by solving HCIP. For determination of temperature dependence of materials thermal conductivity in this activity the method of solving HCIP, designed in ITTF NANU by P.G. Krukovsky, was used [5].

The results of experimental determination of a temperature field in a sample of hexanite-R, and also results of determination of temperature dependence of its thermal conductivity are adduced. The matching with the literary data is held.

Introduced in the given activity the technology also was successfully applied and for research of thermal conductivity of heat-shielding materials with organic resins, compositions on the basis of aluminium-silicon, high-porous blast-furnace slag etc.

References

1. Compendium of Thermophysical Property Measurement Methods. Vol.1. Survey of Measurement Techniques. Ed. Maglic K. D. e.a. London. Pergamon Press, 1984. XVI, 789p.
2. Isayev K.B. and Schur D.V. Study of thermophysical properties of metal-hydrogen system. *Int. J. Hydrogen Energy*, Vol. 21, No. 11/12, pp.1129-1132, 1996.
3. Isayev K.B. Designs of heat receiver for determination of one-dimensional temperature fields in compact and powder materials. *IV Minsk Int. Forum: Heat/Masstransfer-2000*, 3, 394 (2000) (in Russ.).
4. Isayev K.B., Bochko A.V., Lapteva A.K. e. a. Investigation of Thermal Conductivity of Hexanite-R by Solving of Ill-Defined Problems. // *Proceedings of the 1998 Powder Metallurgy World Congress*. Granada, Spain, October 18-22 1998, pp.119-123.
5. Krukovsky P.G. Universal approach to solution of inverse heat-transfer problems (method and software). *30th National Heat Transfer Conf.*, N. Y. (1995), ASME (UEC), 10, 107 (1995).

COMPLEX APPROACH TO ASSESSMENT OF FAILURE MECHANISMS OF STRUCTURAL MATERIALS CONTACTING WITH VISCOUS AGGRESSIVE MEDIUM

Kolotilkin O.

Zaporozhye national technical university, Zaporozhye, Ukraine

Modernization and creating new equipment of high efficiency is one of the reserves in improving the productivity of equipment. But along with increase in productivity the probability of damage and wear of separate parts and assemblies of equipment is sharply growing.

In glass industry, a glass shaping tooling is the basic operational unit of the equipment for processing viscous, chemical active silicate melts and the quality, prime costs of goods produced and efficiency of production equipment by its reliable and durable operation. Analysis of equipment performance at glass plants has proved that glass shaping equipment down time because of change-over of premature failure of tooling makes 30% of yearly service life of equipment that does not meet modern production requirements. Glass shaping tooling of modern machines for manufacturing articles from glass mass comprises rather large group of parts, which at different stages of production process have its peculiarities of operation and character of a damage. Different conditions of tooling service define the use of various structural materials for their manufacturing. For example knives for cutting off the glassmass portion is usually made from rapid steels. It is conditioned by necessity of providing a good quality cut off of molten glass portion with knives working over prolonged periods that is achieved through increased heat-resistance of rapid steels.

To assess physico-chemical and physico-mechanical processes occurring in a zone of contact of metal with silicate melt it has been suggested to research such characteristics as angle of wetting θ , a coefficient of adhesion of silicate melt to metal A , roughness of surface of R_a metal after periodic contact with aggressive medium and the speed of thermochemical erosion of v structural materials in this medium along with mechanical characteristics, viscosity of failure and thermal resistance of alloys.

A new methodology has been worked out for determining mentioned above criterions. For researching the speed of thermo-chemical erosion the installation, was elaborated. It's sample holder was made with additional pipes supplying cooling

water directly to 10x10 x20 mm samples being researched. This prevents samples from being overheated and adhesion of glassmass to them, providing, in this way, the possibility to research structural materials of different heat transfer.

It was suggested to assess the roughness of samples before and after the contact with a silicate melt with the help of highly sensitive profilograph-profilometer with radius of instrument point feeler equals to 0,002 mm and a force at feeling the surface not exceeding 1,0 N.

Wetting is one of the important factor of reliability of structural material for glass shaping tooling. Glass samples of $5 \pm 0,25$ mm diameter and $5 \pm 0,25$ and samples of the material being researched of $20 \pm 0,5$ mm diameter and $10 \pm 0,5$ mm height were used to determine wetting. Wetting was determined by modern installation additionally fitted with heat-insulative screens to prevent distortion of a drop contour when fixing on a film, plumb bob for alignment of sample and system of fine gas purification with respective adsorbents and catalysts. A drop of molten glass was fixed with a help of camera and wetting angle θ was measured on photo enlarged 5 times with microscope, accuracy $\pm 1^\circ$. The method of quantitative assessment of adhesion of melt glass to metal has been proposed for the purpose of widening the scope of processes occurring in a zone of contacting structural material with a viscous melt. Proposed method resides in analysis of coefficient of adhesion A , being determined as ratio of surface area on which adhesion of glassmass to metal occurred to all the surface which a drop of molten glass occupied. The instrument was elaborated on a base of microhardnessmeter to characterize the damage and adhesive properties of oxide layers on materials surface after contacting with glassmass. Principle of operation of the instrument is based on pressing in the revolving around its axis roller into oxide layer. To improve the accuracy of results obtained, the speed of roller displacement relatively to the sample being researched is limited to 1 mm/min and force pressing in the roller into oxide layer is $P=1N$ and length of measurement is 15 mm.

The influence of graphite phase in ferrous-carbon alloy on sensible heat, physical mechanical, and service properties has been studied. It was revealed that with increase of graphite phase quantity from 2,1 up to 18,3 volumetric percent heat conduction increases by 78 %. At the same time surface area of failure with graphite increases from $9 \pm 0,5\%$ to $90 \pm 0,5\%$, so alloy failure occurs mainly in graphite inclusions that explains deterioration of mechanical properties and viscosity of failure. It was found that iron wetting with glass mass, roughness and velocity of thermochemical erosion rises respectively to 65%, 412,5% and 292% with an increase of graphite phase quantity.

The analytical task of determining ultimate strength of heterogeneous material (ferrite + graphite) with growing carbon content from 0,48 up to 4,02% has been solved. It was shown that the failure character of iron-carbon alloys at loading is related to concentration of stresses at points of graphite inclusions. Experimentally it was proved, that when loading at points of graphite inclusions microzones of plastic deformation are being formed. Using numerical-analytical method of finite elements, analytical task in frames of theory of plasticity has been solved enabling to determine sizes of plastic deformation zones which are related to size and shape of inclusion, load and elastoplastic characteristics of inclusions and metallic matrix. Relationship between microdeformed metal factor and parameter of inclusion shape has been ascertained.

It is shown that with the increase of parameters of inclusion shape the share of microdeformed metal grows with exponential relationship.

The idea of cast iron failure mechanism on periodic contact with glassmass melt has been widened. It was found that cast iron wetting with glassmass is related to shape and roughness and velocity of thermochemical erosion to shape and sizes of graphite inclusions. The mechanism of damage of cast iron with different degree of alloying has been studied. It is proved that graphite has a dominant role in failure and formation of cast iron properties regardless of alloying degree. On basis of analysis of regressive relationships of proposed criteria of durability to chemical composition of cast iron, optimum combinations of concentration of carbon and silicon providing required level of mechanical and service characteristics for definite conditions of tools parts operation have been found. It was found that at simultaneous alloying of cast iron with chromium (0,4...0,6%) and aluminum (0,4...0,6%) strength, viscosity of failure and thermal resistance increase that is associated

primarily with finer structure of perlite and relatively low graphite participation in failure. Finer structure of perlite and presence on cast iron of oxide films with chrome and aluminium base offer minimum values of roughness, wetting, adhesive factor, velocity of thermochemical erosion and better resistance to failure of oxide layers. It has been proved the copper content in cast iron should be within limits of 0,15...0,3% to increase heat conductivity of cast iron for the purpose of extraction of heat from working surface of glassmoulding tool. On basis of results obtained compositions of cast iron for parts of glassmoulding tools working in conditions of thermochemical erosion, thermocyclic and mechanical loads have been obtained. Relationships describing the influence of chemical composition of cast high speed steel for knives fragment of glassmass to suggested criteria of reliability and durability have been established. It is shown that carbon content of 0,85-0,95% provides optimum combination of mechanical, operational and technological properties of steel. It has been proved that increasing content of tungsten, molybdenum and vanadium by 5% enhances coefficient of adhesion by 117,4%, 183,3% and 157%, breakage of oxide layers – by 135%, 15% and 55% and roughness – by 293,3%, 206,7% and 220,4% respectively. It has been found out that concentration of tungsten (1%), molybdenum (3%) and vanadium (3%) decrease to maximum the velocity of thermochemical erosion as a consequence of leveling off carbide heterogeneity, desintegration of carbide phase and decrease in electrode potential between carbide phase and metal matrix. On the basis of these obtained results steel has been elaborated for manufacturing knives with prolonged operational resource.

Relationships of influence of basic alloying element of copper, self-fluxing elements of boron and silicon as well as calcium and cerium modifiers to regularity of structure formation and creating mechanical, operational and technological properties of built-up metal on a basis of nickel have been established. It has been proved that silicon content in nickel alloys with 0,5...1,5% of B should not exceed 2% that provides for minimum coefficient of adhesion of glassmass to built-up metal. It has been proved that addition of 12...15% of Cu to nickel alloy with boron and silicon enables decreasing in roughness and adhesion factor. Increase of copper content up to 30% improves the adhesive strength of built-up metal with base one and thermal resistance respectively.

COMBUSTION SYNTHESIS OF STABILIZED ZIRCONIUM OXIDE IN SYSTEM $\text{ZrO}_2\text{-Y}_2\text{O}_3\text{-MgO}$

Hashkovsky S.V., Shilova O.A.

Institute of Silicate Chemistry of Russian Academy of Sciences, St. Petersburg, Russia

Zirconium oxide excels a lot of ceramic structural materials in respect of such important characteristics as high mechanical strength, heat resistance, low heat conductivity, chemical durability and unique electro-physical properties.

Precursor of zirconium ceramic materials, as a rule, is stabilized zirconium oxide. It is known that traditional process of synthesis stabilized ZrO_2 is of long-time character and proceeds at high temperatures, demanding the big power expenses.

Here the opportunity of preparing stabilized zirconium in system $\text{ZrO}_2\text{-Y}_2\text{O}_3\text{-MgO}$ in a mode of combustion synthesis is considered.

The tableted mechanical mixture consisting of powder-like ZrO_2 , Y_2O_3 and metallic Mg was used as a starting composition. The synthesis was carried out in a quartz reactor in atmosphere of oxygen at temperature 800°C .

It was shown using visual examination that process of component interaction has active character and occurs in short-term intervals with a large heat release. The samples prepared looked like fused glassy substance.

X-ray phase analysis was carried out using X-ray-diffractometer D-500/HS (Siemens). It is determined that reaction products consist of large amount of zirconium dioxide of cubic phase and a small amount of magnesium oxide (Fig. 1B). Both the electron probe microanalysis and scanning electron microscopy studies was carried out using Camebax microanalyzer. There are the presence of the features of the structural relief inhomogeneity as well as synthesis products in the form of both a globe and globule on the surface (Fig. 2 and 3). The latters are connected, probably, to a character of interaction of the components in oxygen atmosphere and the techniques of the mixture kindling.

In the following experiment the part of metal magnesium was replaced with magnesium

perchlorate. The synthesis was carried out in the steel reactor under conditions of static environmental stress applied to a sample.

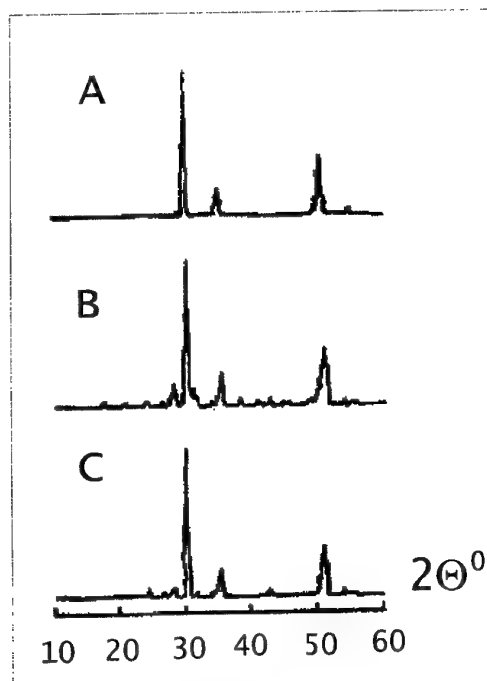


Fig. 1 Rontgenogram describing phase composition of products of component interaction in system $\text{ZrO}_2\text{-Y}_2\text{O}_3\text{-MgO}$ prepared by means of combustion synthesis.

A – a reference sample of stabilized ZrO_2 prepared by traditional methods of ceramic technology.

B – a sample of stabilized ZrO_2 prepared from mix of powder-like ZrO_2 , Y_2O_3 and metallic Mg in an atmosphere of oxygen by means of combustion synthesis

C – a sample stabilized ZrO_2 prepared from mix of powder-like ZrO_2 , Y_2O_3 and metallic Mg in an atmosphere of oxygen by means of combustion synthesis under conditions of static environmental stress.

The reaction was initiated by a supply of heat of tungsten filament. The process of interaction of the components had explosive character with allocation of light-end products of decomposition of magnesium perchlorate.



Fig. 2. A fragment of the sample surface with the globular formations.



Fig. 3. A fragment of the sample surface with the teardrop-shaped formations.

The data of X-ray analysis of the products of interaction evidenced that they consist of zirconium dioxide of a cubic phase and are characterized a presence of magnesium oxide traces (Fig. 1C).

STRUCTURAL - PHASE TRANSFORMATIONS AND DIFFUSION OF NITROGEN IN SUBSURFACE AREAS OF ION ALLOYED MOLYBDENUM

Bodnar O.B., Bdikin I.K.⁽¹⁾, Aristova I.M.⁽¹⁾, Mazilkin A.A.⁽¹⁾, Zamalin E.Yu., Pronina L.N.⁽¹⁾

Moscow State Academy of the Instrument Engineering and Information

⁽¹⁾Institute of Solid State Physics, Russian Academy of Sciences

Purpose of the given research is to study features of structure, properties and diffusion in subsurface layers of a monocrystalline foil of molybdenum after implantation by ions of nitrogen. The technology of ion implantation opens opportunities for changing microstructure and properties of a surface

Experimental

The paper concerns structure investigation of subsurface layers of a molybdenum monocrystalline foil. The initial samples before implantation had orientation of a plane of the surface parallel to a (001) crystallographic plane. The average dislocation density in foils was about 10^8 cm^{-2} . The implantation dose was $5 \cdot 10^{17} \text{ cm}^{-2}$, and energy of implantation was 50 and 100 keV. Diffusion annealing of samples was carried out at temperature 800 – 900°C. Change of surface concentration of nitrogen in ion alloyed molybdenum was investigated by means of Auger electronic spectroscopy and SIMS technique. The estimation of the nitrogen diffusion constant was made by the time of occurrence of a maximum of nitrogen concentration at the sample surface. X-ray investigations were made using DRON-2 diffractometer with copper radiation.

Results and discussion

Technique of the diffusion characteristics of subsurface areas was developed in [1, 2] for ion alloyed materials. The basic features of this technique are to create of cupola-shaped distribution of an impurity inside a sample and to study kinetics of changes of surface concentration at the diffusion annealing. Several diffusion flows with various coefficients of diffusion were detected experimentally in ion alloyed silicon and at least one radiation defect was identified. In present work the technique of diffusion characteristics determination is applied to metals, in particular, to molybdenum.

Initial nitrogen profile after implantation was defined by SIMS with constant speed of etching of 70 Å/min. Annealing of the alloyed samples was carried out in the chamber of Auger spectrometer

with simultaneously determining the nitrogen concentration on the surface.

Fig. 1 is the experimental time dependencies of nitrogen subsurface concentration received for four various annealing temperatures.

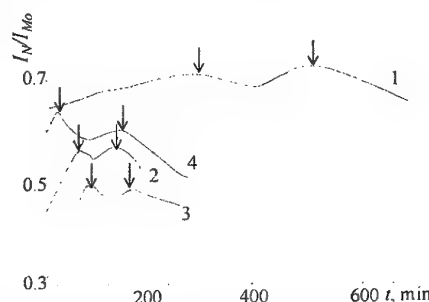


Fig.1. Time dependencies of nitrogen subsurface concentration 1 – $T=1073\text{K}$, $E=50\text{keV}$; 2 – $T=1123\text{K}$, $E=50\text{keV}$; 3 – $T=1148\text{K}$, $E=100\text{keV}$; 4 – $T=1173\text{K}$, $E=100\text{keV}$

All the kinetic curves have two maxima of concentration (shown by arrows in Fig. 1). Their occurrence is connected, apparently, to presence of additional peak of nitrogen in initial distribution [3] (Fig. 2). The additional peak of nitrogen in initial distribution connected authors [3] with the radiation induced diffusion arising because of appreciable target heating at implantation. The estimation of nitrogen diffusion constant in subsurface areas of molybdenum was carried out by a technique described in [2]. Parameters for the initial impurity distribution were defined from Fig. 2. For the main maximum these parameters practically coincide with the data reported in [4]. Nitrogen diffusion constants are given in the table. The diffusion constant D_1 is connected with annealing of radiation damages, and that of D_2 - to the diffusion by volume mechanism.

The nitrogen diffusion constants in molybdenum taken from [5, 6] are also given in the table. It is necessary to note that feature of the received diffusion constants is their low values (6 – 9 orders of magnitude) in comparison with volume diffusion constants of nitrogen in molybdenum solid solution. The solubility of nitrogen in molybdenum [7] is rather small, and

the implantation dose gives the maximal concentration in the initial distribution more than 30 at.%. That it is enough for the nitride Mo_2N formation.

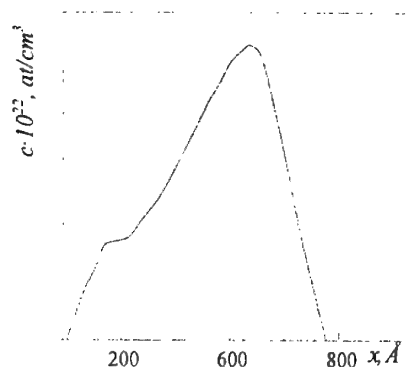


Fig. 2. The initial profile of nitrogen distribution (SIMS). $E=100\text{keV}$, $Q=5 \cdot 10^{17}\text{cm}^{-2}$, $j=20\mu\text{A/cm}^2$

Table 1. Diffusion constants

Implantation energy, keV	50 keV		100 keV		Ref.
T, K	1073	1183	1148	1173	
D_1 , cm^2/s	$2,8 \cdot 10^{-17}$	$2,1 \cdot 10^{-16}$	$7,5 \cdot 10^{-16}$	$2,9 \cdot 10^{-15}$	
D_2 , cm^2/s	$1,1 \cdot 10^{-16}$	$8,7 \cdot 10^{-16}$	$2,3 \cdot 10^{-15}$	$6,2 \cdot 10^{-15}$	
	$2,7 \cdot 10^{-9}$	$9,3 \cdot 10^{-9}$	$1,1 \cdot 10^{-8}$	$1,7 \cdot 10^{-8}$	[5]
D , cm^2/s	$9,5 \cdot 10^{-8}$	$1,7 \cdot 10^{-7}$	$6,2 \cdot 10^{-7}$		[6]

On the $\theta - 2\theta$ diffractogram (Fig. 3) for implanted molybdenum specimens additional diffraction peaks are appeared. Position of these peaks corresponds to that of (200) and (004) reflections for Mo_2N phase (141/amd). Absence of other peaks shows that the received phase has a definite orientation in relation to molybdenum crystal: $(100)\text{Mo} \parallel (100)\text{Mo}_2\text{N}$ and $(100)\text{Mo} \parallel (001)\text{Mo}_2\text{N}$. By the reflections crystallographic parameters of this phase are determined: $a=4.124\text{\AA}$, $c=8.044\text{\AA}$. It is close to the known parameters for a phase $\beta\text{-Mo}_2\text{N}$.

Thus the implanted nitrogen in molybdenum specimens is presented both as a solid solution and as nitride Mo_2N . At the ion implantation there are a lot of radiation damages in molybdenum surface layers [8]. Atoms of nitrogen apparently are condensed on them reducing their mobility. Besides according to the data of [9] at the annealing of implanted specimens with doses

$\geq 10^{17}\text{cm}^{-2}$ interfaces of the nitrides particles can serve as a drain of point defects. Then the measured diffusion constant D_1 characterizes the mobility of the radiation defect bound up with nitrogen atoms, and constant D_2 , apparently is connected to the volume diffusion of nitrogen in the nitride. In this sense the values of constants D_1 and D_2 , considerably smaller than those of diffusion in the solid solution, are seemed to be reasonable enough.

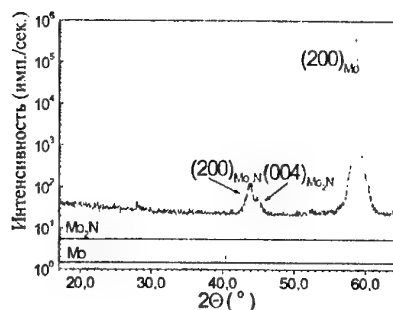


Fig. 3. $\theta - 2\theta$ diffractogram for implanted molybdenum specimens

This work is supported by Russian Foundation for Basic Research (RFFI grant 02 – 02 – 17190)

References

- [1] Zamali E.Yu. Surfase Investigations. No 6. (1995) 116-118.
- [2] Bodnar' O.B., Zamali E.Yu., Mambetov A.K.. Surfase Investigations No 7-8 (1995) 64-67.
- [3] Zamali E.Yu, Bodnar' O.B, Popova T.V. Investigations No 8 (1999) 62-65
- [4] Burenkov A.F., Komarov F.F., Kumakhov M.A. et al. Preprint No 3592/11. Moscow: Institute of Atom Energy, 1982 (in Russian)
- [5] Francfelter R. J. Chem. Phys. v. 48 (1968) 3966.
- [6] Ying-Liang M., Jin-Yihs. Acta Metal. Sinica v. 7 (1964) 68.
- [7] Diffusion in Solid Metals and Alloys, Ed. Mehrer (1990) Springer Verlag
- [8] Thompson M W., Defects Radiation Damage in Metals (1969) Cambridge, University Press[12]
- [9] Tyumentsev et al. Phizica metallov i Metallovedeniye No. 9(1992) 131 – 138 (in Russian)

STUDYING MATERIAL DEGRADATION IN THE COURSE OF OPERATION BY THE METHOD OF LM-HARDNESS

Lebedev A.A., Muzyka N.R., Voltchek N.L.

Institute for Problems of Strength of the National Ac. Sci. of Ukraine 2 Timiryazivs'ka str., 01014, Kyiv, Ukraine

The quality of monitoring the remaining life of active structures depends essentially on the reliability of the data on the current state of materials of the most stressed elements. The assessment of this state at different stages of operation is performed using the results of direct (methods of metallography, weighing, etc.) or indirect (acoustic metallography, electric resistance, etc.) measurements [1].

Application of these methods often involves large errors, because the relation between the measured parameters of a structure and the characteristics of the material properties is ambiguous. Besides, in many cases, measurements require samples of materials to be cut from structures, which is not always possible.

The hardness method based on the assumption that there exists a correlation between the characteristics of hardness and the material properties [2] has received wide acceptance in estimating the material degradation due to damage accumulation. However, in spite of the apparent merits (convenience and simplicity of the equipment, no need for breaking down a structure to fabricate specimens, etc.), the hardness method in its classical form possesses low sensitivity to many structural transformations, i.e., to the degree of damage.

As demonstrated by the investigations performed at the Institute for Problems of Strength of the National Ac. Sci. of Ukraine, some derivatives of the hardness absolute values, in particular, the dispersion of the measurement results obtained using the same instrumentation under identical conditions rather than the absolute values themselves, are more representative for the correlation with the structural state. With the availability of the necessary data set on the hardness of the material studied, the dispersion of its values can be inferred by the parameters of the distribution law describing this dispersion. It turned out that Weibull's distribution [3] widely used in the mechanics of materials, in particular, in elaborating static theories of strength, is the most physically justified law. This distribution contains

the parameter m , i.e., the coefficient of homogeneity describing the degree of dispersion of the characteristics of the property under study. Its determination involves Gumbel's formula [4] transformed into the following form applicable to hardness testing:

$$m = 0.4343d_n \left[\frac{1}{n-1} \sum_{i=1}^n (\lg H_i - \lg H)^2 \right]^{-1/2},$$

where d_n is the quantity determined depending on the number of measurements ($n > 15$) and H is the mean hardness value.

The larger values of the coefficient m correspond to the low values of the dispersion of the hardness characteristics and, therefore, to a better arrangement of the structure and low degree of damage, and vice versa. It should be noted that the level of the characteristic dispersion of the sought property, including hardness, can be matched by other statistic criteria, in particular, the confidence interval, variation coefficient, and others [5].

The above method can be used in studying the non-localized damage accumulation due to operation under conditions of long-term static or cyclic loading as well as under short-term loading depending on the level of plastic strains. This statement is evidenced by the experimental data described below, which were obtained in operational development of the method.

Hardness of the materials was determined by a standard procedure using Vickers' diamond pyramid machine. Indentations were made by a diamond pyramid with a vertex angle of 136° and the load on indenter 150N.

The investigations were performed on three steels in the initial state after a certain operating time: pipe steel 13123 produced in Czechoslovakia after being in operation for a long time in the system of Dashava - Kiev gas

pipeline (a pipe of $\varnothing 508 \times 9.5$ mm), a similar domestic pipe steel 17GS after being in operation under conditions of cyclic loading, and structural steel 20KhN3A after short-term static loading to various levels of deformation.

The results of the investigation revealed that, after long-term (during 48 years) operation, the hardness of steel 13123 changed by about 9%, whereas the value of the coefficient of homogeneity, which characterizes the degree of the material homogeneity, decreased almost three times and this decrease was the largest on the inside of the pipe.

Analogous results, which point to a higher sensitivity of the characteristics of dispersion of the hardness data to the operating time as compared to the average values of the hardness absolute magnitudes can be observed under conditions of cyclic loading. The investigation of steel 17GS after being in operation under conditions of alternating bending to fracture at $\sigma_u = 35$ MPa and $N_u = 0.57 \cdot 10^7$ cycles and without fracture at $\sigma_u = 28$ MPa and $N_u = 10^7$ cycles, similarly to the case of long-term static loading, revealed insignificant increase in hardness. In this case, the contribution of the level of stresses to the increase in hardness is more significant than that of the accumulated operating time. Changes in Weibull's coefficient of

homogeneity are more appreciable and point to the fact that the process of damage accumulation was more intensive at a stress of 35 MPa and at the instant of fracture its intensity was half of the initial one. At a stress of 28 MPa its intensity decreased by no more than 10%, though the material was subjected to 10^7 load cycles.

The accumulation of damages in the material is also well correlated with Weibull's parameter under short-term static loading of steel. Similarly to the case of long-term static and cyclic loading described above, in the course of static short-term deformation hardness does not practically change, whereas the characteristic of dispersion of its values (Weibull's parameter) changes appreciably and the rate of decrease of the latter grows with increasing deformation.

The results described above show that the method of LM-hardness, being highly informative in terms of the degree of damage accumulated in the material, does not require high qualification of the operator and can be realized directly on the object under investigation with little if any damage done to the state of its surface.

REFERENCES

1. Drozd M.C. *Determination of Mechanical Properties of Metals without its Fracture* (in Russian). Metallurgiya, Moscow, 1965. -pp. 147-156.
2. Makhutov N.A., Zatsarinny V.V., Bazaris Z.L., et al. *Statistical Regularities of Low-Cycle Fracture* (in Russian). Nauka, Moscow, 1989.-253 p.
3. Weibull W.A. A statistical distribution function of wide applicability // *J. of Applied Mechanics*.-1951.-vol.18.-No.3.-p. 293-297.
4. Gumbel E. *Statistics of Extreme Values* (in Russian translation). Mir, Moscow, 1965.-450 p.
5. Stepnov M.N. *Statistical Methods of Processing the Results of Mechanical Tests* (in Russian): Handbook.-Mashinostroyeniye, Moscow, 1985.-232 p.

VISUALIZATION OF BORON DISTRIBUTION IN MOLYBDENUM ALLOYS BY PARTICLE-TRACKING AUTORADIOGRAPHY

Fumio MORITO*, Alexander V. KRAJNIKOV⁽¹⁾ and Hideo SAITO⁽²⁾

National Institute for Materials Science, Tsukuba, Japan

⁽¹⁾Institute for Problems of Materials Science, Kiev, Ukraine

⁽²⁾Chiba Institute of Technology, Funabashi, Japan

We have been studied that mechanical properties of molybdenum alloys were improved by a small amount of boron addition [1-4]. In order to understand the state of boron in the matrix, the role of boron and its mechanism, we investigated boron distribution by particle-tracking autoradiography (PTA) [5,6]. To our lesser knowledge, it is for the first time that we could succeed in visualization of boron distribution in molybdenum alloys by means of α -rays tracked etching method using thermal neutron irradiation. In the PTA analysis, fission reaction of the isotope, ^{10}B , takes place when subjected to irradiation of the thermal neutron: $^{10}\text{B} + ^1_0\text{n} \rightarrow ^4_2\text{He} + ^7_3\text{Li}$. The capture area of this reaction can be used as a guide for detecting the existence of boron in a material.

Fig. 1 shows the PTA micrograph of Mo-2.5 ppm B. The black dots corresponded to the etched pits in cellulose acetate detector films. The densities of these dots in the local microstructure were directly proportional to the boron concentration in this area. There were three patterns of the black dots: One was that the dots uniformly distributed in the material, the second was that the dots formed in a black cluster and the third was that the dots clearly existed along grain boundaries. The first pattern corresponded to the boron dissolved in the matrix of the material. The second corresponded to the boron existing in a boron-containing phase. The third corresponded to the boron segregated to grain boundaries. As the boron content increased, the portion of the cluster significantly increased. We also found out that even in molybdenum containing as low as 0.02 ppm B, some clusters still existed. This suggests that the boron rich phase formed very easily in molybdenum

containing boron. As the bulk boron increased, the density of the dots, uniformly distributed in the matrix, decreased. This demonstrates that the content of boron dissolved in the matrix decreased as the bulk boron content increased. Borides with molybdenum in fine needle-like precipitates were also recognized in molybdenum containing more than 50 ppm B.

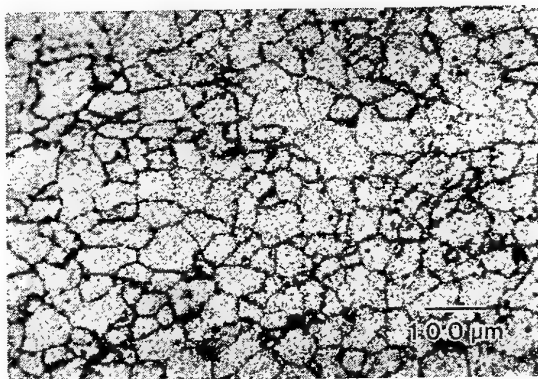


Fig.1 PTA micrograph of Mo-2.5 ppm B.

References

1. F. Morito, Colloque de Physique, C1-51(1990), 281.
2. F. Morito, Surface and Interface Analysis, 15(1990), 427.
3. F. Morito, Scripta Mat., (2002), to be published.
4. F. Morito, T. Noda and A. V. Krajnikov, Proc. Int. Conf. Science for Materials 2002.
5. F. Morito and H. Saito, Scripta Mat., (2002), to be published.
6. H. Saito and F. Morito, ISIJ Int., (2003), to be published.

SIMULATION OF THE CONCENTRATION PROFILES USING AUGER ELECTRON-SPECTROSCOPY AND SECONDARY ION MASS SPECTROMETRY

Vasylyev M.A., Sidorenko S.I.,⁽¹⁾ Voloshko S.M.,⁽¹⁾ Vilkova N.Yu.,⁽¹⁾ Tkachuk A.A.

Institute of Metal Physics NAS, Kiev, Ukraine

⁽¹⁾National Technical University of Ukraine "KPI", Kiev, Ukraine

The calculation of the diffusion coefficients is conducted by a method of simulation in the thin-film system Cu-Ni on experimental concentration profiles obtained by the method of Auger Electron-Spectroscopy using the diffusion model [1] and solution of the Fick second equation for the n -layer system ($n=2$) finite depth. In this model the difference of the diffusion coefficients of components in the different contacting layers is allowed, therefore to definition were subject for other investigated temperatures of an four parameters: D_{11} , D_{22} - self-diffusion coefficients of copper and nickel; D_{12} , D_{21} - partial diffusion coefficients of copper in a nickel and nickel in copper accordingly.

With the purpose of finding the values of the partial diffusion coefficients and the self-diffusion coefficients as much as possible approximating parent distributions obtained within the framework of indicated model, to experimentally found, their adjustment with using of the reliability R -factor. The reliability criterion was determined as follows

$$R = \sum_i \frac{1}{C_{\min}} [C_E - C_T]^2,$$

where C_E , C_T - experimental and theoretical values of the concentration, and C_{\min} - minimum experimentally observed concentration.

The experimental ($T = 573$ K, $\lambda = 900$ eV) and the theoretical concentration profiles at different values of the diffusion coefficients for a thin-film system Cu-Ni with thickness of layers about 100 nm were received. The values of the R -factor conforming to different combinations of a self-diffusion coefficient of copper (D_{11}) and a partial diffusion coefficient (D_{12}) of copper in a nickel (Fig. 1) are calculated also.

The optimization of the calculated values was conducted by a method "network search" in the supposition, that the R -factor is a quadratic function D_{11} and D_{12} in neighborhood of some minimum value R_{\min} . The maximum similarity between the calculated and experimental concentration curves is observed at following

values of diffusion coefficients: $D_{11} = 2 \cdot 10^{-14}$ cm²/s and $D_{12} = 3 \cdot 10^{-13}$ cm²/s ($R_{\min} = 0,082$).

The self-diffusion coefficients Cu and Ni, and also partial diffusion coefficients of the copper atoms in a layer of a nickel and nickel in a layer of copper annealing are similarly calculated. The obtained data for a case of a maximum similarity experimental and theoretical curves testify to predominance of a diffusive flow Cu as contrasted to Ni. The self-diffusion coefficients and partial diffusion coefficients of components of thin-film systems Cr-Cu and Ni-Au with depth of layers about 100 nm also are calculated by a method "network search" with using of the optimized R -factor for the two annealing temperatures of 373 and 573 K. From the obtained data follows, that the partial coefficients $D^{\text{Cu} > \text{Cr}}$ on the order exceed the conforming values $D^{\text{Cr} > \text{Cu}}$ in an investigated temperature region. The values $D^{\text{Ni} > \text{Au}}$ approximately in 4 times are more $D^{\text{Au} > \text{Ni}}$ and on the order - $D^{\text{Cr} > \text{Cu}}$.

The similarly simulation method can be utilised and for the calculation of the diffusion coefficients in thin-film systems under the data of a of Secondary Ion Mass-Spectrometry. The similar calculation is conducted by us for a system Ti-Al with thickness of layers 100 nm and 40 nm accordingly (Fig. 2). In this case solution of a diffusive problem for a system consisting of n -layers under condition of unlimited dissolubility of components and piecewise constant partial diffusion coefficients also utilised.

It is necessary to mark, that the system Ti-Al has the complicated equilibrium diagram, however in the region of the investigated temperatures (773 ... 923 K) and concentrations the intermediate phases miss, i.e. the unlimited dissolubility of components is observed. It was confirmed by both data of X-ray crystallographic analysis, and the behavior of the secondary ion emission, which one is responsive to change of a phase structure of the system. Thus indispensable condition for using of the indicated solution is executed.

The plots of the R -factor changes (example in a Fig. 3) are constructed at exhaustive search of values of the partial diffusion coefficient Ti in Al - D_{12} in some interval and constant value of a self-diffusion coefficient Ti - D_{11} and, to the contrary, exhaustive search D_{11} and constant D_{12} , and the outcomes of calculation R_{\min} for concentration profiles Ti are added at $T = 773$ K, $\tau = 1800$ s. To minimum value of the reliability factor $R_{\min} = 0,01$ there correspond the values $D_{11} = 4 \cdot 10^{-16}$ cm²/s and $D_{12} = 6 \cdot 10^{-16}$ cm²/s, i. e. at these values the maximum similarity between calculated and experimental concentration curves is observed. The outcomes of the similar calculations R_{\min} , D_{11} and D_{12} and for other annealing temperatures are determined. The activation energy and preexponential factor, which one for a case of a self-diffusion Ti are $Q_{11} = 17,73$ kkal and $D_{11}^0 = 3,98 \cdot 10^{-11}$ cm²/s; and for diffusion Ti in Al $Q_{12} = 4,5$ kkal and $D_{12}^0 = 1,12 \cdot 10^{-11}$ cm²/s, accordingly, were determined.

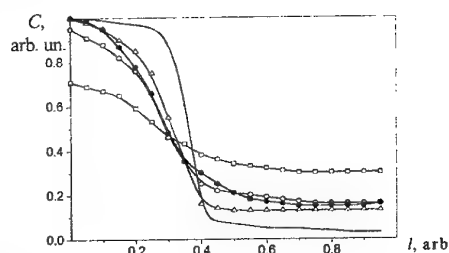


Fig. 1. Simulation of the concentration profiles in the Cu-Ni system. An experimental profile (·) and calculated at the following data:

D_{11} , cm ² /s	D_{12} , cm ² /s	R	
$1 \cdot 10^{-15}$	$1 \cdot 10^{-13}$	1,98	—
$8 \cdot 10^{-15}$	$9 \cdot 10^{-13}$	0,39	Δ
$2 \cdot 10^{-14}$	$3 \cdot 10^{-13}$	0,082	o
$5 \cdot 10^{-13}$	$2 \cdot 10^{-12}$	2,01	

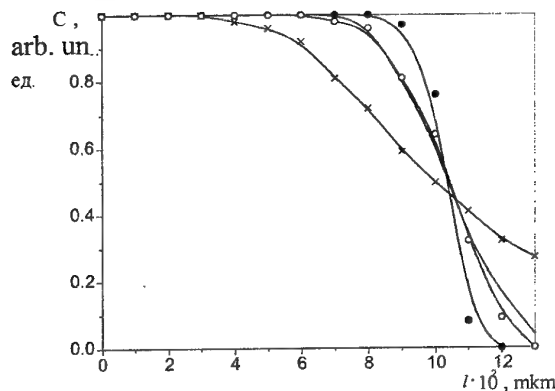


Fig. 2. The experimental concentration profile of Ti in the Ti-Al system for 773 K (—) and calculated one obtained for values: $D_{11} = 3,25 \cdot 10^{-16}$ cm²/s, $D_{12} = 4,6 \cdot 10^{-16}$ cm²/s, $R = 0,03$ (o); $D_{11} = D_{12} = 10^{-16}$ cm²/s, $R = 0,442$ (·); $D_{11} = 10^{-15}$ cm²/s, $D_{12} = 2 \cdot 10^{-15}$ cm²/s, $R = 2,42$ (x).

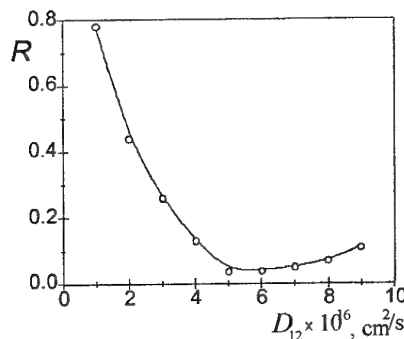


Fig. 3. Relation of the R -factor to a partial diffusion coefficient Ti in Al at fixed value $D_{11} = 5 \cdot 10^{-16}$ cm²/s.

REFERENCE

1. Berezovski A.A., Bondarchuk V.T., Sidorenko S.I. The solution of a diffusion problem for a system consisting of n - of layers of the finite depth // Mathematical research of filtration actions and thermotransfer. - Kiev: Naukova dumka, 1978. - C. 130-136 (in Russian).

Institute for Problems of Material Science, NAS of Ukraine, Kyiv, Ukraine

For aluminum alloys studied was developed atlases of molecular interferences allowing to minimize detrimental effect of interferences.

AES with spark evaporation and excitation of lines is widely used for analysis of alloys. High performance and good detection limit for light elements compared to XRF are advantages of this method. Weak point of this technique is dependence of analytical signal of sample composition and spark generator parameters. Earlier study has show that analytical signal at some generation mode is independent on elemental and structural difference in standards and samples [2]. These effects arise at power density in a spark foot up to 10^{10} W/m². Such mode results in small oxidation of the surface and formation of small grain size structure. Mathematical simulation of plasma parameters show weak dependence of electron concentration and plasma temperature of additions light ionized elements such as REE. Decrease in n_e by 5 - 10% became visible at concentrations REE of about 10% (Fig.3). Concentrations of REE in alloys studied do not exceed 0.5%.

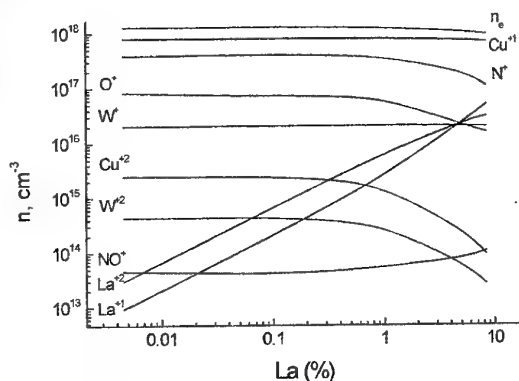


Fig.3.: Concentrations of charged particles on discharge axis against addition of REE in W-Cu composition at constant power.

Calculations show that additions of REE does not increase n_e , as it may be expected a-priori, moreover this results in clearly visible decrease of n_e . The reason of such behaviour is decreasing in electron temperature due to inelastic collisions with excitations of levels. But decrease in n_e is not so high as it may be thought taking into account exponential dependence of electron concentration of T (Saga function). The point is that simultaneously decreases effective ionization potential of the gas mixture E_{eff}^i . Combined effect of these factors results in relatively small decrease in n_e and proportionality between

concentrations of elements in sample, evaporation rate and ion concentration in plasma (Fig.3). Investigation of influence of discharge power on relative intensity of analytical lines of elements to line of Al were performed on a sample with such composition (wt.%) (Mg 3.0, Sc 0.4, Mn 0.4, Cu 2.7, Zn 9.0, Zr 0.2, Y 0.2).

Experiments show that decreasing in power ($C=0.005$ μ F) results in selective evaporation of Y, Mg, Mn. In the Fig.4 as an example is shown kinetic curves for Y.

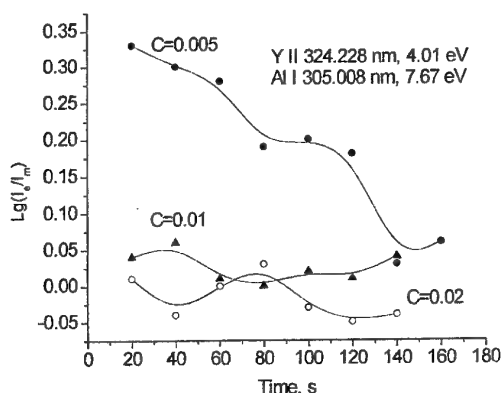


Fig.4. Relative intensities of Y and Al lines as function of discharge time.

Curves for Mg explain the same behaviour but for Mn relative intensity increases with time. In other words low power discharge performs electric etching of the surface. Such results may be used to establish correlation between structure and line intensities. Decreasing in capacity or switching on additional inductance results in structural effects. More powerful discharge, as indicates Fig.4, ($C \geq 0.01$ μ F, $L=0$) gives nonselective flush evaporation allowing to minimize structural and matrix effects.

REFERENCES

1. Курочкин В.Д. // Укр. хім.журн. -1999. - 65. -№3. - С.57-63.
2. Курочкин В.Д., Кравченко Л.Ф. // Тез. докл. конф. "Современные методы спектрального анализа в черной металлургии", Днепропетровск, 1990.
3. Kurochkin V.D. Kravchenko L.P. // High Temperature Materials and Processes. - 2000. -19. - 6.- P.427-433.

ELIMINATION OF STRUCTURAL EFFECTS AT SILICON DETERMINATION IN ALUMINUM ALLOYS USING GD-MS AND X-RAY METHODS

Kravchenko L.P., Kurochkin V.D.

Institute for Problems of Material Science, NAS of Ukraine, Kyiv, Ukraine

GD-MS and X-ray fluorescence techniques are recognized as sensitive methods for analysis of elements distribution over an ingot or for depth profiling of thin surface layers. The intensity of analytical signal strongly depends on crystallite size and phase composition especially in determination of light elements producing major amount of fluorescence radiation from thin layer of a sample. Effect of grain size is negligibly small if the following inequality is true [1]:

$$K(\mu_p(\lambda) - \mu_i(\lambda)) \ll 1, \quad (1)$$

where K is a particle size, $\mu_p(\lambda)$ - the mean absorption coefficient of a sample, $\mu_i(\lambda)$ - absorption coefficient of a phase i . This condition is especially unfavorable for silicon determination in aluminum matrix owing to the high value of $\mu_p(\lambda)$ for Si K_α radiation in aluminum (3630) and small $\mu_i(\lambda)$ for silicon K_α radiation in silicon phase (344). To meet condition (1) the grain size must be less than several microns. This is the reason why the structure of a sample to be analyzed must be as close as possible to that of the standard reference materials.

The nature of structural effects in GD-MS differs from that of X-ray fluorescence and depends on processes in glow discharge. The glow discharge plasma interacts active with the surface of a sample owing to the sputtering by Ar ions and condensation process. The sputter rate of the cathode is for 10% or more due to ions of its own material [2]. The joint action of sputtering and condensation creates a new type of the surface which grows on the initial surface. Nevertheless GD-MS system in contrast to X-ray fluorescence relatively free of structural and matrix effects. Relative sensitivity factors (RSFs) measured with use of a set of standard samples of one matrix could be used for analysis of elements in a different matrix. Our experience in analysis of various types of alloys supports this conclusions but for master alloy with 3% of Si the error of determination appears to be about 300 - 400%.

The commonly used methods for sample preparation in X-ray fluorescence based on remelting in specially designed furnace. Such methods allow to measure only bulk concentration of an element and

do not suit for analysis of elements distribution over an ingot. To preserve high spatial resolution of X-ray and GD-MS methods and to avoid errors the surface of the sample must be modified to obtain small grain size. This study presents a method for preliminary treatment of the sample surface by pulse spark discharge allowing to minimize the structural effects in X-ray fluorescence and GD-MS methods.

Analyses were carried out with use VRA-30 X-ray fluorescence spectrometer (Carl Zeiss, Jena, Germany). VRA-30 is vacuum spectrometer equipped with appropriate X-ray tube. Structural effects were studied on aluminum alloy of the following composition (wt.%): Mg - 0.67, Al - 92.08, Si - 6.0, Ti - 0.16, Mn - 0.04, Fe - 0.15 and master alloy with 3 wt.% of silicon. Samples were prepared as a ring plate 20 mm in diameter. The surface of the sample was given high-polish using the diamond paste.

For GD-MS analysis the VG9000 mass-spectrometer was used. Experiments were carried out using the flat-cell without cooling operated at 1 kV discharge voltage and 2 mA discharge current in Ar. The samples were filed to obtain a fresh surface without any sharp edges, rinsed in ethanol in an ultrasonic bath for 5 min., and finally plasma etched for 20 min. in GD source prior to analysis.

The standard materials analyzed in the course of this study were National aluminum alloy standards of the former Soviet Union. Standards had been prepared in the shape of a rod 8 mm in diameter by casting in a chilled mold. Such technology refines the grain because of high cooling rate and results in homogeneous distribution of elements.

IVS-23 spark generator was used for surface treatment of samples. This generator is used as spectra source in emission spectral analysis of metals. Time of a single pulse was about 10^{-5} s and power density in foot of plasma runs as high as 10^{10} Wm.⁻² [3]. The generator gives nonselective flash evaporation and rapid

quenching of the surface. This process is responsible for fine-grained metal structure. The thickness of flowed layer is about 20 - 50 μ depending on regime of generator.

Effects of the structure were discovered at X-ray silicon determination in aluminum alloys casted in earth mould. The size of silicon crystallites grows proportional to chill time, so the similar increase in measured values of Si was observed. For coarse crystallites (20 - 40 μ) the measured values of Si exceed the true concentrations in 200%. After spark plasma treatment the fine crystallite structure (1-2 μ) was obtained. It is worth to note that connection of even small additional inductance results in increase of discharge time and appearance of structural effects.

In GD-MS method RSF for silicon have been measured using a set of standards of various composition. The calibration graph is strait line passing through the origin. The reason of uniform values of RSF for various standards is that all of them have been produced by the same fabrication technique and have very small grain size. GD-MS analysis of #357 alloy shows no significant structural effects. But at analysis of master alloy with 3% of Si the structural effect appears to be very strong. In Fig.1 are shown dependence of measured silicon content on sputtering time. Initial values exceed the true value in 3-4 times. An equilibrium concentration of Si is established after 30 - 60 min. depending on production route of a sample.

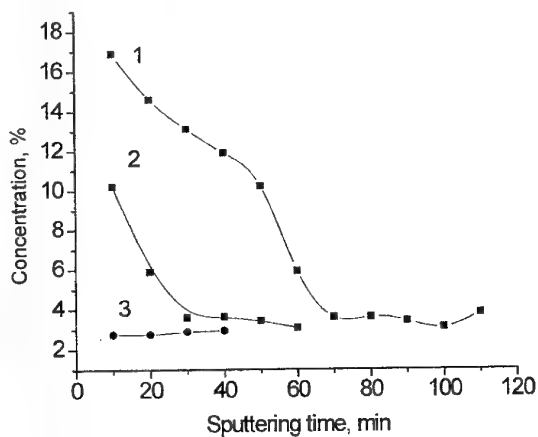


Fig.1. Sputtering kinetic of silicon from aluminum alloys. 1, 2 - master alloys before spark treatment; 3 - alloys after spark treatment.

The thickness of surface layer producing analytical signal depends on discharge parameters and like in X-ray method is about several microns.

Apparently spark plasma treatment leads to the partial dissolution of silicon crystallites in Al matrix. As indicates Table 1 spark plasma process fully eliminates structural effects.

Table 1. Influence of spark plasma process on silicon determination in aluminum alloy.

Methods	Before treatment	After treatment
Alloy #357	%	%
X-Ray	8 - 12	6.0
GD-MS	5.6	5.9
Chemical analysis	6.0	-
Master Alloy		
X-Ray	4.4	2.77
GD-MS	10 - 12	2.8
Chemical analysis	2.8	-

At this stage of investigation it is not clear why effects of structure in GD-MS show itself in master alloy Al-Si and there is no effect in more complex alloys. As it has been mentioned above, the condensation process together with sputtering by Ar^+ ions change the initial structure of the surface. The morphology of the surface creating as a result of condensation depends on nucleating centers. In some aluminum alloys with high Zn concentration a chains of crystallites grow along the grain boundary after preliminary sputtering. Such crystallites grow perpendicular to the surface and are about 20 - 100 μ in high. The crystallite growth rate controlled by dynamic equilibrium of sputtering and condensation.

Structural effects influence also on determination other elements in various matrices so method developed is promising for similar analytical tasks.

REFERENCES

1. Hunter C.B., Rhodes J.R. // X-Ray Spectrom. -1972 - 1. - P. 107.
2. M.Van Straaten and R.Gijbels, in *Application of Plasma Source Mass Spectrometry II*, ed. Grenville H. and A.N.Eaton, Cambridge, RSC. - 1993. -P. 130-139.
3. Kurochkin V.D. Kravchenko L.P. // High Temperature Materials and Processes. - 2000. -19. - 6.- P.427-433.

CERAMIC SOLID ELECTROLYTE DEVICES TO CONTROL AND MAINTAIN OXYGEN PARTIAL PRESSURE

V.A. Dubok, V.V. Lashneva

Frantsevich Institute for Problems of Material Science of the National Academy of Sciences of Ukraine, Kiev, Ukraine

Last decade large scale investigation and tests have been launched out in the field of direct electrochemical conversion of energy of fuel oxidation into electricity with ceramic oxygen-ion-conductors based on ZrO_2 . The efficiency of laboratory and pilot models of such solid ionic generators is almost twice higher than for best industrial electric generators, that makes path of intensive development in this field inevitable for modern power engineering.

Besides power engineering the solid electrolytes devices are widely using all over the world as a basis of numerous devices and instruments for measurement, control and regulation of values, bound with partial pressure and quantity of oxygen: completeness of fuel combustion and regulation of ratio oxidant / fuel in different power systems, engines, boiler etc., control of degree of steel deoxidization or contents of oxygen in melts of non-ferrous metals, control of technological processes, bound with reduction of metals' oxides or processing of different materials and workpieces in gas environment with determined oxygen contents, dosed supply of oxygen, regulation and measurement of oxygen contents in technological and scientific research installations, as well as in physicochemical and thermodynamic researches etc. The object of this report - to summarize researchers and experience accumulated in IPMS NASU in the field of development and application devices on the basis of oxide solid electrolytes. First of all, it is relevantly to remind, that the used now all over the world material for high temperature current-carrying leads of solid electrolyte power systems on the basis of doped chromite of lanthanides, was developed in IPMS NASU by prof. S.G. Tresviatsky. Under his guidance since 1962 the author of this report began study of S.G. Tresviatsky. Under his guidance since 1962 the author of this report began study of solid electrolyte devices for control of a partial pressure of oxygen P_{O_2} in laboratory measuring installations. The necessity of such devices caused by the fact that at high temperature measurements of physical properties of oxides made in equilibrium conditions of

oxide with a gas phase, the partial pressure of oxygen controls deviation of the oxide from stoichiometry, i.e. concentration of electronic defects which determine the electrical conductivity of the most oxides. Thus, the high temperature measurements of many properties of oxides are practically impossible without control and regulation of P_{O_2} .

The device developed and presented in 1963 to Scientific Council of IPMS consist of ceramic test tube made from solid electrolyte - dioxide of zirconium stabilized by calcium oxide, with gas-permeable electrodes made by burned-in platinum paste, platinum current leads and gas leads made of ceramic tubes. Solid electrolyte test tube was sealed in the open part, and the closed part of the test tube with the platinum electrodes burned-in on both sides of the ceramics was heated in special furnace up to 1000 - 1100 °C. The internal electrodes of the device was subjected to flow of gas mixture, P_{O_2} in which one it was necessary to measure, the outside electrode was in air. The tests of this device have shown its high performance and functionability in broad range of oxygen partial pressures from $2 \cdot 10^4$ up to 10^{-18} Pa. It can act also as tiny electrogenerator with short circuit current of about 100 mA. The varieties of this device were manufactured later by industry - first by Angarsk branch of OKBA, where the author has lectured on this topic. Later on the basis of accumulated experience a number of such devices and materials for them have been developed for solution of the particular technical tasks, for example: sensors for control of stainless steel deoxidization on the basis of modified solid electrolyte with diminished n-type conduction (for the Moscow Evening Metallurgical Institute), solid electrolyte materials and devices steady in melts of alkali metals (for SPU "Energy"), sensor for control of oxidation level and kinetics of reduction of metal powders (for Institute of Gas NASU), sensors for the control of completeness of fuel combustion in high-power engines (have been producing by Ukranalit for more than 10 years now), sensors with oxide ceramic electrodes and current-

carrying leads to control completeness of fuel combustion in district boilers (for Minenergo of Ukraine), and some other similar sensors and materials for them. The laboratory device for study nonstoichiometry in oxides was improved

in such way: instead of gas mixture flow through measuring volume and control P_{O_2} at input and output with solid electrolyte sensors, the internal part of ceramic test tube, sealed in the cold part, have been utilized as measuring cell (Fig.1).

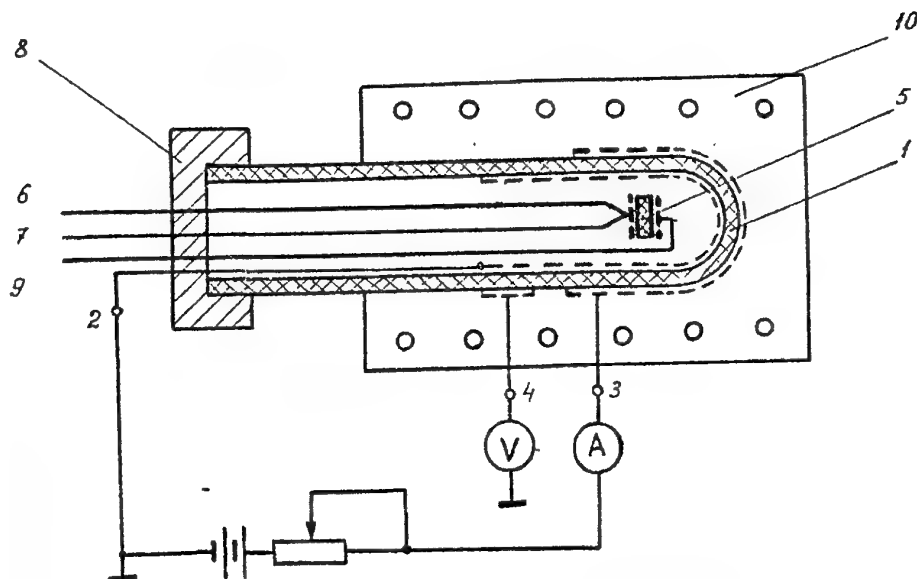


Fig.1. Ceramic solid electrolyte device for regulation and measurement of partial pressure of oxygen.

Inside the test tube 1, made from solid electrolyte with composition $0,85ZrO_2 + 0,15Y_2O_3$, the sample 5 was placed with electrodes and current leads 6,7,9 connected with measuring instrument through hermetical connector 8. The closed part of the test tube was placed into furnace 10 with platinum-rhodium heater. The regulation and control P_{O_2} in a measuring volume was made by two pairs of platinum electrodes: on internal surface of the test tube there was common electrode 2, and on outside surface - two electrodes 3 and 4. The electrodes 2 and 3 worked as the oxygen pump regulating P_{O_2} in the measuring cell, and pair electrodes 2 and 4 - as the P_{O_2} -meter. Total volume of the measuring cell was about 150 cm^3 . The described cell can be used to measure electrical conductivity of

oxides at temperatures up to 1550°C in P_{O_2} range $2 \cdot 10^{-4} - 10^{-15} \text{ Pa}$. Except the measurements, the cell was utilized also for physicochemical experiments - dosed oxidation of the suboxides and other high-melting compounds, dosed partial and full reduction of oxides etc. In particular, by pumping oxygen from a single-crystal of nickel oxide it was found that the oxide has been completely reduced up to metal and was transformed into nickel single-crystal containing about 50 % vol. of ordered nanopores. Such kind of a single-crystal Reley nickel was obtained for the first time.

As the given cell contains electric minigenerator and measuring device, on its basis the original method of estimation efficiency of solid ionic fuel cells was proposed.

PRECISION MEASUREMENT OF LATTICE PARAMETERS IN HIGH-TEMPERATURE X-RAY DIFFRACTOMETRY

Karpets M.V.

I.N. Frantsevich Institute for Problems of Materials Science of NAS of Ukraine, Kiev, Ukraine

Unknown specimen displacements are the most severe errors of an *in situ* high-temperature X-ray diffraction (XRD) method, in particular at elevated temperatures, with respect to positions of the Bragg's reflections characterized by the corresponding diffraction angles, 2θ . Nevertheless, nowadays the XRD method is a very useful tool for investigation of the behaviour of powder materials at non-ambient temperatures.

The specimen surface, which may be in the ideal position at room temperature, in general will not be in this position upon heating. Heating leads to thermal expansion, possibly in association with stress development, and the specimen surface can move. Furthermore, it is necessary to take into account the following diffractometer aberrations: the zero shift, the effect of beam penetrating into a specimen and the effect of specimen transparency.

The zero shift, $\Delta(2\theta)_z$, involves a constant shift of the peak positions over the whole 2θ range. The specimen displacement, s , leads to a peak shift $\Delta(2\theta)_d$ proportionally to $\cos\theta$ [1]:

$$\Delta(2\theta)_d = (2s/R) \cos\theta, \quad (1)$$

where R is the goniometer radius and s is positive for displacement along the perpendicular to the specimen surface. The shift diffraction angle $\Delta(2\theta)_p$ dependence of the beam penetrating into specimen effect and given by the equation:

$$\Delta(2\theta)_p = -(p/R) \sin 2\theta, \quad (2)$$

where p is a depth of X-ray penetration into a specimen. The thickness specimen, t , leads to the specimen transparency effect and peak shift $\Delta(2\theta)_t$, expressed as:

$$\Delta(2\theta)_t = (t/R) \cos\theta \quad (3)$$

It is noted that the effect of specimen transparency, which may be non-neglectable, is effectively incorporated in the specimen displacement parameter determination. The largest errors in 2θ are the zero shift and the specimen displacement. It is evident that the peak shift induced by the specimen displacement can hardly be distinguished from the zero shift for low diffraction angles. In this case, these two errors have been considered as one combined error causing a constant shift of the peak positions.

If both the zero shift and specimen displacement occur, they can be measured at constant temperature by applying standard

materials for which the true peak positions are known. It can be assumed safely that, the zero shift has not been changed when the specimen is exposed to various temperatures in the heating diffractometer chamber. This is not true for the specimen displacement.

In the present work, an *in situ* XRD method was used to study phases of the $\text{Al}_3(\text{Ti}_{1-x}\text{Zr}_x)$ alloy and to determine simultaneously both the zero shift and the specimen displacement using a heating UVD-2000 stage installed in the diffractometer. The alloys were prepared by arc melting in a purified argon atmosphere. An X-ray analysis of specimens, in as cast and grinded in an agate grinder conditions, was carried out using a DRON-UM1 diffractometer with Bragg-Brentano geometry (goniometer radius $R = 192$ mm) in monochromatic $\text{Cu K}\alpha$ radiation. A graphite single crystal used as monochromator was installed on diffracted beam.

High temperature X-ray investigations were performed in helium atmosphere. The room temperature was 293 K. The temperature deviations during measurements were within ± 2 K. A pure silicon powder (unit-cell parameter, $a = 5.43047$ Å, at 293 K), either mixed with the grinded specimen or deposited as a thin layer on the surface of the cast alloy, was used as an internal standard to determine lattice parameters. The diffraction patterns were registered by step scanning in the angle range of $2\theta = 10 - 130^\circ$. Scanning step was $2\theta = 0.05^\circ$, and the exposure time was varied from 5 to 20 s. The PowderCell 2.3 software was used to carry out a full-profile analysis of the diffraction patterns.

Calculations were made for three polycrystalline phases: two tetragonal structures D_{022} (Al_3Ti), D_{023} ($\text{Al}_3(\text{Ti}_{1-x}\text{Zr}_x)$) and FCC structure Si. Pseudo-Voigt1 function was selected as an approximating function of diffraction profiles. Varied in the process of calculation were parameters of crystalline lattice, the half-width of diffraction maximum, the texture factor, the general thermal factor, the zero shift and the specimen displacement. An XRD pattern of Si and the sample ($\text{Al}_3\text{Ti}_{0.84}\text{Zr}_{0.16}$) containing equal quantities of phases with D_{022} and D_{023} structures in as-cast state is presented in Figure 1a.

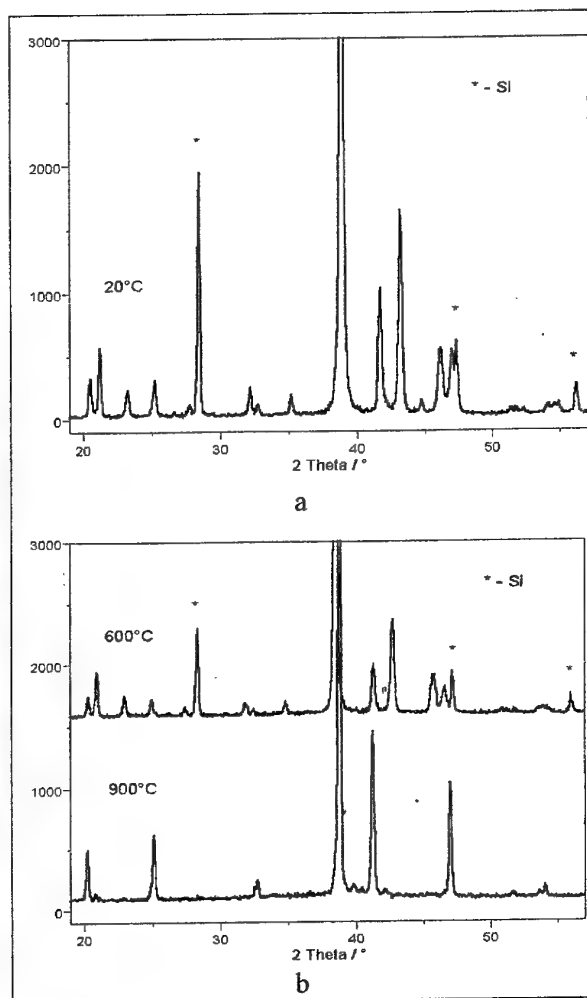


Fig. 1. XRD pattern of the sample $\text{Al}_3(\text{Ti}_{0.84}\text{Zr}_{0.16})$ with Si (*) as an internal standard at different temperatures: 20°C (a) and 600°C, 900°C (b).

In the process of all calculations the unit-cell parameter for Si was fixed. Using values of thermal expansion coefficients, silicon unit-cell parameters at different temperatures were calculated from the expression [2]:

$$a(T) = a_0(1 - 0.071 + \sum_{i=1}^3 a_i(T - T_0)^i), \quad (4)$$

where $a_1 = 1.887 \cdot 10^{-4}$ 1/K, $a_2 = 1.934 \cdot 10^{-7}$ 1/K, $a_3 = -4.544 \cdot 10^{-11}$ 1/K, a_0 is the silicon cell period at temperature $T_0 = 273$ K.

The zero shift at room temperature is determined from the peak position measurements performed with the internal standard material. This zero shift value does not change when the specimen is investigated at elevated temperature. Thus, using the zero shift determined at room temperature and the unit-cell parameter for Si $a(T)$ [cf. equation (4)], the specimen displacement is determined as a function of the temperature. In the

next step, the corrected true peak positions of the structures D0_{22} and D0_{23} are determined for each temperature. The unit-cell parameter was refined by least-squares fitting of Bragg's equation to these corrected values of the peak positions.

The calculations have shown that, at room temperature the half of the unit-cell volume of D0_{23} structure ($V_{23}/2 = 129.41 \text{ \AA}^3$) is bigger than the unit cell volume of D0_{22} ($V_{22} = 129.05 \text{ \AA}^3$). However, already at the temperature of 600°C these volumes are approximately equal (132.00 \AA^3 and 132.07 \AA^3 , correspondingly). Further, the temperature increasing up to 700°C causes the volume $V_{23}/2 = 132.45 \text{ \AA}^3$ to become less than the volume $V_{22} = 132.61 \text{ \AA}^3$.

At the same time the phase transformation of a tetragonal structure D0_{22} into another tetragonal phase D0_{23} was observed (fig.1b). When cooling, this transformation occurred in the temperature range of 600-650°C. The formation of a phase with the D0_{23} structure suggests that this transformation is accelerated by internal stresses. Therefore, a mechanism of the $\text{D0}_{22} \rightarrow \text{D0}_{23}$ phase transformation is related probably with shear processes.

It is of interest to note that during heating a powder of the $\text{Al}_3(\text{Ti}_{0.84}\text{Zr}_{0.16})$ specimen with Si up to 800°C, full disappearance of Si diffraction peaks is observed (fig.1b). In addition, the transformation of the D0_{23} structure into D0_{22} is registered by an X-ray *in situ* investigation. The same transformation has been observed also in the as-cast specimen containing a thin Si layer on its surface. The only distinction that the similar bulk-sample transformation was found to be at 100°C higher temperatures. Therefore, the silicon powder served in this case as a catalyst of the $\text{D0}_{23} \rightarrow \text{D0}_{22}$ structural transformation.

Conclusion

The utilization of an internal standard allows to determine the zero shift and displacement of the sample at elevated temperatures. This method, with simultaneous utilization of the PowderCell 2.3 software, reveals unit-cell parameter values for the specimen investigated that are equal to the true values.

References

1. Rusakov A.A. *Rentgenografiya metallov*, Moscow, Atomizdat, 1977, -479 p.
2. Touloukian, Y.S., Kirby, R.K., Taylor, R. E. & Lee, T.Y.R In *Thermal Expansion, Nonmetallic Solids, Thermophysical Properties of Matter*, Vol. 13, New York: IFI/Plenum, 1977.

INFRARED SPECTROSCOPIC RESEARCH OF STRUCTURAL CHANGES WHEN GRINDING A SILICON CARBIDE

Gilev V.G.

Research center of powder materials science, Perm, Russia

Cheap and available commercial SiC powders, as a rule, are coarse. The most simple method of producing the disperse and active powders is their crushing in various mills. Grinding the ceramic powders is accompanied with significant structural changes which render essential influence on the subsequent sintering. The grinding process data concerning kinetics of crushing and changes of silicon carbide structure and properties are insufficient.

Polytype transformations in a silicon carbide can proceed under various conditions, including various kinds of a loading, for example, shock load [1]. It is known, that when abrading the silicon carbide at room temperature there is a transition 6H \rightarrow 3C [1].

In the present work, changes of particle sizes, phase and polytype composition and structure when grinding with a hard-alloy ball mill the silicon carbide powder manufactured by Volgograd abrasive factory (fraction up to 50 microns) have been investigated.

As the data received by direct diffraction methods, in this case are difficult to interpret due to affinity of SiC polytype structures, they were complemented with studies performed by Infrared Spectroscopy, which can provide additional information on symmetry and structure of crystals.

X-ray structure analysis has shown that the investigated powder in its initial condition consists of 6H, 15R α -SiC and cubic β -SiC polytype mix, and this is a typical composition for commercial powders of silicon carbide [2]. The changes of X-ray diffraction patterns when grinding are scarcely appreciable in view of SiC polytype lattice affinity and line interference, fig. 1. The grinding influences mostly 15R polytype 0.239 nm line which intensity considerably decreases just after 5 h grinding and almost absolutely disappears in 20 hours.

The changes of powder infrared spectra, fig. 2, tab.1, also testify the structural reorganization when grinding the SiC commercial powder.

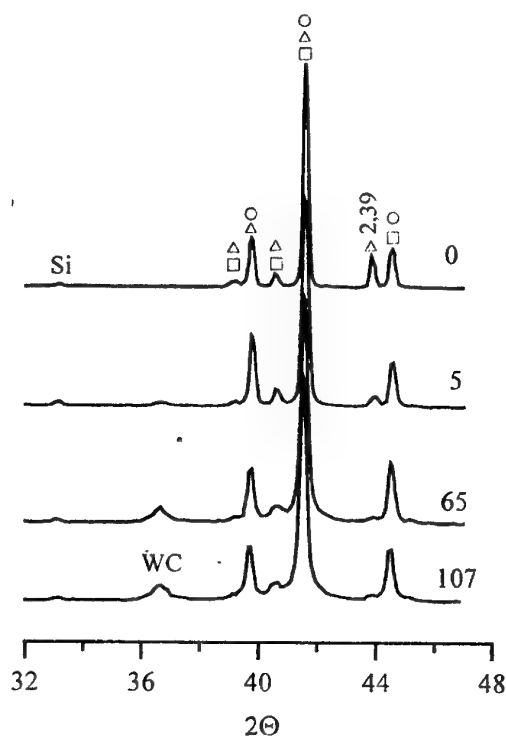


Fig.1. X-ray diffraction patterns of SiC powder after grinding in a ball mill. Figures at a curve on the right are represented a grinding time, hours. Phases: \square - 4H, \circ - 6H, Δ - 15R.

For comparison the table 2 indicates the information on number of bands in SiC polytype infrared spectra according to data [3].

As the grinding time increases from 5 up to 10 and 20 hours, the number of bands, fig. 1, tab.1 is reduced.

Numerous small intensity bands disappear, the intensity of 464, 514, 1092, 1160 cm^{-1} bands decreases, the intensity of 348 cm^{-1} single wide band increases.

The least number of 5 absorption bands corresponds to a spectrum of a sample after 44 hours of a grinding.

Table 1
Positions (wavenumbers, cm^{-1}) and intensity of absorption band in Infrared spectra of silicon carbide powders grinded in a ball mill.

Grinding Time, hours			
5	10	20	44
1164 med.	1160 med.	1160 med.	
1092 str.	1090 med.	1088 med.	
944 med.	936 med.	934 w.	940 med.
830 str.	836 str.	834 str.	842 str.
800 str.			
780 w.			
	730 med.	720 med.	
696 w.			700 med.
648 w.			
	620 w.	622 med.	624 w.
607 w.			604 med.
514 med.	528 w.		
454 str.	462 med.	462 w.	

Band intensity: med. - medium, str.- strong
w.- weak

Table 2
Number of bands in infrared spectra of a silicon carbide polytypes according to data [3]

	n *	Modes active in infrared region**	Shape
3C	2	F_1	cubic
4H	8	$3A_1, 2E_1$	hexagonal
6H	12	$5A_1, 5E_1$	hexagonal
15R	10	$9A_1, 9E_1$	rhombohedral
21R	14	$13A_1, 13E_1$	rhombohedral

* n - number of atoms in an elementary cell,

** $3A_1, 2E_1$ means the following: 3 completely symmetrical vibrations of A_1 type and two twice degenerate vibrations of E_1 type, F_1 — one three times degenerate vibration.

The same appearance of the spectra takes a place when grinding time further increases.

Trend of changes in infrared spectra and the x-ray data testify that there is a gradual transformation of 1RK, 6H polytypes existing in an initial powder into structures of less lamination: 4H and β -SiC polytype.

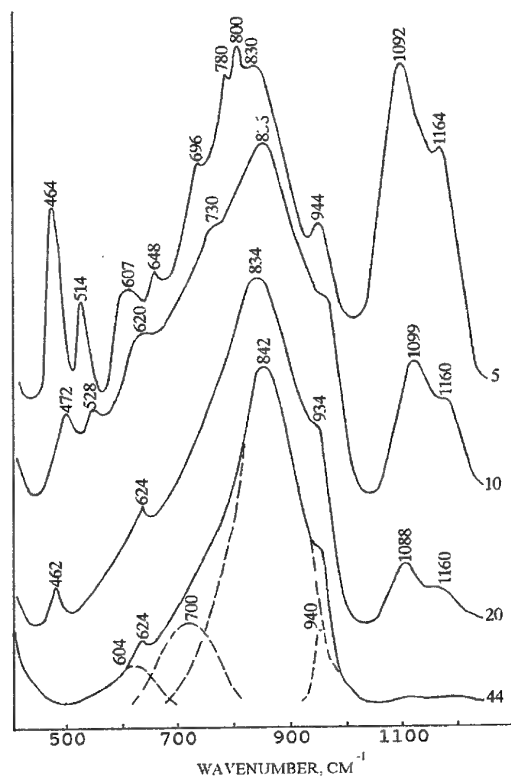


Fig. 2. Infrared spectra of a SiC powder grinded in a hard-alloy ball mill. Figures near curves represent a grinding time, in hours.

So, the process of silicon carbide powder grinding is accompanied with changes of polytype composition consisting in reduction of a multilayer 15R polytype share and increase of share of less laminated structures: 4H and β -SiC polytype, and in this case the number of absorption bands of infrared spectra decreases.

References

1. G.S.Olejnik, N.V.Danilenko. Polytype generation in non-metal substances // Successes of Chemistry. 1997. vol.66, No. 7, p.615-640
2. G.G.Gnesin. Silicon carbide materials. M.: Metallurgy, 1977, p. 216.
3. Application of Raman spectra / Editor: A.Andersen, translated from English, M."Mir", 1977, p.586.

AN OPTICAL METHOD OF INVESTIGATING THE VISCOSITY OF POLYMER SOLUTIONS

Kasheuski S.B., Prokhorov I.V.

A.V. Luikov Heat and Mass Transfer Institute of the National Academy of Sciences of Belarus,
Minsk, 220072, Belarus, E-mail: bekas@itmo.by

The enhancement of electrical conductivity of filled polymer materials (conducting adhesive, films, coating, gaskets, etc.) can be attained by forming, upon application of a magnetic field, clusters of ferromagnetic conductive particles [1]. A new electromagnetic technique based upon the phenomenon of dissipative self-organisation of magnetic particulate system under strongly non-equilibrium conditions [2] can increase the electrical conductivity of a weakly filled composite by a factor of 7-9 orders [3]. The technique involves numerical simulations of the behaviour of many-particle system under the time-varying properties of polymer matrix, and the data are needed on the time dependence of these properties, first of all rheological. During electromagnetic formation of a structured film, the polymer matrix changes its viscosity by several orders of magnitude and is endowed with elasticity. The traditional methods can hardly be used to measure the time-dependent rheological properties when a thin layer of evaporating polymer solution is involved. In addition, for a medium consisting of macromolecules whose size is comparable with that of a filler particle, the macroviscosimetry data may be not a good approximation when describing particle motion.

In order to investigate the changes in the rheological parameters of a polymer solution caused by the solvent evaporation we propose an optical method. It is based on measuring a time variation of light transmission through a thin layer of polymer with ferromagnetic particles when subjected to a pulsed magnetic field. If radiation propagates in the field direction, the layer is bleached. The kinetics of the optical effect that occur with particle motion, provided that particle properties, concentration and initial space distribution, as well as characteristics of a field pulse are specified, is determined by the matrix viscosity. The evaporation alters both polymer properties and filler concentration. To exclude the influence of the latter on the kinetics and the magnitude of the effect, measurements

can be made after the total particle sedimentation. First, one have to prepare several samples being uniform layers of the same thickness and particle concentration. These samples must be sealed and hold for a time interval necessary for complete sedimentation. Then, they have to be unsealed, and the optical measurements with each of these samples have to be made at some time intervals. A practical implementation of this method is associated with solving a number of methodological problems. Among them the sensitivity of the response to particle concentration at the bottom of the layer and to how full sedimentation was. To answer these questions, computer simulations of structure formation and the light transmission were performed. An initial state of a layer is characterised by a uniform distribution of identical spherical particles obtained by a generator of random numbers (the layer height is equal to several particle diameters). The number of particles is assigned by a magnitude of a desired degree of filling the layer bottom with precipitated particles, S , (relative to full square packing of an individual layer). A sedimentation time τ_s is determined in the Stokes approximation. The kinetics of structure formation of the particles in fluid upon application of a field H is considered by the direct numerical simulation of the motion of interacting particles having regard to particles magnetisation M and the fluid matrix viscosity η . In this approximation, the characteristic time of the process is given by the relation $t' = 18\eta/\pi M^2$. In a small field, $M = (3/4\pi)H$ and $t' = 32\pi\eta/H^2$. A lift of particles toward the upper boundary of the layer is calculated. In the approximation of geometrical optics, study is made of the kinetics of light transmission during the structure formation.

The analysis of the numerical data obtained and supported by experiments allow some important conclusions to be made. The initial section of the optical response curve is linear. The curve slope

β to the time axis τ is inversely proportional to the fluid viscosity. At a small number of particles ($s < 1$), the system response is not stabilised by sedimentation time $\tau = \tau_s$, and b still goes down at $\tau > 2\tau_s$. As $s > 1$ the b value as a function of the sedimentation time is stabilised when $\tau = \tau_s$. Calculated and measured variations of b with s is presented in Fig.1.

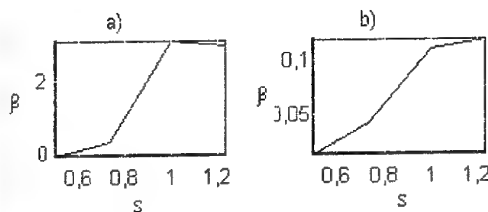


Fig.1. Predicted (a) and experimental (b) curve slopes vs. filling degree

A measured system response is plotted in Fig.2.

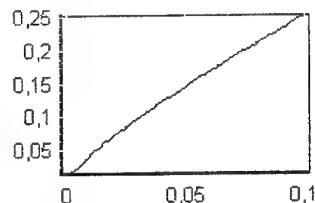


Fig.2. The optical response of a magnetic suspension to a pulse of magnetic field

In experiments it was chosen that $s=1.25$ and $t=1.25t_s$. A possible experimental error in determining these quantities by 10-15% causes an error of the quantity β no more than 10%. In order to determine the viscosity η in terms of the curve slope, the normalised curve was constructed. Experiments were performed with suspensions of 10 mm spherical nickel particles in polyvinilbuteral-cyclohexyl alcohol solution.

The relation is obtained: $\eta = \frac{1}{\alpha} \text{tg} \beta$, where α is the calibration coefficient. In a field of 300Oe, $\alpha=0.043$. The optical method developed for studying the viscosity kinetic during evaporation has appeared to be useful for investigation of rheological parameters of thin polymer films.

The investigation was supported by the Foundation of fundamental research of the Republic of Belarus (Grant T99-246).

References

1. Гуль В.Е., Шенфиль Л.З. Электропроводящие полимерные композиции. - М., 1984.
2. Кашевский Б.Э. Докл. НАН Беларуси. 2000. Т. 44. С.105 – 108.
3. Кашевский Б.Э., Прохоров И.В., Кузьмин В.А, Русалович А.А.. Доклады НАНБ. 2002 (в печати).

CATHODOLUMINESCENCE SPECTRA OF DOPED CUBIC BORON NITRIDE CRYSTALS

Gameza L.M.

The Institute of Machine Reliability of NASB, Minsk, Belarus

Cubic boron nitride (cBN) is a A^3B^5 semiconducting compound with a wide band gap. Due to a number of physical properties it can be considered as an analogue of diamond. The practical application of the material is facilitated by the controlled introduction of electrically and optically active impurities into its crystal lattice. The present note reports the influence of a number of doping impurities on cathodoluminescent (CL) spectra over the range from 200 to 800 nm with the aim of finding optically active impurities introduced into the crystal during its growth.

The studies of cBN have presently been reported in a number of papers [1 – 3]. Attempts have been made at ion implantation of this material [4].

Single crystals were grown using systems with an excess of either nitrogen (BN – Li_3N) or boron (BN – MgB_2) [5 – 8]. The crystals were doped by adding fine dispersed powder dopes to the initial mixture (Na_2O_2 , CaO, MgO, B_2O_3 , Al_2O_3 , Cr_2O_3 , C, Si, LiH, Fe_2N_2 , MgCl were added to the BN – Li_3N system and Si, P, As, Sb, Bi – to the BN – MgB_2 system).

A specially equipped EM-9 electron microscope with the excitation energy of 35 keV was used to excite the CL. The spectra were recorded by a MDR-2 monochromator at 80 K.

With currently available methods of synthesis cBN single crystals are bound to possess nonuniform distribution of defects and impurities over the volume. This causes noticeable differences in the structure of the CL spectra both in crystals obtained in one experiment and at various points of one single crystal (linear dimensions of the single crystals were 0.15 – 0.70 mm), which makes it difficult to find a correlation between the peculiarities of CL spectra of cBN single crystals and the presence of dopes in them. The correlations reported in this note are either explicit or highly probable.

The crystals obtained in the BN – Li_3N system are transparent, colourless, or yellow coloured. Figure 1, spectrum 1 represents a typical CL spectrum of

initial (undoped) crystal grown in the system with nitrogen excess. These samples irradiate over the entire investigated range. The maximum radiation is achieved in the range from 2.50 – 3.10 eV then it decreases monotonously to zero in the range 4.15 – 4.45 eV. In the majority of the spectra of this crystal type the radiation related to the GC-2 center [1] is observed. Some dopes bring about the appearance of the bands the maxima of which are located in the red and ultraviolet ranges. Thus, while adding LiH, Na_2O_2 and P there appear broad bands with maxima in the range of 1.9 eV and when Si, Na_2O_2 , MgO are introduced the maxima are in the range between 3.45 and 4.28 eV. Figure 1, spectrum 2 presents a CL spectrum of the crystal grown in the presence of Na_2O_2 which, in contrast to the spectra of the initial crystals, contains the bands at 1.85 and 3.50 eV.

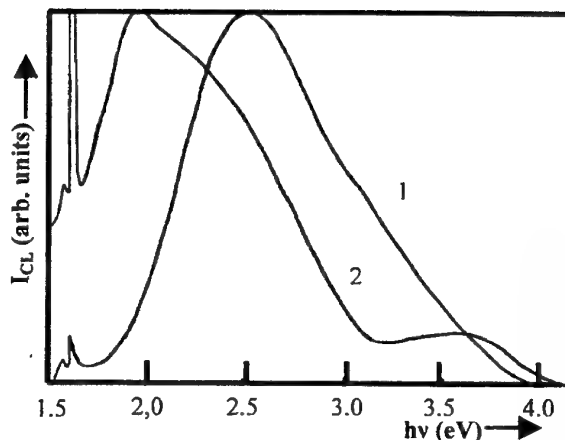


Fig. 1. CL spectra of transparent cBN crystals: 1 – initial; 2 – as doped by Na_2O_2 .

The crystals grown with MgB_2 as a catalyst are black coloured. In the CL spectra of undoped initial crystals of this type the radiation maximum can be located in any part of the spectra ranging from 1.77 to 3.10 eV. The colour of radiation is white or blue-white. The presence of dopes does not influence the nature of the spectrum in visible range but in the ultraviolet range with Si, P and Bi additions there appear bands with maxima in the range 3.87 – 4.35 eV.

In the CL spectra of the crystals investigated by us a number of known and new centers with zero-phonon lines and phonon structures accompanying them have been recorded. The GC-2 center is the most frequently noted in the transparent crystals, which agrees with the assumption that this center is connected with the boron vacancy [1]. It should be noted that the intensity of the GC-2 center rises markedly in the crystals grown in the reaction mixture doped by phosphorus or oxide. In the transparent crystals grown in the presence of CaO all the three centers, reported earlier as radiation induced ones, have also been revealed [2, 4], and in silicon doped crystals two unknown centers at 3.183 and 4.200 eV have been noted (Figure 2).

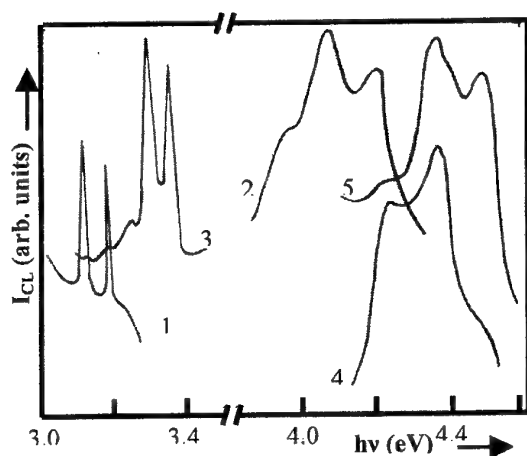


Fig. 2. CL spectrum segments of doped cBN crystals referring to vibronic transits. The numbers of the spectra correspond to those given in Table 1

In the CL spectra of black coloured single crystals new centers have been recorded: at 4.500 eV (BN – MgB_2 – Si system), at 4.365 eV (BN – MgB_2 – P system) and at 3.353 eV (BN – MgB_2 – P or LiH system). A center at 3.353 eV has also been observed in undoped material. It is worthwhile to mention that we have not found any of the centers known earlier in the black coloured single crystals both doped and undoped ones.

Table 1 lists the data on spectral position of the luminescent bands and zero-phonon lines as well as catalysts used in synthesis and dopes. The dopes omitted from Table 1 did not bring about visible changes in the CL spectra of the

corresponding crystals when compared to the spectra of the initial crystals.

The results obtained in this study are tentative and further investigations are needed to interpret the nature of the defects responsible for the peculiarities observed in the CL spectra.

Table 1 Energy position of peculiarities of cBN single crystals grown in different system

N	Catalyst	Dope	Type of spectral peculiarities	Energy position, eV
1	Li_3N	Si	Zero-phonon line	3.183
2	Li_3N	Si	Zero-phonon line	4.210
3	MgB_2	P, LiH	Zero-phonon line	3.353
4	MgB_2	P	Zero-phonon line	4.365
5	MgB_2	Si	Zero-phonon line	4.500
6	Li_3N	Si	Band	3.97 - 4.27
7	Li_3N	Na_2O_2 , MgO	Band	3.45 - 4.00
8	MgB_2	Si	Band	4.35
9	MgB_2	P	Band	4.27
10	MgB_2	Bi	Band	3.87 - 4.00

References

- [1] V.D.Tkachev, V.B.Shipilo, and A.M.Zaitsev, Dokl. Akad. Nauk Beloruss. SSR **29**, 326 (1985).
- [2] A.M.Zaitsev, A.A.Melnikov, V.B.Shipilo, and E.M.Shishonok, Phys. Stat. Sol. (a) **94**, K 125 (1986).
- [3] V.B.Shipilo, A.M.Zaitsev, E.M.Shishonok, and A.A.Melnikov, Zh.prikladnoi spektroskopii **45**, 601 (1986).
- [4] A.M.Zaitsev, A.A.Melnikov, and V.F.Stelmakh, Fiz. Tekh. Poluprov. **21**, 1101 (1987).
- [5] V.B.Shipilo, L.M.Gameza, N.V.Semashko, and T.S.Bartnitskaya, Zh. Fiz. Khimii **63**, 6, 1599 (1989).
- [6] V.B.Shipilo, L.M.Gameza, and E.M.Smolyarenko, Poroshkovaya metallurgiya **1**, 73 (1988).
- [7] V.B.Shipilo, L.M.Gameza, and A.I.Lukomskii, NATO ASI Ser. 3. High Technology, **1**, 397 (1995).
- [8] V.B.Shipilo, L.M.Gameza, N.G.Anichenko, and P.J.Gielisse, J.Wide Bandgap Mat. **7**, 213 (2000)

INVESTIGATION OF METAL SURFACE BY SCAN KELVIN PROBE

Shipitsa N.A., Zharin A.L., Saroka D.I.

Powder Metallurgy Research Institute, Minsk, Belarus

The most promising method for surface control enabling to register properties of a thin superficial layer at quite big area of surface has been a method based on registration of electron work function along the surface of investigated material.

Electron work function, Φ - energy, which should be spent on removing of an electron from solid state into vacuum. If electric-static potential in vacuum is ϕ_0 , in a substance - ϕ_1 and E_F - Fermi energy, electron work function is determined according to the equation [1]:

$$\Phi = (\phi_1 - \phi_0) - E_F = \Delta\phi - E_F = 4\pi P_s - E_F$$

Value of $\Delta\phi$ is the difference between electric-static potentials of the electron inside and outside the metal at a certain point; $\Delta\phi$ - depends on the metal surface condition and, thus, on its structure. At the same time $\Delta\phi = 4\pi P_s$, where P_s - dipole moment of the double layer on a unit of surface area.

Thus, work function depends both on the metal volume condition E_F and its surface condition P_s . This second component depends on crystal-graphic orientation of the surface, surface defects, adsorbed atoms, surface micro-roughness, etc. In case the metal has absolutely flat surface electron cloud inside has no definite boundary because this would correspond to unlimited high power. In practice charge density gradually falls at some distance from the surface because wave function exponentially subsides at the same time. As a result of that the electron cloud expands also outside the surface limits, which leads to the deficit of electrons inside the metal and formation of a corresponding double layer and a step of the potential of the negative terminal outside. The potential along this step is automatically included into the value of the work function, and its presence changes topology of the work function on the metal surface.

From the point of view of non-destructive surface condition inspection, the most suitable method to register changes in the work function is scan Kelvin probe, where measurements are carried out on a contact potential between standard surfaces and the investigated one (Fig.1).

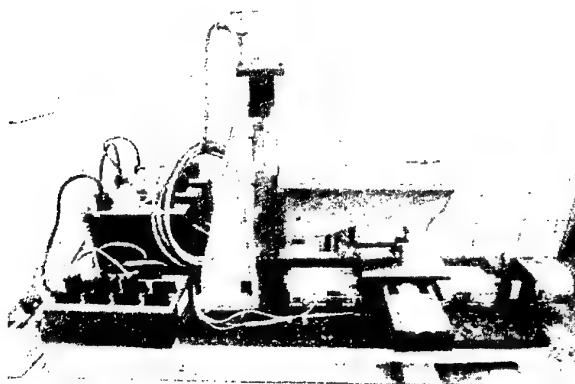


Figure 1. The device for registering topology of the electron work function.

In fig. 1 you can see the device for registering topology of the electron work function. The device consists of a scanning system, a control system, a reading and signal processing system and a Kelvin probe.

The developed device enables to register topology of the electron work function up to 200 x 200 mm at the speed of 50 mm/sec, and determine structural surface non-homogeneities about 100 mkm.

With help of the developed unit localization of deformations during uniaxial tension were investigated.

Samples from steel 45 were tested. They were tested for tension up to the necessary deformation degree. Then they were removed from the tensile-testing machine, topology of the electron work function was registered along the sample surface; after that tests were continued until breaking of the sample.

In Fig. 2 you can see some results of the investigations presented.

The investigations showed minor changes in topology of the electron work function on the surface of a sample not subjected to deformation. At deformation of 1.6% (Fig. 2a) some spread of the electron work function was observed, which, most likely, was caused by non-homogeneous distribution of defects on the material surface at such a deformation. Increasing of deformation causes some smoothing out of the electron work function distribution on the surface and formation of an area with low electron work function within the breaking area (Fig. 2b).

This device enables to carry out investigations of material corrosion, including determination of local corrosion areas, investigate adsorption processes on metals and semi-conductors, and estimate homogeneity of precision surfaces of metals and semi-conductors and also coatings.

References.

1. Жарин А.Л. Метод контактной разности потенциалов и его применение в трибологии. Мн. Бестпринт, 1996. с. 240.



a) $\varepsilon = 1.7\%$

b) before destruction

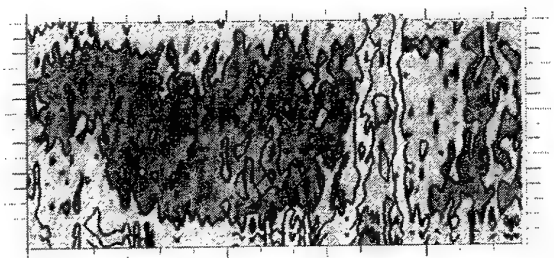


Figure 2. Topology of the surface electron work function during uniaxial tension for Cr 45 (areas of lower electron work function are showed with arrows) a) $\varepsilon = 1.7\%$; b) before destruction.

THE INVESTIGATION OF FERROELECTRIC MATERIALS BY RADIOSPECTROSCOPY METHODS

Bykov I.P., Glinchuk M.D., Laguta V.V., Slipenyuk A.M., Yurchenko L.P.

I.N.Frantsevich Institute for Problems of Materials Science, NASc of Ukraine, Kiev, Ukraine

1. In recent years radiospectroscopy methods (ESR, NMR) have been widely and successfully applied for the study of solid state materials in which structural phase transitions take place. This is related to the fact that these methods permit to obtain information both about macroscopic and local properties of materials. In many cases it is possible to obtain the unique information upon the mechanisms of phase transitions and upon the changes of the properties related to these transitions. Traditional radiospectroscopy methods make it possible to obtain information about the symmetry of crystalline fields, the frequencies of the lattice vibrational spectra, the spin-phonon interaction, times of spin-lattice relaxation, the internal field created by defects, the structure and dynamics of impurities and so on. As a result it is possible to make conclusions about the changes of symmetry and about the values of atomic displacements at phase transitions, to define the temperatures of phase transitions T_c (this is important, for example, for the high-temperature phase transitions, where the traditional dielectric methods are insufficient), to define the value and temperature dependencies of the order parameter. The last point in particular is related to the fact that the crystalline field constants, which are defined by the position of the resonance lines at $T < T_c$, are functions of the order parameter and this is why they have some specific temperature dependence.

In what follows for sake of illustration we shall represent a brief review of physical information we obtained on investigation of ferroelectric materials by ESR method.

2. Incipient ferroelectrics (KTaO_3 , SrTiO_3) properties are extremely sensitive to defects and impurities, which can even induce ferroelectric phase transition. Because of this much attention was paid to these materials investigation by ESR method. Since the external factors like the annealing in different gas atmospheres, illumination by light etc. change the defect structure of the solids (see e.g. [1]), we performed ESR investigation of incipient ferroelectric KTaO_3 under these external factors influence [2,3] as well as nominally pure KTaO_3 [4], where several unavoidable impurities were discovered as one can see below.

The ESR investigation of nominally pure KTaO_3 [4] was carried out at $4,2 \text{ K} < T < 77 \text{ K}$. Two ESR spectra were observed for the first time. The first spectrum with cubic symmetry was shown to be that of Gd^{3+} substituted for K^+ (Fig.1). The analysis of the spectrum line intensities and widths gave no evidence about the quasi-static displacements of tantalum ions in the lattice assumed earlier. The second spectrum had axial symmetry and its source was identified as a new off-center impurity ion Fe^{3+} substituted for K^+ in KTaO_3 . The surrounding oxygen ion displacements were shown to be the main reason for the Fe^{3+} ESR spectra axiality. The estimation of these displacements Δx was carried out in the framework of crystalline-field theory and appeared to be about $0,2 \text{ \AA}$.

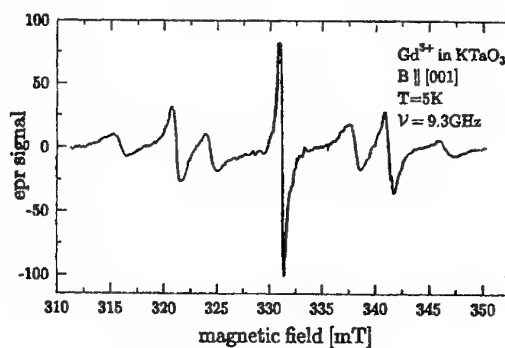


Fig. 1. The Gd^{3+} ESR spectrum in nominally pure KTaO_3

3. The investigation of SrTiO_3 : Ca, Cr, $\text{PbZr}_{0.58}\text{Ti}_{0.42}\text{O}_3$ and PbTiO_3 ferroelectric films on the substrate of Al_2O_3 and MgO single crystals respectively was performed by ESR method [5]. Study of the SrTiO_3 films with the thickness $h = 17000 \text{ \AA}$ and 3500 \AA doped by 0,1 % Cr and 0,2 % Ca was carried out at $T = 18 \text{ K}$ with and without illumination of ultraviolet light ($\lambda = 365 \text{ nm}$). Analysis of the observed spectra (fig.2) had shown that there were two Cr^{3+} ESR lines with g-factors 1,977 and 1,974 in the thick film whereas in thin film there was line with $g = 1,974$ with higher intensity than that in thick film. Calculations lead to the conclusion that the line with smaller g-factor belongs to Cr^{3+} centers nearby films surface. Small intensity line with $g = 2,002$

revealed in the films most probably belongs to O^- center. Its intensity increases after illumination, but it conserves even without illumination contrary to the bulk samples. ESR spectra of PZT and PT films were recorded at $T = 77$ K and 300 K for different orientations of magnetic field. Analysis have shown that the spectra origin is Cr, Mn, V and Fe impurity ions.

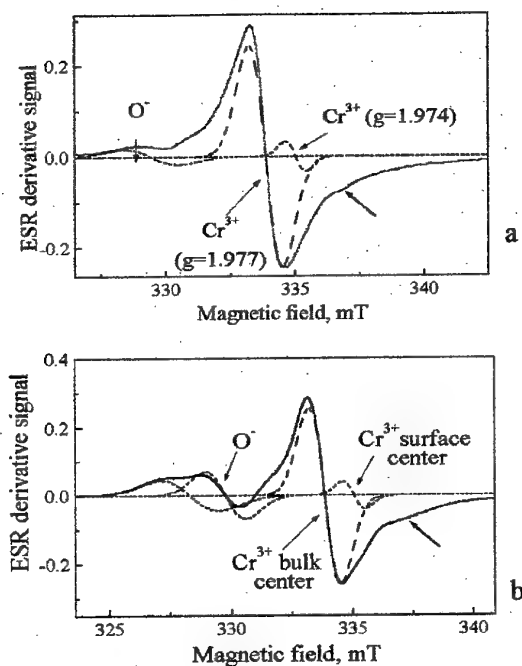


Fig. 2. ESR spectra of $\text{SrTiO}_3\text{:Ca,Cr}$ on Al_2O_3 thick film before (a) and after (b) illumination at 18 K (strange line); dashed line – separated lines of spectra

4. Investigations of impurity centers, electrical resistivity and microstructure of BaTiO_3 ceramics doped with rare-earth ions Y, La, Nd, Sm, Dy and Lu at concentrations $x = 0,001\text{--}0,005$ were carried out [6]. Electron paramagnetic resonance, X-ray diffraction and electron microscopy were used for measurements. The most intensive ESR lines were shown to belong to paramagnetic complexes $\text{Fe}^{3+}\text{-V}_0$ and $\text{Ti}^{3+}\text{-Ln}^{3+}$ (Ln is rare-earth ion, V_0 is oxygen vacancy) (fig.3). A change in symmetry of the center $\text{Fe}^{3+}\text{-V}_0$ at the transition temperature from the ferroelectric to paraelectric phase has been revealed for the first time. Measurements of the dependence of ESR line intensities and electrical resistivity on rare-earth ion concentrations were performed.

The observed correlation in their behaviour showed an essential role of the identified paramagnetic complexes in the appearance of BaTiO_3

ceramic semiconducting properties and the positive temperature coefficient of resistance effect. The latter effect was at a maximum for $x \leq x_c$ where $x_c \approx 0,002\text{--}0,003$ is the critical rare-earth ion concentration which determines the excess charge compensation mechanism.

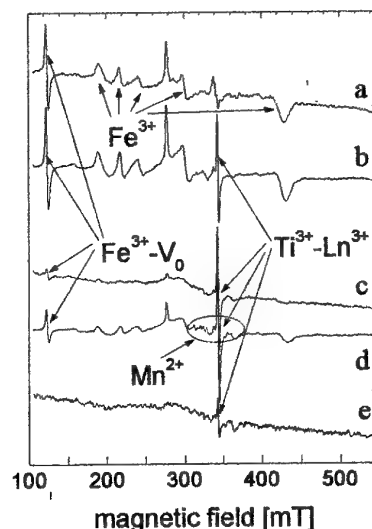


Fig. 3. EPR spectra of pure BaTiO_3 ceramic (a) and BaTiO_3 ceramic doped by 0,001 Lu (b), 0,001 La (c), 0,001 Dy (d), 0,002 Sm (e); $T = 20^\circ\text{C}$

Up to x_c , rare earths investigated (except for the small ion Lu), substitute for barium, and the main compensation mechanism is an electronic mechanism. At high concentrations ($x > x_c$) in the case of large ions (e.g. La) substitution is at barium sites with the creation of titanium vacancies, whereas intermediate ions (e.g. Y) begin to substitute for titanium.

1. V.V.Laguta, M.D.Glinchuk, I.P.Bykov et al., Phys. Rev. B, **54**, 12353 (1996).
2. V.V.Laguta, M.D.Glinchuk, I.P.Bykov et al., Phys. Rev. B, **52**, 7102 (1995).
3. V.V.Laguta, M.I.Zaritskii, M.D.Glinchuk, I.P.Bykov et al., Phys. Rev. B, **58**, 156 (1998).
4. M.D.Glinchuk, V.V.Laguta, I.P.Bykov, J.Rosa, L.Jastrabik, J. Phys.: Condens. Matter, **7**, 2605 (1995).
5. I.P.Bykov, M.D.Glinchuk, V.V.Laguta et al., Integrated Ferroelectrics, **32**, 159 (2001).
6. M.D. Glinchuk, I.P.Bykov, S.M.Kornienko, V.V.Laguta et al., J. Mater. Chem., **10**, 941 (2000).

ATOMIC FORCE MICROSCOPY OF THICK FILM RESISTORS ON THE BASE OF METAL BORIDES

Paustovsky A.V., Rud' B.M., Shelud'ko V.E., Tel'nikov E.Ya., Tsukruk V.V.⁽¹⁾, Luzinov I.A.⁽¹⁾

Frantsevich Institute for Problems of Material Science, NAS of Ukraine, Kiev, Ukraine

⁽¹⁾Iowa State University, Ames, USA

The thick film technology of making of dielectric and conducting layers on the substrates is widely used in the microelectronics. In this way the thick film resistors (TFR) on the base of high-melting compounds, namely, borides of rare-earth and transition metals are produced. The electrophysical properties of TFR depend on many factors, such as surface morphology, structure, and phase constitution of the functional phase etc. By acting of high-energy fluxes (laser irradiation, plasma, electron beam, induction heating) on the mentioned factors one can change electrical resistance, temperature coefficient of resistance (TCR) and other resistor characteristics.

The TFRs on the base of Ni_3B , BaB_6 borides and glass-binder were adopted as the objects for investigation. The making of TFRs was realized with the method of paste mask printing on the dielectric 22XC or BK94 substrates followed by the heat treatment in the travelling ПЭК-8 oven. The specimens were processed with "Квант-15" laser in the following regime: $\lambda = 1.06 \mu m$, $E = 1-2 J$, $\tau = 4 ms$, $\varnothing_s 1 mm$. Nanoscope Digital Instruments D3000 Atomic Force Microscopy was used to characterize in tapping mode the TFR surface before and after the laser treatment.

The principle of investigating of the local microcharacteristics of the solid bodies surface with the aid of AFM consists in detecting molecular forces (Van der Waals' interactions) originating between the surface in study and the probe point – "tip" which is brought near it at a distance of 1–10 Å [1] (Fig.1.). Unlike Scanning Tunnel Microscopy (STM), AFM allows to study the surface microrelief not only conductors but also dielectrics. AFM working occurs in the contact (between the scanning point and specimen surface) regime and non-contact one. Their combination forms so-called "tap regime" – tapping mode (Fig.2.). In scanning of the specimen (the point moves over the surface or the specimen moves under the fixed point) AFM detects the probe point deviation ("height recording"). By this means the data on the surface relief form. In detecting amplitude or cantilever oscillation

frequency one can obtain the distribution of mechanical properties on the specimen surface with the recording of the so-called "phase contrast image".

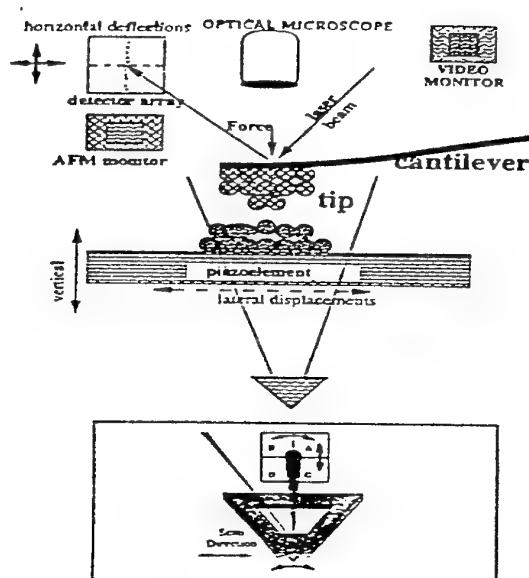


Fig.1. General scheme of AFM instrumentation

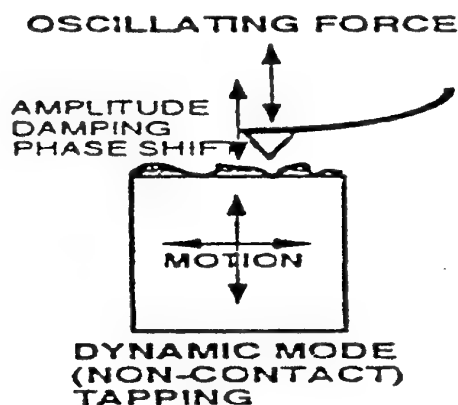


Fig.2. The tapping mode regime

To do this, in the measuring cantilever of AFM working in dynamic regime, or in the specimen, the forced oscillations are modulated. Their frequency changes in accordance with the elastic properties of the scanned surface area. The value of the phase angle ϕ of the cantilever free

oscillations can be recorded (in radians) as a function of the frequency of oscillations ω .

$$\phi = \operatorname{tg}^{-1} \left[\frac{m\omega\omega_0}{Q(k - m\omega^2)} \right], \quad (1)$$

where k – a constant of rigidity; m – cantilever mass; Q – figure of merit, $Q = k/(m\mu)$ where μ – friction factor; ω_0 – the resonance frequency of oscillations, $k = m\omega_0^2$.

The phase angle ϕ_0 for oscillations at the resonance frequency ω_0 is determined by the expression:

$$\phi_0 = \operatorname{tg}^{-1} \left(\frac{k}{Q\sigma} \right), \quad (2)$$

where σ is the sum of the force derivatives for all the forces F_i affecting the cantilever:

$$\sigma = \sum_i \partial F_i / \partial Z, \quad (3)$$

Here Z is the displacement of the tip relative to the specimen.

In recording phase shift between the free and real frequency of the tip oscillations, when contacted to the specimen, the phase contrast image is formed (Fig.3).

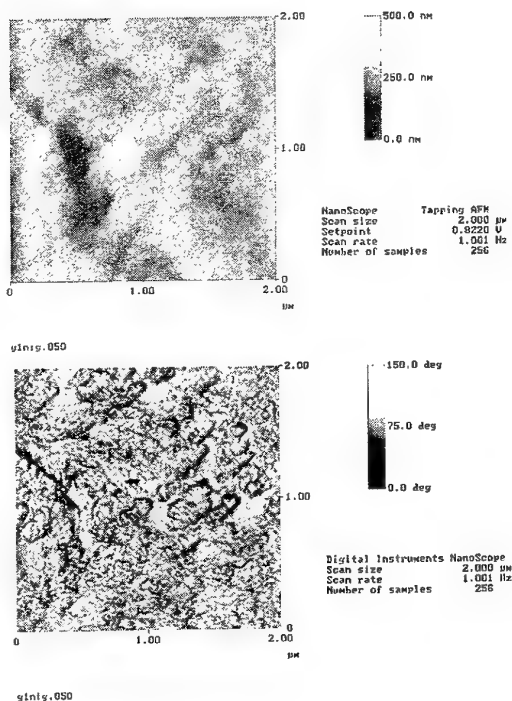


Fig. 3: **top**– topography image of Ni_3B -based TFR
bottom– phase contrast image of mentioned TFR

It presents the change in the rigidity of the surface layers within the area in study, that is defined as:

$$\Delta\phi_0 \approx \varepsilon \langle a \rangle E \left(\frac{Q}{k} \right), \quad (4)$$

where ε – a constant depending on the tip shape, $\varepsilon = 2$ for the sphere; $\langle a \rangle$ – radius of a round contact spot; E – the effective modulus of elasticity.

In order to estimate the surface microrelief it's convenient to draw the section at different directions. For example, the initial surface cross-section analysis shows that the degree of roughness is $R_z = 32.82$ nm. After irradiating with the energy $E = 1$ J the areas with the different roughness (from $R_z = 6.64$ nm to $R_z = 13.77 - 30.81$ nm) form at the surface. With increasing energy to 2 J the degree of roughness rises to 67.73 nm.

The distribution of the surface mechanical properties (rigidity) is studied using the combined image "topography + phase contrast" by means of SurfSoft software.

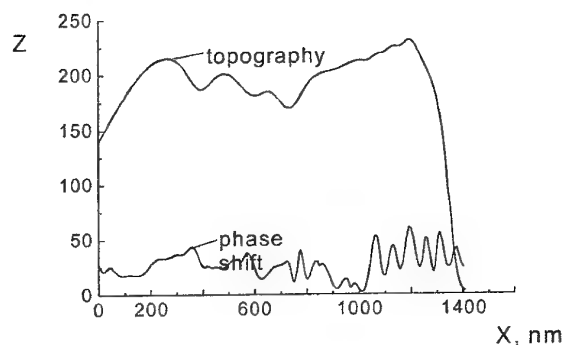


Fig.4. Profile sections for topography and phase contrast image for $(Ni_3B + BaB_6)$ – based TFR

Shown in Fig. 4 are the diagonal sections of topography and phase contrast of the surface area of $(Ni_3B + BaB_6)$ – based TFR before radiating. Attention is drawn to the fact that the more or less regular alternation of the areas with the high rigidity (the areas with the enhanced concentration of borides and metallic nickel) occurs at the site from 1092.5 nm to 1403.1 nm. Between these sites, the less rigid amorphous glass-binder phase is located. Using the data one can estimate the thickness of the dielectric layer between the areas with the functional phase.

The same analysis is carried out for the TFR on the base of Ni_3B and glass-binder.

References

- 1.V.V.Tsukruk. Scanning Probe Microscopy of polymer surfaces // Rubber Chemistry and Technology, **70**, №3, 430–467 (1997)

AUTOMATIC DEVICE FOR DETERMINATION OF POWDER FLOWABILITY AND CALIBRATION OF FUNNELS

Vinnitchenko V.D.

I.N.Frantsevitch Institute for Problems of Material Science, National Academy of Science of Ukraine, str. Krguganovskogo 3, Kiev, 03142 Ukraine

The device is developed and is introduced in I. N. Frantsevitch Institute for Problems of Material Science, National Academy of Science of Ukraine in 1991.

It is recommended for application in scientific organizations and at the enterprises, which work in the field of mechanical engineering, in a particular in a direction of powder metallurgy.

In the countries of CIS the similar devices are not let out. The international standard ISO 4490-1978 /E/ recommends to get a funnel of a Hall (without automatics) and turkish corundum a powder at Alcan Metal Powder Inc., Box 290. Elisabeth N. I. 07207 U. S. A.

The automatic device is based on single crystal computer of a series 1816 with microcircuits of a high degree of integration also consists of the block of measurements, panel of indication and management calibrated funnel with the optical-and-electronic gauge. The device is intended for definition of time of the expiration metal and not metal powders, which freely flow through the calibrated test - aperture of a funnel, and also for calibration of funnels in a manual mode according to the international standard ISO 4490-1978 /E /, and in an automatic mode agrees GOCT 20899-98, which was entered at reconsideration GOCT 20899-75.

The results of measurement after their processing and serial number of measurement are deduced on a digital electronic panel.

Technical Characteristics of the Device (Automatic Mode of Operation)

- accuracy of measurement of flow time $\pm 0,02$ s;
- discreteness of time read-out - 0,01 s;
- maximum value of single measurement 99,99 s;
- setting range of funnel correction factor: 0,98+1,10 with discreteness of 0,001;

- automatic sece exception of results of measurement of pauses from possible breaks of a jet of a powder by duration, s: up to 0,1;
- the distribution of a sound signal in case a difference between the greatest and least meaning in a mode of three and five-multiple measurements will exceed. c: 0,3;
- feed from a network of an alternating current, B: 220;
- power consumption, W, no more: 20;
- overall dimensions, mm: 190 X 180 X 150;
- weight, kg: 10;
- climatic conditions of operation:
- temperature, °C 15 - 35;
- humidity, %, no more than 86;
- automatic introduction of factor corrections of a funnel in all modes of measurement;
- automatic calculation average arithmetic in a mode of three and five-multiple measurement.

Principle of work

Researched powder, following from calibrated of an aperture of a funnel the operation causes the gauge, which includes an electronic stop watch of the block of measurement. Upon termination of the expiration the test - portion of a powder on a panel is deduced time of the expiration in view of factor of correction and serial number of measurement.

Modes of Operation of Measuring Unit

- testing system;
- initial setting (reset);
- setting of funnel correction factor:
- single measurement;
- 3 measurements cycle with computation of arithmetic mean value;
- cycle from five measurements with calculation of average arithmetic meaning;
- control of clock pulse generator.

Algorithm of functioning of the block at various modes robots

- a) The mode of initial installation is intended for reduction of the device in an initial condition after

inclusion in a network, after realization of any procedures of measurement or after a manipulation by the button "CORRECTION" and by the switch "MODE", by whipping off of any results of measurements.

b) The mode of installation of factor of correction is intended for introduction correction factor of correction of a funnel, by installation of concrete importance at its cyclic updating with step-type behaviour 0,01 on the indicator.

c) The mode of individual measurement is intended for realization of control gaugings, by translation of the device by the toggle - switch in a mode "1" and pressing of the button " INITIAL INSTALLATION ". The mode is included at the moment of operation of the optic-electronic gauge. On the indicator the result of measurement is fixed in view of processing and serial number of gauging.

In final result of measurement the casual pauses by size up to 0,1 with. Quantity of possible casual pauses during one measurement are not taken into account do not regulate. A pause by size more than 0,1 with should to be regarded as the end of the previous measurement

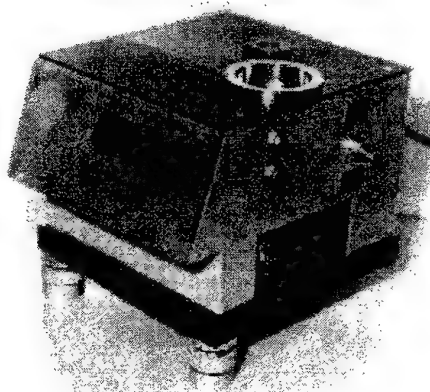
d) The mode of three measurements with calculation of average arithmetic meaning intended for averaging the received meanings, and the algorithm of work of the block and technique of definition of result in each of three individual measurements completely corresponds to a mode of individual measurement. The mode is started at the moment of operation of the optic-electronic gauge. The measurements follow continuously one after another with subsequent of result of measurements. The procedure of calculation of final result is started through 3-4 with the ambassador of end of last specific cycle of measurements. The algorithm of work of the block and technique of definition of result in each of three individual measurements of a cycle completely corresponds to a mode of individual measurement.

e) The mode of five measurements with calculation of average arithmetic importance intended for averaging the received importance, and the algorithm of work of the block and technique of definition of result in each of five individual measurements completely corresponds to a mode of individual measurement. The mode is started at the moment of operation of the optic-electronic gauge. The measurements follow continuously one after another with the subsequent procedure of calculation of final result of measurements. The procedure of calculation of final result is started through 3-4 with the ambassador of end of last specific cycle of measurements. Algorithm of work of the block and technique of definition of result are similar to a mode of three measurements.

f) The verification mode is intended for testing system by submission on a control socket of control frequency of the clock generator of the block, at this procedure of measurement will not be carried out.

Complete Set

The complete set includes the devise with certified funnel and 60 gms weight corundum mounting for periodic funnel calibration



Fax: 38 (044) 516 8519, (044) 444 5613

PECULIARITIES OF THE ELECTRON SPECTRUM FOR $Zr_xHf_{1-x}V_2$

Nemoshkalenko V.V., Shevchenko A. D.

G.V.Kurdyumov Institute for Metal Physics, N.A.S. of the Ukraine,
36 Academician Vernadsky Blvd., UA-03680 Kyyiv-142, Ukraine

Abstract

In the temperature range of 4,2—300 K on the polycrystal $Zr_xHf_{1-x}V_2$ with superconducting transition temperature $T_c \approx 10$ K the magnetic susceptibilities χ and X-ray fluorescent emissive $VK_{\beta_{2,5}}$ — spectra there were investigated. Anomalous dependences χ was discovered below 150 K that may be explained by decrease in the electron states density at the Fermi level $N(E_F)$. The presence of regions with localised electron density in the investigated compounds on the low-energy side of the vanadium emission spectrum at low temperatures ($T=10$ K) indicates an essential rebuilding in the electron spectrum of valence electrons.

Introduction

Ternary superconducting compounds $Zr_xHf_{1-x}V_2$ ($T_c \approx 10$ K) are of great interest for applied superconductivity due to the presence in them the promising combination of such properties as the high current-carrying capacity and radiation steady. Besides, the change of a crystal structure type occur in these compounds at temperatures ≈ 100 K considerably exceeding the temperature of the superconductivity ($T_c \approx 10$ K): the cubic high temperature symmetry decreases to the rhombohedral one for $x > 0,45$ or to the orthorhombic one for $x < 0,4$. The present work is dedicated to the investigation in $Zr_xHf_{1-x}V_2$ system in the temperature range 4,2 — 300 K of the magnetic susceptibility χ and also to the X-ray emission fluorescent $VK_{\beta_{2,5}}$ — spectra to examine the changes occurring in the electron spectrum with the change of the ternary system composition and the temperature.

Procedure experimental

The χ measurement was carried out by means of the Faraday relative method on an electron microbalance with automatic compensation on the set-up previously described by us [1]. The set-up sensitivity in the magnetic field with $m_e H = 7,0$ koE intensity (on the area, where $H dH/dZ = 14$ mm) was $-3 \times 10^{-11} \text{ cm}^3 \text{ g}^{-1}$, which made it possible to carry out the measurements at the samples with a milligram unit weight. The measuring error did not thereby exceed 1%. In the

samples under study the χ did not depend on the magnetic field intensity in all the investigated temperature range ($T_c - 300$) K, which indicates the absence of the impurities with a large magnetic (ferro-or antiferro-) order in the given samples.

The X-ray fluorescent emission K-spectra were obtained on the spectrograph, constructed on the base of the well-known long-wave spectrograph. Our spectrograph has two distinctive properties:

- (1) the X-ray spectrograph and the helium cryostat, on which the investigated sample is fixed, are aligned;
- (2) the sealed X-ray tube and the system of the X-ray screens (nitric and helium ones) allowing to provide the secure thermal insulation of the sample without an attenuation of the X-radiation were used as the X-ray source.

The applied method has allowed to investigate the object ranging from the room temperature to that of the liquid helium. Quartz [the plane (101 0)] was used as a crystal-analyser. The operating conditions of the X-ray tube were 40 kV, 85 mA. The vacuum in the operating volume was $1 \times 10^{-5} - 5 \times 10^{-6}$ torr. The emission spectra were obtained with the resolving power being no worse than 0.16 eV.

Results and discussion

Figure 1 gives the temperature dependence of $\chi(T) = \chi_{lat} + \chi_d(T)$ for ZrV_2 , where χ_{lat} are the Van Vleck orbital paramagnetic and Larmor precession diamagnetic contributions into the magnetic susceptibilities of the crystal lattice which is paramagnetic and does not depend on temperature, and χ_d is the spin paramagnetic magnetic susceptibilities of d — electrons proportional to $N(E_F)$ [2]. A decrease in χ value with the temperature lowering at $T < T_m \approx 135$ K indicates that $N(E_F)$ decreases. The substitution of hafnium by zirconium causes the decrease in the size of the anomaly in $\chi(T)$ (Fig.2). At this time even the temperature dependence sign χ changes within the low temperature range. Figure 3 gives χ in $Zr_xHf_{1-x}V_2$ versus composition at 10 K. As it is seen from the plots, χ passes through the maximum with the change $Zr_xHf_{1-x}V_2$ composition for $x=0,6$. As it was mentioned above, the diminution of χ with temperature

decrease at $T < T_m$ indicates the diminution of $N(E_F)$. Then the increase in χ with the growth of zirconium content in the $HfV_2 - ZrV_2$ system is caused by the increase in $N(E_F)$.

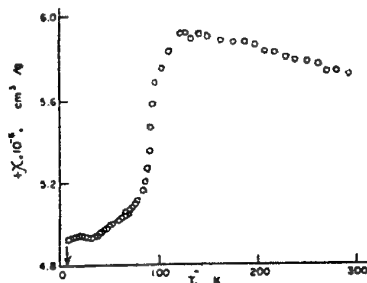


Fig. 1. Magnetic susceptibility vs. temperature for ZrV_2 .

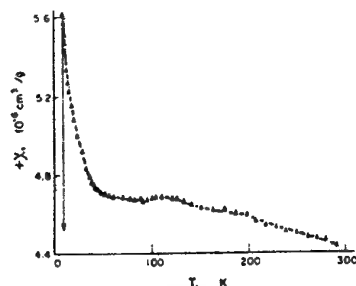


Fig. 2. Magnetic susceptibility vs. temperature for $Zr_{0.6}Hf_{0.4}V_2$.

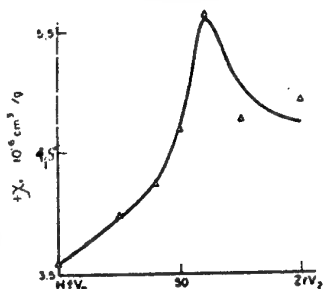


Fig. 3. Magnetic susceptibility vs. temperature for $Zr_xHf_{1-x}V_2$ at 10 K.

The study of the effect of the crystal lattice symmetry lowering upon the electron spectrum of valence electrons was of some interest. Towards this end the X-ray fluorescent emission K-spectra of vanadium were investigated in $Zr_xHf_{1-x}V_2$ system. The obtained spectra of pure vanadium and vanadium in ZrV_2 , $Zr_{0.6}Hf_{0.4}V_2$ are given in Fig. 4 while their main parameters are given in Table. The main maximum position of the $K\beta_{2,5}$ -spectrum of pure vanadium was conditionally adopted as a zero reading of the energy. The spectral line intensity is given in relative units (Fig. 4). The K-spectra of pure vanadium and vanadium in ZrV_2 and $Zr_{0.6}Hf_{0.4}V_2$ Laves phases were studied at 10, 97 and 300 K.

$K\beta_{2,5}$ -emission spectrum of metallic vanadium, which reflects the electron state distribution of d- and partially of asymmetry in the crystal valence zone has been well studied in the works of many authors. Its form and the main parameters at 300 K are given in Fig. 4 and in Table.

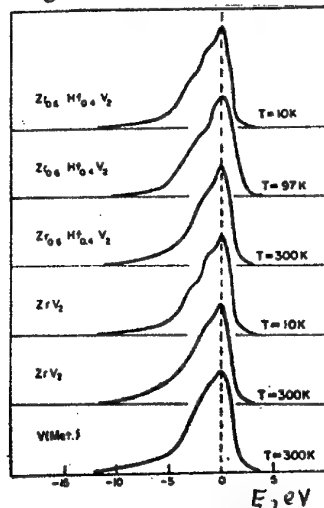


Fig. 4. X-ray fluorescent emission $K\beta_{2,5}$ -spectra of vanadium in $Zr_{0.6}Hf_{0.4}V_2$ and to metallic vanadium.

Remelting vanadium with zirconium being an element of the second transition period with the formation of ZrV_2 Laves phase does not lead to the essential changes of the spectral line main parameters at 300 K. The electron distribution over the valence zone in vanadium atom vicinity by character of the intensity distribution in the density of state curve is well as by its energetic extent remains practically the same as in pure vanadium. The energetic position of the emission spectrum main maximum within the limits of the experimental error is also unaffected. It follows that the vanadium electron structure under the formation of ZrV_2 changes unessentially at 300 K. The data of $\chi(T)$ dependence obtained on the vanadium monocrystals also indicate it. It appeared, that of pure vanadium and ZrV_2 with in the range of 300K are close in value.

The temperature decrease in ZrV_2 to 10K leads to the noticeable change of the spectral line form in this alloy. Two well-defined low-energy maxima make their appearance. Yet the spectral line parameter value changes slightly: some tendency toward the decrease in width and halfwidth of the spectrum is observed.

The formation of $Zr_{0.6}Hf_{0.4}V_2$ phase does not lead to the essential change of the vanadium spectrum form, which indicates, that the distribution

character of the electron density p-component in the valence band of the formed crystal remains practically the same as with pure vanadium. One can observe only some increase in the spectral intensity of $K\beta_{2.5}$ -spectrum though its Integrated intensity within our measuring accuracy remains unaffected. The decrease in the emission spectrum width to the base as well as at one half the maximum intensity is simultaneously observed. The emission spectrum width on the base was measured from the point of the Itoe short-wave bend, conditionally adopted as the Fermi level position, to the intersection point of the linear extrapolation of the spectrum low-energy branch with the hum level.

Table The main parameters of spectral line for $Zr_xHf_{1-x}V_2$

Parameter	T, K	$IK\beta_{2.5}$ $IK\beta_1$ (integral)	$IK\beta_{2.5}$ $IK\beta_1$ maximal	$IK\beta_{2.5}$ $IK\beta_1$ (at the Fermi level)	ΔE (eV)	$\Delta E_{1/2}$ (eV)
V(met.)	300	1.00	1.00	1.00	6.4	4.0
ZrV ₂	300	0.95	1.00	1.06	6.1	3.7
ZrV ₂	10	0.90	1.02	1.00	6.1	3.6
Zr _{0.6} Hf _{0.4} V	300	1.05	1.18	1.18	5.9	3.5
Zr _{0.6} Hf _{0.4} V	97	0.91	1.02	1.05	7.0	4.1
Zr _{0.6} Hf _{0.4} V	10	1.27	1.27	1.54	6.4	3.6
Error:	± 1	± 0.10	± 0.10	± 0.20	± 0.4	± 0.2

The emission spectrum width at one half the maximum intensity has not a definite physical sense but being defined with higher accuracy, it permits to fix more confidently the general trend towards the increase or decrease in the width of the filled part of the crystal valence zone. Invariability at 300 K of the spectral line integral intensity in $Zr_{0.6}Hf_{0.4}V_2$ at some decreases of its width indicates, that the density of filling of the crystal valence spectrum in the vicinity of vanadium atoms practically remains unaffected and only its localization degree slightly increases, that is probably conditioned by the increase in distance between vanadium atoms in the lattice and their bond weakening.

Cooling of $Zr_{0.6}Hf_{0.4}V_2$ to the temperature of liquid nitrogen though does not lead to the essential change in the spectral line main parameters (width, halfwidth, spectral and integrated intensity), but it is followed by the noticeable change in the emission spectrum form, manifesting itself in the "smearing" of the main maximum and in the increase of the distance between the latter and low-energy maximum. The observed in the character of the electron density distribution in the valence band is most likely conditioned by the stacking

process of the structural re-arrangement of a crystal at 97 K.

The subsequent cooling of $Zr_{0.6}Hf_{0.4}V_2$ alloy to 8 K is primarily accompanied by the drastic change in the spectrum form: the ranges of distinct localization develop in the electron density distribution as well as in the case of ZrV_2 . The presence of the localization in the valence electron distribution of p-symmetry in the vicinity of vanadium atoms may be connected with the splitting of p-states by a crystalline field with lower symmetry which arises from the structural transition at $T=100$ K. Such an effect was experimentally observed for example, under the electron-paramagnetic resonance study in the compounds on the transition metal base and described in [3]. It should be noticed, that the marked bend is observed on $Zr_{0.6}Hf_{0.4}V_2$ emission spectrum part which reflects the electron distribution in the range of the Fermi level. The appearance of this bend may be caused by the energy gap formation during transition of the alloy into a superconducting state. Also the spectral line main parameters significantly change for $Zr_{0.6}Hf_{0.4}V_2$ ternary system in comparison with ZrV_2 (Table). A considerable increase in the integral as well as in spectral intensity of the emission spectrum is observed which may indicate the electron density growth in the vicinity of vanadium atoms. The relative intensity of K-spectrum within the range of the Fermi level has also been measured and though this part of the spectrum is the most subjected to the effect of self-absorption with the attendant growth of the experimental error, we managed to fix a considerable growth in the electron state density at the Fermi level. This result agrees with the data being obtained during study in $Zr_xHf_{1-x}V_2$ system at low temperatures (Figs. 2 and 3).

Conclusion

The temperature dependences of magnetic susceptibility χ and the X-ray emission fluorescent $VK\beta_{2.5}$ -spectra were investigated in the polycrystal $Zr_xHf_{1-x}V_2$ with the temperature range 4,2 — 300 K. It is found, that the lowering of the crystal lattice symmetry from structural transformation at the temperatures below 110 K leads to the significant re-arrangement of the electron spectrum of valence electrons, namely: the areas of the electron density localization emerge at the low energy part of the emission spectrum representing the valence electron distribution of p-symmetry in the vicinity of

vanadium atoms; the presence of the localization areas may be connected with the splitting of p-states of the valence electrons by the-crystal field of lower symmetry. An increase in the state electron density at the Fermi level was discovered at low temperatures in the ternary Laves phases as compared to binary ones owing to the investigation data of the magnetic susceptibility and X-ray fluorescent emission K-spectra of vanadium.

References

1. Lashkarev G.V., Migley D.F., Shevchenko A.D., Tovstyuk K.D. Magnetic Susceptibility and Electrical Properties of p- $\text{Pb}_{1-x}\text{Sn}_x\text{Te}$ // Phys. Status Solidi, B. - 1974. - V. 63, No2.-P.663-668.
2. Vonsovskiy S.V. Magnetizm. - Moskva: "Nauka", 1971. - 1032 P.
3. Abragam A., Bliney B. Electronic Paramagnetic Resonance of Transitional Metals. - Moskva: "Mir", 1972. -V.1. - 651 P; 1975. - V.2. - 349 P.

THE USAGE OF SCANNING ELECTRONIC AND ATOMIC-POWER MICROSCOPY METHODS FOR RESEARCH OF THE STRUCTURE OF THIN COMBINED COATINGS

Andreyev M., Markova L., Kuznetsova T., Chekan V.

Powder Metallurgy Institute, Minsk, Belarus

The depositing of protective coatings on a surface of details during several decades is an effective method of increasing their reliability and durability. The last achievements in the field of coating deposition are directed on creation of unknown quantities of properties in a very thin surface layer. The modern concept of creation of protective wear resistant coatings represents by itself combined processing of items with usage of various methods of surface modification [1].

In the given work the structure and morphology of the surface of coatings obtained by combination of method of arc evaporation process in vacuum and processing of surface in nitrogen-hydrogen plasma of the pulsing discharge was studied. The polished surface of a substrate made of steel P6M5 is pre-coated by chromium of 1 micron thickness using arc evaporation method. Further the sample with precoat is exposed to ion nitriding in plasma of pulsing current. The last deposited coating was CrN of 3 microns thickness made by arc evaporation method. The small thickness of coating (up to 4 microns) requires high-resolution methods of its structure research. The most informative for researching of structural elements by a size less than 1 micron is an electronic microscopy in combination with microoentgenspectral analysis. The application of such methods for researching of "thick" vacuum coatings is effective and also allows studying the mechanism of creation and change of structure under effect of the operating conditions [2]. The research of morphology of thin coating surface in scanning electronic microscopy on stages of technological process has allowed to produce structural criterions of valuation of the surface state in each concrete case and to reveal changes in modes of coating nitriding. However for research of structure and revealing of the mechanism of creation of thin wear resistant coatings by scanning electronic microscopy not always is enough (Fig. 1a, c, e).

During the last years the wide development was received with a method of atomic-power microscopy. This method with usage of modes of topography and phase contrast allows to study not only

morphology of a surface after each technological stage of creation, but also to reveal zones with increased micromechanical properties in surface structure (Fig. 1b, d, f).

The combination of the image of transversal structure of coating with concentration distribution curves of Cr, Fe, W, V, Mo allows to study character of interaction of elements in a diffusion zone between coating and basis. The complete absence of Fe diffusion from a basis both in one-micron Cr coating, and in CrN coating in this case is proved practically. In the same time insignificant diffusion of Mo in Cr coating is observed (Fig. 2).

The complex research of structure and properties of thin wear resistant coatings on chromium basis by methods of atomic-power and scanning electronic microscopy with the microoentgenstructure analysis allows to reveal the mechanism of creation of such coatings and to formulate bases for development of the scientific proved highly effective combined technology of coatings deposition.

Literature:

1. Dostanko A.P., Bosyakov M.N., Kucharev S.A. Surface Modification of Solid in Unbalanced Gas Discharge Plasma. - Minsk: Scientific Center of Marketing Researches and Management «Armita», 1996. - 95 p.
2. V.A. Chekan, L. V. Markova. Mechanism of High-Temperature Oxidation and Sulfur Oxide Corrosion of Vacuum Plasma Coating of Me-Cr-Al-Y Type on Heat-Resistant Nickel-Based Alloys in Handbook of Surfaces and Interfaces of Materials (H.S. Nalwa, Ed.), Vol. 4. Academic Press, New York, 2001.
3. Andreyev M.A., Markova L.V., Bosyakov M.N., Kuznetsova T.A., Zhuk D.V. Surface Morphology of Combined Wear-resistant Coatings Based on Titanium. // POWDER METALLURGY, issue 24 • 2001, p. 104-108.

INDEX OF AUTHORS

This Page Intentionally
Left Blank

A

Adeev V.M. 167
Akulitch A.V. 266
Alekseitsev A.V. 234
Alexandrova L.I. 433, 595
Alfintseva R.A. 636
Aliievsky V.M. 48, 206
Ananitch G.V. 621
Andreeva A.F. 516, 517, 518
Andreeva A.V. 131
Andreyev M. 728
Andrievskaya E.R. 312, 42
Andrievski R.A. 25
Andrushchik L.O. 184
Antanovich A.A. 452
Antonova M.M. 638
Antsiferov V.N. 17, 151, 196, 250, 277, 563, 564, 566

Arinkin S.M. 295
Aristova I.M. 117, 695
Artamonov V. 270
Artushkevich A.S. 343
Artyukh L.V. 100, 101, 102, 437
Asnis E.A. 480
Astakhov E.A. 262
Astashynski V. 333
Avramchuk S.K. 169

B

Baginsky I.L. 462
Baglyuk G.A. 478
Balyuk Z.V. 359
Banciu C. 135
Bankovskiy O. 601, 634
Barabash O.M. 188, 473, 476
Barinova A.P. 258, 324, 588, 325
Bashev V.F. 359
Bat'ko I. 227
Bdikin I.K. 695
Bega M.D. 397
Bega N. 367, 601, 634
Bel'skaya G.N. 234
Belchikov E. 264
Beletskaia O.E. 359
Beliaev A.V. 329, 339

Beloborodov I.I. 512
Belots'ky O.V. 679
Belous A.G. 28, 414, 560

Belousova E.E. 281
Belyaev A.V. 619
Belyaeva O.V. 568
Belyavin K.E. 20
Belyavina N.M. 223
Belyavina N.N. 217
Belykh V.D. 325
Bengus V.Z. 373, 454
Berenda V.V. 119
Berezutski V. 193
Besov A.V. 351
Bezhenar M.P. 223

Bezimyanniy Y.G. 674
Biblik I. 85, 659
Bieloborodova O.A. 116, 106
Bilevych Ye.O. 91
Bilous A.M. 371, 506
Bilous O.O. 100, 101, 102, 437

Bilousov M.M. 445
Bilyavina N.M. 56
Blyznuk O.V. 306
Bobba F. 670
Bobet J.L. 638, 640
Bodnar O.B. 695
Bogomol Yu.I. 104
Bohac P. 382
Boldyrev V.V. 258, 324, 325

Boledzyuk V.B. 458
Bolgar A.S. 192, 496, 523

Boltovets N.S. 316
Bondar A.A. 100, 101, 102, 437

Bondar A.M. 135
Bondarenko B.I. 279, 431
Bondarenko M.E. 640
Bondarenko V.P. 21, 480
Bondarev E. 381, 581
Bondarkova G.V. 681
Bondaruk O.N. 353
Bonshtedt B.E. 234
Borodians'ka H.Yu. 447
Borodulia V.A. 266
Borysov D.B. 101
Bovkun G.A. 500
Bozhko S.A. 223
Brinson B. 465
Britun V.F. 23, 399
Brodnikovskij N.P. 493, 539
Bruehne K. 259
Bubnov Yu.Z. 664
Budovskikh E.A. 615
Bukhovets V.L. 633
Bulanov V.Ya. 236
Bulanova M.V. 99, 190, 191

Bunchuk J.P. 575
Burka M.P. 101, 102
Butenko V. 605
Butorin P.E. 68
Buyanov Y. 191
Buzhenets E.I. 389
Byakova A.V. 74, 666
Bykov A.I. 389, 495, 506
Bykov I.P. 26, 718

C

Chekan V. 728
Chernenko A. 579, 630
Chernenko N.M. 11
Chernyshev L.I. 230
Chervonyi I.F. 143
Chevychelova T.M. 549
Chivanov A.V. 136
Chivel Yu. 333
Chomenko E.V. 525
Choo K.Y. 250
Chugunova S.I. 556
Chuistov K.V. 483

Chujko A.A. 554
Churpita Ya.V. 249
Cren T. 670
Csach K. 454
Czopnik A. 227

D

D'yachkovsky P.K. 138
Danilov N.V. 642
Danylenko M.I. 245, 371, 377, 533, 543

Danylenko V.M. 175
Datskevich O. 521
Davydov V.A. 465
Dekhteruk V.I. 502
Demchenko L.D. 210
Demidik A.N. 365
Derev'yanko O.V. 161
Despotuli A. L. 64
Diaconescu M. 482
Dick T.A. 283, 285
Dmitriev A.I. 68
Dmitrovich A.A. 420
Domareva A.S. 275
Dominguez G. 552
Dotsenko F.F. 359
Dotsenko V. 149
Drapak S.I. 129
Drozd V.A. 462
Dub S.N. 539, 541, 543, 556, 595, 406

Dubikiwsky L.F. 547, 539
Dubok V.A. 412, 508, 706

Dubovik T.V. 607, 609
Dubrova O.E. 302
Dubrovskaya G. 643
Dubyna V.M. 116
Dudnik E.V. 177
Duhnenko A.V. 347
Dunin-Barkowski L.R. 685
Dvoynenko O.K. 518
Dymenko V.V. 554
Dziazko A. 460

E

Efimova I.E. 655
Efimova T.V. 483, 582
Efryushina N.P. 56
Egorov S.G. 143
Egorova N.B. 234
Einarsrud M.-A. 627
Ekimov E.A. 452
Enyashin A.N. 597
Eremenko A.M. 208
Eremenko L.I. 308
Ermishkin V.A. 661
Eryomin O.G. 56
Evtushok T.M. 531

F

Fal'kovs'kaja T.I. 306
Fedirko V. 287
Fedorenkova L. 573
Fedorus V.B. 308, 389
Feodorov V.A. 136, 469
Feodorova I.L. 78
Ficshich O.I. 549
Filippov V.B. 347, 404

- | | | | | | |
|-------------------------|--|--------------------|-----------------------------|---------------------|--------------------|
| Filonenko V.P. | 452, 465, 467 | Gridneva I.V. | 389, 495 | Kasheuski S.B. | 712 |
| Firstov S.A. | 12, 14, 99, 100, 437, 504, 521, 550, 558, 601, 623, 632, 634 | Grigorev O.N. | 531, 248, 397, 607 | Kashevarova L.S. | 465 |
| | | Grigorieva T.F. | 323, 324, 258, 325, 588 | Kashyryn V.P. | 443 |
| Fiyalka L.I. | 502 | Grigoryan L. | 429 | Kasumov A.M. | 516, 518 |
| Flachbart K. | 227 | Grigoryan R. | 429 | Kasumov M.M. | 554 |
| Flis A.A. | 304 | Grinkevych K.E. | 506 | Katerynchuk V.M. | 127 |
| Florea C. | 489 | Gromov V.E. | 52, 155, 335, 337, 653, 655 | Kazakevich A.G. | 619 |
| Florea A. | 489 | | | Kazakov S.S. | 589 |
| Fomenko V.V. | 317, 638 | Grushko B. | 39 | Khabashesku V.N. | 465 |
| Formanek B. | 256, 619 | Gryhoryeva O.V. | 204 | Kharlamov A.I. | 317, 638, 640 |
| Frenkel O.A. | 516 | Gubareni N.I. | 317, 640 | Khichenko V.F. | 289 |
| Frolov A.A. | 312 | Gubenko S.I. | 575 | Khina B.B. | 256 |
| Frolov A.G. | 649 | Gubin Yu.V. | 636 | Khitko V.I. | 268 |
| Froyen L. | 343 | Gumenyuk O.R. | 91 | Khomko T.V. | 638 |
| G | | Guslienکو Y.A. | 314 | Khorujaya V.G. | 103 |
| Gab A.I. | 327 | Gvozđ G.V. | 249 | Khotynenko N.G. | 317 |
| Gab I.I. | 300 | H | | Khovavko O.I. | 279 |
| Gagauz V.P. | 335 | Haidarshin A.F. | 319 | Khvadagiani A. | 345 |
| Galieva J.N. | 353 | Hambardzumyan A.F. | 221 | Khyzhun O.Yu. | 668 |
| Gamanovitch N.M. | 487 | Hashkovsky S.V. | 410, 693 | Kildiy A.I. | 262 |
| Gameza L.M. | 714 | Havryliuk V.P. | 629 | Kilimnik A.A. | 552 |
| Garan A.G. | 147 | Hilarov V.L. | 62 | Kim T.W. | 250, 277 |
| Garmash E.P. | 625 | Hirano T. | 447 | Kireev L.S. | 247 |
| Gavrilenko O.N. | 414 | Homenko E.V. | 194 | Kirichenko A.G. | 119 |
| Gavriliu G. | 482 | Homskaia I.V. | 613 | Kirilenko S.N. | 636 |
| Gawalek W. | 406, 595 | I | | Kirillova N.V. | 317 |
| Gierlotka S. | 452 | Ilyasov V. | 198 | Kislyak I. | 149 |
| Gilev V.G. | 196, 564, 710 | Ilyuschenko A.Ph. | 329, 333, 619 | Klein J. | 670 |
| | | | | Klimenko N.S. | 410, 577 |
| Gilyov V.G. | 250, 277 | Isaeva L.P. | 389 | Klochkov L.A. | 495, 607 |
| Giubileo F. | 670 | Isayev K.B. | 689 | Knohin V.N. | 418, 589 |
| Gleevoi Yu.V. | 249 | Ishikawa R. | 74 | Kobylynska O.V. | 321 |
| Glinchuk M.D. | 26, 718 | Istomina T.I. | 302 | Kokorina N.N. | 262 |
| Gnesin G.G. | 529 | Ivanchenko L.A. | 306 | Kolesnik N.F. | 119 |
| Gnyloskurenko S.V. | 74 | Ivanenko K.O. | 163 | Kolin'ko S. | 643 |
| Gogotsi G.A. | 425, 627 | Ivanov M. | 193 | Kolinsnichenko O.V. | 401, 611 |
| Goloubtsova E.S. | 145 | Ivanov V.N. | 316 | Kolmogorov G.L. | 89, 586 |
| Golovkova M.E. | 408 | Ivanov Yu.F. | 655 | Kolobov G.A. | 143 |
| Goltsov V.A. | 35 | Ivanov E.Yu. | 258 | Kolomiets A.T. | 632 |
| Goncharenko V.V. | 249 | Ivanova I.I. | 365, 504 | Kolotilkin O. | 70, 691 |
| Goncharova I.V. | 556 | Ivanovskaya V.V. | 597 | Kondratenko V.M. | 418, 589 |
| Goncharuk L.V. | 192, 523 | Ivanovskii A.L. | 597 | Konovalov S.V. | 335, 337, 653, 655 |
| Goncharuk V.A. | 245 | Ivanyshyn I.M. | 158 | Konstantinova T.E. | 153 |
| Gonzales-Rodriguez J.G. | 552 | Ivashchenko R.K. | 527 | Korchagin M.A. | 323 |
| Gorbachuk N.P. | 192, 496, 523 | Ivshina I.B. | 151 | Kordyuk A.A. | 595 |
| | | J | | Korniyenko K.Ye. | 103 |
| Gorban V. | 260 | Jakimenko I.L. | 179 | Korolev U.M. | 464 |
| Gorbunov A.V. | 487 | Jastrabik L. | 382 | Korovnikova N.I. | 451 |
| Gorbunova V.A. | 487 | Jovanovic Z.D. | 131 | Korsak Yu.V. | 431 |
| Gordienko Yu.G. | 683 | Jurchuk N.A. | 480 | Korzhova N.P. | 188, 473, 476 |
| Gorelik P.N. | 621 | K | | Koscheev S.V. | 664 |
| Gorin A.I. | 475 | Kadushnikov R.M. | 48, 206 | Kosenko N.S. | 202 |
| Gorlova S.N. | 653 | Kakazey M. | 552 | Kosenko P.N. | 202 |
| Gornaya I. | 550, 558 | Kaledin B.A. | 145 | Kosinskaia A.V. | 435 |
| Gorobetz Yu.I. | 681 | Kamalov M.M. | 387 | Kosourukov P.A. | 638 |
| Gorokhov V.M. | 97 | Kanchoukov V.Z. | 114 | Kostenco A.D. | 302, 435, 531, 549 |
| Gorokhov V.U. | 586 | Kaplina G.S. | 262 | Kostenko V.K. | 314 |
| Goryachev Yu.M. | 502, 603 | Kapustnikova S. | 14, 367 | Kostikov V.I. | 11 |
| Gostishev V.V. | 254 | Karamurзов B.S. | 114 | Kostornov A.G. | 18, 435, 512, 549 |
| Goydina S.V. | 317 | Karpets M.V. | 188, 321, 476, 708 | Kostyuk N.N. | 283, 285 |
| Graivoronskaya E.A. | 509, 668 | Kartuzov V.V. | 215, 408 | Kotenko V.A. | 531 |
| Grechishkin E. | 260 | Kasakov S. | 418 | Kotko A.V. | 186, 447 |
| Grevnov L.M. | 563 | | | Kotova N.V. | 116 |

- | | | | | | |
|--------------------|--|-------------------|--|------------------------|--|
| Kotrechko S. | 34, 84, 112,
123, 124,
133 | Kuzin N.N. | 452 | M | |
| Koval A.Y. | 248 | Kuzmenko M.M. | 537, 623 | Macht M. | 454 |
| Koval O.I. | 213, 613 | Kuzmenko N.N. | 478 | Maiboroda V.P. | 95, 163,
165, 167,
171 |
| Koval V.A. | 329 | Kuznechik O.O. | 20 | | |
| Koval' O.Yu. | 537, 623 | Kuznetsov M.V. | 339 | Makara V.A. | 44, 219 |
| Kovalchenko M.S. | 379, 545,
609 | Kuznetsova E.V. | 89 | Makarenko G.N. | 308, 389 |
| Kovalenko L. | 560 | Kyznetsova T.L. | 179, 728 | Maksimiva G.M. | 165, 167 |
| Kovalenko S.V. | 293 | L | | Makurin Yu.N. | 597 |
| Kovalenko V.V. | 335, 337,
653, 655 | Labunets T.F. | 321 | Malakhov V.Ya. | 603 |
| Kovalev A.E. | 89 | Laguta V.V. | 26, 718 | Malashenko I.S. | 186 |
| Kovalyuk Z.D. | 127, 129,
456, 458 | Lakeev V.A. | 274 | Malashenkov S.P. | 554 |
| | | Lakhnenko V.L. | 629 | Malkevich N.G. | 145 |
| Koviazina S.A. | 676 | Lakiza S.M. | 173 | Malochkin O.V. | 384 |
| Kovtunenkov V. | 643 | Lamy R. | 670 | Malyshev V.V. | 327 |
| Kozak S.I. | 349 | Laoui T. | 343 | Malysheva G.V. | 645 |
| Kozhan O.P. | 431 | Lapteva A.V. | 377, 379,
491, 500 | Margolin V.I. | 234 |
| <u>Kozlov A.V.</u> | 272 | Lashkarev G.V. | 68, 422 | Margrave J.L. | 465 |
| Kozlov E.V. | 335, 337,
653, 655 | Lashneva V.V. | 706 | Markiv V.Ya. | 56, 217,
223 |
| Kozlova L.E. | 182 | Latypov M.G. | 562 | Markova L. | 728 |
| Krajnikov A. | 140, 699 | Layshchenko A.B. | 347 | Maroresku I.I. | 625 |
| Krapivka N.A. | 493 | Lazhevskaya O. | 200 | Martsenyuk P.S. | 101, 102,
103 |
| Kravchenko L.P. | 702, 704 | Lebedev A.A. | 697 | | |
| Kravchenko V.M. | 219 | Lebedkina T.A. | 685 | Martusevich E.V. | 615 |
| Kravets A.F. | 681 | Lebuchova N.V. | 254 | Martynova L.M. | 21 |
| Kravtsova J.V. | 125 | Lebyodkin M.A. | 685 | Maslyuk V.A. | 519 |
| Krivchikov A. | 227 | Legkaya T.N. | 188, 473,
476 | Mastepan V.Yu. | 441 |
| Krushinskaya L.A. | 296, 607 | | | Matysina Z.A. | 208 |
| | | Lekishvili K. | 345 | Maximov A.I. | 664 |
| Kruth J.-P. | 343 | Leonidov I.A. | 676 | Maystrenko A.L. | 572 |
| Krutko N.P. | 78 | Leonidova O.N. | 676 | Mazilkin A.A. | 117, 695 |
| Kryachko L.A. | 408, 514,
525 | Lepeshkin Y.D. | 661 | Mazur V. | 14, 367 |
| Kryshanovska A.S. | 451 | Lesnik N.D. | 194 | Meduch R.M. | 314 |
| Kshnjakin V.S. | 611 | Letsko A.I. | 339 | Medvedev A.S. | 387 |
| Kucher O. | 123 | Levashov V.I. | 64 | Medvedeva N.I. | 121 |
| Kud' I.V. | 308 | Levchenko G.V. | 225 | Meleshevich K.A. | 190 |
| Kudin V.G. | 44 | Levina D.A. | 230 | Melnikov V.S. | 406 |
| Kukhareno S. | 381, 577,
581 | Levinson D.I. | 58 | | 595 |
| | | Levitsky M. | 367 | Meshkov Yu. | 34, 84, 112,
124 |
| Kulak L.D. | 14, 99, 478,
521, 550,
558, 601,
623, 634 | Liaschenko V.I. | 310 | Mestnikov N.S. | 138 |
| Kulich V.G. | 572 | Likhoded L.S. | 308 | Mikhailov O.V. | 508 |
| Kulichenko V. | 460 | Likhtorovich S.P. | 462 | Mileshkin M. | 85, 659 |
| Kulik A.I. | 443 | Lipatov Ya. M. | 375 | Milman Y.V. | 12, 15, 188,
245, 371,
377, 473,
476, 506,
527, 533,
535, 543,
556 |
| Kulik O.G. | 147 | Lisnyak V.V. | 232 | | |
| Kulikovskiy V. | 382 | Lisovsky A.F. | 252 | Milutinovic-Nikolic A. | 131 |
| Kulmetyeva V.B. | 568 | Litvin B. | 156 | Minakova R.V. | 194, 349,
408, 525 |
| Kunitskiy Yu.A. | 50, 95 | Litzendorf D. | 406, 595 | | |
| Kunty O.I. | 349 | Liydvinskaya T.A. | 511 | Minko D.V. | 20 |
| Kuprianov I.L. | 326 | Loboda P.I. | 104 | Mintyanskii I.V. | 456 |
| Kuprin V.V. | 533 | Lojkowski W. | 452 | Miracle D. | 12, 14, 99,
100, 188,
367, 371,
437, 476,
521, 533,
550, 558,
601, 623,
634 |
| Kurdyumov A.V. | 23, 296,
382, 399 | Lopato L.M. | 40, 42, 173,
177, 312 | | |
| Kurganskiy M.P. | 431 | | | Miroshnichenko V. | 367 |
| Kurilov G.V. | 439 | Loshak M.G. | 433 | Mischuk O.D. | 416 |
| Kurinnaya T.V. | 636 | Losiev U.A. | 291 | Mishchuk O.A. | 158 |
| Kurkova D.I. | 300 | Lotsko D.V. | 245, 371,
377, 506,
527, 533,
535 | Miskuf J. | 454 |
| Kurochkin V.D. | 677, 702,
704 | | | Mitz I.V. | 262 |
| Kusiak N.V. | 91 | Luchka M.V. | 314 | | |
| Kusmenko N. | 558 | Lugovskoi Y.F. | 87 | | |
| Kutseva N.A. | 359 | Lugovy M.I. | 425 | | |
| | | Lukovich V.V. | 408 | | |
| | | Lunyov A.N. | 341 | | |
| | | Luyckx S. | 556 | | |
| | | Luzinov I.A. | 720 | | |
| | | Lyakhov N.Z. | 323, 325,
588 | | |
| | | Lyashenko V.I. | 296 | | |

- Mkrtychev Yu.G. 642
Moiseev V.F. 186
Mokretzov A.S. 586
Molchanovskaya G.M. 163, 165, 167
Mordovets N.M. 476, 535
Mordyuk B.N. 272, 582
Morito F. 140, 699
Morozov Yu.G. 339
Moshchil V.E. 406, 595
Moshnikov V.A. 664
Mosina T.V. 248
Movchan B.A. 5, 584
Mozkova O.V. 56
Muratov V.B. 496
Muzyka N.R. 697
Mynyk S. 287
Myshlyayev M.M. 387
Myshlyayeva M.M. 387
- N**
Nagorny P.A. 406
Naidich Y.V. 248, 300
Nakamura T. 74
Napara-Volgina S.G. 519
Natsik V.D. 373, 454, 672, 687
Naumenko S.M. 219
Nedilko S.A. 460, 462
Neikov O.D. 371, 377
Nemoshkalenko V.V. 724
Neshpor I.P. 511
Netyaga V.V. 129
Nikolenko S.V. 254, 293, 471
Nikonenko A.P. 143
Nischenko M.M. 462
Noda T. 140
Normatov I.Sh. 490
Nosolev I.K. 153
Novikov G.I. 487
Novikov N.V. 9, 570
Novikov V.V. 72
Novikova V.I. 636
Novytsky V.G. 629
Nurkanov E.Y. 48
Nurkanov E.Y. 206
- O**
Ogenko V.M. 554
Okatova G.P. 339
Okhrimenko G. 547
Okovity V. 333
Okrostvaridze O. 345
Oleynik G.S. 80, 169
Onofrio G. 343
Onoprienko A. 270
Orletskii V.B. 129
Orlov S.A. 599
Orlovskaya N. 425, 627
Oryshch I.V. 493
Oschkaderov S.P. 184
Osipov A.S. 147
Osipova I.I. 529
Ovchar O.V. 416
Ovchinnikov I.N. 661
Ovchinnikov V.I. 213, 613
Ovsyannikov O. 124
- P**
Paderno V.N. 404
Paderno Yu.B. 227, 347, 404
Palosz B. 452
Pal-Val P.P. 672
Panashenko V.M. 609
Panasiyuk A.D. 316, 511
Panin V.E. 7
Panin V.N. 591
Panov V.S. 384
Paschenko E. 200, 577, 579, 630
Pashinskaya E.G. 275
Pashinskaya O.V. 275
Pashkova Y.V. 414
Pashynsky V.V. 441, 443
Paton B.E. 654
Patsyna R.V. 245, 377
Paustovsky A.V. 636, 720
Pavlenko T.P. 161
Pavligo T.M. 391
Pavlikov V.N. 625
Pavlitchuk T.V. 302
Pavlov V.S. 181
Pechkovsky E.P. 504
Perekos A.E. 483, 582
Pereliaeva L.A. 676
Permyakova I.J. 469
Petrosyan G.L. 221
Petrosyan V.G. 221
Petrov S. 260
Petrinin V.A. 155
Petrusha I.A. 399
Pilipenko N.P. 153
Pinchuk N.D. 306
Pirón Abellán J. 395
Pisarenko V.A. 181, 541
Piskalenko V.V. 52
Plekhanov K.A. 642
Pleskach I.V. 625
Pletnev R.N. 212
Plevkov A.V. 337
Plomodyalo L.G. 391
Plomodyalo R.L. 391
Plushnikova T.N. 136
Pluzhnikov V. 227
Podarevskaya O.V. 110
Podchernyaeva I.A. 316
Podrezov Y.N. 367, 385, 473, 476, 623
Pogrebnyak A.D. 331, 401, 611
Pohreliuk I. 287
Pokropivny A.V. 651
Pokropivny V.V. 393, 651
Polikarpov V.M. 464
Polischuk S.S. 584
Polyakov V.A. 591
Ponirko E.F. 249
Ponomarev S.S. 506
Popov V.P. 161
Popovich P. 232
Popovych V.O. 112
Porozova S. 17, 151, 568
Poryadchenko N.E. 493
Potsar N.A. 234
- Poznyak L.A. 241
Prikhna T.A. 406, 595
Prilutskiy E.V. 308, 310
Prokhorov I.V. 712
Prokopenko A.A. 248
Prokopenko G.I. 272, 582
Pronina L.N. 117, 695
Protasova S.G. 66
Pryadko L.F. 50
Pyriya M.M. 458
- Q**
Quadackers W.J. 395
- R**
Rabinovich O.S. 256, 266
Rachek O.P. 535
Radchenko A.K. 513
Radchenko M.V. 68
Ragozin Y. 17
Ragulya A.V. 321, 495
Rakhlin M. 259
Rakhmanina A.V. 465
Rakitsky A.N. 181
Ravi N. 633
Raychenko O.I. 74, 76, 161, 302
Red'ko V.P. 173
Revo S.L. 163
Rimbu G.A. 135
Ristic M.M. 50
Ritchkova M.I. 151
Rodichev D. 670
Rogozinskaya A.A. 298, 607, 609
Rogozinskii A. 298
Rogul T.G. 181, 632
Roik T.A. 617
Romanenko O.M. 702
Romanov G.N. 138
Rosantsev G.M. 281
Ruban A.K. 177
Rud' B.M. 603, 720
Rudenko O.V. 219
Rumyantseva A.I. 664
Ruzhitskaya T.V. 483, 582
Ryabicheva L.A. 125, 289, 291
Ryabtsev A.D. 441
Ryabtsev S.I. 359
Ryumshina T.A. 153
- S**
Sabokar V.K. 247, 361
Sacks W. 670
Safonova A.M. 593
Sahvadze D. 345
Saito H. 699
Sakamoto K. 74
Sakhnenko A.V. 391
Saldan I.V. 438
Saltykov V.A. 190
Samelyuk A.V. 181, 190, 245, 377, 527, 539, 541
Saroka D.I. 657, 716
Sartinska L.L. 529
Sarzhani G.F. 527, 558
Savchuk Ya.M. 406
Savich V.V. 343

Savin Yu.N.	423, 451	Siman M.I.	502	Talijan N.M.	131
Savitskii A.P.	138	Simeonova Y.	549	Tarasov P.P.	138
Savitskii P.I.	456	Sinelichenko A.K.	171	Tarasyuk E.V.	410
Schmidt Ch.	406	Singheiser L.	395	Târdei C.	482
Schubert M.	259	Sirko A.I.	377	Tavadze G.	345
Sckolnii V.K.	163	Sirko O.I.	245, 371,	Tel'nikov E.Ya.	720
Semenyuk N.I.	279		527	Telemko O.V.	158
Semerenko Yu.A.	687	Sitalo V.G.	575	Teplenko M.A.	316
Senkov O.	188, 521,	Skilko A.M.	662	Tereshko N.V.	283
	550, 558,	Skorokhod V.V.	3, 48, 60,	Tichonov A.	17
	601, 634		651	Tikhonovsky M.	149
Senyut V.	485	Skrypai A.A.	496	Timofeeva I.I.	389, 495
Serdyuk G.G.	391	Slavoljubov V.S.	599	Tjalin Yu. I.	136
Sergeyev V.V.	341	Slesarev V.N.	452	Tkachenko L.N.	508
Sergienko N.V.	406, 595	Slipenyuk A.M.	718	Tkachenko V.D.	625
Sergienko O.A.	431	Slipenyuk A.N.	533, 543	Tkachenko V.G.	363
Serov I.N.	234	Slobodyanik N.S.	232	Tkachenko V.M.	275
Sevastyanov E.S.	97	Slys I.	160, 298	Tkachenko Yu.G.	310, 498,
Shalunov E.P.	375, 599	Slyunyayev V.N.	425		500
Shalunova N.B.	375	Smetkin A.A.	319	Tkachuk A.A.	700
Shaposhnikova T.I.	531	Smirnov S.N.	672	Tokhtuev V.G.	377
Shapoval T.O.	101, 102	Smyshlyaeva T.V.	566	Tolmachev A.V.	423, 451
Shapovalov V.I.	46	Sofronov A.A.	597	Tolochko N.K.	343
Sharai E.V.	435	Sokolov A.N.	217	Tomashik V.M.	91
Shatsikh C.K.	317	Solntsev V.P.	60	Tomashik Z.F.	91
Shcherbak I.A.	82	Solntseva T.A.	60	Tomila T.	296, 552
Shcherbakova L.	298	Solonin Yu.M.	30, 509,	Tovarovskiy I.G.	243
Shcheretsky O.A.	629		668	Trapalis Ch.	317
Shchur D.	298	Sorokin U.V.	241	Trebnikov A.G.	285
Sheleg V.K.	20	Sosnin O.V.	653, 655	Tretyachenko L.	99, 190
Shelud'ko V.E.	720	Sozaev V.A.	114	Trofimova L.M.	535
Shemet V.	395	Spiridonov Yu.L.	341	Troyansky A.A.	441
Shestakov S.I.	570, 572	Spiridonova I.	156, 605	Tsellermaer V.V.	653, 655
Shevchenko A.D.	724	Sribny V.M.	349	Tsellermaer V.Ya.	52, 335
Shevchenko A.V.	177	Stamatin I.	135	Tsirkin A.T.	289
Shevchenko E.A.	412	Static-Trosic J.	131	Tsukruk V.V.	720
Shevchenko O.M.	182	Statsenko V.M.	518	Tsurpal L.A.	702
Shevchenko O.V.	40	Steblenko L.P.	219	Tsyganenko N.I.	101, 102
Shevchenko V.	264, 410	Steinhauser S.	333	Tsypanin P.P.	138
Shevchuk U.F.	617	Stepanenko A.V.	397	Tsyrkyn A.T.	291
Shevchyk N.V.	82	Stepanenko N.V.	268, 353	Turkevich V.Z.	54, 147
Shevtsov A.	333	Stepanenko V.N.	266	Tychomyrov S.V.	241
Shilo A.	200, 381,	Stepanov G.V.	141	Tyurin Y.N.	331, 401,
	577, 581	Stetsenko N.	123		611
Shilov V.V.	410	Stetsyuk T.V.	300	Tzellermaer V.Ya.	155
Shilova O.A.	410, 664,	Stovpchenko A.P.	589, 591	U	
	693	Strativnov V.	431	Ulrikh T.A.	586
Shinkaruk A.V.	412	Strekalovsky V.N.	676	Ulshin S.V.	186
Shipitsa N.A.	657, 716	Stukalo V.A.	106	Ulshin V.I.	241
Shipovskiy V.Yu.	640	Stus N.V.	232	Ulyanova T.M.	78
Shirokov A.V.	141	Sudavtsova V.S.	106, 108,	Usakov E.I.	632
Shitsevalova N.	227		110, 232	Usenko N.	193
Shkilko A.	149	Sudnik L.V.	621	Ushakov I.V.	469
Shpak A.P.	50	Sukhostavets S.V.	512	Usherenko S.M.	213, 575,
Shpilevskaya L.E.	593	Sukhova O.	605		613
Shportko A.	367	Sung J.S.	196, 250,	Ushkalov L.N.	638, 640
Shtern M.B.	508		277	Uskova N.N.	327
Shulishova O.I.	82	Sursaeva V.G.	66	Ustinov A.I.	202, 584
Shulzhenko A.A.	217, 223	Surzhenko A.B.	406, 595	Ustinova G.P.	97
Shumikhin V.S.	629	Susidko V.L.	408	<u>Utkin S.V.</u>	516
Shurygina Z.P.	506	Sverdun V.B.	595	V	
Shvartsman O.Y.	502	Svistun L.I.	391	V'yunov O.	560
Sidor O.M.	127	Svyatenko O.M.	279	Vakulenko I.A.	225
Sidorenko S.I.	700	Sydorenko D.G.	443	Varshavskaya I.G.	633
Sidorko V.	191, 192,	T		Varyukhin V.N.	275
	523	Tabachnikova E.D.	373, 454	Vasilevich V.P.	266, 268
Signorelli E.	343	Talako T.L.	339, 619	Vasylyev O.	623, 634
Silantiev V.I.	681	Talanin I.E.	58	Vasylyev M.A.	700
Silchenko Ya.	579, 630	Talanin V.I.	58		

INDEX OF AUTHORS

Ved V.	427	W		Zakharova N.P.	245, 377
Velikanova T.Ya.	39, 99, 100, 437	Wendland St.	375	Zalutskiy V.P.	483
Verbylo D.G.	537	Wendt M.	406	Zamalin E.Yu.	695
Verchoturov A.D.	254, 293, 471	Werheit H.	32	Zamkov V.N.	247, 361
Vilkova N.Yu.	700	Wildemann V.E.	93	Zankevich A.B.	480
Vinnitchenko V.D.	722	Wojciechowski K.W.	72	Zasimchuk E.E.	683
Vinogradov L.M.	266	Y		Zaslavskaya L.V.	281
Vinoviy V.	418	Yagodkin V.V.	175	Zaslonkin A.V.	127, 456
Vityaz P.A.	339	Yakovlev E.N.	465	Zatovskiy V.G.	408
Vlasova M.	552	Yanchuk I.	270	Zatulovskiy A.S.	274, 435
Vlasova N.M.	471	Yaskiv O.	287	Zatulovskiy S.S.	435
Volkogon V.M.	169, 302	Yefimov M.O.	371, 506, 533, 535	Zavaliy I.Yu.	403, 438
Voloshko S.M.	700	Yenevich V.G.	408	Zel'dovich V.I.	613
Voltchek N.L.	697	Yurchenko L.P.	718	Zelyavskii V.B.	296
Voropaev V.S.	245, 377	Yurchuk M.O.	545	Zhabrev V.A.	664
Voropayev V.S.	371	Yuriev A.B.	337	Zharin A.L.	657, 716
Voskoboinik I.V.	188, 473, 476	Yurkova O.I.	679	Zhunkovskii G.L.	531
Vovkotrub N.E.	108	Yuryeva E.I.	212	Zhuravlev V.S.	110, 248
Voynash V.Z.	476	Z		Zibrov I.P.	467
Vrzhyzhevsky E.L.	361	Zadkevich M.L.	331, 401	Zimina G.	133
		Zaginaichenko S.Yu.	208	Zinchenko V.F.	56
		Zagoruiko L.	149	Zinevich T.M.	116
		Zakarjan D.A.	215	Zinkovsky G.	156
				Zubets Y.E.	541
				Zvonarev E.V.	97
				Zyatkevich N.S.	607, 609
				Zykova E.V.	539

LIST OF PARTICIPANTS

**This Page Intentionally
Left Blank**

A

ADEEV V.M.

Frantsevich Institute for Problems of Material
Science, NASU, Kyiv, Ukraine
Tel.: (044) 444-3364

AKULITCH A.V.

Lykov Heat and Mass Transfer Institute, NASB;
Minsk, Belarus
Tel.: (375 017) 284-1057, 284-2775, 284-1057,
284-2480
Fax: (375 017) 232-2513
E-mail: orebi@hmti.ac.by, and@hmti.ac.by,
bor@itmo.by

ALEKSEITSEV A.V.

Research Center of the Fund for Development New
Medical Technologies "AIRES", Saint-Petersburg,
Russia
Tel.: (812) 596-3533
Fax: (812) 596-3551
E-mail: foundation@aires.spb.ru

ALEXANDROVA L.I.

Bakul Institute of Superhard Materials, NASU, Kyiv,
Ukraine
Tel.: (044) 468-8631, 430-1126
Fax: (044) 468-8625
E-mail: prikhna@iptelecom.net.ua,
loshak@ism.kiev.ua

ALFINTSEVA R.A.

Frantsevich Institute for Problems of Material
Science, NASU, Kyiv, Ukraine
Tel.: (044) 444-0256
Fax: (044) 444-2131
E-mail: post@ipms.kiev.ua

ALIEVSKY V.M.

Ural State Technical University, Ekaterinburg,
Russia
Tel.: (3432) 75-9724
Fax: (3432) 75-9407
E-mail: radi@siams.com, bas@siams.com,
nurkanov@siams.com

ANANITCH G.V.

Concern "Planar", Minsk, Belarus
Tel.: (017) 221-7210

ANDREEVA A.F.

Frantsevich Institute for Problems of Material
Science, NASU, Kyiv, Ukraine
Tel.: (044) 444-8218
E-mail: andreeva@ipms.kiev.ua

ANDREEVA A.V.

Institute of Microelectronics Technology RAS,
Chernogolovka, Russia
Tel.: (095) 962-4780
Fax: (095) 962-8047
E-mail: andreeva@ipmt-hpm.ac.ru

ANDREYEV M.

Powder Metallurgy Research Institute, NASB, Minsk,
Belarus
Tel.: (517) 239-9804
Fax: (517) 210-0574
E-mail: pb8361@belsonet.net,
chekan@srpmi.minsk.by, vityaz@srpmi.minsk.by

ANDRIEVSKAYA E.R.

Frantsevich Institute for Problems of Material
Science, NASU, Kyiv, Ukraine
Tel.: (044) 444-3573
Fax: (044) 444-2131
E-mail: ragulya@materials.kiev.ua

ANDRIEVSKI R.A.

Institute of Problems of Chemical Physics, RAS,
Chernogolovka, Russia
Tel.: (7-096) 522-3577
E-mail: ara@icp.ac.ru

ANDRUSHCHIK L.O.

Kurdyumov Institute for Metal Physics, NASU, Kyiv,
Ukraine
Tel.: (044) 444-9586
Fax: (044) 444-9561
E-mail: metall@imp.kiev.ua

ANTANOVICH A.A.

Vereschagin Institute for High Pressure Physics,
RAS, Troitsk, Russia
Tel.: (095) 334-0732
Fax: (095) 334-0012
E-mail: ekimov@hppt.troitsk.ru

ANTSIFEROV V.N.

Research Center of Powder Materials Science,
Perm, Russia
Tel.: (3422) 39-1119, 39-1110
Fax: (3422) 39-1122
E-mail: director@pm.pstu.ac.ru

ARINKIN S.M.

Lykov Heat & Mass Transfer Institute, NASB, Minsk,
Belarus
E-mail: sergey_demidkov@tut.by

ARISTOVA I.M.

Institute of Solid State Physics, RAS,
Chernogolovka, Russia
Tel.: (095) 993-2755
Fax: (096) 524-9701
E-mail: aristova@issp.ac.ru

ARTAMONOV V.

Institute of Semiconductor Physics, NASU, Kyiv, Ukraine

ARTUSHKEVICH A.S.

Belorussian Institute for Postgraduate Medical Education, Minsk, Belarus
Tel.: (375 17) 232-3339
Fax: (375 17) 232-3339

ARTYUKH L.V.

Frantsevich Institute for Problems of Material Science, NASU, Kyiv, Ukraine
Tel.: (044) 444-3090
Fax: (044) 452-55-23
E-mail: velikanova@materials.kiev.ua

ASNIS E.A.

Paton Electric Welding Institute, NASU, Kyiv, Ukraine
Tel.: (044) 227-7246

ASTAKHOV E.A.

Paton Electric Welding Institute, NASU, Kyiv, Ukraine
Tel.: (044) 220-8687
Fax: (044) 220-9215
E-mail: borisov.y@paton.kiev.ua

ASTASHYNSKI V.

Institute of Molecular and Atomic Physics, Minsk, Belarus

AVRAMCHUK S.K.

Frantsevich Institute for Problems of Material Science, NASU, Kyiv, Ukraine
Tel.: (044) 444-3401
E-mail: dep20@ipms.kiev.ua

B

BAGINSKY I.L.

Kiev Taras Shevchenko National University, 64 Vladimirskaya St., Kiev 01033, Ukraine
Tel.: (044) 221-0206
E-mail: nedilko@red-gw.univ.kiev.ua

BAGLYUK G.A.

Frantsevich Institute for Problems of Material Science, NASU, Kyiv, Ukraine
Tel.: (044) 444-3345
Fax: (044) 452-5523
E-mail: rapid@materials.kiev.ua

BALYUK Z.V.

Dnipropetrovsk National University, Dnipropetrovsk, Ukraine
Tel.: (0562) 776-9042
E-mail: metal@ff.dsu.dp.ua

BANCIU C.

Advanced Research Institute for Electrical Engineering, Bucharest, Romania
Tel.: +40 1-346-7283
Fax: +40 1-346-7283
E-mail: electmat@icpe.ro

BANKOVSKIY O.

Frantsevich Institute for Problems of Material Science, NASU, Kyiv, Ukraine
Tel.: (044) 444-3345
Fax: (044) 452-5523
E-mail: dep22@materials.ua

BARABASH O.M.

Kurdyumov Institute for Metal Physics, NASU, Kyiv, Ukraine
Tel.: (044) 444-3061
Fax: (044) 444-3061
E-mail: barabash@imp.kiev.ua

BARINOVA A.P.

Institute of Solid State Chemistry and Mechanochemistry, SB of RAS, Novosibirsk, Russia
E-mail: barinova_ap@mail.ru

BASHEV V.F.

Dnipropetrovsk National University, Dnipropetrovsk, Ukraine
Tel.: (0562) 776-9042
E-mail: metal@ff.dsu.dp.ua

BAT'KO I.

Institute of Experimental Physics, Kosice, Slovakia

BDIKIN I.K.

Institute of Solid State Physics, RAS, Chernogolovka, Russia
Tel.: (095) 993-2755
Fax: (096) 524-9701
E-mail: mazilkin@issp.ac.ru

BEGA M.D.

Frantsevich Institute for Problems of Material Science, NASU, Kyiv, Ukraine
Tel.: (044) 444-0090, 444-1321
Fax: (044) 444-2131, 444-3502
E-mail: oleggrig@materials.kiev.ua, step@materials.kiev.ua

BEGA N.

Frantsevich Institute for Problems of Material Science, NASU, Kyiv, Ukraine
Tel.: (044) 444-0051
E-mail: podrezov@materials.kiev.ua

BEL'SKAYA G.N.

Research Center of the Fund for Development New Medical Technologies "AIRES", Saint-Petersburg, Russia
Tel.: (812) 596-3533
Fax: (812) 596-3551
E-mail: foundation@aires.spb.ru

BELCHIKOV E.

Zaporizhzhya National Technical University,
Zaporizhzhya, Ukraine
Tel.: (0612) 64-44-55
Fax: (0612) 64-2141
E-mail: vshevch@zstu.edu.ua

BELETSKAYA O.E.

Dnipropetrovsk National University, Dnipropetrovsk,
Ukraine
Tel.: (0562) 776-9042
E-mail: metal@ff.dsu.dp.ua

BELIAEV A.V.

Powder Metallurgy Research Institute, NASB, Minsk,
Belarus
Tel.: (375 17) 232-8271, 232-6340
Fax: (375 17) 232-5691, 210-0574
E-mail: Alexil@srpmi.belpak.minsk.by,
beliayev_a@open.by

BELOBORODOV I.I.

Frantsevich Institute for Problems of Material
Science, NASU, Kyiv, Ukraine
Tel.: (044) 444-1571, 444-1124

BELOTS'KY O.V.

National Technical University of Ukraine "Kyiv
Polytechnic Institute", Kyiv, Ukraine
Tel.: (044) 441-1076
E-mail: byakova@vic.com.ua

BELOUS A.G.

Vernadskii Institute of General and Inorganic
Chemistry, NASU, Kyiv, Ukraine
Tel.: (044) 444-2211
Fax: (044) 444-2211
E-mail: belous@ionc.kar.net

BELOUSOVA E.E.

Donetsk National University, Donetsk, Ukraine
Tel.: 91-9238
E-mail: getman@dongu.donetsk.ua, dshe@skif.net

BELYAEV A.V.

Powder Metallurgy Research Institute, NASB, Minsk,
Belarus
Tel.: (375 17) 232-8271, 232-6340, 239-9827
Fax: (375 17) 232-5691, 210-0574
E-mail: beliayev_a@open.by

BELYAEVA O.V.

Regional Clinical Dentistry, Perm, Russia

BELYAVIN K.E.

Powder Metallurgy Research Institute, NASB, Minsk,
Belarus
Tel.: (517) 239-9828
Fax: (517) 210-0574
E-mail: vityaz@srpmi.minsk.by

BELYAVINA N.M.

Taras Shevchenko Kyiv National University, Kyiv,
Ukraine
Tel.: (044) 266-2335
E-mail: be1mar@univ.kiev.ua

BELYAVINA N.N.

Taras Shevchenko Kyiv National University, Kyiv,
Ukraine
Tel.: (044) 266-2335
E-mail: be1mar@univ.kiev.ua

BELYKH V.D.

Institute of Solid State Chemistry and
Mechanochemistry, SB of RAS, Novosibirsk, Russia
E-mail: barinova_ap@mail.ru

BENGUS V.Z.

Verkin Institute for Low Temperature Physics and
Engineering, NASU, Kharkiv, Ukraine
Tel.: (057) 230-0331
Fax: (057) 233-5593
E-mail: BENGUS@ilt.kharkov.ua

BERENDA V.V.

Zaporizhzhya State Engineering Academy,
Zaporizhzhya, Ukraine
Tel.: (0612) 29-7216, 60-1250, 601330
E-mail: kmarkovich@efp.com.ua,
beley_finance@efp.com.ua

BEREZUTSKI V.

Frantsevich Institute for Problems of Material
Science, NASU, Kyiv, Ukraine
Tel.: (044) 444-3090
Fax: (044) 444-2131
E-mail: dep6@materials.kiev.ua

BESOV A.V.

National Technical University of Ukraine "Kyiv
Polytechnic Institute", Kyiv, Ukraine
Tel.: (044) 441-1546
E-mail: oksana@materilas.kiev.ua

BEZHENAR M.P.

Bakul Institute of Superhard Materials, NASU, Kyiv,
Ukraine
Tel.: (044) 430-3506
E-mail: ism1@kibor.kiev.ua

BEZIMYANNIY Y.G.

Frantsevich Institute for Problems of Material
Science, NASU, Kyiv, Ukraine
Tel.: (044) 444-2055, 444-2331
Fax: (044) 444-2131

BIBLIK I.

Podgorny Institute for Mechanical Engineering
Problems, NASU, Kharkiv, Ukraine
Tel.: (0572) 95-9538
Fax: (0572) 94-4635, 94-2914
E-mail: miles@ipmach.kharkov.ua

BIELOBORODOVA O.A.

Taras Shevchenko Kyiv National University, Kyiv, Ukraine
Tel.: (044) 221-0270
E-mail: vovd@ukr.net, vsudavtsova@univ.kiev.ua

BILEVYCH YE.O.

Institute for Semiconductor Physics, National Academy of Sciences of Ukraine, Kyiv, Ukraine
Tel.: 265-5755
Fax: 265-8342
E-mail: tomashyk@isp.kiev.ua, yarri@gmx.ch

BILOUS A.M.

Frantsevich Institute for Problems of Material Science, NASU, Kyiv, Ukraine
Tel.: (044) 444-3061
Факс(044) 444-3061, 452-5523
E-mail: biloys@materials.kiev.ua

BILOUS O.O.

Frantsevich Institute for Problems of Material Science, NASU, Kyiv, Ukraine
Tel.: (044) 444-3090
Fax: (044) 452-55-23
E-mail: velikanova@materials.kiev.ua

BILOUSOV M.M.

Donetsk Physical-Technical Institute, NASU, Donetsk, Ukraine
Tel.: 337-9608
E-mail: slobodina_vera@mail.ru

BILYAVINA N.M.

Taras Shevchenko Kyiv National University, Kyiv, Ukraine
Tel.: (044) 266-2335
E-mail: belmar@mail.kiev.ua

BLYZNUK O.V.

National Technical University of Ukraine "Kyiv Polytechnic Institute", Kyiv, Ukraine

BOBBA F.

Physics Department, University of Salerne, Salerne, Italy

BOBET J.L.

Institute de la Matière Condensée de Bordeaux, Pessac, France

BODNAR O.B.

Moscow State Academy of the Instrument Engineering and Information, Moscow, Russia
Tel.: (095) 269-4622
Fax: (095) 162-0470
E-mail: vep@octava.msk.su

BOGOMOL YU.I.

National Technical University of Ukraine "Kyiv Polytechnic Institute", Kyiv, Ukraine
E-mail: loboda@i.com.ua

BOHAC P.

Institute of Physics, Academy of Sciences of the Czech Republic, Prague, Czech Republic

BOLDYREV V.V.

Institute of Solid State Chemistry and Mechanochemistry, SB of RAS, Novosibirsk, Russia
E-mail: barinova_ap@mail.ru

BOLEDZYUK V.B.

Chernivtsi Department, Frantsevich Institute for Problems of Material Science, NASU, Chernivtsi, Ukraine
Tel.: (03722) 25-155
Fax: (03722) 20-050
E-mail: chimsp@unicom.cv.ua

BOLGAR A.S.

Frantsevich Institute for Problems of Material Science, NASU, Kyiv, Ukraine
Tel.: (044) 444-1290
Fax: (044) 444-2131
E-mail: bas@materials.kiev.ua

BOLTOVETS N.S.

State Plant "Scientific-Research the Institution "Orion", Kyiv, Ukraine
Tel.: (044) 446-5291
E-mail: bms@mvsemicond.kiev.ua

BONDAR A.A.

Frantsevich Institute for Problems of Material Science, NASU, Kyiv, Ukraine
Tel.: (044) 444-3090
Fax: (044) 452-55-23
E-mail: velikanova@materials.kiev.ua

BONDAR A.M.

Advanced Research Institute for Electrical Engineering, Bucharest, Romania
Tel.: +40 1-346-7283
Fax: +40 1-346-7283
E-mail: electmat@icpe.ro

BONDARENKO B.I.

Gas Institute, NASU, Kyiv, Ukraine
E-mail: bond@bond.elan-ua.net

BONDARENKO M.E.

Frantsevich Institute for Problems of Material Science, NASU, Kyiv, Ukraine
Tel.: (044) 444-0256
Fax: (044) 444-2131

BONDARENKO V.P.

Bakul Institute of Superhard Materials, NASU, Kyiv, Ukraine
Tel.: (044) 468-8623
Fax: (044) 468-8632, 468-8624
E-mail:alcon@ism.kiev.ua,almaz@ism.kiev.ua

BONDAREV E.

Bakul Institute of Superhard Materials, NASU, Kyiv, Ukraine
Tel.: (044) 430-76-94
Fax: (044) 430-76-94
E-mail: shilo@ism.kiev.ua, svetlana@ism.kiev.ua

BONDARKOVA G.V.

Institute of Magnetism, NASU, Kyiv, Ukraine
Tel.: (044) 444-1020, 444-9568
E-mail: fmf@ntu-kpi.kiev.ua

BONDARUK O.N.

Research Institute of Radiomaterials, Minsk, Belarus
Tel.: (375 017) 278-4054
Fax: (375 017) 278-3705
E-mail: irma@infonet.by

BONSHTEDT B.E.

Vavilov VNTS GOI, Saint-Petersburg, Russia
Tel.: (812) 596-3533
Fax: (812) 596-3551
E-mail: foundation@aires.spb.ru

BORODIANS'KA H. YU.

Frantsevich Institute for Problems of Material Science, NASU, Kyiv, Ukraine
E-mail: oleganna@svitonline.com

BORODULIA V.A.

Lykov Heat and Mass Transfer Institute, NASB, Minsk, Belarus
Tel.: (375 017) 284-1057, 284-2775, 284-1057, 284-2480
Fax: (375 017) 232-2513
E-mail: orebi@hmti.ac.by, and@hmti.ac.by, bor@itmo.by

BORYSOV D.B.

Frantsevich Institute for Problems of Material Science, NASU, Kyiv, Ukraine
Tel.: (044) 444-3090
Fax: (044) 452-55-23
E-mail: velikanova@materials.kiev.ua

BOVKUN G.A.

Frantsevich Institute for Problems of Material Science, NASU, Kyiv, Ukraine
Tel.: (044) 444-2101
Fax: (044) 444-2131
E-mail: kovalms@ipms.kiev.ua

BOZHKO S.A.

Bakul Institute of Superhard Materials, NASU, Kyiv, Ukraine
Tel.: (044) 430-3506
E-mail: ism1@kibor.kiev.ua

BRINSON B.

Rice University, Houston, TX, USA
Tel.: 713-348-5485
Fax: 713-523-8236
E-mail: brinson@rice.edu, marsrav@rice.edu, khval@ruf.rice.edu

BRITUN V.F.

Frantsevich Institute for Problems of Material Science, NASU, Kyiv, Ukraine
Tel.: (044) 444-3401
E-mail: britun@i.com.ua, dep20@ipms.kiev.ua

BRODNIKOVSKIY N.P.

Frantsevich Institute for Problems of Material Science, NASU, Kyiv, Ukraine
Tel.: (044) 444-8286, 444-2524, 444-0294

BRUEHNE K.

Institute of Physical Electronics, University of Stuttgart, Stuttgart, Germany
E-mail: Michail.Rakhlin@ipe.uni-stuttgart.de

BUBNOV YU.Z.

"Avangard-Microsensor" Co, Saint-Petersburg, Russia
Tel.: (812) 543-9076
E-mail: olgashilova@peterlink.ru

BUDOVSKIKH E.A.

Siberian State University of Industry, Novokuznetsk, Russia
Tel.: (3843) 46-2277
Fax: (3843) 46-5792
E-mail: gromov@physics.sibsiu.ru

BUKHOVETSV.L.

Institute of Physical Chemistry, RAS, Moscow, Russia
Tel.: (095) 955-4673, 955-4470
Fax: (095) 952-5308
E-mail: iravarsh@yahoo.com, buhovet@mail.ru

BULANOV V.YA.

Institute for Metallurgy, UrB of RAS, Ekaterinburg, Russia
Tel.: (3432) 67-8906
Fax: (3432) 67-9186
E-mail: powder@imet.mplik.ru

BULANOVA M.V.

Frantsevich Institute for Problems of Material Science, NASU, Kyiv, Ukraine
Tel.: (044) 444-3090
Fax: (044) 444-02131
E-mail: bulanova@materials.kiev.ua, dep6@materials.kiev.ua

BUNCHUK J.P.

Yuzhnoye State Design Office, Dnipropetrovsk, Ukraine
Tel.: (0562) 92-5113
Fax: (0562) 92-5113
E-mail: kbu@public.ua.net

BURKA M.P.

Frantsevich Institute for Problems of Material Science, NASU, Kyiv, Ukraine
Tel.: (044) 444-3090
Fax: (044) 452-55-23
E-mail: velikanova@materials.kiev.ua

BUTENKO V.

Dnipropetrovsk National University, Dnipropetrovsk, Ukraine
Tel.: (0562) 469-212
E-mail: odm@ff.dsu.dp.ua

BUTORIN P.E.

Frantsevich Institute for Problems of Material Science, NASU, Kyiv, Ukraine
Tel.: (044) 444-3228
Fax: (044) 444-2131
E-mail: lashk@ipms.kiev.ua

BUYANOV Y.

Frantsevich Institute for Problems of Material Science, NASU, Kyiv, Ukraine
Tel.: (044) 444-3090
Fax: (044) 444-02131
E-mail: dep6@materials.kiev.ua

BUZHENETS E.I.

Frantsevich Institute for Problems of Material Science, NASU, Kyiv, Ukraine
Tel.: (044) 444-2371, 444-3061, 444-1501
Fax: (044) 444-3061
E-mail: abykov@materials.kiev.ua, gridneva@materials.kiev.ua

BYAKOVA A.V.

National Technical University of Ukraine "Kyiv Polytechnic Institute", Kyiv, Ukraine
E-mail: byakova@vic.com.ua

BYKOV A.I.

Frantsevich Institute for Problems of Material Science, NASU, Kyiv, Ukraine
Tel.: (044) 444-2371, 444-3415, 444-3061
Fax: (044) 444-3061
E-mail: abykov@materials.kiev.ua,

BYKOV I.P.

Frantsevich Institute for Problems of Material Science, NASU, Kyiv, Ukraine
Tel.: (044) 444-1540
Fax: (044) 444-2131
E-mail: dep4@materials.kiev.ua

C

CARTUZOV V.V.

Frantsevich Institute for Problems of Material Science, NASU, Kyiv, Ukraine
Fax: (044) 444-2131

CHEKAN V.

Powder Metallurgy Research Institute, NASB, Minsk, Belarus
Tel.: (517) 239-9804
Fax: (517) 210-0574
E-mail: chekan@srpmi.minsk.by

CHERNENKO A.

Bakul Institute of Superhard Materials, NASU, Kyiv, Ukraine
Tel.: (044) 430-76-94
Fax: (044) 430-76-94
E-mail: shilo@ism.kiev.ua, svetlana@ism.kiev.ua

CHERNENKO N.M.

Federal Governmental Unitarity Enterprise "The State Research Institute of Graphite-Based Structural Materials" – FGUE "NII Grait", Moscow, Russia
Tel.: (095) 176-2988
Fax: (095) 176-2988
E-mail: grafit@aha.ru

CHERNYSHEV L.I.

Frantsevich Institute for Problems of Material Science, NASU, Kyiv, Ukraine
Tel.: (044) 444-3231, 444-2073
Fax: (044) 444-2131
E-mail: chern@materials.kiev.ua

CHERVONYI I.F.

Zaporizhzhya State Engineering Academy, Zaporizhzhya, Ukraine
Tel.: (80612) 60-1261
E-mail: rot@zgia.zp.ua, al_nik_co@ukr.net

CHEVYCHELOVA T.M.

Frantsevich Institute for Problems of Material Science, NASU, Kyiv, Ukraine
Tel.: (044) 444-1571
Fax: (044) 444-2131
E-mail: dir@ipms.kiev.ua

CHIVANOV A.V.

Derzhavin Tambov State University, Tambov, Russia
Tel.: (0572) 35-2614
Fax: (0752) 710-307
E-mail: plushnik@mail.ru

CHIVEL YU.

Institute of Molecular and Atomic Physics, Minsk, Belarus

CHOMENKO E.V.

Frantsevich Institute for Problems of Material Science, NASU, Kyiv, Ukraine
Tel.: (044) 444-1181, 444-2474
E-mail: 29min@ipms.ua

CHOO K.Y.

Korea Institute of Energy Research, 71-2 Jang-dong, Yoo-song, Daejeon, Korea

CHUGUNOVA S.I.

Frantsevich Institute for Problems of Material Science, NASU, Kyiv, Ukraine
Tel.: (044) 444-3061
Fax: (044) 444-3061
E-mail: Irina@materials.kiev.ua

CHUISTOV K.V.

Kurdyumov Institute for Metal Physics, NASU, Kyiv, Ukraine
Tel.: (044) 44-9546, 444-9531, 444-9532
Fax: (044) 444-2561
E-mail: perekos@imp.kiev.ua, potvora@imp.kiev.ua

CHUJKO A.A.

Institute for Surface Chemistry, NASU, Kyiv, Ukraine
Tel.: (044) 444-1135
Fax: (044) 444-3567
E-mail: user@sufchem.freenet.kiev.ua

CHURPITA YA.V.

National Technical University of Ukraine "Kyiv Polytechnic Institute", Kyiv, Ukraine
E-mail: rchebot@ukr.net

CREN T.

Groupe de Physique des Solides, C.N.R.S., Universités Paris 6 et 7, Paris, France
Tel.: 0144274672
Fax: 0143542878
E-mail: rodichev@gps.jussieu.fr

CSACH K.

Institute of Experimental Physics, Kosice, Slovakia

CZOPNIK A.

Trzebiatowski Institute of Low Temperature and Structure Research of Polish Academy of Sciences, Wroclaw, Poland

D

D'YACHKOVSKY P.K.

Amosov Yakutiya State University, Yakutsk, Russia
Tel.: (4112) 25-3212
Fax: (4112) 26-0934
E-mail: romgeorg@sitc.ru, fz_ema@sitc.ru

DANILOV N.V.

Joint-Skock Company "Uralelektromed", Pyshma, Russia
Tel.: (34368) 46-596
Fax: (34368) 46-344
E-mail: N.Danilov@elem.ru

DANYLENKO M.I.

Frantsevich Institute for Problems of Material Science, NASU, Kyiv, Ukraine
Tel.: (044) 444-2380, 444-3061
Fax: (044)444-3061
E-mail: sery@materials.kiev.ua, nick@ipms.kiev.ua, neiko@svitonline.com

DANYLENKO V.M.

Frantsevich Institute for Problems of Material Science, NASU, Kyiv, Ukraine
Tel.: (044) 444-3364
E-mail: dep40@materials.kiev.ua

DATSKEVICH O.

Frantsevich Institute for Problems of Material Science, NASU, Kyiv, Ukraine
E-mail: rapid@materials.kiev.ua

DAVYDOV V.A.

Vereschagin Institute for High Pressure Physics, RAS, Troitsk, Russia
Tel.: (095) 334-0810, 334-0738, 334-0808
Fax: (095) 334-0012
E-mail: ydavydov@ns.hppi.troitsk.ru

DEKHTERUK V.I.

Frantsevich Institute for Problems of Material Science, NASU, Kyiv, Ukraine
Tel.: (044) 444-2171
E-mail: phil02@ukr.net

DEMCHENKO L.D.

National Technical University of Ukraine "Kyiv Polytechnic Institute", Kyiv, Ukraine
Tel.: (044) 441-1076
E-mail: demles@yahoo.com, sidorenko@uap.ntu-kpi.kiev.ua

DEMIDIK A.N.

Frantsevich Institute for Problems of Material Science, NASU, Kyiv, Ukraine
Tel.: (044) 444-11-24

DEREV'YANKO O.V.

Frantsevich Institute for Problems of Material Science, NASU, Kyiv, Ukraine
Tel.: (044) 444-2255
Fax: (044) 444-2131
E-mail: raitch@ipms.kiev.ua

DESPOTULI A. L.

Institute of Microelectronics Technology, RAS, Chernogolovka, Russia
E-mail: despot@ipmt-hpm.ac.ru

DIACONESCU M.

Advanced Research Institute for Electrical Engineering, Bucharest, Romania
Tel.: 0040-1-346-82-97
Fax: 0040-1-346-82-99
E-mail: magnet@icpe.ro, gavriliu@rol.ro

DICK T.A.

Institute of Applied Physical Problems of Belarus State University, Minsk, Belarus
Tel.: (017) 277-4939
Fax: (017) 278-0417
E-mail: TREBNIKOV@BSU.BY

DMITRIEV A.I.

Frantsevich Institute for Problems of Material Science, NASU, Kyiv, Ukraine
Tel.: (044) 444-3228
Fax: (044) 444-2131
E-mail: lashk@ipms.kiev.ua

DMITROVICH A.A.

Powder Metallurgy Research Institute, NASB, Minsk, Belarus
Tel.: (517) 239-9820
Fax: (517) 210-0574
E-mail: fricom1@inbox.ru, dsaroka@tut.by

DOMAREVA A.S.

Donetsk Physical-Technical Institute, NASU, Donetsk, Ukraine
E-mail: pashinska@mail.ru

DOMINGUEZ G.

Autonomous University of State of Morelos, Cuernavaca, Mexico

DOTSENKO F.F.

Dnipropetrovsk National University, Dnipropetrovsk, Ukraine
Tel.: (0562) 776-9042
E-mail: metal@ff.dsu.dp.ua

DOTSENKO V.

Ukrainian Medical Stomatological Academy, Poltava, Ukraine

DRAPAK S.I.

Chernivtsi Department, Frantsevich Institute for Problems of Material Science, NASU, Chernivtsi, Ukraine
Tel.: (03722) 25-155
Fax: (03722) 20-050
E-mail: chimsp@unicom.cv.ua

DROZD V.A.

Kiev Taras Shevchenko National University, 64 Vladimirskaya St., Kiev 01033, Ukraine
Tel.: (044) 221-0206
E-mail: nedilko@red-gw.univ.kiev.ua

DUB S.N.

Bakul Institute of Superhard Materials, NASU, Kyiv, Ukraine
Tel.: (044) 430-3560
E-mail: sergey_dub@ukrpost.net

DUBIKIWSKY L.

Frantsevich Institute for Problems of Material Science, NASU, Kyiv, Ukraine
Tel.: (044) 295-9613
Fax: (044) 196-1684
E-mail: rym@ipp.adam.kiev.ua

DUBOK V.A.

Frantsevich Institute for Problems of Material Science, NASU, Kyiv, Ukraine
Tel.: (044) 444-7256
E-mail: dubok@ipms.kiev.ua

DUBOVIK T.V.

Frantsevich Institute for Problems of Material Science, NASU, Kyiv, Ukraine
Tel.: (044) 444-0002, 444-3522, 444-2371
Fax: (044) 444-2131
E-mail: imorozov@materials.kiev.ua, grigorev@ipms.kiev.ua, mscoval@ipms.kiev.ua

DUBROVA O.E.

Bakul Institute of Superhard Materials, NASU, Kyiv, Ukraine
Tel.: (044) 430-3529
Fax: (044) 468-8632
E-mail: ceramic@isv.kiev.ua

DUBROVSKAYA G.

State Technological University, Cherkassy, Ukraine
Tel.: (0472) 43-4155
E-mail: zholonko@gate.chiti.uch.net

DUBYNA V.M.

Taras Shevchenko Kyiv National University, Kyiv, Ukraine
Tel.: (044) 221-0270
E-mail: vovd@ukr.net, vsudavtsova@univ.kiev.ua

DUDNIK E.V.

Frantsevich Institute for Problems of Material Science, NASU, Kyiv, Ukraine
Tel.: (044) 444-3573
Fax: (044) 444-2131
E-mail: dep25@materials.kiev.ua

DUHNENKO A.V.

Frantsevich Institute for Problems of Material Science, NASU, Kyiv, Ukraine
Tel.: (044) 444-1367
E-mail: dep60@ipms.kiev.ua

DUNIN-BARKOWSKII L.R.

Institute of Solid State Physics, RAS, Chernogolovka, Russia
Tel.: (09652) 48836
Fax: (09652) 49701
E-mail: dbarkov@issp1.issp.ac.ru

DVOYNNENKO O.K.

Frantsevich Institute for Problems of Material Science, NASU, Kyiv, Ukraine
Tel.: (044) 444-8218
E-mail: andreeva@ipms.kiev.ua

DYMENKO V.V.

Paton Electric Welding Institute, NASU, Kyiv, Ukraine
Tel.: (044) 261-5966
Fax: (044) 286-0486

DZIAZKO A.

Kiev Taras Shevchenko National University, 64 Vladimirskaya St., Kiev 01033, Ukraine
Tel.: (044) 221-0206
E-mail: dziazko@carrier.kiev.ua

E

EFIMOVA I.E.

Siberian State University of Industry, Novokuznetsk, Russia

Tel.: (3843) 46-2277, 46-4000

Fax: (3843) 46-5792

E-mail: gromov@physics.sibsiu.ru

EFIMOVA T.V.

Kurdyumov Institute for Metal Physics, NASU, Kyiv, Ukraine

Tel.: (044) 44-9546, 444-9531, 444-9532

Fax: (044) 444-2561

E-mail: perekos@imp.kiev.ua, potvora@imp.kiev.ua

EFRYUSHINA N.P.

Bogatsky Physico-Chemical Institute, NASU, Odessa, Ukraine

Tel.: (0482) 61-8225, 66-2097

Fax: (0482) 65-2012

E-mail: physchem@paco.net

EGOROV S.G.

Zaporizhzhya State Engineering Academy, Zaporizhzhya, Ukraine

Tel.: (80612) 60-1261

E-mail: egorovsergey@km.ru

EGOROVA N.B.

Research Center of the Fund for Development New Medical Technologies "AIRES", Saint-Petersburg, Russia

Tel.: (812) 596-3533

Fax: (812) 596-3551

E-mail: foundation@aires.spb.ru

EINARSRUD M.-A.

Norwegian University of Science and Technology, Trondheim, Norway

EKIMOV E.A.

Vereschagin Institute for High Pressure Physics, RAS, Troitsk, Russia

Tel.: (095) 334-0732

Fax: (095) 334-0012

E-mail: ekimov@hppi.troitsk.ru

ENYASHIN A.N.

Ural State Technical University, Ekaterinburg, Russia

Tel.: (3432) 55-8340

E-mail: vika@nexcom.ru

EREMENKO A.M.

Dnipropetrovsk National University, Dnipropetrovsk, Ukraine

Tel.: (0562) 45-0717, 93-8949

Fax: (0562) 46-5523

E-mail: optic@ff.dsu.dp.ua

EREMENKO L.I.

Frantsevich Institute for Problems of Material Science, NASU, Kyiv, Ukraine

Tel.: (044) 444-1501

Fax: (044) 450-4030

E-mail: empril@mail.ru

ERMISHKIN V.A.

Bauman Moscow State Technical University, Moscow, Russia

Baikov Institute of Metallurgy and Material Science, RAS, Moscow, Russia

E-mail: iovchin@mx.bmstu.ru

ERYOMIN O.G.

Bogatsky Physico-Chemical Institute, NASU, Odessa, Ukraine

Tel.: (0482) 61-8225, 66-2097

Fax: (0482) 65-2012

E-mail: physchem@paco.net

EVTUSHOK T.M.

Frantsevich Institute for Problems of Material Science, NASU, Kyiv, Ukraine

Tel.: (044) 444-1481, 444-3301, 444-1321

F

FAL'KOVSKAJA T.I.

National Technical University of Ukraine "Kyiv Polytechnic Institute", Kyiv, Ukraine

FEDIRKO V.

Karpenko Physico-Mechanical Institute, NASU, Lviv, Ukraine

Tel.: (0322) 65-4343

E-mail: fedirko@ipm.lviv.ua

FEDORENKOVA L.

Dnipropetrovsk National University, Dnipropetrovsk, Ukraine

Tel.: 469-2112

E-mail: odm@ff.dsu.dp.ua

FEDORUS V.B.

Frantsevich Institute for Problems of Material Science, NASU, Kyiv, Ukraine

Tel.: (044) 444-1501

Fax: (044) 450-4030

E-mail: empril@mail.ru

FEODOROV V.A.

Derzhavin Tambov State University, Tambov, Russia

Tel.: (0572) 35-2614

Fax: (0572) 710-307

E-mail: ushakov@tsu.tmb.ru, feodorov@tsu.tmb.ru

FEODOROVA I.L.

State Institute of System Analyses, Minsk, Belarus

FICSHICH O.I.

Frantsevich Institute for Problems of Material
Science, NASU, Kyiv, Ukraine
Tel.: (044) 444-1571
Fax: (044) 444-2131
E-mail: dir@ipms.kiev.ua

FILIPPOV V.B.

Frantsevich Institute for Problems of Material
Science, NASU, Kyiv, Ukraine
Tel.: (044) 444-1367
Fax: (044) 444-2131
E-mail: dep60@ipms.kiev.ua

FILONENKO V.P.

Vereschagin Institute for High Pressure Physics,
RAS, Troitsk, Russia
Tel.: (095) 334-0732
Fax: (095) 334-0012
E-mail: ekimov@hppi.troitsk.ru

FIRSTOV S.A.

Frantsevich Institute for Problems of Material
Science, NASU, Kyiv, Ukraine
Tel.: (044) 444-0051, 444-3345, 444-3360
Fax: (044) 452-5523
E-mail: fsa@materials.kiev.ua,
dep22@materials.kiev.ua

FIYALKA L.I.

Frantsevich Institute for Problems of Material
Science, NASU, Kyiv, Ukraine
Tel.: (044) 444-2171
E-mail: phil02@ukr.net

FLACHBART K.

Institute of Experimental Physics, Kosice, Slovakia

FLIS A.A.

Frantsevich Institute for Problems of Material
Science, NASU, Kyiv, Ukraine
Tel.: (044) 444-2471
E-mail: flis@imp.kiev.ua

FLOREA A.

University of Petrosani, Romania
E-mail: prorektor2@upet.ro

FOMENKO V.V.

National University of Food Technologies, Kyiv,
Ukraine
Tel.: (044) 221-7833

FORMANEK B.

Silesian University of Technology, Katowice, Poland
Tel.: (+48 32) 255-3225(439)
Fax: (+48 32) 256-3197
E-mail: bforman@polsl.katowice.pl

FRENKEL O.A.

Frantsevich Institute for Problems of Material
Science, NASU, Kyiv, Ukraine
Tel.: (044) 444-8218
E-mail: andreeva@ipms.kiev.ua

FROLOV A.A.

Frantsevich Institute for Problems of Material
Science, NASU, Kyiv, Ukraine
Tel.: (044) 459-59-44, 444-35-73
Fax: (044) 444-2131
E-mail: frolov@edu-ua.net

FROLOV A.G.

Frantsevich Institute for Problems of Material
Science, NASU, Kyiv, Ukraine
Fax: (044) 444-2131
E-mail: frolov@alfacom.net

FROYEN L.

Department of Metallurgy and Materials Engineering,
K.U. Leuven, Leuven, Belgium
Fax: 32 16 32 1992, 32 16 32 2987
E-mail: Ludo.Froyen@kuleuven.ac.be

G

GAB A.I.

Vernadskii Institute of General and Inorganic
Chemistry, NASU, Kyiv, Ukraine
Tel.: (044) 444-0111
Fax: (044) 444-3070
E-mail: GAB@ionc.kar.net

GAB I.I.

Frantsevich Institute for Problems of Material
Science, NASU, Kyiv, Ukraine
Tel.: (044) 444-3017, 444-6201
Fax: (044) 444-3017
E-mail: naidich@ipms.kiev.ua

GAGAUZ V.P.

Siberian State University of Industry, Novokuznetsk,
Russia
Tel.: (3843) 46-2277, 46-4000, 78-4367
Fax: (3843) 46-5792
E-mail: gromov@physics.sibsiu.ru

GALIEVA J.N.

Research Institute of Radiomaterials, Minsk, Belarus
Tel.: (375 017) 278-4054
Fax: (375 017) 278-3705
E-mail: irma@infonet.by

GAMANOVITCH N.M.

Belorussian State University of Technology, Minsk,
Belarus

GAMEZA L.M.

Institute of Machine Reliability, NASB, Minsk,
Belarus
Tel.: (375 17) 284-2401
Fax: (375 17) 284-2401
E-mail: nanotech@inmash.bas-net.by

GARAN A.G.

Bakul Institute of Superhard Materials, NASU, Kyiv,
Ukraine
Tel.: (044) 468-8632, 430-3506
Fax: (044) 468-8625
E-mail: vturk@ism.kiev.ua

GARANIN V.M.

Open Joint-Stock "AMULET", Kyiv, Ukraine
Tel.: (044) 265-2610, 267-6370
Fax: (044) 265-2611
E-mail: amulet@akcecc.kiev.ua

GARMASH E.P.

Frantsevich Institute for Problems of Material
Science, NASU, Kyiv, Ukraine
Tel.: (044) 444-2001
Fax: (044) 444-2131
E-mail: garmasg@materials.kiev.ua

GAVRILENKO O.N.

Vernadskii Institute of General and Inorganic
Chemistry, NASU, Kyiv, Ukraine
Tel.: (044) 444-2211
Fax: (044) 444-2211
E-mail: belous@ionc.kar.net

GAVRILIU G.

Advanced Research Institute for Electrical
Engineering, Bucharest, Romania
Tel.: 0040-1-346-82-97
Fax: 0040-1-346-82-99
E-mail: magnet@icpe.ro, gavriliu@rol.ro

GAWALEK W.

Institut für Physikalische Hochtechnologie, Jena,
Germany
Tel.: (49 36 41) 206103, 206107, 206106
Fax: (49 36 41) 206199
E-mail: Wolfgang.Gawalek@ipht-jena.de

GIERLOTKA S.

High Pressure Research Center, Polish Academy of
Sciences, Warsaw, Poland

GILEV V.G.

Research Center of Powder Materials Science,
Perm, Russia
Tel.: (3422) 391-110, 391-119
Fax: (3422) 391-122
E-mail: mak@pm.pstu.ac.ru, patent@pm.pstu.ac.ru

GIUBILEO F.

Physics Department, University of Salerno, Salerno,
Italy

GLEEVOI YU.V.

National Technical University of Ukraine "Kyiv
Polytechnic Institute", Kyiv, Ukraine
E-mail: rchebot@ukr.net

GLINCHUK M.D.

Frantsevich Institute for Problems of Material
Science, NASU, Kyiv, Ukraine
Tel.: (044) 444-1540
Fax: (044) 444-2131
E-mail: glin@materials.kiev.ua

GNESIN G.G.

Frantsevich Institute for Problems of Material
Science, NASU, Kyiv, Ukraine
Tel.: (044) 444-2371, 444-2471, 216-5371
Fax: (044) 444-2131
E-mail: sart@ipms.kiev.ua

GNYLOSKURENKO S.V.

Institute of Multidisciplinary Research for Advanced
Materials, Tohoku University, Sendai, Japan
Tel.: 81-22-217-5213, 81-22-217-5214
Fax: 81-22-217-5213, 81-22-217-5214
E-mail: ntakashi@tagen.tohoku.ac.jp,
slava@iamp.tohoku.ac.jp

GOGOTSI G.A.

Institute for Problems of Strength, NASU, Kyiv,
Ukraine
Tel.: (044) 295-4464
Fax: (044) 296-1684
E-mail: ggogotsi@ipp.adam.kiev.ua

GOLOUBTSOVA E.S.

Belorussian National Technical University, Minsk,
Belarus
Tel.: (517) 232-7146, 231-0545, 232-5406
Fax: (517) 232-7183
E-mail: egolubtsova@tut.by

GOLOVKOVA M.E.

Frantsevich Institute for Problems of Material
Science, NASU, Kyiv, Ukraine
Tel.: (044) 444-1181
Fax: (044) 444-2131
E-mail: 29min@ipms.ua

GOLTSOV V.A.

Donetsk Physical-Technical Institute, NASU,
Donetsk, Ukraine
Tel.: (0622) 93-6141
Fax: (0622) 93-1278
E-mail: goltsov@physics.dgtu.donetsk.ua

GONCHARENKO V.V.

National Technical University of Ukraine "Kyiv
Polytechnic Institute", Kyiv, Ukraine
E-mail: rchebot@ukr.net

GONCHAROVA I.V.

Frantsevich Institute for Problems of Material Science, NASU, Kyiv, Ukraine
Tel.: (044) 444-3061,
Fax: (044) 444-3061
E-mail: milman@materials.kiev.ua,
Irina@materials.kiev.ua

GONCHARUK L.

Frantsevich Institute for Problems of Material Science, NASU, Kyiv, Ukraine
Tel.: (044) 444-1290, 444-3090
Fax: (044) 444-2131
E-mail: dep6@materials.kiev.ua

GONCHARUK V.A.

Frantsevich Institute for Problems of Material Science, NASU, Kyiv, Ukraine
Tel.: (044) 444-30-61, 444-0294
Fax: (044) 452-5523
E-mail: sery@materials.kiev.ua, nick@ipms.kiev.ua,

GONZALES-RODRIGUEZ J.G.

Autonomous University of State of Morelos, Cuernavaca, Mexico

GORBACHUK N.P.

Frantsevich Institute for Problems of Material Science, NASU, Kyiv, Ukraine
Tel.: (044) 444-1290
Fax: (044) 444-2131
E-mail: dep6@materials.kiev.ua,
bas@materials.kiev.ua

GORBAN V.

Frantsevich Institute for Problems of Material Science, NASU, Kyiv, Ukraine
Fax: (044) 444-2131

GORBUNOV A.V.

Lykov Heat & Mass Transfer Institute, NASB, Minsk, Belarus
Tel.: (017) 284-1223
Fax: (017) 232-2513
E-mail: ptab_hmti@tut.by, gml@hmti.ac.by

GORBUNOVA V.A.

Belorussian State University of Technology, Minsk, Belarus

GORDIENKO YU.G.

Kurdyumov Institute for Metal Physics, NASU, Kyiv, Ukraine
Tel.: (044) 444-9514
E-mail: eezas@imp.kiev.ua

GORELIK P.N.

Concern "Planar", Minsk, Belarus
Tel.: (017) 221-7210

GORIN A.I.

Keldysh Research Center, Moscow, Russia
Tel.: (095) 196-4351
E-mail: thenami@mtu-net.ru

GORLOVA S.N.

Siberian State University of Industry, Novokuznetsk, Russia
Tel.: (3843) 46-2277, 46-4000
Fax: (3843) 46-5792
E-mail: gromov@physics.sibsiu.ru

GORNAYA I.

Frantsevich Institute for Problems of Material Science, NASU, Kyiv, Ukraine
Tel.: (044) 444-0051, 444-3345, 444-3360
Fax: (044) 452-5523
E-mail: rapid@materials.kiev.ua,
dep22@materials.kiev.ua

GOROBETZ YU.I.

Institute of Magnetism, NASU, Kyiv, Ukraine
Tel.: (044) 444-1020, 444-9568
E-mail: fmf@ntu-kpi.kiev.ua

GOROKHOV V.M.

Powder Metallurgy Research Institute, NASB, Minsk, Belarus
Tel.: (017) 239-9842
Fax: (017) 210-0574
E-mail: gorokhov47@mail.ru

GOROKHOV V.U.

Perm State Technical University, Perm, Russia
Tel.: (3422) 39-1340
E-mail: dpm@cpl.pstu.ac.ru

GORYACHEV YU. M.

Frantsevich Institute for Problems of Material Science, NASU, Kyiv, Ukraine
Tel.: (044) 444-2371
Fax: (044) 444-2131
E-mail: phil02@ukr.net,
vlad.malakhov@materials.kiev.ua

GOSTISHEV V.V.

Institutes of Mountain Business, KSC FEB RAS, Khabarovsk, Russia

GOYDINA S.V.

Frantsevich Institute for Problems of Material Science, NASU, Kyiv, Ukraine
Tel.: (044) 444-0256

GRAIVORONSKAYA E.A.

Frantsevich Institute for Problems of Material Science, NASU, Kyiv, Ukraine
Tel.: (044) 444-3364, 444-1533
E-mail: khyzhun@ipms.kiev.ua,
solonin@materials.kiev.ua

GRECHISHKIN E.

Frantsevich Institute for Problems of Material Science, NASU, Kyiv, Ukraine
Fax: (044) 444-2131

GREVNOV L.M.

Research Center of Powder Materials Science,
Perm, Russia
Tel.: (3422) 391-119, 391-127
Fax: (3422) 391-122
E-mail: kpmc@pm.pstu.ac.ru, patent@pm.pstu.ac.ru

GRIDNEVA I.V.

Frantsevich Institute for Problems of Material
Science, NASU, Kyiv, Ukraine
Tel.: (044) 444-2371, 444-3061, 444-1501
Fax: (044) 444-3061
E-mail: gridneva@materials.kiev.ua

GRIGORIEV O.N.

Frantsevich Institute for Problems of Material
Science, NASU, Kyiv, Ukraine
Tel.: (044) 444-1321, 444-3522
Fax: (044) 444-2131
E-mail: grigorev@ipms.kiev.ua

GRIGORIEVA T.F.

Institute of Solid State Chemistry and
Mechanochemistry, SB of RAS, Novosibirsk, Russia
E-mail: barinova_ap@mail.ru

GRIGORYAN L.

Institute of Problems of Chemical Physics, RAS,
Chernogolovka, Russia
Tel.: (096) 252-8514
Fax: +7(096) 514-3244
E-mail: hrant@icp.ac.ru

GRIGORYAN R.

Institute of Structural Macrokinetics and Materials
Science, RAS, Chernogolovka, Russia
Tel.: (0965) 962-8014
Fax: (0965) 962-8025
E-mail: rud@ism.ac.ru

GRINKEVYCH K.E.

Frantsevich Institute for Problems of Material
Science, NASU, Kyiv, Ukraine
Tel.: (044) 444-3061
Fax: (044) 444-3061
E-mail: kevich@materials.kiev.ua

GROMOV V.E.

Siberian State University of Industry, Novokuznetsk,
Russia
Tel.: (3843) 46-2277, 46-4000, 78-4367
Fax: (3843) 46-5792
E-mail: gromov@physics.sibsiu.ru

GRUSHKO B.

Institut für Festkörperforschung, Forschungszentrum
Jülich, Jülich, Germany

GRYHORYEVA O.V.

National Technical University of Ukraine "Kyiv
Polytechnic Institute", Kyiv, Ukraine
Tel.: (044) 441-1076
Fax: (044) 241-6740
E-mail: grigoks@mail.ru, panda@relos.ntu-
kpi.kiev.ua

GUBARENI N.I.

Frantsevich Institute for Problems of Material
Science, NASU, Kyiv, Ukraine
Tel.: (044) 444-0256
Fax: (044) 444-2131

GUBENKO S.I.

National Metallurgical Academy of Ukraine,
Dnipropetrovsk, Ukraine
Tel.: (0562) 92-0866
Fax: (0562) 92-5113
E-mail: bunchuc@a-teleport.com

GUBIN YU.V.

Frantsevich Institute for Problems of Material
Science, NASU, Kyiv, Ukraine
Tel.: (044) 444-0256
Fax: (044) 444-2131
E-mail: post@ipms.kiev.ua

GUMENYUK O.R.

Institute for Semiconductor Physics, National
Academy of Sciences of Ukraine, Kyiv, Ukraine
Tel.: 265-5755
Fax: 265-8342
E-mail: tomashyk@isp.kiev.ua, yarri@gmx.ch

GUSLIENKO Y.A.

Frantsevich Institute for Problems of Material
Science, NASU, Kyiv, Ukraine
Tel.: (044) 444-2055
Fax: (044) 444-2131
E-mail: miron@ipms.ua

GVOZD G.V.

National Technical University of Ukraine "Kyiv
Polytechnic Institute", Kyiv, Ukraine
E-mail: rchebot@ukr.net

H

Haidarshin A.F.

Research Center of Powder Materials Science,
Perm, Russia
Tel.: (3422) 391-110
Fax: (3422) 391-122
E-mail: solid@pm.pstu.ac.ru

HAMBARDZUMYAN A.F.

State Engineering University of Armenia, Yerevan, Armenia

Tel.: (374 1) 56-3217

Fax: (374 1) 54-5843

E-mail: gevorglp@seua.am, afh@seua.am

HASHKOVSKY S.V.

Institute of Silicate Chemistry, RAS, Saint-Petersburg, Russia

Tel.: (812) 328-8596

Fax: (812) 328-5401

E-mail: olgashilova@peterlink.ru

HAVRYLIUK V.P.

Physico-Technological Institute of Metals and Alloys, NASU, Kyiv, Ukraine

Tel.: (044) 444-1065, 444-1212, 444-0280

Fax: (044) 452-9736

E-mail: metal@ptima.kiev.ua, alloy@i.com.ua

HILAROV V.L.

Ioffe Physical Technical Institute, RAS, Saint-Petersburg, Russia

Tel.: (812) 247-9939

E-mail: Vladimir.Hilarov@pop.ioffe.rssi.ru

HIRANO T.

National Institute for Materials Science, Tsukuba, Japan

HOMENKO E.V.

Frantsevich Institute for Problems of Material Science, NASU, Kyiv, Ukraine

Tel.: (044) 444-1181

E-mail: 29min@ipms.ua

HOMSKAJA I.V.

Institute of Metal Physics, Ekaterinburg, Russia

E-mail: zeldovich@imp.uran.ru

ILYASOV V.

Don State Technical University, Rostov-on-Don, Russia

Tel.: (8632) 381-516

Fax: (8632) 327-953

E-mail: victor.ilyasov@rost.ru

ILYUSCHENKO A.PH.

Powder Metallurgy Research Institute, NASB, Minsk, Belarus

Tel.: (375 17) 232-5691

Fax: (375 17) 210-0574

E-mail: alexil@srpmi.belpak.minsk.by

ISAEVA L.P.

Frantsevich Institute for Problems of Material Science, NASU, Kyiv, Ukraine

Tel.: (044) 444-2371, 444-3061, 444-1501

Fax: (044) 444-3061

E-mail: abykov@materials.kiev.ua, gridneva@materials.kiev.ua

ISAYEV K.B.

Frantsevich Institute for Problems of Material Science, NASU, Kyiv, Ukraine

Tel.: (044) 444-0081

E-mail: isayev_k@gala.net

ISHIKAWA R.

Honda R&D CO., LTD., Tochigi, Japan

ISTOMINA T.I.

Frantsevich Institute for Problems of Material Science, NASU, Kyiv, Ukraine

Tel.: (044) 444-2255

Fax: (044) 444-2131

E-mail: raich@ipms.kiev.ua

IVANCHENKO L.A.

Frantsevich Institute for Problems of Material Science, NASU, Kyiv, Ukraine

Tel.: (044) 444-33-64

Fax: (044) 450-44-87

IVANENKO A.A.

Open Joint-Stock "AMULET", Kyiv, Ukraine

Tel.: (044) 265-2610, 267-6370

Fax: (044) 265-2611

E-mail: amulet@akcecc.kiev.ua

IVANENKO K.O.

Taras Shevchenko Kyiv National University, Kyiv, Ukraine

IVANISHINA I.M.

Stefanyk Precarpathian University, Ivano-Frankivsk, Ukraine

Tel.: (0342) 59-6082

E-mail: prk@pu.if.ua, olmi@freemail.com.ua

IVANOV M.

Frantsevich Institute for Problems of Material Science, NASU, Kyiv, Ukraine

Tel.: (044) 444-3090

Fax: (044) 444-2131

E-mail: dep6@materials.kiev.ua

IVANOV V.N.

State Plant "Scientific-Research the Institution "Orion", Kyiv, Ukraine

Tel.: (044) 446-5291

E-mail: bms@mvsemicond.kiev.ua

IVANOV YU.F.

Tomsk State University of Architecture and Construction, Tomsk, Russia

Tel.: (3822)65-4263

E-mail: kozlov@mail.tomsknet.ru

IVANOV E.YU.

Tosoh SMD Inc., Grove City, Ohio, USA

IVANOVA I.I.

Frantsevich Institute for Problems of Material Science, NASU, Kyiv, Ukraine
Tel.: (044) 444-1124
Fax: (044) 452-55-23
E-mail: epp@materials.kiev.ua

IVANOVSKAYA V.V.

Ural State Technical University, Ekaterinburg, Russia
Tel.: (3432) 55-8340
E-mail: vika@nexcom.ru

IVANOVSKII A.L.

Institute of Solid State Chemistry, UrB of RAS, Ekaterinburg, Russia

IVASHCHENKO R.K.

Frantsevich Institute for Problems of Material Science, NASU, Kyiv, Ukraine
Tel.: (044) 444-3061
Fax: (044) 444-3061
E-mail: sery@materials.kiev.ua, nick@ipms.kiev.ua

IVSHINA I.B.

Institute Ecology and Genetics of Microorganisms, UrB of RAS, Perm, Russia
Tel.: (3422) 64-6714
Fax: (3422) 64-6711

J**JAKIMENKO I.L.**

Frantsevich Institute for Problems of Material Science, NASU, Kyiv, Ukraine
Tel.: (044) 444-2524, 444-8286
E-mail: dep53@materials.ua

JASRABIK L.

Institute of Physics, Academy of Sciences of the Czech Republic, Prague, Czech Republic

JOVANOVIC Z.D.

Institute of Chemistry, Technology and Metallurgy, Belgrade, Yugoslavia

JURCHUK N.A.

Bakul Institute of Superhard Materials, NASU, Kyiv, Ukraine
Tel.: (044) 468-8623, 430-3505
E-mail:alcon@ismanu.kiev.ua,almaz@ism.kiev.ua, krasikova_nataly@mail.ru

K**KADUSHNIKOV R.M.**

Ural State Technical University, Ekaterinburg, Russia
Tel.: (3432) 75-9724
Fax: (3432) 75-9407
E-mail: radi@siams.com

KAKAZEY M.

Autonomous University of State of Morelos, Cuernavaca, Mexico

KALEDIN B.A.

Belorussian National Technical University, Minsk, Belarus
Tel.: (517) 232-7146, 231-0545, 232-5406
Fax: (517) 232-7183
E-mail: egolubtsova@tut.by, mitko_gala@mail.ru, metolit@tut.by

KAMALOV M.M.

Institute of Solid State Physics, RAS, Chernogolovka, Russia
Tel.: (096) 522-2066
E-mail: dpx@aha.ru, myshlyae@issp.ac.ru

KANCHOUKOE V.Z.

Kabardino-Balkarian State University, Nalchik, Russia
Tel.: (86622) 50-345, (095) 337-9955
E-mail: bsk@kbsu.ru, sozaevv@ns.kbsu.ru, exp@kbsu.ru

KAPLINA G.S.

Paton Electric Welding Institute, NASU, Kyiv, Ukraine
Tel.: (044) 220-8687
Fax: (044) 220-9215
E-mail: borisov.y@paton.kiev.ua

KAPUSTNIKOVA S.

National Metallurgical Academy of Ukraine, Dnipropetrovsk, Ukraine
Tel.: (0562) 41-0602
Fax: (0562) 67-6977
E-mail: a_mazur@fregat.com

KARAMURZOV B.S.

Kabardino-Balkarian State University, Nalchik, Russia
Tel.: (86622) 50-345, (095) 337-9955
E-mail: bsk@kbsu.ru, sozaevv@ns.kbsu.ru, exp@kbsu.ru

KARPETS M.V.

Frantsevich Institute for Problems of Material Science, NASU, Kyiv, Ukraine
Tel.: (044) 444-3228
Fax: (044) 444-3061
E-mail: karp@materials.kiev.ua

KARTUZOV V.V.

Frantsevich Institute for Problems of Material Science, NASU, Kyiv, Ukraine
Tel.: (044) 444-0102, 444-1181
Fax: (044) 2131
E-mail: 29min@ipms.ua, vvk@materials.kiev.ua

KASAKOV S.

Kuzmin Open Joint-Stock "Electrometallurgical Steel Works "Dneprospetsstal", Zaporizhzhya, Ukraine
Tel.: (0612) 39-7327, 39-7302
Fax: (0612) 13-1780
E-mail: glavin@dss.comint.net, dss@comint.net

KASHEUSKI S.B.

Lykov Heat & Mass Transfer Institute, NASB, Minsk, Belarus
E-mail: bekas@cpl5.itmo.by

KASHEVAROVA L.S.

Vereschagin Institute for High Pressure Physics, RAS, Troitsk, Russia
Tel.: (095) 334-0810, 334-0738, 334-0808
Fax: (095) 334-0012
E-mail: kashevar@ns.hppi.troitsk.ru

KASHYRYN V.P.

Scientific Production Company "Donix", Donetsk, Ukraine
Tel.: (062) 335-1151
Fax: (0622) 93-3262
E-mail: rato@fizmet.dgtu.donetsk.ua

KASUMOV A.M.

Frantsevich Institute for Problems of Material Science, NASU, Kyiv, Ukraine
Tel.: (044) 444-8218
E-mail: andreeva@ipms.kiev.ua

KASUMOV M.M.

Institute for Surface Chemistry, NASU, Kyiv, Ukraine
Tel.: (044) 444-1135
Fax: (044) 444-3567
E-mail: user@sufrchem.freenet.kiev.ua

KATERYNCHUK V.M.

Chernivtsi Department, Frantsevich Institute for Problems of Material Science, NASU, Chernivtsi, Ukraine
Tel.: (03722) 25-155
Fax: (03722) 20-050
E-mail: chimsp@unicom.cv.ua

KAZAKOV S.S.

Kuzmin Open Joint-Stock "Electrometallurgical Steel Works "Dneprospetsstal", Zaporizhzhya, Ukraine
Tel.: (0612) 39-7302, 39-7327
Fax: (0612) 13-1780
E-mail: glavin@dss.comint.net, dss@comint.net

KHABASHESKU V.N.

Zelinsky Institute of Organic Chemistry, RAS, Moscow, Russia

KHABASHESKU V.N.

Rice University, Houston, TX, USA
Tel.: 713-348-5485
Fax: 713-523-8236
E-mail: brinson@rice.edu, marsrav@rice.edu, khval@ruf.rice.edu

KHARLAMOV A.I.

Frantsevich Institute for Problems of Material Science, NASU, Kyiv, Ukraine
Tel.: (044) 444-0256
Fax: (044) 444-2131

KHINA B.B.

Physico-Technical Institute, NASB, Minsk, Belarus
Tel.: (375 17) 268-0741
Fax: (375 17) 263-7693
E-mail: khina@lenta.ru

KHITKO V.I.

Research Institute of Radiomaterials, Minsk, Belarus
Tel.: (375 017) 278-1401
Fax: (375 017) 278-3705
E-mail: irma@infonet.by, and@hmti.ac.by

KHOMKO T.V.

Frantsevich Institute for Problems of Material Science, NASU, Kyiv, Ukraine
Tel.: (044) 444-0256
Fax: (044) 444-2131

KHORUJAYA V.G.

Frantsevich Institute for Problems of Material Science, NASU, Kyiv, Ukraine
E-mail: velikanova@materials.kiev.ua

KHOTYENKO N.G.

Frantsevich Institute for Problems of Material Science, NASU, Kyiv, Ukraine
Tel.: (044) 444-0256

KHOVAVKO O.I.

Gas Institute, NASU, Kyiv, Ukraine
E-mail: bond@bond.elan-ua.net

KHVADAGIANI A.

State Scientific-Technical Center "Delta", Tbilisi, Georgia
Tel.: (99532) 969-248, 923-779, 955-646
Fax: (99532) 956-080
E-mail: argusdel@hotmail.com

KHYZHUN O.YU.

Frantsevich Institute for Problems of Material Science, NASU, Kyiv, Ukraine
Tel.: (044) 444-3364, 444-1533
E-mail: khyzhun@ipms.kiev.ua, solonin@materials.kiev.ua

KILDIY A.I.

Paton Electric Welding Institute, NASU, Kyiv,
Ukraine
Tel.: (044) 220-8687
Fax: (044) 220-9215
E-mail: borisov.y@paton.kiev.ua

KILIMNIK A.A.

State Technical University of Construction and
Architecture, Kyiv, Ukraine

KIM T.W.

Korea Institute of Energy Research, 71-2 Jang-dong,
Yeosong, Daejeon, Korea

KIREEV L.S.

Paton Electric Welding Institute, NASU, Kyiv,
Ukraine
Tel.: (044) 227-1366, 227-4783, 261-5098
Fax: (044) 227-1366, 268-0486
E-mail: zamkov@paton.kiev.ua,
office@paton.kiev.ua

KIRICHENKO A.G.

Zaporizhzhya State Engineering Academy,
Zaporizhzhya, Ukraine
Tel.: (0612) 29-7216, 60-1250, 601330
E-mail: kmarkovich@efp.com.ua,
beley_finance@efp.com.ua

KIRILENKO S.N.

Frantsevich Institute for Problems of Material
Science, NASU, Kyiv, Ukraine
Tel.: (044) 444-0256
Fax: (044) 444-2131
E-mail: post@ipms.kiev.ua

KIRILLOVA N.V.

Taras Shevchenko Kyiv National University, Kyiv,
Ukraine
Tel.: (044) 221-02-16

KISLYAK I.

Verkin Institute for Low Temperature Physics and
Engineering, NASU, Kharkiv, Ukraine
E-mail: BRAUDE@ilt.kharkov.ua

KLEIN J.

Groupe de Physique des Solides, C.N.R.S.,
Universités Paris 6 et 7, Paris, France
Tel.: 0144274672
Fax: 0143542878
E-mail: rodichev@gps.jussieu.fr

KLIMENKO N.

Bakul Institute of Superhard Materials, NASU, Kyiv,
Ukraine
Tel.: (044) 430-76-94
Fax: (044) 430-7694
E-mail: shilo@ism.kiev.ua, svetlana@ism.kiev.ua

KLIMENKO N.S.

Institute of Macromolecular Chemistry, NASU, Kyiv,
Ukraine
Tel.: (044) 559-5500
Fax: (044) 552-4064
E-mail: olgs-s@mail.kar.net, nina@kea.kiev.ua

KLOCHKOV L.A.

Frantsevich Institute for Problems of Material
Science, NASU, Kyiv, Ukraine
Tel.: (044) 444-2371, 444-3415, 444-3061
Fax: (044) 444-3061
E-mail: abykov@materials.kiev.ua,
ragulya@materials.kiev.ua,
gridneva@materials.kiev.ua

KNOHIN V.N.

Kuzmin Open Joint-Stock "Electrometallurgical Steel
Works "Dneprospetsstal", Zaporizhzhya, Ukraine
Tel.: (0612) 39-7302, 39-7327
Fax: (0612) 13-1780
E-mail: glavin@dss.comint.net, dss@comint.net

KOBYLINSKA O.V.

Frantsevich Institute for Problems of Material
Science, NASU, Kyiv, Ukraine
Tel.: (044) 444-1533
Fax: (044) 444-2131
E-mail: olgak@materials.kiev.ua

KOKORINA N.N.

Paton Electric Welding Institute, NASU, Kyiv,
Ukraine
Tel.: (044) 220-8687
Fax: (044) 220-9215
E-mail: borisov.y@paton.kiev.ua

KOLESNIK N.F.

Zaporizhzhya State Engineering Academy,
Zaporizhzhya, Ukraine
Tel.: (0612) 29-7216, 60-1250, 601330
E-mail: kmarkovich@efp.com.ua,
beley_finance@efp.com.ua

KOLIN'KO S.

State Technological University, Cherkassy, Ukraine
Tel.: (0472) 43-4155
E-mail: zholonko@gate.chiti.uch.net

KOLISNICHENKO O.V.

Paton Electric Welding Institute, NASU, Kyiv,
Ukraine
E-mail: ytyurin@i.com.ua

KOLMOGOROV G.L.

Perm State Technical University, Perm, Russia
Tel.: (3414) 39-1340, 22-6596, 90-4188
E-mail: dpm@cpl.pstu.ac.ru

KOLOBOV G.A.

Zaporizhzhya State Engineering Academy,
Zaporizhzhya, Ukraine
Tel.: (80612) 60-1261
E-mail: egorovsergey@km.ru, rot@zgja.zp.ua,
al_nik_co@ukr.net

KOLOMIETS A.T.

Frantsevich Institute for Problems of Material
Science, NASU, Kyiv, Ukraine
Tel.: (044) 444-3301
Fax: (044) 444-2131
E-mail: fsa@materials.kiev.ua

KOLOTILKIN O.

Zaporizhzhya National Technical University,
Zaporizhzhya, Ukraine
Tel.: (0612) 69-8267
E-mail: tamara@zstu.edu.ua

KONDRATENKO V.M.

Nekrasov Iron and Steel Institute, NASU,
Dnipropetrovsk, Ukraine
Tel.: (0562) 47-0312
Fax: (0562) 47-0313
E-mail: postmaster@kondrat.dp.ua

KONOVALOV S.V.

Siberian State University of Industry, Novokuznetsk,
Russia
Tel.: (3843) 46-2277, 46-4000
Fax: (3843) 46-5792
E-mail: zsmk@zsmk.ru, gromov@physics.sibsiu.ru

KONSTANTINOVA T.E.

Donetsk Physical-Technical Institute, NASU,
Donetsk, Ukraine
Tel.: (0622) 55-5121
E-mail: Tatjana@konstant.fti.donetsk

KORCHAGIN M.A.

Institute of Solid State Chemistry and
Mechanochemistry, SB of RAS, Novosibirsk, Russia
E-mail: barinova_ap@mail.ru

KORDYUK A.A.

Kurdyumov Institute for Metal Physics, NASU, Kyiv,
Ukraine
Tel.: (044) 444-9538
E-mail: kord@imp.kiev.ua

KORNIYENKO K.YE.

Frantsevich Institute for Problems of Material
Science, NASU, Kyiv, Ukraine
E-mail: velikanova@materials.kiev.ua

KOROLEV U.M.

Topchiev Institute of Petrochemical Synthesis RAS
Tel.: (095) 955-4242
E-mail: tips@tips.rc.ac.ru

KOROVNIKOVA N.I.

Institute for Single Crystals, NASU, Kharkiv, Ukraine
Tel.: (0572) 30-7977, 30-7989
Fax: (0572) 32-0273
E-mail: nkorovnikova@isc.kharkov.com

KORSAK YU.V.

Gas Institute, NASU, Kyiv, Ukraine
E-mail: bond@bond.elan-ua.net

KORZHOVA N.P.

Frantsevich Institute for Problems of Material
Science, NASU, Kyiv, Ukraine
Tel.: (044) 444-3061, 444-0051
Fax: (044) 444-3061
E-mail: korzhova@materials.kiev.ua

KOSCHEEV S.V.

Saint-Petersburg State Electrotechnical University
"LETI" Saint-Petersburg, Russia
Tel.: (812) 351-0798, 234-3016
E-mail: vamousnikov@mail.eltech.ru

KOSENKO N.S.

Kurdyumov Institute for Metal Physics, NASU, Kyiv,
Ukraine
Tel.: (044) 444-9532
E-mail: kosnik@imp.kiev.ua

KOSENKO P.N.

National Technical University of Ukraine "Kyiv
Polytechnic Institute", Kyiv, Ukraine
Tel.: (044) 467-1976
E-mail: kosnik@imp.kiev.ua

KOSINSKAIA A.V.

Physico-Technological Institute of Metals and Alloys,
NASU, Kyiv, Ukraine
Tel.: (044) 444-3542
Fax: (044) 444-3542
E-mail: kompozit@inec.kiev.ua

KOSOURUKOV P.A.

Frantsevich Institute for Problems of Material
Science, NASU, Kyiv, Ukraine
Tel.: (044) 444-0256
Fax: (044) 444-2131

KOSTENKO A.D.

Frantsevich Institute for Problems of Material
Science, NASU, Kyiv, Ukraine
Tel.: (044) 444-444-3301
Fax: (044) 444-2131
E-mail: raitch@ipms.kiev.ua

KOSTENKO V.K.

Frantsevich Institute for Problems of Material
Science, NASU, Kyiv, Ukraine
Tel.: (044) 444-2055
Fax: (044) 444-2131
E-mail: miron@ipms.ua

KOSTIKOV V.I.

Federal Governmental Unitarity Enterprise "The State Research Institute of Graphite-Based Structural Materials" – FGUE "NII Graft", Moscow, Russia
Tel.: (095) 176-2988
Fax: (095) 176-2988
E-mail: grafit@aha.ru

KOSTORNOV A.G.

Frantsevich Institute for Problems of Material Science, NASU, Kyiv, Ukraine
Tel.: (044) 444-1571, 444-0427
Fax: (044) 444-2131
E-mail: dir@ipms.kiev.ua

KOSTYUK N.N.

Institute of Applied Physical Problems of Belarus State University, Minsk, Belarus
Tel.: (017) 277-4939
Fax: (017) 278-0417
E-mail: TREBNIKOV@BSU.BY

KOTENKO V.A.

Frantsevich Institute for Problems of Material Science, NASU, Kyiv, Ukraine
Tel.: (044) 444-1481, 444-3301, 444-1321

KOTKO A.V.

Frantsevich Institute for Problems of Material Science, NASU, Kyiv, Ukraine
Tel.: (044) 444-0294, 444-0051
E-mail: oleganna@svitonline.com

KOTOVA N.V.

Taras Shevchenko Kyiv National University, Kyiv, Ukraine
Tel.: (044) 221-0270
E-mail: vovd@ukr.net, vsudavtsova@univ.kiev.ua

KOTRECHKO S.O.

Kurdyumov Institute for Metal Physics, NASU, Kyiv, Ukraine
Tel.: (044) 444-9520
E-mail: kotr@imp.kiev.ua

KOVAL O.I.

Research Institute of Impulse Processes, Minsk, Belarus
Tel.: (375 17) 239-3244
Fax: (375 17) 232-8411
E-mail: impuls@bn.by

KOVAL V.A.

Powder Metallurgy Research Institute, NASB, Minsk, Belarus
Tel.: (375 17) 232-8271, 232-6340
Fax: (375 17) 232-5691, 210-0574
E-mail: Alexil@srpmi.belpak.minsk.by, beliaev_a@open.by

KOVAL' O.Yu.

Frantsevich Institute for Problems of Material Science, NASU, Kyiv, Ukraine
Tel.: (044) 444-3360, 444-3345
Fax: (044) 452-5523
E-mail: rapid@materials.kiev.ua

KOVALCHENKO M.S.

Frantsevich Institute for Problems of Material Science, NASU, Kyiv, Ukraine
Tel.: (044) 444-2101
Fax: (044) 444-2131
E-mail: mskoval@ipms.kiev.ua

KOVALENKO L.

Vernadskii Institute of General and Inorganic Chemistry, NASU, Kyiv, Ukraine
Tel.: (044) 444-2211
Fax: (044) 444-2211
E-mail: leo@ionc.kar.net, vyunov@ionc.kar.net, belous@ionc.kar.net

KOVALENKO S.V.

Institute of Material Science, KSC FEB RAS, Khabarovsk, Russia
Tel.: (4212) 71-9956
Fax: (4212) 71-9598
E-mail: imdvo@fe.ru, infarest@pop.redcom.ru

KOVALENKO V.V.

Siberian State University of Industry, Novokuznetsk, Russia
Tel.: (3843) 46-2277, 46-4000
Fax: (3843) 46-5792
E-mail: zsmk@zsmk.ru, gromov@physics.sibsiu.ru

KOVALEV A.E.

Perm State Technical University, Perm, Russia
Tel.: (3414) 39-1340, 22-6596, 90-4188
E-mail: dpm@cpl.pstu.ac.ru

KOVALYUK Z.D.

Chernivtsi Department, Frantsevich Institute for Problems of Material Science, NASU, Chernivtsi, Ukraine
Tel.: (03722) 25-155
Fax: (03722) 20-050
E-mail: chimsp@unicom.cv.ua

KOVIASINA S.A.

Institute of Solid State Chemistry, UrB of RAS, Ekaterinburg, Russia
Tel.: (3432) 49-3387, 49-9161
E-mail: leonidov@imp.uran.ru, florid@rambler.ru

KOVTUNENKO V.

State Technological University, Cherkassy, Ukraine
Tel.: (0472) 43-4155
E-mail: zholonko@gate.chiti.uch.net

KOZAK S.I.

National University "Lviv Politechnik", Lviv, Ukraine
Tel.: 39-8172, 39-8770
E-mail: kunty@polynet.lviv.ua, kunty@ukr.net.ua

KOZHAN O.P.

Gas Institute, NASU, Kyiv, Ukraine
E-mail: bond@bond.elan-ua.net

KOZLOV E.V.

Tomsk State University of Architecture and Construction, Tomsk, Russia
Tel.: (3822)65-4263
E-mail: kozlov@mail.tomsknet.ru

KOZLOVA L.E.

Institute of Magnetism, NASU, Kyiv, Ukraine
Tel.: (044) 444-9591
E-mail: kozlova@im.imag.kiev.ua

KRAJNIKOV A.

Frantsevich Institute for Problems of Material Science, NASU, Kyiv, Ukraine
Tel.: (044) 444-0294
Fax: (044) 444-2078
E-mail: avk@ipms.kiev.ua

KRAPIVKA N.A.

Frantsevich Institute for Problems of Material Science, NASU, Kyiv, Ukraine
Tel.: (044) 444-8286

KRAVCHENKO L.P.

Frantsevich Institute for Problems of Material Science, NASU, Kyiv, Ukraine
Tel.: (044) 444-2024
E-mail: vkur@ipms.kiev.ua

KRAVCHENKO V.M.

Taras Shevchenko Kyiv National University, Kyiv, Ukraine
Tel.: (044) 266-2326, 266-4587
Fax: (044) 266-2326
E-mail: krav@mail.phys.univ.kiev.ua

KRAVETS A.F.

Institute of Magnetism, NASU, Kyiv, Ukraine
Tel.: (044) 444-1020, 444-9568
E-mail: fmf@ntu-kpi.kiev.ua

KRAVTSOVA J.V.

Vladimir Dahl East Ukrainian National University, Lugansk, Ukraine
Tel.: (0642) 46-2233
E-mail: material@snu.edu.ua

KRIVCHIKOV A.

Verkin Institute for Low Temperature Physics and Engineering, NASU, Kharkiv, Ukraine

KRUSHINSKAYA L.A.

Frantsevich Institute for Problems of Material Science, NASU, Kyiv, Ukraine
Tel.: (044) 444-1501
E-mail: tomila@materials.kiev.ua

KRUTH J.-P.

Department of Metallurgy and Materials Engineering, K.U. Leuven, Leuven, Belgium
Fax: 32 16 32 1992, 32 16 32 2987
E-mail: Ludo.Froyen@kuleuven.ac.be, Jean-Pierre.Kruth@mech.kuleuven.ac.be

KRUTKO N.P.

Institute of General and Inorganic Chemistry, NASB, Minsk, Belarus
E-mail: ulya@igic.bas-net.by, IONCH@igic.bas-net.by

KRYACHKO L.A.

Frantsevich Institute for Problems of Material Science, NASU, Kyiv, Ukraine
Tel.: (044) 444-24-74
E-mail: 29min@ipms.ua

KRYSHANOVSKA A.S.

Institute for Single Crystals, NASU, Kharkiv, Ukraine
Tel.: (0572) 30-7977, 30-7989
Fax: (0572) 32-0273
E-mail: alexkryzh@isc.kharkov.com

KSHNJAKIN V.S.

Institute of Surface Modification, Sumy, Ukraine

KUCHER O.

Kurdyumov Institute for Metal Physics, NASU, Kyiv, Ukraine
Tel.: (044) 444-9520
E-mail: kotr@imp.kiev.ua

KUD' I.V.

Frantsevich Institute for Problems of Material Science, NASU, Kyiv, Ukraine
Tel.: (044) 444-1501
Fax: (044) 450-4030
E-mail: emprit@mail.ru

KUDIN V.G.

Taras Shevchenko Kyiv National University, Kyiv, Ukraine
E-mail: vsudavtsova@univ.kiev.ua

KUKHARENKO S.

Bakul Institute of Superhard Materials, NASU, Kyiv, Ukraine
Tel.: (044) 430-7694
Fax: (044) 430-7694
E-mail: shilo@ism.kiev.ua

KULAK L.D.

Frantsevich Institute for Problems of Material Science, NASU, Kyiv, Ukraine
Tel.: (044) 444-3090, 444-3360, 444-3345
Fax: (044) 444-02131
E-mail: fsa@materials.kiev.ua, dep22@materials.kiev.ua

KULICH V.G.

Bakul Institute of Superhard Materials, NASU, Kyiv, Ukraine
Tel.: (044) 432-9544
Fax: (044) 467-5625
E-mail: ism1@kibor.kiev.ua

KULICHENKO V.

Kiev Taras Shevchenko National University, 64
Vladimirska St., Kiev 01033, Ukraine
Tel.: (044) 221-0206
E-mail: dziazko@carrier.kiev.ua

KULIK A.I.

Scientific Production Company "Donix", Donetsk, Ukraine
Tel.: (062) 335-1151
Fax: (0622) 93-3262
E-mail: rato@fizmet.dgtu.donetsk.ua

KULIK O.G.

Bakul Institute of Superhard Materials, NASU, Kyiv, Ukraine
Tel.: (044) 468-8632, 430-3506
Fax: (044) 468-8625
E-mail: vturk@ism.kiev.ua

KULIKOVSKY V.

Frantsevich Institute for Problems of Material Science, NASU, Kyiv, Ukraine
Tel.: (044) 444-3401
E-mail: kulik@materials.kiev.ua, kulikov@fzu.cz

KULMETYEVA V.B.

Research Center of Powder Materials Science, Perm, Russia
Tel.: (3422) 391-110
Fax: (3422) 391-122
E-mail: patent@pm.pstu.ac.ru

KUNITSKY YU.A.

Technical Centre of NASU, Kyiv, Ukraine
Tel.: (044) 434-1301
Fax: (044) 235-3474
E-mail: gfrkiev@carrier.kiev.ua

KUNTY O.I.

National University "Lviv Politechnik", Lviv, Ukraine
Tel.: 39-8172, 39-8770
E-mail: kunty@polynet.lviv.ua, kunty@ukr.net.ua

KUPRIANOV I.L.

Institute of Improvement of Professional Skill, Minsk, Belarus
E-mail: beliyev_a@open.by

KUPRIN V.V.

Frantsevich Institute for Problems of Material Science, NASU, Kyiv, Ukraine
Tel.: (044) 444-3061, 444-0294
Факс: (044) 444-3061, 452-55-23
E-mail: yefimov@materials.kiev.ua, san@materials.kiev.ua, nick@ipms.kiev.ua

KURDYUMOV A.V.

Frantsevich Institute for Problems of Material Science, NASU, Kyiv, Ukraine
Tel.: (044) 444-3401
E-mail: britun@i.com.ua, dep20@ipms.kiev.ua

KURGANSKYI M.P.

Gas Institute, NASU, Kyiv, Ukraine
E-mail: bond@bond.elan-ua.net

KURIOV G.V.

Open Joint-Stock Company Special Design-Technology Office of Submerged Electric Equipment "Potential", Kharkiv, Ukraine
Tel.: (0572) 92-2167
Fax: (0572) 16-2180
E-mail: Kgv_2000@mail.ru, big777@mail.ru

KURINNAYA T.V.

Frantsevich Institute for Problems of Material Science, NASU, Kyiv, Ukraine
Tel.: (044) 444-0256
Fax: (044) 444-2131
E-mail: post@ipms.kiev.ua

KURKOVA D.I.

Frantsevich Institute for Problems of Material Science, NASU, Kyiv, Ukraine
Tel.: (044) 444-3017, 444-6201
Fax: (044) 444-3017
E-mail: naidich@ipms.kiev.ua

KUROCHKIN V.D.

Frantsevich Institute for Problems of Material Science, NASU, Kyiv, Ukraine
Tel.: (044) 444-20-24
E-mail: vkur@ipms.kiev.ua

KUSIAK N.V.

Franko Zhytomyr Pedagogical University, Zhytomyr, Ukraine

KUSMENKO N.

Frantsevich Institute for Problems of Material Science, NASU, Kyiv, Ukraine
E-mail: rapid@materials.kiev.ua

KUTSEVA N.A.

Dnipropetrovsk National University, Dnipropetrovsk, Ukraine
Tel.: (0562) 776-9042
E-mail: metal@ff.dsu.dp.ua

KUZIN N.N.

Vereschagin Institute for High Pressure Physics, RAS, Troitsk, Russia
Tel.: (095) 334-0732
Fax: (095) 334-0012
E-mail: ekimov@hppi.troitsk.ru

KUZMENKO N.N.

Frantsevich Institute for Problems of Material Science, NASU, Kyiv, Ukraine
Tel.: (044) 444-3345
Fax: (044) 452-5523
E-mail: rapid@materials.kiev.ua

KUZNECHIK O.O.

Powder Metallurgy Research Institute, NASB, Minsk, Belarus
Tel.: (517) 239-9828
Fax: (517) 210-0574
E-mail: vityaz@srpmi.minsk.by

KUZNETSOV M.V.

Institute of Structural Macrokinetics and Materials Science, RAS, Chernogolovka, Russia
Tel.: (095) 524-5047
Fax: (095) 962-8025
E-mail: kuznets@ism.ac.ru, morozov@ism.ac.ru

KUZNETSOVA E.V.

Perm State Technical University, Perm, Russia
Tel.: (3414) 39-1340, 22-6596, 90-4188
E-mail: dpm@cpl.pstu.ac.ru

KUZNETSOVA T.

Powder Metallurgy Research Institute, NASB, Minsk, Belarus
Tel.: (517) 239-9804
Fax: (517) 210-0574
E-mail: pb8361@belsonet.net, chekan@srpmi.minsk.by, vityaz@srpmi.minsk.by

KYZNETSOVA T.L.

Frantsevich Institute for Problems of Material Science, NASU, Kyiv, Ukraine
Tel.: (044) 444-2524, 444-8286
E-mail: dep53@materials.ua

L

LABUNETS T.F.

Frantsevich Institute for Problems of Material Science, NASU, Kyiv, Ukraine
Tel.: (044) 444-1533
Fax: (044) 444-2131
E-mail: olgak@materials.kiev.ua

LAGUTA V.V.

Frantsevich Institute for Problems of Material Science, NASU, Kyiv, Ukraine
Tel.: (044) 444-1540
Fax: (044) 444-2131
E-mail: dep4@materials.kiev.ua

LAKEEV V.A.

Physico-Technological Institute of Metals and Alloys, NASU, Kyiv, Ukraine
Tel.: (044) 444-3542
Fax: (044) 444-3542
E-mail: kompozit@inec.kiev.ua

LAKHNENKO V.L.

Physico-Technological Institute of Metals and Alloys, NASU, Kyiv, Ukraine
Tel.: (044) 444-1065, 444-1212, 4440280
Fax: (044) 452-9736
E-mail: metal@ptima.kiev.ua, alloy@i.com.ua

LAKIZA S.M.

Frantsevich Institute for Problems of Material Science, NASU, Kyiv, Ukraine
Tel.: (044) 444-35-73
E-mail: dep25@ipms.kiev.ua

LAMY R.

Groupe de Physique des Solides, C.N.R.S., Universités Paris 6 et 7, Paris, France
Tel.: 0144274672
Fax: 0143542878
E-mail: rodichev@gps.jussieu.fr

LAOUI T.

University of Wolverhampton, Wolverhampton, United Kingdom
Fax: 44 1902 322743
E-mail: t.laoui@wlv.ac.uk

LAPTEV A.V.

Frantsevich Institute for Problems of Material Science, NASU, Kyiv, Ukraine
Tel.: (044) 444-2101
Fax: (044) 444-2131
E-mail: shat@ipms.kiev.ua

LASHKAREV G.V.

Frantsevich Institute for Problems of Material Science, NASU, Kyiv, Ukraine
Tel.: (044) 444-3228
Fax: (044) 4442131
E-mail: lashk@ipms.kiev.ua

LASHNEVA V.V.

Frantsevich Institute for Problems of Material Science, NASU, Kyiv, Ukraine
Tel.: (044) 444-72-56
E-mail: dubok@ipms.kiev.ua

LATYPOV M.G.

Research Center of Powder Materials Science, Perm, Russia
Tel.: (3422) 391-110
Fax: (3422) 391-122
E-mail: patent@pm.pstu.ac.ru

LAYSHCHENKO A.B.

Frantsevich Institute for Problems of Material
Science, NASU, Kyiv, Ukraine
Tel.: (044) 444-1367
E-mail: dep60@ipms.kiev.ua

LAZHEVSKA O.

Bakul Institute of Superhard Materials, NASU, Kyiv,
Ukraine
Tel.: (044) 430-76-94
Fax: (044) 430-76-94
E-mail: svetlana@ism.kiev.ua

LEBEDEV A.A.

Institute for Problems of Strength, NASU, Kyiv,
Ukraine
Tel.: (044) 296-5457
Fax: (044) 296-1684
E-mail: leb@ipp.adam.kiev.ua

LEBEDKINA T.A.

Institute of Solid State Physics, RAS,
Chernogolovka, Russia
Tel.: (09652) 48836
Fax: (09652) 49701
E-mail: lebedkin@issp.ac.ru, tlebyod@issp.ac.ru

LEBUCHOVA N.V.

Institute of Material Science, KSC FEB RAS,
Khabarovsk, Russia
Tel.: (4212) 71-9956
Fax: (4212) 71-9598
E-mail: imdvo@fe.ru, infarest@pop.redcom.ru

LEBYODKIN M.A.

Institute of Solid State Physics, RAS,
Chernogolovka, Russia
Tel.: (09652) 48836
Fax: (09652) 49701
E-mail: lebedkin@issp.ac.ru

LEGKAYA T.N.

Kurdyumov Institute for Metal Physics, NASU, Kyiv,
Ukraine
Tel.: (044) 444-3061
Fax: (044) 444-3061
E-mail: barabash@imp.kiev.ua

LEKISHVILI K.

State Scientific-Technical Center "Delta", Tbilisi,
Georgia
Tel.: (99532) 969-248, 923-779, 955-646
Fax: (99532) 956-080
E-mail: argusdel@hotmail.com

LEONIDOV I.A.

Institute of Solid State Chemistry, UrB of RAS,
Ekaterinburg, Russia
Tel.: (3432) 49-3387, 49-9161
E-mail: leonidov@imp.uran.ru, florid@rambler.ru

LEONIDOVA O.N.

Institute of Solid State Chemistry, UrB of RAS,
Ekaterinburg, Russia
Tel.: (3432) 49-3387, 49-9161
E-mail: leonidov@imp.uran.ru, florid@rambler.ru

LEPESHKIN Y.D.

Bauman Moscow State Technical University,
Moscow, Russia
Baikov Institute of Metallurgy and Material Science,
RAS, Moscow, Russia
E-mail: iovchin@mx.bmstu.ru

LESNIK N.D.

Frantsevich Institute for Problems of Material
Science, NASU, Kyiv, Ukraine
Tel.: (044) 444-1181
E-mail: 29min@ipms.ua

LETSKO A.I.

Powder Metallurgy Research Institute, NASB, Minsk,
Belarus
Tel.: (375 17) 284-0659, 239-9827, 239-9883,
232-6340
Fax: (375 17) 239-3141, 210-0574
E-mail: merkul@presidium.bas-net.by, gppo@mail.ru

LEVASHOV V.I.

Institute of Microelectronics Technology, RAS,
Chernogolovka, Russia
E-mail: despot@ipmt-hpm.ac.ru

LEVCHENKO G.V.

Nekrasov Iron and Steel Institute, NASU,
Dnipropetrovsk, Ukraine
Tel.: (056) 46-2369
Fax: (056 2) 776-5924
E-mail: isi-nasu@a-teleport.com

LEVINA D.A.

Frantsevich Institute for Problems of Material
Science, NASU, Kyiv, Ukraine
Tel.: (044) 444-3231, 444-2073
Fax: (044) 444-2131
E-mail: chern@materials.kiev.ua

LEVINSON D.I.

Zaporizhzhya Institute of State and Municipal
Government, Zaporizhzhya, Ukraine
Tel.: (0612) 63-9973

LEVITSKY M.

Physico-Technological Institute of Metals and Alloys,
NASU, Kyiv, Ukraine
Tel.: (044) 444-2350

LIASHENKO V.I.

Frantsevich Institute for Problems of Material
Science, NASU, Kyiv, Ukraine
Tel.: (044) 444-1501
Fax: (044) 450-4030
E-mail: empril@mail.ru

LIKHODED L.S.

Frantsevich Institute for Problems of Material Science, NASU, Kyiv, Ukraine
Tel.: (044) 444-1501
Fax: (044) 450-4030
E-mail: empril@mail.ru

LIKHTOROVICH S.P.

G.V. Kurdyumov Institute for Metal Physics of the National Academy of Sciences of Ukraine

LIPATOV YA. M.

Scientific and Technological Company TECHMA Ltd, Cheboksary, Russia
Tel.: (8352) 45-3948, 49-8327
Fax: (8352) 45-0901
E-mail: techma@chuvashia.ru

LISNYAK V.V.

Taras Shevchenko Kyiv National University, Kyiv, Ukraine
E-mail: vsudavtsova@univ.kiev.ua

LISOVSKY A.F.

Bakul Institute of Superhard Materials, NASU, Kyiv, Ukraine
Tel.: (044) 468-8625
Fax: (044) 468-8625
E-mail: frd@ism.kiev.ua

LITVIN B.

Dnipropetrovsk National University, Dnipropetrovsk, Ukraine
Tel.: (0562) 469-212, 776-9042
Fax: (0562) 461-697
E-mail: odm@ff.dsu.dp.ua

LITZKENDORF D.

Institut für Physikalische Hochtechnologie, Jena, Germany
Tel.: (49 36 41) 206103, 206107, 206106
Fax: (49 36 41) 206199
E-mail: Doris.Litzkendorf@ipht-jena.de

LIYDVINSKAYA T.A.

Frantsevich Institute for Problems of Material Science, NASU, Kyiv, Ukraine
Tel.: (044) 444-1321

LOBODA P.I.

National Technical University of Ukraine "Kyiv Polytechnic Institute", Kyiv, Ukraine
E-mail: loboda@i.com.ua

LOJKOWSKI W.

High Pressure Research Center, Polish Academy of Sciences, Warsaw, Poland

LOPATO L.M.

Frantsevich Institute for Problems of Material Science, NASU, Kyiv, Ukraine
Tel.: (044) 444-3573
Fax: (044) 444-2131
E-mail: dep25@materials.kiev.ua

LOTSKO D.V.

Frantsevich Institute for Problems of Material Science, NASU, Kyiv, Ukraine
Tel.: (044) 444-3061
Fax: (044) 444-3061
E-mail: lotsko@materials.kiev.ua

LUCHKA M.V.

Frantsevich Institute for Problems of Material Science, NASU, Kyiv, Ukraine
Tel.: (044) 444-2055
Fax: (044) 444-2131
E-mail: miron@ipms.ua

LUGOVSKOI Y.F.

Frantsevich Institute for Problems of Material Science, NASU, Kyiv, Ukraine
Tel.: (044) 456-3483

LUGOVY M.I.

Frantsevich Institute for Problems of Material Science, NASU, Kyiv, Ukraine
Tel.: (044) 444-0051
E-mail: lugovoj@materials.kiev.ua

LUKOVICH V.V.

Frantsevich Institute for Problems of Material Science, NASU, Kyiv, Ukraine
Tel.: (044) 444-1181
Fax: (044) 444-2131
E-mail: 29min@ipms.ua

LUNYOV A.N.

Kazan State Technical University, Kazan, Russia
Tel.: (8432) 384-623
Fax: (8432) 435-935
E-mail: root@una.kazan.ru

LUYCKX S.

University of Witwatersrand, South Africa
Fax: 011-403-1471
E-mail: SLUYCKX@chemeng.chmt.wits.ac.za

LUZINOV I.A.

Iowa State University, Ames, Iowa, USA
Tel.: 515-294-6904, 864-656-5958
Fax: (515) 294-5444, 864-656-5973
E-mail: vladimir@iastate.edu, luzinov@clemson.edu

LYAKHOV N.Z.

Institute of Solid State Chemistry and Mechanochemistry, SB of RAS, Novosibirsk, Russia
E-mail: barinova_ap@mail.ru

LYASHENKO V.I.

Frantsevich Institute for Problems of Material Science, NASU, Kyiv, Ukraine
Tel.: (044) 444-1501
E-mail: tomila@materials.kiev.ua

M**MACHT M.**

Hahn-Meitner Institut, Berlin, Germany

MAIBORODA V.P.

Frantsevich Institute for Problems of Material
Science, NASU, Kyiv, Ukraine
Tel.: (044) 444-3364, 434-1301

MAKARA V.A.

Taras Shevchenko Kyiv National University, Kyiv,
Ukraine
Tel.: (044) 266-2326, 266-4587
Fax: (044) 266-2326
E-mail: krav@mail.phys.univ.kiev.ua

MAKARENKO G.N.

Frantsevich Institute for Problems of Material
Science, NASU, Kyiv, Ukraine
Tel.: (044) 444-1501,
Fax: (044) 450-4030
E-mail: empril@mail.ru

MAKSIMIVA G.M.

Frantsevich Institute for Problems of Material
Science, NASU, Kyiv, Ukraine
Tel.: (044) 444-3364

MAKURIN YU.N.

Ural State Technical University, Ekaterinburg,
Russia
Tel.: (3432) 55-8340
E-mail: vika@nexcom.ru

MALAKHOV V.YA.

Frantsevich Institute for Problems of Material
Science, NASU, Kyiv, Ukraine
Tel.: (044) 444-2371
Fax: (044) 444-2131
E-mail: vlad.malakhov@materials.kiev.ua

MALASHENKO I.S.

Paton Electric Welding Institute, NASU, Kyiv,
Ukraine
Tel.: (044) 261-5281

MALASHENKOV S.P.

Institute for Surface Chemistry, NASU, Kyiv, Ukraine
Tel.: (044) 444-1135
Fax: (044) 444-3567
E-mail: user@sufchem.freenet.kiev.ua

MALKEVICH N.G.

Belorussian National Technical University, Minsk,
Belarus
Tel.: (517) 232-7146, 231-0545, 232-5406
Fax: (517) 232-7183
E-mail: egolubtsova@tut.by, mitko_gala@mail.ru,
metolit@tut.by

MALOCHKIN O.V.

Moscow State Steel and Alloys Institute
(Technological University), Moscow, Russia
Tel.: (095) 230-46-42
Fax: (095) 230-4642
E-mail: olmaloch@shs.misis.ru

MALYSHEV V.V.

National Technical University of Ukraine "Kyiv
Polytechnic Institute", Kyiv, Ukraine
Tel.: (044) 441-1384
Fax: (044) 444-241-9679
E-mail: Koschij@xtf.ntu-kpi.kiev.ua

MALYSHEVA G.V.

Bauman Moscow State Technical University,
Moscow, Russia
E-mail: malyin@mail.ru

MARGOLIN V.I.

Saint-Petersburg State Electrotechnical University
"LETI" Saint-Petersburg, Russia
Tel.: (812) 596-3533
Fax: (812) 596-3551
E-mail: foundation@aires.spb.ru

MARGRAVE J.L.

Rice University, Houston, TX, USA
Tel.: 713-348-5485
Fax: 713-523-8236
E-mail: marsrav@rice.edu, khval@ruf.rice.edu

MARKIV V.YA.

Taras Shevchenko Kyiv National University, Kyiv,
Ukraine
Tel.: (044) 266-2335
E-mail: be1mar@univ.kiev.ua

MARKOVA L.

Powder Metallurgy Research Institute, NASB, Minsk,
Belarus
Tel.: (517) 239-9804
Fax: (517) 210-0574
E-mail: pb8361@belsonet.net,
chekan@srpmi.minsk.by, vityaz@srpmi.minsk.by

MARORESKU I.I.

Frantsevich Institute for Problems of Material
Science, NASU, Kyiv, Ukraine
Tel.: (044) 444-2001
Fax: (044) 444-2131
E-mail: pleskach@i.com.ua

MARTSENYUK P.S.

Frantsevich Institute for Problems of Material
Science, NASU, Kyiv, Ukraine
Tel.: (044) 444-3090
Fax: (044) 452-55-23
E-mail: velikanova@materials.kiev.ua

MARTUSEVICH E.V.

Siberian State University of Industry, Novokuznetsk, Russia
Tel.: (3843) 46-2277
Fax: (3843) 46-5792
E-mail: gromov@physics.sibsiu.ru

MARTYNOVA L.M.

Bakul Institute of Superhard Materials, NASU, Kyiv, Ukraine
Tel.: (044) 468-8623
Fax: (044) 468-8632, 468-8624
E-mail:alcon@ism.kiev.ua, almaz@ism.kiev.ua

MASLYUK V.A.

Frantsevich Institute for Problems of Material Science, NASU, Kyiv, Ukraine
Tel.: (044) 444-8287, 444-1201
E-mail: Maslyuk@materials.kiev.ua

MASTEPAN V.YU.

Donetsk National Technical University, Donetsk, Ukraine
Tel.: (0622) 93-3262
Fax: (0622) 93-3262
E-mail: rato@fizmet.dgtu.donetsk.ua

MATYSINA Z.A.

Dnipropetrovsk National University, Dnipropetrovsk, Ukraine
Tel.: (0562) 45-0717, 93-8949
Fax: (0562) 46-5523
E-mail: optica@ff.dsu.dp.ua

MAXIMOV A.I.

Saint-Petersburg State Electrotechnical University "LETI" Saint-Petersburg, Russia
Tel.: (812) 351-0798, 234-3016
E-mail: vamochnikov@mail.eltech.ru

MAYSTRENKO A.L.

Bakul Institute of Superhard Materials, NASU, Kyiv, Ukraine
Tel.: (044) 432-9544
Fax: (044) 467-5625
E-mail: ism1@kibor.kiev.ua

MAZILKIN A.A.

Institute of Solid State Physics, RAS, Chernogolovka, Russia
Tel.: (095) 993-2755
Fax: (096) 524-9701
E-mail: mazilkin@issp.ac.ru

MAZUR V.

National Metallurgical Academy of Ukraine, Dnipropetrovsk, Ukraine
Tel.: (0562) 41-0602
Fax: (0562) 67-6977
E-mail: a_mazur@fregat.com

MEDUCH R.M.

Frantsevich Institute for Problems of Material Science, NASU, Kyiv, Ukraine
Tel.: (044) 444-2055
Fax: (044) 444-2131
E-mail: miron@ipms.ua

MEDVEDEV A.S.

Institute of Solid State Physics, RAS, Chernogolovka, Russia
Tel.: (096) 522-2066
E-mail: dpx@aha.ru, myshlyae@issp.ac.ru

MEDVEDEVA N.I.

Institute of Solid State Chemistry, UrB of RAS, Ekaterinburg, Russia
Tel.: (3432) 49-3554
Fax: (3432) 74-4495
E-mail: Medvedeva@ihim.uran.ru

MELESHEVICH K.A.

Frantsevich Institute for Problems of Material Science, NASU, Kyiv, Ukraine
Tel.: (044) 444-3090
Fax: (044) 444-02131
E-mail: dep6@materials.kiev.ua

MELNIKOV V.S.

Institute of Geochemistry, Mineralogy and Ore-Formation, Kyiv, Ukraine
Tel.: (044) 444-0570

MESHKOV YU.YA.

Kurdyumov Institute for Metal Physics, NASU, Kyiv, Ukraine
Tel.: (044) 444-9520
E-mail: popovich@imp.kiev.ua

MESTNIKOV N.S.

Amosov Yakutiya State University, Yakutsk, Russia
Tel.: (4112) 25-3212
Fax: (4112) 26-0934
E-mail: romgeorg@sitc.ru, fz_ema@sitc.ru

MIKHAILOV O.V.

Frantsevich Institute for Problems of Material Science, NASU, Kyiv, Ukraine
Tel.: (044) 3039, 444-7256

MILESHKIN M.

Podgorny Institute for Mechanical Engineering Problems, NASU, Kharkiv, Ukraine
Tel.: (0572) 95-9538
Fax: (0572) 94-4635, 94-2914
E-mail: miles@ipmach.kharkov.ua

MILMAN YU.V.

Frantsevich Institute for Problems of Material Science, NASU, Kyiv, Ukraine
Tel.: (044) 444-3061
Fax: (044) 444-3061
E-mail: milman@materials.kiev.ua

MILUTINOVIC-NIKOLIC A.

Institute of Chemistry, Technology and Metallurgy,
Belgrade, Yugoslavia

MINAKOVA R.V.

Frantsevich Institute for Problems of Material
Science, NASU, Kyiv, Ukraine
Tel.: (044) 444-1181
Fax: (044) 444-2131
E-mail: 29min@ipms.ua

MINKO D.V.

Powder Metallurgy Research Institute, NASB, Minsk,
Belarus
Tel.: (517) 239-9828
Fax: (517) 210-0574
E-mail: vityaz@srpmi.minsk.by

MINTYANSKII I.V.

Chernivtsi Department, Frantsevich Institute for
Problems of Material Science, NASU, Chernivtsi,
Ukraine
Tel.: (03722) 25-155
Fax: (03722) 20-050
E-mail: chimsp@unicom.cv.ua

MIRACLE D.

Air Force Research Laboratory, Wright-Patterson,
OH, USA
Tel.: (937) 25-59833
Fax: (937) 25-53007
E-mail: Daniel.Miracle@wpafb.af.mil,
Daniel.Miracle@afri.af.mil

MIROSHNICHENKO V.

Physico-Technological Institute of Metals and Alloys,
NASU, Kyiv, Ukraine
Tel.: (044) 444-2350

MISCHUK O.A.

UkrNDINP "MASMA", Kyiv, Ukraine
Tel.: (044) 444-9291
E-mail: ukrndimasma@svitonline.com,
olmi@freemail.com.ua

MISCHUK O.D.

Vernadskii Institute of General and Inorganic
Chemistry, NASU, Kyiv, Ukraine
Tel.: (044) 444-2211
Fax: (044) 444-2211
E-mail: belous@ionc.kar.net

MISKUF J.

Institute of Experimental Physics, Kosice, Slovakia

MITZ I.V.

Paton Electric Welding Institute, NASU, Kyiv,
Ukraine
Tel.: (044) 220-8687
Fax: (044) 220-9215
E-mail: borisov.y@paton.kiev.ua

MKRTYCHEV YU.G.

Joint-Skock Company "Uralelektromed", Pyshma,
Russia
Tel.: (34368) 46-596
Fax: (34368) 46-344
E-mail: N.Danilov@elem.ru

MOISEEV V.F.

Frantsevich Institute for Problems of Material
Science, NASU, Kyiv, Ukraine
Tel.: (044) 444-0294, 444-0051

MOKRETZOV A.S.

Perm State Technical University, Perm, Russia
Tel.: (3422) 39-1340
E-mail: dpm@cpl.pstu.ac.ru

MOLCHANOVSKAYA G.M.

Frantsevich Institute for Problems of Material
Science, NASU, Kyiv, Ukraine
Tel.: (044) 444-3364

MORDOVETS N.M.

Frantsevich Institute for Problems of Material
Science, NASU, Kyiv, Ukraine
Tel.: (044) 444-3061, 444-0051
Fax: (044) 444-3061
E-mail: korzhova@materials.kiev.ua

MORDYUK B.N.

Kurdyumov Institute for Metal Physics, NASU, Kyiv,
Ukraine
Tel.: (044) 444-9572; 444-0521
E-mail: prokop@imp.kiev.ua

MORITO F.

National Institute for Materials Science, Tsukuba,
Japan
Tel.: 81-298-59-2549
Fax: 81-298-59-2501
E-mail: MORITO.Fumio@nims.go.jp

MOROZOV YU.G.

Institute of Structural Macrokinetics and Materials
Science, RAS, Chernogolovka, Russia
Tel.: (095) 524-5047
Fax: (095) 962-8025
E-mail: morozov@ism.ac.ru

MOSHCHIL V.E.

Bakul Institute of Superhard Materials, NASU, Kyiv,
Ukraine
Tel.: (044) 430-1126, 468-8625
Fax: (044) 468-8625
E-mail: frd@ism.kiev.ua, prikhn@iptelecom.net.ua

MOSHNIKOV V.A.

Saint-Petersburg State Electrotechnical University
"LETI" Saint-Petersburg, Russia
Tel.: (812) 351-0798, 234-3016
E-mail: vamoshnikov@mail.eltech.ru

MOSINA T.V.

Frantsevich Institute for Problems of Material Science, NASU, Kyiv, Ukraine
Tel.: (044) 444-6201, 444-3017, 444-3502

MOVCHAN B.A.

International Center of Electron Beam Technologies of Paton Electric Welding Institute, NASU, Kyiv, Ukraine
Tel.: (044) 269-3917, 227-6041
E-mail: movchan@ic-ebt1.kiev.ua

MOZKOVA O.V.

CDO "Arsenal", Kyiv, Ukraine
Tel.: (044) 254-5908
Fax: (044) 254-5908
E-mail: borisgor@i.com.ua

MURATOV V.B.

Frantsevich Institute for Problems of Material Science, NASU, Kyiv, Ukraine
Tel.: (044) 444-1290
Fax: (044) 444-2131
E-mail: bas@materials.kiev.ua

MUZYKA N.R.

Institute for Problems of Strength, NASU, Kyiv, Ukraine
Tel.: (044) 296-5457
Fax: (044) 296-1684
E-mail: leb@ipp.adam.kiev.ua

MYNYK S.

Karpenko Physico-Mechanical Institute, NASU, Lviv, Ukraine
Tel.: (0322) 65-4343
E-mail: fedirko@ipm.lviv.ua, minnezing@ah.ipm.lviv.ua

MYSHLYAEV M.M.

Baikov Institute of Metallurgy and Material Science, RAS, Moscow, Russia
Tel.: (096) 522-2066
Fax: (096) 524-9701
E-mail: myshlyae@issp.ac.ru

MYSHLYAEVA M.M.

Institute of Solid State Physics, RAS, Chernogolovka, Russia
Tel.: (096) 522-2066
E-mail: myshlyae@issp.ac.ru

N

NAGORNY P.A.

Bakul Institute of Superhard Materials, NASU, Kyiv, Ukraine
Tel.: (044) 430-1126, 468-8625
Fax: (044) 468-8625
E-mail: frd@ism.kiev.ua, prikhna@iptelecom.net.ua

NAIDICH YU.V.

Frantsevich Institute for Problems of Material Science, NASU, Kyiv, Ukraine
Tel.: (044) 444-3017, 444-6201
Fax: (044) 444-3017
E-mail: naidich@ipms.kiev.ua

NAKAMURA T.

Institute of Multidisciplinary Research for Advanced Materials, Tohoku University, Sendai, Japan
Tel.: 81-22-217-5213, 81-22-217-5214
Fax: 81-22-217-5213, 81-22-217-5214
E-mail: ntakashi@tagen.tohoku.ac.jp

NAPARA-VOLGINA S.G.

Frantsevich Institute for Problems of Material Science, NASU, Kyiv, Ukraine
Tel.: (044) 444-8287, 444-1201
E-mail: Maslyuk@materials.kiev.ua

NATSIK V.D.

Verkin Institute for Low Temperature Physics and Engineering, NASU, Kharkiv, Ukraine
Tel.: (0572) 30-0331
Fax: (0572) 32-2370
E-mail: natsik@ilt.kharkov.ua

NAUMENKO S.M.

Taras Shevchenko Kyiv National University, Kyiv, Ukraine
Tel.: (044) 266-2326, 266-4587
Fax: (044) 266-2326
E-mail: krav@mail.phys.univ.kiev.ua

NEDILKO S.A.

Kiev Taras Shevchenko National University, 64 Vladimirskaya St., Kiev 01033, Ukraine
Tel.: (044) 221-0206
E-mail: nedilko@red-gw.univ.kiev.ua

NEIKOV O.D.

Frantsevich Institute for Problems of Material Science, NASU, Kyiv, Ukraine
Tel.: (044) 444-2380, 444-3061
Fax: (044) 444-3061
E-mail: neiko@svitonline.com

NESHPOR I.P.

Frantsevich Institute for Problems of Material Science, NASU, Kyiv, Ukraine
Tel.: (044) 444-1321

NETYAGA V.V.

Chernivtsi Department, Frantsevich Institute for Problems of Material Science, NASU, Chernivtsi, Ukraine
Tel.: (03722) 25-155
Fax: (03722) 20-050
E-mail: chimsp@unicom.cv.ua

NIKOLENKO S.V.

Institute of Material Science, KSC FEB RAS,
Khabarovsk, Russia
Tel.: (4212) 71-9956
Fax: (4212) 71-9598
E-mail: imdvo@fe.ru, infarest@pop.redcom.ru

NIKONENKO A.P.

Zaporizhzhya State Engineering Academy,
Zaporizhzhya, Ukraine
Tel.: (80612) 60-1261
E-mail: al_nik_co@ukr.net

NISCHENKO M.M.

G.V. Kurdyumov Institute for Metal Physics of the
National Academy of Sciences of Ukraine

NODA T.

National Institute for Materials Science, Tsukuba,
Japan
Tel.: 81-298-59-2549
Fax: 81-298-59-2501
E-mail: MORITO.Fumio@nims.go.jp

NORMATOV I.SH.

Institute of Chemistry, Dushanbe, Tajikistan
Tel.: (992372) 245-231
Fax: (992372) 214-911
E-mail: inom@ac.tajik.net

NOSOLEV I.K.

Donetsk Physical-Technical Institute, NASU,
Donetsk, Ukraine
Tel.: (0622) 55-5121
E-mail: Tatjana@konstant.fti.donetsk

NOVIKOV G.I.

Belorussian State University of Technology, Minsk,
Belarus

NOVIKOV N.V.

Bakul Institute of Superhard Materials, NASU, Kyiv,
Ukraine
Tel.: (044) 468-8632, 432-9544
Fax: (044) 468-8625, 467-5625
E-mail: novikiv@ism.kiev.ua, vturk@ism.kiev.ua

NOVIKOV V.V.

Odessa National Polytechnical University
E-mail: novikov@te.net.ua

NOVIKOVA V.I.

Frantsevich Institute for Problems of Material
Science, NASU, Kyiv, Ukraine
Tel.: (044) 444-0256
Fax: (044) 444-2131
E-mail: post@ipms.kiev.ua

NOVYTSKYY V.G.

Physico-Technological Institute of Metals and Alloys,
NASU, Kyiv, Ukraine
Tel.: (044) 444-1065, 444-1212, 4440280
Fax: (044) 452-9736
E-mail: metal@optima.kiev.ua, alloy@i.com.ua

NURKANOV E.Y.

Ural State Technical University, Ekaterinburg,
Russia
Tel.: (3432) 75-9724
Fax: (3432) 75-9407
E-mail: nurkanov@siams.com

O

OGENKO V.M.

Institute for Surface Chemistry, NASU, Kyiv, Ukraine
Tel.: (044) 444-1135
Fax: (044) 444-3567
E-mail: user@sufrchem.freenet.kiev.ua

OKATOVA G.P.

Powder Metallurgy Research Institute, NASB, Minsk,
Belarus
Tel.: (375 17) 284-0659, 239-9827,
239-9883, 232-6340
Fax: (375 17) 239-3141, 210-0574
E-mail: merkul@presidium.bas-net.by, gppo@mail.ru

OKHRIMENKO G.

Institute for Problems of Strength, NASU, Kyiv,
Ukraine
Tel.: (044) 444-2425
Fax: (044) 488-3821
E-mail: chern@materials.kiev.ua

OKOVITY V.

Powder Metallurgy Research Institute, NASB, Minsk,
Belarus
Tel.: (375 17) 232-5691
Fax: (375 17) 210-0574
E-mail: alexil@srpmi.belpak.minsk.by

OKROSTVARIDZE O.

State Scientific-Technical Center "Delta", Tbilisi,
Georgia
Tel.: (99532) 969-248, 923-779, 955-646
Fax: (99532) 956-080
E-mail: argusdel@hotmail.com

OLEYNIK G.S.

Frantsevich Institute for Problems of Material
Science, NASU, Kyiv, Ukraine
Tel.: (044) 444-3401
E-mail: dep20@ipms.kiev.ua

ONOFRIO G.

Istituto per la Tecnologia dei Materiali e dei
Processi Energetici, Milano, Italy
Fax: 39 2 66173321
E-mail: onofrio@tempe.mi.cnr.it

ONOPRIENKO A.

Frantsevich Institute for Problems of Material Science, NASU, Kyiv, Ukraine
Tel.: (044) 444-3401
Fax: 444-2131
E-mail: onopr@materials.kiev.ua

ORLETSKII V.B.

Chernivtsi Department, Frantsevich Institute for Problems of Material Science, NASU, Chernivtsi, Ukraine
Tel.: (03722) 25-155
Fax: (03722) 20-050
E-mail: chimsp@unicom.cv.ua

ORLOV S.A.

Open Joint-Stock Zavolzhsky Engine Plant, Zavolzhje, Russia
Tel.: (83169) 67-022
Fax: (83169) 33-287

ORLOVSKAYA N.A.

Drexel University, Philadelphia, USA
E-mail: nao22@drexel.edu

ORYSHICH I.V.

Frantsevich Institute for Problems of Material Science, NASU, Kyiv, Ukraine
Tel.: (044) 444-8286

OSCHKADEROV S.P.

Kurdyumov Institute for Metal Physics, NASU, Kyiv, Ukraine
Tel.: (044) 444-9586
Fax: (044) 444-9561
E-mail: metall@imp.kiev.ua

OSIPOV A.S.

Bakul Institute of Superhard Materials, NASU, Kyiv, Ukraine
Tel.: (044) 468-8632, 430-3506
Fax: (044) 468-8625
E-mail: vturk@ism.kiev.ua

OSIPOVA I.I.

Frantsevich Institute for Problems of Material Science, NASU, Kyiv, Ukraine
Tel.: (044) 444-2371, 444-2471, 216-5371
Fax: (044) 444-2131
E-mail: sart@ipms.kiev.ua

OVCHAR O.V.

Vernadskii Institute of General and Inorganic Chemistry, NASU, Kyiv, Ukraine
Tel.: (044) 444-2211
Fax: (044) 444-2211
E-mail: belous@ionc.kar.net

OVCHINNIKOV I.N.

Bauman Moscow State Technical University, Moscow, Russia
E-mail: iovchin@mx.bmstu.ru

OVCHINNIKOV V.I.

Research Institute of Impulse Processes, Minsk, Belarus
Tel.: (375 17) 239-3244
Fax: (375 17) 232-8411
E-mail: impuls@bn.by

OVSYANNIKOV O.

Kurdyumov Institute for Metal Physics, NASU, Kyiv, Ukraine
Tel.: (044) 444-9520
E-mail: kotr@imp.kiev.ua

P

PADERNO V.N.

Frantsevich Institute for Problems of Material Science, NASU, Kyiv, Ukraine
Tel.: (044) 444-1367
Fax: (044) 444-2131
E-mail: dep60@ipms.kiev.ua

PADERNO YU.B.

Frantsevich Institute for Problems of Material Science, NASU, Kyiv, Ukraine
Tel.: (044) 444-1367
Fax: (044) 444-2131
E-mail: dep60@ipms.kiev.ua

PALOSZ B.

High Pressure Research Center, Polish Academy of Sciences, Warsaw, Poland

PAL-VAL P.P.

Verkin Institute for Low Temperature Physics and Engineering, NASU, Kharkiv, Ukraine
Tel.: ((0572) 30-0331, 30-8513
Fax: (0572) 32-2370
E-mail: PALVAL@ilt.kharkov.ua

PANASHENKO V.M.

Frantsevich Institute for Problems of Material Science, NASU, Kyiv, Ukraine
Tel.: (044) 444-0002, 444-0101, 444-2101
Fax: (044) 444-2131
E-mail: mscoval@ipms.kiev.ua, imorozov@materials.kiev.ua

PANASYUK A.D.

Frantsevich Institute for Problems of Material Science, NASU, Kyiv, Ukraine
Tel.: (044) 444-2201, 444-3522
E-mail: lavrenko@ipms.kiev.ua

PANIN V.E.

Institute of Strength Physics and Materials Science, SB of RAS, Tomsk, Russia
E-mail: editor@ms.tsc.ru

PANIN V.N.

Engineering-Technical Center "Prometej", Chekhov,
Russia
Tel.: (09672) 62-784
Fax: (09672) 62-784
E-mail: prometej@aha.ru

PANOV V.S.

Moscow State Steel and Alloys Institute
(Technological University), Moscow, Russia
Tel.: (095) 230-46-42
Fax: (095) 230-4642
E-mail: olmaloch@shs.misis.ru

PASCHENKO E.

Bakul Institute of Superhard Materials, NASU, Kyiv,
Ukraine
Tel.: (044) 430-7694
Fax: (044) 430-7694
E-mail: shilo@ism.kiev.ua

PASHINSKAYA E.G.

Donetsk Physical-Technical Institute, NASU,
Donetsk, Ukraine
E-mail: pashinska@mail.ru

PASHINSKAYA O.V.

Donetsk Physical-Technical Institute, NASU,
Donetsk, Ukraine
E-mail: pashinska@mail.ru

PASHKOVA Y.V.

Vernadskii Institute of General and Inorganic
Chemistry, NASU, Kyiv, Ukraine
Tel.: (044) 444-2211
Fax: (044) 444-2211
E-mail: belous@ionc.kar.net

PASHYNSKY V.V.

Donetsk National Technical University, Donetsk,
Ukraine
Tel.: (0622) 93-3262
Fax: (0622) 93-3262
E-mail: rato@fizmet.dgtu.donetsk.ua

PATON B.E.

Paton Electric Welding Institute, NASU, Kyiv,
Ukraine
Tel.: (044) 261-5966
Fax: (044) 286-0486

PATSYNA R.V.

Frantsevich Institute for Problems of Material
Science, NASU, Kyiv, Ukraine
Tel.: (044) 444-2380, 444-3061
Fax: (044) 444-3061
E-mail: neiko@svitonline.com

PAUSTOVSKY A.V.

Frantsevich Institute for Problems of Material
Science, NASU, Kyiv, Ukraine
Tel.: (044) 444-0256
Fax: (044) 444-2131
E-mail: post@ipms.kiev.ua

PAVLENKO T.P.

Frantsevich Institute for Problems of Material
Science, NASU, Kyiv, Ukraine
Tel.: (044) 444-2255
Fax: (044) 444-2131
E-mail: raich@ipms.kiev.ua

PAVLIGO T.M.

Frantsevich Institute for Problems of Material
Science, NASU, Kyiv, Ukraine
Tel.: (044) 444-3255
E-mail: gena@ipms.kiev.ua

PAVLIKOV V.N.

Frantsevich Institute for Problems of Material
Science, NASU, Kyiv, Ukraine
Tel.: (044) 444-2001
Fax: (044) 444-2131
E-mail: pavlikov@materials.kiev.ua

PAVLITCHUK T.V.

Frantsevich Institute for Problems of Material
Science, NASU, Kyiv, Ukraine
Tel.: (044) 444-2255
Fax: (044) 444-2131
E-mail: raich@ipms.kiev.ua

PAVLOV V.S.

National Scientific Centre "Kharkiv Institute of
Physics & Technology", NASU, Kharkiv, Ukraine

PECHKOVSKY E.P.

Frantsevich Institute for Problems of Material
Science, NASU, Kyiv, Ukraine
Tel.: (044) 444-0294, 444-1124, 444-0051
Fax: (044) 452-55-23
E-mail: fsa@materials.kiev.ua,
epp@materials.kiev.ua

PEREKOS A.E.

Kurdyumov Institute for Metal Physics, NASU, Kyiv,
Ukraine
Tel.: (044) 44-9546, 444-9531, 444-9532
Fax: (044) 444-2561
E-mail: perekos@imp.kiev.ua

PERELIAEVA L.A.

Institute of Solid State Chemistry, UrB of RAS,
Ekaterinburg, Russia
Tel.: (3432) 49-3387, 49-9161
E-mail: leonidov@imp.uran.ru, florid@rambler.ru

PERMYAKOVA I.J.

Derzhavin Tambov State University, Tambov, Russia
Tel.: (0572) 35-2614
Fax: (0572) 710-307
E-mail: ushakov@tsu.tmb.ru, feodorov@tsu.tmb.ru

PETROSYAN G.L.

State Engineering University of Armenia, Yerevan,
Armenia
Tel.: (374 1) 56-3217
Fax: (374 1) 54-5843
E-mail: gevorglp@seua.am, afh@seua.am

PETROSYAN V.G.

State Engineering University of Armenia, Yerevan,
Armenia
Tel.: (374 1) 56-3217
Fax: (374 1) 54-5843
E-mail: gevorglp@seua.am, afh@seua.am

PETROV S.

Scientific Production Association "TOPAC", Kyiv,
Ukraine
Tel.: (044) 467-3549

PETRUNIN V.A.

Siberian State University of Industry, Novokuznetsk,
Russia
Tel.: (3843) 462-277
Fax: (3843) 465-792
E-mail: gromov@physics.sibsiu.ru

PETRUSHA I.A.

Bakul Institute of Superhard Materials, NASU, Kyiv,
Ukraine

PILIPENKO N.P.

Donetsk Physical-Technical Institute, NASU,
Donetsk, Ukraine
Tel.: (0622) 55-5121
E-mail: Tatjana@konstant.fti.donetsk

PINCHUK N.D.

Frantsevich Institute for Problems of Material
Science, NASU, Kyiv, Ukraine
Tel.: (044) 444-33-64
Fax: (044) 450-44-87

PIRÓN ABELLÁN J.

Institute for Materials and Processes in Energy
Systems, Forschungszentrum Jülich, Germany
Tel.: +49-2461-615560
Fax: +49-2461-613699
E-mail: v.shemet@fz-juelich.de

PISARENKO V.A.

Frantsevich Institute for Problems of Material
Science, NASU, Kyiv, Ukraine
Tel.: (044) 444-8286, 444-2524, 444-0294
E-mail: dep53@ipms.kiev.ua

PISKALENKO V.V.

Siberian State University of Industry, Novokuznetsk,
Russia
Tel.: (3843) 46-2277
Fax: (3843) 46-5792
E-mail: gromov@physics.sibsiu.ru

PLEKHANOV K.A.

Joint-Skock Company "Uralelektromed", Pyshma,
Russia
Tel.: (34368) 46-596
Fax: (34368) 46-344
E-mail: N.Danilov@elem.ru

PLESKACH I.V.

Frantsevich Institute for Problems of Material
Science, NASU, Kyiv, Ukraine
Tel.: (044) 444-2001
Fax: (044) 444-2131
E-mail: pleskach@i.com.ua

PLETNEV R.N.

Institute of Solid State Chemistry, UrB of RAS,
Ekaterinburg, Russia
Tel.: (3432) 74-5331, 74-5691
Fax: (3432) 74-4495
E-mail: pletnev@ihim.uran.ru, Yuryeva@ihim.uran.ru

PLEVKOV A.V.

Tomsk State University of Architecture and
Construction, Tomsk, Russia
Tel.: (3822)65-4263
E-mail: kozlov@mail.tomsknet.ru

PLOMODYALO L.G.

Technological Enterprise "Tool", Krasnodar, Russia
Tel.: 56-6410
Fax: 56-6410

PLOMODYALO R.L.

Kuban State Technological University, Krasnodar,
Russia

PLUSHNIKOVA T.N.

Derzhavin Tambov State University, Tambov, Russia
Tel.: (0572) 35-2614
Fax: (0752) 710-307
E-mail: plushnik@mail.ru

PLUZHNIKOV V.

Verkin Institute for Low Temperature Physics and
Engineering, NASU, Kharkiv, Ukraine

PODAREVSKAYA O.V.

National University of Food Technologies, Kyiv,
Ukraine

PODCHERNYAEVA I.A.

Frantsevich Institute for Problems of Material
Science, NASU, Kyiv, Ukraine
Tel.: (044) 444-2201, 444-3522
E-mail: lavrenko@ipms.kiev.ua

PODREZOV Y.N.

Frantsevich Institute for Problems of Material
Science, NASU, Kyiv, Ukraine
Tel.: (044) 444-3061, 444-0051
Fax: (044) 444-3061
E-mail: podrezov@materials.kiev.ua

POGREBNJAK A.D.

Institute of Surface Modification, Sumy, Ukraine

POHRELIUK I.

Karpenko Physico-Mechanical Institute, NASU, Lviv, Ukraine
Tel.: (0322) 65-4343
E-mail: fedirko@ipm.lviv.ua, minnezing@ah.ipm.lviv.ua

POKROPIVNY A.V.

Frantsevich Institute for Problems of Material Science, NASU, Kyiv, Ukraine
Tel.: (263) 36401
Fax: (044) 444-2131
E-mail: pokr@ipms.kiev.ua

POKROPIVNY V.V.

Frantsevich Institute for Problems of Material Science, NASU, Kyiv, Ukraine
Tel.: (263) 36401
Fax: (044) 444-2131
E-mail: pokr@ipms.kiev.ua

POLIKARPOV V.M.

Derzavin Tambov State University
Tel.: (075) 248-3751
E-mail: polikarpovt@mail.ru

POLISCHUK S.S.

Kurdyumov Institute for Metal Physics, NASU, Kyiv, Ukraine
Tel.: (044) 444-9532
E-mail: cuba@imp.kiev.ua

POLYAKOV V.A.

Nekrasov Iron and Steel Institute, NASU, Dnipropetrovsk, Ukraine
Tel.: (0562) 47-3826

PONIRKO E.F.

National Technical University of Ukraine "Kyiv Polytechnic Institute", Kyiv, Ukraine
E-mail: rchebot@ukr.net

PONOMAREV S.S.

Frantsevich Institute for Problems of Material Science, NASU, Kyiv, Ukraine
Tel.: (044) 444-0294
Fax: (044) 452-5523
E-mail: nick@ipms.kiev.ua

POPOV V.P.

Frantsevich Institute for Problems of Material Science, NASU, Kyiv, Ukraine
Tel.: (044) 444-2255
Fax: (044) 444-2131
E-mail: raitch@ipms.kiev.ua

POPOVICH P.

Carls Eberhard Tuebingen Universität, Tuebingen, Deutschland

POPOVYCH V.O.

Kurdyumov Institute for Metal Physics, NASU, Kyiv, Ukraine
Tel.: (044) 444-9520
E-mail: popovich@imp.kiev.ua

POROZOVA S.E.

Research Center of Powder Materials Science, Perm, Russia
Tel.: (3422) 39-1119, 39-1110
Fax: (3422) 39-1122
E-mail: patent@pm.pstu.ac.ru, director@pm.pstu.ac.ru

PORYADCHENKO N.E.

Frantsevich Institute for Problems of Material Science, NASU, Kyiv, Ukraine
Tel.: (044) 444-8286

POTSAR N.A.

Saint-Petersburg State Electrotechnical University "LETI" Saint-Petersburg, Russia
Tel.: (812) 596-3533
Fax: (812) 596-3551
E-mail: foundation@aires.spb.ru

POZNYAK L.A.

Frantsevich Institute for Problems of Material Science, NASU, Kyiv, Ukraine
Tel.: (044) 444-2034, 444-1534
E-mail: celt@materials.kiev.ua

PRIKHNA T.A.

Bakul Institute of Superhard Materials, NASU, Kyiv, Ukraine
Tel.: (044) 430-1126, 468-8625
Fax: (044) 468-8625
E-mail: frd@ism.kiev.ua, prikhna@iptelecom.net.ua

PRILUTSKIY E.V.

Frantsevich Institute for Problems of Material Science, NASU, Kyiv, Ukraine
Tel.: (044) 444-1501
Fax: (044) 450-4030
E-mail: empril@mail.ru

PROKHOROV I.V.

Lykov Heat & Mass Transfer Institute, NASB, Minsk, Belarus
E-mail: bekas@cpl5.itmo.by

PROKOPENKO A.A.

Frantsevich Institute for Problems of Material Science, NASU, Kyiv, Ukraine
Tel.: (044) 444-6201, 444-3017, 444-3502

PROKOPENKO G.I.

Kurdyumov Institute for Metal Physics, NASU, Kyiv, Ukraine
Tel.: (044) 444-9572; 444-0521
E-mail: prokop@imp.kiev.ua

PRONINA L.N.

Institute of Solid State Physics, RAS,
Chernogolovka, Russia
Tel.: (095) 993-2755
Fax: (096) 524-9701
E-mail: pronina@issp.ac.ru

PROTASOVA S.G.

Institute of Solid State Physics, RAS,
Chernogolovka, Russia
Tel.: (095) 993-2755
Fax: (096) 524-9701
E-mail: sveta@issp.ac.ru

PRYADKO L.F.

Frantsevich Institute for Problems of Material
Science, NASU, Kyiv, Ukraine
Tel.: (044) 277-9253
Fax: (044) 235-3474
E-mail: lfp@ukr.net

PYRLYA M.M.

Chernivtsi Department, Frantsevich Institute for
Problems of Material Science, NASU, Chernivtsi,
Ukraine
Tel.: (03722) 25-155
Fax: (03722) 20-050
E-mail: chimsp@unicom.cv.ua

Q**QUADAKKERS W.J.**

Institute for Materials and Processes in Energy
Systems, Forschungszentrum Jülich, Germany
Tel.: +49-2461-615560
Fax: +49-2461-613699
E-mail: v.shemet@fz-juelich.de

R**RABINOVICH O.S.**

Lykov Heat & Mass Transfer Institute, NASB, Minsk,
Belarus
Tel.: (375 17) 284-2775
Fax: (375 17) 232-2513
E-mail: orabi@hmti.ac.by

RACHEK O.P.

Frantsevich Institute for Problems of Material
Science, NASU, Kyiv, Ukraine
Tel.: (044) 444-3061
Fax: (044) 444-3061

RADCHENKO A.K.

Frantsevich Institute for Problems of Material
Science, NASU, Kyiv, Ukraine
Tel.: (044) 444-2155
E-mail: ArRadch@ipms.kiev.ua

RADCHENKO M.V.

Frantsevich Institute for Problems of Material
Science, NASU, Kyiv, Ukraine
Tel.: (044) 444-3228
Fax: (044) 444-2131
E-mail: lashk@ipms.kiev.ua

RAGOZIN Y.

Perm State Technical University, Perm, Russia
Tel.: (3422) 64-8826

RAGULYA A.V.

Frantsevich Institute for Problems of Material
Science, NASU, Kyiv, Ukraine
Tel.: (044) 444-2371, 444-3415, 444-3061
Fax: (044) 444-3061
E-mail: ragulya@materials.kiev.ua

RAKHLIN M.

Institute of Physical Electronics, University of
Stuttgart, Stuttgart, Germany
E-mail: Michail.Rakhlin@ipe.uni-stuttgart.de

RAKHMENINA A.V.

Vereschagin Institute for High Pressure Physics,
RAS, Troitsk, Russia
Tel.: (095) 334-0810, 334-0738, 334-0808
Fax: (095) 334-0012
E-mail: rakhman@ns.hppi.troitsk.ru

RAVI N.

International Advanced Research Center for Powder
Metallurgy and New Materials, Hyderabad, India
Tel.: 91-40-4441075
Fax: 91-40-4442699
E-mail: nukravi@yahoo.com

RAYCHENKO O.I.

Frantsevich Institute for Problems of Material
Science, NASU, Kyiv, Ukraine
Tel.: (044) 444-2255
Fax: (044) 444-2131
E-mail: raitch@ipms.kiev.ua

RED'KO V.P.

Frantsevich Institute for Problems of Material
Science, NASU, Kyiv, Ukraine
Tel.: (044) 444-35-73
E-mail: dep25@ipms.kiev.ua

REVO S.L.

Taras Shevchenko Kyiv National University, Kyiv,
Ukraine
Tel.: (044) 266-2357

RIMBU G.A.

Advanced Research Institute for Electrical
Engineering, Bucharest, Romania
Tel.: +40 1-346-7283
Fax: +40 1-346-7283
E-mail: electmat@icpe.ro

RISTIC M.M.

Institute of Technical Science of Serbian ASA,
Belgrade, Serbian
Tel.: +381 11 637367
Fax: +381 11 637239
E-mail: risticm@mi.sanu.ac.yu

RITCHKOVA M.I.

Institute Ecology and Genetics of Microorganisms,
UrB of RAS, Perm, Russia
Tel.: (3422) 64-6714
Fax: (3422) 64-6711

RODITCHEV D.

Groupe de Physique des Solides, C.N.R.S.,
Universités Paris 6 et 7, Paris, France
Tel.: 0144274672
Fax: 0143542878
E-mail: rodichev@gps.jussieu.fr

ROGOZINSKAYA A.A.

Frantsevich Institute for Problems of Material
Science, NASU, Kyiv, Ukraine
Tel.: (044) 444-0002, 444-0101, 444-2101
Fax: (044) 444-2131
E-mail: mscoval@ipms.kiev.ua,
imorozov@materials.kiev.ua

ROGOZINSKII A.

Frantsevich Institute for Problems of Material
Science, NASU, Kyiv, Ukraine
Tel.: (044) 444-8286
E-mail: ba-ua@yahoo.co.uk

ROGUL T.G.

Frantsevich Institute for Problems of Material
Science, NASU, Kyiv, Ukraine
Tel.: (044) 444-2524, 444-0294
E-mail: dep53@ipms.kiev.ua

ROIK T.A.

State Scientific and Technical Center of Artillery-Rifle
Arms, Kyiv, Ukraine
Tel.: (044) 241-8756
Fax: (044) 456-2834
E-mail: kba@kba.kiev.ua

ROMANENKO O.M.

Frantsevich Institute for Problems of Material
Science, NASU, Kyiv, Ukraine
Tel.: (044) 444-2024
E-mail: vkur@ipms.kiev.ua

ROMANOV G.N.

Kuibyshev Tomsk State University, Tomsk, Russia
Tel.: (4112) 25-3213
Fax: (4112) 26-0934
E-mail: romgeorg@sitc.ru, fz_ema@sitc.ru

ROSANTSEV G.M.

Donetsk National University, Donetsk, Ukraine
Tel.: 91-9238
E-mail: getman@dongu.donetsk.ua, dshe@skif.net

RUBAN A.K.

Frantsevich Institute for Problems of Material
Science, NASU, Kyiv, Ukraine
Tel.: (044) 444-3573
Fax: (044) 444-2131
E-mail: dep25@materials.kiev.ua

RUD` B.M.

Frantsevich Institute for Problems of Material
Science, NASU, Kyiv, Ukraine
Tel.: (044) 444-0256, 444-2371
Fax: (044) 444-2131
E-mail: post@ipms.kiev.ua

RUDEKO O.V.

Taras Shevchenko Kyiv National University, Kyiv,
Ukraine
Tel.: (044) 266-2326, 266-4587
Fax: (044) 266-2326
E-mail: krav@mail.phys.univ.kiev.ua

RUMYANTSEVA A.I.

Saint-Petersburg State Electrotechnical University
"LETI" Saint-Petersburg, Russia
Tel.: (812) 351-0798, 234-3016
E-mail: vamochnikov@mail.eltech.ru

RUZHITSKAYA T.V.

Kurdyumov Institute for Metal Physics, NASU, Kyiv,
Ukraine
Tel.: (044) 44-9546, 444-9531, 444-9532
Fax: (044) 444-2561
E-mail: perekos@imp.kiev.ua, potvora@imp.kiev.ua

RYABICHEVA L.A.

Vladimir Dahl East Ukrainian National University,
Lugansk, Ukraine
Tel.: (0642) 46-2233
E-mail: material@snu.edu.ua

RYABTSEV A.D.

Donetsk National Technical University, Donetsk,
Ukraine
Tel.: (0622) 93-3262
Fax: (0622) 93-3262
E-mail: rato@fizmet.dgtu.donetsk.ua

RYABTSEV S.I.

Dnipropetrovsk National University, Dnipropetrovsk,
Ukraine
Tel.: (0562) 776-9042
E-mail: metal@ff.dsu.dp.ua

RYUMSHINA T.A.

Donetsk National Technical University, Donetsk,
Ukraine
Tel.: (0622) 910-381, 559-515
E-mail: Ryumshina@donapex.net

S

SABOKAR V.K.

Paton Electric Welding Institute, NASU, Kyiv, Ukraine

Tel.: (044) 227-1366, 227-4783, 261-5098

Fax: (044) 227-1366, 268-0486

E-mail: zamkov@paton.kiev.ua,
office@paton.kiev.ua

SACKS W.

Groupe de Physique des Solides, C.N.R.S.,
Universités Paris 6 et 7, Paris, France

Tel.: 0144274672

Fax: 0143542878

E-mail: rodichev@gps.jussieu.fr

SAFONOVA A.M.

Institute of General and Inorganic Chemistry, NASB,
Minsk, Belarus

Tel.: (375 17) 284-1009

Fax: (375 17) 284-2703

E-mail: safonova@igic.bas-net.by

SAHVADZE D.

State Scientific-Technical Center "Delta", Tbilisi,
Georgia

Tel.: (99532) 969-248, 923-779, 955-646

Fax: (99532) 956-080

E-mail: argusdel@hotmail.com

SAITO H.

Chiba Institute of Technology, Funabashi, Japan

SAKAMOTO K.

Keihin Corporation, Kakuta, Japan

SAKHNENKO A.V.

Frantsevich Institute for Problems of Material
Science, NASU, Kyiv, Ukraine

Tel.: (044) 444-3255

E-mail: gena@ipms.kiev.ua

SALDAN I.V.

Karpenko Physico-Mechanical Institute, NASU, Lviv,
Ukraine

Tel.: (0322) 65-4833

Fax: (0322) 64-9427

E-mail: zavalij@ipm.lviv.ua

SALTYKOV V.A.

Frantsevich Institute for Problems of Material
Science, NASU, Kyiv, Ukraine

Tel.: (044) 444-3090

Fax: (044) 444-02131

E-mail: dep6@materials.kiev.ua

SAMELYUK A.V.

Frantsevich Institute for Problems of Material
Science, NASU, Kyiv, Ukraine

Tel.: (044) 444-2380, 444-3061

Fax: (044)444-3061

E-mail: neiko@svitonline.com

SAROKA D.I.

Powder Metallurgy Research Institute, NASB, Minsk,
Belarus

Tel.: (375 17) 239-9892

Fax: (375 17) 210-0574

E-mail: dsaroka@tut.by

SARTINSKA L.L.

Frantsevich Institute for Problems of Material
Science, NASU, Kyiv, Ukraine

Tel.: (044) 444-2371, 444-2471, 216-5371

Fax: (044) 444-2131

E-mail: sart@ipms.kiev.ua

SARZHAN G.F.

Frantsevich Institute for Problems of Material
Science, NASU, Kyiv, Ukraine

Tel.: (044) 444-3061, 444-0294

Fax: (044) 444-3061, 452-5523

E-mail: sery@materials.kiev.ua, nick@ipms.kiev.ua

SAVCHUK YA.M.

Bakul Institute of Superhard Materials, NASU, Kyiv,
Ukraine

Tel.: (044) 430-1126, 468-8625

Fax: (044) 468-8625

E-mail: frd@ism.kiev.ua, prikhna@iptelecom.net.ua

SAVICH V.V.

Powder Metallurgy Research Institute, NASB, Minsk,
Belarus

Tel.: (375 17) 232-2526

Fax: (375 17) 210-00574

E-mail: Chekan@srpmi.minsk.by

SAVIN YU.N.

Institute for Single Crystals, NASU, Kharkiv, Ukraine

Tel.: (0572) 30-7977, 30-7989

Fax: (0572) 32-0273

E-mail: savin@isc.kharkov.com

SAVITSKII A.P.

Institute of Strength Physics and Materials Science,
SB of RAS, Tomsk, Russia

Tel.: (3822) 25-8138

Fax: (3822) 26-0934

E-mail: savitskii@hotmail.com

SAVITSKII P.I.

Chernivtsi Department, Frantsevich Institute for
Problems of Material Science, NASU, Chernivtsi,
Ukraine

Tel.: (03722) 25-155

Fax: (03722) 20-050

E-mail: chimsp@unicom.cv.ua

SCHMIDT CH.

Institut für Physikalische Hochtechnologie, Jena,
Germany
Tel.: (49 36 41) 206103, 206107, 206106
Fax: (49 36 41) 206199
E-mail: Oleksiy.Surzhenko@ipht-jena.de,
Wolfgang.Gawalek@ipht-jena.de

SCHUBERT M.

Institute of Physical Electronics, University of
Stuttgart, Stuttgart, Germany
E-mail: Michail.Rakhlin@ipe.uni-stuttgart.de

SCKOLNIY V.K.

Frantsevich Institute for Problems of Material
Science, NASU, Kyiv, Ukraine
Tel.: (044) 444-3364, 266-2357

SEMENYUK N.I.

Gas Institute, NASU, Kyiv, Ukraine
E-mail: bond@bond.elan-ua.net

SEMERENKO YU.A.

Verkin Institute for Low Temperature Physics and
Engineering, NASU, Kharkiv, Ukraine
Tel.: (0572) 30-0331
Fax: (0572) 32-2370
E-mail: natsik@ilt.kharkov.ua,
semerenko@ilt.kharkov.ua

SENKOV O.N.

Air Force Research Laboratory, Wright-Patterson,
OH, USA

SENYUT V.

Institute of Machine Reliability, NASB, Minsk,
Belarus
Tel.: (017) 284-2401
Fax: (017) 284-2401
E-mail: nanotech@inmash.bas-net.by

SERDYUK G.G.

Frantsevich Institute for Problems of Material
Science, NASU, Kyiv, Ukraine
Tel.: (044) 444-3255
E-mail: gena@ipms.kiev.ua

SERGEYEV V.V.

Scientific-Industrial Complex Closed Joint-Stock
"Yuna", Kazan, Russia
Tel.: (8432) 435-935
Fax: (8432) 435-935
E-mail: root@una.kazan.ru, irina_ch@una.kazan.ru

SERGIENKO N.V.

Bakul Institute of Superhard Materials, NASU, Kyiv,
Ukraine
Tel.: (044) 430-1126, 468-8625
Fax: (044) 468-8625
E-mail: frd@ism.kiev.ua, prikhna@iptelecom.net.ua

SERGIENKO O.A.

Gas Institute, NASU, Kyiv, Ukraine
E-mail: bond@bond.elan-ua.net

SEROV I.N.

Research Center of the Fund for Development New
Medical Technologies "AIRES", Saint-Petersburg,
Russia
Tel.: (812) 596-3533
Fax: (812) 596-3551
E-mail: foundation@aires.spb.ru

SEVASTYANOV E.S.

Powder Metallurgy Research Institute, NASB, Minsk,
Belarus
Tel.: (017) 239-9842
Fax: (017) 210-0574
E-mail: gorokhov47@mail.ru

SHALUNOV E.P.

Scientific and Technological Company TECHMA Ltd,
Cheboksary, Russia
Tel.: (8352) 45-3948
Fax: (8352) 45-0901
E-mail: techma@chuvashia.ru

SHALUNOVA N.B.

Scientific and Technological Company TECHMA Ltd,
Cheboksary, Russia
Tel.: (8352) 45-3948, 49-8327
Fax: (8352) 45-0901
E-mail: techma@chuvashia.ru

SHAPOSHNIKOVA T.I.

Frantsevich Institute for Problems of Material
Science, NASU, Kyiv, Ukraine
Tel.: (044) 444-1481, 444-3301, 444-1321

SHAPOVAL T.O.

Frantsevich Institute for Problems of Material
Science, NASU, Kyiv, Ukraine
Tel.: (044) 444-3090
Fax: (044) 452-55-23
E-mail: velikanova@materials.kiev.ua

SHAPOVALOV V.I.

Sandia National Laboratories, USA
Tel.: 505-275-1626
Fax: 505-845-3430
E-mail: Oshapoval@aol.com

SHARAI E.V.

Physico-Technological Institute of Metals and Alloys,
NASU, Kyiv, Ukraine
Tel.: (044) 444-3542
Fax: (044) 444-3542
E-mail: kompozit@inec.kiev.ua

SHATSCIKH C.K.

Frantsevich Institute for Problems of Material
Science, NASU, Kyiv, Ukraine
Tel.: (044) 444-0256

SHCHERBAK I.A.

Frantsevich Institute for Problems of Material Science, NASU, Kyiv, Ukraine
Tel.: (044) 444-1290
Fax: (044) 444-2131
E-mail: bas@materials.kiev.ua

SHCHERBAKOVA L.

Frantsevich Institute for Problems of Material Science, NASU, Kyiv, Ukraine
Tel.: (044) 444-8286
E-mail: ba-ua@yahoo.co.uk

SHCHERETSKY O.A.

Physico-Technological Institute of Metals and Alloys, NASU, Kyiv, Ukraine
Tel.: (044) 444-1065, 444-1212, 4440280
Fax: (044) 452-9736
E-mail: metal@ptima.kiev.ua, alloy@i.com.ua

SHCHUR D.

Frantsevich Institute for Problems of Material Science, NASU, Kyiv, Ukraine
Tel.: (044) 444-8286
E-mail: ba-ua@yahoo.co.uk

SHELEG V.K.

Powder Metallurgy Research Institute, NASB, Minsk, Belarus
Tel.: (517) 239-9828
Fax: (517) 210-0574
E-mail: vityaz@srpmi.minsk.by

SHELUD'KO V.E.

Frantsevich Institute for Problems of Material Science, NASU, Kyiv, Ukraine
Tel.: (044) 444-0256, 444-2371
Fax: (044) 444-2131
E-mail: post@ipms.kiev.ua

SHEMET V.

Institute for Materials and Processes in Energy Systems, Forschungszentrum Jülich, Germany
Tel.: +49-2461-615560
Fax: +49-2461-613699
E-mail: v.shemet@fz-juelich.de

SHESTAKOV S.I.

Bakul Institute of Superhard Materials, NASU, Kyiv, Ukraine
Tel.: (044) 432-9544
Fax: (044) 467-5625
E-mail: ism1@kibor.kiev.ua

SHEVCHENKO A.D.

Kurdyumov Institute for Metal Physics, NASU, Kyiv, Ukraine
Tel.: (044) 444-1005
Fax: (044) 444-2561

SHEVCHENKO A.V.

Frantsevich Institute for Problems of Material Science, NASU, Kyiv, Ukraine
Tel.: (044) 444-3573
Fax: (044) 444-2131
E-mail: dep25@materials.kiev.ua

SHEVCHENKO E.A.

Frantsevich Institute for Problems of Material Science, NASU, Kyiv, Ukraine
Tel.: (044) 444-7256
E-mail: dubok@ipms.kiev.ua

SHEVCHENKO O.M.

Frantsevich Institute for Problems of Material Science, NASU, Kyiv, Ukraine
Tel.: (044) 444-3364

SHEVCHENKO O.V.

Frantsevich Institute for Problems of Material Science, NASU, Kyiv, Ukraine
Tel.: (044) 444-3573
Fax: (044) 444-2131
E-mail: dep25@materials.kiev.ua

SHEVCHENKO V.

Zaporizhzhya National Technical University, Zaporizhzhya, Ukraine
Tel.: (0612) 64-44-55
Fax: (0612) 64-2141
E-mail: vshevch@zstu.edu.ua

SHEVCHENKO V.V.

Institute of Macromolecular Chemistry, NASU, Kyiv, Ukraine
Tel.: (044) 559-5500
Fax: (044) 552-4064
E-mail: olgs-s@mail.kar.net, nina@kea.kiev.ua

SHEVCHUK U.F.

Frantsevich Institute for Problems of Material Science, NASU, Kyiv, Ukraine
Tel.: (044) 444-1124

SHEVCHYK N.V.

Frantsevich Institute for Problems of Material Science, NASU, Kyiv, Ukraine
Tel.: (044) 444-1290
Fax: (044) 444-2131
E-mail: bas@materials.kiev.ua

SHEVTSOV A.

Powder Metallurgy Research Institute, NASB, Minsk, Belarus
Tel.: (375 17) 232-5691
Fax: (375 17) 210-0574
E-mail: alexil@srpmi.belpak.minsk.by

SHILO A.

Bakul Institute of Superhard Materials, NASU, Kyiv, Ukraine
Tel.: (044) 430-7694
Fax: (044) 430-7694
E-mail: shilo@ism.kiev.ua

SHILOV V.V.

Institute of Macromolecular Chemistry, NASU, Kyiv, Ukraine
Tel.: (044) 559-5500
Fax: (044) 552-4064
E-mail: olgs-s@mail.kar.net, nina@kea.kiev.ua

SHILOVA O.A.

Institute of Silicate Chemistry, RAS, Saint-Petersburg, Russia
Тел. (812) 328-8596
Fax: (812) 328-5401
E-mail: olgashilova@peterlink.ru

SHINKARUK A.V.

Frantsevich Institute for Problems of Material Science, NASU, Kyiv, Ukraine
Tel.: (044) 444-7256
E-mail: dubok@ipms.kiev.ua

SHIPITSA N.A.

Powder Metallurgy Research Institute, NASB, Minsk, Belarus
Tel.: (375 17) 239-9892
Fax: (375 17) 210-0574
E-mail: shipitsa_nik@mail.ru

SHIPOVSKIY V.YU.

Frantsevich Institute for Problems of Material Science, NASU, Kyiv, Ukraine
Tel.: (044) 444-0256
Fax: (044) 444-2131

SHIROKOV A.V.

Institute for Problems of Strength, NASU, Kyiv, Ukraine
E-mail: STEP@ipp.adam.kiev.ua

SHITSEVALOVA N.Y.

Frantsevich Institute for Problems of Material Science, NASU, Kyiv, Ukraine
Tel.: (044) 444-1367
Fax: (044) 444-2131
E-mail: dep60@ipms.kiev.ua

SHKILKO A.

Ukrainian Engineering Pedagogical Academy, Kharkiv, Ukraine

SHPAK A.P.

Kurdyumov Institute for Metal Physics, NASU, Kyiv, Ukraine
Tel.: (044) 444-3010
E-mail: lfp@ukr.net

SHPILEVSKAYA L.E.

Institute of General and Inorganic Chemistry, NASB, Minsk, Belarus
Tel.: (375 17) 284-1009
Fax: (375 17) 284-2703
E-mail: safonova@igic.bas-net.by

SHPORTKO A.

National Metallurgical Academy of Ukraine, Dnipropetrovsk, Ukraine
Tel.: (0562) 41-0602
Fax: (0562) 67-6977
E-mail: a_mazur@fregat.com

SHTERN M.B.

Frantsevich Institute for Problems of Material Science, NASU, Kyiv, Ukraine
Tel.: (044) 444-3039, 444-7256

SHULISHOVA O.I.

Frantsevich Institute for Problems of Material Science, NASU, Kyiv, Ukraine
Tel.: (044) 444-1290
Fax: (044) 444-2131
E-mail: bas@materials.kiev.ua

SHULZHENKO A.A.

Bakul Institute of Superhard Materials, NASU, Kyiv, Ukraine
Tel.: (044) 430-3506
Fax: (044) 266-2335
E-mail: ism1@kibor.kiev.ua

SHUMIKHIN V.S.

Physico-Technological Institute of Metals and Alloys, NASU, Kyiv, Ukraine
Tel.: (044) 444-1065, 444-1212, 444-0280
Fax: (044) 452-9736
E-mail: metal@ptima.kiev.ua, alloy@i.com.ua

SHURYGINA Z.P.

Frantsevich Institute for Problems of Material Science, NASU, Kyiv, Ukraine
Tel.: (044) 444-3061
Fax: (044) 444-3061

SHVARTSMAN O.Y.

Frantsevich Institute for Problems of Material Science, NASU, Kyiv, Ukraine
Tel.: (044) 444-2171
E-mail: phil02@ukr.net

SIDOR O.M.

Chernivtsi Department, Frantsevich Institute for Problems of Material Science, NASU, Chernivtsi, Ukraine
Tel.: (03722) 25-155
Fax: (03722) 20-050
E-mail: chimsp@unicom.cv.ua

SIDORENKO S.I.

National Technical University of Ukraine "Kyiv Polytechnic Institute", Kyiv, Ukraine
Tel.: (044) 441-1645, 441-1331
E-mail: vasil@imp.kiev.ua

SIDORKO V.R.

Frantsevich Institute for Problems of Material Science, NASU, Kyiv, Ukraine
Tel.: (044) 444-1290, 444-3090
Fax: (044) 444-2131
E-mail: dep6@materials.kiev.ua

SIGNORELLI E.

Istituto per la Tecnologia dei Materiali e dei Processi Energetici, Milano, Italy
Fax: 39 2 66173321
E-mail: onofrio@tempe.mi.cnr.it, signorel@tempe.mi.cnr.it

SILANTIEV V.I.

Institute of Magnetism, NASU, Kyiv, Ukraine
Tel.: (044) 444-1020, 444-9568
E-mail: fmf@ntu-kpi.kiev.ua

SILCHENKO YA.

Bakul Institute of Superhard Materials, NASU, Kyiv, Ukraine
Tel.: (044) 430-7694
Fax: (044) 430-7694
E-mail: shilo@ism.kiev.ua

SIMAN M.I.

Frantsevich Institute for Problems of Material Science, NASU, Kyiv, Ukraine
Tel.: (044) 444-2171
E-mail: phil02@ukr.net

SIMEONOVA Y.

Space Research Institute, Bulgaria Academy of Sciences, Sofia, Bulgaria

SINELNICHENKO A.K.

Frantsevich Institute for Problems of Material Science, NASU, Kyiv, Ukraine
Tel.: (044) 444-33-64

SINGHEISER L.

Institute for Materials and Processes in Energy Systems, Forschungszentrum Jülich, Germany
Tel.: +49-2461-615560
Fax: +49-2461-613699
E-mail: v.shemet@fz-juelich.de

SIRKO A.I.

Frantsevich Institute for Problems of Material Science, NASU, Kyiv, Ukraine
Tel.: (044) 444-2380, 444-3061
Fax: (044) 444-3061
E-mail: neiko@svitonline.com

SITALO V.G.

Yuzhnoye State Design Office, Dnipropetrovsk, Ukraine
Tel.: (0562) 92-5113
Fax: (0562) 92-5113
E-mail: kbu@public.ua.net

SKILKO A.M.

Ukrainian Engineering Pedagogical Academy, Kharkiv, Ukraine
Tel.: (0572) 20-6454
Fax: (0572) 712-7236
E-mail: fed@postmaster.co.uk

SKOROKHOD V.V.

Frantsevich Institute for Problems of Material Science, NASU, Kyiv, Ukraine
Tel.: (044) 444-2264, 444-1201
Fax: (044) 444-2131
E-mail: dir@materials.kiev.ua

SKRYPAI A.A.

Frantsevich Institute for Problems of Material Science, NASU, Kyiv, Ukraine
Tel.: (044) 444-1290
Fax: (044) 444-2131
E-mail: bas@materials.kiev.ua

SLAVOLJUBOV V.S.

Open Joint-Stock DIESELPROM, Cheboksary, Russia
Tel.: (8352) 55-5072
Fax: (8352) 55-5072

SLESAREV V.N.

Vereschagin Institute for High Pressure Physics, RAS, Troitsk, Russia
Tel.: (095) 334-0732
Fax: (095) 334-0012
E-mail: ekimov@hppi.troitsk.ru

SLIPENYUK A.M.

Frantsevich Institute for Problems of Material Science, NASU, Kyiv, Ukraine
Tel.: (044) 444-1540
Fax: (044) 444-2131
E-mail: dep4@materials.kiev.ua

SLIPENYUK A.N.

Frantsevich Institute for Problems of Material Science, NASU, Kyiv, Ukraine
Tel.: (044) 444-3061, 444-0294
Факс(044) 444-3061, 452-55-23
E-mail: san@materials.kiev.ua, nick@ipms.kiev.ua

SLOBODYANIK N.S.

Taras Shevchenko Kyiv National University, Kyiv, Ukraine
E-mail: vsudavtsova@univ.kiev.ua

SLYS I.G.

Frantsevich Institute for Problems of Material Science, NASU, Kyiv, Ukraine
Tel.: (044) 444-1124
E-mail: slys@materials.kiev.ua

SLYUNYAYEV V.N.

Institute for Problems of Strength, NASU, Kyiv, Ukraine
Tel.: (044) 295-4464
Fax: (044) 296-1684
E-mail: ggogotsi@ipp.adam.kiev.ua

SMETKIN A.A.

Research Center of Powder Materials Science, Perm, Russia
Tel.: (3422) 391-110
Fax: (3422) 391-122
E-mail: solid@pm.pstu.ac.ru

SMIRNOV S.N.

Verkin Institute for Low Temperature Physics and Engineering, NASU, Kharkiv, Ukraine
Tel.: (0572) 30-0331, 30-8513
Fax: (0572) 32-2370
E-mail: smirnov@ilt.kharkov.ua

SMYSHLYAEVA T.V.

Institute of Technical Chemistry, UrB of RAS, Perm, Russia
Tel.: (3422) 391-110
Fax: (3422) 391-122
E-mail: patent@pm.pstu.ac.ru

SOFRONOV A.A.

Ural State Technical University, Ekaterinburg, Russia
Tel.: (3432) 55-8340
E-mail: vika@nexcom.ru

SOKOLOV A.N.

Bakul Institute of Superhard Materials, NASU, Kyiv, Ukraine
Tel.: (044) 430-3506
Fax: (044) 266-2335
E-mail: ism1@kibor.kiev.ua

SOLNTSEV V.P.

Frantsevich Institute for Problems of Material Science, NASU, Kyiv, Ukraine
Tel.: (044) 444-2264, 444-1201
Fax: (044) 444-2131
E-mail: solntsev_kutuz@mail.ru

SOLNTSEVA T.A.

Frantsevich Institute for Problems of Material Science, NASU, Kyiv, Ukraine
Tel.: (044) 444-2264, 444-1201
Fax: (044) 444-2131
E-mail: solntsev_kutuz@mail.ru

SOLOVIN YU.M.

Frantsevich Institute for Problems of Material Science, NASU, Kyiv, Ukraine
Tel.: (044) 444-33-15
E-mail: solonin@materials.kiev.ua

SOROKIN U.V.

Frantsevich Institute for Problems of Material Science, NASU, Kyiv, Ukraine
Tel.: (044) 444-2034, 444-1534
E-mail: celt@materials.kiev.ua

SOSNIN O.V.

Siberian State University of Industry, Novokuznetsk, Russia
Tel.: (3843) 46-2277, 46-4000
Fax: (3843) 46-5792
E-mail: gromov@physics.sibsiu.ru

SOZAEV V.A.

Kabardino-Balkarian State University, Nalchik, Russia
Tel.: (86622) 50-345, (095) 337-9955
E-mail: bsk@kbsu.ru, sozaevv@ns.kbsu.ru, exp@kbsu.ru

SPIRIDONOV YU.L.

Scientific-Industrial Complex Closed Joint-Stock "Yuna", Kazan, Russia
Tel.: (8432) 435-935
Fax: (8432) 435-935
E-mail: root@una.kazan.ru, irina_ch@una.kazan.ru

SPIRIDONOVA I.

Dnipropetrovsk National University, Dnipropetrovsk, Ukraine
Tel.: (0562) 469-212, 776-9042
Fax: (0562) 461-697
E-mail: odm@ff.dsu.dp.ua

SRIBNY V.M.

State Enterprise "Argentum", Lviv, Ukraine
Tel.: 70-2596
E-mail: argentum@litech.lviv.ua

STAMATIN I.

Advanced Research Institute for Electrical Engineering, Bucharest, Romania
Tel.: +40 1-346-7283
Fax: +40 1-346-7283
E-mail: electmat@icpe.ro

STATIC-TROSIC J.

Institute of Chemistry, Technology and Metallurgy, Belgrade, Yugoslavia

STATSENKO V.M.

Frantsevich Institute for Problems of Material Science, NASU, Kyiv, Ukraine
Tel.: (044) 444-8218
E-mail: andreeva@ipms.kiev.ua

STEBLENKO L.P.

Taras Shevchenko Kyiv National University, Kyiv, Ukraine
Tel.: (044) 266-2326, 266-4587
Fax: (044) 266-2326
E-mail: krav@mail.phys.univ.kiev.ua

STEINHAUSER S.

Technical University, Chemnitz, Germany

STEPANENKO A.V.

Frantsevich Institute for Problems of Material Science, NASU, Kyiv, Ukraine
Tel.: (044) 444-0090, 444-1321
Fax: (044) 444-2131, 444-3502
E-mail: oleggrig@materials.kiev.ua, step@materials.kiev.ua

STEPANENKO N.V.

Belorussian State University of Informatics and Radioelectronics, Minsk, Belarus
Tel.: (375 017) 260-8007, 202-1132
Fax: (375 017) 234-7959
E-mail: irma@infonet.by, Solarsys@gw.bsuir.unibel.by

STEPANENKO V.N.

Research Institute of Radiomaterials, Minsk, Belarus
Tel.: (375 017) 278-3710
Fax: (375 017) 278-3705
E-mail: irma@infonet.by

STEPANOV G.V.

Institute for Problems of Strength, NASU, Kyiv, Ukraine
E-mail: STEP@ipp.adam.kiev.ua

STETSENKO N.

Kurdyumov Institute for Metal Physics, NASU, Kyiv, Ukraine
Tel.: (044) 444-9520
E-mail: kotr@imp.kiev.ua

STETSYUK T.V.

Frantsevich Institute for Problems of Material Science, NASU, Kyiv, Ukraine
Tel.: (044) 444-3017, 444-6201
Fax: (044) 444-3017
E-mail: naidich@ipms.kiev.ua

STOVPCHENKO A.P.

National Metallurgical Academy of Ukraine, Dnipropetrovsk, Ukraine
Tel.: (0562) 41-0347
Fax: (0562) 47-4461
E-mail: dmeti@dmeti.dp.ua

STRATIVNOV V.

Gas Institute, NASU, Kyiv, Ukraine
E-mail: bond@bond.elan-ua.net

STREKALOVSKY V.N.

Institute of Hightemperature Electrochemistry, UrB of RAS, Ekaterinburg, Russia
Tel.: (3432) 49-3504
Fax: (3432) 74-5992
E-mail: Vstrek@ihte.uran.ru

STUKALO V.A.

Taras Shevchenko Kyiv National University, Kyiv, Ukraine
E-mail: vsudavtsova@univ.kiev.ua

STUS N.V.

Taras Shevchenko Kyiv National University, Kyiv, Ukraine
E-mail: vsudavtsova@univ.kiev.ua

SUDAVTSOVA V.S.

Taras Shevchenko Kyiv National University, Kyiv, Ukraine
E-mail: vsudavtsova@univ.kiev.ua

SUDNIK L.V.

Powder Metallurgy Research Institute, NASB, Minsk, Belarus
Tel.: (017) 239-9801
Fax: (017) 210-0574
E-mail: vityaz@srpmi.minsk.by

SUKHONOSOV A.F.

Open Joint-Stock "AMULET", Kyiv, Ukraine
Tel.: (044) 265-2610, 267-6370
Fax: (044) 265-2611
E-mail: amulet@akcecc.kiev.ua

SUKHOSTAVETS S.V.

Frantsevich Institute for Problems of Material Science, NASU, Kyiv, Ukraine
Tel.: (044) 444-1571, 444-1124

SUKHOVA O.

Dnipropetrovsk National University, Dnipropetrovsk, Ukraine
Tel.: (0562) 469-212
E-mail: odm@ff.dsu.dp.ua

SUNG J. S.

Korea Institute of Energy Research, 71-2 Jang-dong, Yoosong, Daejeon, Korea

SURSAEVA V.G.

Institute of Solid State Physics, RAS, Chernogolovka, Russia
Tel.: (095) 993-2755
Fax: (096) 524-9701
E-mail: sursaeva@issp.ac.ru

SURZHENKO A.B.

Institut für Physikalische Hochtechnologie, Jena, Germany
Tel.: (49 36 41) 206103, 206107, 206106
Fax: (49 36 41) 206199
E-mail: Wolfgang.Gawalek@ipht-jena.de, Oleksiy.Surzhenko@ipht-jena.de, Doris.Litzkendorf@ipht-jena.de

SUSIDKO V.L.

"Ukrzaliznytsia", Kyiv, Ukraine
Tel.: (044) 223-0515
Fax: (044) 2230517
E-mail: cshtekh@lotus.uz.gov.ua

SVERDUN V.B.

Bakul Institute of Superhard Materials, NASU, Kyiv, Ukraine
Tel.: (044) 430-1126
Fax: (044) 468-8625
E-mail: prikhna@iptelecom.net.ua

SVISTUN L.I.

Kuban State Technological University, Krasnodar, Russia

SVYATENKO O.M.

Gas Institute, NASU, Kyiv, Ukraine
E-mail: bond@bond.elan-ua.net

SYDORENKO D.G.

Scientific Production Company "Donix", Donetsk, Ukraine
Tel.: (062) 335-1151
Fax: (0622) 93-3262
E-mail: rato@fizmet.dgtu.donetsk.ua

T

TABACHNIKOVA E.D.

Verkin Institute for Low Temperature Physics and Engineering, NASU, Kharkiv, Ukraine
Tel.: (057) 230-0331
Fax: (057) 233-5593
E-mail: TABACHNIKOVA@ilt.kharkov.ua

TALAKO T.L.

Powder Metallurgy Research Institute, NASB, Minsk, Belarus
Tel.: (375 17) 232-8271, 232-6340, 239-9827
Fax: (375 17) 232-5691, 210-0574
E-mail: talako@tut.by

TALANIN I.E.

Zaporizhzhya State Engineering Academy, Zaporizhzhya, Ukraine
Tel.: (0612) 60-1498, 60-1240
Fax: (0612) 60-1498
E-mail: rio@zgia.zp.ua

TALANIN V.I.

Zaporizhzhya State Engineering Academy, Zaporizhzhya, Ukraine
Tel.: (0612) 60-1498, 60-1240
Fax: (0612) 60-1498
E-mail: rio@zgia.zp.ua

TALIJEAN N.M.

Institute of Chemistry, Technology and Metallurgy, Belgrade, Yugoslavia

TARASOV P.P.

Amosov Yakutiya State University, Yakutsk, Russia
Tel.: (4112) 25-3212
Fax: (4112) 26-0934
E-mail: romgeorg@sitc.ru, fz_ema@sitc.ru

TARASYUK E.V.

Institute of Silicate Chemistry, RAS, Saint-Petersburg, Russia
Tel.: (812) 328-85-96
Fax: (812) 328-5401
E-mail: olgashilova@peterlink.ru, ISCLANC@yandex.ru

ȚÂRDEI C.

Advanced Research Institute for Electrical Engineering, Bucharest, Romania
Tel.: 0040-1-346-82-97
Fax: 0040-1-346-82-99
E-mail: magnet@icpe.ro, gavriliu@rol.ro

TAVADZE G.

State Scientific-Technical Center "Delta", Tbilisi, Georgia
Tel.: (99532) 969-248, 923-779, 955-646
Fax: (99532) 956-080
E-mail: argusdel@hotmail.com

TEL'NIKOV E.YA.

Frantsevich Institute for Problems of Material Science, NASU, Kyiv, Ukraine
Tel.: (044) 444-0256, 444-2371
Fax: (044) 444-2131
E-mail: post@ipms.kiev.ua

TELEMKO A.V.

UkrNDINP "MASMA", Kyiv, Ukraine
Tel.: (044) 444-9291
E-mail: ukrndimasma@svitonline.com, olmi@freemail.com.ua

TEPLENKO M.A.

Frantsevich Institute for Problems of Material Science, NASU, Kyiv, Ukraine
Tel.: (044) 444-2201, 444-3522
E-mail: lavrenko@ipms.kiev.ua

TERESHKO N.V.

Institute of Applied Physical Problems of Belarus State University, Minsk, Belarus
Tel.: (017) 277-4939
Fax: (017) 278-0417
E-mail: TREBNIKOV@BSU.BY

TICHONOV A.

Perm State Technical University, Perm, Russia
Tel.: (3422) 64-8826

TIKHONOVSKY M.

National Scientific Centre "Kharkiv Institute of Physics & Technology", NASU, Kharkiv, Ukraine

TIMOFEEVA I.I.

Frantsevich Institute for Problems of Material Science, NASU, Kyiv, Ukraine
Tel.: (044) 444-2371, 444-3415, 444-3061
Fax: (044) 444-3061
E-mail: abykov@materials.kiev.ua, gridneva@materials.kiev.ua

TJALIN YU. I.

Derzhavin Tambov State University, Tambov, Russia
 Tel.: (0572) 35-2614
 Fax: (0752) 710-307
 E-mail: plushnik@mail.ru

TKACHENKO L.N.

Frantsevich Institute for Problems of Material
 Science, NASU, Kyiv, Ukraine
 Tel.: (044) 3039, 444-7256

TKACHENKO V.D.

Frantsevich Institute for Problems of Material
 Science, NASU, Kyiv, Ukraine
 Tel.: (044) 444-2001
 Fax: (044) 444-2131
 E-mail: pavlikov@materials.kiev.ua,
 garmasg@materials.kiev.ua

TKACHENKO V.G.

Frantsevich Institute for Problems of Material
 Science, NASU, Kyiv, Ukraine
 Tel.: (044) 444-11-90
 E-mail: icems@materials.kiev.ua

TKACHENKO V.M.

Donetsk Physical-Technical Institute, NASU,
 Donetsk, Ukraine
 E-mail: pashinska@mail.ru

TKACHENKO YU.G.

Frantsevich Institute for Problems of Material
 Science, NASU, Kyiv, Ukraine
 Tel.: (044) 444-2101
 Fax: (044) 444-2131
 E-mail: kovalms@ipms.kiev.ua

TKACHUK A.A.

Kurdyumov Institute for Metal Physics, NASU, Kyiv,
 Ukraine
 Tel.: (044) 444-2520
 E-mail: vasil@imp.kiev.ua

TOKHTUEV V.G.

Frantsevich Institute for Problems of Material
 Science, NASU, Kyiv, Ukraine
 Tel.: (044) 444-2380, 444-3061
 Fax: (044) 444-3061
 E-mail: neiko@svitonline.com

TOLMACHEV A.V.

Institute for Single Crystals, NASU, Kharkiv, Ukraine
 Tel.: (0572) 30-7977, 30-7989
 Fax: (0572) 32-0273
 E-mail: avtol@isc.kharkov.com

TOLOCHKO N.K.

Institute of Technical Acoustics, NASB, Vitebsk,
 Belarus
 Tel.: (375 212) 246-389
 Fax: (275 212) 243953
 E-mail: lkm_ita@vitebsk.by

TOMASHIK V.M.

Institute for Semiconductor Physics, National
 Academy of Sciences of Ukraine, Kyiv, Ukraine
 Tel.: 265-5755
 Fax: 265-8342
 E-mail: tomashyk@isp.kiev.ua

TOMASHIK Z.F.

Institute for Semiconductor Physics, National
 Academy of Sciences of Ukraine, Kyiv, Ukraine
 Tel.: 265-5755
 Fax: 265-8342
 E-mail: tomashyk@isp.kiev.ua

TOMILA T.V.

Frantsevich Institute for Problems of Material
 Science, NASU, Kyiv, Ukraine
 Tel.: (044) 444-1501
 E-mail: tomila@materials.kiev.ua

TOVAROVSKIY I.G.

Nekrasov Iron and Steel Institute, NASU,
 Dnipropetrovsk, Ukraine
 Tel.: (0562) 47-4548
 Fax: (056) 776-5324
 E-mail: iosif@tig.dp.ua

TRAPALIS CH.

Institute of Materials Science, Athens, Greece
 Tel.: 3-01-65-03-336

TREBNIKOV A.G.

Institute of Applied Physical Problems of Belarus
 State University, Minsk, Belarus
 Tel.: (017) 277-4939
 Fax: (017) 278-0417
 E-mail: TREBNIKOV@BSU.BY

TRETYACHENKO L.A.

Frantsevich Institute for Problems of Material
 Science, NASU, Kyiv, Ukraine
 Tel.: (044) 444-3090
 Fax: (044) 444-02131
 E-mail: dep22@materials.kiev.ua,
 dep6@materials.kiev.ua

TROFIKOVA L.M.

Kurdyumov Institute for Metal Physics, NASU, Kyiv,
 Ukraine
 Tel.: (044) 444-9565

TROSCHENKO V.T.

Institute for Problems of Strength, NASU, Kyiv,
 Ukraine
 Tel.: (044) 295-1687
 Fax: (044) 296-1684
 E-mail: vtt@ipp.adam.kiev.ua, trt@ipp.adam.kiev.ua

TROYANSKY A.A.

Donetsk National Technical University, Donetsk,
 Ukraine
 Tel.: (0622) 93-3262
 Fax: (0622) 93-3262
 E-mail: rato@fizmet.dgtu.donetsk.ua

TSELLERMAER V.V.

Siberian State University of Industry, Novokuznetsk,
Russia
Tel.: (3843) 46-2277, 46-4000
Fax: (3843) 46-5792
E-mail: gromov@physics.sibsiu.ru

TSELLERMAER V.YA.

Siberian State University of Industry, Novokuznetsk,
Russia
Tel.: (3843) 46-2277, 46-4000, 78-4367
Fax: (3843) 46-5792
E-mail: gromov@physics.sibsiu.ru

TSUKRUK V.V.

Iowa State University, Ames, Iowa, USA
Tel.: 515-294-6904, 864-656-5958
Fax: (515) 294-5444, 864-656-5973
E-mail: vladimir@iastate.edu, luzinov@clemson.edu

TSURPAL L.A.

Frantsevich Institute for Problems of Material
Science, NASU, Kyiv, Ukraine
Tel.: (044) 444-2024
E-mail: vkur@ipms.kiev.ua

TSYGANENKO N.I.

Frantsevich Institute for Problems of Material
Science, NASU, Kyiv, Ukraine
Tel.: (044) 444-3090
Fax: (044) 452-55-23
E-mail: velikanova@materials.kiev.ua

TSYPANDIN P.P.

Amosov Yakutiya State University, Yakutsk, Russia
Tel.: (4112) 25-3212
Fax: (4112) 26-0934
E-mail: romgeorg@sitc.ru, fz_ema@sitc.ru

TSYRKYN A.T.

Vladimir Dahl East Ukrainian National University,
Lugansk, Ukraine
Tel.: (0642) 46-2233
E-mail: material@snu.edu.ua

TURKEVICH V.Z.

Bakul Institute of Superhard Materials, NASU, Kyiv,
Ukraine
Tel.: (044) 468-8632
Fax: (044) 468-8625
E-mail: vturk@ism.kiev.ua

TYCHOMYROV S.V.

Frantsevich Institute for Problems of Material
Science, NASU, Kyiv, Ukraine
Tel.: (044) 444-2034, 444-1534
E-mail: celt@materials.kiev.ua

TYURIN Y.N.

Paton Electric Welding Institute, NASU, Kyiv,
Ukraine
E-mail: ytyurin@i.com.ua

U

ULRIKH T.A.

Perm State Technical University, Perm, Russia
Tel.: (3422) 39-1340
E-mail: dpm@cpl.pstu.ac.ru

ULSHIN S.V.

Kurdyumov Institute for Metal Physics, NASU, Kyiv,
Ukraine
Tel.: (044) 444-0120
Fax: (044) 444-0120
E-mail: ulshin@imp.kiev.ua

ULSHIN V.I.

Frantsevich Institute for Problems of Material
Science, NASU, Kyiv, Ukraine
Tel.: (044) 444-2034, 444-1534
E-mail: celt@materials.kiev.ua

ULYANOVA T.M.

Institute of General and Inorganic Chemistry, NASB,
Minsk, Belarus
E-mail: ulya@igic.bas-net.by, IONCH@igic.bas-
net.by

USAKOV E.I.

Frantsevich Institute for Problems of Material
Science, NASU, Kyiv, Ukraine
Tel.: (044) 444-3301
Fax: (044) 444-2131
E-mail: fsa@materials.kiev.ua

USENKO N.

Frantsevich Institute for Problems of Material
Science, NASU, Kyiv, Ukraine
Tel.: (044) 444-3090
Fax: (044) 444-2131
E-mail: dep6@materials.kiev.ua

USHAKOV I.V.

Derzhavin Tambov State University, Tambov, Russia
Tel.: (0572) 35-2614
Fax: (0752) 710-307
E-mail: ushakov@tsu.tmb.ru, feodorov@tsu.tmb.ru

USHERENKO S.M.

Research Institute of Impulse Processes, Minsk,
Belarus
Tel.: (375 17) 239-3244
Fax: (375 17) 232-8411
E-mail: impulsca@bn.by

USHKALOV L.N.

Frantsevich Institute for Problems of Material
Science, NASU, Kyiv, Ukraine
Tel.: (044) 444-0256
Fax: (044) 444-2131

USKOVA N.N.

Vernadskii Institute of General and Inorganic Chemistry, NASU, Kyiv, Ukraine
 Tel.: (044) 444-0111
 Fax: (044) 444-3070
 E-mail: GAB@ionc.kar.net, shakhnin@p5com.com, Synthesis@ionc.kar.net

USTINOV A.I.

Kurdyumov Institute for Metal Physics, NASU, Kyiv, Ukraine
 Tel.: (044) 444-9532, 269-3917
 E-mail: ustinov@imp.kiev.ua, cuba@imp.kiev.ua

USTINOVA G.P.

Powder Metallurgy Research Institute, NASB, Minsk, Belarus
 Tel.: (017) 239-9842
 Fax: (017) 210-0574
 E-mail: gorokhov47@mail.ru

V**V'YUNOV O.**

Vernadskii Institute of General and Inorganic Chemistry, NASU, Kyiv, Ukraine
 Tel.: (044) 444-2211
 Fax: (044) 444-2211
 E-mail: vyunov@ionc.kar.net

VAKULENKO I.A.

Nekrasov Iron and Steel Institute, NASU, Dnipropetrovsk, Ukraine
 Tel.: (056) 46-2369
 Fax: (056 2) 776-5924
 E-mail: isi-nasu@a-teleport.com

VARSHAVSKAYA I.G.

Institute of Physical Chemistry, RAS, Moscow, Russia
 Tel.: (095) 955-4673, 955-4470
 Fax: (095) 952-5308
 E-mail: iravarsh@yahoo.com, buhovet@mail.ru

VARYUKHIN V.N.

Donetsk Physical-Technical Institute, NASU, Donetsk, Ukraine
 E-mail: pashinska@mail.ru

VASILEVICH V.P.

Belorussian State University of Informatics and Radioelectronics, Minsk, Belarus
 Tel.: (375 017) 260-8007, 202-1132
 Fax: (375 017) 234-7959
 E-mail: Solarsys@gw.bsuir.unibel.by

VASYLYEV O.

Frantsevich Institute for Problems of Material Science, NASU, Kyiv, Ukraine
 Tel.: (044) 444-3345, 444-3360
 Fax: (044) 452-5523
 E-mail: dep22@materials.ua

VASYLYEV M.A.

Kurdyumov Institute for Metal Physics, NASU, Kyiv, Ukraine
 Tel.: (044) 444-2520
 E-mail: vasil@imp.kiev.ua

VED V.

National Technical University "Kharkiv Polytechnic Institute", Kharkiv, Ukraine
 Tel.: (0572) 40-0894
 Fax: (0572) 40-0632
 E-mail: ulm@kpi.kharkov.ua

VELIKANOVA T.YA.

Frantsevich Institute for Problems of Material Science, NASU, Kyiv, Ukraine
 Tel.: (044) 444-3090
 Fax: (044) 452-55-23
 E-mail: velikanova@materials.kiev.ua

VERBYLO D.G.

Frantsevich Institute for Problems of Material Science, NASU, Kyiv, Ukraine
 E-mail: rapid@materials.kiev.ua

VERCHOTUROV A.D.

Institute of Material Science, KSC FEB RAS, Khabarovsk, Russia
 Tel.: (4212) 71-9956
 Fax: (4212) 71-9598
 E-mail: imdvo@fe.ru, infarest@pop.redcom.ru

VILKOVA N.YU.

National Technical University of Ukraine "Kyiv Polytechnic Institute", Kyiv, Ukraine
 Tel.: (044) 441-1645, 441-1331
 E-mail: vasil@imp.kiev.ua

VINNITCHENKO V.D.

Frantsevich Institute for Problems of Material Science, NASU, Kyiv, Ukraine
 Tel.: (044) 444-2541
 Fax: (044) 444-2078
 E-mail: imsa@skif.kiev.ua

VINOGRADOV L.M.

Lykov Heat and Mass Transfer Institute, NASB, Minsk, Belarus
 Tel.: (375 017) 284-1057, 284-2775, 284-1057, 284-2480
 Fax: (375 017) 232-2513
 E-mail: orebi@hmti.ac.by, and@hmti.ac.by, bor@itmo.by

VINOVIY V.

"New Technologies & Materials Institute" Ltd,
Dnipropetrovsk, Ukraine
Tel.: (0562) 47-0313
Fax: (0562) 47-0313
E-mail: postmaster@kondrat.dp.ua

VITYAZ P.A.

Powder Metallurgy Research Institute, NASB, Minsk,
Belarus
Tel.: (375 17) 232-2526
Fax: (375 17) 210-00574
E-mail: vityaz@srpmi.minsk.by

VLASOVA M.

Autonomous University of State of Morelos,
Cuernavaca, Mexico

VLASOVA N.M.

Institute of Material Science, KSC FEB RAS,
Khabarovsk, Russia
Tel.: (4212) 71-9956
Fax: (4212) 71-9598
E-mail: imdvo@fe.ru, infarest@pop.redcom.ru

VOLKOGON V.M.

Frantsevich Institute for Problems of Material
Science, NASU, Kyiv, Ukraine
Tel.: (044) 444-2255, 444-3401
Fax: (044) 444-2131
E-mail: dep20@ipms.kiev.ua, raitch@ipms.kiev.ua

VOLOSHKO S.M.

National Technical University of Ukraine "Kyiv
Polytechnic Institute", Kyiv, Ukraine
Tel.: (044) 441-1645, 441-1331
E-mail: vasil@imp.kiev.ua

VOLTCHER N.L.

Institute for Problems of Strength, NASU, Kyiv,
Ukraine
Tel.: (044) 296-5457
Fax: (044) 296-1684
E-mail: leb@ipp.adam.kiev.ua

VOROPAEV V.S.

Frantsevich Institute for Problems of Material
Science, NASU, Kyiv, Ukraine
Tel.: (044) 444-2380, 444-3061
Fax: (044) 444-3061
E-mail: neiko@svitonline.com

VOSKOBOINIK I.V.

Frantsevich Institute for Problems of Material
Science, NASU, Kyiv, Ukraine
Tel.: (044) 444-3228
Fax: (044) 444-3061
E-mail: karp@materials.kiev.ua,
korzhova@materials.ua

VOVKOTRUB N.E.

Taras Shevchenko Kyiv National University, Kyiv,
Ukraine
E-mail: vsudavtsova@univ.kiev.ua

VOYNASH V.Z.

Kurdyumov Institute for Metal Physics, NASU, Kyiv,
Ukraine
Tel.: (044) 444-3180
E-mail: barabash@imp.kiev.ua

VRZHYZHEVSKY E.L.

Paton Electric Welding Institute, NASU, Kyiv,
Ukraine
Tel.: (044) 227-1366, 261-5098
Fax: (044) 227-1366

W

WENDLAND ST.

RÖTECH G.m.b.H., Mülheim-an-der-Ruhr,
Germany
Tel.: +49-208-4442167
Fax: +49-208-478117
E-mail: Dienstleistungs.Wendland@t-online.de

WENDT M.

Institut für Physikalische Hochtechnologie, Jena,
Germany
Tel.: (49 36 41) 206103, 206107, 206106
Fax: (49 36 41) 206199
E-mail: Doris.Litzkendorf@ipht-jena.de,
Oleksiy.Surzhenko@ipht-jena.de,
Wolfgang.Gawalek@ipht-jena.de

WERHEIT H.

Gerhard Mercator University, Duisburg, Germany
E-mail: h.werheit@uni-duisburg.de,
helmut.werheit@koeln.de

WILDEMANN V.E.

Perm State Technical University, Perm, Russia
Tel.: (3422) 39-1294
Fax: (3422) 19-8035
E-mail: wildemann@pstu.ac.ru

WOJCIECHOWSKI K.W.

Institute of Molecular Physics, Polish Academy of
Sciences, Poznań, Poland
E-mail: kww@man.poznan.pl

Y

YAGODKIN V.V.

Frantsevich Institute for Problems of Material
Science, NASU, Kyiv, Ukraine
Tel.: (044) 444-3364
E-mail: dep40@materials.kiev.ua

YAKOVLEV E.N.

Vereschagin Institute for High Pressure Physics,
RAS, Troitsk, Russia
Tel.: (095) 334-0810, 334-0738, 334-0808
Fax: (095) 334-0012
E-mail: yakovlev@ns.hppi.troitsk.ru

YANCHUK I.

Institute of Semiconductor Physics, NASU, Kyiv,
Ukraine

YASKIV O.

Karpenko Physico-Mechanical Institute, NASU, Lviv,
Ukraine
Tel.: (0322) 65-4343
E-mail: fedirko@ipm.lviv.ua,
minnezing@ah.ipm.lviv.ua

YEFIMOV M.O.

Frantsevich Institute for Problems of Material
Science, NASU, Kyiv, Ukraine
Tel.: (044) 444-3061
Fax: (044) 444-3061
E-mail: yefimov@materials.kiev.ua

YENEVICH V.G.

Frantsevich Institute for Problems of Material
Science, NASU, Kyiv, Ukraine
Tel.: (044) 444-1181
E-mail: 29min@ipms.ua

YURCHENKO L.P.

Frantsevich Institute for Problems of Material
Science, NASU, Kyiv, Ukraine
Tel.: (044) 444-1540
Fax: (044) 444-2131
E-mail: dep4@materials.kiev.ua

YURCHUK M.O.

Bakul Institute of Superhard Materials, NASU, Kyiv,
Ukraine
Tel.: (044) 430-3505

YURIEV A.B.

Siberian State University of Industry, Novokuznetsk,
Russia
Tel.: (3843) 46-2277, 46-4000
Fax: (3843) 46-5792
E-mail: zsmk@zsmk.ru, gromov@physics.sibsiu.ru

YURKOVA O.I.

National Technical University of Ukraine "Kyiv
Polytechnic Institute", Kyiv, Ukraine
Tel.: (044) 441-1076
E-mail: byakova@vic.com.ua

YURYEVA E.I.

Institute of Solid State Chemistry, UrB of RAS,
Ekaterinburg, Russia
Tel.: (3432) 74-5331, 74-5691
Fax: (3432) 74-4495
E-mail: pletnev@ihim.uran.ru, Yuryeva@ihim.uran.ru

Z**ZABOLOTIN S.P.**

Paton Electric Welding Institute, NASU, Kyiv,
Ukraine
Tel.: (044) 227-7246

ZAGINAICHENKO S.YU.

Frantsevich Institute for Problems of Material
Science, NASU, Kyiv, Ukraine
Tel.: (044) 444-0381
Fax: (044) 444-0381
E-mail: shurzag@ipms.kiev.ua

ZAGORUIKO L.

Ukrainian Engineering Pedagogical Academy,
Kharkiv, Ukraine

ZAKARJAN D.A.

Frantsevich Institute for Problems of Material
Science, NASU, Kyiv, Ukraine
Tel.: (044) 444-0102
Fax: (044) 2131
E-mail: vvk@materials.kiev.ua

ZAKHAROVA N.P.

Frantsevich Institute for Problems of Material
Science, NASU, Kyiv, Ukraine
Tel.: (044) 444-2380, 444-3061
Fax: (044) 444-3061, 452-5523
E-mail: sery@materials.kiev.ua,
neiko@svitonline.com

ZALUTSKIY V.P.

Kurdyumov Institute for Metal Physics, NASU, Kyiv,
Ukraine
Tel.: (044) 44-9546, 444-9531, 444-9532
Fax: (044) 444-2561
E-mail: perekos@imp.kiev.ua, potvora@imp.kiev.ua

ZAMALIN E.YU.

Moscow State Academy of the Instrument
Engineering and Information, Moscow, Russia
Tel.: (095) 269-4622
Fax: (095) 162-0470
E-mail: vep@octava.msk.su

ZAMKOV V.N.

Paton Electric Welding Institute, NASU, Kyiv,
Ukraine
Tel.: (044) 227-1366, 227-4783, 261-5098
Fax: (044) 227-1366, 268-0486
E-mail: zamkov@paton.kiev.ua,
office@paton.kiev.ua

ZANKEVICH A.B.

Bakul Institute of Superhard Materials, NASU, Kyiv,
Ukraine
Tel.: (044) 468-8623, 430-3505
E-mail: alcon@ismanu.kiev.ua, almaz@ism.kiev.ua,
krasikova_natally@mail.ru

ZASIMCHUK E.E.

Kurdyumov Institute for Metal Physics, NASU, Kyiv, Ukraine
Tel.: (044) 444-9514
E-mail: eezas@imp.kiev.ua

ZASLAVSKAYA L.V.

Donetsk National University, Donetsk, Ukraine
Tel.: 91-9238
E-mail: getman@dongu.donetsk.ua, dshe@skif.net

ZASLONKIN A.V.

Chernivtsi Department, Frantsevich Institute for Problems of Material Science, NASU, Chernivtsi, Ukraine
Tel.: (03722) 25-155
Fax: (03722) 20-050
E-mail: chimsp@unicom.cv.ua

ZATOVSKIY V.G.

Frantsevich Institute for Problems of Material Science, NASU, Kyiv, Ukraine
Tel.: (044) 444-1181
Fax: (044) 444-2131
E-mail: 29min@ipms.ua

ZATULOVSKY A.S.

Physico-Technological Institute of Metals and Alloys, NASU, Kyiv, Ukraine
Tel.: (044) 444-3542
Fax: (044) 444-3542
E-mail: kompozit@inec.kiev.ua

ZATULOVSKY S.S.

Physico-Technological Institute of Metals and Alloys, NASU, Kyiv, Ukraine
Tel.: (044) 444-3542
Fax: (044) 444-3542
E-mail: kompozit@inec.kiev.ua

ZAVALIY I.YU.

Karpenko Physico-Mechanical Institute, NASU, Lviv, Ukraine
Tel.: (0322) 65-4833
Fax: (0322) 64-9427
E-mail: zavalii@ipm.lviv.ua

ZEL'DOVICH V.I.

Institute of Metal Physics, Ekaterinburg, Russia
E-mail: zeldovich@imp.uran.ru

ZELYAVSKII V.B.

Frantsevich Institute for Problems of Material Science, NASU, Kyiv, Ukraine
Tel.: (044) 444-1501
E-mail: tomila@materials.kiev.ua

ZHABREV V.A.

Institute of Silicate Chemistry, RAS, Saint-Petersburg, Russia
Tel.: (812) 328-8596
Fax: (812) 328-5401
E-mail: olgashilova@peterlink.ru

ZHARIN A.L.

Powder Metallurgy Research Institute, NASB, Minsk, Belarus
Tel.: (375 17) 239-9892
Fax: (375 17) 210-0574
E-mail: zharin@hotmail.com

ZHUNKOVSKII G.L.

Frantsevich Institute for Problems of Material Science, NASU, Kyiv, Ukraine
Tel.: (044) 444-1481, 444-3301, 444-1321

ZHURAVLEV V.S.

Frantsevich Institute for Problems of Material Science, NASU, Kyiv, Ukraine
Tel.: (044) 444-6201, 444-3017, 444-3502

ZIBROV I.P.

Institute of Crystallography, RAS, Moscow, Russia
Tel.: (095) 330-7883
Fax: (095) 135-1011
E-mail: zibrov@ns.crys.ras.ru,

ZIMINA G.

Kurdyumov Institute for Metal Physics, NASU, Kyiv, Ukraine
Tel.: (044) 444-9520
E-mail: kotr@imp.kiev.ua

ZINCHENKO V.F.

Bogatsky Physico-Chemical Institute, NASU, Odessa, Ukraine
Tel.: (0482) 61-8225, 66-2097
Fax: (0482) 65-2012
E-mail: physchem@paco.net

ZINEVICH T.M.

Taras Shevchenko Kyiv National University, Kyiv, Ukraine
Tel.: (044) 221-0270
E-mail: vovd@ukr.net, vsudavtsova@univ.kiev.ua

ZINKOVSKY G.

Dnipropetrovsk National University, Dnipropetrovsk, Ukraine
Tel.: (0562) 469-212, 776-9042
Fax: (0562) 461-697
E-mail: odm@ff.dsu.dp.ua

ZUBETS Y.E.

Frantsevich Institute for Problems of Material Science, NASU, Kyiv, Ukraine
Tel.: (044) 444-8286, 444-2524, 444-0294
E-mail: dep53@ipms.kiev.ua

ZVONAREV E.V.

Powder Metallurgy Research Institute, NASB, Minsk, Belarus
Tel.: (017) 239-9842
Fax: (017) 210-0574
E-mail: gorokhov47@mail.ru

ZYATKEVICH N.S.

Frantsevich Institute for Problems of Material
Science, NASU, Kyiv, Ukraine
Tel.: (044) 444-1501, 444-2101
Fax: (044) 444-2131
E-mail: imorozov@materials.kiev.ua

ZYKOVA E.V.

Frantsevich Institute for Problems of Material
Science, NASU, Kyiv, Ukraine
Tel.: (044) 444-8286, 444-2524, 444-0294

JOINING OF POROUS AND COMPACT TITANIUM WITH LASER WELDING AND PLASTIC DEFORMATION

Savich V.V., Pilinevich L.P., Tumilovich M.V., Tolochko N.K.⁽¹⁾

Powder Metallurgy Research Institute of the NAS of Belarus, Minsk, Belarus

⁽¹⁾Technical Acoustics Research Institute of the NAS of Belarus, Vitebsk, Belarus

Titanium filters have gained wide application for cleaning food liquids, chemical solutions, medical preparations [1]. Porous titanium elements are used as parts of surgical implants [2]. These parts often look like built-in constructions, consisting of porous elements and different main and auxiliary parts (flanges, connecting pipes, etc.). As a rule, they use welding for their assembling. But conventional methods of argon and electron-beam welding of titanium, which are widely used in aircraft and space industries [3, 4] for welding of porous parts do not provide necessary quality of welded joints.

The present paper modes of laser welding and conditions of preliminary preparation of joint surfaces, influencing quality of a weld during their welding porous parts produced from technically pure titanium powder ITX2-1 with parts from compact technically pure titanium BT1-0 are studied.

In a sheet of compact titanium there was cut out a hole with diameter $\varnothing 185$ mm in which there was tightly inserted a porous disc of the same diameter. These parts were welded by laser along the joint perimeter.

Impulse Nd:YAG laser ($\lambda=1.06$ μm) was used as a source of laser radiation. The best quality of welded joints characterized by absence of pores and cavities, smooth and flat surface of solidified metal in a weldpool, the same dimensions along the whole weld perimeter were obtained at the following conditions: impulse radiation energy - 2-4 J, impulses time - 4 milliseconds, frequency of impulses repetition - 5 Hz, diameter of laser spot - 0.7-1.1 mm, speed of laser spot motion - 30-50 mm/min.

Treatment of titanium in technological processes, characterized by thermal effect is carried out in vacuum or inert protective gas environment [5]. But our experiments have showed that you can achieve appropriate quality of a titanium weld in the air when using impulse laser radiation.

In Figure 1 you can see a photo of such a welding joint of porous and compact titanium after etching.



Figure 1. Cross-section metallographic specimen of a welded joint of compact and porous titanium after etching. $\times 50$

In Fig. 1 you can determine that at optimal treatment modes the weld is dense and smooth. Its width is 1.5-1.7 mm and depth 1.1-1.3 mm. The weld is recessed below the welded parts surface at the depth of about 200 μm , which is connected with titanium melting and the melt infiltration into pores. Preliminary mechanical treatment of porous titanium, due to its high viscosity and plasticity, leads to compaction of the materials in the zone of cutting and «smoothing out» of pores. As an effect of that reduction of the material shrinkage degree during welding and limitation of the melt infiltration into pores takes place, which reduces possibility of formation of the mentioned defect.

The weld metal heats to the temperature higher than the melting point and after cooling has plate structure of fast-cooled casted metal of martensite type [6]. As for near-weld zone, it is typical to observe partial melting of grains boundaries. Average width of this zone is 90-105 μm . Zone of thermal influence includes a zone of phase refining, where the metal got a meta-stable α' -transformed structure, and a transformation zone from α' -transformed structure to the basic metal structure.

Multi-zone type of the weld structure was proved by results of hardness measuring.

During tensile testing of all the samples under investigation we have observed breaking not in the place of a weld but along the body of porous elements. Equivalent tensile strength was 50-70 MPa, and strength of the weld was, accordingly, higher than this number.

We have also carried out investigations of the process of a permanent joint from compact and porous titanium production by expansion [7]. This method enables to join easily parts having different plastic properties. Due to the fact that compact titanium has higher hardness and stiffness, a porous part should be deformed. According to this hypothesis the porous part is the one under straddling, so the other one should have a cut pit, with a closed groove inside along its perimeter. This groove should be «filled in» with the material of the porous part due to local plastic deformation.

There was carried out a number of experiments on models, which scheme is presented in Figure 2.

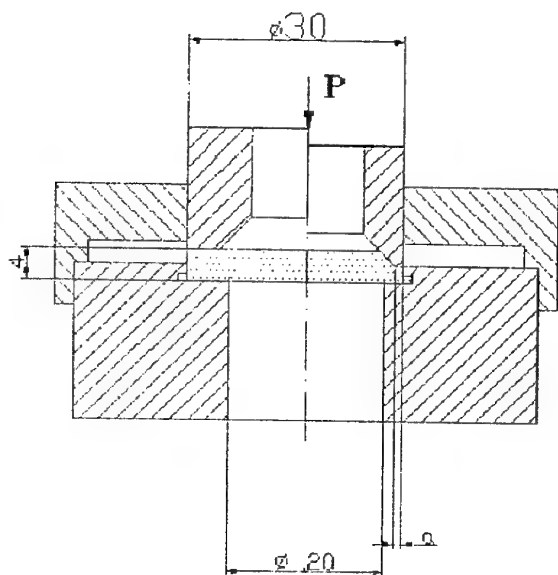


Figure 2. Scheme of expansion of a model porous sample into a compact mandrel.

For our experiments we were using porous discs from titanium powder with height 4 mm and diameter $30_{-0.1}^{+0.05}$ mm calibrated along their diameter. We were cutting standard cartridges with central hole 20 mm in diameter, pits $30_{-0.05}^{+0.05}$ mm in diameter of different depth with square grooves along their sides. The outer diameter of the groove was the same for all the cartridges (34 mm). Only 2 pa-

rameters were under variation - depth of the pit and height of the groove. With the help of special ring punches, mounted directly along the axes of the cartridges and porous discs, we have carried out local inserting of the discs to the level of the cartridge surfaces. As for the punches we were varying width of deformed ring surface and degree of deformation. Height of the groove was 12, 24 and 36% of the disc height.

After shrinkage and compacting the porous discs into the cartridge we were measuring force of ejecting a disc out of the cartridge.

The results of the investigations carried out have showed that optimal ejecting force (higher than 700-750 N) is achieved at the following parameters: relative deformation degree - 2-3 mm; relative groove height - 35-38%.

The achieved results can be used for optimizing processes of joining porous and compact materials.

References

1. Vityaz P.A., Kaptsevich V.M., Sheleg V.K. Porous Powder Materials and Parts Made from Them // Minsk. «Vysheishaya Shkola» Publishers, 1987, 164 p. (in Russian).
2. V. Savich, A. Ilyuschenko Porous and Nonporous Titanium for Surgical Implants of Various Application // Proceedings of the 1998 Powder Metallurgy World Congress & Exhibition. Granada, Spain. 1998, vol.5, p.352-356.
3. Technology for Production of Titanium Aircraft Parts // A.G. Bratukhin, B.A. Kolachev, V.V. Sadkov and others / M., «Mashinostroyeniye» Publishers. 1995, 448p. (in Russian).
4. G.Yu. Pinchuk. Laser Welding of Porous Materials // «New Materials and Technologies». Theses of reports at Republican Scientific-Technical Conf., Minsk. 1994, p.186 (in Russian).
5. Technology of Non-ferrous Metals and Alloys Thermal Treatment // B.A. Kolachev, R.M. Gabidulin, Yu.V. Piguzov / M., «Metallurgy» Publishers. 1992, 272 p. (in Russian).
6. Laser Welding of Porous and Compact Titanium Elements // N.K. Tolochko, V.V. Savich, L.P. Pilinovich and others / Physics and Chemistry of Materials Treatment, 2000, #4, p.75-78 (in Russian).
7. Permanent Joint of Implant Parts from Compact and Porous Titanium Produced by Their Cold Plastic Deformation // V.V. Savich, S.A. Bedenko / Powder Metallurgy, 2001, issue 24, p.79-82 (in Russian).

COMPOSITE METAL-POLYMER POROUS MATERIALS FOR GASES DEHUMIDIFICATION AND FUEL DEWATERING

Ilyuschenko A.Ph., Pilinevich L.P., Tumilovich M.V., Savich V.V., Kravtsov A.G.⁽¹⁾, Ryabchenko I.A.⁽¹⁾

Powder Metallurgy Research Institute of the NAS of Belarus (Minsk, Belarus)

⁽¹⁾Mechanics of Metal-Polymer Systems Research Institute of the NAS of Belarus (Gomel, Belarus)

Complex cleaning and dewatering of gases, fuel and lubricants from mechanical impurities is a promising application for porous permeable materials (PPM) which are determined by their structural and capillary properties [1].

Effectiveness of removing mechanical impurities by porous materials is determined by shape and sizes of pores and material thickness. Moisture separation depends, first of all, on capillary properties of pores surface. Adhesion interaction takes place during the contact between water and hard surface, which influences effectiveness of moisture separation.

Characteristics of adhesion between a compact hard body and a liquid are not the same as compared to adhesion between a porous body and a liquid. On porous surface edge angle θ is not true, but is a seeming edge angle. Porosity of a hard surface increases a seeming edge angle, if the true one is less than 90° . Higher porosity of a hard surface may lead to significant reduction of wetting even in a case of hydrophilic surfaces. That's why water-repellency is not a function only of a wetting angle and for its estimation we need to use parameters of porous structures correlating to water-repellency.

A porous material is usually considered as a system of open cylinder capillaries with an average diameter of d . Capillary pressure $P = 4\sigma \cos\theta/d$ (σ - surface tension) causes suction of liquid into a capillary. In conditions of complete wetting $\theta = 0$, $\cos\theta = 1$, and P is maximal. At non-complete wetting, when $\theta > 0^\circ$, $\cos\theta < 1$, value of P reduces. At $\theta > 90^\circ$, $\cos\theta$ changes its sign and, correspondingly, capillary pressure changes its direction as well preventing ingress of moisture into pores (anti-capillary pressure). Cosine of edge wetting angle for porous and polymer materials, determined according to method [2] is presented in Figure 1.

In Fig.1 you can see that bronze has the least value of $\cos\theta$ from all metals, and PTFE - from polymers. The following investigations [3] showed that the least moisture-absorption capacity was determined for PPM from bronze and PTFE

powders, and the highest - for PPM from titanium and copper powders. At the same time porous titanium holds moisture at the highest temperature comparing to other materials. Investigations of water yielding capacity of different PPM during their drying at 100°C showed that PPM from titanium powder have high moisture capacity and high ability to hold it [3].

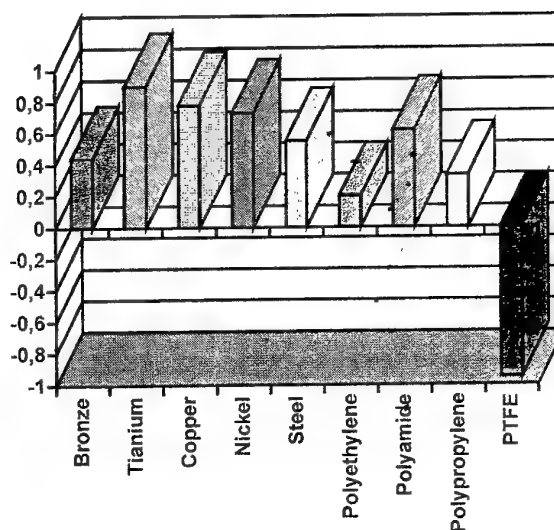


Figure 1. Cosine of edge water wetting angle for different materials.

Taking all the mentioned above into consideration at least two PPM with different parameters of porous structure and physical and physical-chemical properties are necessary for effective separation of water vapor and droplets from fuel, lubricants and compressed gases.

Thus, for cleaning and dewatering fuel a composite metal-polymer PPM (MPPM) was developed consisting of two layers. Substrate was made of sintered bronze powder (thickness 3-4 mm) which provides mechanical strength, necessary cleaning fineness and permeability, and a thin selective hydrophobic layer is precipitated in vacuum when a PTFE block is exposed to focused

CO₂-laser radiation and generation at certain modes of ultra-fine fibre [4]. Porosity of a fibre PTFE layer can reach 80-90%, it can be formed on quite complex-shaped parts. Technology enables to control porosity according to thickness. A MPPM like that enables to separate water from fuel and liquid oil. At the same time PTFE serves as a water-repellent, which is practically not permeable for water and other polar liquids. General look and structure of a filter element are presented in Fig. 2.

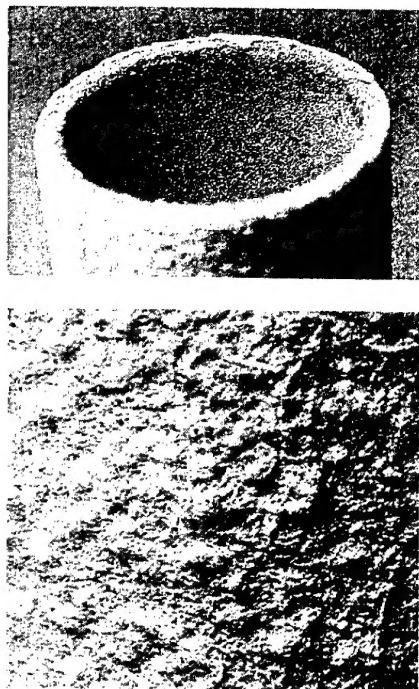


Figure 2. Structure of porous material «PTFE - bronze» for fuel dewatering.

A test sample of filter element from this MPPM was tested at Minsk Motor Works on summer diesel fuel with density of 0.84 g/cm³ and viscosity of 3.6 cSt for its corresponding to standard requirements for filters of rough and fine cleaning. Test results have showed that cleaning completeness for mechanical impurities was 95-98 % and can be increased by optimization of porous structure of metal porous layer, and completeness of moisture separation from diesel fuel was 100 % at any test mode.

To dry compressed air and other gases we have developed two types of double-layer MPPM based on porous titanium - with a selective PTFE layer produced according to the technology mentioned before, and a selective layer from HPPE fibre deposited according to «Melt-blowing» method [5]. A selective layer provides cleaning from mechanical impurities and moisture droplets. A layer from porous titanium with big pores has high moisture absorption and moisture capacity to pro-

vide vapour condensation and holding of formed droplets in pores. Tests have showed close character of both types of MPPM, and lower cost of MPPM with a selective layer from HPPE. In Figure 3 you can see general look and structure of a filter from the last material.

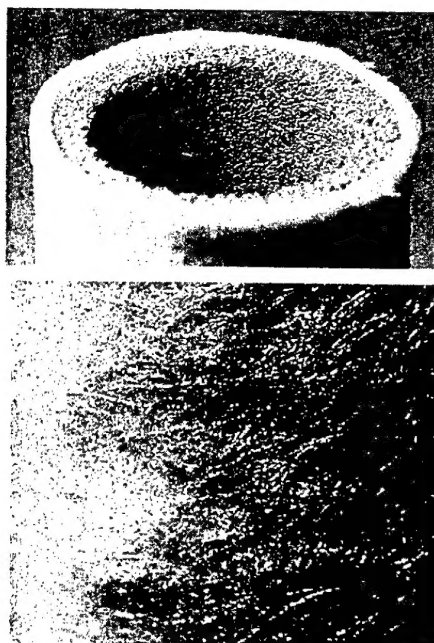


Figure 3. Structure of porous «HPPE - titanium» material for drying compressed air.

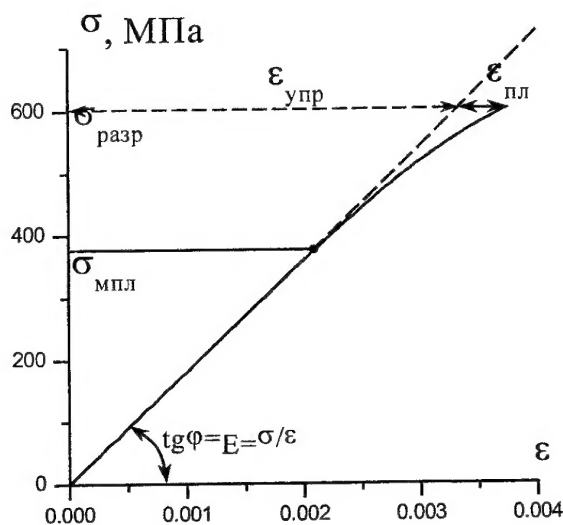
Dew point when drying air with MPPM with a selective layer from HPPE fibre reduces to -5 °C, completeness of cleaning from droplets and vapors reaches 99.99 %.

The investigations carried out have showed that MPPM «PTFE - bronze» is the most effective for water separation from fuel and lubricants; «PTFE - titanium» or «HPPE - titanium» - for drying compressed gases.

1. P.A. Vityaz, V.M. Kaptsevich, V.K. Sheleg. Porous Powder Materials and Parts Made from Them // Minsk. «Vysheishaya Shkola», 1987, 164 p. (in Russian).
2. A.Ph. Ilyuschenko, L.P. Pilinevich, M.V. Tumilovich. Porous Powder Materials for Effective Cleaning Gases and Liquids // Proceedings of PM2001 Congress & Exhibition, Nice, France, 22-24 October, 2001, vol.1, p. 369-374.
3. P.A. Vityaz, V.K. Sheleg, V.V. Savich and others. Definition of Edge Angle for Capillary-Porous Materials // «Zavodskaya Laboratoriya».- vol.51, 1985, #4, p. 53-55 (in Russian).
4. L.F. Ivanov. Physics and Technology of Laser Processing PTFE into Fibre-Porous Materials // Theses for Ph.D. degree, Gomel, IMMS, 1998 (in Russian).
5. V.A. Goldade, A.V. Makarevich, L.I. Pinchuk and others. Polymer Fibre «Melt-Blowing» Materials // Gomel, IMMS, 2000, p.254 (in Russian).

ЛАБОРАТОРИЯ МЕХАНИЧЕСКИХ ИСПЫТАНИЙ Института проблем материаловедения им. И.Н. Францевича НАН Украины проводит испытания керамики, металлов и других материалов на **изгиб, растяжение, сжатие, длительную прочность, индентирование** в широком интервале температур с определением комплекса механических свойств (**модуль упругости**, предел текучести, разрушающее напряжение, пластическая деформация, трещиностойкость, твердость и т.д.) на **современных компьютеризированных испытательных машинах**, в том числе есть возможность наблюдения эволюции структуры материала в процессе нагружения в **сканирующем электронном микроскопе T20**.

Испытания проводятся в соответствии с ГОСТами, международными стандартами ISO, CEN, ASTM или по техническим условиям заказчика.



**Мы точно
определим,
какое напряжение
выдержит Ваш
материал!**

Оперативность проведения испытаний, их высокая точность — отличительные характеристики нашей работы.

Оплата по договоренности.

Контакты:

Заведующий лабораторией
докт. физ.-мат. наук, профессор
Подрезов Юрий Николаевич

e-mail: podrezov@materials.kiev.ua
телефон: (044) 444-00-51

Главный инженер
Вербило Дмитрий Григорьевич

e-mail: ver@materials.kiev.ua
телефон: (044) 444-00-51

Адрес в интернете:

http://ru.ipms.kiev.ua/Departments/Dep-22/SECM/SECM_eng.htm